VNIVERSITAT DE VALÈNCIA

Doctorado en Física

$\overline{K}^0 - K^0$, $\overline{D}^0 - D^0$ and $\overline{B}^0 - B^0$ oscillations in the Standard Model and beyond from unquenched Twisted Mass Lattice QCD

PhD dissertation by

Nuria Carrasco Vela

Thesis director

Vicent Giménez Gómez

Departamento de Física Teórica, Facultad de Física
IFIC (Instituto de Física Corpuscular CSIC/UV)

Valencia, Spain
May 2013

Vicent Giménez Gómez, Catedrático de la Universidad de Valencia,

CERTIFICA:

Que la presente memoria,
"$\overline{K}^0 - K^0$, $\overline{D}^0 - D^0$ and $\overline{B}^0 - B^0$ oscillations in the Standard Model and Beyond from unquenched Twisted Mass Lattice QCD" ha sido realizada bajo su dirección en el Departamento de Física Teórica de la Universidad de Valencia-IFIC, por **Nuria Carrasco Vela** y constituye su Tesis para optar al grado de Doctora en Física.

Y para que así conste, en cumplimiento de la legislación vigente, presenta en el Departamento de Física Teórica la referida Tesis Doctoral y firma el presente certificado en Valencia, a 30 de Mayo de 2013.

Firma del director de tesis

Vicent Giménez Gómez

Agradecimientos

Quiero agradecer, en primer lugar, a Vicent por haber confiado en mi para llevar a cabo este proyecto, por orientarme y por apoyar mi formación permitiéndome asistir a cursos, reuniones de la ETMC y conferencias. Gracias también por la corrección y revisión de esta tesis.

Questa tesi è anche un po' italiana. Un grazie particolare va a tutte le persone che ho trovato a Roma e con cui ho condiviso questo progetto di ricerca. Questo lavoro è il frutto della collaborazione con loro. Non potrò mai ringraziare abbastanza Petros Dimopoulos, per l'ospitalità, per la sua constante disponibilità, per tutto ciò che mi ha insegnato e per avermi seguito e consigliato durante quasi tutto il percorso di dottorato. Ringrazio inoltre Roberto Frezzotti, Giancarlo Rossi, Vittorio Lubicz, Silvano Simula e Cecilia Tarantino. Grazie per l'accoglienza a Roma, per le interessanti discussioni e per avermi coinvolto in tanti lavori. Infine ringrazio Francesco Sanfilippo che, oltre alla straordinaria collaborazione scientifica, è presto diventato un amico.

Aún en Roma, pero con un pie en Valencia, quisiera mencionar a David Palao con quien he tenido la suerte de encontrarme en mis dos estancias en Roma.

A mis compañeros del departamento de Física Teórica de la Universidad de Valencia. Son muchas las personas con las que he tenido el placer de coincidir durante estos últimos años y que poco a poco me han ido enriqueciendo. Enumerarlos uno a uno sería demasiado largo. En pocas palabras, gracias a todos. No obstante, quisiera acordarme de Felip A.Nadal por las tantas veces que ha dedicado su tiempo a resolver mis problemas informáticos y dudas burocráticas. Y, como no, gracias a David Ibañez que me ha soportado en la mesa de al lado durante casi tres años lo cual, en ocasiones, no debe haber sido fácil.

Por supuesto mil gracias a Ana Doblas, Vicent Ferrando y Vicent Marín, por convertir las comidas en Burjassot en uno de los mejores momentos del día.

Y por último, mi familia: mi hermano, mi sobrina Paula y mis padres. Mi gratitud va más allá de lo que pueda expresar aquí en un par de lineas. Así que, simplemente, gracias.

The work presented here is part of the rich flavour phenomenology program of the ETM Collaboration. I gratefully acknowledge all the members for the fruitful collaboration. My PhD thesis is based on their experience, ideas and projects and it would not have been possible without them.

I would also like to mention the members of my thesis evaluation committee: Francisco Botella, Petros Dimopoulos, Vittorio Lubicz, Juan Nieves, Elisabetta Pallante and Cecilia Tarantino. Thanks for accepting the proposal of reading and evaluating a thesis of almost 300 pages.

This work had been supported by the Spanish MCEI under the grants No. FPA2008-03373 and No. FPA2011-23897.

I acknowledge the CSIC (*Consejo Superior de Investigaciones Científicas*) and the IFIC *(Instituto de Física Corpuscular* mixed centre CSIC/UV) for the financial support provided by a *JAE-Predoctoral* grant and the financial aids for short stays at foreign institutions.

CPU time for this work was made available to the ETMC by the PRACE Research Infrastructure resource JUGENE based in Germany at Forschungzentrum Juelich (FZJ) under the project PRA027 “QCD Simulations for Flavor Physics in the Standard Model and Beyond” and the Italian SuperComputing Resource Allocation (ISCRA) under the class A project HP10A7IBG7 "A New Approach to B-Physics on Current Lattices" and the class C project HP10CJTSNF "Lattice QCD Study of B-Physics" at the CINECA supercomputing service. We acknowledge the BSC on MareNostrum in Barcelona, the North-German Supercomputing Alliance (HLRN), the AuroraScience, Donald Smits center for information technology, University of Groningen, IDRIS, INFN/apeNEXT, GENCI Grant 052271 and CC-IN2P3 for partial computing support.

Contents

Introducción

El Modelo Estándar de la física de partículas es la mejor teoría que los físicos tenemos a día de hoy para describir las partículas elementales y sus interacciones no gravitatorias. Recapitulemos muy brevemente: El Modelo Estándar es una teoría cuántica de campos que describe la interacción de los fermiones mediada por bosones de gauge y las interacciones de los bosones de gauge entre ellos. Es capaz de explicar tres de las cuatro fuerzas fundamentales de la naturaleza: la interacción fuerte o Cromodinámica Cuántica (QCD), la interacción electromagnética o Electrodinámica Cuántica (QED) y la interacción débil unificada con el electromagnetismo en la llamada interacción electrodébil [1, 2].

Las partículas elementales, en el sentido que no poseen estructura interna, son los leptones y quarks, mientras que los hadrones son partículas con estructura interna formados por quarks. Los quarks existen solamente dentro de los hadrones donde están confinados por la fuerza fuerte. Los quarks y los leptones son por tanto los constituyentes básicos de la materia fermiónica que vienen agrupados en tres familias. Hay seis quarks: up (u), down (d), charm (c), strange (s), top (t) y bottom (b). Los quarks son tripletes del grupo gauge SU(3) y por tanto transportan una carga adicional, llamada color, que es la responsable de la interacción fuerte. Además a cada uno de ellos se le asigna una carga de sabor diferente que se considera un número cuántico conservado bajo QCD pero no bajo las interacciones electrodébiles. Las tres familias de quarks están mezcladas, es decir los autoestados de masa no corresponden con los autoestados de interacción. Esta mezcla está parametrizada por la matriz de Cabibbo-Kobayashi-Maskawa (CKM). Asimismo, hay seis leptones: el electrón (e), el muón (μ), el tau (τ) y los tres correspondientes neutrinos (ν_e, ν_μ y ν_τ). Los leptones no poseen carga de color y por tanto no participan en las interacciones fuertes.

La interacción entre las partículas viene mediada por bosones: los ocho gluones no masivos que median en la interacción fuerte entre las partículas con carga de color, es decir los quarks; el fotón, sin masa, responsable de la interacción electromagnética y las partículas masivas $W^{\pm}$ y Z de la interacción débil. El mecanismo de Higgs es el responsable de que los bosones débiles adquieran masa a través de la rotura del grupo de simetría $SU(2) \otimes U(1)$ que describe la interacción electrodébil.

Con esta simple descripción el Modelo Estándar ha sido capaz de describir la mayor parte de los datos experimentales. Durante los últimos cuarenta años numerosos experimentos lo han puesto a prueba obteniendo un acuerdo realmente espectacular con las predicciones teóricas. Es más, en el último año, un nueva partícula con masa entorno a 125 GeV y las propiedades del bosón de Higgs ha sido observada por Atlas y CMS [3, 4]. Después de años de una intensa búsqueda experimental, éste podría ser el bosón de Higgs del Modelo Estándar, la única partícula del modelo que faltaba por descubrir.

No obstante, a pesar del éxito del Modelo Estándar para describir con precisión una gran variedad de resultados experimentales, existen varias razones para creer que ésta no es la teoría definitiva de la física de partículas sino otro paso más hacia una teoría más general. Una de las principales dificultades del Modelo Estándar es que no incluye la interacción gravitatoria. Otra es que no explica el 95% del Universo que no está compuesto por materia ordinaria sino por materia oscura (~27%) y energía oscura (~68%). ¿Cuál es la partícula que constituiría la materia oscura? ¿Cuál es el origen de la energía oscura? son preguntas que el Modelo Estándar no puede responder.

A parte de estos, hay otra serie de problemas relacionados con la estructura de sabor del Modelo Estándar: ¿Cual es la naturaleza de las oscilaciones de neutrinos? ¿Por qué el universo está hecho de materia y no de antimateria? ¿Cual es el origen de la violación de CP? ¿Por qué la interacción fuerte es invariante CP mientras que la interacción débil no lo es?

Finalmente, aunque el Modelo Estándar es auto consistente contiene muchos parámetros que no predice el modelo y que deben ser medidos experimentalmente: las tres constantes de acoplamiento α_s, $\alpha_{\rm em}$ y G_F de la fuerza fuerte, electromagnética y débil respectivamente; las masas de los seis quarks, tres leptones y tres neutrinos (en el caso en que son masivos); la masa del bosón Z que establece la escala de la interacción débil; la masa del Higgs, los ángulos de mezcla bajo la interacción débil y el parámetro de violación de CP. 18 parámetros si los neutrinos no tienen masa, es decir en el Modelo Estándar estrictamente hablando, pero 7 más, 25 en total, si los neutrinos son masivos: las tres masas de neutrinos, tres ángulos de mezcla y una fase. El Modelo Estándar nos dice como interactúan las partículas pero no nos dice nada de sus propiedades intrínsecas: ¿Por qué hay tres familias de fermiones? ¿Por qué las partículas tienen esas masas y no otras? ¿Por qué las masas de los neutrinos son mucho menores que las de los otros leptones? Todo esto nos lleva a pensar que debe existir otra teoría que nos diga por qué dichos parámetros tienen precisamente los valores que tienen.

Desde la misma invención del Modelo Estándar, a principios de los años setenta, la física teórica ha intentado encontrar una alternativa o extensión del Modelo Estándar que pueda dar respuesta a estas cuestiones todavía no resueltas: diversos modelos de supersimetría, teorías con dimensiones adicionales, tecnicolor etc... Con este amplio abanico de teorías a nuestra disposición son necesarios datos experimentales capaces de confirmar o descartar sus predicciones.

Con la puesta en marcha del LHC estamos viviendo un momento de gran expectación en física de partículas. Los nuevos datos experimentales proporcionan una valiosa información que nos permitirá entender si el Modelo Estándar es todo lo que podemos ver por ahora en los experimentos o si se revelan ya señales de nueva física. Sin embargo,

la observación directa de nuevas partículas en colisionadores de altas energías, como el LHC, no es la única forma de descubrir nueva física. Paradójicamente, mediciones de precisión en procesos a bajas energías pueden explorar regiones de energía más allá de las accesibles en el LHC y podrían también escudriñar señales de nueva física. Esto no es más que uno de los aspectos no intuitivos de la teoría cuántica de campos: partículas de gran masa aún no descubiertas podrían contribuir a procesos de bajas energías a través de correcciones cuánticas.

Desviaciones respecto a las predicciones del Modelo Estándar revelarían el intercambio de partículas virtuales pesadas involucrando escalas de energías a las que el LHC es completamente ciego. Por ello, medidas de precisión de procesos suprimidos en el Modelo Estándar como los procesos de FCNC, donde por consiguiente los efectos de nueva física podrían ser competitivos, proporcionan un interesante marco experimental y teórico para estudiar la consistencia del Modelo Estándar y aportan una información de gran valor sobre la estructura de la nueva teoría que reemplazará al Modelo Estándar.

Retornemos con más detalle a uno de los problemas cruciales del Modelo Estándar: la asimetría materia-antimateria. El universo, al menos el que hemos observado, está compuesto en su mayoría por partículas (protones, neutrones y electrones principalmente) y no por antipartículas. Por tanto, deben existir procesos elementales que favorezcan la materia sobre la antimateria: los procesos de violación de CP.

Matemáticamente, la operación conjugación de carga (C) cambia el signo de todos los números cuánticos aditivos (carga eléctrica, hypercarga, extrañeza...) mientras que paridad (P) invierte las coordenadas espaciales. En el Modelo Estándar, QED y QCD conservan C y P separadamente. En cambio, las interacciones electrodébiles rompen la simetría bajo C y P. Sin embargo, la invariancia se recupera casi en su totalidad si en vez de considerar C o P consideramos la combinación CP.

La simetría bajo CP se consideró exacta hasta 1964 cuando la violación bajo CP se observó por primera vez en el sistema de kaones [5]. Esta fue la primera prueba de violación de CP indirecta. La primera evidencia de violación de CP directa se encontró en los años noventa en la desintegración de los kaones neutros por el experimento NA31 del CERN [6] y fue posteriormente confirmada en 1999 por el experimento KTeV en Fermilab [7] y NA48 en el CERN [8]. En 2001 los experimentos BaBar en SLAC y Belle en KEK, las llamadas factorías de B, confirmaron la violación de CP en el sector de la física del B [9, 10] mostrando que ésta no estaba confinada al sector de los kaones. Recientemente, en el 2011, la primera evidencia de violación de CP en la desintegración de mesones D neutros ha sido observada en el LHCb [11].

De acuerdo con el Modelo Estándar, la violación de CP solo puede ocurrir en las interacciones débiles, más específicamente, con neutrinos sin masa, la violación de CP solo puede tener lugar en procesos con cambio de sabor de quarks (con neutrinos masivos la violación de CP en el sector leptónico es también posible). De hecho, la interacción débil es la única en el Modelo Estándar que puede cambiar el sabor de los quarks. Estos procesos de cambio de sabor dependen típicamente de las masas de los quarks involucrados y del acoplamiento entre los quarks de diferentes sabores. Este acoplamiento entre los quarks bajo la interacción electrodébil vienen descrito mediante una matriz unitaria denominada la matriz de Cabibbo-Kobayashi-Maskawa (CKM) [12]

$$V_{CKM} = \begin{pmatrix} V_{ud} & V_{us} & V_{ub} \\ V_{cd} & V_{cs} & V_{cb} \\ V_{td} & V_{ts} & V_{tb} \end{pmatrix}$$

La matriz CKM debe ser unitaria y viene parametrizada con tres ángulos y una fase compleja. Esta fase compleja es la única fuente de violación de CP en el Modelo Estándar lo que restringe los fenómenos de violación de CP permitidos. Si los acoplamientos rompen la condición de unitariedad o el valor de fase de violación de CP difiere entre las predicciones teóricas y el experimento, entonces contribuye algún proceso desconocido que podría estar indicando nueva física.

Por ejemplo, con una cuarta generación de quarks, la matriz CKM reducida 3x3 no sería unitaria o si nuevas partículas no incluidas en el Modelo Estándar cambiasen el sabor de los quarks, la relación que el Modelo Estándar predice entre la medida experimental relacionada con un cierto observable de cambio de sabor y la matriz CKM no sería cierta. Por esta razón, se está realizando un gran esfuerzo experimental y teórico para medir los elementos de la matriz de CKM con precisión suficiente para detectar estas posibles desviaciones.

Actualmente, la violación de CP es un fenómeno físico confirmado en las desintegraciones débiles de kaones y mesones B consistente con la explicación teórica que proporciona la matriz CKM. Sin embargo, aunque la presencia de una sola fase de violación de CP, como predice el Modelo Estándar, es capaz de explicar los fenómenos observados en el laboratorio, el mecanismo CKM sigue sin explicar por qué la materia domina sobre la antimateria. De forma más precisa, la matriz CKM predice una densidad de numero bariónico que está varios ordenes de magnitud por debajo del valor observado actualmente [13].

Además, experimentalmente CP no se viola en las interacciones fuertes. Este hecho experimental conlleva un problema de ajuste fino, o *fine tuning*, de los parámetros. En principio, nada nos impide añadir un término en el Lagrangiano de QCD de la forma $\mathcal{L}_\theta \sim \theta \epsilon^{\mu\nu\rho\sigma} F_{\mu\nu} F_{\rho\sigma}$ que viola explícitamente CP. Este término induce un momento dipolar eléctrico para el neutrón proporcional a θ. Sin embargo, la cota experimental para el valor del momento dipolar eléctrico del neutrón conduce al valor $\theta \leq 10^{-11}$[14]. Este ajuste fino se conoce como el problema fuerte de CP, o *strong CP problem* en inglés, y la razón por la cual es necesario es un misterio. Aunque no es un problema en sí mismo, parece poco natural ya que existen de modo natural términos que violarían CP en el Lagrangiano de QCD y fijarlos a cero a posteriori no proporciona ninguna simetría adicional.

Estas evidencias, la asimetría materia-antimateria y el problema fuerte de CP, nos hacen pensar que deben existir fuentes de violación de CP más allá del mecanismo de la matriz CKM. En este ámbito, la precisión en física del sabor resulta ser una buena estrategia para mirar más allá del Modelo Estándar.

El enfoque para estudiar los procesos electrodébiles a bajas energías está basado en la observación de que la masa del bosón W es del orden de 100 GeV mientras que las escalas hadrónicas típicas son del orden de 1 GeV. Por tanto, la masa del W se puede considerar mucho mayor que cualquier escala hadrónica relevante en el proceso. Junto con

el desarrollo en producto de operadores (OPE), esta hipótesis conduce a la construcción de un Hamiltoniano efectivo débil en el que las amplitudes físicas vienen expresadas como sumas sobre elementos de matriz de operadores locales.

En este tipo de análisis de precisión de procesos electrodébiles, la medida precisa de un experimento, por ejemplo un tiempo de desintegración, debe ser comparado con la expresión analítica del mismo proceso predicha por el Modelo Estándar. El OPE factoriza la expresión teórica en tres partes: una combinación de ciertos parámetros del Modelo Estándar, el elemento de matriz no perturbativo del Hamiltoniano efectivo electrodébil y ciertos factores peturbativos, los llamados coeficientes de Wilson. Por tanto, por cada oportuna medición experimental obtenemos una restricción sobre una cierta combinación de parámetros del Modelo Estándar siempre que el elemento de matriz hadrónico que controla el proceso sea conocido.

Los coeficientes de Wilson contienen los efectos de corta distancia que incluyen los efectos físicos desde las escalas de energías altas, como la escala electrodébil M_W o la posible escala de nueva física, hasta la escala hadrónica. Mientras que estos coeficientes se pueden calcular en teoría de perturbaciones, los métodos perturbativos pierden su validez en el cálculo del elemento de matriz hadrónico a bajas energías. Esto es debido a que las correcciones no perturbativas de QCD a los procesos electrodébiles a bajas energías pueden ser grandes debido al intercambio de gluones entre el estado inicial y final. En otras palabras, para describir con precisión estos elementos de matriz, el efecto de confinar los quarks dentro de hadrones, es decir las correcciones de QCD, deben ser incluidas.

Pero, ¿Por qué las interacciones fuertes son no perturbativas en el mundo hadrónico mientras que los efectos electrodébiles se pueden calcular en teoría de perturbaciones? En su formulación QED y QCD son muy similares: ambas son teorías de campos invariantes gauge. Pero mientras que QED está basada en una teoría invariante gauge U(1) abeliana y local, QCD está construida sobre una teoría gauge SU(3) y por tanto no abeliana. Es sorprendente como esta diferencia en su formulación tiene enormes consecuencias para la fenomenología: mientras que los fotones son neutros y por tanto no interaccionan directamente entre ellos, los gluones transportan carga de color y en consecuencia interactúan no solo con los quarks sino también entre ellos mismos. Esta aparentemente pequeña diferencia es la raíz de la complejidad de QCD: a altas energías el acoplamiento de QCD α_s es pequeño, lo que se conoce como la libertad asintótica de QCD, por lo que son posibles los cálculos perturbativos; en cambio a bajas energías α_s es grande dando lugar al confinamiento de los quarks dentro de los hadrones neutros en color (como protones, neutrones y otros hadrones).

El confinamiento es precisamente el origen de la masa del mundo que nos rodea: mientras que la masa de los quarks up y down ronda los 3.5 MeV (en un cierto esquema y a una cierta escala de renormalización), la masa del protón o el neutrón, compuestos por estos quarks, es de aproximadamente 940 MeV. Es decir, el mecanismo de Higgs es irrelevante en la masa de los nucleones y el resto de hadrones. Su masa es debida a las interacciones de QCD. Estas interacciones a bajas energías se pueden describir solo mediante un método no perturbativo.

QCD en el retículo, *Lattice* QCD, proporciona una óptima herramienta para el análisis

del espectro hadrónico así como para el cálculo de los elementos de matriz no perturbativos que aparecen en los procesos electrodébiles. De hecho, se suele decir que *Lattice* QCD juega un papel protagonista en la física del sabor. La fase y todas las magnitudes de la matriz CKM son accesibles a través de desintegraciones leptónicas y semileptónicas u oscilaciones de mesones. Todos ellos son procesos para los cuales el análisis del correspondiente elemento de matriz esta actualmente bajo control mediante cálculos en el retículo. Los factores de forma de las transiciones leptónicas $\pi \to l\nu$, $K \to l\nu$, $D_{(s)} \to l\nu$ o $B \to \tau\nu$ y semileptónicas como $K \to \pi l\nu$, $D \to \pi l\nu$, $D \to K l\nu$, $B \to \pi l\nu$, $B \to D l\nu$, $B \to D^* l\nu$ o $t \to bW \to bl\nu$ son sensibles a los ángulos de mezcla mientras que las oscilaciones $\overline{K}^0 - K^0$ son sensibles a la fase de violación CP y $\overline{B}^0_{(s)} - B^0_{(s)}$ determina $|V_{td}|$ y $|V_{ts}|$. Gracias a las factorías de Bs, otros procesos independientes de *Lattice* QCD proporcionan información extra sobre la matriz CKM de tal modo que en última instancia es posible combinar toda la información teórica y experimental para sobredeterminar el valor de los elementos de la matriz CKM y comprobar su consistencia.

La unitariedad de la matriz CKM define un conjunto de nueve ecuaciones complejas. Las seis condiciones obtenidas con elementos de matriz fuera de la diagonal se pueden ver como triángulos en el plano complejo, todos con la misma área relacionada con la única fase de violación de CP en el Modelo Estándar. En ausencia de violación de CP, estos triángulos degenerarían en segmentos a lo largo del eje real. Entre estas seis condiciones, la más restrictiva corresponde a $V^*_{ub}V_{ud} + V^*_{cb}V_{cd} + V^*_{tb}V_{td} = 0$ pues involucra un triángulo de lados del mismo orden de magnitud. Las diferentes restricciones experimentales sobre este triángulo se representan de modo gráfico a través del llamado triángulo de unitariedad. Si el mecanismo CKM describe todos los procesos de mezcla entre quarks, todas las medidas deberían ser compatibles y converger en un solo vértice para el triángulo de unitariedad.

Una de las restricciones del triángulo de unitariedad se obtiene a partir de ϵ_K que mide experimentalmente la violación de CP indirecta en las oscilaciones de mesones neutros $\overline{K}^0 - K^0$. Otras restricciones independientes se obtienen de la diferencia de masa entre los dos mesones B neutros, ΔM_B. ϵ_K y ΔM_B son medidas experimentales que pueden expresarse teóricamente en términos del Hamiltoniano efectivo que describe las oscilaciones $\overline{K}^0 - K^0$ y $\overline{B}^0 - B^0$.

Aunque los últimos análisis parecen indicar que los efectos de nueva física en las oscilaciones $\overline{K}^0 - K^0$ y $\overline{B}^0 - B^0$ están muy suprimidos [15, 16], los futuros datos experimentales necesitarán medidas precisas, del orden del 1%, de los parámetros hadrónicos no perturbativos para confirmar este resultado.

En otro orden de cosas, el interés por la física del charm ha resurgido en los últimos años desde que se observó la primera evidencia de la oscilación $\overline{D}^0 - D^0$ [17, 18, 19]. Las oscilaciones de mesones en el sector del charm están a día de hoy bien establecidas desde el punto de vista experimental. Aunque los datos experimentales parecen consistentes con las predicciones del Modelo Estándar [20], aún existe la posibilidad de una ventana de nueva física. Es más, el sector del charm se ha convertido en la actualidad en un sector muy prometedor para estudiar los efectos de física más allá del Modelo Estándar. Por ello en esta tesis hemos generalizado el estudio de las oscilaciones de mesones también al sistema de mesones D^0.

Centrándonos ya en el tema central de esta tesis, el valor esperado del Hamiltoniano efectivo para las oscilaciones $\overline{K}^0 - K^0$, $\overline{D}^0 - D^0$ y $\overline{B}^0 - B^0$ se calcula numéricamente en términos de los parámetros B. Los parámetros B miden la desviación entre el cálculo analítico del elemento de matriz del operador de cuatro fermiones local que describe el Hamiltoniano efectivo en la llamada aproximación de inserción de vacío (VIA) y el valor físico que incluye todas las correcciones de QCD.

Debido a las simetrías del Modelo Estándar el Hamiltoniano efectivo responsable de las oscilaciones de mesones neutros contiene sólo un operador de cuatro fermiones y por lo tanto existe solo un parámetro B que debemos calcular. El análisis del triángulo de unitariedad se puede generalizar de modo que incluya también posibles extensiones de nueva física considerando el Hamiltoniano efectivo más general que contiene, además de la contribución del Modelo Estándar, los operadores que aunque están ausentes en el Modelo Estándar pueden contribuir en los modelos de nueva física.

El Hamiltoniano electrodébil más general que contribuye a las oscilaciones de mesones incluye cinco operadores locales de cuatro fermiones locales dando lugar a cinco parámetros B que pueden ser calculados no perturbativamente independientemente del modelo de nueva física considerado. De este modo, combinando el cálculo de los parámetros B con las restricciones experimentales sobre los procesos FCNC es posible acotar la escala de nueva física y restringir qué extensiones del Modelo Estándar son viables.

Como ya he discutido, el cálculo del valor esperado del Hamiltoniano efectivo electrodébil, y más en concreto de los parámetros B, requiere un método no perturbativo. Hoy en día el retículo proporciona la única formulación no perturbativa y matemáticamente bien definida de QCD a partir de primeros principios. *Lattice* QCD es básicamente QCD formulada en una red espacio-temporal discreta y Euclídea con espaciado a. El espaciado del *lattice* actúa como un corte límite o *cutoff* y por tanto es un esquema valido de regularización no perturbativa. Las simulaciones numéricas en el retículo están basadas en integraciones de Monte Carlo sobre la integral de camino Euclídea usando métodos completamente análogos a los usados en Mecánica Estadística. Las simulaciones numéricas permiten calcular los elementos de matriz entre estados hadrónicos en términos de grados de libertad de quarks y gluones. Los parámetros de entrada de cualquier simulación en el retículo son la constante de acoplamiento α_s y las masas de quarks desnudas. Por tanto, como no hay nuevos parámetros o campos en la simulación, *Lattice* QCD retiene todas las propiedades fundamentales de QCD.

No obstante, el proceso de discretización no es único y diferentes acciones en la red son posibles. La discretización directa de los fermiones en el continuo conduce al problema de multiplicidad de fermiones, que consiste en la generación de modos fermionicos no físicos. El problema de la multiplicidad se puede resolver con diversos métodos cada uno con sus ventajas y desventajas. Los fermiones de Wilson solucionan el problema de la multiplicidad del modo más sencillo posible añadiendo a la acción un término, el llamado término de Wilson, con una derivada de segundo orden proporcional al espaciado del *lattice* de tal forma que en el límite al continuo los fermiones no físicos se desacoplan. La acción *Twisted Mass*, que hemos usado en las simulaciones analizadas en esta tesis, es una variante de la acción original de Wilson donde el término de Wilson ha sido rotado

quiralmente. Esto nos permite llevar a cabo simulaciones con masas de quarks más ligeras y con ello más cercanas a su valor físico que con fermiones puros de Wilson y reducir de forma casi automática los errores de discretización. Otras posibles regularizaciones, actualmente en uso por diferentes colaboraciones de *lattice* en diversos proyectos con simulaciones a gran escala, son los fermiones *staggered* o *Domain Wall*, explicados de modo general en muchos libros de texto como [21, 22].

Lattice QCD es una disciplina muy prometedora. Las simulaciones en el retículo están alcanzando un estado en el cual todos los errores sistemáticos presentes en las simulaciones numéricas pueden estar bajo control. Por una parte, gracias a las mejoras en los algoritmos y el diseño de la acción, simulaciones con pequeños espaciados del retículo, grandes volúmenes y masas ligeras en el régimen de la teoría quiral son posibles en la actualidad. Debido al coste computacional que supone incluir los efectos de creación de pares quark-antiquarks en las simulaciones, históricamente muchos cálculos se han llevado a cabo en la aproximación *quenched* en la que los bucles quark-antiquark se omitían. A pesar de que con frecuencia se ha encontrado que en la práctica esta aproximación tiene un pequeño impacto, el error que supone es difícil de cuantificar a priori. La inclusión de los efectos físicos de los quarks del mar ha sido uno de los grandes avances en las simulaciones de QCD en el retículo en los últimos años. Simulaciones dinámicas con $N_f = 2$ sabores de quarks (u y d), $N_f = 2 + 1$ (u, d y s) o $N_f = 2 + 1 + 1$ (u, d, s y c) están siendo analizadas por prácticamente todas las colaboraciones internacionales.

Por otra parte, muchos observables físicos requieren un procedimiento de renormalización. Aunque en principio la renormalización podría realizarse en teoría de perturbaciones, la renormalización no perturbativa, actualmente usada en la mayor parte de los cálculos en el retículo, evita los problemas debidos al truncamiento de la serie perturbativa permitiendo un mejor control de los errores sistemáticos. Por último, pero no por ello menos importante, las arquitecturas modernas de superordenadores permiten obtener un numero considerable de configuraciones gauge con las características que hemos citado.

Como resultado de todos estos factores, muchas cantidades físicas son calculadas a día de hoy con gran precisión estadística y con errores sistemáticos bajo control. Esto nos conduce a una nueva era de física de precisión en las simulaciones de QCD en la red. Tal perspectiva es muy emocionante ya que no solo conducirá a una mejor comprensión de QCD en si misma sino que también abrirá una ventana hacia el descubrimiento de nueva física más allá del Modelo Estándar.

Siguiendo esta idea, la colaboración internacional de *lattice* ETMC, cuyo nombre viene de las siglas en inglés de *European Twisted Mass Collaboration*, ha hecho un enorme esfuerzo para generar y analizar un número significativo de configuraciones gauge que incluyen los efectos dinámicos de quarks en el mar.

La ETMC es una colaboración internacional de diferentes grupos de investigación europeos de QCD en el retículo que utilizamos conjuntamente fermiones *Twisted Mass* para simulaciones dinámicas de QCD a gran escala. En una primera fase sus proyectos estuvieron centrados en la inclusión de los quarks ligeros up y down, la denominada simulación $N_f = 2$. En una segunda fase, la ETMC pasó a la inclusión dinámica de los quarks *strange* y *charm*, la llamada simulación $N_f = 2 + 1 + 1$. La inclusión de $N_f = 2+1+1$ sabores de quarks dinámicos es un paso fundamental hacia una simulación

completamente realista.

La inclusión de los quarks *strange* y *charm* en la simulación introduce un problema potencial en la renormalización: en las simulaciones $N_f = 2 + 1 + 1$ las masas de los los quarks *strange* y *charm* se fijan cercanas a su valor físico mientras que en el proceso de renormalización el límite quiral de todas las masas de quarks debe realizarse. Por ello son necesarias simulaciones con $N_f = 4$ sabores degenerados de quarks. La ETMC ha producido y analizado con este objetivo simulaciones expresamente dedicadas para la renormalización con cuatro sabores de quarks dinámicos en el mar.

El cálculo en el lattice de los parámetros B requiere un proceso de renormalización no perturbativa, al igual que otras cantidades calculadas en el retículo, como las masas de quarks. Sin embargo, debido a la rotura explicita de la simetría quiral por el término de Wilson de la acción, la renormalización de los parámetros B requiere una atención especial. Con fermiones de Wilson el conjunto de operadores en el retículo que debemos considerar es mayor que en el continuo debido a que la teoría tiene menos simetrías. De forma más precisa, el operador local de cuatro fermiones relevante en el cálculo de los parámetros B se mezcla con otros operadores de cuatro fermiones de dimensión seis que pertenecen a una representación distinta de quiralidad.

En nuestro análisis, hemos esquivado esta complicación usando una acción mixta donde adoptamos diferentes regularizaciones para los quarks del mar, es decir los responsables de la polarización del vacío, y los quarks de valencia, es decir los involucrados en la interacción. Más concretamente, como fue propuesto por primera vez en [23], usamos la acción *Twisted Mass* para los quarks del mar mientras que para los quarks de valencia la acción de *Osterwalder-Seiler*, una variante de la acción *Twisted Mass*, ha sido implementada. Esta inteligente estrategia proporciona un marco computacional sin mezcla con operadores locales de distinta quiralidad y al mismo tiempo libre de efectos de discretización de orden del espaciado del lattice, es decir $\mathcal{O}(a)$.

Siguiendo esta estrategia en esta tesis hemos abordado el cálculo de los parámetros B que controlan las oscilaciones $\overline{K}^0 - K^0$, $\overline{D}^0 - D^0$ y $\overline{B}^0 - B^0$ usando las configuraciones de gauge con $N_f = 2$ sabores de quarks dinámicos producidos por la ETMC.

El estudio de las oscilaciones $\overline{B}^0 - B^0$ en el retículo presenta ciertos problemas ya que con la potencia computacional disponible hoy en día aún no podemos simular un quark b físico propagándose en el lattice controlando al mismo tiempo los efectos de volumen finito y los errores de discretización del retículo. Para superar este problema hemos usado el método de los cocientes, el llamado *ratio method,* propuesto por la ETMC [24].

Finalmente, también presentaremos un estudio preliminar de las oscilaciones $\overline{K}^0 - K^0$ usando las simulaciones $N_f = 2+1+1$ de la ETMC. Este análisis requiere previamente el cálculo de las constantes de renormalización de dos y cuatro fermiones que será también discutido.

Esta tesis se organiza en siete capítulos. Los capítulos del 1 al 3 están dedicados a un repaso del Modelo Estándar y la violación de CP, QCD en el retículo, la acción *Twisted Mass* y la extracción teórica de los parámetros B a partir de las funciones de correlación de dos y tres puntos. Más en detalle:

- En el capítulo 1 empezaremos con una breve descripción del Modelo Estándar y la violación de CP con el objetivo de motivar el cálculo de los parámetros B. Discutiré a continuación la violación de CP en los tres sistemas de mesones neutros $\overline{K}^0 - K^0$, $\overline{D}^0 - D^0$ y $\overline{B}^0 - B^0$.

- En el capítulo 2 presentaré un resumen de los aspectos de QCD en el retículo que usaremos en el resto del trabajo. En este capítulo nos centraremos en las propiedades principales y las ventajas de la acción *Twisted Mass*.

- En el capítulo 3 derivaré todas las fórmulas necesarias para el cálculo de los parámetros B en el lattice a partir de las funciones de correlación de dos y tres puntos. Discutiré en detalle el patrón de renormalización de los operadores de dos y cuatro fermiones obtenido al usar la acción Osterwalder-Seiler y mostraré como podemos evitar la mezcla con los operadores de distinta quiralidad.

Los capítulos del 4 al 7 contienen los trabajos originales de esta tesis:

- En el capítulo 4 describiré en primer lugar la renormalización no perturbativa usando el conocido método de RI-MOM. Aplicaré dicho método, por primera vez, al cálculo de las constantes de renormalización no perturbativa de los operadores de dos y cuatro fermiones provenientes de las simulaciones $N_f = 4$.

- En el capítulo 5 mostraré y discutiré nuestros resultados para los parámetros B en las oscilaciones $\overline{K}^0 - K^0$ y $\overline{D}^0 - D^0$ con la simulación $N_f = 2$. Los parámetros B discutidos aquí son de gran interés fenomenológico ya que se trata de los primeros resultados *unquenched* (con sabores dinámicos de quarks) y extrapolados al límite del continuo.

- En el capítulo 6 me centraré en la física del b, más conocida como *B-physics*. En primer lugar, presentaré el ya conocido *ratio method* que es el método que hemos aplicado para tratar el quark b en el retículo. Tras aplicar este método al calculo de m_b, f_B y f_{B_s}, pasaré al cálculo de los parámetros B que controlan las oscilaciones $\overline{B}^0 - B^0$ que es otro de los principales trabajos originales de esta tesis.

- En el capítulo 7 presentaré finalmente un análisis, todavía preliminar, de los parámetros B en el sistema $\overline{K}^0 - K^0$ obtenidos a partir de configuraciones gauge $N_f = 2 + 1 + 1$ de la ETMC. Para ello usaré las constantes de renormalización de dos y cuatro fermiones que previamente he discutido en el capítulo 4.

Finalmente, en las conclusiones resumiré los principales resultados, compararé nuestros resultados con los obtenidos mediante otros cálculos alternativos en el retículo y repasaré las perspectivas futuras.

Esta tesis incluye ocho apéndices que contienen los detalles técnicos de la simulación y el análisis así como tablas detalladas de nuestros resultados. Están organizados del siguiente modo:

- El apéndice A describe brevemente algunos detalles técnicos sobre el smearing y las técnicas estocásticas que han sido aplicadas para el cálculo de los propagadores de quarks en las simulaciones $N_f = 2$.
- El apéndice B está dedicado al análisis de algunas simetrías discretas de la acción *Twisted Mass* usadas en el capítulo 3.
- El apéndice C repasa las características básicas de las ecuaciones del Grupo de Renormalización que gobiernan la evolución de los operadores de dos y cuatro fermiones.
- El apéndice D contiene detalles técnicos sobre la sustracción de los artefactos del retículo $\mathcal{O}(a^2 g^2)$ en los bilineares y operadores de cuatro fermiones.
- El apéndice E trata los detalles de la evolución o *matching* entre QCD y la teoría del quark pesado, la llamada HQET, necesario en los pasos intermedios del *ratio method*.
- El apéndice F contiene todos los resultados numéricos para las masas de mesones, constantes de desintegración y parámetros B obtenidos con la simulación $N_f = 2$. El método que hemos usado para mejorar las funciones de correlación a dos puntos está descrito también en este apéndice.
- El apéndice G resume los resultados de las constantes de renormalización necesarias en la simulación $N_f = 2$. El método para calcularlas ha sido discutido y aplicado en detalle en el caso de $N_f = 4$ en el capítulo 4 así que aquí me centraré solamente en los resultados principales de la simulación $N_f = 2$.
- El apéndice H contiene las tablas con las masas de mesones y parámetros B relevantes en el análisis de los parámetros B con la simulación $N_f = 2 + 1 + 1$ realizado en el capítulo 7.

Introduction

The Standard Model (SM) is the best theory with which theoretical physicists describe elementary particles and their interactions, excluding gravity. The SM is a quantum field theory which describes the interaction of fermions through the mediation of gauge bosons and the interactions of gauge bosons among themselves. It provides an elegant theoretical framework to describe three of the four forces in the nature: the strong or Quantum Chromodynamics (QCD), the electromagnetic or Quantum Electrodynamics (QED) and the weak interactions, unified with the electromagnetism in the so-called electroweak theory [1, 2].

Elementary particles, without internal structure, are leptons and quarks, while the hadrons are particles with internal structure composed by quarks. Quarks exist inside the hadrons where they are confined by the strong interaction. Quarks and leptons are thereby the basic constituents of fermionic matter. They are grouped into three families. There are six quarks: up (u), down (d), charm (c), strange (s), top (t) and bottom (b). Quarks are triplets of the SU(3) group gauge and consequently they have an additional charge, colour, which is the responsible for the strong interaction. Each one of them is given a flavour charge which is conserved under QCD but not under the electroweak interactions. The three families of quarks are mixed, i.e mass eigenstates are not weak eigenstates. This mixing is parametrized by the Cabibbo-Kobayashi-Maskawa (CKM) matrix. Likewise, there are six leptons: the electron (e), the muon (μ), the tau (τ) and the three neutrinos (ν_e, ν_μ,ν_τ). Leptons do not have colour charge hence they do not participate in the strong interactions.

The interaction is mediated by bosons: eight massless gluons mediate the strong interactions; the photon, massless, responsible for the electromagnetic interactions and the massive $W^{\pm}$ and Z mediate weak interactions. The weak bosons acquire mass through the Higgs mechanism which breaks the electroweak symmetry group $SU(2) \otimes U(1)$.

With this description the SM has been able to describe most of the experimental data. During the past forty years many experiments have tested it obtaining very good agreement with theoretical predictions. Furthermore, in the last year a new particle with mass around 125 GeV and showing Higgs boson properties has been observed by ATLAS

and CMS [3, 4]. After years of intense experimental search, it could be the Higgs boson of the SM, the last missing particle of the model to be discovered.

Despite its success in describing with high precision a wide variety of experimental results there are several reasons to believe that the SM is not the final theory of particle interactions but a step towards a more general theory. One of the most striking limits of the SM is that it does not incorporate gravity. More than that it does not explain 95% of the Universe mass energy which is not made of ordinary matter but of dark matter (~27%) and dark energy (~68%). Which is the particle responsible for the dark matter? Which is the origin of dark energy? These are important questions that the SM can not answer.

Beyond these questions, there are other problems related with the flavour structure of the SM: Which is the nature of the neutrino oscillations? Why the universe is made of matter and not antimatter? Which is the origin of the CP violation? Why the strong interaction is invariant under CP while the electroweak interaction is not?

Finally, although the SM is theoretically self-consistent, it contains many parameters that should be obtained experimentally: the three coupling constants α_s, α_{em} and G_F responsible for the strong, electromagnetic and weak interactions respectively; the masses of the six quarks, three leptons and three neutrinos; the mass of the Z boson which fixes the electroweak scale; the Higgs mass, the mixing angles under the weak interactions and the CP violating phase. 18 parameters if the neutrinos are massless, i.e in the SM strictly speaking, but 7 more, 25 in total, if they are massive: three neutrino masses, three mixing angles and one phase. The SM tells us how particles interact but says nothing about their intrinsic properties: Why are there three families of fermions? How can elementary particle masses be explained? Why neutrino masses are much smaller than other lepton masses? All of which leads us to believe that it should exist a more general theory than the SM.

Since the formulation of the SM, in the early seventies, physicists have been trying to find a convincing alternative or extension of the SM that could resolve these issues: several supersymmetric models, extra dimensions, technicolor... With such huge spectrum of possibilities new experimental data is needed in order to confirm or exclude their predictions.

With the LHC operating we are living in a very exciting era in particle physics. The new experimental data helps us to understand whether the SM is all we can see in current experiments or if there are insights of New Physics (NP). However, the observation of new particles at high-energy colliders, as the LHC, is not the only way for NP to be discovered. It can also be unveiled through high precision measurements of low energy observables. These processes are able to explore energy scales higher than those that can be achieved in the LHC. This non intuitive fact is just a consequence of quantum field theory: heavy particles still undiscovered could contribute to low energy processes via quantum corrections.

Such deviation from the SM predictions could reveal the exchange of virtual new heavy particles involving scales where the LHC is completely blind. Consequently, precise measurement of SM suppressed flavour changing processes as FCNC, where NP effects may be competitive and consequently visible, provide an excellent framework where one

can test the SM and furnish very valuable information about the more general theory which could replace the SM.

We come back to one of the crucial problems of the SM: the matter-antimatter asymmetry. The observed universe is mainly composed of matter (principally protons, neutrons and electrons) and not of antimatter. Hence, one needs elementary processes favoring matter over antimatter. Such processes are the CP violating interactions.

Explicitly, the C operation reverses all additive quantum number (electric charge, hypercharge, strangeness...) while the P transformation inverts the spatial coordinates. In the SM, QED and QCD conserve C and P separately. On the contrary, the electroweak interactions break C and P. But invariance is almost recovered if we consider not just C or P but the combined transformation CP.

The CP symmetry was believed to be exact until 1964 when CP violation was firstly established in the kaon sector [5]. This was the first evidence of indirect CP violation. The first indication of direct CP violation was found in the decay of neutral kaons in the 1990s at the NA31 experiment at CERN [6] and it was confirmed in 1999 by the KTeV experiment at Fermilab [7] and the NA48 experiment at CERN [8]. In 2001, the BaBar experiment in SLAC and Belle in KEK, the so-called B-factories, confirmed CP violation in the B sector [9, 10] showing that it is not confined to the kaon sector. Recently, in 2011, a first evidence of CP violation in neutral D meson decays was reported by the LHCb experiment at CERN [11].

According to the SM, CP violation can only occur in weak interactions and more specifically, with massless neutrinos, CP violation can only take place in flavour changing processes involving quarks (with massive neutrinos CP violation can also occur in the leptonic sector although its size is strongly suppressed by the smallness of neutrino masses). In fact, the weak interaction is the only one in the SM which can change the flavour of quarks. These flavour physics phenomena typically depend on the quark masses and the couplings between quarks of different flavours. These couplings are described in terms of a unitary matrix known as the Cabibbo-Kobayashi-Maskawa (CKM) matrix [12]

$$V_{CKM} = \begin{pmatrix} V_{ud} & V_{us} & V_{ub} \\ V_{cd} & V_{cs} & V_{cb} \\ V_{td} & V_{ts} & V_{tb} \end{pmatrix}$$

The CKM matrix must be unitary and it can be parametrized using three angles and one complex phase. This complex phase is the only source of CP violation in the SM. If couplings break the unitary conditions, or the size of the CP violating phase differs between theoretical predictions and experiment, then some unknown process, which would indicate NP, is contributing.

For instance, with a fourth generation of quarks, the 3x3 CKM matrix would not be unitary or if other non SM particles change quark flavour, then the SM relation between the flavour changing process and the CKM matrix would be spoiled. For this reason, an intense experimental and theoretical effort is under way to measure the CKM matrix elements precisely enough to detect such departures from unitarity.

Currently, CP violation is a well establish phenomenon in weak decays in the strange and beauty sectors which seems to be consistent with the CKM description of CP viola-

tion. However, although there is a reasonably good agreement with the SM prediction of a single CP-violating phase, as predicted by the CKM matrix, the CKM mechanism continues to fail to explain why the matter dominates over the antimatter. More precisely, the CKM mechanism predicts a baryon number density many orders of magnitude below the observed value [13].

Furthermore, CP is not violated in the strong interactions. This is an experimental fact and leads to a fine tuning problem since in principle one can add a term in the QCD Lagrangian of the form $\mathcal{L}_\theta \sim \theta \epsilon^{\mu\nu\rho\sigma} F_{\mu\nu} F_{\rho\sigma}$, which explicitly violates CP. $\mathcal{L}_\theta$ would induce a electric dipole moment of the neutron proportional to θ. However, the experimental bound on the electric dipole moment for the neutron leads to a value of $\theta \leq 10^{-11}$[14]. Such delicate fine tunning of θ to this extremely small value, the so-called strong CP problem, is still a mystery. Although it is not a problem itself, it seems quite unnatural. Considering their contribution to be near zero does not attribute to the theory any additional symmetry.

These evidences, i.e the matter-antimatter asymmetry and the strong CP problem, suggest that there must exist sources of CP violation beyond the CKM mechanism of the SM. In this sense, the high precision measurements in flavour physics may turn out to be an excellent strategy to look beyond the SM.

The approach to the study of flavour processes is based on the observation that the mass of the W boson mass, M_W, is $\sim \mathcal{O}(100$ GeV) while the typical hadronic scale is $\mathcal{O}(1$ GeV). Therefore, M_W can be considered much larger than any relevant hadronic scale and the W boson can be integrated out. Together with the Operator Product Expansion formalism (OPE), this assumption leads to an effective weak Hamiltonian in which the physical amplitudes can be expressed as a sum over matrix elements of local operators.

Typically, the result of an experiment, for instance a decay rate, should be compared with the analytical expression for the same process. The OPE decomposes this theoretical expression into three parts: a combination of some SM parameters, the non perturbative matrix element of the effective weak hamiltonian between the initial and final states and some perturbative factors, the so-called Wilson coefficients. In this way, for each experimental constraint one gets a constraint over a particular combination of SM parameters provided the hadronic matrix elements that control the corresponding quark flavour process are known.

The Wilson Coefficients contain the short distance effects including all relevant physics from the highest scales, such as the weak scale M_W or some new physics scale, down to the relevant hadronic scale. They can be computed in perturbation theory. In contrast, perturbative methods are no longer valid for the computation of the hadronic matrix elements at low energy. The reason is that the non perturbative QCD long distance corrections to the weak process could be large due to the exchange of soft gluons between the initial and final states. In other words, in order to accurately describe the hadronic matrix elements responsible for weak interactions involving quarks, the confinement effects of quarks into hadrons, i.e the QCD corrections, must be included.

At the typical hadronic scale, where electroweak effects can be studied in a perturbative way, QCD effects are non perturbative. Why? In their formulation QED are

QCD are very similar: both are gauge-invariant field theories. Nevertheless, while QED is based on the abelian and local U(1) gauge invariance, QCD is based on a non-abelian SU(3) gauge symmetry. That difference has big consequences for phenomenology: while photons are neutral and they cannot interact directly with each other, gluons carry colour charge so they can interact directly with each other as well as with quarks. This apparently innocent difference is the root of the QCD complexity. At high energies the QCD coupling constant α_s is small, we have asymptotic freedom and it is possible to carry out perturbative calculations. On the contrary at low energies α_s is large giving rise to the confinement of quarks into colour neutral hadrons like protons and neutrons.

Confinement is essentially the phenomenon responsible for the mass of the world. The average mass of the up and down quark is around 3.5 MeV (in some scale and scheme of renormalization), but the mass of the proton or neutron is around 940 MeV. That is, the Higgs mechanism is irrelevant for the mass of the proton and neutron. Its mass is due to the QCD interactions at low energies. These interactions can only be described through a non perturbative approach.

Lattice QCD provides an optimal tool for the analysis of the hadronic spectrum and the computation of the non perturbative matrix elements relevant in electroweak processes. In fact, lattice QCD calculations play a key role in flavour physics. The phase and all the magnitudes of the CKM matrix can be obtained via leptonic and semileptonic decays or meson-antimeson oscillations. All of them are processes for which the corresponding hadronic weak matrix elements are, at present, under good control by lattice QCD computations. Leptonic transitions for $\pi \to l\nu$, $K \to l\nu$, $D_{(s)} \to l\nu$ and $B \to \tau\nu$ and semileptonic transitions such as $K \to \pi l\nu$, $D \to \pi l\nu$, $D \to Kl\nu$, $B \to \pi l\nu$, $B \to Dl\nu$, $B \to D^* l\nu$ and $t \to bW \to bl\nu$ are sensitive to the mixing angles while $\overline{K}^0 - K^0$ mixing is sensitive to the CP-violating phase and $\overline{B}^0_{(s)} - B^0$ mixing determines $|V_{td}|$ and $|V_{ts}|$. Other processes, which do not need lattice QCD computations, provide extra information on the CKM matrix so at the end of the day one can use all the experimental and theoretical information to over determine the CKM matrix and test its consistency.

The unitarity of the CKM matrix defines a set of nine complex equations that the matrix elements should satisfy. The six off-diagonal unitarity constraints can be visualized as triangles in the complex plane. All the unitarity triangles have the same area, related to the unique CP violating phase in the SM. In the absence of CP violation, these triangles would degenerate into segments along the real axis. Among the six unitarity triangles, the most stringent one corresponds to $V^*_{ub}V_{ud} + V^*_{cb}V_{cd} + V^*_{tb}V_{td} = 0$ since it involves sides of the same order. The different experimental constraints on this triangle are translated in the so-called unitarity triangle (UT). If the CKM mechanism describes exclusively all the quark mixing processes then all the measurements should converge on a single apex of the UT.

One of the constraints in the UT is obtained from the ϵ_K which measures experimentally the indirect CP violation in the $\overline{K}^0 - K^0$ neutral meson oscillations. Independent constraints can be obtained from the difference of mass between the two neutral B meson, ΔM_B. The experimental measurements of ϵ_K and ΔM_B are related with the expectation value of the effective Hamiltonian describing the $\overline{K}^0 - K^0$ and $\overline{B}^0 - B^0$ mixing.

Although the most recent analyses seem to indicate that NP effects in the $\overline{K}^0 - K^0$ and $\overline{B}^0 - B^0$ meson-antimeson mixing are constrained to be highly suppressed [15, 16] further measurements will need precise calculations of non perturbative hadronic matrix elements, at the level of $\sim$1%, to confirm these results.

At the same time, there has been a resurgence of interest for the charm physics in the past few years since evidence for $\overline{D}^0 - D^0$ mixing was first observed [17, 18, 19]. Mixing in the charm sector is now well-established at a level which is consistent with SM expectations but at the upper bound of it [20]. Moreover, the charm sector is now a promising place to probe for the effects of physics beyond the SM. For these reasons in this thesis we have generalized the study of the neutral meson oscillations to also include the D^0 system.

Focusing on the main topic of this thesis, the expectation value of the effective Hamiltonian for the $\overline{K}^0 - K^0$, $\overline{D}^0 - D^0$ and $\overline{B}^0 - B^0$ mixing are computed numerically through the so-called B-parameters or bag parameters. The B-parameters measure the deviation between the analytical computation of the matrix element of the local four-fermion operator describing the effective Hamiltonian performed in the so-called Vacuum Insertion Approximation (VIA) and the physical value including the QCD corrections.

Due to SM symmetries the effective Hamiltonian responsible for the neutral meson oscillations contains only one four-fermion operator and thus there is only one B-parameter to be computed. The UT analysis can be generalized in order to include possible NP contributions by considering the most general effective Hamiltonian which includes, besides the SM local four-fermion operator, also the operators which, although they are absent in the SM, could contribute in some NP model.

The most general effective weak Hamiltonian includes five local four-fermion operators, leading to the computation of five B-parameters. These B-parameters are computed non perturbatively in a model independent way while the Wilson coefficients depend on the properties of the specific NP model under study. Based on the experimental constraints on FCNC processes, together with the B-parameter, one can derive lower bounds on the scale of NP and constrain which extensions of the SM are viable.

As I discussed before, the computation of the expectation value of the effective weak Hamiltonian, and in particular the computation of B-parameters, requires a non perturbative method. Up to now the lattice approach is the only known non perturbative and mathematically well defined first principles formulation of QCD. Lattice QCD is formulated on a discrete Euclidean space-time grid of lattice spacing a. The lattice spacing acts as an ultraviolet cutoff and consequently offers a non perturbative regularization scheme. Numerical simulations of lattice QCD are based on Monte Carlo integrations over the Euclidean path integral using analogous methods as the ones used for Statistical Mechanics systems. These lattice simulations allow us to compute matrix elements between hadronic states in terms of fundamentals quark and gluon degrees of freedom. The inputs of any lattice simulation are the coupling constant α_s and bare quark masses. Therefore, since no new parameters or fields are introduced, lattice QCD retains all the fundamental properties of QCD.

Nevertheless, the discretization procedure is not straightforward and different lattice

actions are possible. The naive discretization of the continuum fermions leads to the so-called doubling-fermion problem, consisting in the onset of non-physical fermionic modes. The doubling problem could be solved in various ways, each with their advantages and disadvantages. The Wilson fermions solve the doubling problem in the simplest way by adding to the action a second order derivative term proportional to the lattice spacing, the so-called Wilson term, in such a way that in the continuum limit the non physical fermionic modes vanish. The Twisted Mass action, used in the simulations analyzed in this thesis, is a variant of the Wilson action where the Wilson term has been rotated. This allows us to safely perform simulations with lighter quark masses and under certain conditions has the advantage to reduce automatically the discretization errors $\mathcal{O}(a^2)$. Other possible fermion regularizations, currently used by different lattice collaborations for large-scale projects are the staggered or Domain Wall fermions, fully explained in many text books as [21, 22].

Lattice QCD is a very promising research field. Lattice simulations are approaching nowadays a stage in which all systematic uncertainties present in numerical calculations can be set under control. On the one hand, thanks to algorithm and action improvements, simulations at small lattice spacings with large volumes and light quark masses in the Chiral Perturbation Theory regime are now feasible. Due to the computational cost of including sea quarks on lattice simulations, until late 90s many lattice QCD calculations have been carried out in the quenched approximation in which the sea quark loops are omitted. Although it was often found that the predictions of quenched approximation are not so far from the real ones, the error entailed in them is difficult to quantify a priori. The inclusion of physical effects from sea quarks has been one of the main advances in lattice QCD simulations over the last few years. Dynamical simulations with $N_f = 2$ degenerate flavours (u and d), $N_f = 2 + 1$ (u, d and s) and $N_f = 2 + 1 + 1$ (u, d, s and c) are currently being performed by essentially all lattice collaborations.

On the other hand, many observables, such as quark masses or B-parameters, require a renormalization procedure. Although the renormalization could in principle be performed in perturbation theory, non perturbative renormalization overcomes the problems due to truncation errors in lattice perturbation theory avoiding large systematic errors. Last, but not least, modern supercomputer architectures allow us to obtain a high number of gauge field configurations.

As a result of these factors, many physical results are currently computed with a very good statistical accuracy and well controlled systematic errors. This clearly opens a new era of precision physics for lattice QCD simulations. Such a perspective is extremely exciting since it will not only lead to a better understanding of QCD itself but it may open the window to discover NP beyond the SM.

In this sense, the international lattice QCD collaboration ETMC, European Twisted Mass Collaboration, has made a determinant effort in order to generate and analyze a significant number of gauge configurations including all the dynamical effects of sea quarks.

The ETMC is a collaboration from different lattice European research centers that uses maximally Twisted Mass Wilson fermions in large-scale dynamical QCD simulations. In a first stage the ETMC projects were focused in the inclusion of the two light quarks

up and down, the so-called $N_f = 2$ simulations. In a second stage, the ETMC investigations involve the generation and analysis of gauge configurations including also dynamical strange and charm quarks, the so-called $N_f = 2 + 1 + 1$ simulations.

The inclusion of the strange and charm quarks in the simulations introduces a potential problem in the renormalization: in the $N_f = 2+1+1$ the strange and charm quark masses are fixed close to their physical values while in the renormalization procedure, for mass independent renormalization constants, the chiral limit of all quarks must be performed. Because of that, dedicated simulations with $N_f = 4$ degenerate quarks have been also produced.

The computation on the lattice of the B-parameters requires a renormalization procedure as well as other quantities like quark masses. However, special attention is required due to the breaking of chiral symmetry by the Wilson term which leads to a complication in the renormalization pattern of the four-fermion operators. With Wilson fermions the set of lattice operators to be considered is larger than those in the continuum theory because the theory has less symmetries. More accurately, the four-fermion operators relevant in the computation of the B-parameter mix with dimension-six four-fermion operators which belong to a different representation of the chiral group.

The ETMC bypass this complication with the use of a mixed action setup where we adopt different regularizations for sea quarks and valence quarks. In particular, as it was proposed in [23], we introduce the Twisted Mass action for the sea quarks while on the valence the Osterwalder-Seiler action, a variant of the Twisted Mass action, is implemented. This strategy provides a computation framework without wrong chirality mixing effects and free of $\mathcal{O}(a)$ discretization effects.

This thesis is focused in the computation of the B-parameters in the $\overline{K}^0 - K^0$, $\overline{D}^0 - D^0$ and $\overline{B}^0 - B^0$ systems using the $N_f = 2$ dynamical gauge configurations generated by the ETMC.

The study of the $\overline{B}^0 - B^0$ oscillations on the lattice is complicated because, with present computer power facilities, we cannot study the propagation of a physical b-quark on the lattice. In order to overcome this problem I use the ratio-method proposed by the ETMC [24].

Finally, a preliminary analysis of the $\overline{K}^0 - K^0$ bag parameters with the $N_f = 2+1+1$ ETMC dynamical gauge configurations has been also performed. This analysis requires the computation of the non perturbative renormalization constants of the relevant two- and four-fermion operator which will also be discussed.

The thesis is organized in seven chapters. Chapters from 1 to 3 are devoted to a review of the SM and CP violation, lattice QCD, the Twisted Mass action and the extraction of B-parameters from the two- and three-point correlation functions. More in detail:

- In Chapter 1 I will provide a brief description of the SM and CP violation in order to motivate the computation of the B-parameters. The CP violation in the three neutral meson systems $\overline{K}^0 - K^0$, $\overline{D}^0 - D^0$ and $\overline{B}^0 - B^0$ will be also briefly reviewed.

- In Chapter 2 a summary of the lattice QCD issues used in the rest of the thesis will be given. The chapter is devoted to the main aspects and advantages of the Twisted Mass QCD action.

- In Chapter 3 I will derive all the needed formulae for the computation of the B-parameters on the lattice from two and three-point correlators. The renormalization pattern for the two- and four-fermion when the Osterwalder-Seiler regularization is employed will be discussed in detail showing how we can avoid the wrong chirality mixing.

Chapters from 4 to 7 contain the main original works developed within this thesis:

- In Chapter 4 the non perturbative renormalization of lattice operators, following the well-known RI-MOM method, is firstly reviewed. For the first time, we apply this method to the computation of the two- and four-fermion renormalization constants for the $N_f = 4$ simulations.

- In Chapter 5 I will show our results for the B-parameters analysis in the $\overline{K}^0 - K^0$ and $\overline{D}^0 - D^0$ oscillations with $N_f = 2$ simulations. The B-parameters discussed here are phenomenologically very interesting since they are the first unquenched results extrapolated to the chiral and continuum limit.

- In Chapter 6 I will focus in B-physics. First, I will present the so-called ratio method. Then I will describe its application for the computation of the b-quark mass and the f_B and f_{B_s} decay constants. Finally, I will discuss the computation of the B-parameters controlling the $\overline{B}^0 - B^0$ oscillations.

- In Chapter 7 I will present a preliminary analysis of the B-parameters controlling the $\overline{K}^0 - K^0$ oscillations with $N_f = 2 + 1 + 1$ simulations. Here I will use the two- and four-fermion renormalization constants previously computed in chapter 4.

Finally, I will end with some conclusions where I summarize the main results, I compare them with the ones provided by alternative lattice computations and I will overview the future perspectives.

This thesis includes also eight appendices containing technical details of the simulations and analysis as well as detailed tables of our results. They are organized as follows:

- Appendix A describes briefly some technical details about the smearing and stochastic techniques which have been applied in the $N_f = 2$ simulations.

- Appendix B is dedicated to the lattice discrete symmetries of the Twisted Mass action useful in Chapter 3.
- Appendix C reviews the basic features of the Renormalization Group Equations which govern the evolution of bilinear and four-fermion operators.
- Appendix D contains the technical details about the subtraction of $\mathcal{O}(a^2 g^2)$ lattice artifacts to the bilinears and four-fermion operators.
- Appendix E is devoted to the technical details of the QCD-HQET matching necessary in the intermediate steps of the ratio method.
- Appendix F contains all the numerical results for meson masses, decay constants and B-parameters obtained the $N_f = 2$ simulations. The method used to improve the two-point correlators will be described here.
- Appendix G summarizes the results for the $N_f = 2$ RCs. The method to compute the $N_f = 4$ RCs is discussed and applied in detail in chapter 4.
- Appendix H collects the tables of meson masses and bare B-parameters relevant for the preliminary analysis of the $N_f = 2 + 1 + 1$ B-parameters presented in chapter 7.

Chapter 1

Standard Model and CP Violation

In this chapter, I will start with a brief review of the Standard Model and the CKM mechanism. At the end of the section, I will focus on the role of Lattice QCD in the Unitarity Triangle Analysis (UTA). In a second part of this chapter, I will discuss the CP violation in the three neutral meson systems: $\overline{K}^0 - K^0$, $\overline{D}^0 - D^0$ and $\overline{B}^0 - B^0$.

1.1 SM and quark flavour mixing

The SM is the gauge theory describing strong, weak and electromagnetic interactions [1, 2]. It is based on the gauge group

$$SU(3)_c \otimes SU(2)_L \otimes U(1)_Y$$

where $SU(3)_C$ is the colour gauge group of QCD and $SU(2)_L \otimes U(1)_Y$ is the group describing the electroweak interactions. The subindex L refers to left-handed fields while Y is the electroweak hypercharge. The weak gauge symmetry is spontaneously broken by the vacuum (SSB) in the electromagnetic subgroup

$$SU(3)_c \otimes SU(2)_L \otimes U(1)_Y \xrightarrow{\text{SSB}} SU(3)_C \otimes U_{QED}(1)_Q$$

being Q the electric charge generator.

The fermionic matter contents of the SM is made up by the known leptons and quarks organized in three families

$$\begin{bmatrix} \nu_e & u \\ e^- & d' \end{bmatrix} \quad \begin{bmatrix} \nu_\mu & c \\ \mu^- & s' \end{bmatrix} \quad \begin{bmatrix} \nu_\tau & t \\ \tau^- & b' \end{bmatrix}$$

where the left-handed leptons and quarks are put into $SU(2)_L$ doublets and the right-handed fields transform as singlets under $SU(2)_L$. The primes denote weak eigenstates. That is, for each family we have

$$\begin{bmatrix} \nu_l & q_u \\ l^- & q_d \end{bmatrix} \equiv \begin{pmatrix} \nu_l \\ l^- \end{pmatrix}_L, \begin{pmatrix} q_u \\ q_d \end{pmatrix}_L, l_R^-, q_{uR}, q_{dR}$$

For simplicity, we introduce the following identifications

$$\begin{array}{lll} L_{L1} = \begin{pmatrix} \nu_e \\ e^- \end{pmatrix}_L & L_{L2} = \begin{pmatrix} \nu_\mu \\ \mu^- \end{pmatrix}_L & L_{L3} = \begin{pmatrix} \nu_\tau \\ \tau^- \end{pmatrix}_L \\ E_{R1} = e_R^- & E_{R2} = \mu_R^- & E_{R3} = \tau_R^- \\ Q_{L1} = \begin{pmatrix} u \\ d' \end{pmatrix}_L & Q_{L2} = \begin{pmatrix} c \\ s' \end{pmatrix}_L & Q_{L3} = \begin{pmatrix} t \\ b' \end{pmatrix}_L \\ U_{R1} = u_R & U_{R2} = c_R & U_{R3} = t_R \\ D_{R1} = d'_R & D_{R2} = s'_R & D_{R3} = b'_R \end{array}$$

The Lagrangian describing the free Dirac fermions of all these particles, i.e the kinetic terms of the Lagrangian, is

$$\mathcal{L}_K^0 = i\sum_{j=1}^{3} \left\{ \sum_{\psi=Q_L,U_R,D_R} \overline{\psi}_j \partial\!\!\!/ \psi_j + \sum_{\psi=L_L,E_R} \overline{\psi}_j \partial\!\!\!/ \psi_j \right\} \tag{1.1.1}$$

which is invariant under global $SU(3)_C \otimes SU(2)_L \otimes U(1)_Y$ transformations.

Gauge invariance requires the Lagrangian to be also invariant under local $SU(3)_C \otimes SU(2)_L \otimes U(1)_Y$. To satisfy this requirement, the standard derivative in Eq.1.1.1 should be replaced with the covariant derivative, responsible for the interactions between matter and gauge fields

$$\partial^\mu \rightarrow D^\mu = \left(\partial^\mu + ig_s \frac{\lambda^a}{2} G_a^\mu + ig \frac{\sigma^b}{2} W_b^\mu + ig' Y B^\mu \right)$$

with G_a^μ the eight gluon fields, W_i^μ the three weak interaction bosons and B^μ the single hypercharge boson. λ_a and σ_a are the Gell-Mann matrices and the Pauli matrices respectively. Obviously, the terms proportional to g and g_s are present only if the field is not a singlet of $SU(2)_L$ and $SU(3)_C$. This implies

$$\begin{array}{l} \overline{Q}_L D\!\!\!/ Q_L = \overline{Q}_L \gamma_\mu \left(\partial^\mu + ig_s \frac{\lambda^a}{2} G_a^\mu + ig \frac{\sigma^b}{2} W_b^\mu + ig' Y_{Q_L} B \right) Q_L \\ \overline{U}_R D\!\!\!/ U_R = \overline{U}_R \gamma_\mu \left(\partial^\mu + ig_s \frac{\lambda^a}{2} G_a^\mu + ig' Y_{U_R} B^\mu \right) U_R \\ \overline{D}_R D\!\!\!/ D_R = \overline{D}_R \gamma_\mu \left(\partial^\mu + ig_s \frac{\lambda^a}{2} G_a^\mu + ig' Y_{D_R} B^\mu \right) D_R \\ \overline{L}_L D\!\!\!/ L_L = \overline{L}_L \gamma_\mu \left(\partial^\mu + ig \frac{\sigma^b}{2} W_b^\mu + ig' Y_{L_L} B^\mu \right) L_L \\ \overline{E}_R D\!\!\!/ E_R = \overline{E}_R \gamma_\mu \left(\partial^\mu + ig' Y_{E_R} B^\mu \right) E_R \end{array}$$

Therefore the Lagrangian containing the interactions is given by

$$\mathcal{L}_K^I = i\sum_{j=1}^{3} \left\{ \sum_{\psi=Q_L,U_R,D_R} \overline{\psi}_j D\!\!\!/ \psi_j + \sum_{\psi=L_L,E_R} \overline{\psi}_i D\!\!\!/ \psi_i \right\}$$

The term containing the $SU(2)_L$ matrix can be written as

$$\frac{\sigma_b}{2}W_\mu^b = \frac{1}{2}\begin{pmatrix} W_\mu^3 & \sqrt{2}W_\mu^\dagger \\ \sqrt{2}W_\mu & -W_\mu^3 \end{pmatrix}$$

with $W_\mu = (W_\mu^1 + iW_\mu^2)/\sqrt{2}$ and since W_μ^3 and B_μ are both neutral they can mix through

$$\begin{pmatrix} W_\mu^3 \\ B_\mu \end{pmatrix} = \begin{pmatrix} \cos\theta_W & \sin\theta_W \\ -\sin\theta_W & \cos\theta_W \end{pmatrix}\begin{pmatrix} Z_\mu \\ A_\mu \end{pmatrix}$$

the interaction Lagrangian gives rise to a charged-current interaction ($\mathcal{L}_{CC}$) and a neutral-current interaction ($\mathcal{L}_{NC}$)

$$\mathcal{L}^{EW} = \mathcal{L}_{CC} + \mathcal{L}_{NC}$$

with

$$\mathcal{L}_{CC} = \frac{g}{\sqrt{2}}\left[W_\mu^\dagger J^\mu + W_\mu J^{\mu\dagger}\right]$$

and

$$\mathcal{L}_{NC} = \mathcal{L}_{QED} + \mathcal{L}_{NC}^Z$$

where each term is given by

$$\mathcal{L}_{QED} = \quad eA_\mu J_{QED}^\mu$$

$$\mathcal{L}_{NC}^Z = \quad \frac{g}{2\cos\theta_W}Z^\mu J_\mu^0$$

In the previous expressions, the electromagnetic, charged and neutral currents are, respectively

$$J_{QED}^\mu = \sum_f Q_f \overline{f}\gamma^\mu f$$

$$J^\mu = \overline{Q}_L\gamma^\mu\tau^\dagger Q_L + \overline{L}_L\gamma^\mu\tau^\dagger L_L$$

$$J^{\mu,0} = \overline{Q}_L\tau^3\gamma^\mu Q_L + \overline{L}_L\tau^3\gamma^\mu L_L - 2\sin^2\theta_W J_{QED}^\mu$$

with $e = g'\cos\theta_W$ in order to recover QED. Applying the step operator $\tau^\dagger = (\tau^1 + i\tau^2)/\sqrt{2}$ and with $\psi_L = (1-\gamma_5)\,\psi/2$, the charged current is straightforwardly rewritten as

$$J^\mu = \tfrac{1}{2}\left[\overline{\mathbf{u}}\gamma_\mu(1-\gamma_5)\mathbf{d}' + \overline{\nu}\gamma^\mu(1-\gamma_5)\mathbf{l}^-\right]$$

where

$$\mathbf{u} = \begin{pmatrix} u \\ c \\ t \end{pmatrix} \quad \mathbf{d}' = \begin{pmatrix} d' \\ s' \\ b' \end{pmatrix} \quad \nu = \begin{pmatrix} \nu_e \\ \nu_\mu \\ \nu_\tau \end{pmatrix} \quad \mathbf{l} = \begin{pmatrix} e \\ \mu \\ \tau \end{pmatrix}$$

	ν_L	e_L^-	e_R^-	u_L	d_L	u_R	d_R
Q	0	-1	-1	2/3	-1/3	2/3	-1/3
T_3	1/2	-1/2	0	1/2	-1/2	0	0
Y	-1/2	-1/2	-1	1/6	1/6	2/3	-1/3

Table 1.1.1: Electroweak charges. To get QED from the mixing between W_μ^3 and B_μ one has to impose $Y = Q - T_3$

On the other hand, the neutral current becomes $J^{\mu,0} = \sum_f \overline{f}\gamma^\mu(v_f - a_f\gamma_5)f$ with $a_f = T_{3,f}$ and $v_f = T_{3,f}(1 - 4|Q_f|\sin^2\theta_W)$. For completeness, the electroweak charges are collected in table Table 1.1.1

If one wants the introduced boson gauge fields to be true propagating fields, one needs to add the corresponding gauge invariant kinetic terms

$$\mathcal{L}_K = \mathcal{L}_K^I - \frac{1}{4}\left[G_a^{\mu\nu}G_{\mu\nu}^a + W_i^{\mu\nu}W_{\mu\nu}^i + B^{\mu\nu}B_{\mu\nu}\right]$$

Here,

$$\begin{aligned} G^{\mu\nu} &= \tfrac{-i}{g_s}[D_\mu, D_\nu] = \partial^\mu G^\nu - \partial^\nu G^\mu + ig_s[G^\mu, G^\nu] = \tfrac{\lambda_a}{2}G_a^{\mu\nu} \\ W^{\mu\nu} &= \tfrac{-i}{g}[D_\mu, D_\nu] = \partial^\mu W^\nu - \partial^\nu W^\mu + ig[W^\mu, W^\nu] = \tfrac{\sigma_i}{2}W_i^{\mu\nu} \\ B^{\mu\nu} &= \partial^\mu B^\nu - \partial^\nu B^\mu \end{aligned}$$

The gauge symmetry forbids a mass term for the gauge bosons. However, physical $W^\pm$ and Z bosons should be heavy objects. In order to generate masses, we need to break the gauge symmetry in a special way. Spontaneous symmetry breaking takes place in the Higgs sector.

Let us consider an $SU(2)_L$ doublet of complex scalar fields

$$\phi(x) \equiv \begin{pmatrix} \phi^+(x) \\ \phi^0(x) \end{pmatrix}$$

which obeys the Lagrangian

$$\mathcal{L}_H = (D^\mu\phi)^\dagger(D_\mu\phi) - \mu^2\phi^\dagger\phi - \lambda(\phi^\dagger\phi)^2 \quad \lambda{>}0,\ \mu^2 < 0$$

with

$$D^\mu\phi = \left[\partial^\mu + ig\frac{\sigma^a}{2}W_a^\mu + ig'Y_\phi B^\mu\right]\phi$$

The potential has an infinite set of degenerate states with minimum energy

$$\left|\langle 0|\phi^0|0\rangle\right| = \sqrt{\frac{-\mu^2}{2\lambda}} \equiv \frac{v}{\sqrt{2}}$$

We can parametrize the scalar doublet in the form

$$\phi(x) = \exp\left\{i\frac{\sigma_a}{2}\theta^a(x)\right\}\frac{1}{\sqrt{2}}\begin{pmatrix} 0 \\ v + H(x) \end{pmatrix}$$

with four degrees of freedom: $\theta^a(x)$ and $H(x)$. The local $SU(2)_L$ invariance of the Lagrangian allows us to rotate $\theta^a(x)$. In the unitary gauge, $\theta^a(x) = 0$, we get

$$\phi(x) = \frac{1}{\sqrt{2}}\begin{pmatrix} 0 \\ v + H(x) \end{pmatrix}$$

and the covariant derivative takes the form

$$(D^\mu\phi)^\dagger(D_\mu\phi) \to \frac{1}{2}\partial^\mu H\partial_\mu H + (v+H)^2\left\{\frac{g^2}{4}W_\mu^\dagger W^\mu + \frac{g^2}{8\cos^2\theta_W}Z_\mu Z^\mu\right\}$$

where one can see that the vacuum expectation value of the neutral scalar has generated a mass term for the $W^\pm$ and the Z.

We know experimentally that there are six different quark flavours and three different leptons with the corresponding neutrinos. These can be organized in families with the same $SU(2)_L \otimes U(1)_Y$ structure but different masses. In order to allow non zero values for the masses the Yukawa terms are introduced. The most general Yukawa Lagrangian allowed by the gauge symmetry is

$$\mathcal{L}_Y = -Y_{ij}^D\overline{Q}_{Li}\phi D_{Rj} - Y_{ij}^U\overline{Q}_{Li}\widetilde{\phi}U_{Rj} - Y_{ij}^E\overline{L}_{Li}\widetilde{\phi}E_{Rj} + \text{h.c}$$

where $\widetilde{\phi} = i\tau^2\phi^*$, Y^U, Y^D and Y^E are 3x3 complex matrices and i, j=1,2,3 refer to the three generations of fermions.

After SSB, the Yukawa Lagrangian becomes

$$\mathcal{L}_Y = -\left(1+\frac{H}{v}\right)\left\{\overline{\mathbf{d}}'_{\mathbf{L}}\mathbf{M}'_{\mathbf{d}}\mathbf{d}'_{\mathbf{R}} + \overline{\mathbf{u}}'_{\mathbf{L}}\mathbf{M}'_{\mathbf{u}}\mathbf{u}'_{\mathbf{R}} + \overline{\mathbf{l}}'_{\mathbf{L}}\mathbf{M}'_{\mathbf{l}}\mathbf{l}'_{\mathbf{R}} + \text{h.c}\right\}$$

where $\mathbf{d}'$,$\mathbf{u}'$ and $\mathbf{l}'$ are 3-vectors representing weak eigenstates and $\mathbf{M}'_{\mathbf{d}}$, $\mathbf{M}'_{\mathbf{u}}$ and $\mathbf{M}'_{\mathbf{l}}$ are 3x3 complex matrices. As far as $\mathbf{M}'_{\mathbf{f}} \neq 0$ we can always decompose

$$\mathbf{M}'_{\mathbf{f}} = \mathbf{H}_{\mathbf{f}}\mathbf{U}_{\mathbf{f}} = \mathbf{S}_{\mathbf{f}}^\dagger\mathcal{M}_{\mathbf{f}}\mathbf{S}_{\mathbf{f}}\mathbf{U}_{\mathbf{f}}$$

where $\mathbf{H}_{\mathbf{f}} = \sqrt{\mathbf{M}'_{\mathbf{f}}\mathbf{M}'^\dagger_{\mathbf{f}}}$, $\mathbf{U}_{\mathbf{f}}$ and $\mathbf{S}_{\mathbf{f}}$ are unitary and the resulting matrix $\mathcal{M}_{\mathbf{f}}$ is diagonal

$$\mathcal{M}_d = \text{diag}(m_d, m_s, m_b) \quad \mathcal{M}_u = \text{diag}(m_u, m_c, m_t) \quad \mathcal{M}_l = \text{diag}(m_e, m_\mu, m_\tau)$$

Then, the Yukawa Lagrangian in terms of the mass eigenstates reads

$$\mathcal{L}_Y = -\left(1+\frac{H}{v}\right)\left\{\overline{\mathbf{d}}\mathcal{M}_d\mathbf{d} + \overline{\mathbf{u}}\mathcal{M}_u\mathbf{u} + \overline{\mathbf{l}}\mathcal{M}_l\mathbf{l}\right\}$$

where the mass eigenstates are defined in terms of the weak eigenstates as

$$\mathbf{f_L} \equiv \mathbf{S_f f'_L}$$
$$\mathbf{f_R} \equiv \mathbf{S_f U_f f'_R}$$

with $\mathbf{f} = \mathbf{d}, \mathbf{u}, \mathbf{l}$.

1.1.1 The Cabibbo-Kobayashi-Maskawa Mechanism

The Cabbibo-Kobayashi-Maskawa (CKM) matrix, $\mathbf{V}$, is the mixing matrix that relates (primed) weak eigenstates to (unprimed) mass eigenstates

$$\mathbf{\overline{u}'_L d'_L} = \mathbf{\overline{u}_L S_u S_d^\dagger d_L} \equiv \mathbf{\overline{u}_L V d_L} \rightarrow \mathbf{V} = \mathbf{S_u S_d^\dagger}$$

It is a non-diagonal 3x3 unitary matrix of the form

$$\mathbf{V} = \begin{pmatrix} V_{ud} & V_{us} & V_{ub} \\ V_{cd} & V_{cs} & V_{cb} \\ V_{td} & V_{ts} & V_{tb} \end{pmatrix}$$

Consequently, $W^\pm$ bosons couple quarks mass eigenstates of different generations in weak interactions[1]

$$J^\mu = \tfrac{1}{2}\left[\mathbf{\overline{u}}\gamma_\mu(1-\gamma_5)\mathbf{d'} + \overline{\nu}_\mathbf{e}\gamma^\mu(1-\gamma_5)\mathbf{e}^-\right] = \frac{1}{2}\left[\mathbf{\overline{u}}\gamma_\mu(1-\gamma_5)\mathbf{V d} + \overline{\nu}_\mathbf{e}\gamma^\mu(1-\gamma_5)\mathbf{e}^-\right] \tag{1.1.2}$$

This charged current is the responsible for Flavour Changing Neutral Currents (FCNC). FCNC are neutral currents which violate flavour. In the SM, they can appear only at loop level because the only flavour changing current is the charged current J^μ, hence in order to have a neutral current violating flavour more than one current insertion is necessary.

1.1.2 CP violation in the SM

All terms in the SM are CP invariant except the one given by the charged current term Eq.1.1.2

$$\mathcal{L}_{CC} = \frac{g}{\sqrt{2}}\left[W_\mu^\dagger J^\mu + W_\mu J^{\mu\dagger}\right]$$

Under parity

$$W_\mu(x) \xrightarrow{P} W^\mu(x^P)$$

here, $x^P = (x^0, -\vec{x})$. Under charge conjugation

[1] We note that, because the neutrinos are assumed to be massless in the SM, there is no mixing matrix for leptons. In general the leptonic CKM matrix would have the form $\mathbf{V}^l = \mathbf{S}_\nu \mathbf{S}_l^\dagger$. With massless neutrinos we are free to chose $\mathbf{S}_\nu = \mathbf{S}_l$ and the leptonic analog of the CKM matrix is the identity matrix.

$$W_\mu(x) \xrightarrow{C} -W_\mu^\dagger(x)$$

Therefore

$$W_\mu(x) \xrightarrow{CP} -W^{\mu\dagger}(x^P)$$

In the Weyl or chiral representation we have

$$\gamma^0 = \begin{pmatrix} 0 & I_2 \\ I_2 & 0 \end{pmatrix} \quad \vec{\gamma} = \begin{pmatrix} 0 & \vec{\sigma} \\ -\vec{\sigma} & 0 \end{pmatrix} \quad \gamma^5 = \begin{pmatrix} -I_2 & 0 \\ 0 & I_2 \end{pmatrix}$$

$$P_L = \begin{pmatrix} I_2 & 0 \\ 0 & 0 \end{pmatrix} \quad P_R = \begin{pmatrix} 0 & 0 \\ 0 & I_2 \end{pmatrix}$$

where I_2 is the 2x2 identity matrix. Thus, under parity

$$\psi(x) = \begin{pmatrix} \psi_L \\ \psi_R \end{pmatrix}(x) \xrightarrow{P} \gamma^0\psi(x^P) = \begin{pmatrix} \psi_R \\ \psi_L \end{pmatrix}(x^P)$$

and under charge conjugation

$$\psi(x) = \begin{pmatrix} \psi_L \\ \psi_R \end{pmatrix}(x) \xrightarrow{C} \underbrace{i\gamma^2\gamma^0}_{C}\overline{\psi}^T(x) = \begin{pmatrix} i\sigma^2\psi_R^* \\ -i\sigma^2\psi_L^* \end{pmatrix}$$

and consequently under CP

$$\psi(x) = \begin{pmatrix} \psi_L \\ \psi_R \end{pmatrix}(x) \xrightarrow{CP} \gamma^0 C\overline{\psi}^T = \begin{pmatrix} -i\sigma^2\psi_L^* \\ i\sigma^2\psi_R^* \end{pmatrix}(x^P)$$

Using the Pauli matrix identity $\sigma^2\sigma^i\sigma^2 = -\sigma^i$ and the anticonmutation of fermionic fields we have

$$J^\mu = \frac{1}{2}\overline{u}_i\gamma^\mu(1-\gamma^5)V_{ij}d_j = \overline{u}_{Li}\gamma^\mu V_{ij}d_{Lj} \xrightarrow{CP} \overline{d}_{Lj}\gamma_\mu V_{ij}u_{Li}$$

Finally, in matrix notation

$$\begin{aligned}\mathcal{L}_{CC} = \tfrac{g}{\sqrt{2}}\left[W_\mu^\dagger J^\mu + W_\mu J^{\mu\dagger}\right] \quad &= \tfrac{g}{\sqrt{2}}\left[\overline{\mathbf{u}}_L \not{W}^\dagger \mathbf{V}\mathbf{d}_L + \overline{\mathbf{d}}_L \not{W}\mathbf{V}^\dagger\mathbf{u}_L\right] \\ &\xrightarrow{CP} \tfrac{g}{\sqrt{2}}\left[\overline{\mathbf{d}}_L \not{W}\mathbf{V}^{\mathbf{T}}\mathbf{u}_L + \overline{\mathbf{u}}_L \not{W}^\dagger \mathbf{V}^*\mathbf{d}_L\right]\end{aligned}$$

Consequently, the SM is CP invariant only if the CKM matrix is real: $\mathbf{V} = \mathbf{V}^*$, while in the presence of a non vanishing phase, CP is potentially violated in the SM.

The source of CP violation in the quark sector of the SM is related with the number of degrees of freedom in the CKM matrix which defines the presence or not of this phase. A generic NxN complex matrix has $2N^2$ free parameters. If V is unitary we have the following relation

$$\sum_{k=1}^{N} V_{ik} V_{kj}^{*} = \delta_{ij} \tag{1.1.3}$$

giving N^2 constrains. Thus, a NxN unitary complex matrix has $2N^2 - N^2 = N^2$ real parameters. We can always choose arbitrary quark phases through the redefinition

$$\begin{array}{l} u_i \to e^{i\phi_i} u_i \\ d_j \to e^{i\theta_j} d_j \end{array} \quad i,j = 1,...,N$$

Thus, the CKM matrix change as

$$\mathbf{V}_{ij} \to \mathbf{V}_{ij} e^{i(\theta_j - \phi_i)}$$

Therefore $2N-1$ phases can be eliminated since they are unobservable, and only the overall phase remains. Finally, the number of free parameters gets reduced to $N^2 - 2(N-1) = (N-1)^2$. As it is a unitary matrix it must have $N(N-1)/2$ real rotational angles and thereby remain $(N-1)(N-2)/2$ phases.

In the case of three generations $N = 3$, the number of free parameters is $(3-1)^2 = 4$, three of them are (real) angles and one phase. This complex phase is the only source of CP violation in the SM. On the contrary, with only two fermion generations $N = 2$ and the quark mixing mechanism cannot give rise to CP violation. CP violation effects can only appear when the three generation of quarks play an active role.

Different but equivalent representations of the CKM matrix are possible. In the Wolfenstein parametrization, the CKM matrix is expressed in terms of four parameters: A, λ, ρ and η, as an expansion in the small parameter λ, which is just the sinus of the Cabibbo angle, and making explicitly the experimental hierarchy pattern. This hierarchy is based on the following experimental features:

- The diagonal elements are very close to one
- The mixing between the first and second generation is the sinus of the Cabibbo angle

$$V_{us} = \lambda = \sin(\theta_c) \simeq 0.223$$

- The mixing between the second and third generations is of order λ^2 and the mixing between the first and the third is even smaller, of order λ^3

Up to $\mathcal{O}(\lambda^5)$, as required by the present level of theoretical and experimental accuracy, the Wolfenstein parametrization of the CKM matrix is given by

$$V = \begin{pmatrix} 1 - \frac{1}{2}\lambda^2 - \frac{1}{8}\lambda^4 & \lambda & A\lambda^3(\rho - i\eta) \\ -\lambda + \frac{1}{2}A^2\lambda^5\left[1 - 2(\rho + i\eta)\right] & 1 - \frac{\lambda^2}{2} - \frac{1}{8}\lambda^4\left(1 + 4A^2\right) & A\lambda^2 \\ A\lambda^3\left[1 - (\rho + i\eta)\left(1 - \frac{1}{2}\lambda^2\right)\right] & -A\lambda^2 + \frac{1}{2}A\left(1 - 2\rho\right)\lambda^4 - i\eta A\lambda^4 & 1 - \frac{1}{2}A\lambda^4 \end{pmatrix} \tag{1.1.4}$$

1.1.3 The Unitarity Triangle

The CP violation mechanism is based on the unitarity of the CKM matrix Eq.1.1.3. Among the nine unitarity conditions, the following is convenient

$$V_{ub}^* V_{ud} + V_{cb}^* V_{cd} + V_{tb}^* V_{td} = 0$$

since all sides have similar sizes $\mathcal{O}(\lambda^3)$. The unitarity triangle (UT) is rescaled by dividing its side by $V_{cb}^* V_{cd}$

$$\frac{V_{ub}^* V_{ud}}{V_{cb}^* V_{cd}} + \frac{V_{cb}^* V_{cd}}{V_{cb}^* V_{cd}} + \frac{V_{tb}^* V_{td}}{V_{cb}^* V_{cd}} = 0 \tag{1.1.5}$$

in such a way that the vertices are now fixed at (0,0) (1,0) and[2]

$$(\overline{\rho}, \overline{\eta}) \equiv (1 - \lambda^2/2)(\rho, \eta) \tag{1.1.6}$$

The UT is sketched in Figure 1.1.1 in the $(\overline{\rho}, \overline{\eta})$ plane. The sides R_u and R_d are

$$R_u = \sqrt{\overline{\rho}^2 + \overline{\eta}^2}, \quad R_t = \sqrt{(1-\overline{\rho})^2 + \overline{\eta}^2}$$

and the third size is normalized to one. The three angles of the UT are defined by

$$\alpha = \arg\left[-\frac{V_{td}V_{tb}^*}{V_{ud}V_{ub}^*}\right] \qquad \beta = \arg\left[-\frac{V_{cd}V_{cb}^*}{V_{td}V_{tb}^*}\right] \qquad \gamma = \arg\left[-\frac{V_{ud}V_{ub}^*}{V_{cd}V_{cb}^*}\right]$$

The relation between the angles and the $(\overline{\rho}, \overline{\eta})$ coordinates is given by

$$\cos\gamma = \frac{\bar{\rho}}{R_u} \qquad \sin\gamma = \frac{\bar{\eta}}{R_u}$$

$$\cos\beta = \frac{(1-\bar{\rho})}{R_t} \qquad \sin\beta = \frac{\bar{\eta}}{R_t}$$

$$\alpha = \pi - \beta - \gamma$$

1.1.4 The Unitarity Triangle Analysis and the role of Lattice QCD in flavour physics

Many experimental measurements can be interpreted as constraints in the $(\bar{\rho}, \bar{\eta})$ plane. The sides and angles of the triangle defined by the unitarity condition Eq.1.1.5 can be constrained from these measurements and consequently the CKM parameters $\bar{\rho}$ and $\bar{\eta}$ can be determined. This procedure is what it is usually known as the Unitarity Triangle Analysis (UTA).

[2] $\bar{\rho}$ and $\bar{\eta}$ are defined as the vertex of the UT. Eq.1.1.6 is valid up to $\mathcal{O}\left(\lambda^4\right)$

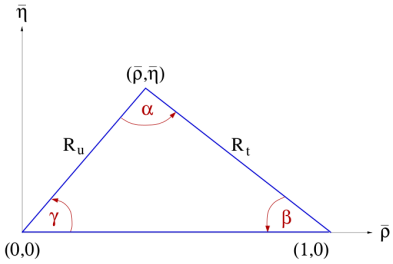

Figure 1.1.1: UT in the Wolfenstein parametrization

Within the UTA several constraints are included, provided by the comparison of the theoretical prediction with the experimental measurement of flavour observables depending on $\bar{\rho}$ and $\bar{\eta}$. These constraints define curves in the $(\bar{\rho}, \bar{\eta})$ plane which, because of the experimental and theoretical uncertainties, are designed as bands. SM consistency requires that all bands intersect each other in the same region. The aim of the UTA is over constraining $(\bar{\rho}, \bar{\eta})$ with high precision from as many independent processes as possible. If theoretical and experimental results are sufficiently precise, a possible inconsistency in the determination of $(\bar{\rho}, \bar{\eta})$ could reveal insights in flavour physics of still undiscovered NP beyond the SM.

Many of these constraints require the computation of non perturbative QCD quantities. In general, every experimental quantity can be expressed in terms of some perturbative known factors, the product of some CKM matrix elements and some non perturbative quantity. The dominant uncertainty in the theoretical prediction of flavour observables comes from the hadronic parameters enclosing the non perturbative QCD contributions. Lattice QCD provides an optimal tool to compute these non perturbative inputs with controlled systematic errors.

The standard analysis of the UTA involves a simultaneous fit to several quantities in which the hadronic parameters required are:

- The bag-parameter B_K entering in the theoretical prediction of ϵ_K defined in subsection 1.2.4
- The semileptonic form factors are required for the extraction of $|V_{ub}|$ and $|V_{cb}|$. From their ratio one determines:

$$\left|\frac{V_{ub}}{V_{cb}}\right| = \frac{\lambda}{1-\lambda^2/2}\sqrt{\bar{\rho}^2+\bar{\eta}^2} = \frac{\lambda}{1-\lambda^2/2}R_u \tag{1.1.7}$$

- The combination of $B_{(s)}$ meson decay constant and bag parameters f_{B_s}, f_{B_s}/f_B, B_{B_s} and B_{B_s}/B_{B_d}, which enter in the theoretical predictions of the B-physics observables ΔM_{B_d} , $\Delta M_{B_d}/\Delta M_{B_s}$ (see subsection 1.2.6) and $\mathrm{Br}(B \to \tau\nu)$.

Consequently, lattice results for hadronic parameters play a crucial role in the UTA. Besides the five UTA constraints that rely on Lattice QCD results, i.e ϵ_K, $\mathrm{Br}(B \to \tau\nu)$,

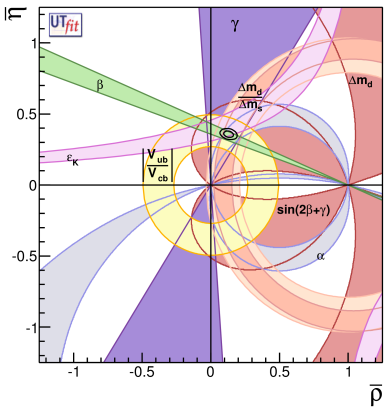

Figure 1.1.2: Results of the UTA within the SM from the UTfit collaboration.

ΔM_{B_d} , $\Delta M_{B_d}/\Delta M_{B_s}$ and V_{ub}/V_{cb} complementary information about the UT angles has also been obtained from the B decay modes, being available from the B factories: $B \to \psi K$ $(\sin 2\beta)$, $B \to \pi\pi, \rho\pi, \rho\rho$ (α) and $B \to DK$ (γ) .

The main results of the UTA [25], performed by the UTfit collaboration assuming the validity of the SM, up to Summer 2012, are summarized in Figure 1.1.2 showing superimposed the constraints coming from the individual constraints. The curves representing the UTA constraints intersect in a single allowed region for $(\bar{\rho}, \bar{\eta})$ proving that the CKM parameters are consistently over constrained. The parameters $\bar{\rho}$ and $\bar{\eta}$ turn out to be $\bar{\rho} = 0.139 \pm 0.021$ and $\bar{\eta} = 0.352 \pm 0.016$.

The UTfit collaboration uses a Bayesian method for the treatment of errors, see [26]. Other statistical approaches are based on a frequentist understanding of systematic theoretical uncertainties, which cannot be treated as statistically distributed quantities. In this framework, two main approaches can be distinguished: the Rfit [27] and the Scanning method [28]. At the moment, the CKMfitter group [29] is also performing a global analysis of measurements determining the CKM matrix with the Rfit treatment for the theoretical uncertainties.

Although, there is a reasonably good agreement with the SM prediction of a single CP-violating phase, as encoded in the CKM matrix, some tensions have been point out in the previous years [30, 31, 32]. As was first pointed out by [30] this tension is primarily given between the three most precise constraints on the unitarity triangle: $\sin(2\beta)$, $\mathrm{Br}(B \to \tau\nu)$ and ϵ_K. The comparison between input value and SM prediction for the UTA constraints performed by the UTfit is shown in [25]. For most of the constrains the $\sigma-$discrepancy is smaller than one, showing that there is a very good agreement between the input value and the UTA prediction. For the observables $\sin(2\beta)$, $\mathrm{Br}(B \to \tau\nu)$ and ϵ_K, instead, there is some tension in the UT fit given by a discrepancy larger than one σ between the input value and the UTA prediction (for a recent review of the UTfit collaboration see [33]).

1.2 Neutral Meson Oscillations

Flavour mixing of neutral mesons is a well known phenomenon in particle physics. In 1964 predictions of the existence of two kinds of neutral kaons with different lifetimes and masses had been confirmed experimentally [34]. The same year the decay $K_{\text{long}} \to \pi\pi$ was discovered [5] establishing CP violation in the kaon sector. Historically, the charm quark was predicted before the first evidence of J/ψ in order to eliminate large tree-level FCNC couplings in conflict with the experiment (the GIM mechanism). In 1987 the ARGUS experiment at DESY observed $B^0_d - \overline{B}^0_d$ mixing at an unexpectedly large rate [35]. This finding was the first hint of the existence of the heavy top quark which enters in its box diagram. The later was possible due to the sensitivity of meson-antimeson mixing to heavy virtual particles propagating in the internal loop of the transition. First evidences of $B^0_s - \overline{B}^0_s$ mixing was found in 2006 by the CDF experiment [36]. While for the D sector, even though many searches, the small scale at which both amplitude and frequency of the $D^0 - \overline{D}^0$ oscillations took place made difficult any observation. It was only in 2007 when BABAR [17] and Belle [18, 19] gave first evidence for mixing in that sector. These results were later confirmed by the CDF [37] and recently by the LHCb experiment [20].

The neutral K^0, D^0, B^0_d and B^0_s mesons are the only mesons which mix with their antiparticles: $\overline{K}^0$, $\overline{D}^0$, $\overline{B}^0_d$ and $\overline{B}^0_s$. The quark content of these mesons is

$$K^0 \sim \bar{s}d \qquad D^0 \sim c\bar{u} \qquad B^0_d \sim \bar{b}d \qquad B^0_s \sim \bar{b}s$$

$$\overline{K}^0 \sim s\bar{d} \qquad \overline{D}^0 \sim \bar{c}u \qquad \overline{B}^0_d \sim b\bar{d} \qquad B^0_s \sim b\bar{s}$$

Top quarks decay before they can hadronize and without top hadrons $T^0 - \overline{T}^0$ oscillations cannot occur. Hadrons built with d and $\overline{d}$ or u and $\overline{u}$ quarks like π^0 or η are their own antiparticle, thus there can not exist oscillations as $\pi^0 - \pi^0$.

Neutral meson mixing belongs to the class of FCNC processes, involving different flavours with the same electric charge. Within the SM they can occur through a weak interaction of second order with the mediation of a W boson. Oscillations in the kaon and beauty sector are dominated by the box diagrams shown in Figure 1.2.1, while in the charm sector the box diagram is doubly Cabibbo supressed and also GIM supressed. Thus in $\overline{D}^0 - D^0$ mixing long distance effects dominate over the short distance contribution given by the box diagram in Figure 1.2.1.

The absence of FCNC at tree level in the SM turns out these processes into an excellent framework to test the SM and look for NP effects. In fact, $\Delta F = 2$ transitions provide some of the most stringent constraints of NP.

In the following I will use the generic notation $M = K^0, D^0, B^0_d$ or B^0_s. $|M\rangle$ and $|\overline{M}\rangle$ will represent the quantum state of the corresponding particle and antiparticle respectively.

In the absence of weak forces $|M\rangle$ and $|\overline{M}\rangle$ are two mass degenerate mesons carrying definite flavour (S for K^0, C for D^0 and B for B^0 mesons) $+1$ and -1, respectively, since the strong and electromagnetic forces conserve this quantum number. Thus, $|M\rangle$ and

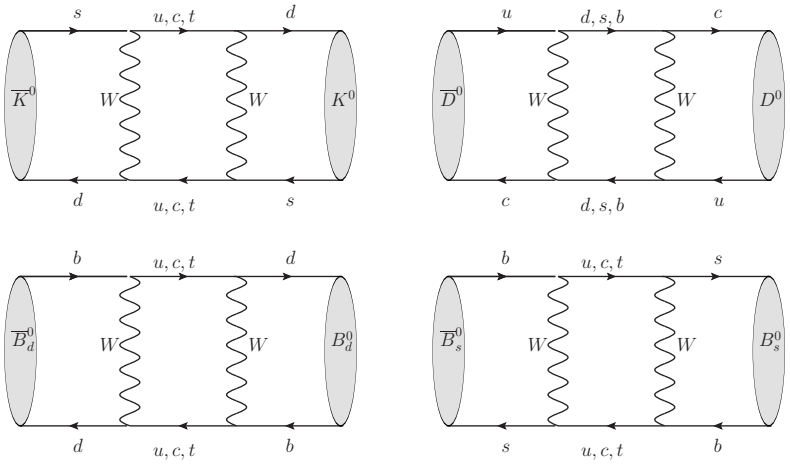

Figure 1.2.1: Box diagrams for $K^0 - \overline{K}^0$, $D^0 - \overline{D}^0$, $B^0_d - \overline{B}^0_d$ and $B^0_s - \overline{B}^0_s$ mixing. These are the s-channel diagrams and for each one of them it exists also the t-channel one (see Figure 1.2.2).

$|\overline{M}\rangle$ are eigenstates of the strong and electromagnetic interactions with definite flavour. If only the strong and electromagnetic interactions existed $|M\rangle$ and $|\overline{M}\rangle$ would be stable and form a particle-antiparticle pair with common mass. With the addition of weak forces flavour is no longer conserved. The new mass eigenstates are a superposition of $|M\rangle$ and $|\overline{M}\rangle$ which do not carry definite flavour. The flavour violation lifts the degeneracy and we have two physical states $|M_H\rangle$ and $|M_L\rangle$ with different masses and lifetimes.

1.2.1 Quantum mechanical two-state system

Let us consider first the case of absence of mixing, as it happens for the charged meson such as K^+, D^+ or B^+. The state at $t = 0$, denoted by $|M^+\rangle$, will evolve into a superposition of all states allowed by energy-momentum conservation

$$|M^+(t)\rangle = e^{-iM_M t - \Gamma t/2}|M^+\rangle$$

The first term in the exponential is the usual time evolution of a stable particle represented by a plane wave. The second term corresponds to the probability to find the initial meson $|M^+\rangle$ at a time t

$$|\langle M^+|M^+(t)\rangle|^2 = e^{-\Gamma t}$$

This evolution is the solution of the free Schrödinger equation

$$i\frac{d}{dt}|M^+(t)\rangle = H|M^+(t)\rangle \tag{1.2.1}$$

with $H = M_M - i\Gamma/2$.

We can generalize Eq.1.2.1 to the two system state describing the neutral meson mixing

$$i\frac{d}{dt}\begin{pmatrix} |M(t)\rangle \\ |\overline{M}(t)\rangle \end{pmatrix} = H\begin{pmatrix} |M(t)\rangle \\ |\overline{M}(t)\rangle \end{pmatrix}$$

The transition matrix element H for the quantum-mechanical two-state system meson-antimeson can be defined by

$$-i\,(2\pi)^4\,\delta^{(4)}\left(p_M - p_{\overline{M}}\right)H = \frac{\langle M(\vec{p}_M)|S|\overline{M}(\vec{p}_{\overline{M}})\rangle}{2M_M}$$

where S denotes the S-matrix which is usually given in terms of the time-ordered exponential

$$S = \boldsymbol{T}\exp\left[-i\int d^4x H_{\rm int}^{\rm SM}\right]$$

where $H_{\rm int}^{\rm SM}$ is the Hamiltonian encoding all the interactions in the SM.

Owing H to be a non-diagonal 2x2 matrix, M and $\overline{M}$ mix and are no more mass eigenstates. The two mass eigenstates are linear combinations of M and $\overline{M}$. They can be denoted by M_H and M_L, where "H" and "L" stands for "heavy" and "light" respectively. But they not only differ in their masses but also in their lifetimes. If we produce a state of meson M at time $t = 0$, the corresponding state evolves into a superposition of M and $\overline{M}$ at times $t > 0$ showing meson-antimeson oscillations.

Any matrix can be written as the sum of an hermitian plus an antihermitian matrix $H = M - i\Gamma/2$, where M is the mass matrix and Γ the decay matrix. In matrix form, the hamiltonian is

$$H = \begin{pmatrix} M_{11} - i\Gamma_{11}/2 & M_{12} - i\Gamma_{12}/2 \\ M_{21} - i\Gamma_{21}/2 & M_{22} - i\Gamma_{22}/2 \end{pmatrix}$$

The diagonal elements M_{11} and M_{22} correspond to the masses of $|M\rangle$ and $|\overline{M}\rangle$, generated from the quark mass term in the lagrangian and from the binding energy of the strong interaction. In contrast, M_{12}, M_{21} and all elements of Γ come from the weak interaction and therefore are small compared with M_{11} and M_{22}. M and Γ are hermitian matrices having positive real eigenvalues, thus $H_{21} = H_{12}^*$. In addition, due to CPT $H_{11} = H_{22}$. In other words H can be rewritten as

$$H = \begin{pmatrix} M - i\Gamma/2 & M_{12} - i\Gamma_{12}/2 \\ M_{12}^* - i\Gamma_{12}^*/2 & M - i\Gamma/2 \end{pmatrix} \tag{1.2.2}$$

Now we can diagonalize the system. The eigenvalues are given by the secular equation

$$\left(M - i\frac{\Gamma}{2} - \lambda\right)^2 = Q^2 \tag{1.2.3}$$

with

$$Q = \sqrt{\left(M_{12} - i\frac{\Gamma_{12}}{2}\right)\left(M_{12}^* - i\frac{\Gamma_{12}^*}{2}\right)}$$

The two solutions of the secular equation are

$$\lambda_{H,L} = M - i\frac{\Gamma}{2} \pm Q \equiv M_{H,L} - i\frac{\Gamma_{H,L}}{2}$$

where

$$M_{H,L} = M \pm \mathrm{Re}Q \qquad \Gamma_{H,L} = \Gamma \mp 2\mathrm{Im}Q \tag{1.2.4}$$

The following definitions for the average has been adopted

$$M = \frac{M_H + M_L}{2} \equiv M_{11} = M_{22} \qquad \Gamma = \frac{\Gamma_H + \Gamma_L}{2} \equiv \Gamma_{11} = \Gamma_{22}$$

From Eq.1.2.4

$$\Delta M \equiv M_H - M_L = 2\mathrm{Re}Q \qquad \Delta\Gamma \equiv \Gamma_H - \Gamma_L = -4\mathrm{Im}Q$$

The corresponding eigenstates are a superposition of $|M\rangle$ and $|\overline{M}\rangle$

$$|M_{H,L}\rangle = p|M\rangle \pm q|\overline{M}\rangle \equiv \frac{|M\rangle \pm \chi|\overline{M}\rangle}{\sqrt{1+|\chi|^2}}$$

where by definition $q/p = \chi$ and its explicit value is

$$\frac{q}{p} = \frac{Q^2}{2M_{12} - i\Gamma_{12}} = \frac{\Delta M - i\frac{\Delta\Gamma}{2}}{2M_{12} - i\Gamma_{12}} = \sqrt{\frac{M_{12}^* - i\frac{\Gamma_{12}^*}{2}}{M_{12} - i\frac{\Gamma_{12}}{2}}} \tag{1.2.5}$$

Contrary to what happens with $|M\rangle$ and $|\overline{M}\rangle$, $|M_{H,L}\rangle$ have exponential evolution laws with well-defined masses and decay widths

$$|M_H(t)\rangle = e^{-iM_H t - \Gamma_H t/2}|M_H\rangle$$

$$|M_L(t)\rangle = e^{-iM_L t - \Gamma_L t/2}|M_L\rangle$$

If CP is conserved in the $\Delta F = 2$ transitions the weak eigenstates have to be CP eigenstates.

It is clear that $|M\rangle$ and $|\overline{M}\rangle$ are not CP eigenstates since

$$CP|M\rangle = -|\overline{M}\rangle \qquad CP|\overline{M}\rangle = -|M\rangle$$

The CP eigenstates must satisfy

$$CP|M_{CP}\rangle = \eta_{CP}|M_{CP}\rangle$$

with $\eta_{CP} = \pm 1$. They are

$$\text{CP=+1} \qquad |M_+\rangle = \frac{1}{\sqrt{2}}\left(|M\rangle - |\overline{M}\rangle\right)$$

$$\text{CP=-1} \qquad |M_-\rangle = \frac{1}{\sqrt{2}}\left(|M\rangle + |\overline{M}\rangle\right)$$

In terms of the CP eigenstates, the eigenstates of the Hamiltonian are

$$|M_H\rangle = \frac{|M_+\rangle - \bar{\epsilon}|M_-\rangle}{\sqrt{1+|\epsilon|^2}} \qquad |M_L\rangle = \frac{|M_+\rangle + \bar{\epsilon}|M_-\rangle}{\sqrt{1+|\epsilon|^2}}$$

with

$$\chi = q/p = \frac{1-\bar{\epsilon}}{1+\bar{\epsilon}}$$

From the secular equation Eq.1.2.3 taking the real and imaginary part it is easy to obtain the following relations

$$\begin{aligned} (\Delta M)^2 - \frac{1}{4}(\Delta\Gamma)^2 &= 4|M_{12}|^2 - |\Gamma_{12}|^2 \\ \Delta M \Delta\Gamma &= -4\text{Re}\left(M_{12}\Gamma_{12}^*\right) = 4|M_{12}|\,|\Gamma_{12}|\cos\phi \end{aligned} \tag{1.2.6}$$

with

$$\phi = \arg\left(-\frac{M_{12}}{\Gamma_{12}}\right)$$

On the other hand, from Eq.1.2.5

$$\left(\frac{q}{p}\right)^2 = \frac{M_{12}^* - i\frac{\Gamma_{12}^*}{2}}{M_{12} - i\frac{\Gamma_{12}}{2}} = \frac{M_{12}^*}{M_{12}}\frac{1 + i\left|\frac{\Gamma_{12}}{2M_{12}}\right|e^{i\phi}}{1 + i\left|\frac{\Gamma_{12}}{2M_{12}}\right|e^{-i\phi}} \tag{1.2.7}$$

Here, we identify the phase ϕ as the responsible for the CP violation in the meson mixing. If $\phi \neq 0, \pi$ then $|q/p| \neq 1$ and $|M_{H,L}\rangle$ are not CP eigenstates. If $\phi = 0$ or π then $\chi = 1$ and $\bar{\epsilon} = 0$ so $|M_H\rangle = |M_+\rangle$ and $|M_L\rangle = |M_-\rangle$ which implies that the eigenstates of weak interaction, denoted as $|M_{H,L}\rangle$, are CP eigenstates with the same contribution of each one of the flavour states $|M\rangle$ and $|\overline{M}\rangle$.

1.2.2 Short and Long Distance Contributions

In order to determine the elements in the effective hamiltonian Eq.1.2.2, we can decompose the Hamiltonian into a QCD+QED part plus an effective weak interaction H_W responsible for the oscillations. Considering the weak Hamiltonian H_W and working to second order

$$H_{ij} = M_M \delta_{ij} + \frac{\langle i|H_W|j\rangle}{2M_M} + \frac{1}{2M_M}\sum_n \frac{\langle i|H_W|n\rangle\langle n|H_W|j\rangle}{M_M - E_n + i\epsilon}$$

where the states $|i\rangle$ and $|j\rangle$ would represent the mesons $|M\rangle$ and $|\overline{M}\rangle$, M_M is the mass common to $|M\rangle$ and $|\overline{M}\rangle$ states given by QCD and QED and E_n is the energy of the intermediate states $|n\rangle$.

The Cauchy theorem implies

$$\frac{1}{M_M - E_n + i\epsilon} = P\left(\frac{1}{M_M - E_n}\right) - i\pi\delta\left(E_n - M_M\right)$$

where P stands for principal part. The real part corresponds to the dispersive contribution to the hamiltonian while the imaginary part corresponds to the absorptive contribution. The off-diagonal element of the mass matrix reads

$$M_{12} = \frac{\langle M|H^{\Delta F=2}|\overline{M}\rangle}{2M_M} + \frac{1}{2M_M} P\sum_n \frac{\langle M|H^{\Delta F=1}|n\rangle\langle n|H^{\Delta F=1}|\overline{M}\rangle}{M_M - E_n}$$

where we have written explicitly the contribution of H_W which gives a non-zero matrix element: $H^{\Delta F=2}$. The first term with $H^{\Delta F=2}$ Hamiltonian corresponds to the short distance contribution computed through the box diagrams while the term with the double insertion $\Delta F = 1$ Hamiltonian give rise to long distance contributions, with $|n\rangle$ being for instance a $\pi\pi$ state.

Finally, the off-diagonal element of the width matrix is given theoretically by the absorptive part

$$\Gamma_{12} = \frac{1}{2M_M}\sum_n \langle M|H^{\Delta F=1}|n\rangle\langle n|H^{\Delta F=1}|\overline{M}\rangle(2\pi)\delta(E_n - M_M)$$

1.2.3 $\Delta F = 2$ effective weak Hamiltonian

The matrix elements responsible for the short distance contributions in the neutral meson system $\langle M|H^{\Delta F=2}|\overline{M}\rangle$ can be computed using the formalism of the effective Hamiltonian. The effective Hamiltonian approach consists in integrating out the heavy degrees of freedom of the theory. Weak processes of mesons are multi-scale processes, involving separated scales. These scales can be disentangled to separate short distance QCD, described by the exchange of quarks and gluons, from the long distance hadronic physics. The basic idea consists in separate the physics associated with the scale m_{heavy}, from the one associated to $m_{\text{light}} \ll m_{\text{heavy}}$.

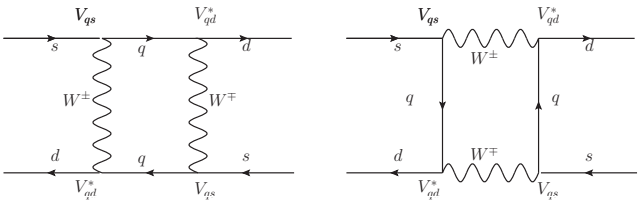

Figure 1.2.2: Box diagrams responsible for $K^0 - \overline{K}^0$ mixing in the SM

In the OPE formalism [38] the transition amplitude $A_{i\to j}$ corresponding to the transition $i \to j$ induced by the operator O is given by $A_{i\to j} = C_W(\mu)\langle f|O(\mu)|i\rangle$. The short distance contributions are contained in the Wilson coefficients $C_W(\mu)$ while the long distance ones are contained in the renormalized matrix element $\langle f|O(\mu)|i\rangle$. In order to guarantee the correct matching both, Wilson coefficients and matrix elements must be renormalized at the same scale μ with the same renormalization scheme. The effective Hamiltonian $H_{\text{eff}}^{\Delta F=2}$ must be designed to reproduce the S-matrix elements of the SM up to corrections of order $(m_{\text{light}}/m_{\text{heavy}})^n$

$$\langle f|T\exp\left[-i\int d^4x H_{\text{int}}^{\text{SM}}(x)\right]|i\rangle = \langle f|T\exp\left[-i\int d^4x H_{\text{int}}^{\text{eff}}(x)\right]|i\rangle\left[1+\mathcal{O}\left(\frac{m_{\text{light}}}{m_{\text{heavy}}}\right)^n\right]$$

$\Delta S = 2$ effective weak Hamiltonian

$K^0 - \overline{K}^0$ mixing in the SM occurs at one loop through the box diagram in Figure 1.2.2 Figure 1.2.2.

Setting the external four-momenta to zero, the amplitude of the diagram in the SM is

$$\begin{aligned}\mathcal{M}^{\Delta S=2} &= \frac{g^4}{2}\int\frac{d^4k}{(2\pi)^4}D_{\mu\nu}(k)D_{\rho\sigma}(k)\\ &\times\left[\bar{d}\gamma^\mu\tfrac{(1-\gamma_5)}{2}S(k)\gamma^\sigma\tfrac{(1-\gamma_5)}{2}s\right]\left[\bar{d}\gamma^\nu\tfrac{(1-\gamma_5)}{2}S(k)\gamma^\rho\tfrac{(1-\gamma_5)}{2}s\right]\end{aligned}$$

where $D_{\mu\nu}(k)$ is the W propagator

$$D_{\mu\nu}(k) = \frac{-g_{\mu\nu} + k_\mu k_\nu/k^2}{k^2 - M_W^2 + i\epsilon}$$

and $S(k)$ is the sum of all the quark propagators in the loop with the corresponding CKM matrix elements

$$S(k) = \sum_{q=u,c,t}\frac{\lambda_q}{\not{k} - M_W + i\epsilon}$$

with $\lambda_q = V_{qs}V_{qd}^*$. Due to the unitarity of the CKM matrix $\lambda_u + \lambda_c + \lambda_t = 0$, so we can rewrite the quark propagator as

$$S(k) = \sum_{q=c,t} \lambda_q \left(\frac{1}{\not{k} - m_q + i\epsilon} - \frac{1}{\not{k} - m_u + i\epsilon} \right)$$

After some Dirac algebra, the result can be straightforwardly identified with an effective four-fermion interaction expressed in terms of the effective Hamiltonian

$$H_{\text{eff}}^{\Delta S=2} = \frac{G_F^2 M_W^2}{16\pi^2} \mathcal{F}^0 Q^{\Delta S=2}$$

where G_F is the Fermi coupling, M_W the W-boson mass and $Q^{\Delta S=2}$ is the vectorial-axial dimension-six four-fermion operator

$$Q^{\Delta S=2} \equiv Q_1 \equiv \left[\bar{d}\gamma^\mu(1-\gamma_5)s\right]\left[\bar{d}\gamma_\mu(1-\gamma_5)s\right] \tag{1.2.8}$$

and the function $\mathcal{F}^0$ is given by

$$\mathcal{F}^0 = \lambda_c^2 S_0(x_c) + \lambda_t^2 S_0(x_t) + 2\lambda_c\lambda_t S_0(x_c, x_t)$$

The functions $S_0(x_c)$, $S_0(x_t)$ and $S_0(x_c, x_t)$ are the Inami-Lim functions [39] computed in terms of $x_q = m_q^2/M_W^2$. The Inami-Lim functions express the electroweak loop contributions of the quarks without QCD corrections

$$S_0(x_q, x_{q'}) = \int \frac{d^4k}{(2\pi)^4} \frac{1 - 2k^2/M_W^2 + (k^2/M_W^2)^2}{k^2(1 - k^2/M_W^2)^2} \frac{m_q^2}{k^2 - m_q^2} \frac{m_{q'}^2}{k^2 - m_{q'}^2}$$

with $S_0(x_q) \equiv S_0(x_q, x_q)$.

At leading order in m_c/M_W, one can set $k^2/M_W^2 \simeq 0$ and in terms of $x_q = m_q^2/M_W^2$ we have

$$\begin{aligned} S_0(x_c) &\sim \left\{x_c + \mathcal{O}(x_c^2)\right\} \\ S_0(x_c, x_t) &\sim \left\{x_c \left[\log\frac{x_t}{x_c} - \frac{3x_t}{4(1-x_t)} - \frac{3x_t \log x_t}{4(1-x_t)^2}\right] + \mathcal{O}(x_c^2 \log x_c)\right\} \end{aligned}$$

These two terms are tiny because $x_c \sim 10^{-4}$. This consequence of CKM unitarity is called the GIM suppression, related to the vanishing of FCNCs in the limit of small internal quark masses. In contrast, $S_0(x_t)$ is much larger because of the no GIM suppression in the top loops

$$S_0(x_t) \sim \left\{\frac{4x_t - 11x_t^2 + x_t^3}{4(1-x_t)^2} - \frac{3x_t^3 \log x_t}{2(1-x_t)^3}\right\}$$

However, the top contribution involved in $S_0(x_t)$ appears in the effective Hamiltonian suppressed by the small CKM factor so the three contributions, $S_0(x_c)$, $S_0(x_t)$ and $S_0(x_c, x_t)$, could be of comparable size.

When strong interactions are included, the transition can not longer be discussed at quark level. The effective Hamiltonian should be considered between meson states

$$\begin{aligned}\langle \overline{K}^0|H_{\text{eff}}^{\Delta S=2}|K^0\rangle = & \frac{G_F^2 M_W^2}{16\pi^2}\left[\lambda_c^2 S_0\left(x_c\right)\eta_1 + \lambda_t^2 S_0\left(x_t\right)\eta_2 + 2\lambda_c\lambda_t S_0\left(x_c,x_t\right)\eta_3\right] \\ & \times\left(\frac{\alpha(\mu)}{4\pi}\right)^{\frac{-\gamma_0}{2\beta_0}}\left\{1+\frac{\alpha(\mu)}{4\pi}J\right\}\langle \overline{K}^0|\hat{Q}^{\Delta S=2}(\mu)|K^0\rangle\end{aligned} \tag{1.2.9}$$

where $\hat{Q}^{\Delta S=2}(\mu)$ is the renormalized four-fermion operator renormalized in some regularization scheme at the scale μ and the terms involving $\alpha(\mu)$ contain the renormalization running.γ_0 and J are the anomalous dimension matrix at one loop and two loops (see Appendix C and the references in it for more details). Eq.1.2.9 is valid for energy scales below the charm threshold, after all heavier flavours have been integrated out

The short distance QCD contributions in the box diagrams are included through the correction factors η_1, η_2 and η_3 multiplying the Inami-Lim functions. Their numerical values are known at NLO [40, 41, 42][3]

$$\eta_1 = 1.51 \pm 0.24 \qquad \eta_2 = 0.5765 \pm 0.0065 \qquad \eta_3 = 0.47 \pm 0.04 \quad \text{@NLO}$$

In Eq.1.2.9 the terms proportional to the $\eta_{1,2,3}$ multiplied by the evolution correspond to the Wilson coefficient in the OPE formalism. The OPE factorizes perturbative contributions from the non perturbative ones in such a way that the expectation value of the effective Hamiltonian between the kaon and the antikaon state can be rewritten as

$$\langle \overline{K}^0|H_{\text{eff}}^{\Delta S=2}|K^0\rangle = \frac{G_F^2 M_W^2}{16\pi^2} C_W\left(\mu\right)\langle \bar{K}^0|\hat{Q}^{\Delta S=2}(\mu)|K^0\rangle \tag{1.2.10}$$

Short distance contributions, contained in the Wilson coefficients of the OPE $C_W(\mu)$, can be estimated in perturbation theory. Its dependence on the renormalization scheme and scale μ is canceled by that of the matrix element which must be computed using a non perturbative method.

As we will see in section 3.2, for historical and practical reasons the matrix element of the four-fermion operator is written in terms of the bag parameter B_K which contains the non perturbative contribution in the matrix element

$$\langle \bar{K}^0|\hat{Q}^{\Delta S=2}(\mu)|K^0\rangle = \frac{8}{3} f_K^2 M_K^2 \hat{B}_K(\mu) \tag{1.2.11}$$

Here, $B_K = 1$ corresponds to a vacuum saturation approximation and it refers to a situation where inserting the vacuum intermediate state into $\langle \bar{K}^0|\hat{Q}^{\Delta S=2}(\mu)|K^0\rangle$ reproduces the result $\frac{8}{3} f_K^2 M_K^2$ after contracting all the quark lines.

[3] The theoretical errors comes from the uncertainties due to the μ dependence at $\mathcal{O}(\alpha_S^2)$ and $\Lambda_{\overline{MS}}$. See [43] for a recent calculation of η_3 up to N^{2}LO

The renormalization group independent bag parameter, the so-called RGI B_K , usually denoted as $\hat{B}_K$, is simply related with $\hat{B}_K(\mu)$ at next-to-leading log (NLL) by

$$\hat{B}_K^{\rm RGI} = \left(\frac{\alpha(\mu)}{4\pi}\right)^{\frac{-\gamma_0}{2\beta_0}} \left\{1 + \frac{\alpha(\mu)}{4\pi} J\right\} \hat{B}_K(\mu) \tag{1.2.12}$$

which is just the scale-independent product at NLL of all the $\mu-$dependent quantities in Eq.1.2.9.

1.2.4 Indirect CP violation in $\overline{K}^0 - K^0$ system : ϵ_K

There is a crucial difference between the neutral kaon system and the other neutral meson systems. The lifetimes of the two eigenstates of mixing are very different. Because of that, it is usual to distinguish the eigenstates of mixing in the K system by their lifetimes instead of distinguishing them by their masses. The reason is the following: the only available nonleptonic channel for the CP odd kaon K_-, which is the dominant component of K_H, is the 3 pion channel for which it has barely enough mass. Consequently, the lifetime of $K_H = K_{\rm long}$ is rather larger than the one of $K_L = K_{\rm short}$, $\tau_{\rm short} \sim 10^{-10}s$ against $\tau_{\rm long} \sim 10^{-8}s$.

In the absence of CP violation, the two physical neutral kaon states would be also CP eigenstates. In other words $|K_{\rm short}\rangle$ and $|K_{\rm long}\rangle$ would correspond to $|K_+\rangle$ and $|K_-\rangle$ respectively. However, in nature CP is only nearly conserved so one expect a small contamination of $|K_-\rangle$ in $|K_{\rm short}\rangle$ and of $|K_+\rangle$ in $|K_{\rm long}\rangle$ determined by the value of $\bar{\epsilon}$.

Since a two pion final state is CP even while a three pion state is CP odd, if we consider only CP conserving decay modes, $K_{\rm short}$ and $K_{\rm long}$ will decay via the following dominant modes

$$K_{\rm short} \to 2\pi\,(\text{via } K_+) \qquad K_{\rm long} \to 3\pi\,(\text{via } K_-)$$

But $K_{\rm long}$ ($K_{\rm short}$) acquires a small CP even (odd) component proportional to $\bar{\epsilon}|K_+\rangle$ ($\bar{\epsilon}|K_-\rangle$) due to $\overline{K}^0 - K^0$ mixing. Therefore a small branching ratio through the following modes is also expected

$$K_{\rm short} \to 3\pi\,(\text{via } K_-) \qquad K_{\rm long} \to 2\pi\,(\text{via } K_+)$$

This is the so-called indirect CP violation because it comes from the mixing of the dominant CP state with a small component of the opposite one. However, if CP is directly violated in the decay a CP even state can decay into a CP odd one and viceversa. This is what we call direct CP violation and allows us to have also these modes

$$K_{\rm short} \to 3\pi\,(\text{via } K_+) \qquad K_{\rm long} \to 2\pi\,(\text{via } K_-)$$

The direct and indirect CP violation are parametrized by the small numbers ϵ' and ϵ_K respectively as it is illustrated in Figure 1.2.3.

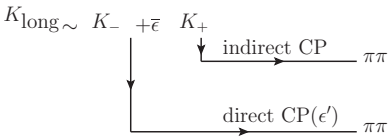

Figure 1.2.3: Schematic representation of ϵ_K and ϵ'

$\bar{\epsilon}$ is a phase dependent quantity since one can always redefine with a phase the CP eigenstates. However, it is easily related to the physical measurable quantity ϵ_K which is independent of the phase convention [44]

$$\epsilon_K \simeq \bar{\epsilon} + i\xi$$

where ξ is the weak phase of the $K^0 \to (2\pi)_{I=0}$ amplitude,

$$\xi = \frac{\text{Im}A_0}{\text{Re}A_0}, \quad A_0 = A\left[K^0 \to (2\pi)_{I=0}\right]$$

ϵ_K can be found by measuring

$$\epsilon_K \equiv \frac{2\eta_{+-} + \eta_{00}}{3} \tag{1.2.13}$$

where η_{+-} and η_{00} are the CP violating amplitude ratios for two-pion final states

$$\eta_{00} = \frac{\langle \pi^0\pi^0|\mathcal{H}|K_{\text{long}}\rangle}{\langle \pi^0\pi^0|\mathcal{H}|K_{\text{short}}\rangle} \qquad \eta_{+-} = \frac{\langle \pi^+\pi^-|\mathcal{H}|K_{\text{long}}\rangle}{\langle \pi^+\pi^-|\mathcal{H}|K_{\text{short}}\rangle}$$

Experimentally, ϵ_K has been measured with high precision. The updated result is [45] $|\epsilon_K| = (2.228 \pm 0.011) \times 10^{-3}$.

On the other hand, it is possible to derive the following theoretical formula for ϵ_K [46]

$$\epsilon_K = \sin\phi_\epsilon \left[\frac{\text{Im } M_{12}}{\Delta M_K} + \xi\right] e^{i\phi_\epsilon} \tag{1.2.14}$$

where the phase ϕ_ϵ is given by

$$\phi_\epsilon = \arctan\left(\frac{\Delta M_K}{\Delta\Gamma_K/2}\right)$$

and $\phi_\epsilon = 43.51(5)^o$, $\Delta M_K = 3.483(6) \times 10^{-12}$MeV and $\Delta\Gamma_K = 7.335(4) \times 10^{-15}$ s have been also determined experimentally [45].

Eq.1.2.14 allows us to calculate ϵ_K by computing $\text{Im}M_{12}$ and ξ theoretically in the SM and taking ϕ_ϵ and ΔM_K from experiment. Under reasonable estimates for the long distance contributions to both the dispersive and absorptive parts of the Hamiltonian ϵ_K is given by [47]

$$\epsilon_K = \kappa_\epsilon \frac{e^{i\phi_\epsilon}}{\sqrt{2}} \left[\frac{\text{Im } M_{12}}{\Delta M_K} \right]$$

where the factor $\kappa_\epsilon = 0.94(2)$ incorporates phenomenologically the long distance contributions and the corrections due to $\phi_\epsilon \neq 45^o$. The calculation of $\text{Im}M_{12}$ (its short distance contributions) is performed in the OPE approach. As described in subsection 1.2.2

$$M_{12}^* = \frac{\langle \bar{K}^0 | H^{\Delta S=2} | K^0 \rangle}{2M_K}$$

which yields

$$|\epsilon_K| = \kappa_\epsilon C_\epsilon |V_{cb}|^2 \lambda^2 \bar{\eta} \left[\left(1 - \frac{\lambda^2}{2} \right) S_0(x_t)\, \eta_2 + |V_{cb}|^2 \lambda^2 (1-\bar{\rho}) S_0(x_t)\, \eta_2 + S_0(x_c, x_t)\, \eta_3 \right] \hat{B}_K^{\text{RGI}} \tag{1.2.15}$$

with $C_\epsilon = \frac{G_F^2 M_W^2 f_K^2 M_K}{6\sqrt{2}\pi^2 \Delta M_K}$. The hyperbola defined by Eq.1.2.15 can be used to constrain the vertex of the unitarity triangle in the $(\bar{\rho}, \bar{\eta})$ plane, as shown in the UTA analysis of Figure 1.1.2, with a precision which depends on the quality of the estimates of λ, $|V_{cb}|$ and $\hat{B}_K$. While the numerical value of the former is known with very good precision [48], the estimate of $|V_{cb}|$ [49] is still given with an uncertainty of $\sim 2\%$ which is amplified four times since $|V_{cb}|$ enters in Eq.1.2.15 at the fourth power. $\hat{B}_K$ in the past used to be the largest uncertainty but in the last years has been computed in the previous years from several lattice collaborations with an error smaller than 4%. This is a consequence of using unquenched simulations with two (up and down), three (up, down and strange) and very recently also four (including also the charm quark) dynamical sea quarks together with simulations at light quark masses and using non perturbative methods for the computation of the renormalization constants.

As was first pointed out by Lunghi and Soni [50], there is a (2-3)σ tension, depending whether one uses exclusive or inclusive determinations of $|V_{cb}|$, between the average lattice determination of the $\hat{B}_K$ parameter and its prediction from the SM coming from the χ^2 minimization of the UT fit excluding the direct input of $\hat{B}_K$. The tension between the ϵ_K band and the other constraints is enhanced by the inclusion of the correction κ_ϵ, which decreases the SM prediction of ϵ_K about an 8%. After averaging between exclusive and inclusive determinations of $|V_{cb}|$ and considering the difference as a systematic error to be conservative, the UTfit collaboration is reporting currently a 1.4σ agreement between the lattice input value of ϵ_K and the SM prediction [33].

1.2.5 Neutral Kaon Oscillations beyond the SM

In order to extend the SM Hamiltonian $H^{\Delta S=2}$ in Eq.1.2.10 with NP contributions, one needs to consider the operators which, though absent in the SM, may appear in some of its extensions. This can be done by considering the *most general* effective Hamiltonian for $\Delta S = 2$ transitions considering the complete basis of dimension-six $\Delta S = 2$ four-fermion

operators which mix under renormalization [51]. The most general $\Delta S = 2$ effective Hamiltonian adopts the general form

$$H_{\text{eff}}^{\Delta S=2} = \frac{G_F^2 M_W^2}{16\pi^2} \left\{ \sum_{i=1}^{5} C_i(\mu) Q_i + \sum_{i=1}^{3} \tilde{C}_i(\mu) \tilde{Q}_i \right\} \tag{1.2.16}$$

where in the so-called SUSY basis, the four-fermion operators in Eq.1.2.16 are

$$\begin{array}{ll} Q_1 = \left[\bar{h}^a \gamma^\mu (1-\gamma_5) l^a\right]\left[\bar{h}^b \gamma_\mu (1-\gamma_5) l^b\right] & \tilde{Q}_1 = \left[\bar{h}^a \gamma^\mu (1+\gamma_5) l^a\right]\left[\bar{h}^b \gamma_\mu (1+\gamma_5) l^b\right] \\ Q_2 = \left[\bar{h}^a (1-\gamma_5) l^a\right]\left[\bar{h}^b (1-\gamma_5) l^b\right] & \tilde{Q}_2 = \left[\bar{h}^a (1+\gamma_5) l^a\right]\left[\bar{h}^b (1+\gamma_5) l^b\right] \\ Q_3 = \left[\bar{h}^a (1-\gamma_5) l^b\right]\left[\bar{h}^a (1-\gamma_5) l^b\right] & \tilde{Q}_3 = \left[\bar{h}^a (1+\gamma_5) l^b\right]\left[\bar{h}^a (1+\gamma_5) l^b\right] \\ Q_4 = \left[\bar{h}^a (1-\gamma_5) l^a\right]\left[\bar{h}^b (1+\gamma_5) l^b\right] & \\ Q_5 = \left[\bar{h}^a (1-\gamma_5) l^b\right]\left[\bar{h}^b (1+\gamma_5) l^a\right] & \end{array} \tag{1.2.17}$$

here, h, l are weak interaction eigenstates and denote the quark content of the meson $M \sim \bar{h}l$. In the case of the kaon $h \sim s$ and $l \sim d$. The indices a and b denote colour while spin indices are implicitly contracted within the square brackets.

Notice that $\tilde{Q}_{1,2,3}$ are obtained from $Q_{1,2,3}$ by exchanging the sign in both helicity projectors. Since the parity-even parts of the operators $\tilde{Q}_{1,2,3}$ and $Q_{1,2,3}$ coincide, due to parity conservation in the strong interactions, it is enough to consider only the matrix elements $\langle \overline{K}^0 | Q_i | K^0 \rangle$ with $i = 1...5$. On the other hand $Q_1 = Q^{\Delta S=2}$, so this is the only one contributing in the SM.

The Wilson coefficients appearing in Eq.1.2.16 match the full theory with the effective one. There are several models for physics Beyond the SM which lead to possible $\Delta S = 2$ processes.

1.2.6 $\overline{B}^0 - B^0$ mixing

The phenomenological situation is simpler in the $\overline{B}^0 - B^0$ mixing due to the large separation of energy scales $m_t > M_W \gg m_b \gg \Lambda_{QCD}$, that is, the flavour changing dynamics plays out in a scale of energies much larger than the scale of QCD, governing the size of the meson binding energies and the hadronic physics, but at the same time sufficiently smaller compared with M_W to still work with an effective theory.

Here, all the products of CKM matrix elements are of the same order while the contribution of the box diagram grows with the internal quark mass. As a consequence, the contribution with internal top quarks vastly dominates over the others. Moreover, since short distance contributions dominate over long distance, M_{12} is mainly given by the contribution of the box diagram[4]

$$M_{12} = \frac{G_F^2 M_W^2}{6\pi^2} f_{B_q}^2 M_B \left(V_{tb} V_{tq}^*\right)^2 S^0(x_t) \eta_B \hat{B}_{B_q}^{\text{RGI}} \tag{1.2.18}$$

[4] Eq.1.2.18 is valid for energy scales below the top threshold.

where the subindex q stands for d or s quarks and $\hat{B}_{B_q}^{\rm RGI}$ is the RGI bag parameter defined from

$$\langle \bar{B}^0|\hat{Q}^{\Delta B=2}(\mu)|B^0\rangle = \frac{8}{3} f_{B_q}^2 M_{B_q}^2 \hat{B}_{B_q}(\mu)$$

with $\hat{Q}^{\Delta B=2}$ analogous to $\hat{Q}^{\Delta S=2}$ in Eq.1.2.8 but with b quark content.

As the mass of the top quark is much larger than M_{B_q}, B meson can not decay to any top hadron. Therefore, Γ_{12} is dominated by $M_{B_q}^2 \sim m_b^2$ while $M_{12} \sim S^0(x_t)\,\eta_B \propto m_t^2$. Thus, one arrives to the theoretical prediction $|\Gamma_{12}/M_{12}| \sim m_b^2/m_t^2 \sim 10^{-3}$. Expanding $(q/p)^2$ in Eq.1.2.7 in terms of Γ_{12}/M_{12} we find that

$$1 - \left(\frac{q}{p}\right)^2 = \left|\frac{\Gamma_{12}}{M_{12}}\right| \sin\phi$$

And together with the experimental observation $\Delta M \gg \Delta\Gamma$, from Eq.1.2.7 we have

$$\Delta M_B \simeq 2|M_{12}| \qquad \Delta\Gamma_B \simeq 2|\Gamma_{12}|\cos\phi$$

up to corrections $\mathcal{O}\left(|\Gamma_{12}/M_{12}|^2\right)$. Therefore, ΔM_B is simply given by[5]

$$\Delta M_{B_q} = 2|M_{12}| = \frac{G_F^2 M_W^2}{6\pi^2} f_{B_q}^2 M_B \left(V_{tb}V_{tq}^*\right)^2 S^0(x_t)\,\eta_B \hat{B}_{B_q} \tag{1.2.19}$$

where η_B contains the QCD radiative corrections. It depends smoothly on $x_t = m_t^2/M_W^2$ and in practice it can be treated as a constant number [52]

$$\eta_B = 0.551(07)$$

Since

$$\left(V_{tb}V_{tq}^*\right)^2 \simeq A^2\lambda^6\left[(1-\rho)^2+\eta^2\right] \simeq |V_{us}|^2|V_{cb}|^2\left[(1-\rho)^2+\eta^2\right]$$

with $\lambda = |V_{us}|$ and $A = |V_{cb}|/|V_{us}|^2$ well determined experimentally, one can use Eq.1.2.19 to constrain $\sqrt{(1-\rho)^2+\eta^2}$ through the experimental measurement of ΔM_{B_q} and M_{B_q} and the lattice computation of $f_{B_q}$and B_{B_q}. Within the error the previous constraint correspond in the $(\bar{\rho},\bar{\eta})$ plane to the area in between two circumferences with center in $(\rho,\eta) = (1,0)$.

Alternatively, the experimental value of $\Delta M_{B_s}/\Delta M_B$ turns out to provide a stronger constraint on the $(\bar{\rho},\bar{\eta})$ plane

$$\frac{\Delta M_{B_s}}{\Delta M_B} \simeq \frac{f_{B_s}^2}{f_B^2}\frac{B_{B_s}}{B_B}\frac{M_{B_s}}{M_B}\left|\frac{V_{ts}}{V_{td}}\right|^2 = \xi^2\frac{M_{B_s}}{M_B}\left|\frac{V_{ts}}{V_{td}}\right|^2$$

where

[5] Note hat ΔM_K can not be computed from M_{12} due to the long distance effects which instead are negligible in the B system

$$\xi = \frac{f_{B_s}\sqrt{B_{B_s}}}{f_B\sqrt{B_B}}$$

1.2.7 $\overline{D}^0 - D^0$ mixing

In the $\overline{D}^0 - D^0$ mixing the effective Hamiltonian could be written as

$$\begin{aligned}\langle \overline{D}^0|H_{\text{eff}}^{\Delta C=2}|D^0\rangle = \; & \frac{G_F^2 M_W^2}{16\pi^2}\Big[\left(V_{cb}V_{ub}^*\right)^2 S_0\left(x_b\right) + \left(V_{cs}V_{us}^*\right)^2 S_0\left(x_s\right) \\ & +2V_{cb}V_{ub}^*V_{cs}^*V_{us}S_0\left(x_b,x_s\right)\Big] \\ & \times\left(\frac{\alpha(\mu)}{4\pi}\right)^{\frac{-\gamma_0}{2\beta_0}}\left\{1+\frac{\alpha(\mu)}{4\pi}J\right\}\langle \overline{D}^0|\hat{Q}^{\Delta C=2}(\mu)|D^0\rangle\end{aligned} \tag{1.2.20}$$

where the four-fermion operator $Q^{\Delta C=2}$ is defined as in Eq.1.2.8 but with charm and up quark content.

$\overline{D}^0 - D^0$ mixing is phenomenologically very interesting since it provides new information about processes with down-type quarks in the mixing loop diagrams not available in the K^0 or B^0 sector. Therefore it is sensitive to a new sector of NP. However, from the theoretical point of view it has the disadvantage that long distance contributions dominate over the short distance ones.

This is so because, on the one hand, box diagrams with internal b quarks are highly CKM suppressed by a factor $\left(V_{cb}V_{ub}^*\right)^2$ (see Eq.1.2.20), while the dominant box diagrams with internal d and s quarks are GIM suppressed. Therefore, short distance contributions from mixing box diagrams are expected to be small and long distance effects as the one in Figure 1.2.4 dominate.

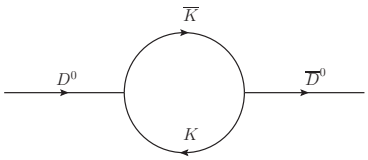

Figure 1.2.4: $D^0 \to KK \to \overline{D}^0$ long distance effect.

The long distance contributions to $\overline{D}^0 - D^0$ mixing are inherently non perturbative. Their theoretical estimates provide only order of magnitude estimates ($\sim \sin\theta_c^2 \times$ [SU(3) breaking]) and they are at the level of the experimental constraints which prevent us to determine whether oscillations in the neutral D system arise from a SM long distance effects or a NP short distance effects. In spite of that, there could still be a significant window between the experimental limits and the theoretical SM estimates such that significant constraints can be put on the NP parameter space. These NP contributions are short distance and they can be computed on the lattice by considering the complete basis of four-fermion operator presented in subsection 1.2.5.

Chapter 2

Twisted Mass Lattice QCD

In this chapter I will introduce the basic concepts about lattice QCD used in the rest of the work. First the lattice discretization of the QCD action à la Wilson with $\mathcal{O}(a)$ improvement is presented as it can be found in many textbooks such as [21, 53]. Motivated by the problems of the Wilson regularization, I will introduce the Twisted Mass QCD action in the continuum and its discretized version, the Wilson Twisted Mass QCD action, following the references [54, 55]. I will start with $N_f = 2$ degenerate quarks and then I will generalize the action for $N_f = 2 + 1 + 1$, a degenerate light quark doublet and a splitted heavy quark doublet. The Twisted Mass action presents a number of interesting advantages, which will be discussed here. Finally, I will show how one can compute observables in Lattice QCD from Monte Carlo simulations and I will briefly discuss the error analysis.

2.1 Lattice regularization of QCD

LQCD method is a first principle non perturbative implementation of field theory using the Feynman path integral approach. The starting point for the path integral formalism is the partition function in the Minkowski space

$$Z = \int \left[\prod_{x,r} d\phi^r \right] e^{iS[\phi]}$$

By replacing the continuum space-time by a discrete grid of spacing a and extension aL (aT) in the spatial (time) directions the infinite degrees of freedom of the continuum theory are reduced to a discrete set which can be numerically treated. The inverse of the lattice spacing provides an intrinsic cutoff scale, regularizing ultraviolet divergences. Therefore, the lattice provides a regularization scheme.

In the Minkowski space, the paths are weighted with a highly oscillating function $e^{iS[\phi]}$. For this reason, this path integral representation is not suited for numerical calculations. To overcome this difficulty LQCD makes use the Euclidean action in which the paths are weighted by a Boltzmann factor. The Euclidean action is obtained from the Minkowskian one by performing a Wick rotation to imaginary time[1]. In order that Euclidean correlation functions can be analytically continued back from the Euclidean to Minkowski space they have to obey a positivity condition, called reflection positivity, as it is discussed in [21]. The Wilson action [56] and the Twisted Mass Wilson action [57] satisfy this property under certain conditions. All these issues are discussed in the previous references.

2.1.1 Fermionic Action: Doubling Problem

In contrast with gauge fields, for which the replacement of the vector potential by the link brings us from the continuum to the lattice, the naive discretization for fermions is problematic because of the onset of non-physical modes [21, 53, 58].

Consider the action for a free fermion with mass M in the continuum

$$S_F^{\text{cont}}\left[\psi,\bar{\psi}\right] = \int d^4x \bar{\psi}(x)(\gamma_\mu \partial_\mu + M)\psi(x) \tag{2.1.1}$$

Its version in a discretized and finite space-time box can be constructed by replacing the derivatives with symmetric differences

$$\partial_\mu \psi(x) \to \frac{1}{2a}\left[\psi(x+a\hat{\mu}) - \psi(x-a\hat{\mu})\right] = \frac{1}{2}\left(D_\mu + D_\mu^*\right)\psi(x) \tag{2.1.2}$$

where $\hat{\mu}$ denotes the unit vector in direction μ, x is now the discretized lattice sites and

$$D_\mu \psi(x) = \frac{\left[\psi(x+a\hat{\mu}) - \psi(x)\right]}{a} \qquad D_\mu^* \psi(x) = \frac{\left[\psi(x) - \psi(x-a\hat{\mu})\right]}{a}$$

The lattice discretized version of Eq.2.1.1 reads

$$S_F\left[\psi,\bar{\psi}\right] = a^4 \sum_x \bar{\psi}(x)\left[\sum_\mu \frac{1}{2}\gamma_\mu\left(D_\mu + D_\mu^*\right) + M\right]\psi(x) \tag{2.1.3}$$

The equation above is usually rewritten in the form

$$S_F\left[\psi,\bar{\psi}\right] = a^4 \sum_{x,y} \bar{\psi}(x) Q\left(x,y\right)\psi(y)$$

where the Dirac free operator is

[1] The Wick rotation to imaginary time is obtained trough the replacement [53] $x_0 \to i x_0$, $p_0 \to -i p_0$ and $A_0^a \to = i A_0^a$, where A is the gauge field. In the Euclidean space, all the scalar products are performed using the four-dimensional Euclidean metric $\delta_{\mu\nu}$ rather than the Minkowski metric $g_{\mu\nu}$, which removes the need of lowering and raising indices.

$$Q\left(x,y\right)=\sum_{\mu}\frac{1}{2}\gamma_{\mu}\left(\left[D_{xy}\right]_{\mu}+\left[D^{*}_{xy}\right]_{\mu}\right)+M\delta_{xy}$$

and

$$\left[D_{xy}\right]_{\mu}=\frac{1}{a}\left(\delta_{x+a\hat{\mu},y}-\delta_{x,y}\right)\qquad\left[D^{*}_{xy}\right]_{\mu}=\frac{1}{a}\left(\delta_{x,y}-\delta_{x-a\hat{\mu},y}\right)$$

The free propagator $S(x,y)=\langle\psi(x)\bar{\psi}(y)\rangle$ is given by $S(x,y)=Q^{-1}$ where Q^{-1} is determined from the equation $\sum_z Q(x,z)Q^{-1}(z,y)=\delta_{xy}$. The inverse matrix Q^{-1} is easily computed using the Fourier transform formalism in momentum space. Imposing periodic boundary conditions one easily finds

$$S(x,y)=Q^{-1}(x,y)=\lim_{a\to 0}\int_{-\pi/a}^{\pi/a}\frac{d^4p}{(2\pi)^4}\frac{\left[-i\sum_{\mu}\gamma_{\mu}\tilde{p}_{\mu}+M\right]}{\sum_{\mu}\tilde{p}_{\mu}^2+M^2}e^{ip(x-y)}$$

with $\tilde{p}_{\mu}=\sin(p_{\mu}a)/a$. There exist sixteen regions in each Brillouin Zone, $[-\pi/a,\pi/a]$, in which $\tilde{p}_{\mu}$ take a finite value in the limit $a\to 0$ ($p_{\mu}=0$ and $p_{\mu}=\pm\pi/a$). This is the famous *doubling fermion problem*. The doubling problem can be solved by adding to the action a second order derivative term proportional to the lattice spacing a, the *Wilson term*, which explicitly breaks chiral symmetry [58]

$$S_F^W\left[\psi,\bar{\psi}\right]=\;\;S_F\left[\psi,\bar{\psi}\right]+a^4\sum_x a\frac{r}{2}\bar{\psi}(x)D^{*}_{\mu}D_{\mu}\psi(x)=a^4\sum_x\bar{\psi}(x)\left[D_W+M\right]\psi(x)\tag{2.1.4}$$

with r the *Wilson parameter* and S_F the naive discretized action. The free *Wilson-Dirac operator* is

$$Q(x,y)=\sum_{\mu}\frac{1}{2}\gamma_{\mu}\left(\left[D_{xy}\right]_{\mu}+\left[D^{*}_{xy}\right]_{\mu}\right)+\frac{a}{2}r\left[\Box_{xy}\right]_{\mu}+M\delta_{xy}$$

with

$$\left[\Box_{xy}\right]_{\mu}=\frac{1}{a^2}\left(\delta_{x+a\hat{\mu},y}+\delta_{x-a\hat{\mu},y}-2\delta_{xy}\right)$$

leading to the following propagator

$$S(x,y)=Q(x,y)^{-1}=\int_{-\pi/a}^{\pi/a}\frac{d^4p}{(2\pi)^4}\frac{\left[-i\sum_{\mu}\gamma_{\mu}\tilde{p}_{\mu}+M(p)\right]}{\sum_{\mu}{\tilde{p}_{\mu}}^2+M(p)^2}\tag{2.1.5}$$

where

$$M(p) = M + \frac{2r}{a}\sum_{\mu}\sin^2\left(\frac{p_\mu a}{2}\right) \tag{2.1.6}$$

$M(p)$ approaches M in the continuum limit except near $p_\mu = \pm\pi/a$ where $M(p)$ diverges when $a \to 0$. This eliminates the presence of fermion non-physical modes at the expense that the chiral symmetry of the original action is broken.

2.1.2 Wilson QCD Action

Fermionic action

In the continuum QED or QCD actions are obtained by gauging the global symmetry of the free fermionic action and adding a kinetic term for the gauge fields. The lattice version of QCD can be obtained following the same reasoning with the lattice fermionic action as the starting point and imposing local gauge invariance over SU(3) of colour.

Consider the Wilson action for $a = 1, 2, 3$ fermions ψ^a, where a is the colour index. The action Eq.2.1.4 is still valid if ψ is a 3-component vector field

$$\psi = \begin{pmatrix} \psi^1 \\ \psi^2 \\ \psi^3 \end{pmatrix} \quad \bar{\psi} = \begin{pmatrix} \psi^1 & \psi^2 & \psi^3 \end{pmatrix} \tag{2.1.7}$$

The Wilson action is invariant under the global non-abelian group SU(3), $\psi(x) \to G\psi(x)$, where G is an element of SU(3). It can be generalized to local invariance by introducing the links variables U_μ on the lattice which link, in a covariant way, the lattice site x with the neighbor site $x + a\hat{\mu}$ in the direction μ

$$S_F^W\left[\psi, \bar{\psi}, U\right] = \; a^4\sum_x \bar{\psi}(x)Q(x,y)\psi(y) = a^4\sum_x \bar{\psi}(x)\left[D_W\left[U\right] + M\right]\psi(x) \tag{2.1.8}$$

here, the Wilson Dirac operator $D_W\left[U\right]$ is the same as in the free theory replacing the derivative symmetric D_μ with the covariant derivative ∇_μ

$$D_W\left[U\right] = \sum_\mu \frac{1}{2}\gamma_\mu\left(\nabla_\mu + \nabla_\mu^*\right) + a\frac{r}{2}\nabla_\mu^*\nabla_\mu \tag{2.1.9}$$

where ∇_μ and ∇_μ^* are the forward and the backward covariant lattice derivatives, respectively, defined by

$$\nabla_\mu\psi(x) = \frac{\left[U_\mu(x)\psi(x + a\hat{\mu}) - \psi(x)\right]}{a}$$

$$\nabla_\mu^*\psi(x) = \frac{\left[\psi(x) - U_\mu^{-1}(x - a\hat{\mu})\psi(x - a\hat{\mu})\right]}{a}$$

$U_\mu(x)$ takes the explicit form $U_\mu(x) = e^{i\phi_\mu(x)}$ where $\phi_\mu(x)$ is an hermitian matrix belonging to the Lie algebra of SU(3). In terms of the lattice field $A_\mu(x)$ and the bare coupling constant g_0 it takes the form $\phi_\mu(x) = g_0 a A_\mu(x)$. Since A_μ is an element of the Lie algebra of SU(3), it can be written in the base of the Gell Mann matrices $A_\mu(x) = \sum_{i=1}^{8} A^i_\mu(x)\lambda_i/2$.

In this way, the action Eq.2.1.8 is invariant under the local gauge transformations for $\psi(x)$: $\psi(x) \to G(x)\psi(x)$ and $\bar{\psi}(x) \to G^{-1}(x)\bar{\psi}(x)$, while the link variables transform as

$$U_\mu(x) \to G(x)U_\mu(x)G^{-1}(x+\hat{\mu})$$
$$U^\dagger_\mu(x) \to G(x+\hat{\mu})U^\dagger_\mu(x)G^{-1}(x)$$

Chiral symmetry of the Wilson action

For vanishing fermion mass the QCD continuum action is invariant under the global chiral transformation

$$\psi \to e^{i\alpha\gamma_5}\psi \qquad \bar{\psi} \to \bar{\psi}e^{i\alpha\gamma_5} \tag{2.1.10}$$

On the lattice, writing the naive fermionic action with $M = 0$ as $S_F = \sum_{xy} \bar{\psi}(x)\,[D_{xy}\,[U]]\psi(y)$, it is straightforward to see that if

$$\{\gamma_5, D\} = 0 \tag{2.1.11}$$

then the action is invariant under Eq.2.1.10.

Instead, the $r-$term in the Wilson action breaks explicitly the chiral symmetry even for massless fermions. The connection between the doubler contributions (i.e the doubling fermion problem) and the chiral symmetry breaking is expressed by the the *no-go* theorem of Nielsen-Ninomiya. The theorem states that the the following properties for the Fourier transform $\tilde{D}(p)$ cannot hold simultaneously (for a proof see [59])

1. $\tilde{D}(p)$ is an analytic periodic function of momenta p_μ with period $2\pi/a$.
2. For momenta far below the cutoff π/a, we have $\tilde{D}(p) = i\gamma_\mu p_\mu$ up to terms of order ap^2
3. $\tilde{D}(p)$ is invertible at all non-zero momenta
4. D anti-commutes with γ_5

Property (1) guarantees that D is a local operator, while (2) and (3) are necessary if we want to recover the correct continuum limit. Finally, as we have pointed before, (4) ensures that the action is invariant under global chiral transformations. The Wilson approach satisfy (1), (2) and (3) but at the expense of breaking explicitly chiral symmetry.

Gauge action

Given the transformation of the links $U_\mu(x)$ under $G(x)$ the simplest gauge invariant quantity one can build from the group elements U_μ is the trace of the path ordered product of link variables along the boundary of an elementary plaquette P

$$\begin{aligned} U_P \equiv U_{\mu\nu} &= U_\mu(x)U_\nu(x+\hat{\mu})U_\mu^\dagger(x+\hat{\nu})U_\nu^\dagger(x) \\ &= U_\mu(x)U_\nu(x+\hat{\mu})U_{-\mu}(x+\hat{\mu}+\hat{\nu})U_{-\nu}(x+\hat{\mu}) \end{aligned}$$

where we have used the equivalence between the link variable in the negative $\hat{\mu}$ direction $U_{-\mu}(x)$ and pointing from x to $x-\hat{\mu}$ and the positively oriented link variable $U_\mu(x-\hat{\mu})$: $U_{-\mu}(x) \equiv U_\mu(x-\hat{\mu})^\dagger$.

The *Wilson Gauge Action* is defined in terms of the sum over all paquettes as

$$S_G = \beta \sum_P \left[1 - \frac{1}{6}\mathrm{Tr}(U_P + U_P^\dagger)\right] \tag{2.1.12}$$

with $\beta = 6/g_0^2$ and $\sum_P = \sum_x \sum_{\mu<\nu}$. It is easy to see that Eq.2.1.12 reaches the continuum expression with $\mathcal{O}(a^2)$ discretization errors.

The Wilson LQCD action is given by $S_{QCD} = S_G[U] + S_F^W[\psi, \bar{\psi}, U]$ with S_G and S_F^W from Eq.2.1.12 and Eq.2.1.8 respectively.

2.1.3 Wilson action properties

The chiral symmetry breaking of the Wilson action has the following consequences detailed in [21]. Here we just enumerate them:

1. The quark mass term is not protected against additive renormalization. The renormalized quark mass is of the form $m_R = Z_m(m - m_{cr})$ where the critical mass is linearly divergent with $a \to 0$.

2. The massive Dirac operator $D_W + M$ is not protected against zero modes unless the bare parameter M is positive. Due to the additive term in the quark mass renormalization the masses of the light quarks can be negative bare parameters which leaves the Dirac operator unprotected against zero modes which are considered unphysical.

3. Due to the Wilson term, the leading cutoff effects with Wilson-type fermions are $\mathcal{O}(a)$ cutoff effects. $\mathcal{O}(a)$ improvement is achieved following the Symanzik's on-shell improvement program [60] adding suitable counter-terms not only to the lattice action but also to the operators and determining the improvement coefficients. Close to the continuum limit the lattice theory may be described in terms of a local effective theory with action

$$S = \int d^4x \left\{\mathcal{L}_0(x) + a\mathcal{L}_1(x) + a^2\mathcal{L}_2(x) + ...\right\} = S_0 + aS_1 + \mathcal{O}(a^2)$$

where $\mathcal{L}_0(x)$ denotes the continuum QCD Lagrangian and $\mathcal{L}_k(x)$ with $k \geq 1$ are linear combinations of local operators of dimension $4+k$. Fom the list of all possible terms which contribute to $\mathcal{L}_k(x)$ one only needs to consider those which are invariant under gauge transformations and respect the symmetries of the lattice theory. In particular, the $\mathcal{O}(a)$ effective Lagrangian $\mathcal{L}_1(x)$ must be a linear combination of the fields

$$\begin{aligned} &\mathcal{O}_1 = \bar{\psi}\sigma_{\mu\nu}F_{\mu\nu}\psi \\ &\mathcal{O}_2 = M\mathrm{Tr}\left[F_{\mu\nu}F_{\mu\nu}\right] \qquad &&\mathcal{O}_3 = M^2\bar{\psi}\psi \\ &\mathcal{O}_4 = M\bar{\psi}\left[\overleftrightarrow{\not{D}} + M\right]\psi \qquad &&\mathcal{O}_5 = \bar{\psi}\left[\overleftrightarrow{\not{D}} + M\right]^2\psi \end{aligned} \tag{2.1.13}$$

where $\overleftrightarrow{\not{D}} + m$ is a shorthand for the lattice Wilson-Dirac operator. Operators $\mathcal{O}_2$ and $\mathcal{O}_3$ can be reabsorbed in a redefinition of the bare coupling constant and the mass: $g_0^2 \to g_0^2(1+b_g M)$ and $M \to M(1+b_M M)$. On the other hand operators $\mathcal{O}_4$ and $\mathcal{O}_5$ can be eliminated using the classical equation of motion. The only remaining operator is $\mathcal{O}_1$ which gives us the Sheikholeslami-Wohlert clover operator. It should be added to the original Wilson action with a coefficient c_{SW} in order to achieve the $\mathcal{O}(a)$ improvement. The coefficient c_{SW} is not a new free parameter of the theory, it is uniquely determined by the value of β. It can be calculated in perturbation theory or in a non perturbative way. However, action improvement is not enough, $\mathcal{O}(a)$ improvement also requires the improvement of composite operators. The procedure is similar to the one followed for the action improvement. The first step is to compute the composite operator in perturbation theory. One then should identify the lowest order in a, and subtract its contribution by adding *irrelevant*[2] effective operators to the action.

2.1.4 Gauge action improvement

The $\mathcal{O}(a)$ Symanzik improvement program can be extended to the gauge action to remove the remaining $\mathcal{O}(a^2)$ cutoff effects by adding *irrelevant* effective operators to the gauge action. Gauge invariance restricts the irrelevant operators one can add to the gauge action. As we have seen there is only one dimension-four operator

$$O_4 = \sum_{\mu\nu} \mathrm{Tr} F_{\mu\nu}F_{\mu\nu}$$

There are no dimension-five operators but three dimension-six operators

$$\begin{aligned} O_{6,1} &= \sum_{\mu\nu} \mathrm{Tr} D_\mu F_{\mu\nu} D_\mu F_{\mu\nu} \qquad O_{6,2} = \sum_{\mu\nu,\rho} \mathrm{Tr} D_\mu F_{\nu\rho} D_\mu F_{\nu\rho} \\ O_{6,3} &= \sum_{\mu\nu,\rho} \mathrm{Tr} D_\mu F_{\mu\rho} D_\nu F_{\nu\rho} \end{aligned}$$

[2] irrelevant in the sense that their contribution must go to zero when $a \to 0$

In fact, the expansion of the plaquette in terms of the lattice spacing a also involves all the previous operators

$$\sum_P \left[1-\tfrac{1}{2}\mathrm{Tr}\left[U_P + U_P^\dagger\right]\right] = \frac{1}{2}a^4 O_4 + \frac{1}{6}a^6 \sum_{i=1}^{3} r_i O_{6,i} + ...$$

Any gauge action involving the previous operators must be of the form:

$$S_G = \beta \sum_i c_i S_i \tag{2.1.14}$$

where S_i are the gauge invariant actions corresponding to the operators $O_{6,1}, O_{6,2}, O_{6,3}$ and O_4:

$$S_i = \sum_P \left[1 - \frac{1}{6}\mathrm{Tr}\left(U_{\mathcal{P}_i} + U_{\mathcal{P}_i}^\dagger\right)\right]$$

and $U_{\mathcal{P}_i}$ the corresponding plaquettes constructed by calculating, in addition to the four link plaquette term, also the six link long closed curves coming from $O_{6,\{1,2,3\}}$ shown in figure Figure 2.1.1. Eq.2.1.14 defines several improved actions, by choosing appropriate constants c_i. To fix the coefficients one must choose some improvement criterion. Nevertheless, an overall normalization condition is defined by setting the constant appearing in the gluonic part of the action to one for all orders of g_0^2: $c_0 + 8c_1 + 16c_2 + 8c_3 = 1$.

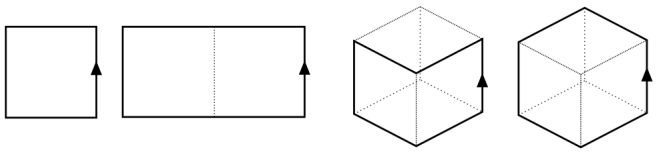

Figure 2.1.1: Curves corresponding to the O_4 operator, the plaquette, with coefficient c_0 and the six link long closed curves corresponding to $O_{6,\{1,2,3\}}$ which are the rectangle, the chair and the parallelogram respectively, with coefficients c_1, c_2 and c_3

The Symanzik improvement program was applied by Weisz in [61] to the Yang-Mills action, by calculating the 2-point Green function of the gauge field, i.e the gluon propagator, and removing the $\mathcal{O}(a^2)$ dependence. At tree-level, the previous cancellation gives us the coefficients at zero order of g_0^2 which defines the *tree-level Symanzik improved action*: $c_0 = 5/3$, $c_1 = -1/12$ and $c_2 + c_3 = 0$. It is convenient to choose $c_2 = 0$ since the multiplicity of *chair* loops per site is higher than that of the other operators. The perturbative Symanzik improvement is found to greatly improve lattice simulations in practice although we should remark that this method does not completely remove cutoff effects, since the $\mathcal{O}(a^2)$ dependence comes also from non perturbative sources. A non perturbative improvement where the cutoff dependence is computed non perturbatively [27] is also possible. Non perturbative improvement requires parameterizing both the action and the operators. To achieve $\mathcal{O}(a)$ improvement there is only one parameter to

tune in the action, the clover term mentioned previously. The coefficient c_{SW} can be fixed imposing the cancellation of $\mathcal{O}(a)$ lattice corrections in the Axial Ward Identity [62]. A conceptually different approach is based on the *renormalization group inspired* actions. The key idea is to incorporate the degrees of freedom above the lattice cutoff in suitable terms of the lattice action. There are two renormalization group inspired action widely considered in the literature, both consisting only on the plaquette and the rectangle terms with the normalization condition $c_0 + 8c_1 = 1$: The Iwasaki action [63] with $c_1 = -0.331$ and DBW2 action [64] with $c_1 = -1.4088$.

2.2 Twisted Mass

Having introduced in the last section the Wilson action and its problems, now I will introduce the twisted mass regularization of LQCD which has significant advantages compared to its untwisted counterpart. Historically, the twisted mass was designed to eliminate the unphysical zero modes in the quenched approximation [65]. The twisted mass term provides an infrared regulator allowing to simulate substantially smaller quark masses compared to Wilson fermion. However, it was soon realized that Twisted Mass has other interesting properties. Frezzotti and Rossi observed [23, 66] that automatic $\mathcal{O}(a)$ improvement is obtained after tuning to the so-called maximal twist without the need of all the $\mathcal{O}(a)$ counter terms required with standard Wilson quarks. Automatic $\mathcal{O}(a)$ improvement is obtained only by tuning one parameter: the bare untwisted quark mass has to be tuned to the critical mass.

2.2.1 Twisted Mass QCD in the continuum

The continuum form of the fermionic QCD action for a doublet $N_f = 2$ mass degenerate quarks, u and d, given in a vector

$$\psi = \begin{pmatrix} \psi_u \\ \psi_d \end{pmatrix}$$

takes the explicit form

$$S_F\left[\psi, \bar{\psi}, A_\mu\right] = \int d^4x \bar{\psi}\left[\gamma_\mu \mathcal{D}_\mu + M\right]\psi \tag{2.2.1}$$

with $\mathcal{D}_\mu$ the covariant derivative in the continuum $\mathcal{D}_\mu = \partial_\mu - ig_0 \frac{\lambda^a}{2} A^a_\mu$.

Performing the axial transformation:

$$\begin{aligned} \psi(x) \to \psi'(x) &= \exp\left\{i\omega\gamma^5 \tfrac{\tau^3}{2}\right\}\chi(x) \\ \bar{\psi}(x) \to \bar{\psi}'(x) &= \bar{\chi}(x)\exp\left\{i\omega\gamma^5 \tfrac{\tau^3}{2}\right\} \end{aligned} \tag{2.2.2}$$

where τ^3 is the third Pauli matrix acting in the flavour space, the fermionic action becomes

$$S_F\left[\chi,\bar{\chi},A^\mu\right]=\int d^4x\bar{\chi}(x)\left[\gamma_\mu\mathcal{D}_\mu+m_q+i\mu_q\gamma_5\tau^3\right]\chi(x) \tag{2.2.3}$$

while the gauge action remains invariant. The *untwisted* m_q and *twisted mass* μ_q are related with the so-called *polar mass* M via $M\mathrm{e}^{i\omega\gamma_5\tau_3}=m_q+i\mu_q\gamma_5\tau^3$ which lead to the following relations:

$$\begin{cases} m_q=M\cos\omega \\ \mu_q=M\sin\omega \end{cases} \rightarrow \begin{cases} M=\sqrt{m_q^2+\mu_q^2} \\ \tan\omega=\frac{\mu_q}{m_q} \end{cases} \tag{2.2.4}$$

This relation generates a family of equivalent theories parametrized by the twist angle ω. In particular the standard Wilson QCD action is obtained from the twisted one by setting $\omega=0$.

In the continuum the Twisted Mass QCD action is just a rewriting of the standard QCD one in a different basis and consequently they should share all the symmetries. The physical basis $\{\psi,\bar{\psi}\}$ is the basis where the continuum QCD action takes the standard form Eq.2.2.1 and the twisted basis $\{\chi,\bar{\chi}\}$ is the one where it takes the form Eq.2.2.3. The symmetry transformations in the twisted basis, the so-called twisted symmetries, are just a transcription of the standard symmetries using Eq.2.2.2 and Eq.2.2.4. For example, the discrete symmetries parity, time reversal and charge conjugation in the twisted basis, $\mathcal{P}_\omega$, $\mathcal{T}_\omega$ and $\mathcal{C}_\omega$ respectively, become

$$\mathcal{P}_\omega:\begin{cases} x_\mu=(x_0,\vec{x})\rightarrow x'_\mu=(x_0,-\vec{x}) \\ A_\mu(x)\rightarrow A_\mu(x') \\ \chi(x)\rightarrow\gamma_0 e^{i\omega\gamma_5\tau_3}\chi(x') \\ \bar{\chi}(x)\rightarrow\bar{\chi}(x')e^{i\omega\gamma_5\tau_3}\gamma_0 \end{cases}$$

$$\mathcal{T}_\omega:\begin{cases} x_\mu=(x_0,\vec{x})\rightarrow x'_\mu=(-x_0,\vec{x}) \\ A_\mu(x)\rightarrow A_\mu(x') \\ \chi(x)\rightarrow i\gamma_0\gamma_5 e^{i\omega\gamma_5\tau_3}\chi(x') \\ \bar{\chi}(x)\rightarrow -i\bar{\chi}(x')e^{i\omega\gamma_5\tau_3}\gamma_5\gamma_0 \end{cases}$$

$$C_\omega:\begin{cases} A_\mu(x)\rightarrow A_\mu(x)^* \\ \chi(x)\rightarrow C^{-1}\bar{\chi}(x)^T \\ \bar{\chi}(x)\rightarrow -\chi(x)^T C \end{cases}$$

where C must satisfy $-\gamma_\mu^T=C\gamma_\mu C^{-1}$, $\gamma_5=C\gamma_5C^{-1}$ being $C=i\gamma_0\gamma_2$ a possible choice. Note that C does not depend on the twist angle.

On the other hand, vector and axial chiral transformation become

$$
\begin{aligned}
SU(2)_V : & \begin{cases} \chi(x) \to \exp(-i\frac{\omega}{2}\gamma_5\tau_3)\exp(i\frac{\alpha_V^a}{2}\tau_a)\exp(i\frac{\omega}{2}\gamma_5\tau_3)\chi(x) \\ \bar{\chi}(x) \to \bar{\chi}(x)\exp(i\frac{\omega}{2}\gamma_5\tau_3)\exp(-i\frac{\alpha_V^a}{2}\tau_a)\exp(-i\frac{\omega}{2}\gamma_5\tau_3) \end{cases} \\
SU(2)_A : & \begin{cases} \chi(x) \to \exp(-i\frac{\omega}{2}\gamma_5\tau_3)\exp(i\frac{\alpha_A^a}{2}\gamma_5\tau_a)\exp(i\frac{\omega}{2}\gamma_5\tau_3)\chi(x) \\ \bar{\chi}(x) \to \bar{\chi}(x)\exp(i\frac{\omega}{2}\gamma_5\tau_3)\exp(i\frac{\alpha_V^a}{2}\gamma_5\tau_a)\exp(-i\frac{\omega}{2}\gamma_5\tau_3) \end{cases}
\end{aligned}
\tag{2.2.5}
$$

The form of the Ward identities in the twisted basis is also slightly different from the standard form. The infinitesimal local $SU_V(2) \times SU_A(2)$ chiral transformations of the fermionic fields are defined as

$$
\begin{aligned}
\delta\chi(x) &= i\left[\alpha_V^a(x) + \alpha_A^a(x)\gamma_5\right]\tfrac{\tau^a}{2}\chi(x) \\
\delta\bar{\chi}(x) &= i\bar{\chi}(x)\tfrac{\tau^a}{2}\left[-\alpha_V^a(x) + \alpha_A^a(x)\gamma_5\right]
\end{aligned}
$$

where we consider either $\alpha_V = 0$, $\alpha_A \neq 0$ (axial transformation) or $\alpha_A = 0$, $\alpha_V \neq 0$ (vectorial transformation). The invariance of the action gives the so-called partially conserved axial current (PCAC) and partially conserved vector current (PCVC) relations:

$$
\begin{aligned}
\partial_\mu \mathcal{A}_\mu{}^a &= 2m_q\mathcal{P}^a + i\mu_q\delta^{3a}\mathcal{S}^0 \\
\partial_\mu \mathcal{V}_\mu^a &= -2\mu_q\epsilon^{3ab}\mathcal{P}^b
\end{aligned}
\tag{2.2.6}
$$

It is straightforward to verify that if we set $\omega = 0$ we obtain the Ward Identities in their standard form

$$
\begin{aligned}
\partial_\mu A_\mu^a &= 2MP^a(x) \\
\partial_\mu V_\mu^a &= 0
\end{aligned}
$$

A very interesting case is when we work at maximal twist which corresponds to $\omega{=}\pi/2$. In this particular case $m_q = 0$ and the role of the physical mass is played by the twisted mass μ_q.

2.2.2 Twisted Mass QCD in the lattice

The lattice action for $N_f = 2$ degenerate flavours represented by the $SU(2)$ twisted doublet

$$
\chi_\ell = \begin{pmatrix} \chi_u \\ \chi_d \end{pmatrix}
$$

in the twisted basis is given by the discretized version of Eq.2.2.3

$$
(S_F)_\ell = a^4\sum_x \bar{\chi}_\ell(x)\left[D_W\left[U\right] + m_0 + i\mu_q\gamma_5\tau^3\right]\chi_\ell(x) \tag{2.2.7}
$$

where $D_W\left[U\right]$ is defined in Eq.2.1.9 and the subindex ℓ stands for *light quarks*.

As in the continuum, the twisted doublet is related by a chiral rotation with the doublet in the physical basis via

$$\psi_\ell(x) = \exp\left\{i\omega\gamma^5\tfrac{\tau^3}{2}\right\}\chi_\ell(x)$$
$$\bar{\psi}_\ell(x) = \bar{\chi}_\ell(x)\exp\left\{i\omega\gamma^5\tfrac{\tau^3}{2}\right\}$$

In the continuum, the symmetries of the Twisted Mass QCD are only a transcription of the standard QCD symmetries, via the axial transformation. In the lattice, instead, the Wilson term breaks some of the symmetries of the continuum action so the exact equivalence between the Wilson action with vanishing and non-vanishing twisted mass is lost. In other words, in the lattice Wilson and Wilson Twisted Mass are different regularizations of QCD.

In particular, the Wilson term breaks twisted parity $\mathcal{P}_\omega$, twisted time reversal $\mathcal{T}_\omega$ and twisted vector symmetry $SU_V(2)_\omega$ but shares with the standard Wilson theory invariance under gauge transformations, lattice rotations, translations and twisted charge conjugation $\mathcal{C}_\omega$.

The standard parity $\mathcal{P}_\omega$ becomes a symmetry of the action if combined either with a discrete flavour rotation

$$\mathcal{P}^{1,2}_{\mathcal{F}} : \begin{cases} x_\mu = (x_0, \vec{x}) \to x'_\mu = (x_0, -\vec{x}) \\ U_0(x) \to U_0(x') \\ U_k(x) \to U_{-k}(x') \equiv U_k^{-1}(x') \quad k = 1,2,3 \\ \chi(x) \to \gamma_0 e^{i\omega\gamma_5\tau_3}\tau_{1,2}\chi(x') \\ \bar{\chi}(x) \to \bar{\chi}(x') e^{i\omega\gamma_5\tau_3}\tau_{1,2}\gamma_0 \end{cases}$$

or with a sign change of the twisted mass term

$$\mathcal{P}_\mu = \mathcal{P}_\omega \times [\mu_q \to -\mu_q]$$

The same holds for the ordinary time reversal $\mathcal{T}_\omega$, which is only a symmetry when combined with the flavour rotation

$$\mathcal{T}^{1,2}_{\mathcal{F}} : \begin{cases} x_\mu = (x_0, \vec{x}) \to x'_\mu = (-x_0, \vec{x}) \\ U_0(x) \to U_0^{-1}(x') \\ U_k(x) \to U_k(x') \quad k = 1,2,3 \\ \chi(x) \to i\gamma_0\gamma_5 e^{i\omega\gamma_5\tau_3}\tau_{1,2}\chi(x') \\ \bar{\chi}(x) \to -i\bar{\chi}(x') e^{i\omega\gamma_5\tau_3}\tau_{1,2}\gamma_5\gamma_0 \end{cases}$$

or with

$$\mathcal{T}_\mu = \mathcal{T}_\omega \times [\mu_q \to -\mu_q]$$

Therefore $\mathcal{CPT}$ is a good symmetry of the Wilson Twisted Mass lattice action.

The Wilson term breaks explicitly the axial symmetry at finite lattice spacing [21]. Consequently the bare untwisted quark mass is subject to an additive renormalization constant in addition to the multiplicative one:

$$\hat{m}_q = Z_m m_q = Z_m\big(m_0 - m_{\text{crit}}\big)$$

The critical mass m_{crit} is the value of m_0 where the untwisted quark mass vanish. By imposing axial Ward Identities as normalization conditions one fixes the multiplicative renormalization for the mass term equal to the inverse of the scalar one $Z_m = Z_S^{-1}$. In contrast, the twisted mass μ_q renormalizes only multiplicatively. The PCVC relation Eq.2.2.6 holds exactly with the lattice Twisted Mass action with the replacement of the local vector current by the point-split vector current $\tilde{V}_\mu^a$ [3]. This implies that the product of the twisted mass μ_q and pseudoscalar density P is renormalization group invariant. Thus Z_P^{-1} renormalizes μ_q

$$\hat{\mu}_q = Z_\mu \mu_q = Z_P^{-1}\mu_q \tag{2.2.8}$$

With these conventions, the twist angle is given through the following ratio of renormalized quantities

$$\tan\omega = \frac{\hat{\mu}_q}{\hat{m}_q} = \frac{Z_S\mu_q}{Z_P\big(m_0 - m_{\text{crit}}\big)} \tag{2.2.9}$$

Tuning to maximal twist

One of the main advantages of the Twisted Mass Action, as discussed in subsection 2.2.4.2, is that automatic $\mathcal{O}(a)$ improvement can be achieved by working at maximal twist ($\omega = \pi/2$) by tunning only one parameter, the bare quark mass m_0, to its critical value m_{crit}.

The method to tune to maximal twist consists in choosing a parity odd operator and determine am_{crit} such that the operator has vanishing expectation value in the limit $\mu_q \to 0$. One appropriate quantity is the PCAC light quark mass

$$m_{\text{PCAC}} = \frac{\sum_x \langle \partial_0 A_0^a(\vec{x},t) P^a(\mathbf{0})\rangle}{2\sum_x \langle P^a(\vec{x},t) P^a(\mathbf{0})} \quad a = 1,2$$

where A and P are the axial and pseudoscalar currents defined in chapter 3.

In practice, we compute m_{PCAC} at large enough time separations in order to isolate the pion ground state and we demand $m_{\text{PCAC}} = 0$. The numerical precision required for the tuning of m_{PCAC} to zero is discussed in [67].

[3] $\tilde{V}_\mu^a$ is the conserved vector current on the lattice

$$\tilde{V}_\mu^a = \frac{1}{2}\left[\bar{\psi}(x)\gamma_\mu U_\mu^a(x)\psi(x+\mu) + \bar{\psi}(x+\mu)\gamma_\mu U_\mu^{a\dagger}(x)\psi(x)\right]$$

2.2.3 Twisted Mass with non degenerate quarks

The strange quark can be introduced in the Twisted Mass action by adding a twisted heavy mass-split doublet

$$\chi_h = \begin{pmatrix} \chi_c \\ \chi_s \end{pmatrix}$$

which in the framework of the Twisted Mass action implies also the addition of the charm quark. The twisted lattice fermionic action of a $SU(2)$ pair of mass non-degenerate quarks can be written in the form

$$(S_F)_h = a^4 \sum_x \bar{\chi}_h(x) \left[D_W[U] + m_q + i\mu_\sigma \gamma_5 \tau_1 + \mu_\delta \tau_3 \right] \chi_h(x) \tag{2.2.10}$$

where h stands for heavy, m_q is the untwisted bare quark mass for the heavy doublet, μ_σ the bare Twisted Mass and μ_δ the mass splitting along the τ_3 direction. As it is shown in [68], a real and strictly positive determinant of the Dirac operator is achieved once the mass splitting is taken to be orthogonal in isospin space to the twist direction with $\mu_\sigma^2 > \mu_\delta^2$. Physical values of the strange and the charm quark mass can be achieved by tunning the parameters μ_σ and μ_δ such that the simulated K and D mesons have their physical masses [69].

The chiral rotation analogous to the one in the light sector, Eq.2.2.2, transforming the heavy quark doublet from the twisted to the physical basis implies a rotation along the τ_1 direction and it is given by

$$\psi_h(x) = \exp\left\{ i\omega_h \gamma^5 \tfrac{\tau^1}{2} \right\} \chi_h(x)$$
$$\bar{\psi}_h(x) = \bar{\chi}_h(x) \exp\left\{ i\omega_h \gamma^5 \tfrac{\tau^1}{2} \right\}$$

The bare parameters μ_σ and μ_δ for the non-degenerate heavy doublet are related to the physical renormalised strange and charm quarks through [23]

$$\hat{m}_s = Z_P^{-1}\left(\mu_\sigma - \frac{Z_P}{Z_S}\mu_\delta\right)$$
$$\hat{m}_c = Z_P^{-1}\left(\mu_\sigma + \frac{Z_P}{Z_S}\mu_\delta\right)$$

2.2.4 Advantages and drawbacks of Lattice Twisted Mass QCD

Twisted Mass fermions share with Wilson ones most of their properties, in particular the solution of the doubling fermion problem, but in addition they provide important advantages compared with the properties of the Wilson action enumerated in subsection 2.1.3:

1. The twisted mass μ_q, the only relevant mass parameter working at maximal twist, is related directly with the physical mass and, unlike the untwisted mass m_0, it renormalizes multiplicatively.

2. Pseudoscalar decay constants need no renormalization constants when they are computed using Ward Identities.

3. In some cases operator mixing under renormalization is simplified. In particular,one can extract the matrix elements of the parity conserving part of the $\Delta F = 2$ weak effective Hamiltonian without contamination from mixing with operators of wrong chirality or parity mixing. To achieve this remarkable property a particular choice of the flavour structure and regularization of the valence quarks has to be made as it will be exhaustively described in subsection 3.4.2.

4. Unphysical zero modes and therefore exceptional configurations are avoided since the spectrum of the fermionic operator $D_W[U] + m_0 + i\mu_q\gamma_5\tau^3$ is bounded from below.

5. Working at maximal twist, physical observables are almost automatically $\mathcal{O}(a)$ improved without the need of any counterterm.

The price to pay is that the Twisted Mass regularization breaks at finite lattice spacing parity and flavour symmetries. This breaking is $\mathcal{O}(a^2)$ and it is recovered in the continuum limit.

Due to the relevance of the previous advantages of the Twisted Mass action we will describe here the last two properties which make it so competitive.

2.2.4.1 Unphysical zero modes

The first motivation for introducing the twisted mass term in the Wilson action was the problem of the *unphysical zero modes:* the quark propagator is obtained inverting the massive Wilson Dirac operator $\big[D_W[U] + M\big]$ but, due to the presence of an additive term in the quark mass renormalization ($\hat{m}_q = Z_P\big(m_0 - m_{crit}\big)$), the masses of the light quarks are typically negative parameters leaving the Wilson Dirac operator unprotected against unphysical zero modes.

Let us consider the two-point correlator (see chapter 3)

$$C^{(2)}_{PP}(x) = -\langle\bar{\psi}(x)\gamma_5\psi(x)\bar{\psi}(0)\gamma_5\psi(0)\rangle = -\langle Q^{-1}(x,0)Q^{-1}(x,0)\rangle$$

where $\langle ...\rangle$ stands for the vacuum expectation value and $Q = \gamma_5\big[D_W[U]+M\big]$. In the path integral formalism, the value of the corresponding observable is obtained after integrating over the fermionic degrees of freedom

$$C^{(2)}_{PP} \sim \int [DU] e^{-S_G} \det\big[Q^\dagger Q\big]\, \mathrm{Tr}[Q^{-1}(x,0)Q^{-1}(x,0)]$$

Denoting the eigenfunctions of Q for a given eigenvalue λ_i by ϕ_i, the r.h.s of the previous expression becomes

$$C^{(2)}_{PP} \sim \int [DU] e^{-S_G} (\prod \lambda_i)^2 \sum \lambda_j^{-1}\lambda_k^{-1}\phi_j(x)\phi_j^*(0)\phi_k(x)\phi_k^*(0)$$

Therefore, the functional integral cannot diverge: the eigenvalues in the denominator are always compensated by corresponding factors from the determinant. The problem arises in the so-called *quenched* approximation where the fermionic determinant is neglected. The functional may then become singular giving rise to the *exceptional configurations*. The approach to the chiral limit in the quenched approximation for Wilson quarks is limited by this unphysical zero modes forbidding simulations at masses lower than around half the strange quark mass. The problem is expected to disappear completely once the quark determinant is properly included. But, actually, one is in practice interested in varying the valence quark masses independently of the sea quark ones, the so-called *partially quenched approximation*, or one can also have different numbers of sea and valence quark masses of a different type. However, the presence of the non-zero twisted mass term $i\mu_q\gamma_5\tau_3$ protects the Dirac operator against very small eigenvalues since it eliminates any unphysical zero mode:

$$\begin{aligned} \det\left[Q^\dagger Q\right] &= \det[(D_W + m_0 - i\mu_q\gamma_5\tau_3)\overbrace{\gamma_5\gamma_5}^{I}(D_W + m_0 + i\mu_q\gamma_5\tau_3)] \\ &= \det\left[(D_W + m_0)^2 + \mu_q^2\right] > 0 \end{aligned}$$

2.2.4.2 $\mathcal{O}(a)$ improvement

Estimation of physical results from lattice measurements are obtained after performing the continuum limit. In practice, this is done by simulating at several values of the lattice spacing a and extrapolating to the continuum limit $a \to 0$. Due to the Wilson term, results are affected by $\mathcal{O}(a)$ lattice artefacts. $\mathcal{O}(a)$ improvement can be achieved applying Symanzik's improvement.

The Twisted Mass formulation of Lattice QCD is of particular interest because one can show that $\mathcal{O}(a)$ cutoff effects are absent from the average of correlators with opposite sign of the Wilson parameter r and a common value of the subtracted unrenormalized lattice quark mass m_q, the so-called Wilson Average (WA).

$\mathcal{O}(a)$ improvement can be proved in different ways just considering the symmetries of the action. Firstly, I will overview the first proof of $\mathcal{O}(a)$-improvement given in [66].

Let us consider the $\mathcal{R}_5$ symmetry

$$\mathcal{R}_5 : \begin{cases} \chi(x_0, \vec{x}) \to & \gamma_5\chi(x_0, \vec{x}) \\ \bar{\chi}(x_0, \vec{x}) \to & -\bar{\chi}(x_0, \vec{x})\gamma_5 \end{cases}$$

As $\left[\mathcal{R}_5\right]^2 = I$, two-fermion operators will be either even or odd under $\mathcal{R}_5$. This parity is the so-called $\mathcal{R}_5$-parity and it is given by $(-1)^{P_{\mathcal{R}_5}}$.

The Wilson Twisted Mass on the lattice remain invariant if after a $\mathcal{R}_5$ transformation of the fields we change also the sign on the Wilson term and the mass term. In particular the lattice action Eq.2.2.7 is invariant under the *spurionic* transformation

$$\mathcal{R}_5^{sp} \equiv \mathcal{R}_5 \times \left[r \to -r\right] \times \left[m_q \to -m_q\right] \times \left[\mu_q \to -\mu_q\right] \tag{2.2.11}$$

On lattice correlators the spurionic symmetry $\mathcal{R}_5^{sp}$ takes the form

$$\langle O\rangle^{\omega}_{(r,m_q,\mu_q)} = (-1)^{P_{\mathcal{R}_5}}\langle O\rangle^{\omega}_{(-r,-m_q,-\mu_q)}$$

As it is detailed in [66], as a consequence of $\mathcal{R}_5^{sp}$ all the terms of $\mathcal{O}(a)$ in the Symanzik expansion have opposite properties under $r \to -r$ and the average of multi-local operators with opposite r is free of $\mathcal{O}(a)$ discretization effects. To show this conclusion let us expand the bare operator O in powers of a in terms of renormalized continuum operators

$$\langle O\rangle^{\omega}_{(r,m_q,\mu_q)} = \big[\zeta_O(r)+am_q\xi_O(r)\big]\langle O\rangle_{0,(r,m_q,\mu_q)}+a\sum_j (m_q)^{n_j}\eta_{O,j}(r)\langle O_j\rangle_{0,(r,m_q,\mu_q)}+\mathcal{O}(a^2) \tag{2.2.12}$$

where $\langle ...\rangle_0$ means vacuum expectation value with respect the continuum action S_0 and ζ_O, ξ_O and η_O are a finite functions of r and g_0^2 necessary to match the lattice operator on the l.h.s with the continuum one on the r.h.s.

We apply the $\mathcal{R}_5^{sp}$ transformation to the operator

$$\begin{aligned}
\langle O\rangle^{\omega}_{(r,m_q)} &= (-1)^{P_{\mathcal{R}_5}(O)}\Big\{\big[\zeta_O(-r)-am_q\xi_O(-r)\big]\langle O\rangle^{\omega}_{(-r,-m_q,-\mu_q)}\Big\} \\
&\quad +(-1)^{P_{\mathcal{R}_5}(O_j)}\left\{a\sum_j(-m_q)^{n_j}\eta_{O,j}(-r)\langle O_j\rangle^{\omega}_{(-r,-m_q,-\mu_q)}\right\}+\mathcal{O}(a^2) \\
&= (-1)^{P_{\mathcal{R}_5}(O)}\Big\{\big[\zeta_O(-r)-am_q\xi_O(-r)\big]\langle O\rangle^{\omega}_{(-r,-m_q,-\mu_q)}\Big\} \\
&\quad +\Big\{a\sum(-1)^{P_{\mathcal{R}_5}(O_j)+n_j}(m_q)^{n_j}\eta_{O,j}(-r)\langle O_j\rangle^{\omega}_{(-r,-m_q,-\mu_q)}\Big\}+\mathcal{O}(a^2)
\end{aligned} \tag{2.2.13}$$

Equaling Eq.2.2.12 and Eq.2.2.13 at each order of a:

$$\begin{aligned}
0 &= \zeta_O(r)-\zeta_O(-r) \\
0 &= am_q\big[\xi_O(r)+\xi_O(-r)\big]\langle O\rangle_{0,(r,m_q,\mu_q)}+a\sum_j(m_q)^{n_j}\big[\eta_{O,j}(r)+\eta_{O,j}(-r)\big]\langle O\rangle_{0,(r,m_q,\mu_q)}
\end{aligned}$$

The last equation is just the $\mathcal{O}(a)$ term one gets by averaging the correlator calculated with r and $-r$ so the Wilson Average satisfies

$$\frac{1}{2}\big[\langle O\rangle^{\omega}_{(r,m_q,\mu_q)}+\langle O\rangle^{\omega}_{(-r,m_q,\mu_q)}\big] = \zeta_O(r;\omega)\langle O\rangle_{0,(m_q,\mu_q)}+\mathcal{O}(a^2) \tag{2.2.14}$$

Automatic $\mathcal{O}(a)$ improvement at maximal twist

In case of maximal twist one can obtain $\mathcal{O}(a)$ improvement without the averaging procedure [54]. The Twisted Mass action for a light doublet at maximal twist reads

$$S = a^4\sum_x\bar{\chi}_\ell(x)\left[D_W\big[U\big]+m_{\rm crit}+i\mu_q\gamma_5\tau^3\right]\chi_\ell(x) \tag{2.2.15}$$

while on the physical basis it reads

$$S = a^4 \sum_x \bar{\psi}_\ell(x) \left[\gamma_\mu \left(\frac{\nabla_\mu + \nabla^*_\mu}{2} \right) - i\gamma_5\tau_3(-\frac{a}{2}\nabla_\mu\nabla^*_\mu + m_{\rm crit}) + M_0 \right] \bar{\psi}_\ell(x)$$

with $M_{0,f} = \sqrt{{m_{\rm crit}}^2 + \mu_q^2}$.

The twisted parity transformation $\mathcal{P}_\omega$ at maximal twist

$$\mathcal{P} \equiv \mathcal{P}_{\omega=\pi/2} : \begin{cases} x_\mu = (x_0, \vec{x}) \to x'_\mu = (x_0, -\vec{x}) \\ A_\mu(x) \to A_\mu(x') \\ \chi(x) \to i\tau_3\gamma_0\gamma_5\chi(x') \\ \bar{\chi}(x) \to i\bar{\chi}(x')\tau_3\gamma_5\gamma_0 \end{cases}$$

is a symmetry of Eq.2.2.15 when it is combined with a change of sign in the Wilson parameter[4]

$$\mathcal{P} \times \left[r \to -r \right]$$

This symmetry implies that the expectation value of any operator must satisfy

$$\langle O \rangle^{\pm\pi/2}_{(-r,\mu_q)} = \eta_O \langle O \rangle^{\pm\pi/2}_{(r,\mu_q)}$$

with η_O the intrinsic parity of O. In this situation the two terms in the l.h.s of Eq.2.2.14 are identical or with opposite sign, so averaging is not necessary to obtain $\mathcal{O}(a)$ improved quantities.

The extension to mass non-degenerate quarks is straightforward since the symmetries we have used, with obvious modifications, remain valid.

An alternative proof of the automatic $\mathcal{O}(a)$ improvement based on the usage of symmetries which are not spontaneously broken in infinite volume continuum QCD is sketched in [54].

Let us introduce the following spurionic symmetries

$$\mathcal{R}^{1,2}_5 : \begin{cases} \chi(x) \to & i\gamma_5\tau^{1,2}\chi(x) \\ \bar{\chi}(x) \to & \bar{\chi}(x)\gamma_5 i\tau^{1,2}\gamma_5 \end{cases}$$

$$\mathcal{D} : \begin{cases} \chi(x) \to & e^{i3\pi/2}\chi(-x) \\ \bar{\chi}(x) \to & \bar{\chi}(-x)e^{i3\pi/2} \end{cases}$$

$$\mathcal{F}_{\mu_q} : \ \mu_q \to -\mu_q$$

and construct the global transformation[5]:

[4] Note that $m_{\rm crit}$ must be chosen to maintain the spurionic invariance. From this simple but crucial point we conclude that the critical mass is an odd function in r: $m_{\rm crit}(-r) = -m_{\rm crit}$

[5] Note that the $\mathcal{D}$ transformation essentially counts the dimension d of the operator.

$$\mathcal{G} = \mathcal{R}_5^{1,2} \times \mathcal{D} \times \left[\mu_q \to -\mu_q\right] \tag{2.2.16}$$

The Twisted Mass action at maximal twist Eq.2.2.15 is invariant under Eq.2.2.16. Moreover, the gauge action is also invariant under $\mathcal{G}$, so one conclude that the whole lattice QCD action is invariant under $\mathcal{G}$. According to the Symanzick program, the effective action is given by

$$S = S_0 + aS_1 + \mathcal{O}(a^2)$$

where S_0 is the continuum maximally twisted QCD action

$$S_0\left[\chi, \bar{\chi}, F_{\mu\nu}\right] = \frac{1}{2}\int d^4x \,\mathrm{Tr}(F_{\mu\nu}F^{\mu\nu}) + \int d^4x \bar{\chi}(x)\left[\gamma_\mu \mathcal{D}_\mu + i\mu_q\gamma_5\tau^3\right]\chi(x)$$

and S_1 is a dimension one action containing all the operators of dimension five which share the same symmetries of the continuum action S_0

$$S_1\left[\chi, \bar{\chi}, F_{\mu\nu}\right] = \int d^4x \sum_i C_i\mathcal{O}_i$$

At maximal twist there are only two operators

$$\mathcal{O}_1 = \bar{\chi}\sigma_{\mu\nu}F_{\mu\nu}\chi$$
$$\mathcal{O}_2 = \mu^2\bar{\chi}\chi$$

$\mathcal{O}(a)$ improvement is achieved if $m_q = \mathcal{O}(a)$ at most. This uncertainty is described by a dimension five operator parameterizing $\mathcal{O}(a)$ uncertainties in the critical mass: $\mathcal{O}_0 = \Lambda^2\bar{\chi}\chi$, where Λ is some energy scale depending of the critical mass, for example it can be Λ^2_{QCD}.

On the other hand, the vacuum expectation value of the multi-local operator is given by

$$\langle O\rangle = \langle O_0\rangle_0 + a\langle O_1\rangle_0 - a\langle S_1O_0\rangle_0 + \mathcal{O}(a^2) \tag{2.2.17}$$

where

- O_0 is the continuum target operator of dimension d and O_k are operators of dimension $d+k$ which respect the same symmetries as O_0.
- S is the lattice action, so:

$$S_0 \xrightarrow{\mathcal{G}} S_0$$
$$S_1 \xrightarrow{\mathcal{G}} S_1$$

- S_0 is the continuum action, thus, since $\mathcal{R}_5^{1,2}$ is part of the vector symmetry which is restored in the continuum, it fulfills that: $S_0 \xrightarrow{\mathcal{R}_5^{1,2}} S_0$

- S_1 depends only quadratically on μ through $\mathcal{O}_2$, then: $S_1 \xrightarrow{\mathcal{R}_5^{1,2}\times\mathcal{D}} S_1$.Since S_1 is dimension one: $S_1 \xrightarrow{D} -S_1$, so necessarily $S_1 \xrightarrow{\mathcal{R}_5^{1,2}} -S_1$.

Suppose now that we choose an operator O of even/odd dimension d independent from μ

a) with positive $\mathcal{R}_5^{1,2}$ parity:

from $O = O_0 + aO_1 + \mathcal{O}(a^2)$ we conclude that

$$O_0 \xrightarrow{\mathcal{R}_5^{1,2}} O_0 \qquad O_1 \xrightarrow{\mathcal{R}_5^{1,2}} -O_1$$

while

$$O_0 \xrightarrow{\mathcal{D}} \pm O_0 \qquad O_1 \xrightarrow{\mathcal{D}} \mp O_1$$

The expectation values $\langle O_1\rangle_0$ and $\langle S_1 O_0\rangle_0$ are

$$\langle O_1\rangle_0 = \frac{1}{Z}\int D\chi D\bar{\chi} DU e^{-S_0} O_1$$
$$\langle S_1 O_0\rangle_0 = \frac{1}{Z}\int D\chi D\bar{\chi} DU e^{-S_0} S_1 O_0$$

Here, e^{-S_0} is parity even while O_1 and $S_1 O_0$ are parity odd, then

$$\langle O_1\rangle_0 \xrightarrow{\mathcal{R}_5^{1,2}} -\langle O_1\rangle_0$$
$$\langle S_1 O_0\rangle_0 \xrightarrow{\mathcal{R}_5^{1,2}} -\langle S_1 O_0\rangle_0$$

But since $\mathcal{R}_5^{1,2}$ is just a change of variables in the above expressions, these expectation values must vanish[6]

$$\langle O_1\rangle_0 = \langle S_1 O_0\rangle_0 = 0$$

so that Eq.2.2.17 reduces to

$$\langle O\rangle = \langle O_0\rangle_0 + \mathcal{O}(a^2) \tag{2.2.18}$$

b) with negative $\mathcal{R}_5^{1,2}$ parity:

In this situation

$$O_0 \xrightarrow{\mathcal{D}} \pm O_0 \qquad O_1 \xrightarrow{\mathcal{D}} \mp O_1$$

while

$$O_0 \xrightarrow{\mathcal{R}_5^{1,2}} -O_0 \qquad O_1 \xrightarrow{\mathcal{R}_5^{1,2}} O_1$$

[6]The same is true if we consider $\mathcal{O}(a^{2k+1})$ effects (k integer)

Thus, now

$$\langle O_0 \rangle_0 = 0$$

but it is also true that $\langle O_{2k} \rangle_0 = 0$ so first corrections arises at $\mathcal{O}(a^3)$,consequently we have:

$$\langle O \rangle = \; a\langle O_1 \rangle_0 - a\langle S_1 O_0 \rangle_0 + \mathcal{O}(a^3) \tag{2.2.19}$$

Finally, from Eq.2.2.18 and Eq.2.2.19 we may conclude that even if the Twisted Mass action Eq.2.2.15 is not improved, the expectation value of operators which are invariant under $\mathcal{R}_5^{1,2}$ is automatically $\mathcal{O}(a)$ improved, while those with odd $\mathcal{R}_5^{1,2}$ vanish in the continuum limit. This is what we expected because $\mathcal{R}_5^{1,2}$ is part of the twisted symmetry $SU_V(2)_\omega$ so what these equations are telling us is that operators invariant under $SU_V(2)$, that is the physical ones, are automatically $\mathcal{O}(a)$ improved, while those which are not invariant under $SU_V(2)$ vanish in the continuum limit.

2.2.5 Osterwalder-Seiler regularization and partially quenched theory

The *Osterwalder-Seiler* (OS) regularization proposed in [70] is closely related to the lattice Twisted Mass (TM) action. The OS action breaks parity but not flavour, i.e for the OS regularization different flavours are all twisted with the same twisted angle, while in the TM one different flavours are combined in a doublet and the twist angle involves the τ^3 Dirac matrix, so they have opposite twist angles.

The OS action for an arbitrary number of flavours is simply given in the twisted basis by

$$\begin{aligned} S_F^{OS}\left[\chi_f, \bar{\chi}_f, U\right] \quad &= a^4 \sum_f \sum_x \bar{\chi}_f(x) \left[D_W\left[U\right] + M_f e^{i\omega_f \gamma_5}\right] \chi_f(x) \\ &= a^4 \sum_f \sum_x \bar{\chi}_f(x) \left[D_W\left[U\right] + m_{0,f} + i\mu_f \gamma_5\right] \chi_f(x) \end{aligned} \tag{2.2.20}$$

with

$$m_{0,f} = M_f \cos\omega_f \qquad \mu_f = M_f \sin\omega_f$$

For two degenerate flavours, it is useful the following compact form for the fermionic action of a doublet of quarks $\chi = \begin{pmatrix} \chi_1 \\ \chi_2 \end{pmatrix}$

$$S_F\left[\chi_f, \bar{\chi}_f, U\right] = a^4 \sum_x \sum_{f=1}^{2} \bar{\chi}_f(x) \left[D_W\left[U\right] + m_0 + i r_f \mu_q \gamma_5\right] \chi_f(x) \tag{2.2.21}$$

with $r_1 = -r_2$ for a TM doublet while $r_1 = r_2$ for a OS doublet of quarks.

The action Eq.2.2.20 is used in [23] to construct a *partially quenched* theory where the action from the valence is different to the action from the sea. Although the unitarity of the theory on the lattice is spoiled, the unitarity is guaranteed in the continuum limit because OS and TM doublets are being renormalized with the same renormalization constants.

The splitted action is

$$S = S_G\big[U\big] + S_F^{(\mathrm{sea})}\big[\chi_l, \bar{\chi}_l, \chi_h, \bar{\chi}_h, U\big] + S_F^{(\mathrm{val})}\big[q_f, \bar{q}_f, U\big] + S_F^{(\mathrm{gh})}\big[\phi_f, U\big] \tag{2.2.22}$$

where the first two terms are the lattice gauge action and the Wilson Twisted Mass action at maximal twist. The third term, $S_F^{(\mathrm{val})}\big[q_f, \bar{q}_f, U\big]$, describes the valence quarks. As we will see in detail in subsection 3.4.2, one can choose the twisting of the quarks involved in the valence action in order to simplify the renormalization pattern of the four fermion operators[23]. The action for each OS valence flavour q_f reads

$$S_f^{(\mathrm{val})OS} = a^4 \sum_x \bar{q}_f(x)\left[D_W(r_f) + m_{0,f} + i\mu_f\gamma_5\right] q_f(x)$$

The last term in Eq.2.2.22 is the ghost action, introduced in order to cancel the fermionic determinant, coming from the integration over the q_f and $\bar{q}_f$ valence degrees of freedom. The ghost action in terms of the scalar fields ϕ and the link variables U reads

$$S^{(\mathrm{gh})}\big[\phi_f, U\big] = a^4 \sum_x \phi_f^\dagger(x)\left[D_W(r_f) + m_f + i\mu_f\gamma_5\right]\phi_f(x)$$

In the path integral formalism the generating functional of the theory is:

$$\begin{aligned} Z = \quad & \int [D\chi_l][D\bar{\chi}_l][D\chi_h][D\bar{\chi}_h] e^{-S_G - S_F^{(\mathrm{sea})}} \\ & \times \int \prod_f [Dq_f][D\bar{q}_f] e^{-S_F^{(\mathrm{val})}} \int \prod_f [D\phi_f][D\phi_f^\dagger] e^{-S^{(\mathrm{gh})}} \end{aligned}$$

Being q_f Grassmann fields:

$$\int \prod_f [Dq_f][D\bar{q}_f] e^{-S_F^{(\mathrm{val})}} = \prod_f \det\left[D_W(r_f) + m_f + i\mu_f\gamma_5\right]$$

On the other hand, with ϕ_f scalar fields:

$$\int \prod_f [D\phi_f][D\phi_f^\dagger] e^{-S^{(\mathrm{gh})}} = \prod_f \left\{\det\left[D_W(r_f) + m_f + i\mu_f\gamma_5\right]\right\}^{-1}$$

Thus, the fermionic determinants exactly cancels and the generating functional arising from Eq.2.2.22 reproduces QCD.

2.3 Lattice simulations

To conclude this chapter, in this section I will explain, without going into the details, the procedure to compute estimators of physical quantities from lattice simulations. The first subsection describes briefly the relevant aspects of Monte Carlo simulations while the second and third subsection are devoted to the statistical and systematic errors respectively.

2.3.1 Importance sampling

Any physical quantity on the lattice is obtained from a Green function defined as the matrix element between vacuum states of an operator O. In the formalism of the path integral it reads

$$\langle 0|O|0\rangle = \frac{1}{Z}\int [\mathcal{D}U][\mathcal{D}\psi][\mathcal{D}\bar{\psi}] O e^{-S_{QCD}}$$

with Z the quantum partition function:

$$Z = \int [\mathcal{D}U][\mathcal{D}\psi][\mathcal{D}\bar{\psi}] e^{-S_{QCD}}$$

After integrating out the fermionic fields represented by Grassman variables[7] one needs to evaluate

$$\langle 0|O|0\rangle = \frac{\int [DU] O(U) \det\left[Q^\dagger Q\right] e^{-S_G[U]}}{\int [DU] \det\left[Q^\dagger Q\right] e^{-S_G[U]}} = \frac{\int [dU] O(U) P[U]}{\int [dU] P[U]} \tag{2.3.1}$$

with $Q = \gamma_5 \left[D_W[U] + M\right]$ and $P[U]$ is the probability distribution for generating gauge configurations, analogous to the Boltzmann factor in the partition functions of statistical mechanic systems, given by: $P[U] = e^{-S_G[U] + \log\det Q^\dagger Q}$. The fermionic contribution is contained in the non-local term $\det Q^\dagger Q$ and the expectation value of the operator becomes an integral over only background gauge configurations.

The quenched approximation consists in neglecting the contribution of $\log\det Q^\dagger Q$ in the probability distribution $P[U]$. This amounts to setting $\det QQ^\dagger = 1$, and hence $P[U]_{\text{Quenched}} = e^{-S_G[U]}$. Physically the quenched approximation amounts to neglect vacuum polarization effects in the Wilson loop, arising from the dynamical fermions. This approximation is only motivated by limited computer resources. Systematic errors arising from the quenched approximation are difficult to estimated and are the main motivation to introduce dynamical sea quarks in lattice simulations.

Numerically the expectation value involves a huge number of integrations. However, most of the link gauge configurations have an action that takes large values and fortunately only a small fraction of them will make a significant contribution to the integral. That is, the distribution is highly peaked about configurations that minimize the action.

[7] With Grassman variables one has: $\int [d\psi][d\bar{\psi}] e^{-\bar{\psi} M \psi} = \det M$. With a light doublet the fermionic determinant is given by $\det Q^\dagger Q$

Consequently in any lattice simulation we use a representative set of gauge configurations, called *importance sampling*, generated with a probability distribution given by the Boltzmann factor $P[U^i] = e^{-S_G[U^i]+\log\det[Q^\dagger Q]}$. This ensemble of gauge configurations $\{U^i\}$ is generated by a Markov chain where each configuration U^i is obtained from the preceding one U^{i-1} using an algorithm satisfying the detailed balance condition

$$P(U^{i-1} \to U^i)P[U^{i-1}] = P(U^i \to U^{i-1})P[U^i] \tag{2.3.2}$$

where $P(U \to U')$ is the probability of generating the configuration U' from the configuration U.

Once we have a set of $\{U^i\}$ generated by a Markov process the expectation value can be approximated by a simple average over the set of important sampling configurations

$$\langle O \rangle = \frac{1}{N}\sum_{i=1}^{N} O(U^i) \tag{2.3.3}$$

The Hybrid Monte Carlo (HMC) and Polinomial Hybrid Monte Carlo (PHMC) algorithm, used for the generation of gauge configurations in the ETMC, combine Molecular Dynamics (MD) and the Metropolis accept/reject method to build the Markov chain of gauge configurations. For more details regarding the (P)HMC algorithm and even/odd mass preconditioning improvement we refer to [71] and the references in it.

2.3.2 Statistical errors: Jacknife and Bootstrap

Typical error analysis does not apply to lattice simulations since we are not dealing with statistical independent measurements. The configurations has been generated following a Markov chain so the ith configuration depends on the (i-1)th configuration. Consequently, first of all, one should update the algorithm a sufficiently large number of steps until *thermalization* is achieved, i.e until the system has lost all memory of the initial configuration. Once thermalization is raised we select a set of gauge configurations $\{U^i\}$ separated by an adequate number of Monte Carlo trajectories in order to reduce the autocorrelation between measurements.

We are interested in derived quantities. Even if gauge configurations are not autocorrelated, derived quantities depending on different primary quantities measured over the same ensemble are correlated. Therefore the typical standard deviation is not a realistic error. The Jacknife method is a statistical method for estimating the propagation of error from the original data to derived quantities which takes correlation into account.

The following procedure provides us a method to treat correlation and autocorrelation simultaneously: Let us begin with an observable depending directly on the gauge configuration $\{P_i\} = \{P(U_i)\}$ where $i = 1...N$ denotes the gauge configuration. We begin by throwing out the first N_j measurements, leaving a data set of $N - N_j$ values. The statistical analysis is done on the reduced cluster giving a mean value $\bar{P}_{c_1}$. Then a new re-sampling is done throwing out the next N_j measurements and computing the corresponding $\bar{P}_{c2}$. The process is repeated $N_{\text{clust}} = N/N_j$ times, until the original ensemble

is completely scanned, resulting in a set of $N_{\text{clust}}+1$ values $\{\bar{P}_{c_1}, \bar{P}_{c_2}....\bar{P}\}$ where the last value is the mean value over the full ensemble. Consider now a derived quantity $f = f(P,Q)$ from two primary quantities $\{P_i\}$ and $\{Q_i\}$. We can construct the two sets $\{\bar{P}_{c_1}, \bar{P}_{c_2}....\bar{P}\}$ and $\{\bar{Q}_{c_1}, \bar{Q}_{c_2}....\bar{Q}\}$. A new ensemble $\{\bar{f}_{c_1}, \bar{f}_{c_2}....\bar{f}\}$ with $\bar{f}_{c_i} = f(\bar{P}_{c_i}, \bar{Q}_{c_i})$ and $\bar{f} = f(\bar{P}, \bar{Q})$ is straightforwardly computed and the jacknife error of $\bar{f}$ is estimated by

$$\sigma_f^2 = \frac{N_{\text{clust}}-1}{N_{\text{clust}}} \sum_{i=1}^{N_{\text{clust}}} \left(\bar{f}_{c_i} - \bar{f}\right)^2 \tag{2.3.4}$$

An alternative to the jacknife method is the bootstrap. In the bootstrap method we generate a data set of N_B values $\{P'_1, P'_2...., P'_{N_B}\}$ where each one of the values P'_i is one measurement of the original ensemble $\{P_i\}$ and N_B is large enough. The error associated is

$$\sigma_P^2 = \frac{1}{N_B - 1} \sum_{i=1}^{N_B} \left(P'_i - \bar{P}\right)^2$$

2.3.3 Systematic Errors

The statistical errors coming from the Monte Carlo simulation are under control and can be estimated with the jacknife or bootstrap methods. In fact, the statistical error is expected to decrease with $1/\sqrt{N}$ where N is the number of measurements. However, numerical simulations of Lattice QCD are characterized also by a systematic error, coming from the technical and theoretical uncertainties, which we have to take into account when quoting lattice results. In the following I list the systematic errors one has to quantify in any lattice computation:

Discretization errors Estimators for the physical quantities are extracted from the lattice in the continuum limit. To perform the continuum limit one has to simulate at several values of the lattice spacing a and then extrapolate to $a \to 0$.

Scale setting Scale setting is required to translate dimensional quantities produced in the lattice in physical units. The results of lattice calculations are dimensionless quantities, i.e expressed in lattice units. For instance, having calculate a hadron mass aM on the lattice it can be related with the experimental value of M in order to determine the lattice spacing a and convert other lattice data to physical units. The lattice spacing a determines the relative lattice spacings of computations performed at different values of the bare coupling. Several quantities can be used to set the scale, for example: the Sommer parameter [72], the pion mass, the nucleon mass, the pseudoscalar decay constants, etc.

Finite Volume All numerical lattice results are obtained in finite volumes. Because of the lattice finite volume, periodic, anti-periodic or twisted boundary conditions are imposed for the field, so every observable one computes on the lattice is affected by unphysical contributions of mirror states. In some cases these finite-volume corrections to the correlators fall exponentially with the lattice length $L = Na$ and usually they are negligible for $L \gtrsim 3/m_\pi$ (see [73]).

Chiral extrapolations Lattice simulations are often performed at unphysically large quark masses and eventually one wants to approach the physical quark masses corresponding to the physical pion mass, the so-called physical point. The chiral inspired extrapolations from the simulated regime to the physical point introduces a systematic error to the lattice computation. However, thanks to the algorithm and action improvements, simulations at physical light quark masses are possible nowadays though CPU expensive.

Heavy quarks The b quark is very heavy to be simulated on the lattice. To solve this problem several approaches can be adopted: one can simulate quarks with mass smaller than the physical one and then extrapolate to the physical mass guided by the *Heavy Quark Effective Theory* (HQET) or one can implement directly HQET on the lattice and consider the heavy quark as a static quark.

Matching between lattice and continuum scheme Renormalization Constants provide the link between matrix element regularized on the lattice, and the one renormalized in the continuum. The operators we simulate are bare operators regularized with the lattice spacing a which can be interpreted as an ultraviolet cutoff. Therefore RCs can be computed perturbatively since it only involves short-distance contributions. In practice, perturbation theory on the lattice is much more complex than in the continuum so the computations are rarely extended beyond one loop order. Moreover, lattice perturbation theory usually converges rather slowly so the accuracy of perturbative RCs is limited. Therefore, non perturbative methods as RI-MOM described in chapter 4 are required. The full systematic associated with the renormalization procedure will be described in detail in chapter 4.

Quenching This approximation is the hardest to justify and quantify. It was only motivated by the limited computational power. In recent years, almost all lattice collaborations include the effects of dynamical quarks in their lattice simulations.

Excited states contamination When computing the correlator function one can suffer the contribution of some excited states (see Eq.3.1.7). These contributions can be suppressed using the smearing techniques described in the following chapters.

Chapter 3

Bag parameters from the lattice

In this chapter I will describe how to extract pseudoscalar masses, decay constants and finally B-parameters from suitable two- and three-point correlation functions. To this end, I will start with the study of the two-point correlation functions and the computation of the pseudoscalar meson masses and decay constants. The signal-to-noise ratio is greatly enhanced by summing over the spatial position of the quarks and antiquarks fields so for reader convenience all formulae will be directly derived using the so-called *meson walls* we have implemented in our numerical simulations. In the second section I will present the strategy for the computation of B-parameters and the involved three-point correlation functions. All formulae will be obtained first in terms of the renormalized correlation functions. Then, I will overview the renormalization pattern for both two- and four-fermion operators. Finally, with all these ingredients I will obtain the renormalized formulae for the B-parameters showing how one can get ride of wrong chirality and parity mixing obtaining a simplified renormalization pattern. The Appendix A contains the details regarding smearing techniques and the construction of stochastic propagators.

3.1 Pseudoscalar mesons

In this section, I proceed to construct the correlation functions, involving the operators necessary to evaluate the pseudoscalar meson masses, pseudoscalar decay constants and bag parameters.

3.1.1 Two-point correlation functions

At a reference time slice y_0 we define a spatial-summed source, the so-called *meson wall,* with pseudoscalar quantum numbers and h and l quark fields, namely

$$\mathcal{P}_{y_0} = \left(\frac{a}{L}\right)^3 \sum_{\vec{y}} \bar{h}\left(\vec{y}, y_0\right) \gamma_5 \, l\left(\vec{y}, y_0\right) = \left(\frac{a}{L}\right)^3 \sum_{\vec{y}} P_5\left(\vec{y}, y_0\right)$$

The non-renormalized two point correlators we need to compute are:

$$\begin{aligned} C^{(2)}_{PP}\left(x_0\right) = & \left(\frac{a}{L}\right)^3 \sum_{\vec{x}} \langle 0 | P_5^\dagger\left(x\right) \mathcal{P}_{y_0} | 0 \rangle \\ C^{(2)}_{PA}\left(x_0\right) = & \left(\frac{a}{L}\right)^3 \sum_{\vec{x}} \langle 0 | A_0^\dagger\left(x\right) \mathcal{P}_{y_0} | 0 \rangle \end{aligned} \tag{3.1.1}$$

where the pseudoscalar and axial currents located in the sinks are[1]

$$\begin{aligned} P_5\left(x\right) = & \bar{h}(x)\gamma_5 l(x) \\ A_0\left(x\right) = & \bar{h}(x)\gamma_0\gamma_5 l(x) \end{aligned}$$

The signal-to-noise ratio has been improved by summing over the spatial position at the time slice y_0 randomly chosen for each gauge configuration. The second spatial sum in $\vec{x}$ gives further signal improvement. These spatial sums were implemented and carried out at a reasonably low computational price using the stochastic technique discussed in Appendix A.

In order to write Eq.3.1.1 in terms of the fermionic propagators the fields should be first Wick contracted. By making use of the H-discrete symmetry (see Appendix B) Eq.3.1.1 is finally rewritten in terms of the stochastic propagators ϕ defined in Appendix A as

$$\begin{aligned} C^{(2)}_{PP}\left(x_0\right) = & -\left(\frac{a}{L}\right)^3 \sum_{\vec{x}} \mathrm{Tr}[\phi_h(\vec{x}, x_0; r)\phi_l^\dagger(\vec{x}, x_0; r')] \\ C^{(2)}_{PA}\left(x_0\right) = & -\left(\frac{a}{L}\right)^3 \sum_{\vec{x}} \mathrm{Tr}[\phi_h(\vec{x}, x_0; r)\gamma_0\phi_l^\dagger(\vec{x}, x_0; r')] \end{aligned}$$

where in the correlators defined as above $r = r'$ for the TM and $r = -r'$ for the OS doublets and the $-$ sign comes from the anticonmutation of the fermionic fields.

[1] In the numerical simulation we compute the two-point correlators with all possible combinations of Γ structures in the source and in the sink

$$C^{(2)}_{\Gamma^a\Gamma^b}\left(x_0\right) = \left(\frac{a}{L}\right)^6 \sum_{\vec{x}\vec{y}} \langle 0 | \left[\bar{h}\Gamma^a l\right]^\dagger \left(\vec{x}, x_0\right) \left[\bar{h}\Gamma^b l\right] \left(\vec{y}, y_0\right) | 0 \rangle$$

with

$$\begin{aligned} \Gamma^a \otimes \Gamma^b = & \{\gamma_5 \otimes \gamma_5, \gamma_5 \otimes \gamma_\mu\gamma_5, \gamma_\mu\gamma_5 \otimes \gamma_5, \gamma_\mu \otimes \gamma_\mu, \gamma_5\gamma_\mu \otimes \gamma_5\gamma_\mu, I \otimes I, \sigma_{\mu\nu} \otimes \sigma_{\mu\nu}, \\ & \sigma_{\mu\nu}\gamma_5 \otimes \sigma_{\mu\nu}\gamma_5, I \otimes \gamma_\mu, \gamma_\mu \otimes I, \gamma_5 \otimes I, I \otimes \gamma_5, \gamma_5 \otimes \gamma_0, \gamma_0 \otimes \gamma_5, I \otimes \gamma_0\gamma_5, \gamma_0\gamma_5 \otimes I\} \end{aligned}$$

However, for our purposes only $C^{(2)}_{PP}\left(x_0\right)$ and $C^{(2)}_{PA}\left(x_0\right)$ are necessary.

Two-point correlation functions in the continuum

Let us consider the non-renormalized two-point correlation function without momentum insertion, computed at the source time-slice y_0, in a non-discretized Euclidean infinite volume. Formally, the two point correlator is obtained from the vacuum expectation value of the time-ordered product of the two operators after Wick rotation to Euclidean times

$$\begin{aligned} C^{(2)}_{PP}(x_0) &= \int d^3\vec{x} d^3\vec{y}\, \langle 0|T\left\{P_5^\dagger(\vec{x},x_0)P_5(\vec{y},y_0)\right\}|0\rangle \\ C^{(2)}_{PA}(x_0) &= \int d^3\vec{x} d^3\vec{y}\, \langle 0|T\left\{A_0^\dagger(\vec{x},x_0)P_5(\vec{y},y_0)\right\}|0\rangle \end{aligned} \tag{3.1.2}$$

The time-ordered product can be written as [21]

$$\langle 0|T\left\{P_5^\dagger(\vec{x},x_0)P_5(\vec{y},y_0)\right\}|0\rangle = \frac{1}{Z_T}\begin{cases} \mathrm{Tr}\left[P_5^\dagger e^{-(x_0-y_0)H}P_5 e^{-(T-x_0+y_0)H}\right] & x_0 \geq y_0 \\ \mathrm{Tr}\left[P_5 e^{-(y_0-x_0)H}P_5^\dagger e^{-(T-y_0+x_0)H}\right] & x_0 < y_0 \end{cases} \tag{3.1.3}$$

and respectively

$$\langle 0|T\left\{A_0^\dagger(\vec{x},x_0)P_5(\vec{y},y_0)\right\}|0\rangle = \frac{1}{Z_T}\begin{cases} \mathrm{Tr}\left[A_0^\dagger e^{-(x_0-y_0)H}P_5 e^{-(T-x_0+y_0)H}\right] & x_0 \geq y_0 \\ \mathrm{Tr}\left[P_5 e^{-(y_0-x_0)H}A_0^\dagger e^{-(T-y_0+x_0)H}\right] & x_0 < y_0 \end{cases} \tag{3.1.4}$$

where H is the Hamiltonian operator, T will be eventually taken $T \to \infty$. The normalization factor, i.e partition function, Z_T is given by[2]

$$Z_T = \mathrm{Tr}\left[e^{-TH}\right] \equiv \mathrm{Tr}\left[S^T\right] = \sum_n \langle n|e^{-TH}|n\rangle = \sum_n e^{-TE_n}$$

where $S = e^{-H}$ is the so-called transfer matrix [21].

Inserting in the trace a complete set of states

$$I = \sum_n \frac{|n\rangle\langle n|}{2M_n} \tag{3.1.5}$$

normalized as $\langle n|\, n'\rangle = 2M_n\delta_{n,n'}$ with $H|n\rangle = E_n|n\rangle$, the trace of the operators can be evaluated in a similar way. With a generic notation one has

$$\begin{aligned} \mathrm{Tr}\left[\hat{O}_1 e^{-tH}O_2 e^{-(T-t)H}\right] &= \sum_m \langle m|\hat{O}_1 e^{-tH}O_2 e^{-(T-t)H}|m\rangle \\ &= \sum_{m,n} e^{-tE_n}\frac{\langle m|\hat{O}_1|n\rangle e^{-(T-t)E_m}\langle n|\hat{O}_2|m\rangle}{2M_n} \end{aligned}$$

[2]The trace of an operator $\hat{O}$ is defined as $\mathrm{Tr}\left[\hat{O}\right] = \sum_n \langle n|\hat{O}|n\rangle$ where the sum runs over the vector of an orthonormal basis.

This leads to

$$\frac{1}{Z_T}\mathrm{Tr}\left[\hat{O}_1 e^{-tH} O_2 e^{-(T-t)H}\right] = \sum_{m,n}\frac{1}{2M_n}\frac{\langle m|\hat{O}_1|n\rangle\langle n|\hat{O}_2|m\rangle}{1+e^{-TE_1}+e^{-TE_2}+...}e^{-tE_n}e^{-(T-t)E_m} \tag{3.1.6}$$

where the energy E_0 of the vacuum $|0\rangle$ is normalized to zero.

In the limit $T\to\infty$ the denominator is equal to 1 and in the numerator only those terms with $|m\rangle = |0\rangle$ survives

$$\lim_{T\to\infty}\frac{1}{Z_T}\mathrm{Tr}\left[\hat{O}_1 e^{-tH} O_2 e^{-(T-t)H}\right] = \sum_n \frac{\langle 0|\hat{O}_1|n\rangle\langle n|\hat{O}_2|m\rangle}{2M_n}e^{-tE_n}$$

Again with the specific operators in Eq.3.1.3 and Eq.3.1.4 and integrating the $\vec{x},\vec{y}$ dependence through the delta function, Eq.3.1.2 reads

$$\begin{aligned} C^{(2)}_{PP}(x_0) &= \sum_n \frac{\langle 0|P_5^\dagger|n\rangle\langle n|P_5|0\rangle}{2M_n}e^{-E_n(x_0-y_0)} \\ C^{(2)}_{PA}(x_0) &= \sum_n \frac{\langle 0|A_0^\dagger|n\rangle\langle n|P_5|0\rangle}{2M_n}e^{-E_n(x_0-y_0)} \end{aligned} \tag{3.1.7}$$

with $A_0 \equiv A_0\left(\vec{0},0\right)$ and $P_5 \equiv P_5\left(\vec{0},0\right)$ and we are assuming $x_0 \geq y_0$.

In the limit $y_0 \ll x_0$, only the states with smaller masses will survive the exponential decay. The state with smaller mass is the pseudoscalar one. In this limit the correlator is dominated by the exponential associated with the lightest pseudoscalar state with energy $E_1 \equiv M_{PS}$, i.e the pseudoscalar meson mass

$$\begin{aligned} C^{(2)}_{PP}(x_0) &\xrightarrow[y_0\ll x_0,]{} \frac{\langle 0|P_5^\dagger|M\rangle\langle\overline{M}|P_5|0\rangle}{2M_{PS}}e^{-M_{PS}(x_0-y_0)} \\ C^{(2)}_{PA}(x_0) &\xrightarrow[y_0\ll x_0,]{} \frac{\langle 0|A_0^\dagger|M\rangle\langle\overline{M}|P_5|0\rangle}{2M_{PS}}e^{-M_{PS}(x_0-y_0)} \end{aligned} \tag{3.1.8}$$

Two-point correlation functions on the lattice

On the lattice, instead of working in an infinite volume we work in a finite discretized volume $V = L^3\times T$ and $\vec{x},\vec{y}$ become discretized variables

$$\begin{aligned} C^{(2)}_{PP}(x_0) &= \left(\frac{a}{L}\right)^6\sum_{\vec{x}}\sum_{\vec{y}}\langle 0|T\left\{P_5^\dagger(\vec{x},x_0)P_5(\vec{y},y_0)\right\}|0\rangle \\ C^{(2)}_{PA}(x_0) &= \left(\frac{a}{L}\right)^6\sum_{\vec{x}}\sum_{\vec{y}}\langle 0|T\left\{A_0^\dagger(\vec{x},x_0)P_5(\vec{y},y_0)\right\}|0\rangle \end{aligned}$$

The time-ordered products are defined in Eq.3.1.3 and Eq.3.1.4 where T is now the lattice extension with antiperiodic boundary conditions [74].

In the limit $0 \ll |x_0 - y_0| \ll T$ only the lightest state dominates. In this case, Eq.3.1.6 with a finite value of T leads automatically to

$$\langle 0|T\left\{P_5^\dagger(\vec{x},x_0)P_5(\vec{y},y_0)\right\}|0\rangle \xrightarrow[|0\ll|x_0-y_0|\ll T]{} \begin{cases} c_{PP}e^{-(x_0-y_0)M_{PS}} + c'_{PP}e^{-(T-y_0-x_0)M_{PS}} & x_0 \geq y_0 \\ c'_{PP}e^{-(y_0-x_0)M_{PS}} + c_{PP}e^{-(T-x_0-y_0)M_{PS}} & x_0 < y_0 \end{cases}$$

with

$$c_{PP} = \frac{\langle 0|P_5^\dagger|M\rangle\langle\overline{M}|P_5|0\rangle}{2M_{PS}} \qquad c_{PP'} = \frac{\langle 0|P_5|M\rangle\langle\overline{M}|P_5^\dagger|0\rangle}{2M_{PS}}$$

while

$$\langle 0|T\left\{A_0^\dagger(\vec{x},x_0)P_5(\vec{y},y_0)\right\}|0\rangle \xrightarrow[0\ll|x_0-y_0|\ll T]{} \begin{cases} c_{AP}e^{-(x_0-y_0)M_{PS}} + c_{PA}e^{-(T-y_0-x_0)M_{PS}} & x_0 \geq y_0 \\ c_{PA}e^{-(y_0-x_0)M_{PS}} + c_{AP}e^{-(T-x_0-y_0)M_{PS}} & x_0 < y_0 \end{cases}$$

with

$$c_{AP} = \frac{\langle 0|A_0^\dagger|M\rangle\langle\overline{M}|P_5|0\rangle}{2M_{PS}} \qquad c_{PA} = \frac{\langle 0|P_5|M\rangle\langle\overline{M}|A_0^\dagger|0\rangle}{2M_{PS}}$$

where we identified again the lightest state with the pseudoscalar meson and its energy with M_{PS}.

Using the symmetries of the action, in Appendix B we show that $C^{(2)}_{PP}$ is even under time inversion while $C^{(2)}_{AP}$ is odd. In other words, we have to impose the following conditions

$$\begin{aligned} C^{(2)}_{PP}(T/2 - x_0) &= C^{(2)}_{PP}(T/2 + x_0) \\ C^{(2)}_{PA}(T/2 - x_0) &= -C^{(2)}_{PA}(T/2 + x_0) \end{aligned} \tag{3.1.9}$$

which fixes

$$c_{PP} = c'_{PP} \qquad c_{AP} = -c_{PA}$$

so that assuming $x_0 > y_0$, the correlation functions on the lattice have the behaviour

$$\begin{aligned} C^{(2)}_{PP}(x_0) &\xrightarrow[0\ll x_0-y_0\ll T]{} \frac{\langle 0|P_5^\dagger|M\rangle\langle\overline{M}|P_5|0\rangle}{2M_{PS}} e^{-M_{PS}\frac{T}{2}} \cosh\left[M_{PS}\left(\frac{T}{2} - x_0\right)\right] \\ &= \frac{G_{PP}}{2M_{PS}} e^{-M_{PS}\frac{T}{2}} \cosh\left[M_{PS}\left(\frac{T}{2} - x_0\right)\right] \\ C^{(2)}_{PA}(x_0) &\xrightarrow[0\ll x_0-y_0\ll T]{} \frac{\langle 0|A_0^\dagger|M\rangle\langle\overline{M}|P_5|0\rangle}{2M_{PS}} e^{-M_{PS}\frac{T}{2}} \sinh\left[M_{PS}\left(\frac{T}{2} - x_0\right)\right] \\ &= \frac{G_{AP}}{2M_{PS}} e^{-M_{PS}\frac{T}{2}} \sinh\left[M_{PS}\left(\frac{T}{2} - x_0\right)\right] \end{aligned} \tag{3.1.10}$$

3.1.2 Pseudoscalar mass

The pseudoscalar mass M_{PS} can be computed from the correlation functions $C^{(2)}_{PP}(x_0)$ or $C^{(2)}_{PA}(x_0)$. However, in practice $C^{(2)}_{PP}$ has better signal-to-noise ratio so we prefer to use the latter. A fit in x_0 to Eq.3.1.10 allows to extract the estimates of the pseudoscalar mass M_{PS} and the corresponding non renormalized factors $\langle \overline{M}|P_5|0\rangle$ or $\langle 0|A_0^\dagger|M\rangle$.

Alternatively one can evaluate the so-called effective mass. In the continuum Eq.3.1.8 leads to

$$\log\left[\frac{C_i^{(2)}(x_0)}{C_i^{(2)}(x_0+1)}\right] = M_{PS} \equiv M_{\text{eff}} \quad x_0 \gg 0 \tag{3.1.11}$$

so a plateau should be reached for large x_0. Instead, on the lattice, using Eq.3.1.10

$$\frac{C_i^{(2)}(x_0)}{C_i^{(2)}(x_0+1)} = \frac{e^{-M_{PS}x_0}}{e^{-M_{PS}(x_0+1)}}\left\{\frac{1 \pm e^{-M_{PS}T+2M_{PS}x_0}}{1 \pm e^{-M_{PS}t+2M_{PS}(x_0+1)}}\right\} \tag{3.1.12}$$

where the $\pm$ sign corresponds to the $i = PP$ and $i = PA$ two-point correlators, respectively. Hence

$$M_{PS}\,(x_0) = \log\left\{\frac{C_i^{(2)}(x_0)}{C_i^{(2)}(x_0+1)}\frac{1 \pm e^{-M_{PS}x_0+2M_{PS}(x_0+1)}}{1 \pm e^{-M_{PS}T+2M_{PS}x_0}}\right\} \quad 0 \ll x_0 \ll T \tag{3.1.13}$$

The equation Eq.3.1.13 is a transcendental equation in M_{PS} which can be solved numerically using an iterative method for each x_0. The main advantage of computing M_{PS} from the effective mass formula, i.e Eq.3.1.13, is that once $M_{PS}\,(x_0)$ has been determined only a constant fit, i.e a weighted average, in the interval of x_0 where the plateaux exists is needed to obtain the final estimate while using Eq.3.1.10 directly requires a fit with two parameters.

3.1.3 Decay constant

The pseudoscalar decay constant f_{PS} can be evaluated in two different ways:

- From the renormalized two-point correlation function $\hat{C}^{(2)}_{PA}$ and the well-known definition of f_{PS}.
- From the renormalized two-point correlation function $\hat{C}^{(2)}_{PP}$ and using the Partially Conserved Axial Ward Identity (PCAC WI).

From the definition of f_{PS}:

The definition of the pseudoscalar decay meson f_{PS} in the Euclidean space is given by

$$\langle 0|\hat{A}^\dagger_\mu(x)|M(p)\rangle = p_\mu f_{PS} e^{-px} \tag{3.1.14}$$

where $\hat{A}$ stands for the renormalized axial current. In the center of mass system where $\vec{p}=0$ and $p_\mu=(M_{PS},0)$ it reduces to

$$\langle 0|\hat{A}_0^\dagger(x)|M\rangle = M_{PS} f_{PS} e^{-M_{PS}x_0} \rightarrow f_{PS} = \frac{\langle 0|\hat{A}_0^\dagger|M\rangle}{M_{PS}}$$

with $\hat{A}_0 \equiv \hat{A}_0\left(\vec{0},0\right)$. Using the renormalized expressions of G_{PP} and G_{PA}, read from Eq.3.1.10

$$\begin{aligned}\hat{G}_{PP} &\equiv \langle 0|\hat{P}_5^\dagger|M\rangle\langle\overline{M}|\hat{P}_5|0\rangle \\ \hat{G}_{PA} &\equiv \langle 0|\hat{A}_0^\dagger|M\rangle\langle\overline{M}|\hat{P}_5|0\rangle\end{aligned}$$

where $\hat{P}_5 \equiv \hat{P}_5\left(\vec{0},0\right)$. Therefore, we have

$$f_{PS} = \frac{\hat{G}_{PA}}{\sqrt{\hat{G}_{PP}}M_{PS}} \tag{3.1.15}$$

The non-renormalized values of G_{PP} and G_{PA} are extracted from Eq.3.1.10 in the limit $0 \ll t \ll T$ where the $\cosh -$ and $\sinh -$functions reach a plateaux. However, to perform the explicit calculation one still has to determine the renormalization constants of the axial operator A_0.

From the PCAC WI:

In field theory, the PCAC WI for a non-degenerate quark doublet reads

$$\partial_\mu\langle M|\hat{A}_\mu(x)|0\rangle = (\hat{m}_h+\hat{m}_l)\langle M|\hat{P}_5(x)|0\rangle$$

where m_h and m_l are the (polar) quark masses of the h and l fermionic fields.

Taking ∂_μ in the definition of the pseudoscalar decay constant in Eq.3.1.14 and fixing $x=0$ one arrives to

$$f_{PS} = \frac{(\hat{m}_h+\hat{m}_l)}{M_{PS}^2}\langle 0|\hat{P}_5^\dagger|M\rangle$$

and finally

$$f_{PS} = \frac{(\hat{m}_h+\hat{m}_l)}{M_{PS}^2}\sqrt{\hat{G}_{PP}} \tag{3.1.16}$$

3.2 Bag parameters

Bag parameters measure the deviation from it physical value of the matrix element of the five four-fermion operators Q_i defined in Eq.1.2.17 between a meson and an antimeson state computed through the *Vacuum Insertion Approximation* (VIA), also called *Vacuum Saturation Approximation*, i.e

$$\langle \overline{M}|N\{\hat{Q}_i\}|M\rangle = \langle \overline{M}|N\{\hat{Q}_i\}|M\rangle_{VIA}\hat{B}_i \text{ with } i = 1, ..., 5$$

where $N\{Q_i\}$ represents the *normal ordering* of the operator Q_i, which places each creation operator on the left of each annihilation operator and the hats denote renormalized quantities.

The matrix elements $\langle \overline{M}|N\{\hat{Q}_i\}|M\rangle$ cannot be computed analytically due to the hadronization mechanism, i.e they are non perturbative quantities. The problem arises from the fact that all operators Q_i are written in terms of quark fields, while the physical asymptotic states are hadrons. Non-numerical computations are only possible through the VIA or some equivalent approximation. In this framework, for historical reasons, it was natural to introduce bag parameters as the deviation of the matrix elements computed in the VIA approximation from the physical value which must take into account hadronization effects.

In this section I will first describe the three-point correlation functions from where each one of the five bag parameters can be obtained. Second, I will focus on the computation of the matrix element in the VIA approximation. To this end, I will transform the operators Q_i in the supersymmetric basis to the lattice basis, more suitable for a lattice implementation. Then I will introduce the normal ordering procedure which will allow us to compute the bag parameters in the VIA approximation. Finally, I will express the $\hat{B}_i$ in terms of renormalized two- and three-point corelation functions.

As it will be described in section 3.4, we use a mixed fermion action on the valence adopting different regularizations for sea and valence quarks, firstly presented in [23], as a way of setting up a a computational framework that is both automatically $\mathcal{O}(a)$ improved and free of wrong chirality mixings. Finally in subsection 3.4.3, I will present the formulae for the renormalized bag parameters with absence of wrong chirality mixing.

3.2.1 Three-point correlation functions

The non-renormalized three-point correlation function for the operator Q_i between a creation and a annihilation pseudoscalar operators is defined on the lattice as

$$C^{(3)}_{Q_i}(x_0) = \left(\frac{a}{L}\right)^3 \sum_{\vec{x}} \langle 0|\mathcal{P}_{y_0} Q_i(\vec{x}, x_0)\mathcal{P}_{y_0+T_{\text{sep}}}|0\rangle \tag{3.2.1}$$

where y_0 is fixed randomly for each gauge configuration in order to avoid autocorrelation and improve the signal-to-noise ratio. In Eq.3.2.1 two pseudoscalar meson walls separated by T_{sep} time-slices, $\mathcal{P}_{y_0}$ and $\mathcal{P}_{y_0+T_{\text{sep}}}$, have been defined. These currents create a meson state from the vacuum at the time-slice y_0 and $y_0 + T_{\text{sep}}$ respectively. The local four-fermion operator is inserted between them at position $(\vec{x}, x_0)$. In general, they are given in term of quark fields as

$$Q_i(\vec{x}, x_0) \sim \left[\overline{h}(\vec{x}, x_0)\Gamma_i l(\vec{x}, x_0)\right] . \left[\overline{h}(\vec{x}, x_0)\Gamma'_i l(\vec{x}, x_0)\right]$$

The physical situation is represented in figure Figure 3.2.1 where the pseudoscalar current operator in the right side of the lattice, at time y_0, creates a pseudoscalar meson

from the vacuum. The four-fermion operator acts in $(\vec{x}, x_0)$ while the current operator in the left side annihilates the pseudoscalar antimeson at time $y_0 + T_{\rm sep}$. Note that this digram is just the one corresponding Figure 1.2.1 obtained after integrating the $W^{\pm}$ mesons.

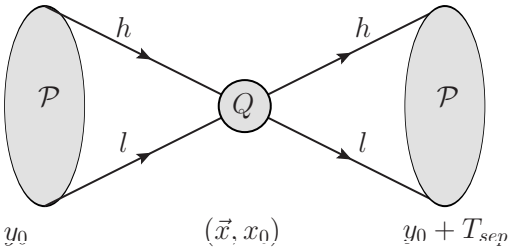

Figure 3.2.1: Feynman diagram for the three-point correlation functions contributing to the $M - \overline{M}$ oscillations

For future use, it is convenient to generalize the formulae to four species of OS quark flavours (ψ_f, $f = 1, ..., 4$), rather than only the heavy and light quarks h,l. Two of them (ψ_1 and ψ_3) will represent the valence heavy quark while the other two (ψ_2 and ψ_4) will be identified with the light quark. This choice will allow us to simplify the renormalization pattern of bag parameters. In section 3.4 I will show that, in the physical basis, parity-even four-fermion operators mix under renormalization while the parity-odd ones mix only through a block diagonal matrix. In order to take profit of the previously mentioned advantage of the parity-odd operators to renormalize the parity-even ones, from which B-parameters are obtained, we will look for a transformation which maps the parity-even operators in the parity-odd ones. As it is detailed in subsection 3.4.3 this transformation is achieved if the Wilson parameter satisfy the relation $r_1 = r_2 = r_3 = -r_4$ or an equivalent one. In our particular setup, we achieve a continuum like renormalization pattern by having different mesons in each side of the lattice. The M-meson consists of a quark-antiquark pair with, say, the same Wilson parameter, while the $\overline{M}$-meson has necessarily a quark-antiquark pair with opposite Wilson parameter.

The three-point correlator in the theory with four quarks reads

$$C^{(3)}_{Q_i}(x_0) = \left(\frac{a}{L}\right)^3 \sum_{\vec{x}} \langle 0|\mathcal{P}^{21}_{y_0} Q_i(\vec{x}, x_0) \mathcal{P}^{43}_{y_0+T_{\rm sep}}|0\rangle \tag{3.2.2}$$

with the currents defined in term of the quark fields

$$\mathcal{P}^{ij}_{y_0} = \left(\frac{a}{L}\right)^3 \sum_{\vec{y}} \bar{\psi}_i\left(\vec{y}, y_0\right) \gamma_5 \psi_j\left(\vec{y}, y_0\right) = \left(\frac{a}{L}\right)^3 \sum_{\vec{y}} P^{ij}_5\left(\vec{y}, y_0\right)$$

and

$$Q_i(\vec{x}, t_x) \sim \left[\overline{\psi}_1(\vec{x}, x_0)\Gamma_i\psi_2(\vec{x}, x_0)\right] . \left[\overline{\psi}_3(\vec{x}, x_0)\Gamma'_i\psi_4(\vec{x}, x_0)\right]$$

Performing the Wick contractions we find that the three-point correlation function is given in terms of the corresponding propagators as the sum of two traces that we usually call the *eight* or connected piece and the *half-eight* or disconnected piece and which are schematically represented as Feynman diagrams in Figure 3.2.2. In terms of the ϕ-propagator defined in Eq.A.2.4, the stochastic three-point correlation function reads

$$C^{(3)}_{Q_i}(x_0) = \left(\frac{a}{L}\right)^6 \sum_{\vec{y},\vec{z}} \Big\{ \mathrm{Tr}\left[\phi_1(\vec{y},y_0)\Gamma_i\tilde{\phi}_2(\vec{z},y_0+T_{\mathrm{sep}})\gamma_5\phi_3(\vec{z},y_0+T_{\mathrm{sep}})\Gamma_i\tilde{\phi}_4(\vec{y},y_0)\gamma_5\right] \\ -\mathrm{Tr}\left[\phi_1(\vec{y},y_0)\Gamma_i\tilde{\phi}_2(\vec{y},y_0)\gamma_5\right] \times \mathrm{Tr}\left[\tilde{\phi}_3(\vec{z},y_0+T_{\mathrm{sep}})\Gamma_i\phi_4(\vec{z},y_0+T_{\mathrm{sep}})\gamma_5\right] \Big\} \tag{3.2.3}$$

where $\tilde{\phi}$ comes from the H-discrete symmetry described in Appendix B

$$\tilde{\phi}_r = \gamma_5 \phi^\dagger_{-r} \gamma_5$$

The implementation of meson walls to describe the creation and anhilitation meson states is translated in Eq.3.2.3 in the two spatial sums while the temporal position of both sources is fixed at y_0 and $y_0 + T_{\mathrm{sep}}$.

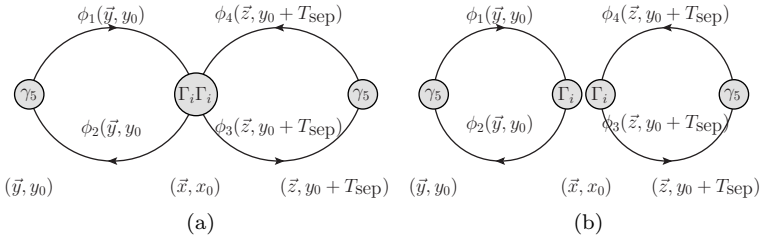

Figure 3.2.2: Connected (a) and disconnected (b) contributions to the three-point correlator, also called *eight* and *half eight*, for meson-antimeson mixing

Three-point correlation function formulae on the continuum

The three-point correlation function with zero momentum is defined formally in terms of the time-ordered product of the operators

$$C^{(3)}_{Q_i}(x_0) = \int d^3\vec{x}d^3\vec{y}d^3\vec{z}\,\langle 0|T\left\{P_5^{21}(\vec{y},y_0)Q_i(\vec{x},x_0)P_5^{43}(\vec{z},y_0+T_{\mathrm{sep}})\right\}|0\rangle \tag{3.2.4}$$

In order to relate Eq.3.2.4 to the matrix elements we are interested in, we express this correlation function in terms of the trace involving the transfer matrix. In the case $y_0 \leq x_0 \leq y_0 + T_{\mathrm{sep}}$, the time-ordered product is

$$\begin{aligned}&\langle 0|T\left\{P_5^{43}(\vec{y},y_0)Q_i(\vec{x},x_0)P_5^{21}(\vec{z},y_0+T_{\rm sep})\right\}|0\rangle\\&=\frac{1}{Z_T}\sum_n\langle n|\left[P_5^{43}e^{-(y_0+T_{sep}-x_0)H}Q_ie^{-(x_0-y_0)H}P_5^{21}e^{-(T-T_{sep})H}\right]|n\rangle\end{aligned}\tag{3.2.5}$$

where $Q_i(\vec{0},0)\equiv Q_i$.

In the continuum, $T\to\infty$, $Z_T=1$ and only the state $|n\rangle=0$ contributes. As we did in the case of the two-point correlators, we insert twice a complete set of states Eq.3.1.5. If the time differences are chosen sufficiently large, $y_0\ll x_0\ll y_0+T_{\rm sep}$, we can restrict to the lowest contributing states and the three-point correlator reads

$$\begin{aligned}C^{(3)}_{Q_i}(x_0)\to\quad&\langle 0|P_5^{43}|M^{34}\rangle\langle M^{34}|Q_i|M^{21}\rangle\langle M^{21}|P_5^{21}|0\rangle\\&\times\frac{1}{4M_{PS}^{34}M_{PS}^{12}}\exp\left[-M_{PS}^{12}(x_0-y_0)\right]\exp\left[-M_{PS}^{34}(y_0+T_{\rm sep}-x_0)\right]\end{aligned}\tag{3.2.6}$$

where $|M^{ij}\rangle$ denotes a zero three-momentum pseudoscalar state with quark content q_i and $\bar{q}_j$ and mass M_{PS}^{ij}.

We need to consider the following two-point correlation

$$\begin{aligned}C^{(2)}_{PP}(x_0)&=\left(\frac{a}{L}\right)^3\sum_{\vec{x}}\langle 0|P_5^{12}(x)\,\mathcal{P}_{y_0}^{21}|0\rangle\qquad C'^{(2)}_{PP}(x_0)=\left(\frac{a}{L}\right)^3\sum_{\vec{x}}\langle 0|\mathcal{P}_{y_0+T_{\rm sep}}^{43}P_5^{34}(x)\,|0\rangle\\C^{(2)}_{PA}(x_0)&=\left(\frac{a}{L}\right)^3\sum_{\vec{x}}\langle 0|A_0^{12}(x)\,\mathcal{P}_{y_0}^{21}|0\rangle\qquad C'^{(2)}_{PA}(x_0)=\left(\frac{a}{L}\right)^3\sum_{\vec{x}}\langle 0|\mathcal{P}_{y_0+T_{\rm sep}}^{43}A_0^{34}(x)\,|0\rangle\end{aligned}$$

The explicit time evolution of each two-point correlators is

$$C^{(2)}_{PP}(x_0)\to\frac{\langle 0|P_5^{12}|M^{21}\rangle\langle M^{21}|P_5^{21}|0\rangle}{2M_{PS}^{12}}e^{-M_{PS}^{12}(x_0-y_0)}$$

$$C'^{(2)}_{PP}(x_0)\to\frac{\langle 0|P_5^{43}|M^{34}\rangle\langle M^{34}|P_5^{34}|0\rangle}{2M_{PS}^{34}}e^{-M_{PS}^{34}(y_0+T_{\rm sep}-x_0)}$$

$$C^{(2)}_{PA}(x_0)\to\frac{\langle 0|A_0^{12}|M^{21}\rangle\langle M^{21}|P_5^{21}|0\rangle}{2M_{PS}^{12}}e^{-M_{PS}^{12}(x_0-y_0)}$$

$$C'^{(2)}_{PA}(x_0)\to\frac{\langle 0|P_5^{43}|M^{34}\rangle\langle M^{34}|A_0^{34}|0\rangle}{2M_{PS}^{34}}e^{-M_{PS}^{34}(y_0+T_{\rm sep}-x_0)}$$

In such a way that the exponential evolution in Eq.3.2.6 is canceled by considering the ratios

$$\begin{aligned} \frac{C^{(3)}_{Q_i}(x_0)}{C^{(2)}_{PP}(x_0)C'^{(2)}_{PP}(x_0)} &\xrightarrow[y_0\ll x_0\ll y_0+T_{\rm sep}]{} \frac{\langle M^{34}|Q_i|M^{21}\rangle}{\langle M^{34}|P_5^{34}|0\rangle\langle 0|P_5^{12}|M^{21}\rangle} \\ \frac{C^{(3)}_{Q_i}(x_0)}{C^{(2)}_{PA}(x_0)C'^{(2)}_{PA}(x_0)} &\xrightarrow[y_0\ll x_0\ll y_0+T_{\rm sep}]{} \frac{\langle M^{34}|Q_i|M^{21}\rangle}{\langle M^{34}|A_0^{34}|0\rangle\langle 0|A_0^{12}|M^{21}\rangle} \end{aligned} \tag{3.2.7}$$

from where bag parameters can be directly obtained as we will see in the following subsections.

Three-point correlation function formulae with periodic boundary conditions

The three-point correlation function on the lattice is

$$C^{(3)}_{Q_i}(x_0) = \left(\frac{a}{L}\right)^9 \sum_{\vec{x}\vec{y}\vec{z}} \langle 0|T\left\{P_5^{21}(\vec{y},y_0)Q_i(\vec{x},x_0)P_5^{43}(\vec{z},y_0+T_{\rm sep})\right\}|0\rangle$$

where operators Q_i and P_5 are now restricted in a time range at most of period T. It is easy to convince oneself that on the lattice the same relation Eq.3.2.7 holds if $y_0 \ll x_0 \ll y_0 + T_{\rm sep}$ with $T_{\rm sep} \ll T$. In practice, we take $T_{\rm sep} \leq T/2$ and only one half of the period, at maximum, can be used to isolate the ground state.

3.2.2 From Supersymmetric to Lattice basis

The complete set of operators Q_i appearing in Eq.3.2.4 is given by Eq.1.2.17

$$\begin{aligned} Q_1 &= \left[\bar{h}^a\gamma^\mu(1-\gamma_5)l^a\right]\left[\bar{h}^b\gamma_\mu(1-\gamma_5)l^b\right] \\ Q_2 &= \left[\bar{h}^a(1-\gamma_5)l^a\right]\left[\bar{h}^b(1-\gamma_5)l^b\right] \\ Q_3 &= \left[\bar{h}^a(1-\gamma_5)l^b\right]\left[\bar{h}^a(1-\gamma_5)l^b\right] \\ Q_4 &= \left[\bar{h}^a(1-\gamma_5)l^a\right]\left[\bar{h}^b(1+\gamma_5)l^b\right] \\ Q_5 &= \left[\bar{h}^a(1-\gamma_5)l^b\right]\left[\bar{h}^a(1+\gamma_5)l^b\right] \end{aligned} \tag{3.2.8}$$

expressed in the *supersymmetric basis*, where each operator comes directly from a supersymmetric diagram. For reader convenience, we work again in terms of the heavy and light quark field (h and l).

An alternative basis more suitable for a lattice implementation is the *lattice basis* constructed from parity-even operators: $O^{ii} = \left[\bar{h}\Gamma^i l\right]\left[\bar{h}\Gamma^i l\right]$ with color and spin indices contracted inside each bracket.

A complete set of parity-even operators is achieved through

$$
\begin{aligned}
O^{SS} &= \left[\bar{h}l\right]\left[\bar{h}l\right] \\
O^{VV} &= \left[\bar{h}\gamma_\mu l\right]\left[\bar{h}\gamma_\mu l\right] \\
O^{TT} &= \left[\bar{h}\sigma_{\mu\nu} l\right]\left[\bar{h}\sigma_{\nu\mu} l\right] \ \text{with}\, \mu > \nu \\
O^{AA} &= \left[\bar{h}\gamma_\mu\gamma_5 l\right]\left[\bar{h}\gamma_\mu\gamma_5 l\right] \\
O^{PP} &= \left[\bar{h}\gamma_5 l\right]\left[\bar{h}\gamma_5 l\right]
\end{aligned}
$$

The lattice basis is constructed with the following combinations of the above operators

$$
\mathbf{O} = \begin{pmatrix} O^{VV} + O^{AA} \\ O^{VV} - O^{AA} \\ O^{SS} - O^{PP} \\ O^{SS} + O^{PP} \\ O^{TT} \end{pmatrix}
$$

In order to find the link between the supersymmetric and the lattice basis one first has to rewrite the operators in the supersymmetric basis as the sum of a parity-even and a parity-odd contribution

$$
\begin{aligned}
Q_1 &= \overbrace{\left[\bar{h}\gamma_\mu l\right]\left[\bar{h}\gamma_\mu l\right] + \left[\bar{h}\gamma_\mu\gamma_5 l\right]\left[\bar{h}\gamma_\mu\gamma_5 l\right]}^{\text{parity-even contributions}} &+ \quad & \text{parity-odd contribution} \\
Q_2 &= \left[\bar{h}l\right]\left[\bar{h}l\right] + \left[\bar{h}\gamma_5 l\right]\left[\bar{h}\gamma_5 l\right] &+ \quad & \text{"} \\
Q_3 &= \left[\bar{h}^a l^b\right]\left[\bar{h}^b l^a\right] + \left[\bar{h}^a\gamma_5 l^b\right]\left[\bar{h}^b\gamma_5 l^a\right] &+ \quad & \text{"} \\
Q_4 &= \left[\bar{h}l\right]\left[\bar{h}l\right] - \left[\bar{h}\gamma_5 l\right]\left[\bar{h}\gamma_5 l\right] &+ \quad & \text{"} \\
Q_5 &= \left[\bar{h}^a l^b\right]\left[\bar{h}^b l^a\right] - \left[\bar{h}^a\gamma_5 l^b\right]\left[\bar{h}^b\gamma_5 l^a\right] &+ \quad & \text{"}
\end{aligned}
$$

where spin indices are implicitly contracted within brackets, a and b color indices and when they are not indicated it means that they are also contracted within each bracket.

Parity-odd contributions are not relevant in our case since parity is a conserved symmetry in QCD. As parity is a symmetry of QCD, all the parity-odd contributions to Q_i gives no contribution when computing the path integral of the matrix elements. Thus,

we can redefine Q_i only with its parity-even contributions

$$\begin{aligned} Q_1 &= \left[\bar{h}\gamma_\mu l\right]\left[\bar{h}\gamma_\mu l\right] + \left[\bar{h}\gamma_\mu\gamma_5 l\right]\left[\bar{h}\gamma_\mu\gamma_5 l\right] \\ Q_2 &= \left[\bar{h}l\right]\left[\bar{h}l\right] + \left[\bar{h}\gamma_5 l\right]\left[\bar{h}\gamma_5 l\right] \\ Q_3 &= \left[\bar{h}^a l^b\right]\left[\bar{h}^b l^a\right] + \left[\bar{h}^a\gamma_5 l^b\right]\left[\bar{h}^b\gamma_5 l^a\right] \\ Q_4 &= \left[\bar{h}l\right]\left[\bar{h}l\right] - \left[\bar{h}\gamma_5 l\right]\left[\bar{h}\gamma_5 l\right] \\ Q_5 &= \left[\bar{h}^a l^b\right]\left[\bar{h}^b l^a\right] - \left[\bar{h}^a\gamma_5 l^b\right]\left[\bar{h}^b\gamma_5 l^a\right] \end{aligned} \tag{3.2.9}$$

It is straightforward now that

$$\begin{aligned} Q_1 &= O^{VV} + O^{AA} \\ Q_2 &= O^{SS} + O^{PP} \\ Q_4 &= O^{SS} - O^{PP} \end{aligned}$$

While for Q_3 and Q_5 the situation is less straightforward due to the color indices crossing. In these cases, one has to use the Fierz theorem to rewrite $Q_{3,5}$ as not color crossed combinations of operators. Let us rewrite the generic color-crossed four-fermion operator as

$$\left[\bar{h}^a\Gamma^i l^b\right]\left[\bar{h}^a\Gamma^i l^b\right] = -\bar{h}^a_\alpha l^a_\delta \bar{h}^b_\gamma l^b_\beta \left[\Gamma^i\right]_{\alpha\beta}\left[\Gamma^i\right]_{\gamma\delta} \tag{3.2.10}$$

where greek indices are spin indices and the minus sign arises from the anticonmutation of fermionic fields. According to the Fierz theorem Dirac matrices Γ^i can be rewritten as

$$\left[\Gamma^i\right]_{\alpha\beta}\left[\Gamma^i\right]_{\gamma\delta} = \sum_k F_{ik}\left[\Gamma^k\right]_{\alpha\delta}\left[\Gamma^k\right]_{\gamma\beta} \quad k = S, V, T, A, P \tag{3.2.11}$$

After some Dirac algebra[3], each coefficient in the Fierz matrix F_{ik} in the basis $\{S, V, T, A, P\}$ and in the Euclidean space can be evaluated explicitly, finding that

$$F = \frac{1}{4}\begin{pmatrix} 1 & 1 & -1 & -1 & 1 \\ 4 & -2 & 0 & -2 & -4 \\ -6 & 0 & -2 & 0 & -6 \\ -4 & -2 & 0 & -2 & 4 \\ 1 & -1 & -1 & 1 & 1 \end{pmatrix} \tag{3.2.12}$$

Thus Eq.3.2.10 takes the form

[3] Multiplying Eq.3.2.11 by $\left[\Gamma^j\right]_{\delta\alpha}\left[\Gamma^j\right]_{\beta\gamma}$ and using the orthogonality relation between each pair of Dirac matrices $\frac{1}{4}\mathrm{Tr}\left[\Gamma^i\Gamma^j\right] = \delta^{ij}$ we immediately infer $F_{ik} = 16\mathrm{Tr}\left[\Gamma^i\Gamma^k\Gamma^i\Gamma^k\right]$.

$$\left[\bar{h}^a\Gamma^i l^b\right]\left[\bar{h}^a\Gamma^i l^b\right] = -\sum_k F_{ik}\left[\bar{h}\Gamma^k l\right]\left[\bar{h}\Gamma^k l\right]$$

In particular for the combinations appearing in Q_3 and Q_5

$$\begin{aligned}\left[\bar{h}^a l^b\right]\left[\bar{h}^b l^a\right] = & -\big[\big(\bar{h}l\big)\big(\bar{h}l\big) + \big(\bar{h}\gamma_\mu l\big)\big(\bar{h}\gamma_\mu l\big) - \big(\bar{h}\sigma_{\mu\nu} l\big)\big(\bar{h}\sigma_{\mu\nu} l\big) \\ & + \big(\bar{h}\gamma_5\gamma_\mu l\big)\big(\bar{h}\gamma_5\gamma_\mu l\big) + \big(\bar{h}\gamma_5 l\big)\big(\bar{h}\gamma_5 l\big)\big]\big] \\ \left[\bar{h}^a\gamma_5 l^b\right]\left[\bar{h}^b\gamma_5 l^a\right] = & -\big[\big(\bar{h}l\big)\big(\bar{h}l\big) - \big(\bar{h}\gamma_\mu l\big)\big(\bar{h}\gamma_\mu l\big) - \big(\bar{h}\sigma_{\mu\nu} l\big)\big(\bar{h}\sigma_{\mu\nu} l\big) \\ & - \big(\bar{h}\gamma_5\gamma_\mu l\big)\big(\bar{h}\gamma_5\gamma_\mu l\big) + \big(\bar{h}\gamma_5 l\big)\big(\bar{h}\gamma_5 l\big)\big]\end{aligned}$$

Hence we have Q_3 and Q_5 in terms of operators in the lattice basis

$$Q_3 = -\tfrac{1}{2}\big[\big(\bar{h}l\big)\big(\bar{h}l\big) - \big(\bar{h}\sigma_{\mu\nu} l\big)\big(\bar{h}\sigma_{\mu\nu} l\big) + \big(\bar{h}\gamma_5 l\big)\big(\bar{h}\gamma_5 l\big)\big] = -\frac{1}{2}\left(O^{SS} - O^{TT} + O^{PP}\right)$$

$$Q_5 = -\tfrac{1}{2}\big[\big(\bar{h}\gamma_\mu l\big)\big(\bar{h}\gamma_\mu l\big) - \big(\bar{h}\gamma_5\gamma_\mu l\big)\big(\bar{h}\gamma_5\gamma_\mu l\big)\big] = -\frac{1}{2}\left(O^{VV} - O^{AA}\right)$$

To sum up

$$\begin{aligned} Q_1 &= O^{VV} + O^{AA} \\ Q_2 &= O^{SS} + O^{PP} \\ Q_3 &= -\frac{1}{2}\left(O^{SS} - O^{TT} + O^{PP}\right) \\ Q_4 &= O^{SS} - O^{PP} \\ Q_5 &= -\frac{1}{2}\left(O^{VV} - O^{AA}\right) \end{aligned} \tag{3.2.13}$$

Finally, we can construct the change of basis matrix R from the supersymmetric to the lattice basis

$$\begin{pmatrix} Q_1 \\ Q_2 \\ Q_3 \\ Q_4 \\ Q_5 \end{pmatrix} = \underbrace{\begin{pmatrix} 1 & 0 & 0 & 0 & 0 \\ 0 & 0 & 0 & 1 & 0 \\ 0 & 0 & 0 & -\frac{1}{2} & \frac{1}{2} \\ 0 & 0 & 1 & 0 & 0 \\ 0 & -\frac{1}{2} & 0 & 0 & 0 \end{pmatrix}}_{\mathbf{R^{-1}}} \begin{pmatrix} O^{VV} + O^{AA} \\ O^{VV} - O^{AA} \\ O^{SS} - O^{PP} \\ O^{SS} + O^{PP} \\ O^{TT} \end{pmatrix} \tag{3.2.14}$$

whose inverse is

$$\begin{pmatrix} O^{VV} + O^{AA} \\ O^{VV} - O^{AA} \\ O^{SS} - O^{PP} \\ O^{SS} + O^{PP} \\ O^{TT} \end{pmatrix} = \underbrace{\begin{pmatrix} 1 & 0 & 0 & 0 & 0 \\ 0 & 0 & 0 & 0 & -2 \\ 0 & 0 & 0 & 1 & 0 \\ 0 & 1 & 0 & 0 & 0 \\ 0 & 1 & 2 & 0 & 0 \end{pmatrix}}_{\mathbf{R}} \begin{pmatrix} Q_1 \\ Q_2 \\ Q_3 \\ Q_4 \\ Q_5 \end{pmatrix} \tag{3.2.15}$$

3.2.3 Normal ordering

Thanks to Eq.3.2.14 the computation of the matrix element $\langle\overline{M}|Q_i|M\rangle$ is reduced to the computation of matrix elements such as $\langle\overline{M}|O^{ii}|M\rangle = \langle\overline{M}|\left[\bar{h}\Gamma^i l\right]\left[\bar{h}\Gamma^i l\right]|M\rangle$. Each operator O^{ii} contains a combination of terms with quark creation and quark annihilation operators. Nevertheless, when an annihilation operator of flavour q acts on a state which does not contain q, the result is zero. Therefore, we need to reorder the four-fermion operator O^{ii} in such a way that each creation operator is placed on the left of each annihilation operator. This is the so-called *normal ordering,* indicated as $N\{O^{ii}\}$.

In order to normal ordering the operator O^{ii} we have first to split each quark field q in its creation q^+ and annihilation part q^-

$$O^{ii} = \left(\bar{h}^+ + \bar{h}^-\right)\Gamma^i\left(l^+ + l^-\right)\left(\bar{h}^+ + \bar{h}^-\right)\Gamma^i\left(l^+ + l^-\right)$$

Since O^{ii} is sandwiched between a meson and antimeson state only the operators containing $\bar{h}^+$, $\bar{h}^-$, l^+ and l^- will give a non zero result

$$\langle\overline{M}|N\{O^{ii}\}|M\rangle = 2\langle\overline{M}|\left[\bar{h}^+\Gamma^i l^+\right]\left[\bar{h}^-\Gamma^i l^-\right] + N\left\{\left[\bar{h}^-\Gamma^i l^+\right]\left[\bar{h}^+\Gamma^i l^-\right]\right\}|M\rangle \tag{3.2.16}$$

The second term can be written explicitly as

$$\left[\bar{h}^-\Gamma^i l^+\right]\left[\bar{h}^+\Gamma^i l^-\right] = -\left(\overline{h}^-\right)^a_\alpha\left(l^-\right)^c_\delta\left(\overline{h}^+\right)^b_\gamma\left(l^+\right)^d_\beta\left[\Gamma^i\right]_{\alpha\beta}\left[\Gamma^i\right]_{\gamma\delta}\delta_{ad}\delta_{cb}$$

where greek and latin letters stands for spin and color indices. In order to have a normal ordered term with both Dirac and color indices contracted in each bracket we use again the Fierz theorem Eq.3.2.11 together with the relation between the Gell-Mann matrices

$$\delta_{ad}\delta_{cb} = \frac{1}{3}\delta_{ac}\delta_{bd} + \frac{1}{2}\sum_{n=1}^{8}\left(\lambda_n\right)_{ac}\left(\lambda_n\right)_{bd} \tag{3.2.17}$$

We obtain

$$\left[\bar{h}^-\Gamma^i l^+\right]\left[\bar{h}^+\Gamma^i l^-\right] \simeq -\frac{1}{3}\sum_{j=1}^{5}F_{ij}\left[\bar{h}^+\Gamma^j l^+\right]\left[\bar{h}^-\Gamma^j l^-\right]$$

where we have neglected the color structure contribution given by the second term in Eq.3.2.17 since it forbids the VIA approximation.

At the end of the story, Eq.3.2.16 reads

$$\begin{aligned}\langle\overline{M}|N\{O^{ii}\}|M\rangle &= 2\langle\overline{M}|\left[\bar{h}^+\Gamma^i l^+\right]\left[\bar{h}^-\Gamma^i l^-\right] + \left(-\frac{1}{3}\right)\sum_{j=1}^{5}F_{ij}\left[\bar{h}^+\Gamma^j l^+\right]\left[\bar{h}^-\Gamma^j l^-\right]|M\rangle \\ &= \frac{2}{3}\sum_{j=1}^{5}\left(3 - F_{ij}\right)\langle\overline{M}|\left[\bar{h}^+\Gamma^i l^+\right]\left[\bar{h}^-\Gamma^i l^-\right]|M\rangle\end{aligned}$$

With this prescription and using the numerically explicit values of F_{ij} given in Eq.3.2.12 it is straightforward to express each $\langle\overline{M}|N\{O^{ii}\}|M\rangle$ in terms of normal ordered terms of the form $\left[\bar{h}^{+}\Gamma^{i}l^{+}\right]\left[\bar{h}^{-}\Gamma^{i}l^{-}\right]$. Performing the change of basis from the lattice to the supersymmetric one as indicated in Eq.3.2.13 one arrives to

$$\begin{aligned}
\langle\overline{M}|N\{Q_1\}|M\rangle &= \frac{8}{3}\langle\overline{M}|N\{V_\mu V_\mu\}|M\rangle + \frac{8}{3}\langle\overline{M}|N\{A_\mu A_\mu\}|M\rangle \\
\langle\overline{M}|N\{Q_2\}|M\rangle &= \frac{5}{3}\langle\overline{M}|N\{SS\}|M\rangle + \frac{1}{3}\langle\overline{M}|N\{T_{\mu\nu}T_{\mu\mu}\}|M\rangle + \frac{5}{3}\langle\overline{M}|N\{P_5P_5\}|M\rangle \\
\langle\overline{M}|N\{Q_3\}|M\rangle &= -\frac{1}{3}\langle\overline{M}|N\{SS\}|M\rangle - \langle\overline{M}|N\{T_{\mu\nu}T_{\mu\mu}\}|M\rangle - \frac{1}{3}\langle\overline{M}|N\{P_5P_5\}|M\rangle \\
\langle\overline{M}|N\{Q_4\}|M\rangle &= 2\langle\overline{M}|N\{SS\}|M\rangle - \frac{1}{3}\langle\overline{M}|N\{V_\mu V_\mu\}|M\rangle + \frac{1}{3}\langle\overline{M}|N\{A_\mu A_\mu\}|M\rangle \\
&\quad -2\langle\overline{M}|N\{P_5P_5\}|M\rangle \\
\langle\overline{M}|N\{Q_5\}|M\rangle &= \frac{2}{3}\langle\overline{M}|N\{SS\}|M\rangle - \langle\overline{M}|N\{V_\mu V_\mu\}|M\rangle + \langle\overline{M}|N\{A_\mu A_\mu\}|M\rangle \\
&\quad -\frac{2}{3}\langle\overline{M}|N\{P_5P_5\}|M\rangle
\end{aligned} \tag{3.2.18}$$

where we defined $N\{\Gamma^i\Gamma^i\} = \left[\bar{h}^{+}\Gamma^{i}l^{+}\right]\left[\bar{h}^{-}\Gamma^{i}l^{-}\right]$.

3.2.4 VIA approximation

Armed with this normal-ordered matrix elements we can directly apply the VIA approximation. It consists in separating the four-fermion matrix elements

$$\langle\overline{M}|\left[\bar{h}^{+}\Gamma^{i}l^{+}\right]\left[\bar{h}^{-}\Gamma^{i}l^{-}\right]|M\rangle$$

into the product of two two-fermion matrix elements by inserting the vacuum state in the middle of the four-fermion operator

$$\begin{aligned}
\langle\overline{M}|\left[\bar{h}^{+}\Gamma^{i}l^{+}\right]\left[\bar{h}^{-}\Gamma^{i}l^{-}\right]|M\rangle &\backsimeq \langle\overline{M}|\left[\bar{h}^{+}\Gamma^{i}l^{+}\right]|0\rangle\langle 0|\left[\bar{h}^{-}\Gamma^{i}l^{-}\right]|M\rangle \\
&\equiv \langle\overline{M}|\left[\bar{h}^{+}\Gamma^{i}l^{+}\right]\left[\bar{h}^{-}\Gamma^{i}l^{-}\right]|M\rangle_{VIA}
\end{aligned} \tag{3.2.19}$$

The new two-fermion matrix elements
$\langle\overline{M}|O^i|0\rangle \equiv \langle\overline{M}|\bar{h}^{+}\Gamma^{i}l^{+}|0\rangle$ and $\langle 0|O^i|M\rangle \equiv \langle 0|\bar{h}^{-}\Gamma^{i}l^{-}|M\rangle$ can be computed exactly

Scalar: $O^i = \bar{h}l$

The operator $O^i = \bar{h}l$ transforms under parity, P, as a scalar: $\bar{h}l \xrightarrow{P} \bar{h}l$. Also the vacuum state is a scalar: $\langle 0| \xrightarrow{P} \langle 0|$ and $|0\rangle \xrightarrow{P} |0\rangle$. Instead, the meson and antimeson are pseudoscalar states: $\langle M| \xrightarrow{P} -\langle M|$ and $|\overline{M}\rangle \xrightarrow{P} -|\overline{M}\rangle$. Thus

$$\langle\overline{M}|\bar{h}l|0\rangle \xrightarrow{P} -\langle\overline{M}|\bar{h}l|0\rangle \qquad \langle 0|\bar{h}l|M\rangle \xrightarrow{P} -\langle 0|\bar{h}l|M\rangle$$

But as parity is a symmetry of QCD the only possibility is

$$\langle \overline{M}|\bar{h}l|0\rangle = \langle 0|\bar{h}l|M\rangle = 0$$

Vectorial: $O^i = \bar{h}\gamma_\mu l$

The vectorial operator should satisfy the Ward Identity in the momentum space. Thus

$$p_\mu \langle 0|\bar{h}\gamma_\mu l|M\rangle = -(m_h - m_l)\langle 0|\bar{h}l|M\rangle = 0$$

and we conclude again that

$$\langle \overline{M}|\bar{h}\gamma_\mu l|0\rangle = \langle 0|\bar{h}\gamma_\mu l|M\rangle = 0$$

Tensorial: $O^i = \bar{h}\sigma_{\mu\nu} l$

In general one can write the matrix element in terms of the most general antisymmetric rank 2 tensor one can construct with $g_{\mu\nu}$, p_μ and $\epsilon_{\mu\nu\rho\sigma}$

$$\langle 0|\bar{h}\sigma_{\mu\nu}l|M\rangle = A\epsilon_{\mu\nu\rho\sigma}p_\rho p_\sigma e^{-ipx}$$

This is the product of a symmetric and an antisymmetric tensor so it is zero

$$\langle 0|\bar{h}\sigma_{\mu\nu}l|M\rangle = \langle \overline{M}|\bar{h}\sigma_{\mu\nu}l|0\rangle = 0$$

Axial: $O^i = \bar{h}\gamma_\mu\gamma_5 l$

One can set

$$\langle 0|\bar{h}\gamma_\mu\gamma_5 l|M(p)\rangle \equiv \langle 0|A^\dagger_\mu(x)|M(p)\rangle = \langle 0|e^{px}A^\dagger_\mu(0)e^{-px}|M(p)\rangle \equiv f_{PS}p_\mu e^{-px} \quad (3.2.20)$$

where $p^\mu = (E, \vec{p})$ is the four-momentum carried by the on-shell meson and in the center of mass system $p^\mu = (M_{PS}, \vec{0})$. Applying charge conjugation

$$\langle \overline{M}|A^\dagger_\mu(x)|0\rangle = \langle \overline{M}(p)|e^{px}A^\dagger_\mu(0)e^{-px}|0\rangle = f_{PS}p_\mu e^{px} \quad (3.2.21)$$

and consequently in the center of mass

$$\langle \overline{M}|A^\dagger_0|0\rangle\langle 0|A^\dagger_0|M\rangle = f^2_{PS}M^2_{PS} \quad (3.2.22)$$

Pseudoscalar: $O^i = \bar{h}\gamma_5 l$

Applying the four-momentum operator $p_\mu \equiv \partial_\mu$ to the matrix elements $\langle 0|A^\dagger_\mu(x)|M\rangle$ and $\langle \overline{M}|A^\dagger_\mu(x)|0\rangle$ in Eq.3.2.20 and Eq.3.2.21 one obtains

$$\partial_\mu \langle 0|A^\dagger_\mu(x)|M\rangle = -f_{PS}p^2 e^{-px} \qquad \partial_\mu \langle \overline{M}|A^\dagger_\mu(x)|0\rangle = f_{PS}p^2 e^{px}$$

But according to the PCAC Ward Identity $\partial_\mu A_\mu = (m_h + m_l)P_5$. Hence, in the center of mass system where $\vec{p} = 0$ and $p = (M_{PS}, 0)$

$$\langle 0|P^\dagger_5|M\rangle = -\frac{f_{PS}M^2_{PS}}{m_h + m_l} \qquad \langle \overline{M}|P^\dagger_5|0\rangle = \frac{f_{PS}M^2_{PS}}{m_h + m_l}$$

and finally

$$\langle \overline{M}|P^\dagger_5|0\rangle\langle 0|P^\dagger_5|M\rangle = -\frac{f^2_{PS}M^4_{PS}}{(m_h + m_l)^2} \tag{3.2.23}$$

With the above prescription Eq.3.2.18 becomes in the VIA approximation Eq.3.2.19

$$\begin{aligned}
\langle \overline{M}|N\{Q_1\}|M\rangle_{VIA} &= \frac{8}{3} f^2_{PS}M^2_{PS} \\
\langle \overline{M}|N\{Q_2\}|M\rangle_{VIA} &= -\frac{5}{3}\left(\frac{M_{PS}}{m_h + m_l}\right)^2 f^2_{PS}M^2_{PS} \\
\langle \overline{M}|N\{Q_3\}|M\rangle_{VIA} &= \frac{1}{3}\left(\frac{M_{PS}}{m_h + m_l}\right)^2 f^2_{PS}M^2_{PS} \\
\langle \overline{M}|N\{Q_4\}|M\rangle_{VIA} &= 2\left[\frac{1}{6} + \left(\frac{M_{PS}}{m_h + m_l}\right)^2\right] f^2_{PS}M^2_{PS} \\
\langle \overline{M}|N\{Q_5\}|M\rangle_{VIA} &= \frac{2}{3}\left[\frac{3}{2} + \left(\frac{M_{PS}}{m_h + m_l}\right)^2\right] f^2_{PS}M^2_{PS}
\end{aligned} \tag{3.2.24}$$

Since the definition of B-parameters is conventional[4], without loss of generality we usually omit terms present in the previous definition and we define the bag parameters through

[4] To illustrate that the definition of B-parameters is conventional let us imagine that at some renormalization scale $\overline{\mu}$, as $m_s \to \infty$, we have $\langle \overline{K}^0|Q_{4,5}|K^0\rangle = \langle \overline{K}^0|Q_{4,5}|K^0\rangle_{VIA}$. Under these hypotheses we get that the B-parameters defined in Eq.3.2.25 would be $B_4 = 7/2$ and $B_5 = 5/2$ instead the standard results $B_{4,5} = 1$ we would get if we have used Eq.3.2.24.

$$\begin{aligned}
\langle \overline{M}|N\{Q_1\}|M\rangle &= \frac{8}{3} f_{PS}^2 M_{PS}^2 B_1 \\
\langle \overline{M}|N\{Q_2\}|M\rangle &= -\frac{5}{3}\left(\frac{M_{PS}}{m_h+m_l}\right)^2 f_{PS}^2 M_{PS}^2 B_2 \\
\langle \overline{M}|N\{Q_3\}|M\rangle &= \frac{1}{3}\left(\frac{M_{PS}}{m_h+m_l}\right)^2 f_{PS}^2 M_{PS}^2 B_3 \\
\langle \overline{M}|N\{Q_4\}|M\rangle &= 2\left(\frac{M_{PS}}{m_h+m_l}\right)^2 f_{PS}^2 M_{PS}^2 B_4 \\
\langle \overline{M}|N\{Q_5\}|M\rangle &= \frac{2}{3}\left(\frac{M_{PS}}{m_h+m_l}\right)^2 f_{PS}^2 M_{PS}^2 B_5
\end{aligned} \tag{3.2.25}$$

In the above formula the normal ordering for the operators Q_i is still explicitly written but for simplicity in the following we will drop it.

The reason why we prefer the B-parameter definition given in Eq.3.2.25 rather than the standard one coming from Eq.3.2.24 is the following: Ignoring for simplicity the mixing under renormalization between operators $Q_2 - Q_3$ and $Q_4 - Q_5$, B_i parameters defined in Eq.3.2.25 must obey the renormalization group equation

$$\mu \frac{dB_1}{d\mu} = \left(\gamma_{Q_1} - 2\gamma_A\right) B_1(\mu)$$

$$\mu \frac{dB_i}{d\mu} = \left(\gamma_{Q_i} - 2\gamma_P\right) B_i(\mu) \quad i = 2, ..., 5$$

with $\mu d/d\mu = \mu\partial/\partial\mu + \beta(\alpha_s)\partial/\partial\alpha_s$, and γ_A , γ_P and γ_{Q_i} are the anomalous dimension of the axial, pseudoscalar and the operators Q_i. The physical amplitude is then given by

$$\begin{aligned}
\langle \overline{M}|H_{\text{eff}}|M\rangle &= C_i(M_W/\mu)\langle \overline{M}|\hat{Q}_i(\mu)|M\rangle \\
&\propto C_i(M_W/\mu) \times B_i(\mu) \times \left(\frac{M_{PS}}{m_h+m_l}\right)^2 f_{PS}^2 M_{PS}^2 \\
&\sim \left(\frac{\alpha_s(M_W)}{\alpha_s(\mu)}\right)^{-\gamma_{Q_i}/2\beta_0} \times (\alpha_s(\mu))^{\left(\gamma_{Q_i}-2\gamma_P\right)/2\beta_0} \times (\alpha_s(\mu))^{\gamma_P/\beta_0}
\end{aligned} \tag{3.2.26}$$

where in the last expression we have only shown the leading behavior of the different factors, that is, the Wilson coefficient, the B-parameter and the quark masses. Eq.3.2.26 shows explicitly the cancellation of the μ-dependence in the amplitude. However, with the standard definition of the B-parameters from Eq.3.2.24, the scaling properties of $B_4(\mu)$ and $B_5(\mu)$ would have been more complicated due to the two pieces on the right hand side, one which scales as the squared pseudoscalar density and another proportional to the axial density which is renormalization group invariant. The μ-independence of the final result would then have been recovered in a intricate way. Consequently, as the definition of B-parameter is a convention, we prefer to use Eq.3.2.25, for which the scaling properties of all B-parameters are the simplest ones. Moreover, note that, with this choice, in the chiral limit both definitions are equivalents.

3.2.5 Extracting B-parameters from lattice correlation functions

Using the relations in Eq.3.2.22 and Eq.3.2.23, we can divide each one of the matrix elements in Eq.3.2.25 either by $\langle \overline{M}^0|A_0^\dagger|0\rangle\langle 0|A_0^\dagger|M^0\rangle$ or $\langle \overline{M}|P_5^\dagger|0\rangle\langle 0|P_5^\dagger|M\rangle$ finding that

$$\begin{aligned} \xi_1 B_1 &= \frac{\langle \overline{M}|Q_1|M\rangle}{\langle \overline{M}|A_0^\dagger|0\rangle\langle 0|A_0^\dagger|M\rangle} \\ \xi_i B_i &= -\frac{\langle \overline{M}|Q_i|M\rangle}{\langle \overline{M}|P_5^\dagger|0\rangle\langle 0|P_5^\dagger|M\rangle} \qquad i=2,...,5 \end{aligned} \tag{3.2.27}$$

with $\xi_i = \{\frac{8}{3}, -\frac{5}{3}, \frac{1}{3}, 2, \frac{2}{3}\}$ and the relative sign between B_1 and B_i with $i = 2,3,4,5$ comes from the relative sign between Eq.3.2.22 and Eq.3.2.23.

Finally, considering again Eq.3.2.7, recovering the renormalized version and the theory with four OS quark fields it is straightforward that

$$\begin{aligned} &\frac{1}{\xi_1}\frac{\hat{C}^{(3)}_{Q_1}(x_0)}{\hat{C}^{(2)}_{PA}(x_0)\hat{C}'^{(2)}_{PA}(x_0)} \xrightarrow[y_0\ll x_0\ll y_0+T_{\rm sep}]{} \frac{1}{\xi_1}\frac{\langle M^{34}|\hat{Q}_1|M^{21}\rangle}{\langle M^{34}|\hat{A}_0^{34}|0\rangle\langle 0|\hat{A}_0^{12}|M^{21}\rangle} = \hat{B}_1 \\ &\frac{1}{\xi_i}\frac{\hat{C}^{(3)}_{Q_i}(x_0)}{\hat{C}^{(2)}_{PP}(x_0)\hat{C}'^{(2)}_{PP}(x_0)} \xrightarrow[y_0\ll x_0\ll y_0+T_{\rm sep}]{} \frac{1}{\xi_i}\frac{\langle M^{34}|\hat{Q}_i|M^{21}\rangle}{\langle M^{34}|\hat{P}_5^{34}|0\rangle\langle 0|\hat{P}_5^{12}|M^{21}\rangle} = \hat{B}_i \quad i=2,...,5 \end{aligned} \tag{3.2.28}$$

So, at the end of the day, Eq.3.2.28 express the renormalized bag parameters in terms of renormalized two- and three-point correlation functions. But, in order to apply them, we need to rewrite these formulae in terms of bare correlation functions coupled with their relative renormalization constants. In the following sections we will consider the renormalization pattern of the four-fermion operators Q_i and then by choosing a particular fermionic basis we will show that we are able to reduce the number of renormalization constants needed.

3.3 Renormalization pattern for bilinear operators

3.3.1 Mapping of two-fermion operators

In this section we will show how two-fermion operators transform under the axial rotation of the quark fields, from the physical basis where $O_{\Gamma,ij} = \bar{\psi}_i\Gamma\psi_j$ to the twisted basis $\mathcal{O}_{\Gamma,ij} = \bar{\chi}_i\Gamma\chi_j$.

In particular, we will focus on the following operators in the physical basis

$$
\begin{aligned}
A_{\mu,ij} &= \bar{\psi}_i \gamma_\mu \gamma_5 \psi_j \\
V_{\mu,ij} &= \bar{\psi}_i \gamma_\mu \psi_j \\
P_{ij} &= \bar{\psi}_i \gamma_5 \psi_j \\
S_{ij} &= \bar{\psi}_i \psi_j
\end{aligned}
$$

while the corresponding ones in the twisted basis are

$$
\begin{aligned}
\mathcal{A}_{\mu,ij} &= \bar{\chi}_i \gamma_\mu \gamma_5 \chi_j \\
\mathcal{V}_{\mu,ij} &= \bar{\chi}_i \gamma_\mu \chi_j \\
\mathcal{P}_{ij} &= \bar{\chi}_i \gamma_5 \chi_j \\
\mathcal{S}_{ij} &= \bar{\chi}_i \chi_j
\end{aligned}
$$

Let us recall that TM quark doublet transforms as

$$
\begin{aligned}
\psi(x) &= \exp\left\{ i\frac{\omega}{2}\gamma^5\tau^3 \right\} \chi(x) \\
\bar{\psi}(x) &= \bar{\chi}(x) \exp\left\{ i\frac{\omega}{2}\gamma^5\tau^3 \right\}
\end{aligned}
\tag{3.3.1}
$$

while for the OS quark doublet we write

$$
\begin{aligned}
\psi(x) &= \exp\left\{ i\frac{\omega}{2}\gamma^5 \right\} \chi(x) \\
\bar{\psi}(x) &= \bar{\chi}(x) \exp\left\{ i\frac{\omega}{2}\gamma^5 \right\}
\end{aligned}
$$

Both expressions can be written in a combined way using the Wilson parameter r_i

$$
\begin{aligned}
\psi_i(x) &= \exp\left\{ i\frac{\omega}{2}\gamma^5 r_i \right\} \chi_i(x) \\
\bar{\psi}_i(x) &= \bar{\chi}_i(x) \exp\left\{ i\frac{\omega}{2}\gamma^5 r_i \right\}
\end{aligned}
\tag{3.3.2}
$$

The Wilson parameters are $r_i = -r_j = 1$ for the standard TM case and $r_i = r_j$ for the OS quark fields.Using Eq.3.3.2, the generic two-fermion operator $\bar{\psi}_i \Gamma^a \psi_j$ is mapped in the twisted basis as

$$
\bar{\psi}_i \Gamma^a \psi_j = \bar{\chi}_i \exp\left\{ i\frac{\omega}{2}\gamma^5 r_i \right\} \Gamma^a \exp\left\{ i\frac{\omega}{2}\gamma^5 r_j \right\} \chi_j \tag{3.3.3}
$$

with $\Gamma^a = \{I, \gamma_\mu, \gamma_5, \gamma_5\gamma_\mu, \sigma_{\mu\nu}\}$ and each Γ^a satisfies one of the following relations

$$
[\Gamma^a, \gamma_5] = 0 \quad \text{or} \quad \{\Gamma^a, \gamma_5\} = 0
$$

Thus Eq.3.3.3 can be written as

$$\bar{\psi}_i \Gamma^a \psi_j = \bar{\chi}_i \Gamma^a \exp\left\{ i \frac{\omega}{2} \gamma^5 \left(r_i + \eta_{\Gamma^a} r_j \right) \right\} \chi_j \tag{3.3.4}$$

where

$$\eta_{\Gamma^a} = \begin{cases} +1 & \text{if } [\Gamma^a, \gamma_5] = 0 \\ \\ -1 & \text{if } \{\Gamma^a, \gamma_5\} = 0 \end{cases} \tag{3.3.5}$$

Now using the known trigonometric formula for the cosinus and sinus of the double angle and the explicit value of η_{Γ^a}

$$\begin{aligned} [\mathbb{I}, \gamma_5] = 0 \quad &\rightarrow \quad \eta_S = +1 \\ \{\gamma_\mu, \gamma_5\} = 0 \quad &\rightarrow \quad \eta_V = -1 \\ [\gamma_5, \gamma_5] = 0 \quad &\rightarrow \quad \eta_P = +1 \\ \{\gamma_\mu \gamma_5, \gamma_5\} = 0 \quad &\rightarrow \quad \eta_A = -1 \\ [\sigma_{\mu\nu}, \gamma_5] = 0 \quad &\rightarrow \quad \eta_T = +1 \end{aligned} \tag{3.3.6}$$

one obtains the following expressions for the mapping at a general value of ω and the corresponding ones at maximal twist

- TM case: $r_i = -r_j = \pm 1$

$$\begin{aligned} S_{ij} &= \mathcal{S}_{ij} & & S_{ij} = \mathcal{S}_{ij} \\ V_{\mu,ij} &= \cos\omega \mathcal{V}_{\mu,ij} \pm i \sin\omega \mathcal{A}_{\mu,ij} & & V_{\mu,ij} = \pm i \mathcal{A}_{\mu,ij} \\ P_{ij} &= \mathcal{P}_{ij} & \xrightarrow{\omega=\pi/2} \quad & P_{ij} = \mathcal{P}_{ij} \\ A_{\mu,ij} &= \cos\omega \mathcal{A}_{\mu,ij} \pm i \sin\omega \mathcal{V}_{\mu,ij} & & A_{\mu,ij} = \pm i \mathcal{V}_{\mu,ij} \\ T_{ij} &= \mathcal{T}_{ij} & & T_{ij} = \mathcal{T}_{ij} \end{aligned}$$

- OS case: $r_i = r_j = \pm 1$

$$\begin{aligned} S_{ij} &= \cos\omega \mathcal{S}_{ij} \pm i \sin\omega \mathcal{P}_{ij} & & S_{ij} = \pm i \mathcal{P}_{ij} \\ V_{\mu,ij} &= \mathcal{V}_{\mu,ij} & & V_{\mu,ij} = \mathcal{V}_{\mu,ij} \\ P_{ij} &= \cos\omega \mathcal{P}_{ij} \pm i \sin\omega \mathcal{P}_{ij} & \xrightarrow{\omega=\pi/2} \quad & P_{ij} = \pm i \mathcal{S}_{ij} \\ A_{\mu,ij} &= \mathcal{A}_{\mu,ij} & & A_{\mu,ij} = \mathcal{A}_{\mu,ij} \\ T_{ij} &= \cos\omega \mathcal{T}_{ij} \pm i \sin\omega \tilde{\mathcal{T}}_{ij} & & T_{ij} = \pm i \tilde{\mathcal{T}}_{ij} \end{aligned} \tag{3.3.7}$$

with $\tilde{\mathcal{T}} = \gamma_5\sigma_{\mu\nu}$ and the $\pm$ sign corresponds to the sign of r.

The axial transformation Eq.3.3.2 transform the TM and OS actions into the action in Eq.2.2.21 where instead the Wilson term we have a mass term taking the form

mass term TM $\sim (i\mu_1\bar{\chi}_1\gamma_5\chi_1 - i\mu_2\bar{\chi}_2\gamma_5\chi_2)$

or mass term OS $\sim (i\mu_1\bar{\chi}_1\gamma_5\chi_1 + i\mu_2\bar{\chi}_2\gamma_5\chi_2)$

This implies, that the RCs for the operators in the twisted basis, defined in the chiral limit, as RI-MOM, are the same for the Wilson, TM and OS cases.

For convention, Renormalization Constants (RCs) of bilinear operators are named after the twisted rotation, that is, once the Wilson term has the standard form. Following this convention together with the two-fermion operator mapping just found the operator renormalization pattern in the physical and twisted basis is given in Table 3.3.1 for both OS and TM formulations at maximal twist.

OS	TM
$\hat{A}_{\mu,ij} = Z_A A_{\mu,ij} = Z_A \mathcal{A}_{\mu,ij}$	$\hat{A}_{\mu,ij} = Z_V A_{\mu,ij} = \pm i Z_V \mathcal{V}_{\mu,ij}$
$\hat{V}_{\mu,ij} = Z_V V_{\mu,ij} = Z_V \mathcal{V}_{\mu,ij}$	$\hat{V}_{\mu,ij} = Z_A V_{\mu,ij} = \pm i Z_A \mathcal{A}_{\mu,ij}$
$\hat{P}_{ij} = Z_S P_{ij} = \pm i Z_S \mathcal{S}_{ij}$	$\hat{P}_{ij} = Z_P P_{ij} = Z_P \mathcal{P}_{ij}$
$\hat{S}_{ij} = Z_P S_{ij} = \pm i Z_P \mathcal{P}_{ij}$	$\hat{S}_{ij} = Z_S S_{ij} = Z_S \mathcal{S}_{ij}$
$\hat{T}_{\mu\nu,ij} = Z_T T_{\mu\nu,ij} = \pm i Z_T \tilde{\mathcal{T}}_{\mu\nu,ij}$	$\hat{T}_{\mu\nu,ij} = Z_T T_{\mu\nu,ij} = Z_T \mathcal{T}_{\mu\nu,ij}$

Table 3.3.1: Renormalization pattern of bilinear quark operators for the OS and TM case at maximal twist. As usual, calligraphic letters refer to operators in the twisted basis.

3.3.2 Renormalized pseudoscalar decay constant

Renormalized pseudoscalar decay constants, from maximal twisted Wilson fermions, are determined using the bilinear renormalization mapping together with

1. The definition in term of the axial current

$$F_{PS} = \frac{\hat{G}_{PA}}{\sqrt{\hat{G}_{PP}} M_{PS}} = \begin{cases} F_{PS}^{OS} = Z_A \dfrac{G_{PA}^{OS}}{\sqrt{G_{PP}^{OS}} M_{PS}} \\ F_{PS}^{TM} = Z_V \dfrac{G_{PA}^{TM}}{\sqrt{G_{PP}^{TM}} M_{PS}} \end{cases}$$

2. The PCAC WI and the renormalization of the twisted quark mass μ_q, the only one relevant at maximal twist, according to Eq.2.2.8

$$F_{PS} = \frac{(\hat{\mu}_h + \hat{\mu}_l)}{M_{PS}^2}\sqrt{\hat{G}_{PP}} = \begin{cases} F_{PS}^{OS} = \dfrac{Z_S}{Z_P}\dfrac{(\mu_h + \mu_l)}{M_{PS}^2}\sqrt{G_{PP}^{OS}} \\ F_{PS}^{TM} = \dfrac{(\mu_h + \mu_l)}{M_{PS}^2}\sqrt{G_{PP}^{TM}} \end{cases}$$

Note that one of the great advantage of the f_{PS} computation from the PCAC WI is that for the TM correlator the renormalization constant is not needed. In other words, we are able to obtain the decay constant f_{PS} just from bare correlators. In addition, only the $C_{PP}^{(2)}$ correlator is involved while Eq.3.1.15 requires also $C_{PA}^{(2)}$. For this reason f_{PS} is usually determined from the PCAC WI using TM correlators.

3.4 Renormalization pattern for four-fermion operators

In this section we will study the mixing of generic four-fermion operators in the presence of explicit chiral symmetry breaking induced by the Wilson term. Following [75] we obtain the complete basis of dimension-six four-fermion operators which mix under renormalization relying on the operator classification according to their discrete symmetries.

I will show that, in the physical basis, using Wilson fermions parity-even four-fermion operators mix under renormalization while the parity-odd ones mix only through a block diagonal matrix. In order to take profit of the previous mentioned advantage of the parity-odd operators we will look for a setup which maps the parity-even operators in the parity-odd ones. As it is detailed in subsection 3.4.3 this transformation is achieved by choosing a particular set of twist angles for the four ψ_f quarks.

3.4.1 Mixing of dimension-six four-fermion operators

A complet set of Lorentz invariant four-fermion operators is defined as

$$\begin{aligned} O_{\Gamma^a\Gamma^b} &= \left(\bar{\psi}_1\Gamma^a\psi_2\right)\left(\bar{\psi}_3\Gamma^b\psi_4\right) \\ O_{t^c\Gamma^a t^c\Gamma^b} &= \left(\bar{\psi}_1 t^c\Gamma^a\psi_2\right)\left(\bar{\psi}_3 t^c\Gamma^b\psi_4\right) \\ O^S_{\Gamma^a\Gamma^b} &= \left(\bar{\psi}_1\Gamma^a\psi_4\right)\left(\bar{\psi}_3\Gamma^b\psi_2\right) \\ O^S_{t^c\Gamma^a t^c\Gamma^b} &= \left(\bar{\psi}_1 t^c\Gamma^a\psi_4\right)\left(\bar{\psi}_3 t^c\Gamma^b\psi_2\right) \end{aligned} \tag{3.4.1}$$

where t^c are the color group generator matrix of $SU(N_c)$ with $N_c = 3$ and Γ^a and Γ^b are two compatible Dirac matrices, i.e, $\Gamma_b = \Gamma_a$ for parity-even operators and $\Gamma_b = \gamma_5\Gamma_a$ for parity-odd. The 16 Euclidean Dirac 4x4 matrices which form a complete basis are denoted by $\Gamma = \left\{\Gamma^S, \Gamma^V, \Gamma^P, \Gamma^A, \Gamma^T\right\}$ with

$$\Gamma^S = I$$

$$\Gamma^{V_\mu} = \gamma_\mu$$

$$\Gamma^P = \gamma_5$$

$$\Gamma^{A_\mu} = \gamma_\mu\gamma_5$$

$$\Gamma^{T_{\mu\nu}} = \sigma_{\mu\nu} = \frac{1}{2}[\gamma_\mu, \gamma_\nu]$$

Moreover, it is also convenient to define the dual tensorial matrix

$$\Gamma^{\tilde{T}_{\mu\nu}} = \sigma_{\mu\nu}\gamma_5 = \epsilon_{\mu\nu\rho\sigma}\sigma_{\rho\sigma} \ \ (\rho < \sigma)$$

Note that the operators O^S_{ab} are those obtained from O_{ab} by applying the so called *switching symmetry* $\mathcal{S}$

$$\mathcal{S} : \psi_2 \leftrightarrow \psi_4 \tag{3.4.2}$$

In order to find a complete basis of operator mixing under renormalization, we do not need to consider the operators $O_{t^c\Gamma^a t^c\Gamma^b}$ and $O^S_{t^c\Gamma^a t^c\Gamma^b}$ since they can be expressed in terms of $O_{\Gamma^a\Gamma^b}$ and $O^S_{\Gamma^a\Gamma^b}$. In other words, $O_{t^c\Gamma^a t^c\Gamma^b}$ and $O^S_{t^c\Gamma^a t^c\Gamma^b}$ are not independent. This can be easily seen by applying the color identity

$$t^c_{AB}t^c_{CD} = -\frac{1}{2N_c}\delta_{AB}\delta_{CD} + \frac{1}{2}\delta_{AD}\delta_{CB}$$

which gives

$$O_{t^c\Gamma^a t^c\Gamma^b} = -\frac{1}{2N_c}O_{\Gamma^a\Gamma^b} + \frac{1}{2}\sum_{n,m} C_{nm}O^S_{\Gamma^a\Gamma^b}$$

where the factors C_{nm} are the constants of the Fierz transformation of the Dirac matrices. Analogously we can express $O^S_{t^c\Gamma^a t^c\Gamma^b}$ in terms of $O_{\Gamma^a\Gamma^b}$ and $O^S_{\Gamma^a\Gamma^b}$. So, in the following, we can focus only on the mixing $O_{\Gamma^a\Gamma^b}$ and $O^S_{\Gamma^a\Gamma^b}$, which form a complete basis of independent operators. This form a set of 20 independent operators: the 5 parity-even, or parity conserving, operators $O_{\Gamma^a\Gamma^a}$, the 5 parity-odd, or parity violating, ones $O_{\Gamma^a(\gamma_5\Gamma^a)}$ and their 10 switching counterparts O^S

parity-even	parity-odd
O_{VV}	O_{VA}
O_{AA}	O_{AV}
O_{PP}	O_{SP}
O_{SS}	O_{PS}
O_{TT}	$O_{T\tilde{T}}$

3.4.1.1 Operator classification according to discrete symmetries

Let us start the classification of the four-fermion dimension-six operators according to their discrete symmetries. First of all, they cannot mix with operators of lower dimensionality since such operators do not have the four-flavour content of the original ones. Therefore, $O_{\Gamma^a\Gamma^b}$ ($O^S_{\Gamma^a\Gamma^b}$) can mix with any other dimension-six operator, provided it has the same symmetries of $O_{\Gamma^a\Gamma^b}$ ($O^S_{\Gamma^a\Gamma^b}$) and of the action. That is, any symmetry of any operator can be used to establish its renormalization pattern only if the same transformation is a symmetry of the action.

The symmetries of the generic QCD Wilson action with four degenerate quarks to be considered are parity $\mathcal{P}$ and charge conjugation $\mathcal{C}$. The switching symmetry $\mathcal{S}$ defined in Eq.3.4.2 and the additional ones

$$\mathcal{S}' : \quad \left(\psi_1 \leftrightarrow \psi_2\right)\left(\psi_3 \leftrightarrow \psi_4\right)$$

$$\mathcal{S}'' : \quad \left(\psi_1 \leftrightarrow \psi_4\right)\left(\psi_2 \leftrightarrow \psi_3\right)$$

can also be used to establish the renormalization pattern of the four-fermion operators $O_{\Gamma^a\Gamma^b}$.

Table 3.4.1 summarize the behavior of $O_{\Gamma^a\Gamma^b}$ under $\mathcal{P}$, $\mathcal{CS}'$, $\mathcal{CS}''$, $\mathcal{CPS}'$ and $\mathcal{CPS}''$. Since $\mathcal{S}$ transforms $\mathcal{S}'$ into $\mathcal{S}''$ and viceversa the quantum numbers of $O^S_{\Gamma^a\Gamma^b}$ are obtained from the ones of $O_{\Gamma^a\Gamma^b}$ by exchanging $\mathcal{S}'$ and $\mathcal{S}''$ columns.

	$\mathcal{P}$	$\mathcal{CS}'$	$\mathcal{CS}$"	$\mathcal{CPS}$'	$\mathcal{CPS}$"
O_{VV}	+1	+1	+1	+1	+1
O_{AA}	+1	+1	+1	+1	+1
O_{PP}	+1	+1	+1	+1	+1
O_{SS}	+1	+1	+1	+1	+1
O_{TT}	+1	+1	+1	+1	+1
O_{VA}	-1	-1	$-O_{AV}$	+1	O_{AV}
O_{AV}	-1	-1	$-O_{VA}$	+1	O_{VA}
O_{SP}	-1	+1	O_{PS}	-1	$-O_{PS}$
O_{PS}	-1	+1	O_{SP}	-1	$-O_{SP}$
$O_{T\tilde{T}}$	-1	+1	+1	-1	-1

Table 3.4.1: Classification of $O_{\Gamma^a\Gamma^b}$ four-fermion operator according to $\mathcal{P}$, $\mathcal{S}$ and adequate products of the discrete symmetries $\mathcal{P}$, $\mathcal{C}$, $\mathcal{S}$, $\mathcal{S}'$ and $\mathcal{S}''$

However, operators $O_{\Gamma^a\Gamma^b}$ are not eigenstates of $\mathcal{S}$, so it is convenient to rotate our basis into a new one in which operators are eigenstates of $\mathcal{S}$ with eigenvalue $\pm$ respectively which will help us to establish the renormalization pattern

$$O^{\pm}_{\Gamma^a\Gamma^b} = \frac{1}{2}\left[O_{\Gamma^a\Gamma^b} \pm O^{S}_{\Gamma^a\Gamma^b}\right] \tag{3.4.3}$$

$$\frac{1}{2}\left[\left(\bar{\psi}_1\Gamma^a\psi_2\right)\left(\bar{\psi}_3\Gamma^b\psi_4\right) \pm \left(\bar{\psi}_1\Gamma^a\psi_4\right)\left(\bar{\psi}_3\Gamma^b\psi_2\right)\right]$$

Table 3.4.2 shows how the 20 operators $O^{\pm}_{\Gamma^a\Gamma^b}$ behave under $\mathcal{P}$, $\mathcal{CS}'$, $\mathcal{CS}''$, $\mathcal{CPS}'$ and $\mathcal{CPS}''$, which are symmetries of the action in the chiral limit[5]. From this table we conclude that the original basis of 20 operators can be decomposed into smaller independent bases. The first decomposition is into 2 basis, of 10 operators each, with definite parity $\mathcal{P} = \pm 1$. The second one comes from the $\mathcal{S}$ symmetry which splits each parity defined basis into 5 independent operators corresponding to $\mathcal{S} = \pm 1$. In the following we will study the renormalization matrix of this four sets of 5 independent operators.

[5]The renormalization process in the RI'-MOM scheme is performed in the chiral limit, so in order to establish the renormalization pattern we can consider any symmetry of the action in the chiral limit.

$O^{\pm}_{\Gamma^a\Gamma^b}$	$\mathcal{P}$	$\mathcal{S}$	$\mathcal{CS}'$	$\mathcal{CS}''$	$\mathcal{CPS}'$	$\mathcal{CPS}'$
$O^{\pm}_{VV}$	+1	±1	+1	+1	+1	+1
$O^{\pm}_{AA}$	+1	±1	+1	+1	+1	+1
$O^{\pm}_{PP}$	+1	±1	+1	+1	+1	+1
$O^{\pm}_{SS}$	+1	±1	+1	+1	+1	+1
$O^{\pm}_{TT}$	+1	±1	+1	+1	+1	+1
$O^{\pm}_{VA}$	-1	±1	$-\frac{1}{2}\left\{O_{VA} \pm O^{S}_{AV}\right\}$	$-\frac{1}{2}\left\{O_{AV} \pm O^{S}_{VA}\right\}$	$\frac{1}{2}\left\{O_{VA} \pm O^{S}_{AV}\right\}$	$\frac{1}{2}\left\{O_{AV} \pm O^{S}_{VA}\right\}$
$O^{\pm}_{AV}$	-1	±1	$-\frac{1}{2}\left\{O_{AV} \pm O^{S}_{VA}\right\}$	$-\frac{1}{2}\left\{O_{VA} \pm O^{S}_{AV}\right\}$	$\frac{1}{2}\left\{O_{AV} \pm O^{S}_{VA}\right\}$	$\frac{1}{2}\left\{O_{VA} \pm O^{S}_{AV}\right\}$
$O^{\pm}_{SP}$	-1	±1	$\frac{1}{2}\left\{O_{SP} \pm O^{S}_{PS}\right\}$	$\frac{1}{2}\left\{O_{PS} \pm O^{S}_{SP}\right\}$	$-\frac{1}{2}\left\{O_{SP} \pm O^{S}_{PS}\right\}$	$-\frac{1}{2}\left\{O_{PS} \pm O^{S}_{SP}\right\}$
$O^{\pm}_{PS}$	-1	±1	$\frac{1}{2}\left\{O_{PS} \pm O^{S}_{SP}\right\}$	$\frac{1}{2}\left\{O_{SP} \pm O^{S}_{PS}\right\}$	$-\frac{1}{2}\left\{O_{PS} \pm O^{S}_{SP}\right\}$	$-\frac{1}{2}\left\{O_{SP} \pm O^{S}_{PS}\right\}$
$O^{\pm}_{T\tilde{T}}$	-1	±1	+1	+1	-1	-1

Table 3.4.2: Classification of $O^{\pm}_{\Gamma^a\Gamma^b}$ four-fermion operator according to $\mathcal{P}$, $\mathcal{S}$ and adequate products of the discrete symmetries $\mathcal{P}$, $\mathcal{C}$, $\mathcal{S}$, $\mathcal{S}'$ and $\mathcal{S}''$

Parity-even (conserving) operators: $\mathcal{P} = +1$ The usual supersymmetric basis we are interested in can be built from the parity-even operators as

$$\begin{aligned} Q_1^{\mathtt{PC}\pm} &= O^{\pm}_{VV} + O^{\pm}_{AA} \\ Q_2^{\mathtt{PC}\pm} &= O^{\pm}_{SS} + O^{\pm}_{PP} \\ Q_3^{\mathtt{PC}\pm} &= -\frac{1}{2}\left\{O^{\pm}_{SS} - O^{\pm}_{TT} + O^{\pm}_{PP}\right\} \\ Q_4^{\mathtt{PC}\pm} &= O^{\pm}_{SS} - O^{\pm}_{PP} \\ Q_5^{\mathtt{PC}\pm} &= -\frac{1}{2}\left\{O^{\pm}_{VV} - O^{\pm}_{AA}\right\} \end{aligned} \tag{3.4.4}$$

where clearly Eq.3.2.13 is recovered from Eq.3.4.4 using the operators Q_i^+ corresponding to $\mathcal{S} = +1$. Since $Q_i^{\mathtt{PC}\pm}$ are linear combination of parity-even operators $O^{\pm}_{\Gamma^a\Gamma^a}$, which

are $\mathcal{P}$, $\mathcal{S}$, $\mathcal{CS}'$, $\mathcal{CS}''$, $\mathcal{CPS}'$ and $\mathcal{CPS}''$ eigenstates, they are also eigenstates of the same transformations as it is summarized in table Table 3.4.3.

	$\mathcal{P}$	$\mathcal{S}$	$\mathcal{CS}'$	$\mathcal{CS}$"	$\mathcal{CPS}$'	$\mathcal{CPS}$"
$Q_1^{\mathtt{PC}\pm}$	$+1$	± 1	$+1$	$+1$	$+1$	$+1$
$Q_2^{\mathtt{PC}\pm}$	$+1$	± 1	$+1$	$+1$	$+1$	$+1$
$Q_3^{\mathtt{PC}\pm}$	$+1$	± 1	$+1$	$+1$	$+1$	$+1$
$Q_4^{\mathtt{PC}\pm}$	$+1$	± 1	$+1$	$+1$	$+1$	$+1$
$Q_5^{\mathtt{PC}\pm}$	$+1$	± 1	$+1$	$+1$	$+1$	$+1$

Table 3.4.3: $Q_i^{\mathtt{PC}\pm}$ parity conserving operator quantum numbers

Renormalization mixes operators sharing the same quantum numbers. Thus, operators $Q_i^{\mathtt{PC}\pm}$ do not mix with the parity-odd operators since they have opposite parity. Moreover, operators with opposite switching symmetry do not mix between them, so any $Q_i^{\mathtt{PC}+}$ do not mix with $Q_i^{\mathtt{PC}-}$. But table Table 3.4.3 shows that each parity-even operator shares its quantum numbers with the rest of parity-even operators with the same switching symmetry, so, in principle they mix with each other under renormalization

$$\begin{pmatrix} \hat{Q}_1 \\ \hat{Q}_2 \\ \hat{Q}_3 \\ \hat{Q}_4 \\ \hat{Q}_5 \end{pmatrix}^{\mathtt{PC}\pm} = \begin{pmatrix} Z_{11} & Z_{12} & Z_{13} & Z_{14} & Z_{15} \\ Z_{21} & Z_{22} & Z_{23} & Z_{24} & Z_{25} \\ Z_{31} & Z_{32} & Z_{33} & Z_{34} & Z_{35} \\ Z_{41} & Z_{42} & Z_{43} & Z_{44} & Z_{45} \\ Z_{51} & Z_{52} & Z_{53} & Z_{54} & Z_{55} \end{pmatrix}^{\mathtt{PC}\pm} \begin{pmatrix} Q_1 \\ Q_2 \\ Q_3 \\ Q_4 \\ Q_5 \end{pmatrix}^{\mathtt{PC}\pm} \tag{3.4.5}$$

where $Z_{ij}^{\mathtt{PC}\pm}$ is in general different from zero.

Parity-odd (-violating) operators $\mathcal{P} = -1$ We consider the following basis, related with the supersymmetric basis

$$
\begin{aligned}
Q_1^{\mathtt{PV}\pm} &= O_{VA}^{\pm} + O_{AV}^{\pm} \\
Q_2^{\mathtt{PV}\pm} &= O_{SP}^{\pm} + O_{PS}^{\pm} \\
Q_3^{\mathtt{PV}\pm} &= -\frac{1}{2}\left\{O_{PS}^{\pm} - O_{\tilde{T}T}^{\pm} + O_{SP}^{\pm}\right\} \\
Q_4^{\mathtt{PV}\pm} &= O_{SP}^{\pm} - O_{PS}^{\pm} \\
Q_5^{\mathtt{PV}\pm} &= -\frac{1}{2}\left\{O_{VA}^{\pm} - O_{AV}^{\pm}\right\}
\end{aligned}
\tag{3.4.6}
$$

From Table 3.4.2 it is easy to obtain the symmetries of $Q_i^{\mathtt{PV}\pm}$ operators. They are summarized in table Table 3.4.4.

	$\mathcal{P}$	$\mathcal{S}$	$\mathcal{CS}'$	$\mathcal{CS}$"	$\mathcal{CPS}$'	$\mathcal{CPS}$"
$Q_1^{\mathtt{PV}\pm}$	-1	$\pm$1	-1	-1	+1	+1
$Q_2^{\mathtt{PV}\pm}$	-1	$\pm$1	+1	+1	-1	-1
$Q_3^{\mathtt{PV}\pm}$	-1	$\pm$1	+1	+1	-1	-1
$Q_4^{\mathtt{PV}\pm}$	-1	$\pm$1	$+Q_4^{\mathtt{PV}\mp}$	$-Q_4^{\mathtt{PV}\mp}$	$-Q_4^{\mathtt{PV}\mp}$	$+Q_4^{\mathtt{PV}\mp}$
$Q_5^{\mathtt{PV}\pm}$	-1	$\pm$1	$-Q_5^{\mathtt{PV}\mp}$	$+Q_5^{\mathtt{PV}\mp}$	$+Q_5^{\mathtt{PV}\mp}$	$-Q_5^{\mathtt{PV}\mp}$

Table 3.4.4: $Q_i^{\mathtt{PV}\pm}$ parity violation operator quantum numbers

The original basis of parity-even four-fermion operator $Q_i^{\mathtt{PV}\pm}$ can be decomposed into two bases, of 5 operators each, with definite $\mathcal{S} = \pm 1$. In addition from Table 3.4.4 we deduce that

- $Q_1^{\mathtt{PV}\pm}$ renormalizes multiplicatively since there are no other operators with the same symmetries.
- $Q_2^{\mathtt{PV}\pm}$ and $Q_3^{\mathtt{PV}\pm}$ share their quantum numbers which are different from those of the other operators. So they form a subset of two operators which mix between them but not with the others.
- $Q_4^{\mathtt{PV}\pm}$ and $Q_5^{\mathtt{PV}\pm}$ have not definite $\mathcal{CS}'$, $\mathcal{CS}''$, $\mathcal{CPS}'$ or $\mathcal{CPS}''$. However, they are eigenstates of $\mathcal{S}$ with definite eigenvalue $\mathcal{S} = \pm 1$, thus there is mixing between the two operators with $\mathcal{S} = 1$, i.e $Q_4^{\mathtt{PV}+}$ and $Q_5^{\mathtt{PV}+}$, and between the two operators with $\mathcal{S} = -1$, i.e $Q_4^{\mathtt{PV}-}$ and $Q_5^{\mathtt{PV}-}$.

Hence, according to the allowed mixing the parity-odd renormalization matrix is a block diagonal matrix of the form:

$$\begin{pmatrix} \hat{Q}_1 \\ \hat{Q}_2 \\ \hat{Q}_3 \\ \hat{Q}_4 \\ \hat{Q}_5 \end{pmatrix}^{\text{PV}\pm} = \begin{pmatrix} Z_{11} & 0 & 0 & 0 & 0 \\ 0 & Z_{22} & Z_{23} & 0 & 0 \\ 0 & Z_{32} & Z_{33} & 0 & 0 \\ 0 & 0 & 0 & Z_{44} & Z_{45} \\ 0 & 0 & 0 & Z_{44} & Z_{55} \end{pmatrix}^{\text{PV}\pm} \begin{pmatrix} Q_1 \\ Q_2 \\ Q_3 \\ Q_4 \\ Q_5 \end{pmatrix}^{\text{PV}\pm} \tag{3.4.7}$$

Chiral symmetry and Operator subtraction It is important to notice that in a chirally invariant regularization, the mixing pattern of both parity-odd and parity-even operators have the simplified block structure. However, on the lattice, because of the Wilson term, chiral symmetry is broken and parity-even operators mix through Eq.3.4.5.

In order to understand better the renormalization pattern of parity-even operators we will separate their mixing into

- Mixing induced by the chiral symmetry breaking due to the Wilson term, giving rise to the lattice subtracted operators.
- Mixing that survives in the continuum and has the same block structure than in the parity-odd sector.

To perform this separation, let us use a hypothetical regularization scheme which respects chiral symmetry, called χRS for short notation. With this scheme we can use chiral symmetry to establish new quantum number providing us new selection rules.

We can consider two discrete axial symmetries of the χRS. The first one acts only on flavours 2 and 4

$$\chi_{24}: \begin{cases} \psi_2 \to i\gamma_5\psi_2 \quad ; \quad \bar{\psi}_2 \to i\bar{\psi}_2\gamma_5 \\ \\ \psi_4 \to i\gamma_5\psi_4 \quad ; \quad \bar{\psi}_4 \to i\bar{\psi}_4\gamma_5 \end{cases}$$

While the second one acts only over on the flavours 1 and 2

$$\chi_{12}: \begin{cases} \psi_1 \to i\gamma_5\psi_1 \quad ; \quad \bar{\psi}_1 \to i\bar{\psi}_1\gamma_5 \\ \\ \psi_2 \to i\gamma_5\psi_2 \quad ; \quad \bar{\psi}_2 \to i\bar{\psi}_2\gamma_5 \end{cases}$$

It is straightforward to obtain the transformation of operators $O_{\Gamma^a\Gamma^b}$

$$O_{\Gamma^a\Gamma^b} \xrightarrow{\chi_{24}} -\left(\bar{\psi}_1\Gamma^a\gamma_5\psi_2\right)\left(\bar{\psi}_3\Gamma^b\gamma_5\psi_4\right)$$

$$O_{\Gamma^a\Gamma^b} \xrightarrow{\chi_{12}} -\left(\bar{\psi}_1\gamma_5\Gamma^a\gamma_5\psi_2\right)\left(\bar{\psi}_3\Gamma^b\psi_4\right)$$

$$O^S_{\Gamma^a\Gamma^b} \xrightarrow{\chi_{24}} -\left(\bar{\psi}_1\Gamma^a\gamma_5\psi_4\right)\left(\bar{\psi}_3\Gamma^b\gamma_5\psi_2\right)$$

$$O^S_{\Gamma^a\Gamma^b} \xrightarrow{\chi_{12}} -\left(\bar{\psi}_1\gamma_5\Gamma^a\psi_4\right)\left(\bar{\psi}_3\Gamma^b\gamma_5\psi_4\right)$$

The particular results for each Γ matrix is given in table Table 3.4.5

	O_{VV}	O_{AA}	O_{SS}	O_{PP}	O_{TT}	O_{VA}	O_{AV}	O_{SP}	O_{PS}	$O_{T\tilde{T}}$
χ_{24}	$-O_{AA}$	$-O_{VV}$	$-O_{PP}$	$-O_{SS}$	-1	$-O_{AV}$	$-O_{VA}$	$-O_{PS}$	$-O_{SP}$	-1
χ_{12}	+1	+1	-1	-1	-1	+1	+1	-1	-1	-1

	O^S_{VV}	O^S_{AA}	O^S_{SS}	O^S_{PP}	O^S_{TT}	O^S_{VA}	O^S_{AV}	O^S_{SP}	O^S_{PS}	$O^S_{T\tilde{T}}$
χ_{24}	$-O^S_{AA}$	$-O^S_{VV}$	$-O^S_{PP}$	$-O^S_{SS}$	-1	$-O^S_{AV}$	$-O^S_{VA}$	$-O^S_{PS}$	$-O^S_{SP}$	-1
χ_{12}	O^S_{AA}	O^S_{VV}	$-O^S_{PP}$	$-O^S_{SS}$	+1	O^S_{AV}	O^S_{VA}	$-O^S_{PS}$	$-O^S_{SP}$	+1

Table 3.4.5: $O_{\Gamma^a\Gamma^b}$ behavior under χ_{12} and χ_{24}. We have used the identities $O_{\tilde{T}\tilde{T}} = O_{TT}$ and $O_{T\tilde{T}} = O_{\tilde{T}T}$

Under these transformation the parity-even and parity-odd four-fermion operators defined in Eq.3.4.4 transform as shown in table Table 3.4.6. The χRS symmetry imposes that $Q_1^{\mathtt{PC}\pm}$ renormalizes multiplicatively because there is not any other parity-even operator with the same quantum numbers while $Q_2^{\mathtt{PC}\pm}$ and $Q_3^{\mathtt{PC}\pm}$ mix between them for the same reason. On the other hand, $Q_4^{\mathtt{PC}\pm}$ and $Q_5^{\mathtt{PC}\pm}$ do not have definite χ_{12} but from χ_{24} symmetry we deduce that at worst $Q_4^{\mathtt{PC}\pm}$ and $Q_5^{\mathtt{PC}\pm}$ mix. Therefore the renormalization pattern of parity-even four-fermion operator in the χRS system is similar to the one of the parity-odd ones (see Eq.3.4.7)

$$\begin{pmatrix} \hat{Q}_1 \\ \hat{Q}_2 \\ \hat{Q}_3 \\ \hat{Q}_4 \\ \hat{Q}_5 \end{pmatrix}^{\mathtt{PC}\pm} = \begin{pmatrix} Z_{11} & 0 & 0 & 0 & 0 \\ 0 & Z_{22} & Z_{23} & 0 & 0 \\ 0 & Z_{32} & Z_{33} & 0 & 0 \\ 0 & 0 & 0 & Z_{44} & Z_{45} \\ 0 & 0 & 0 & Z_{44} & Z_{55} \end{pmatrix}^{\mathtt{PC}\pm}_{\chi} \begin{pmatrix} Q_1 \\ Q_2 \\ Q_3 \\ Q_4 \\ Q_5 \end{pmatrix}^{\mathtt{PC}\pm}_{\chi}$$

where $\left(Q_i\right)_{\chi_{RS}}$ represent the bare operators in the χ_{RS} scheme. In matrix form we can write

$$\hat{\mathbf{Q}}^{\mathtt{PC}\pm} = \mathbf{Z}^{\mathtt{PC}\pm}_{\chi} \mathbf{Q}^{\mathtt{PC}\pm}_{\chi} \tag{3.4.8}$$

In presence of the Wilson term we also have some lattice subtracted operators in such a way that

$$\hat{\mathbf{Q}}^{\mathtt{PC}\pm} = \mathbf{Z}^{\mathtt{PC}\pm}_{\chi} \left[\mathbf{1} + \mathbf{\Delta}^{\pm}\right] \mathbf{Q}^{\mathtt{PC}\pm}$$

	$Q_1^{\mathtt{PC}\pm}$	$Q_2^{\mathtt{PC}\pm}$	$Q_3^{\mathtt{PC}\pm}$	$Q_4^{\mathtt{PC}\pm}$	$Q_5^{\mathtt{PC}\pm}$	$Q_1^{\mathtt{PV}\pm}$	$Q_2^{\mathtt{PV}\pm}$	$Q_3^{\mathtt{PV}\pm}$	$Q_4^{\mathtt{PV}\pm}$	$Q_5^{\mathtt{PV}\pm}$
χ_{24}	-1	-1	-1	+1	+1	-1	-1	-1	+1	+1
χ_{12}	+1	-1	-1	$-Q_4^{\mathtt{PC}\mp}$	$Q_5^{\mathtt{PC}\mp}$	+1	-1	-1	$-Q_4^{\mathtt{PV}\mp}$	$Q_5^{\mathtt{PV}\mp}$

Table 3.4.6: Classification of four-fermion parity-even and parity-odd operators according to the χRS discrete symmetries. Note that parity-violating operators transform in the same way.

where

$$\Delta^{\pm} = \begin{pmatrix} 0 & \Delta_{12} & \Delta_{13} & \Delta_{14} & \Delta_{15} \\ \Delta_{11} & 0 & 0 & \Delta_{24} & \Delta_{25} \\ \Delta_{31} & 0 & 0 & \Delta_{34} & \Delta_{35} \\ \Delta_{41} & \Delta_{42} & \Delta_{43} & 0 & 0 \\ \Delta_{51} & \Delta_{52} & \Delta_{53} & 0 & 0 \end{pmatrix}^{\pm}$$

We stress that, since the renormalized theory must have the desired chiral properties, the chiral renormalization pattern in Eq.3.4.8 should be recovered in the continuum limit. The remaining lattice subtracted operators Δ are due to the presence of the Wilson term, so, they should vanish in the continuum limit.

Moreover, it is also easy to convince oneself that in the chiral limit the parity-even and parity-odd renormalization constants should satisfy: $Z_{ij}^{\mathtt{PC}\pm} = Z_{ij}^{\mathtt{PV}\pm}$.

From lattice to supersymmetric basis The parity conserving operators in the lattice basis are defined as

$$\begin{aligned} O_1^{\mathtt{PC}\pm} &= O_{VV}^{\pm} + O_{AA}^{\pm} \\ O_2^{\mathtt{PC}\pm} &= O_{VV}^{\pm} - O_{AA}^{\pm} \\ O_3^{\mathtt{PC}\pm} &= O_{SS}^{\pm} - O_{PP}^{\pm} \\ O_4^{\mathtt{PC}\pm} &= O_{SS}^{\pm} + O_{PP}^{\pm} \\ O_5^{\mathtt{PC}\pm} &= O_{TT}^{\pm} \end{aligned} \tag{3.4.9}$$

while the parity violating are

$$\begin{aligned} O_1^{\mathtt{PV}\pm} &= O_{VA}^{\pm} + O_{AV}^{\pm} \\ O_2^{\mathtt{PV}\pm} &= O_{VA}^{\pm} - O_{AV}^{\pm} \\ O_3^{\mathtt{PV}\pm} &= O_{SP}^{\pm} - O_{PS}^{\pm} \\ O_4^{\mathtt{PV}\pm} &= O_{SP}^{\pm} + O_{PS}^{\pm} \\ O_5^{\mathtt{PV}\pm} &= O_{T\tilde{T}}^{\pm} \end{aligned} \tag{3.4.10}$$

A parallel analysis to the one in the previous section is followed in [75] to obtain the renormalization pattern of the four-fermion operators in the lattice basis which is also of the form

$$\begin{aligned} \hat{\mathbf{O}}^{\mathtt{PC}\pm} &= \mathbf{Z}_{\chi}^{\mathtt{PC}\pm} \left[\mathbf{I} + \mathbf{\Delta}^{\pm}\right] \mathbf{O}^{\mathtt{PC}\pm} \\ \hat{\mathbf{O}}^{\mathtt{PV}\pm} &= \mathbf{Z}_{\chi}^{\mathtt{PV}\pm} \mathbf{O}^{\mathtt{PV}\pm} \end{aligned}$$

Although the lattice basis is more suitable for numerical implementations, at the end of the day we are interested in the renormalization matrix of the parity-conserving-plus operators in the supersymmetric basis (i.e $Z_{ij}^{\mathtt{PC}+}$). Renormalization matrix in the supersymmetric basis can be obtained from the previous one in the lattice basis using the change of basis matrix $\mathbf{R}$ defined in Eq.3.2.15 through the common relation

$$\{\mathbf{Z}_{\chi}\}_{\mathbf{Q}} = \mathbf{R}^{-\mathbf{1}} \{\mathbf{Z}_{\chi}\}_{\mathbf{O}} \mathbf{R}$$

where $\{\mathbf{Z}_{\chi}\}_{\mathbf{Q}}$ refers to the block renormalization matrix in the supersymmetric basis while $\{\mathbf{Z}_{\chi}\}_{\mathbf{O}}$ refers to the corresponding one in the lattice basis.

3.4.2 Mapping of four-fermion operator

In the last section we have seen that in the absence of chiral symmetry, the parity-odd four-fermion operators in the physical basis have simpler renormalization pattern than the parity-even ones. However, we can find a setup which maps parity-even operators into parity-odd ones, allowing us to renormalize the parity-even operators, that is the ones we are interested in, in a simpler way.

Let us consider the generalized four-fermion operator defined in Eq.3.4.3. Using Eq.3.3.4, Eq.3.4.3 is rewritten in the twisted basis as

$$O_{\Gamma^a\Gamma^b}^{\pm} = \frac{1}{2}\left[\left(\bar{\chi}_1 \Gamma^a e^{i\frac{\omega}{2}\gamma_5(r_1+\eta_{\Gamma^a} r_2)}\chi_2\right)\left(\bar{\chi}_3 \Gamma^b e^{i\frac{\omega}{2}\gamma_5(r_3+\eta_{\Gamma^b} r_4)}\chi_4\right) + 2 \leftrightarrow 4\right]$$

where r_i are the Wilson parameters and η is defined in Eq.3.3.5.

Our purpose is to obtain a mapping between parity-even and parity-odd operators. In order to do that, we choose maximally twisted quarks which implies

$$\omega = \pi/2$$

with the set of Wilson parameters[6]

$$r_1 = r_2 = r_3 = -r_4 \tag{3.4.11}$$

Then one gets

$$\begin{aligned} O^{\pm}_{\Gamma^a\Gamma^b} = \; & \frac{1}{2}\Big[\left(\bar{\chi}_1\Gamma^a e^{i\frac{\pi}{4}\gamma_5(1+\eta_{\Gamma^a})}\chi_2\right)\left(\bar{\chi}_3\Gamma^b e^{i\frac{\pi}{4}\gamma_5(1-\eta_{\Gamma^b})}\chi_4\right) \\ & + \left(\bar{\chi}_1\Gamma^a e^{i\frac{\pi}{4}\gamma_5(1-\eta_{\Gamma^a})}\chi_4\right)\left(\bar{\chi}_3\Gamma^b e^{i\frac{\pi}{4}\gamma_5(1+\eta_{\Gamma^b})}\chi_2\right)\Big] \end{aligned}$$

Now, using the explicit form of η_{Γ^a} given in Eq.3.3.6 it is straightforward to obtain that

$$\begin{aligned} O^{\pm}_{PP} &= \frac{i}{2}\left[\mathcal{O}_{SP} \pm \mathcal{O}^S_{PS}\right] \\ O^{\pm}_{SS} &= \frac{i}{2}\left[\mathcal{O}_{PS} \pm \mathcal{O}^S_{SP}\right] \\ O^{\pm}_{VV} &= \frac{i}{2}\left[\mathcal{O}_{VA} \pm \mathcal{O}^S_{AV}\right] \\ O^{\pm}_{AA} &= \frac{i}{2}\left[\mathcal{O}_{AV} \pm \mathcal{O}^S_{VA}\right] \\ O^{\pm}_{TT} &= i\mathcal{O}_{\tilde{T}T} \end{aligned}$$

where operators denoted with a calligraphic letter $\mathcal{O}_{\Gamma^a\Gamma^b}$ are the same operators as $O_{\Gamma^a\Gamma^b}$ defined in Eq.3.4.1 but in the twisted basis, i.e with ψ_i replaced by χ_i

$$\begin{aligned} \mathcal{O}_{\Gamma^a\Gamma^b} &= \left(\bar{\chi}_1\Gamma^a\chi_2\right)\left(\bar{\chi}_3\Gamma^b\chi_4\right) \\ \mathcal{O}^S_{\Gamma^a\Gamma^b} &= \left(\bar{\chi}_1\Gamma^a\chi_4\right)\left(\bar{\chi}_3\Gamma^b\chi_2\right) \end{aligned} \tag{3.4.12}$$

Since, eventually, we are interested in the even-operators in the supersymmetric basis, one should consider the linear combinations

$$\begin{aligned} Q_1^{\mathtt{PC}\pm} &= O^{\pm}_{VV} + O^{\pm}_{AA} &&= i\left[\mathcal{O}^{\pm}_{VA} + \mathcal{O}^{\pm}_{AV}\right] \\ Q_2^{\mathtt{PC}\pm} &= O^{\pm}_{SS} + O^{\pm}_{PP} &&= i\left[\mathcal{O}^{\pm}_{PS} + \mathcal{O}^{\pm}_{SP}\right] \\ Q_3^{\mathtt{PC}\pm} &= -\frac{1}{2}\left\{O^{\pm}_{SS} - O^{\pm}_{TT} + O^{\pm}_{PP}\right\} &&= -\frac{i}{2}\left[\mathcal{O}^{\pm}_{PS} - \mathcal{O}^{\pm}_{\tilde{T}T} + \mathcal{O}^{\pm}_{SP}\right] \\ Q_4^{\mathtt{PC}\pm} &= O^{\pm}_{SS} - O^{\pm}_{PP} &&= i\left[\mathcal{O}^{\mp}_{PS} - \mathcal{O}^{\mp}_{SP}\right] \\ Q_5^{\mathtt{PC}\pm} &= -\frac{1}{2}\left\{O^{\pm}_{VV} - O^{\pm}_{AA}\right\} &&= -\frac{i}{2}\left[\mathcal{O}^{\mp}_{VA} - \mathcal{O}^{\mp}_{AV}\right] \end{aligned} \tag{3.4.13}$$

Alternatively in the lattice basis one gets

[6] or one of the eight equivalent permutation choices with one r_i with opposite sign.

$$
\begin{aligned}
O_1^{\mathtt{PC}\pm} &= O_{VV}^{\pm} + O_{AA}^{\pm} &&= i\left[\mathcal{O}_{VA}^{\pm} + \mathcal{O}_{AV}^{\pm}\right] \\
O_2^{\mathtt{PC}\pm} &= O_{VV}^{\pm} - O_{AA}^{\pm} &&= i\left[\mathcal{O}_{VA}^{\mp} - \mathcal{O}_{AV}^{\mp}\right] \\
O_3^{\mathtt{PC}\pm} &= O_{SS}^{\pm} - O_{PP}^{\pm} &&= i\left[\mathcal{O}_{PS}^{\mp} - \mathcal{O}_{SP}^{\mp}\right] \\
O_4^{\mathtt{PC}\pm} &= O_{SS}^{\pm} + O_{PP}^{\pm} &&= i\left[\mathcal{O}_{PS}^{\pm} + \mathcal{O}_{SP}^{\pm}\right] \\
O_5^{\mathtt{PC}\pm} &= O_{TT}^{\pm} &&= i\mathcal{O}_{\tilde{T}T}^{\pm}
\end{aligned}
\tag{3.4.14}
$$

In the last equality of Eq.3.4.13 and Eq.3.4.14 we identify the parity violating operators in the twisted basis $\mathcal{Q}_i^{\mathtt{PV}}$ and $\mathcal{O}_i^{\mathtt{PV}}$ respectively defined in Eq.3.4.6 and Eq.3.4.10 but now written in terms of twisted quarks χ_i instead of ψ_i. That is

$$
\begin{aligned}
Q_1^{\mathtt{PC}\pm} &= i\mathcal{Q}_1^{\mathtt{PV}\pm} & O_1^{\mathtt{PC}\pm} &= i\mathcal{O}_1^{\mathtt{PV}\pm} \\
Q_2^{\mathtt{PC}\pm} &= i\mathcal{Q}_2^{\mathtt{PV}\pm} & O_2^{\mathtt{PC}\pm} &= i\mathcal{O}_2^{\mathtt{PV}\mp} \\
Q_3^{\mathtt{PC}\pm} &= i\mathcal{Q}_3^{\mathtt{PV}\pm} & O_3^{\mathtt{PC}\pm} &= -i\mathcal{O}_3^{\mathtt{PV}\mp} \\
Q_4^{\mathtt{PC}\pm} &= -i\mathcal{Q}_4^{\mathtt{PV}\mp} & O_4^{\mathtt{PC}\pm} &= i\mathcal{O}_4^{\mathtt{PV}\pm} \\
Q_5^{\mathtt{PC}\pm} &= i\mathcal{Q}_5^{\mathtt{PV}\mp} & O_5^{\mathtt{PC}\pm} &= i\mathcal{O}_5^{\mathtt{PV}\pm}
\end{aligned}
\tag{3.4.15}
$$

Note that the switching parity $(\pm)$ becomes $(\mp)$ for Q_4, Q_5 and O_2, O_3 and notice also the presence of the minus sign between PC and PV for Q_4 and O_3.

3.4.3 Renormalized B_i without wrong chirality mixings

To derive the renormalized formulae for bag parameters one has to specify the flavour of each one of the fields ψ_i appearing in Eq.3.4.1 so that parity-even operators in $Q_i^{\pm}$ Eq.3.4.4 reduce to the original Q_i operators for the $\overline{M} - M$ neutral pseudoscalar meson oscillations in the supersymmetric basis Eq.3.2.9. Since the parity-even operators maps into the parity-odd if one of the valence quarks has different Wilson parameter one can not set simply $\psi_2 = \psi_4 = l$ and $\psi_1 = \psi_3 = h$. For this reason we are led to introduce *replicas* of the usual h and l quarks, denoted by h' and l' . The identification we require is: $\psi_1 = h$, $\psi_2 = l$, $\psi_3 = h'$ and $\psi_4 = l'$. In order to obtain correlators that in the continuum are equal to those of the standard action without replicas we must require: $m_h = m_{h'}$ and $m_l = m_{l'}$. According to Eq.3.4.11 the Wilson parameters of the valence heavy and light fields are taken to be

$$
r_1 = r_2 = r_3 = -r_4 \;\rightarrow\; r_l = r_h = r_{l'} = -r_{h'} = 1 \tag{3.4.16}
$$

Let us now briefly overview how the three-point correlator in the theory with only two flavour (h and l) could contain the same information as the one in the theory with

four species of OS quarks.

The generic three-point correlator in the theory with four quarks is given by

$$C^{(3)}_{O^{+}_{\Gamma\Gamma}(h,h',l,l')}(x_0) = 2\sum_{\vec{y}}\langle 0|\mathcal{P}^{12}_{y_0}O^{+}_{\Gamma\Gamma}(\vec{x},x_0)\mathcal{P}^{34}_{y_0+T_{\rm sep}}|0\rangle \tag{3.4.17}$$

where $O^{+}_{\Gamma\Gamma}$ is the local four-fermion operator

$$\begin{aligned} O^{+}_{\Gamma\Gamma} &= \left[\left(\bar{\psi}_1\Gamma\psi_2\right)\left(\bar{\psi}_3\Gamma\psi_4\right) + \left(\bar{\psi}_1\Gamma\psi_4\right)\left(\bar{\psi}_3\Gamma\psi_2\right)\right] \\ &= \left[\left(\bar{h}\Gamma l\right)\left(\bar{h}'\Gamma l'\right) + \left(\bar{h}\Gamma l'\right)\left(\bar{h}'\Gamma l\right)\right] \end{aligned}$$

while considering only two flavours

$$C^{(3)}_{O_{\Gamma\Gamma}(h,l)} = \sum_{\vec{y}}\langle 0|\mathcal{P}_{y_0}O_{\Gamma\Gamma}(\vec{x},x_0)\mathcal{P}_{y_0+T_{\rm sep}}|0\rangle$$

with

$$O_{\Gamma\Gamma} = \left(\bar{\psi}_1\Gamma\psi_2\right)\left(\bar{\psi}_1\Gamma\psi_2\right) = \left(\bar{h}\Gamma l\right)\left(\bar{h}\Gamma l\right)$$

If $\psi_1,...,\psi_4$ have different flavours, both terms in $O^{\pm}_{\Gamma\Gamma}$, the normal one and the switched, are needed to give rise to the connected and disconnected three-point correlation functions which spontaneously arise in the two-flavours theory with only h and l flavours. On the other hand, the factor 2 in Eq.3.4.17 has been introduced in order to take into account the double Wick contraction arising in $C^{(3)}_{O_{\Gamma\Gamma}(h,l)}$. Thus, by an elementary application of the Wick theorem one has $C^{(3)}_{O^{+}_{\Gamma\Gamma}(h,h',l,l')} = C^{(3)}_{O_{\Gamma\Gamma}(h,l)}$.

Finally, considering also the renormalization pattern of the TM and OS bilinear operators in Table 3.3.1 one easily arrives to

$$\begin{aligned} &\frac{1}{\xi_1}\frac{Z_{11}}{Z_A Z_V}\frac{C^{(3)}_{Q_1}(x_0)}{C^{(2)}_{PA}(x_0)C^{\prime(2)}_{PA}(x_0)} \xrightarrow[y_0\ll x_0\ll y_0+T_{\rm sep}]{} \hat{B}_1 \\ &\frac{1}{\xi_i}\frac{Z_{ij}}{Z_P Z_S}\frac{C^{(3)}_{Q_i}(x_0)}{C^{(2)}_{PP}(x_0)C^{\prime(2)}_{PP}(x_0)} \xrightarrow[y_0\ll x_0\ll y_0+T_{\rm sep}]{} \hat{B}_i \;\; i=2,...,5 \end{aligned} \tag{3.4.18}$$

To conclude this chapter, I would like to stress again that both $\mathcal{O}(a)$ improvement and continuum-like renormalization pattern are achieved at a low CPU cost by using a different regularization for the internal (sea) quarks, responsible for the QCD corrections, and boundary (valence) quarks, which describe the interactions, as it was introduced in subsection 2.2.5. Sea quarks are introduced in pairs satisfying the twisted mass action at maximal twist in order to avoid $\mathcal{O}(a)$ discretization errors as it was shown in subsection 2.2.4.2. On the valence sector, by replicating the valence flavours and regularizing them according to the OS action Eq.2.2.20 with Wilson coefficients r_i of suitably signs, mixing with operators of wrong chirality or parity is avoided.

Chapter 4

Non perturbative renormalization of lattice operators

The renormalization constants (RCs) computation of lattice operators is a necessary ingredient to obtain most physical results from numerical simulations. In the OPE formalism, any physical amplitude induced by the operator is given by [38]

$$M_{\alpha\to\beta} = c_W(\mu) Z_O(\mu, g(a)) \langle\alpha|O(a)|\beta\rangle$$

where $c_W(\mu)$ is the Wilson coefficient calculated in perturbation theory at the renormalization scale μ and $\langle\alpha|O(a)|\beta\rangle$ is the matrix element of the bare lattice operator $O(a)$. The renormalization constant Z_O is the link between the matrix element regularized on the lattice, and the one renormalized in the continuum.

Several methods have been implemented in the lattice in order to compute the non perturbative matrix element

- Lattice Perturbation Theory (PT)[76, 77, 78, 79]
- Non Perturbative (NP) methods:
  - In some limited cases, lattice Ward Identities (WI) provide a fully non perturbative determination of RCs [80, 81]. RCs are computed by requiring that renormalized lattice Green functions satisfy the proper chiral WI. This approach can be applied only to scale independent RCs such as the vectorial or axial currents.
  - Renormalization conditions imposed on quark and gluon Green functions with operator insertions at a given scale. In the RI-MOM method, proposed in [82] renormalization conditions are imposed for large external momenta, while in the Schrödinger Functional (SF) they are imposed for small volume [83].

In the following I will overview and use the RI-MOM method proposed in [82] which completely avoids lattice perturbation theory providing us a non perturbative determination of the renormalization constants of any operator, essential in lattice QCD calculations which aim at a percent level of accuracy.

RI-MOM method consists in *imposing renormalization conditions non perturbatively directly on quark and gluon Green functions, in a fixed gauge, with given off-shell external states to calculate the renormalization constants of lattice operators.*

This chapter is organized as follows: In the first section I will review the basic ideas of the RI-MOM method. In the second section I will discuss the RI-MOM approach applied to bilinear operators. The discussion will be generalized to the $\Delta F = 2$ four-fermion operators in the third section. Finally, I will focus on the numerical results for the $N_f = 4$ RCs.

Numerical results for the RCs with $N_f = 2$, relevant for the renormalization of the bag parameters in the following chapters, will not be discussed here. RCs of bilinear operators are well-known and publish [84]. I will only update these results including an extra finer lattice spacing. The analysis of the RCs of the four fermion operators in the $N_f = 2$ simulation follows similar techniques as the ones presented here in the case of $N_f = 4$. For this reason, I will limit myself to present the main results for the RCs of $N_f = 2$ in Appendix G and use them on chapter 5 and chapter 6.

4.1 RI-MOM method

The RI-MOM method consists in mimicking on the lattice what one usually does in the continuum perturbation theory to renormalize operators. Renormalization conditions are fixed by imposing that Green functions of a certain operator on momentum space, computed between external off-shell quark states, in a fixed gauge and at a given scale μ, coincide with their tree-level value. Schematically we impose the renormalization condition

$$\langle p'|O(\mu)|p\rangle|_{\,p^2=-\mu^2} = \langle p'|O|p\rangle|_{\,\text{tree-level}} \tag{4.1.1}$$

The renormalization condition depends on the external states and on the gauge, which must be fixed. In general, one has the freedom to choose the external quark states with different momenta, the so-called SMOM scheme [85, 86], but for simplicity we have considered Green's functions where all external quark legs have the same momentum p.

Physical results are obtained by combining the matrix element of the renormalized operator $O(\mu)$ with the corresponding Wilson coefficient computed in the same renormalization scheme and at the same scale. This matching requires perturbation theory. As a consequence, renormalization conditions need to be imposed at large p^2 in order to keep under control non perturbative effects in the matching. The RI-MOM method is expected to work if the *window* $\Lambda_{\text{QCD}} \ll \mu \ll a^{-1}$ exists, where the left inequality is required to allow the perturbative matching while the right one is necessary to avoid $\mathcal{O}(a)$ discretization effects.

To facilitate the renormalization procedure operators can be classified into three main classes, according to their ultraviolet behaviour as $a \to 0$

Logarithmically divergent operators This is a large family of operators including the scalar, pseudoscalar and tensorial densities or $\Delta F = 2$ four-fermion operators. We will outline the fermion bilinear RCs in section 4.2. The extension to four-fermion operators and the operator-mixing will be discussed in detail in section 4.3.

Finite operators These operators include some particular cases as the vector and axial currents as well as the ratio of the scalar and pseudoscalar renormalization constants. In this case we do not have the freedom of fixing the renormalization conditions in an arbitrary way. The renormalization conditions are acceptable only if they are compatible with the WI.

Power divergent operators Operators are divergent in $1/a$ when mixing with lower dimensional operators is possible. Examples are encountered in the operators relevant to deep inelastic scattering, in the $\Delta I = 1/2$ transitions or in operators of order $1/m$ in HQET.

Since power divergent operators do not appear in the neutral meson mixing we will restrict ourselves only to logarithmically divergent and finite operators.

4.1.1 $\mathcal{O}(a)$ improvement of RI-MOM renormalization constants at maximal twist

At maximal twist the RI-MOM form factors from which RCs are extracted are automatically $\mathcal{O}(a)$ improved at all p^2 values. The proof of automatic $\mathcal{O}(a)$ improvement for the RI-MOM RCs in maximally twisted QCD is based on the exact invariance of the Twisted Mass action at maximal twist under $P \times D \times (M_0 \to -M_0)$ and was firstly presented in appendix A of [87].

The proof follows the same steps as in subsection 2.2.4.2. RCs are parity-even. But, the invariance of the maximally twisted QCD action under $P \times D \times (M_0 \to -M_0)$ implies, as shown in [87], that $\mathcal{O}(a^{2k+1})$ discretization errors on lattice correlators arise, in their Symanzik expansion, from the insertion of parity-odd Symanzik operators. Therefore, $\mathcal{O}(a^{2k+1})$ cutoff effects must be absent in the Symanzik expansion of parity-even form factors, as RCs are.

4.2 Renormalization constants of bilinear operators

Let us consider the two fermion operators corresponding to a twisted doublet of quarks[1] (u, d) with $r_u = -r_d = 1$

$$O_\Gamma = \bar{u}\Gamma d$$

where Γ is one of the Dirac matrices. The renormalization constant Z_Γ is defined by

[1] As pointed out in subsection 3.3.1, RCs for $O_\Gamma = \bar{u}\Gamma d$ with $r_u = -r_d = 1$ and $O_\Gamma = \bar{u}\Gamma u$, that is for OS and TM formulations differ by cutoff effects of $\mathcal{O}(a^2)$ at maximal twist. For convenience, we will derive all expressions considering a twisted doublet.

$$O_\Gamma(\mu) = Z_\Gamma(\mu, g(a))O_\Gamma(a) \tag{4.2.1}$$

Projecting Eq.4.1.1 on tree-level and considering the trace over color and spin

$$Z_\Gamma(\mu, g(a))Z_q^{-1}(\mu, g(a))\mathrm{Tr}(\Lambda_\Gamma(ap)P_\Gamma)\big|_{p^2=-\mu^2} = 1 \tag{4.2.2}$$

where Z_q, is the quark field RC and Λ_Γ is the amputed Green function calculated from the *expectation value* of the non amputated Green function G_Γ and the quark propagators in momentum space as

$$\Lambda_\Gamma(ap) = S_u(ap)^{-1}G_\Gamma(ap)S_d(ap)^{-1} \tag{4.2.3}$$

Here, P_Γ is a suitable projector on the tree-level operator. For instance, $P_\Gamma = I\,(\gamma_5)$ for the scalar (pseudoescalar) case. *Expectation value* of the non-amputed Green function means that one averages the Green functions over the gauge field configurations generated by the Monte Carlo simulation

$$G_\Gamma(x,y) = \langle u(x)O_\Gamma(0)\bar{d}(y)\rangle = \frac{1}{N}\sum_{i=1}^{N} S_u^i(x,0)\Gamma S_d^i(0,y) \tag{4.2.4}$$

here, i=1,...,N denotes the gauge field configurations. From Eq.4.2.4 one gets the Green function Fourier transform in momentum space

$$G_\Gamma(ap) \equiv a^8 \sum_{x,y} e^{-ip(x-y)}G_\Gamma(x,y) = \frac{1}{N}\sum_{i=1}^{N} S_u^i(ap|0)\Gamma(\gamma_5 S_u^{i\dagger}(ap|0)\gamma_5) \tag{4.2.5}$$

where we used the hermiticity of the quark propagator (see Appendix B) over one single configuration

$$\sum_y e^{ipy}S_d(0,y) = \gamma_5 S_u(p)^\dagger\gamma_5$$

We have defined

$$S_q(ap|y) = a^4\sum_x S_q(x,y)e^{-ipx} \tag{4.2.6}$$

and the propagator in momentum space is also computed averaging over the configurations

$$S_q(ap) = \frac{1}{N}\sum_{i=1}^{N} S_q^i(ap|0)$$

The renormalization condition defined in Eq.4.2.2 defines a renormalization constant which is independent of the regularization scheme, in fact the name of RI-MOM stands for Regularization Independent MOMentum subtraction. However, it still depends on the gauge due to the gauge dependence of the matrix elements and quark-gluon states. As

a consequence, the gauge field configurations which are generated with a gauge-invariant algorithm have to be gauge-fixed, in particular our gauge configurations are fixed to the Landau gauge [88][2] in order to calculate the propagators $S_q(x,0)$.

RCs are named after the twisted rotation at maximal twist where the Wilson term has its standard form, i.e having no γ_5, while the operator $O_\Gamma = \bar{u}\Gamma d$ is expressed in the physical quark basis. Thus, in practice Eq.4.2.2 is implemented by

$$Z_\Gamma(ap)Z_q^{-1}(ap)\mathcal{V}_\Gamma(ap)\big|_{p^2=-\mu^2} = 1 \tag{4.2.7}$$

where

$$\mathcal{V}_\Gamma(ap) \equiv \mathrm{Tr}(\Lambda_{\tilde{\Gamma}}(ap)P_\Gamma)/12 \tag{4.2.8}$$

is the amputated projected Green function and

$$\tilde{\Gamma} = e^{-i\gamma_5\pi/4}\Gamma e^{i\gamma_5\pi/4}$$

In the RI'-MOM scheme[3] Z_q is given by

$$Z_q(a\tilde{p}) = -\frac{i}{12}\mathrm{Tr}\left[\frac{\tilde{\not{p}}S(ap)^{-1}}{\tilde{p}^2}\right]\Bigg|_{p^2=-\mu^2} \tag{4.2.9}$$

where $\tilde{p}$ is introduced in the numerical calculation in order to minimize discretization effects

$$a^2p^2 \to \sum_{\nu=1}^{4}\sin^2(ap_\nu) \equiv \sum_{\nu=1}^{4} a^2\tilde{p}^2 \qquad a\not{p} \to \textstyle\sum_{\nu=1}^{4}\gamma_\nu \sin(ap_\nu) \equiv a\tilde{\not{p}} \tag{4.2.10}$$

The quark propagator $S_q(p)$ together with the amputated vertex $\Lambda_\Gamma(p)$ are the necessary Green functions for the RI-MOM determination of RCs of bilinear quark operators.

With twisted mass fermions, the explicit breaking of parity at finite lattice spacing allows for the presence in the quark propagator of parity violating contributions which are absent in the Wilson case. By neglecting Euclidean symmetry $O(4)$ violating effects,

[2]The gauge is fixed to Landau through $U_\mu^G(x) = G(x)U_\mu(x)G^\dagger(x+\mu)$, where G is the gauge transformation projecting the links in the Landau gauge: $\partial_\mu A_\mu^G = 0+$ periodic boundary conditions. The gauge fixing algorithm is based on the minimization of a functional $F_U[G]$ constructed in such a way that its extrema are the gauge fixing transformations corresponding to the gauge condition. The standard form for the Landau gauge is $F_U[G] = -\mathrm{Re}\,\mathrm{Tr}\sum_{\mu,x} U_\mu^{G(x)}(x)$ and the transformation G for which $\partial F/\partial G = 0$ rotates the links to the gauge $\partial_\mu A_\mu^G = 0$.

[3]Strictly speaking, the renormalization condition of equation Eq.4.2.9 defines the so called RI'-MOM scheme while

$$Z_q = -\frac{i}{12}\mathrm{Tr}\left[\frac{\partial S(p)^{-1}}{\partial\not{p}}\right]|_{p^2=-\mu^2}$$

defines the original RI-MOM scheme. The main advantage of the RI'-MOM definition is that it avoids the computation of the derivate. In the Landau gauge, the two schemes differ at the N^2LO.

which appear at $\mathcal{O}(a^2)$ or higher, the inverse quark propagator in the physical basis can be expressed in terms of three scalar form factors as

$$S_q(a^2\tilde{p}^2) = i\not{p}\Sigma_1(a^2\tilde{p}^2) + \Sigma_2(a^2\tilde{p}^2) - i\gamma_5\Sigma_3(a^2\tilde{p}^2) \tag{4.2.11}$$

which can be evaluated from

$$\begin{aligned}
\Sigma_1(a^2\tilde{p}^2) = &\quad -\frac{i}{12N(p)}\mathrm{Tr}\left[\sum_\rho{}' \left(\gamma_\rho S_q(a^2\tilde{p}^2)^{-1}\right)/\tilde{p}_\rho\right] \\
\Sigma_2(a^2\tilde{p}^2) = &\quad \frac{1}{12}\mathrm{Tr}\left[S\right] \\
\Sigma_3(a^2\tilde{p}^2) = &\quad \frac{i}{12}\mathrm{Tr}\left[\gamma_5 S\right]
\end{aligned}$$

where the sum $\sum_\rho{}'$ only runs over the Lorentz indices for which p_ρ is different from zero and $N(p) = \sum_\rho{}' 1$. Σ_1 is equivalent to the definition of Z_q in Eq.4.2.9 up to $\mathcal{O}(a)$ terms and it is adopted as our definition for the quark field RC, Z_q.

On the other hand, at large p^2, Σ_2 is related to the renormalized quark mass and the parity violating term proportional to Σ_3 represents an $\mathcal{O}(a)$ discretization effect, induced by the twisted Wilson term in the action.

The procedure described above implicitly involves two main steps: the extrapolation of the RCs computed at a fixed coupling and renormalization scale to the chiral limit and the study of the renormalization scale dependence. Both points will be described in detail in subsection 4.4.3 where the analysis of $N_f = 4$ RCs is discussed.

4.2.1 Bilinear GB-pole contribution

The renormalization condition Eq.4.2.2, which defines the RI-MOM scheme, is implemented in the chiral limit. For getting a mass independent renormalization scheme. Since numerically the RCs are obtained at non vanishing values of the quark masses, an extrapolation of the results to the chiral limit both in the valence and in the sea must be performed. However, the validity of the RI-MOM approach relies on the fact that non perturbative contributions to Green functions vanish asymptotically at large p^2 so, in this region, the Green functions are expected to be smooth functions of the quark masses. The condition $\mu \gg \Lambda_{QCD}$ ensures that non perturbative contributions remain under control. However, among the bilinear quark operators specific care must be taken in the study of the pseudoscalar Green function $\mathcal{V}_P$ since in this case, due to the coupling with the Goldstone boson, the leading power suppressed contribution is divergent in the chiral limit [82] and the condition $\mu \gg \Lambda_{QCD}$ may not be enough.

The existence of these GB-pole contribution can be understood as follows. At asymptotically large p^2, non perturbative effects giving contributions potentially divergent in the chiral limit to the Green functions do vanish and the latter turns out to have a polynomial dependence in the quark mass parameters. At finite values of p^2, however, the contributions to the spectral decomposition of these Green functions from one Goldstone

boson intermediate state with momentum q and mass M_{PS} give rise to terms proportional to $(q^2 + M_{PS}^2)^{-1}$ suppressed by some power of $1/p^2$.

Such non perturbative contributions to the Green function, though suppressed by a factor $1/p^2$, are divergent in the chiral limit and therefore they must be disentangled and removed.

Let us consider the Fourier transform of the Green function of $O_\Gamma(0) = \bar{\psi}(0)\Gamma\psi(0)$

$$G_\Gamma(p,p') = \int d^4x\, d^4y\, e^{-ipx+ip'y} \langle 0|T\left[\psi(x)O_\Gamma(0)\bar{\psi}(y)\right]|0\rangle = \langle 0|T\left[\psi(p)O_\Gamma(0)\bar{\psi}(p')\right]|0\rangle \tag{4.2.12}$$

The Lehmann-Symanzik-Zimmermann (LSZ) reduction formula can be used to reduce interacting fields in a Green function and replace them by the projector on an intermediate state of the spectrum of the field multiplicated by the momentum space propagator of the particle. In particular, if the operator O_Γ couples to the pion, using the LSZ theorem Eq.4.2.12 can be reduced to

$$G_\Gamma(p,p') = \langle 0|T\left[\psi(p)\bar{\psi}(p')\right]|P(q)\rangle \frac{1}{q^2 + M_{PS}^2} \langle P(q)|O_\Gamma(0)|0\rangle + ... \tag{4.2.13}$$

where $q = p - p'$ and $|P(q)\rangle$ is the GB which we can identify with the π meson. The dots indicate terms which have no pion poles. From Eq.4.2.13 it is clear that an infrared divergence can appear when working at exceptional momenta $p_\mu = p'_\mu \;\rightarrow\; q_\mu = 0$.

The axial operator couples to the pion state through

$$\langle 0|A(0)|P(q)\rangle \sim f_{PS}\, q_\mu \tag{4.2.14}$$

But if we insert Eq.4.2.14 in Eq.4.2.13 and then we impose exceptional momenta $q_\mu = 0$, the contribution of the GB-pole vanish when taking the continuum limit.

However, for the pseudoscalar operator one has

$$\langle 0|P_5(0)|P(q)\rangle \sim \frac{\langle\bar{\psi}\psi\rangle}{f_{PS}}$$

where due to spontaneous breaking of $SU(3)_A$, the chiral condensate takes a non zero value in the chiral limit. In this case the matrix element of the operator between a pion and a vacuum state goes to a non zero constant. Therefore, when taking $q_\mu = 0$ Eq.4.2.13 gives a $1/M_{PS}^2$ pole.

A further reduction is possible for large p^2. Using the OPE formalism the behavior of $\langle 0|T\left[\psi(p)\bar{\psi}(p')\right]|P(q)\rangle$ can be computed in perturbation theory (see appendix A of [82])

$$\langle 0|T\left[\psi(p)\bar{\psi}(p')\right]|P(q)\rangle \rightarrow c\Lambda_{QCD}^4 \frac{\ln^\delta(p^2/\mu^2)}{p^2} \tag{4.2.15}$$

which indicates that the non perturbative contribution of the GB-pole is suppressed by a factor $1/p^2$.

4.3 Renormalization constants of four-fermion operators

Now we come to the case of the RCs for $\Delta F = 2$ four-fermions operators, which enter in the effective Hamiltonian of weak interactions controlling the neutral meson oscillations. As discussed in section 3.4 due to the explicit breaking of chiral symmetry induced by the Wilson term, four-fermion operators mix with operators of the same dimension but different chirality. As showed there, the renormalization pattern of parity violating operators defined in Eq.3.4.10 follows the continuum one

$$\hat{\mathbf{O}}^{\mathtt{PV}\pm} = \mathbf{Z}_\chi{}^{\mathtt{PV}\pm}\mathbf{O}^{\mathtt{PV}\pm} \tag{4.3.1}$$

while for the parity conserving defined in Eq.3.4.9 the explicit breaking of the chiral symmetry induces an additional mixing parametrized by $\mathbf{\Delta}$

$$\hat{\mathbf{O}}^{\mathtt{PC}\pm} = \mathbf{Z}_\chi{}^{\mathtt{PC}\pm}\left[\mathbf{1} + \mathbf{\Delta}^{\pm}\right]\mathbf{O}^{\mathtt{PC}\pm} \tag{4.3.2}$$

The procedure to implement the non perturbative RI-MOM computation of the four-fermion RCs has been presented in [75] and it is just a generalization of that explained for bilinears. Here we overview the formulae in [75] including the peculiarities of our approach with four OS species characterized by their Wilson parameters r_1, r_2, r_3 and r_4 satisfying the relation $r_1 = r_2 = r_3 = -r_4$.

The lattice bare non amputated Green function of the operator $O^{\pm}_{\Gamma_1\Gamma_2}$ can be computed through

$$G^{\pm}_{\Gamma_{(1)}\Gamma_{(2)}}(x_1,x_2,x_3,x_4) = \langle\psi_1(x_1)\bar{\psi}_2(x_2)O^{\pm}_{\Gamma_{(1)}\Gamma_{(2)}}\psi_3(x_3)\bar{\psi}_4(x_4)\rangle \tag{4.3.3}$$

where $\langle ...\rangle$ stands for the expectation value obtained by averaging over the gauge configurations. The generic four-fermion operator $O^{\pm}_{\Gamma_{(1)}\Gamma_{(2)}}$ placed at the origin reads

$$O^{\pm}_{\Gamma_{(1)}\Gamma_{(2)}}(0) = \frac{1}{2}\left[\bar{\psi}_1(0)\Gamma_{(1)}\psi_2(0)\bar{\psi}_3(0)\Gamma_{(2)}\psi_4(0) \pm \bar{\psi}_1(0)\Gamma_{(1)}\psi_4(0)\bar{\psi}_3(0)\Gamma_{(2)}\psi_2(0)\right] \tag{4.3.4}$$

with $\Gamma_{(1)} = \Gamma_{(2)}$ for PC operators and $\Gamma_{(1)} \neq \Gamma_{(2)}$ for the PV ones. For notational economy we are dropping the super-index PC and PV when it is not necessary.

The Fourier transform of the non amputated Green function Eq.4.3.3 at equal external momenta takes the explicit form

$$G^{\pm}_{\Gamma_{(1)}\Gamma_{(2)}}(ap)^{ABCD}_{\alpha\beta\gamma\delta} = \frac{1}{2}\left[\langle G^{r_1,r_3}_{\Gamma_{(1)}}(ap)^{AB}_{\alpha\beta}G^{r_2,r_4}_{\Gamma_{(2)}}(ap)^{CD}_{\gamma\delta}\rangle \mp \langle G^{r_1r_4}_{\Gamma_{(1)}}(ap)^{AD}_{\alpha\delta}G^{r_2,r_3}_{\Gamma_{(2)}}(ap)^{CB}_{\gamma\beta}\rangle\right]$$

where the change of sign with respect Eq.4.3.4 is due to the commutation of fields ψ, which are Grassman variables, and $G_{\Gamma_{(i)}}(p)$ denotes the Fourier transform of the bilinear amputated Green function

$$G^{r_1,r_2}_{\Gamma_{(i)}}(ap)^{AB}_{\alpha\beta} = S_{r_1}(ap|0)^{AR}_{\alpha\rho}\,(\Gamma_i)_{\rho\sigma}\,S_{r_2}(0|ap)^{RB}_{\sigma\beta}$$

with the short hand notation $S_{r_2}(0|ap)^{RB}_{\sigma\beta} = \left(\gamma_5 S^{\dagger}_{-r_2}(ap|0)\gamma_5\right)^{RB}_{\sigma\beta}$ and $S(ap|0)$ given in Eq.4.2.6. The amputated Green function is obtained by multiplying $G^{\pm}_{\Gamma_1\Gamma_2}$ by the four inverse quark propagators

$$\begin{aligned}\Lambda^{\pm}_{\Gamma_{(1)}\Gamma_{(2)}}(ap)^{RSR'S'}_{\rho\sigma\rho'\sigma'} = \; & S^{-1}_{r_1}(0|ap)^{RA}_{\rho\alpha} S^{-1}_{r_3}(0|ap)^{R'C}_{\rho'\gamma} \\ & \times G^{\pm}_{\Gamma_{(1)}\Gamma_{(2)}}(ap)^{ABCD}_{\alpha\beta\gamma\delta} \\ & \times S^{-1}_{r_2}(ap|0)^{BS}_{\beta\sigma} S^{-1}_{r_4}(ap|0)^{DS'}_{\delta\sigma'}\end{aligned} \tag{4.3.5}$$

As in the case of bilinear operators we now have to consider the tree-level projectors which should satisfy the orthogonality relation

$$\mathrm{Tr}\left[\mathbf{\Lambda}^{\pm(0)}_i \mathbf{P}^{\pm}_k\right] = \delta_{ik}$$

with the labels i and k running over all the operators of the basis and $\Lambda^{\pm(0)}_i$ denotes the tree-level amputated Green function. The explicit form of the projectors is given in [75]. The parity conserving ones are

$$\mathbf{P}^{\mathtt{PC}\pm}_1 \equiv +\frac{1}{64N_c(N_c \pm 1)}\left(\mathbf{P}_{VV} + \mathbf{P}_{AA}\right)$$

$$\mathbf{P}^{\mathtt{PC}\pm}_2 \equiv +\frac{1}{64(N_c^2-1)}\left(\mathbf{P}_{VV} - \mathbf{P}_{AA}\right) \pm \frac{1}{32N_c(N_c^2-1)}\left(\mathbf{P}_{SS} - \mathbf{P}_{PP}\right)$$

$$\mathbf{P}^{\mathtt{PC}\pm}_3 \equiv \pm\frac{1}{32N_c(N_c^2-1)}\left(\mathbf{P}_{VV} - \mathbf{P}_{AA}\right) + \frac{1}{16(N_c^2-1)}\left(\mathbf{P}_{SS} - \mathbf{P}_{PP}\right)$$

$$\mathbf{P}^{\mathtt{PC}\pm}_4 \equiv +\frac{(2N_c \pm 1)}{32N_c(N_c^2-1)}\left(\mathbf{P}_{SS} + \mathbf{P}_{PP}\right) \mp \frac{1}{32N_c(N_c^2-1)}\mathbf{P}_{TT}$$

$$\mathbf{P}^{\mathtt{PC}\pm}_5 \equiv \mp\frac{1}{32N_c(N_c^2-1)}\left(\mathbf{P}_{SS} + \mathbf{P}_{PP}\right) + \frac{(2N_c \mp 1)}{96N_c(N_c^2-1)}\mathbf{P}_{TT}$$

while the parity violating are

$$\mathbf{P}_1^{\text{PV}\pm} \equiv -\frac{1}{64N_c(N_c \pm 1)}\left(\mathbf{P}_{VA} + \mathbf{P}_{AV}\right)$$

$$\mathbf{P}_2^{\text{PV}\pm} \equiv -\frac{1}{64(N_c^2-1)}\left(\mathbf{P}_{VA} - \mathbf{P}_{AV}\right) \mp \frac{1}{32N_c(N_c^2-1)}\left(\mathbf{P}_{SP} - \mathbf{P}_{PS}\right)$$

$$\mathbf{P}_3^{\text{PV}\pm} \equiv \mp\frac{1}{32N_c(N_c^2-1)}\left(\mathbf{P}_{VA} - \mathbf{P}_{AV}\right) - \frac{1}{16(N_c^2-1)}\left(\mathbf{P}_{SP} - \mathbf{P}_{PS}\right)$$

$$\mathbf{P}_4^{\text{PV}\pm} \equiv +\frac{(2N_c \pm 1)}{32N_c(N_c^2-1)}\left(\mathbf{P}_{SP} + \mathbf{P}_{PS}\right) \mp \frac{1}{32N_c(N_c^2-1)}\mathbf{P}_{T\tilde{T}}$$

$$\mathbf{P}_5^{\text{PV}\pm} \equiv \mp\frac{1}{32N_c(N_c^2-1)}\left(\mathbf{P}_{SP} + \mathbf{P}_{PS}\right) + \frac{(2N_c \mp 1)}{96N_c(N_c^2-1)}\mathbf{P}_{T\tilde{T}}$$

The RI-MOM renormalization condition in matrix notation is simply given by

$$\hat{\mathbf{\Lambda}}^{\pm}(p)|_{p^2=-\mu^2} = \mathbf{\Lambda}^{\pm(0)}$$

Since the amputated Green function renormalizes as

$$\hat{\mathbf{\Lambda}}^{\pm}(p) = Z_q^{-2}(p)\mathbf{\Lambda}^{\pm}(p)\left[\mathbf{Z}^{\pm}(p)\right]^T$$

the RI-MOM renormalization condition reads

$$Z_q^{-2}(ap)\mathbf{\Lambda}^{\pm}(ap)\left[\mathbf{Z}^{\pm}(ap)\right]^T\Big|_{p^2=-\mu^2} = \mathbf{\Lambda}^{\pm(0)} \tag{4.3.6}$$

The bare Green function is usually expressed in terms of a "dynamics" matrix D which factorizes out the tree-level amputated Green function

$$\mathbf{\Lambda}^{\pm} = \mathbf{\Lambda}^{\pm(0)}\mathbf{D}^{\pm}$$

where we are omitting the momentum dependence. Projecting the previous expression on tree-level and taking into account the orthogonality relation one can find $D_{ij}^{\pm}$ from

$$\mathbf{D}^{\pm} = \mathbf{P}^{\pm}\mathbf{\Lambda}^{\pm} \tag{4.3.7}$$

and the RI-MOM renormalization condition Eq.4.3.6 becomes $Z_q^{-2}\mathbf{D}^{\pm}\mathbf{Z}^{\pm T} = \mathbf{I}$, from which we obtain $Z_{ij}^{\pm}$ in terms of the known quantities Z_q and D_{ij}

$$\mathbf{Z}^{\pm} = Z_q^{-2}\left[\mathbf{D}^{\pm T}\right]^{-1}$$

Note that since $\mathbf{D}^{\pm}$ determines the dynamics of the bare operators, it should have the same block diagonal structure as $Z^{\pm}$. Parity violating operator renormalizes with Eq.4.3.1 through a block diagonal matrix. In this case the RI-MOM condition takes the form

$$\mathbf{Z}_\chi{}^{\mathtt{PV}\pm} = Z_q^{-2}\left[\left(\mathbf{D}^{\mathtt{PV}\pm}\right)^T\right]^{-1}$$

while the parity conserving renormalize with Eq.4.3.2 so the RI-MOM condition becomes

$$\mathbf{Z}_\chi{}^{\mathtt{PC}\pm} = Z_q^{-2}\left[I+\mathbf{\Delta}\right]^{-1}\left[\left(\mathbf{D}^{\mathtt{PC}\pm}\right)^T\right]^{-1} \tag{4.3.8}$$

In the strategy proposed in [23] and followed in this thesis, four species of OS quark flavours are introduced with the corresponding Wilson parameters obeying the relation $r_1 = r_2 = r_3 = -r_4$ or an equivalent permutation. The great advantage of our setup is that, as shown in subsection 3.4.2, *wrong chirality mixing* terms Δ_{ij} are reduced to only $\mathcal{O}(a^2)$ effects. Moreover, following the four-fermion mapping found in Eq.3.4.15 the renormalization matrix of the parity-conserving-plus operators in the lattice basis $\{\mathbf{O}_i\}$ can be related with the parity-violating operators in the lattice basis with twisted χ-quarks $\{\mathcal{O}_i\}$

$$\mathbf{Z}_\chi{}^{\mathtt{PC}+} = \begin{pmatrix} \mathcal{Z}_{11}^+ & 0 & 0 & 0 & 0 \\ 0 & \mathcal{Z}_{22}^- & -\mathcal{Z}_{23}^- & 0 & 0 \\ 0 & -\mathcal{Z}_{32}^- & \mathcal{Z}_{33}^- & 0 & 0 \\ 0 & 0 & 0 & \mathcal{Z}_{44}^+ & \mathcal{Z}_{45}^+ \\ 0 & 0 & 0 & \mathcal{Z}_{44}^+ & \mathcal{Z}_{55}^+ \end{pmatrix}^{\mathtt{PV}}_{\chi} \tag{4.3.9}$$

This is a very important advantage of our approach, which we will implement in practice using the following strategy: compute the quark propagators in the physical basis ψ, in which the Wilson term is twisted. Renormalization conditions are imposed on the operators $\{\mathbf{O}_i\}$ and renormalization matrix $\mathbf{Z}_\chi{}^{\mathtt{PC}+}$, which renormalizes the physical relevant $\Delta F = 2$ operators, is extracted from Eq.4.3.8. Finally, we also compute the mixing matrix Δ and we check that they are only $\mathcal{O}(a^2)$ discretization effects.

4.3.1 Four-fermion GB-pole contribution

As discussed in subsection 4.2.1 for the case of the bilinear pseudoscalar operator, a possible difficulty in the implementation on the chiral limit comes from the coupling of the operators to the GB-pole. The main difference with respect to the case of bilinear pseudoscalar operator is that in the case of four-fermion operators both single and double poles can appear in the chiral limit of the relevant Green functions and their associated vertex D_{ij}.

Let us now consider the Fourier transform of the amputated Green function $O^{\pm}_{\Gamma_{(1)}\Gamma_{(2)}}(0)$ with the exceptional momentum configuration $q^2 = 0$, where $q = p - p'$

$$
\begin{aligned}
G^{\pm}_{\Gamma_{(1)}\Gamma_{(2)}}(p,p') &= \int d^4x_1 d^4x_2 d^4x_3 d^4x_4 e^{-ip(x_1+x_3)+ip'(x_2+x_4)} \\
&\quad \times \langle 0|T\left[\psi_1(x_1)\bar{\psi}_2(x_2)O^{\pm}_{\Gamma_{(1)}\Gamma_{(2)}}(0)\psi_3(x_3)\bar{\psi}_4(x_4)\right]|0\rangle \\
&\equiv \langle 0|T\left[\psi_1(p)\bar{\psi}_2(p')O^{\pm}_{\Gamma_{(1)}\Gamma_{(2)}}(0)\psi_3(p')\bar{\psi}_4(p)\right]|0\rangle
\end{aligned}
$$

By applying twice the LSZ reduction formula we see that the dynamics matrix D_{ij} should have the following three kind of GB-pole contributions

$$
\begin{aligned}
&(i) \qquad \sim \langle 0|\psi_1(p)\bar{\psi}_2(p')|P_{12}(q)\rangle \frac{1}{M_{12}^2}\langle P_{12}(q)|O^{\pm}_{\Gamma_{(1)}\Gamma_{(2)}}(0)\psi_3(p)\bar{\psi}_4(p')|0\rangle \\
&(ii) \qquad \sim \langle 0|\psi_1(p)\bar{\psi}_2(p')O^{\pm}_{\Gamma_{(1)}\Gamma_{(2)}}(0)|P_{34}(q)\rangle \frac{1}{M_{34}^2}\langle P_{34}(q)|\psi_3(p)\bar{\psi}_4(p')|0\rangle \\
&(iii) \qquad \sim \frac{\langle 0|\psi_1(p)\bar{\psi}_2(p')|P_{12}(q)\rangle}{M_{34}^2}\langle P_{34}(q)|O^{\pm}_{\Gamma_{(1)}\Gamma_{(2)}}(0)|P_{12}(q)\rangle \frac{\langle P_{34}(q)|\psi_3(p)\bar{\psi}_4(p')|0\rangle}{M_{12}^2}
\end{aligned}
$$

The additional reduction given by Eq.4.2.15 can also be applied here. Therefore, one finds that the GB pole contributions are of the form

$$
\begin{aligned}
&(i) \qquad \sim \frac{\Lambda^4_{\rm QCD}}{p^2}\frac{1}{M_{12}^2}\langle P_{12}(q)|O^{\pm}_{\Gamma_{(1)}\Gamma_{(2)}}(0)\psi_3(p)\bar{\psi}_4(p')|0\rangle \\
&(ii) \qquad \sim \frac{\Lambda^4_{\rm QCD}}{p^2}\frac{1}{M_{34}^2}\langle 0|\psi_1(p)\bar{\psi}_2(p')O^{\pm}_{\Gamma_{(1)}\Gamma_{(2)}}(0)|P_{34}(q)\rangle \\
&(iii) \qquad \sim \frac{\Lambda^8_{\rm QCD}}{(p^2)^2}\frac{1}{M_{12}^2 M_{34}^2}\langle P_{34}(q)|O^{\pm}_{\Gamma_{(1)}\Gamma_{(2)}}(0)|P_{12}(q)\rangle
\end{aligned}
$$

This result implies that single and double GB-pole contributions are suppressed by $1/p^2$ or $1/(p^2)^2$ factors respectively.

In the case of parity violating operators, $\langle P_{34}(q)|O^{\mathtt{PV}\pm}_{\Gamma_{(1)}\Gamma_{(2)}}(0)|P_{12}(q)\rangle$ vanish in the continuum since parity is a symmetry of QCD and it is $\mathcal{O}(a)$ on the lattice. Hence, double poles are suppressed.

Regarding the case of parity conserving operators, for the case of $Q_1^{\mathtt{PC}+} = O_{VV}+O_{AA}$ an important simplification occurs. Thanks to our setup $r_1 = r_2 = r_3 = -r_4$ the lattice axial current $\bar{\psi}_4\gamma_\mu\gamma_5\psi_3$ is exactly conserved (only broken by soft mass term) while the OS axial current $\bar{\psi}_1\gamma_\mu\gamma_5\psi_2$ is not conserved due to $\mathcal{O}(a^2)$ lattice artifacts (see [66]). From the form of $Q_1^{\mathtt{PC}+}$ one deduces that[4]

$$
\begin{aligned}
&\langle 0|\psi_1(p)\bar{\psi}_2(p')O^{\pm}_{\Gamma_{(1)}\Gamma_{(2)}}(0)|P_{34}(q)\rangle \to M_{34}^2 \\
&\langle P_{12}(q)|O^{\pm}_{\Gamma_{(1)}\Gamma_{(2)}}(0)\psi_3(p)\bar{\psi}_4(p')|0\rangle \to M_{12}^2 \\
&\langle P_{34}(q)|O^{\pm}_{\Gamma_{(1)}\Gamma_{(2)}}(0)|P_{12}(q)\rangle \to \Lambda^2_{\rm QCD}M_{34}^2
\end{aligned}
\tag{4.3.10}
$$

[4] using the soft pion theorem

with the TM pseudoscalar mass $M_{34}^2 \sim \mu_3 + \mu_4$ in the chiral limit up to $\mathcal{O}(a^2\mu)$ while the OS one satisfies $M_{12}^2 = \mu_1 + \mu_2 + a^2\Lambda_{QCD}^3$ in the chiral limit.

Hence, for the $Q_1^{\mathtt{PC+}}$ operator the term (ii) vanish in the chiral limit up to $\mathcal{O}(a^2\mu)$ while the OS GB-pole in (i) survives although it is suppressed by a factor of the kind a^2/p^2. Moreover, the double pole in (iii) becomes a single pole with the OS M_{12}^2 mass double suppressed by a factor $1/(p^2)^2$. In other words, only single GB-pole with the OS pseudoscalar meson mass occurs but suppressed either by a^2/p^2 or $1/(p^2)^2$.

For the case of $Q_i^{\mathtt{PC+}}$ with $i = 2, 3, 4, 5$ the chiral properties are such that all the matrix elements in Eq.4.3.10 do not vanish in the chiral limit and no GB-pole simplification occurs: both double and single pole with OS and TM contributions can occur.

4.4 $\mathbf{N_f = 4}$ Renormalization Constants

A special effort is required to obtain non perturbative RCs relevant to renormalize bare lattice data from simulations with dynamical (u,d) degenerate and (s,c) non-degenerate quarks. The unquenched $N_f = 2+1+1$ simulations with fixed m_s and m_c dynamical sea quark masses are not well suited for the computation of mass-independent RCs. Rather, one has to generate further dedicated gauge configurations with $N_f = 4$ degenerate sea quarks.

One of the principal advantages of the Twisted Mass action is that automatic $\mathcal{O}(a)$ improvement is achieved by setting the PCAC mass to zero. This feature has been exploited to compute the $N_f = 2$ RCs. However, in practice this turns to be difficult for $N_f = 4$ simulations due to the instabilities in the tuning to maximal twist [89, 90]. In order to overcome this problem we work out of maximal twist where one can avoid the metastable region and measure the twisted angle with good precision. This comes at the price of a moderate increase of the quark mass M_f and of a slightly more complicated analysis implying the θ-average of the RC estimators as it is explained in the previous subsection.

4.4.1 RI-MOM out of maximal twist

As already presented in [23], one can achieve $\mathcal{O}(a)$ improvement though being far from maximal twist at the prize of doubling the reasonable low CPU time cost for producing gauge simulations at non-zero standard and twisted quark masses.

The $N_f = 4$ Twisted Mass action in the twisted basis reads

$$S_F\left[\chi_f, \bar{\chi}_f, U\right] = a^4 \sum_x \sum_{f=1}^{4} \bar{\chi}_f(x) \left[D_W\left[U\right] + m_{0,f} + i r_f \mu_f \gamma_5\right] \chi_f(x) \tag{4.4.1}$$

where χ_f denotes a single-flavour field. The setup considered for $N_f = 4$, i.e two twisted mass doublet, implies $r_1 = -r_2$ and $r_3 = -r_4$ and $M_{0,f} = M_0$, $\mu_f = \mu$. The lattice action in Eq.4.4.1 can be expressed in the physical quark basis as usual through

$$\begin{aligned}\psi_f(x) &= \exp\left\{\frac{i}{2}\omega\gamma^5 r_f\right\}\chi_f(x) = \exp\left\{\frac{i}{2}\left(\frac{\pi}{2}-\theta_0\right)\gamma_5 r_f\right\}\chi_f(x)\\ \bar{\psi}_f(x) &= \bar{\chi}_f(x)\exp\left\{\frac{i}{2}\omega\gamma^5 r_f\right\} = \bar{\chi}_f(x)\exp\left\{\frac{i}{2}\left(\frac{\pi}{2}-\theta_0\right)\gamma^5 r_f\right\}\end{aligned} \tag{4.4.2}$$

which gives

$$\begin{aligned}&S_F\left[\psi_f,\bar{\psi}_f,U\right] =\\ &a^4\textstyle\sum_x\sum_{f=1}^4\bar{\psi}_f(x)\left[\gamma_\mu\left(\frac{\nabla_\mu+\nabla^*_\mu}{2}\right)-i\gamma_5 r_f e^{i\theta_{0,f}\gamma_5}(-\frac{a}{2}\nabla_\mu\nabla^*_\mu+m_{\text{crit}})+M_{0,f}\right]\psi_f(x)\end{aligned} \tag{4.4.3}$$

The bare mass parameters and the angle θ are given by

$$M_{0,f} = \sqrt{(m_{0,f}-m_{\text{crit}})^2+\mu_f^2} \qquad \sin\theta_f = \frac{m_{0,f}-m_{\text{crit}}}{M_0} \qquad \cos\theta_f = \frac{\mu_f}{M_{0,f}}$$

In practice we make use of m_{PCAC} to estimate $(m_{0,f}-m_{\text{crit}})$. In this way we take as the renormalised quantity the polar quark mass

$$\hat{M}_f = Z_P^{-1}M_f = \sqrt{Z_A^2 m^2_{\text{PCAC}}+\mu_f^2}$$

and the angle θ_f, complementary to the twisted angled ω_f ($\theta_f \equiv \pi/2-\omega_f$), given by

$$\tan\theta_f = Z_A m_{\text{PCAC}}/\mu_f$$

Since we use four mass degenerate quark flavours, the knowledge of the parameters $M^{\text{sea}},\theta^{\text{sea}},M^{\text{val}},\theta^{\text{val}}$ is sufficient to describe our RC computation. The angle θ corresponds to the angle of the upper component of each twisted mass doublet, i.e $\theta_{1,3} = r_{1,3}\theta = \theta$, while the lower components are associated to the angle $\theta_{2,4} = r_{2,4}\theta = -\theta$.

The proof of the cancellation of $\mathcal{O}(a^{2k+1})$ when performing the average of correlators computed at opposite values of θ is analogous to the one given for maximal twist, i.e $\theta = 0$, in appendix A of [87] and outlined in the previous section, with P now replaced by $P\times(\theta\to-\theta)$. The proof follows from the observation that the lattice action in Eq.4.4.3 is invariant under the spurionic transformation

$$P\times(\theta\to-\theta)\times D\times(M_0\to-M_0)$$

The local effective action that allows for a description à la Symanzik of the lattice artifacts in the operators will inherit this invariance of the lattice action. As a straightforward result, $\mathcal{O}(a^{2k+1})$ artifacts occurring in the vacuum expectation values of operators that are invariant under $P\times(\theta\to-\theta)$ are quantities that change sign upon changing the sign of θ. Hence, $\mathcal{O}(a^{2k+1})$ artifacts are absent in the arithmetic average of parity-even correlators under $P\times(\theta\to-\theta)$ computed at opposite values of θ (or equivalently m_{PCAC}). In particular, this holds for the RC estimators.

4.4.2 Simulation details

Within the ETM collaboration we have produced dedicated $N_f = 4$ dynamical quark gauge configurations in the Landau gauge employing the Iwasaki gauge action and the twisted mass fermionic action. The inversions in the valence sector have been performed using point-like sources randomly located on the lattice for each gauge configuration. We have produced data at three values of the inverse gauge coupling, $\beta = 1.90$, 1.95 and 2.10. For each β and for a sequence of $M^{\rm sea}$ values, we produced two ensembles with (nearly) opposite values of $\theta^{\rm sea}$. We label them as Ep/m, where E = 1, 2... and p/m refers to the sign($\theta^{\rm sea}$). On each ensemble Ep/m, with $(M^{\rm sea,Ep/m}, \theta^{\rm sea,Ep/m})$ we compute the RC-estimators for several values of the valence mass parameters $\left(M_j^{\rm val}, \theta_j^{\rm val}\right)$ and $(a\tilde{p})^2$ as summarized in Table 4.4.1.

In order to minimize discretization effects, we select momenta with components $p_\nu = (2\pi/L_\nu)\, n_\nu$ with $\nu = 1, 2, 3, 4$ and L_ν the lattice size in the direction ν, in the intervals

$$n_\nu = \begin{cases} ([0,2]\,,[0,2]\,,[0,2]\,,[0,3]) \\ ([2,3]\,,[2,3]\,,[2,3]\,,[4,7]) \end{cases} \quad , \text{ for } \beta = 1.95$$

and

$$n_\nu = \begin{cases} ([0,2]\,,[0,2]\,,[0,2]\,,[0,3]) \\ ([2,5]\,,[2,5]\,,[2,5]\,,[4,9]) \end{cases} \quad , \text{ for } \beta = 1.90 \text{ and } 2.10$$

where n_4 corresponds to the time direction.

For $\beta = 1.95$ and $\beta = 2.10$ we consider only the standard Fourier transform propagator, i.e the one with momenta components $(n_1, n_2, n_3; n_4)$ with $n_\nu \geq 0$. We refer to this standard momenta with the schematic momenta structure $(+,+,+;+)$. However, in general fifteen extra equivalent momenta configurations could be computed corresponding to the schematic momenta structure $(\pm,\pm,\pm;\pm)$. We found that the jacknife error of the $\beta = 1.90$ RCs is reduced in 25-50%, depending on the Z_Γ, when averaging over the eight momenta configurations with positive n_4 (even components) or by averaging over the eight momenta configurations with negative n_4 (odd components) but in practice error is not further reduced if we consider the average over the sixteen components. For this reason, the RCs at $\beta = 1.90$ are averaged over the eight momenta configuration $(\pm,\pm,\pm;+)$ for each $\tilde{p}^2$, valence and sea quark mass before the $\theta-$average.

The time component of the four-momentum is shifted by π/T in order to take into account the use of antiperiodic boundary conditions on the quark fields in the time direction.

In addition, to minimize the contribution of Lorentz non invariant discretization effects we have only considered for the final RI-MOM analysis the momenta satisfying the cut

$$\Delta_4(p) \equiv \frac{\sum_\rho \tilde{p}_\rho^4}{\left(\sum_\rho \tilde{p}_\rho^2\right)^2} < 0.28 \tag{4.4.4}$$

ensemble	$a\mu^{\rm sea}$	$am^{\rm sea}_{\rm PCAC}$	$aM_0^{\rm sea}$	$\theta^{\rm sea}$	$a\mu^{\rm val}$	$am^{\rm val}_{\rm PCAC}$
$\beta = 1.90$ $a \sim 0.09$ fm $a^{-1} \sim 2.19$ GeV $L = 24$ $T = 48$						
A4m	0.0080	-0.0390(01)	0.0285(01)	-1.286(01)	{0.0060, 0.0080, 0.0120,	-0.0142(02)
A4p		0.0398(01)	0.0290(01)	+1.291(01)	0.0170, 0.0210,0.0260}	+0.0147(02)
A3m	0.0080	-0.0358(02)	0.0263(01)	-1.262(02)	{0.0060, 0.0080, 0.0120,	-0.0152(02)
A3p		0.0356(02)	0.0262(01)	+1.260(02)	0.0170, 0.0210,0.0260}	+0.0147(03)
A2m	0.0080	-0.0318(01)	0.0237(01)	-1.226(02)	{0.0060, 0.0080, 0.0120,	-0.0155(02)
A2p		+0.0310(02)	0.0231(01)	+1.218(02)	0.0170, 0.0210,0.0260}	+0.0154(02)
A1m	0.0080	-0.0273(02)	0.0207(01)	-1.174(03)	{0.0060, 0.0080, 0.0120,	-0.0163(02)
A1p		+0.0275(04)	0.0209(01)	+1.177(05)	0.0170, 0.0210,0.0260}	+0.0159(02)
$\beta = 1.95$ $a \sim 0.08$fm $a^{-1} \sim 2.50$ GeV $L = 24$ $T = 48$						
1m	0.0085	-0.0413(02)	0.0329(01)	-1.309(01)	{0.0085, 0.0150, 0.0203,	-0.0216(02)
1p		+0.0425(02)	0.0338(01)	+1.317(01)	0.0252, 0.0298}	+0.0195(02)
7m	0.0085	-0.0353(01)	0.0285(01)	-1.268(01)	{0.0085, 0.0150, 0.0203,	-0.0180(02)
7p		+0.0361(01)	0.0285(01)	+1.268(01)	0.0252, 0.0298}	+0.0181(01)
8m	0.0020	-0.0363(01)	0.0280(01)	-1.499(01)	{0.0085, 0.0150, 0.0203,	-0.0194(01)
8p		+0.0363(01)	0.0274(01)	+1.498(01)	0.0252, 0.0298}	+0.0183(02)
3m	0.0180	-0.0160(02)	0.0218(01)	-0.601(06)	{0.0060,0.0085,0.0120,0.0150,	-0.0160(02)
3p		+0.0163(02)	0.0219(01)	+0.610(06)	0.0180,0.0203,0.0252,0.0298}	+0.0162(02)
2m	0.0085	-0.0209(02)	0.0182(01)	-1.085(03)	{0.0085, 0.0150, 0.0203,	-0.0213(02)
2p		+0.0191(02)	0.0170(02)	+1.046(06)	0.0252, 0.0298}	+0.0191(02)
4m	0.0085	-0.0146(02)	0.0141(01)	-0.923(04)	{0.0060,0.0085,0.0120,0.0150,	-0.0146(02)
4p		+0.0151(02)	0.0144(01)	+0.940(07)	0.0180,0.0203,0.0252,0.0298}	+0.0151(02)
$\beta = 2.10$ $a \sim 0.06$ fm $a^{-1} \sim 3.23$ GeV $L = 32$ $T = 64$						
5m	0.0078	-0.00821(11)	0.0102(01)	-0.700(07)	{0.0048,0.0078,0.0119,	-0.0082(01)
5p		+0.00823(08)	0.0102(01)	+0.701(05)	0.0190,0.0242,0.0293}	+0.0082(01)
4m	0.0064	-0.00682(13)	0.0084(01)	-0.706(09)	{0.0039,0.0078,0.0119,	-0.0068(01)
4p		+0.00685(12)	0.0084(01)	+0.708(09)	0.0190,0.0242,0.0293}	+0.0069(01)
3m	0.0046	-0.00585(08)	0.0066(01)	-0.794(07)	{0.0025,0.0046,0.0090,0.0152,	-0.0059(01)
3p		+0.00559(14)	0.0064(01)	+0.771(13)	0.0201,0.0249,0.0297}	+0.0056(01)
2m	0.0030	-0.00403(14)	0.0044(01)	-0.821(17)	{0.0013,0.0030,0.0080,0.0143,	-0.0040(01)
2p		+0.00421(13)	0.0045(01)	+0.843(15)	0.0195,0.0247,0.0298}	+0.0042(01)

Table 4.4.1: Simulation details of the Laundau gauge ensembles analyzed at $\beta = 1.90$, 1.95 and 2.10

Finally, in order to improve the statistical accuracy we have computed the RCs by averaging the results obtained from the correlation functions of the operators $O_\Gamma = \bar{u}\Gamma d$ and $O'_\Gamma = \bar{d}\Gamma u$ where the quarks (u, d) of the operator belong to a twisted doublet of quarks, regularized by the TM action with $r_u = -r_d = 1$. Similarly, the quark field RC, Z_q, have been computed by averaging the results obtained for the up and down quark propagators.

4.4.3 Bilinear RCs

Here I present the computation and results using the RI-MOM method for the RCs of bilinear quark operators using the propagators generated by the ETMC simulation with $N_f = 4$ dynamical quark flavours.

Our procedure for the bilinear operators goes from the following analysis steps

1. Compute the RC estimators according to Eq.4.2.7 for each β, each momenta, each ensemble Ep/m (or equivalently each sea quark mass), each valence quark mass in the case of Z_q or each pair of non-equivalent quark masses in the case of the bilinears. That is the basic ingredient of our calculation is the lattice RC estimators

$$Z_q^{\mathrm{Ep/m}}\left(M_0^{\mathrm{sea}}, \theta_0^{\mathrm{sea}}; M^{\mathrm{val}}; a^2\tilde{p}^2; \beta\right)$$
$$Z_\Gamma^{\mathrm{Ep/m}}\left(M_0^{\mathrm{sea}}, \theta_0^{\mathrm{sea}}; M_1^{\mathrm{val}}, M_2^{\mathrm{val}}; a^2\tilde{p}^2; \beta\right)$$

2. Subtract the $\mathcal{O}(a^2 g^2)$ cutoff effects, calculated non perturbatively in [91].

3. Average over equivalent momenta, i.e over momenta ap_ν with the same $(a\tilde{p})^2$.

4. Build the $\mathcal{O}(a)$ improved estimators which is achieved by performing the θ-average of the RC estimators. This is the basic ingredient of our calculation and the main difference with respect to the analysis in the case $N_f = 2$ RCs

$$Z_\Gamma^{\mathrm{E}}(M^{\mathrm{sea,E}}, |\theta^{\mathrm{sea,E}}|) = \frac{1}{2}\left[Z_\Gamma^{\mathrm{Ep}}(M^{\mathrm{sea,Ep}}, \theta^{\mathrm{sea,Ep}}) + Z_\Gamma^{\mathrm{Em}}(M^{\mathrm{sea,Em}}, \theta^{\mathrm{seaEm}})\right]$$

5. Extrapolate to the valence chiral limit using a linear fit of the RC estimators in $M_j^{\mathrm{val,E}}$ for each $(a\tilde{p})^2$, where $M_j^{\mathrm{val,E}} = \left[M_j^{\mathrm{val,Ep}} + M_j^{\mathrm{val,Em}}\right]/2$, with $M_j^{\mathrm{val,Ep/m}}$ the valence polar mass

$$M_j^{\mathrm{val,Ep/m}} = \sqrt{\left(Z_A m_{\mathrm{PCAC}}^{\mathrm{val,Ep/m}}\right)^2 + \left(\mu_j^{\mathrm{val,E}}\right)^2}$$

   For $\Gamma = P$ we proceed in a rather different way to keep into account the contributions $\propto 1/\left(M_{PS}^{\mathrm{val}}\right)^2$ coming from the GB-pole. Before performing the θ-average we remove the GB-pole contribution, which depending directly on the lattice pseudoscalar meson mass, happens to be slightly different for p and m estimators of the same ensemble. The subtraction of the GB-pole is performed together with the valence chiral extrapolation. Once the contribution of the GB-pole has been subtracted for each p and m ensemble separately we perform the θ-average.

6. Extrapolate to the sea chiral limit using a linear fit in $\left(M^{\text{sea,E}}\right)^2$ where $M^{\text{sea,E}} = \left[M^{\text{sea,Ep}} + M^{\text{sea,Em}}\right]/2$ with

$$M^{\text{sea,Ep/m}} = \sqrt{\left(Z_A m_{\text{PCAC}}^{\text{sea,Ep/m}}\right)^2 + \left(\mu^{\text{sea,E}}\right)^2}$$

7. Evolve, via the known perturbative evolution [92], the RCs to a common reference scale: $\tilde{p}^2 = (1/a)^2$.

8. Subtract the residual $\mathcal{O}(a^2\tilde{p}^2)$ lattice artefacts according to the so-called M1 and M2 methods described in the following sections.

In general this is an iterative analysis since the value of Z_A ,which is necessary to renormalize M_0^{sea} through $M^{\text{sea}} = \sqrt{\left(Z_A m_{\text{PCAC}}^{\text{sea}}\right)^2 + \left(\mu^{\text{sea}}\right)^2}$, is an output of the procedure. However, in practice, one step is enough to achieve a consistent value of Z_A.

The previous procedure involves two main steps: the chiral limit extrapolation of the RCs and the study of the renormalization scale dependence. This two steps will be described in the following subsections.

4.4.3.1 Chiral extrapolations

The chiral fit ansätz are inspired in the mass dependence expected from the Symmanzik analysis of lattice artifacts. For the valence chiral extrapolation we consider as a fit function of the $\mathcal{O}(a)$ improved estimator Z_Γ^{E} a linear fit in M^{val}

$$\begin{aligned} Z_q^{\text{E}}\left(\mu^{\text{val,E}}; a^2\tilde{p}^2\right) &= A_q^{\text{E}}(a^2\tilde{p}^2) + B_q^{\text{E}}(a^2\tilde{p}^2) M^{\text{val,E}} \\ Z_\Gamma^{\text{E}}\left(\mu_1^{\text{val,E}}, \mu_2^{\text{val,E}}; a^2\tilde{p}^2\right) &= A_\Gamma(a^2\tilde{p}^2) + B_\Gamma(a^2\tilde{p}^2)\left(M_1^{\text{val,E}} + M_2^{\text{val,E}}\right) \end{aligned}$$

We checked that our results do not change in practice by using more complicated fit functions involving $\left(M^{\text{val}}\right)^2$, $M^{\text{val}}\cos\left(\theta^{\text{val}}\right)$ or $\left(M^{\text{val}}\cos\left(\theta^{\text{val}}\right)\right)^2$.

In the case of Z_P, in order to subtract properly the contribution of the GB-pole we fit the value of the amputated projected Green function $\Gamma_P^{\text{Ep/m}}$ for each p/m ensemble to the ansätz

$$\mathcal{V}_P^{\text{Ep/m}}\left(\mu_1^{\text{val,E}}, \mu_2^{\text{val,E}}; a^2\tilde{p}^2\right) = A_P^{\text{Ep/m}}(a^2\tilde{p}^2) + B_P^{\text{Ep/m}}(a^2\tilde{p}^2)\left[M_{PS}^{\text{val,Ep/m}}\right]^2 + \frac{C_P^{\text{Ep/m}}(a^2\tilde{p}^2)}{\left[M_{PS}^{\text{val,Ep/m}}\right]^2}$$

where $M_{PS}^{\text{val,Ep/m}}$ is the pseudoscalar meson mass composed by valence quarks $\mu_1^{\text{val,E}}$ and $\mu_2^{\text{val,E}}$ for the Ep/m ensemble.

In Figure 4.4.1 we show the GB-pole removal and the residual valence mass dependence in the analysis of Z_P. The dependence of Z_S, Z_V, Z_A, Z_T and Z_q, which are not affected by the GB-pole contribution, on the polar valence quark masses is illustrated in Figure 4.4.2 and Figure 4.4.3.

Once the RCs are extrapolated to the chiral limit in the valence we continue with the chiral limit on the sea. At fixed β and $(a\tilde{p})^2$, we fit the RC to a first order polynomial in $(M^{\rm sea})^2$. This choice is dictated by the expectation that effects of spontaneous chiral symmetry, which may induce a dependence on $M^{\rm sea}$ are strongly suppressed. As it is shown in Figure 4.4.4 we find that our RC estimators show a very mild dependence on the sea quark mass squared. Our final estimates are obtained extrapolating to the chiral limit in the sea with a linear fit in $\left(M^{\rm sea,E}\right)^2$. Finally, we also checked that chiral extrapolations based on a first or second order polynomial fit in $M^{\rm sea,E}$ lead to compatible results.

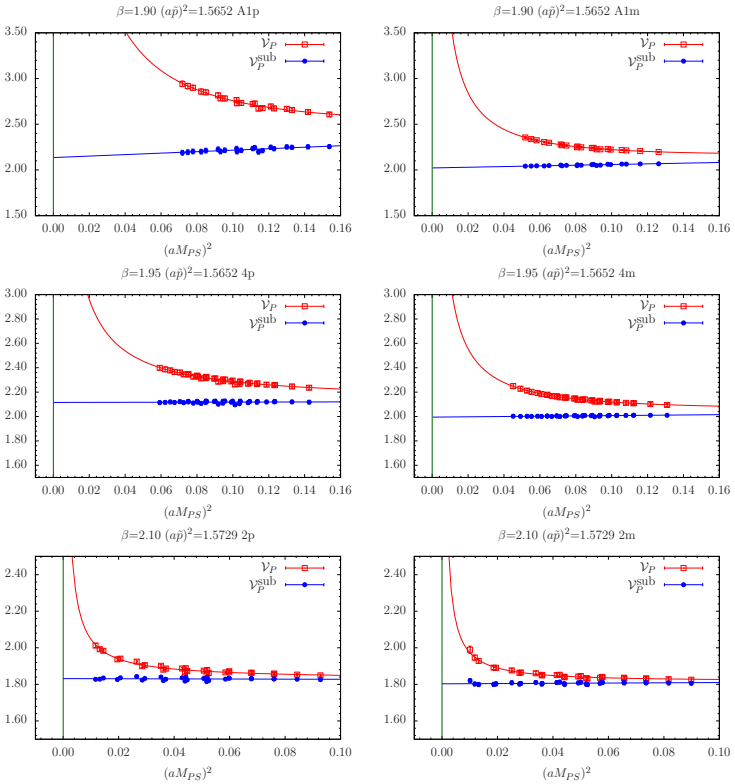

Figure 4.4.1: Amputated Green function $\mathcal{V}_P$ and subtracted amputated Green function $\mathcal{V}_P^{\rm sub}$ evaluated at $(a\tilde{p})^2 \simeq 1.5$, as a function of the pseudoscalar meson mass squared for the lightest polar sea mass at each β-value. Left panels correspond to p ensembles while right one correspond to m ensembles.

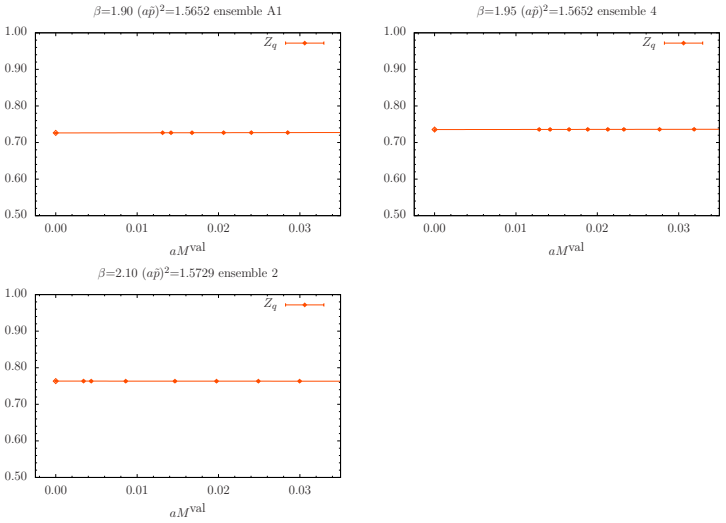

Figure 4.4.2: Valence chiral extrapolations for Z_q against $M^{\rm val}$ at $(a\tilde{p})^2 \simeq 1.5$ for the lightest polar sea mass at each β-value. θ-average have been previously performed.

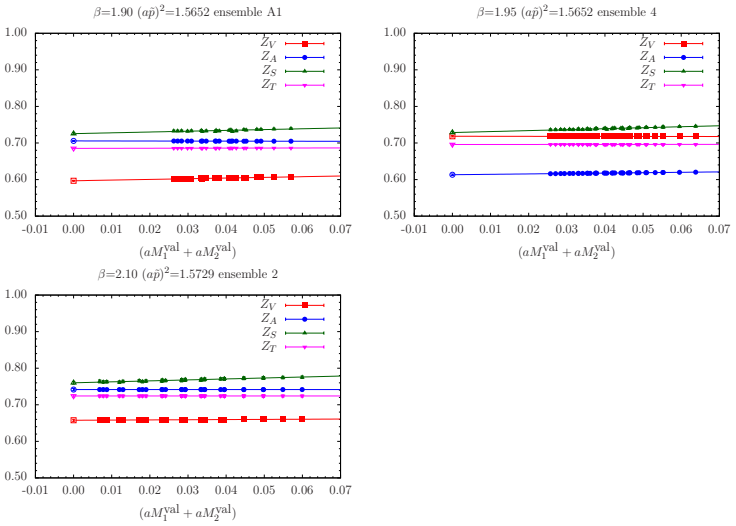

Figure 4.4.3: Valence chiral extrapolations for Z_V, Z_A, Z_S and Z_T at $(a\tilde{p})^2 \simeq 1.5$ for the lightest polar sea mass at each β-value. θ-average have been previously performed. All non equivalent combination of diagonal and non-diagonal valence quark masses $\left(M_1^{\rm val}, M_2^{\rm val}\right)$ have been considered for the valence chiral extrapolation.

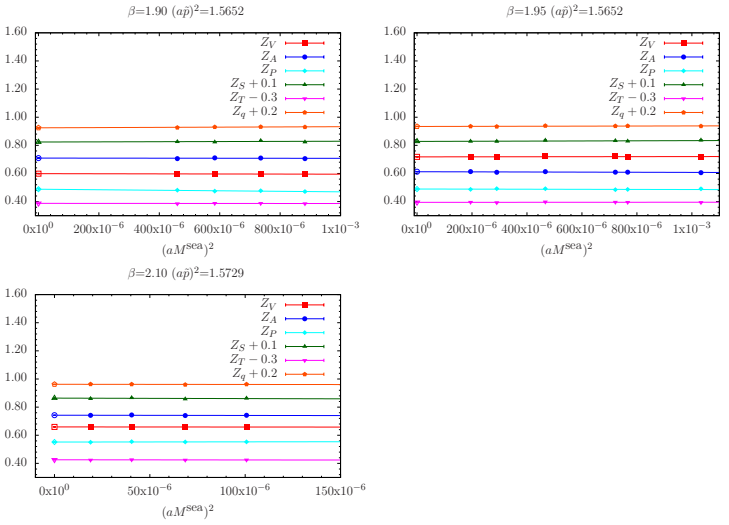

Figure 4.4.4: Sea chiral extrapolation in terms of the polar sea quark mass of the θ-averaged RC estimators of for Z_V, Z_A, Z_P, Z_S, Z_T and Z_q at $(a\tilde{p})^2 \simeq 1.5$.

4.4.3.2 Renormalization scale dependence and subtraction of $\mathcal{O}(a^2g^2)$ discretization effects

Once the RCs have been extrapolated to the chiral limit, we can analyze their dependence on the renormalization scale. It is crucial to notice that following the RI-MOM method RCs are computed on a selected interval of momenta. RCs computed at different values of $(a\tilde{p})^2$ are evolved to a reference scale $\mu_0 = 1/a$ using the well-known evolution functions C_Γ in the RI'-MOM scheme.

$$Z_\Gamma(\mu_0; g(a)) = C_\Gamma(\mu_0, \mu) Z_\Gamma(\mu^2 = a^2\tilde{p}^2; g(a)) \equiv \frac{C_\Gamma(\mu_0)}{C_\Gamma(\mu)} Z_\Gamma(\mu; g(a))$$

The evolution function $C_\Gamma(\mu)$ is related to the beta function $\beta(\alpha)$ and to the anomalous dimension of the relevant operator $\gamma_\Gamma(\alpha)$ by

$$C_\Gamma = \exp\left[\int_{\alpha(\mu_0)}^{\alpha(\mu)} d\alpha\, \gamma_\Gamma(\alpha)/\beta(\alpha)\right]$$

In the RI-MOM scheme, these functions are known at the N^{2}LO for Z_T [93] and N^{3}LO for Z_S and Z_P [92]. For reader convenience, the explicit formulae are collected in Appendix C. In their numerical computation we have fixed $\Lambda_{QCD}^{N_f=4} = 296(10)$MeV [45]. Instead, Z_V, Z_A and the ratio Z_P/Z_S, being scale independent, have a vanishing anomalous dimension and so $C_\Gamma(\mu_0, \mu) = 1$.

In the numerical calculation, the RCs evolved to a reference scale $\mu_0 = 1/a$ still have a dependence on the renormalization scale $a^2\tilde{p}^2$ at which they have been initially computed.

This residual dependence signals the presence of either $\mathcal{O}(a^2)$ discretization effects or of higher-order perturbative corrections not included in the evolution function C_Γ. We can keep track of this dependence by denoting these RCs as $Z_\Gamma(\mu_0; a^2\tilde{p}^2; g(a))$ where

$$Z_\Gamma(\mu_0; a^2\tilde{p}^2; g(a)) = Z_\Gamma(\mu_0; g(a)) + \lambda_\Gamma a^2 \tilde{p}^2$$

The coefficients λ_Γ start at $\mathcal{O}(g^2)$ in perturbation theory. The one loop correction $\mathcal{O}(g^2 a^2)$ of the amputated projected Green function $\mathcal{V}_\Gamma(p) = \mathrm{Tr}\left[\Lambda_\Gamma P_\Gamma\right]$ has been computed using perturbation theory in [91] having the simple and general one-loop expression

$$\begin{aligned}\mathcal{V}_\Gamma(p)^{\mathrm{pert.}} = \; & 1 + \tfrac{g^2}{12\pi^2}\{b_\Gamma^{(1)} + b_\Gamma^{(2)}\, \ln(a^2\, p^2) + a^2\left[p^2\left(c_\Gamma^{(1)} + c_\Gamma^{(2)}\, \ln(a^2\, p^2)\right) + c_\Gamma^{(3)} \frac{\sum_\rho p_\rho^4}{p^2}\right]\} \\ & + \mathcal{O}(a^4\, g^2, g^4)\end{aligned}$$

and a similar expression can be found for the quark propagator.

In order to reduce the size of discretization errors, we analytically subtract from the quark propagator Eq.4.2.11 and the amputated vertex functions Eq.4.2.8 these $\mathcal{O}(a^2 g^2)$ contributions

$$\begin{aligned}\mathcal{V}_\Gamma(p)^{\mathrm{corr.}} &= \mathcal{V}_\Gamma(p) - \tfrac{g^2}{12\pi^2} a^2 \left[\tilde{p}^2\left(c_\Gamma^{(1)} + c_\Gamma^{(2)}\, \ln(a^2\, \tilde{p}^2)\right) + c_\Gamma^{(3)} \frac{\sum_\rho \tilde{p}_\rho^4}{\tilde{p}^2}\right] \\ \Sigma_1(p)^{\mathrm{corr.}} &= \Sigma_1(p) - \tfrac{g^2}{12\pi^2} a^2 \left[\tilde{p}^2\left(c_q^{(1)} + c_q^{(2)}\, \ln(a^2\, \tilde{p}^2)\right) + c_q^{(3)} \frac{\sum_\rho \tilde{p}_\rho^4}{\tilde{p}^2}\right]\end{aligned} \tag{4.4.5}$$

The specific values of the coefficients $b_\Gamma^{(i)}$ and $c_\Gamma^{(i)}$ depends on the action. They are computed in the chiral limit in [91]. They are collected in Appendix D in the case of Iwasaki gluon action in the Landau gauge.

The $\mathcal{O}(a^2)$ terms depend not only on $a^2\tilde{p}^2$ but also on the direction of the momentum, p_ρ, via $\sum_\rho \tilde{p}_\rho^4$. As a consequence, the subtraction of the $\mathcal{O}(a^2 g^2)$ effects must be performed before the average over momenta with the same $a^2\tilde{p}^2$. In the numerical evaluation of the perturbative correction we set g^2 to be the simple boosted coupling defined as $\tilde{g}^2 = g_0^2/\langle P\rangle$, where $\langle P\rangle$ is the average non perturbative plaquette. The numerical values are [0.573, 0.584, 0.613] for β =1.90, 1.95 and 2.10 respectively.

The effect of the subtraction is illustrated in Figure 4.4.5, which shows the $a^2\tilde{p}^2$ dependence of the RCs before and after the perturbative subtraction. We find that the slope λ_Γ is significantly reduced by the perturbative subtraction as it is numerically shown in Table 4.4.2. For Z_S we find that the slope increase after the subtraction as it was also found in the $N_f = 2$ analysis [84].

	before subtraction			after subtraction		
	1.90	1.95	2.10	1.90	1.95	2.10
Z_V	33(03)	28(02)	23(01)	12(03)	05(02)	03(01)
Z_A	09(04)	07(03)	08(02)	-12(04)	-12(03)	-10(02)
Z_S	-02(04)	-01(04)	02(02)	39(05)	38(04)	38(03)
Z_P	20(03)	26(02)	29(01)	12(04)	16(02)	22(01)
Z_T	20(03)	17(03)	16(02)	-06(03)	-08(03)	-06(02)
Z_q	33(03)	30(02)	24(01)	06(03)	04(02)	01(01)

Table 4.4.2: Slope λ_Γ $\left(\times 10^{-3}\right)$ for each Z_Γ before and after the perturbative subtraction of $\mathcal{O}(a^2 g^2)$ effects.

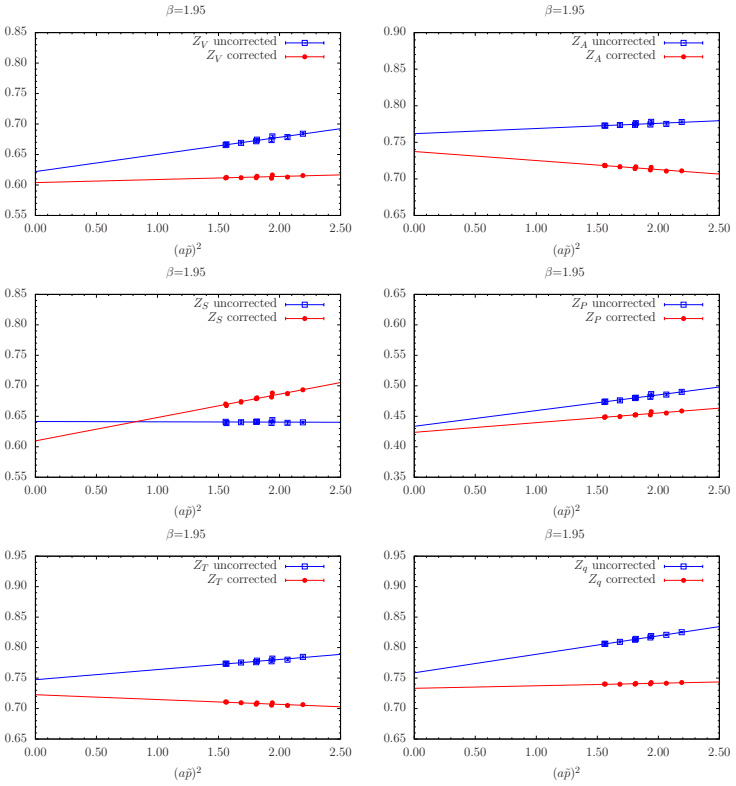

Figure 4.4.5: Perturbative corrected and uncorrected RCs $Z_\Gamma(\mu_0 = 1/a; a^2\tilde{p}^2)$ at $\beta = 1.95$, evaluated at $\mu_0 = 1/a$, as a function of the original renormalization scale $(a\tilde{p})^2$. Only data in the M1 interval and satisfying the cut in Eq.4.4.4 is plotted. The solid lines are linear fits to the data.

In order to take into account residual discretization effects in the calculation of the RCs two different approaches can be followed:

Extrapolation method (M1) After subtracting the $\mathcal{O}(a^2g^2)$ we extrapolate the RCs linearly to $a^2p^2 \to 0$. In practice, we fit $Z_\Gamma^{\text{corr.}}$ vs $a^2\tilde{p}^2$ in a large fixed momentum region $1.5 \leq a^2\tilde{p}^2 \leq 2.2$,which is included in the window $\Lambda_{\text{QCD}} \ll \mu \ll a^{-1}$, using

$$Z_\Gamma^{\text{corr.}}(\mu_0; a^2\tilde{p}^2; g(a)) = Z_\Gamma(\mu_0; g(a)) + \lambda_\Gamma a^2\tilde{p}^2 \tag{4.4.6}$$

The slope λ_Γ shows a very mild dependence on the coupling which can be parametrized by performing a simultaneous extrapolation for the different values of the lattice spacing and writing the slope as

$$\lambda_\Gamma(g^2) = \lambda_\Gamma(g_0^2) + \lambda'_\Gamma(g_0^2)(g^2 - g_0^2)$$

where g_0 is the coupling corresponding to a reference lattice spacing that we set equal to $\beta = 1.95$. The intercept of the extrapolation fit in Eq.4.4.6 determines the final estimate of the RC at $\mu_0 = 1/a$. The combined fit is illustrated in Figure 4.4.6.

p^2-window method (M2) In this method we do not perform any additional subtraction of discretization effects besides the perturbative ones. The final estimates of the RCs are computed by averaging the results of $Z_\Gamma^{\text{corr.}}(\mu_0; a^2\tilde{p}^2; g(a))$ in a small window of rather high $\tilde{p}^2$ values in physical units, the same for all βs. In practice, this is done by performing a weighted average of the RCs in the momentum interval $\tilde{p}^2 \in [11.3 : 13.8]\,\text{GeV}^2$, which translated into lattice units reads: $\left(a^2\tilde{p}^2\right)\big|_{\beta=1.90} \in [2.39 : 2.67]$, $\left(a^2\tilde{p}^2\right)\big|_{\beta=1.95} \in [1.80 : 2.20]$ and $\left(a^2\tilde{p}^2\right)\big|_{\beta=2.10} \in [1.10 : 1.23]$.

The idea behind the compatibility of both approaches is that, in order to construct the physical observables, RCs are combined with bare quantities. The residual $\mathcal{O}(a^2)$ discretization effects affecting both RCs and bare matrix elements will be corrected when extrapolating the physical renormalized quantities to the continuum limit. As an example, we show in Figure 4.4.7 the continuum extrapolation of the pseudoscalar mass squared computed at a fixed value of the renormalized quark mass μ_ℓ. The renormalization of μ_ℓ has been done using the M1 and M2 estimates for Z_P. Although the two estimators differ by $\mathcal{O}(a^2)$ discretization effects at finite lattice spacing the continuum limit results of the pseudoscalar mass squared are consisted within the two determinations.

The final results for the bilinear quark operators and quark field RCs, obtained with the RI-MOM method are collected in Table 4.4.3.

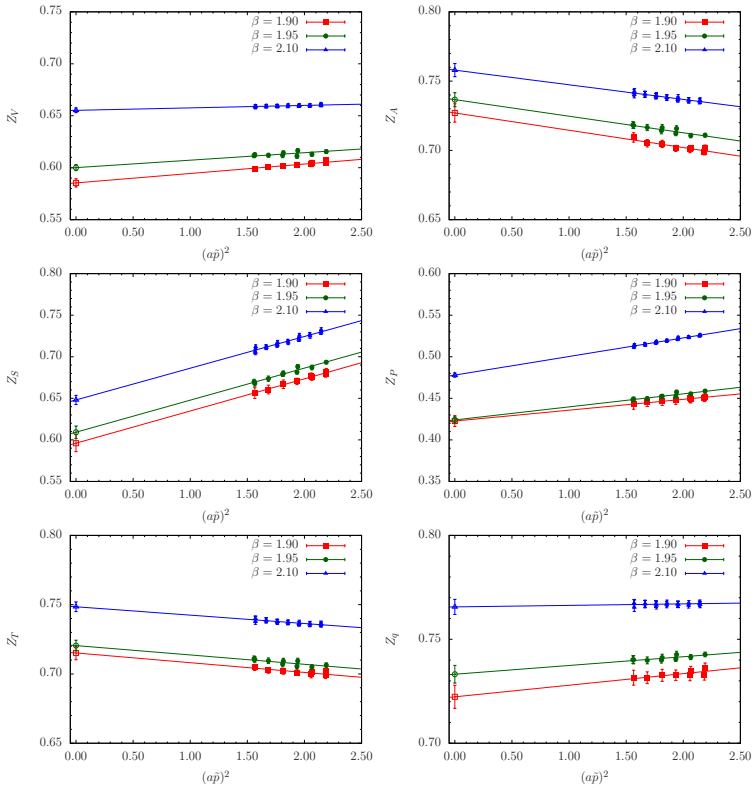

Figure 4.4.6: RCs $Z_\Gamma\left(\mu_0 = a^{-1}; a^2\tilde{p}^2\right)$ plotted against the original value of $a^2\tilde{p}^2$ for the three values of β. Solid lines correspond to fits to the data according to Eq.4.4.6. Open symbols corresponds to the final RC estimator.

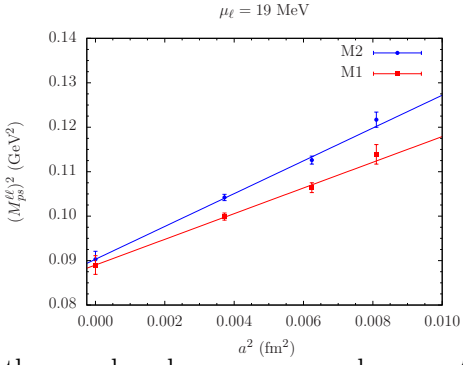

Figure 4.4.7: Scaling of the pseudoscalar mass squared, computed at fixed value of the quark mass. The M1 and M2 determinations of $Z_\mu = Z_P^{-1}$ lead to compatible results in the continuum limit.

Z_A			
	1.90	1.95	2.10
M1	0.726(8)	0.737(6)	0.758(5)
M2	0.698(2)	0.713(2)	0.749(3)
M1(g^2)	0.727(7)	0.737(5)	0.758(5)
Z_V			
	1.90	1.95	2.10
M1	0.580(5)	0.604(4)	0.655(2)
M2	0.611(3)	0.614(2)	0.658(1)
M1(g^2)	0.585(4)	0.600(3)	0.655(2)
WI	0.5920(04)	0.6095(03)	0.6531(02)
$Z_P(\mu_0 = a^{-1})$			
	1.90	1.95	2.10
M1	0.424(12)	0.424(5)	0.478(3)
M2	0.457(4)	0.455(2)	0.503(2)
M1(g^2)	0.422(7)	0.424(4)	0.478(3)
$Z_S(\mu_0 = a^{-1})$			
	1.90	1.95	2.10
M1	0.594(13)	0.610(9)	0.648(5)
M2	0.699(3)	0.686(2)	0.690(3)
M1(g^2)	0.596(10)	0.609(8)	0.648(5)
$Z_T(\mu_0 = a^{-1})$			
	1.90	1.95	2.10
M1	0.713(6)	0.723(5)	0.748(3)
M2	0.702(3)	0.707(2)	0.744(2)
M1(g^2)	0.715(5)	0.721(4)	0.748(3)
$Z_q(\mu_0 = a^{-1})$			
	1.90	1.95	2.10
M1	0.722(8)	0.733(5)	0.766(4)
M2	0.737(2)	0.741(1)	0.767(2)
M1(g^2)	0.723(5)	0.733(4)	0.766(4)
Z_P/Z_S			
	1.90	1.95	2.10
M1	0.709(21)	0.692(7)	0.737(6)
M2	0.655(6)	0.664(3)	0.728(3)
M1(g^2)	0.701(14)	0.693(7)	0.736(6)

Table 4.4.3: Values of Z_A, Z_V, Z_P, Z_S, Z_T , Z_q and Z_P/Z_S obtained with the RI-MOM methods M1 and M2. The one labeled as M1 corresponds to a linear fit in $\left(a^2\tilde{p}^2\right)$ while the $M1(g^2)$ correspond to a combined fit according to Eq.4.4.6.

4.4.3.3 Z_V from the Ward Identity

As proposed in [84], Z_V can be computed using only Twisted Mass two point correlators via the Axial Ward Identity relation. Expressing the correlators in the physical basis the relation reads

$$Z_V \partial_0 C^{(2)}_{A0P5}(t) = \left[\mu_1^{\text{val}} + \mu_2^{\text{val}}\right] C^{(2)}_{P5P5}(t)$$

where ∂_0 is the symmetric lattice time derivative while μ_1^{val} and μ_2^{val} are the pair of valence quark masses. The involved bare correlators have been computed for a pair of valence quark masses equal to the sea quark mass, i.e $\mu_1^{\text{val}} = \mu_2^{\text{val}} = \mu^{\text{sea}}$, using stochastic propagators with sources placed at randomly located time-slices[5]. A typical plot on the data quality of Z_V is shown in Figure 4.4.8.

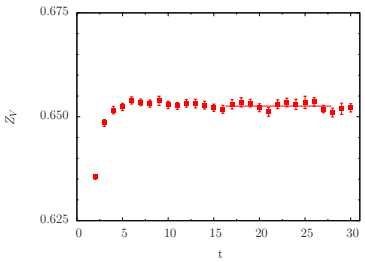

Figure 4.4.8: Example of quality plateau of Z_V computed from the Ward Identity at $\beta = 2.10$ and $\mu^{\text{sea}} = \mu_1^{\text{val}} = \mu_2^{\text{val}} = 0.0046$. The θ-average has been previously performed.

The chiral limit is reached after a linear extrapolation in $(M^{\text{sea}})^2$ as illustrated in Figure 4.4.9. Final results are collected in Table 4.4.3 compared with the determination of the Z_V from the RI-MOM method.

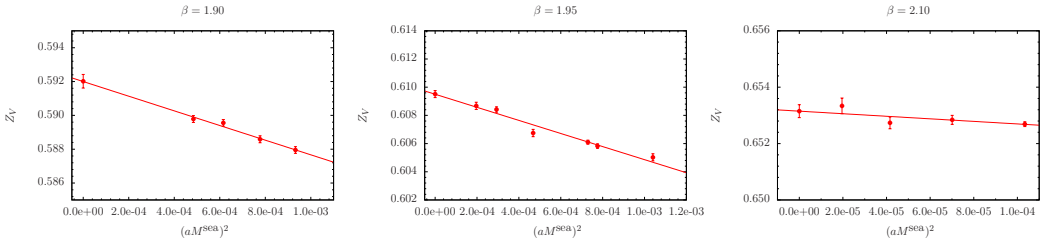

Figure 4.4.9: Sea chiral extrapolation in terms of the polar sea quark mass of the Z_V RC computed from the WI

[5] These correlators have been produced in the $N_f = 2 + 1 + 1$ run with stochastic sources for the computation of the B_K bag parameter

4.4.4 Four-fermion RCs

The computation of the RCs of the four-fermion operators in the RI-MOM method is similar to the one followed in the case of the bilinears. As indicated in section 4.3, for the renormalization of the bag parameters, we are only interested in the computation of the RC for the PC+ operators. The procedure for extracting $\mathbf{Z}^{\mathtt{PC+}}$ can be summarized in the following steps

1. Compute the amputated Green function $\mathbf{\Lambda}^{\mathtt{PC+}}$ defined in Eq.4.3.5 and from it, the dynamical matrix $\mathbf{D}^{\mathtt{PC+}}$ for each β, each ensemble Ep/m and each valence quark mass in the set of discrete lattice momenta specified in subsection 4.4.2.

2. In order to reduce the statistical error, we average our estimators for the dynamical matrix over two equivalent pattern of Wilson parameters (r_1, r_2, r_3, r_4), namely $(1, 1, 1, -1)$ and $(-1, -1, -1, 1)$. Given the structure of Eq.4.3.5, it is straightforward to notice that these are the only two patterns of Wilson parameters providing different results. Consequently, averaging over them is completely equivalent to average over the eight possible Wilson pattern.

3. Subtraction of $\mathcal{O}(a^2 g^2)$ cutoff effects from $\mathbf{D}^{\mathtt{PC+}}$, computed with one-loop perturbation theory on the lattice in [94].

4. Average over equivalent momenta, i.e over momenta p_ν with the same $\tilde{p}^2$. We have checked that performing the average over equivalent Wilson parameters and equivalent momenta before and after the chiral extrapolation leads to consistent results.

5. Extrapolate to the valence chiral limit keeping into account the contributions $\propto 1/\left(M_{PS}^{\mathrm{val}}\right)^2$ and possible $\propto 1/\left(M_{PS}^{\mathrm{val}}\right)^4$ coming from the simple and double GB-pole.

6. Build the $\mathcal{O}(a)$ improved estimators by performing the θ-average.

7. Compute $\mathbf{Z}^{\mathtt{PC+}}$ from Eq.4.3.8. In the practice, we check that the mixing matrix $\mathbf{\Delta}$ behaves as a $\mathcal{O}(a^2)$ artifact and vanish within errors in the range of $\tilde{p}^2$ that we use for extract the RCs. For these reasons, the effect of $\mathbf{\Delta}$ in Eq.4.3.8 is neglected and we assume a continuum-like renormalization pattern for the four-fermion operator.

8. Extrapolate to the sea chiral limit using a linear fit in $\left(M^{\mathrm{sea,E}}\right)^2$.

9. Evolve, using the known perturbative evolution [95], the RCs to a common reference scale: $\tilde{p}^2 = (1/a)^2$.

10. Subtract the residual $\mathcal{O}(a^2\tilde{p}^2)$ lattice artefacts according to the so-called M1 and M2 methods.

4.4.4.1 Chiral extrapolations

According to the conclusions in subsection 4.3.1, in order to properly subtract the GB-pole contribution and perform the valence chiral extrapolation, we fit the dynamic matrix $D_{ij}^{\mathtt{PC+}}$ for each $a^2\tilde{p}^2$, for each β and each ensemble Ep/m to the ansätz[6]

$$\begin{aligned} D_{ij}^{\mathrm{Ep/m}}\left(\mu^{\mathrm{val,E}};a^2\tilde{p}^2\right) = \; & A_{ij}^{\mathrm{Ep/m}}\left(a^2\tilde{p}^2\right) + B_{ij}^{\mathrm{Ep/m}}\left(a^2\tilde{p}^2\right) M^{\mathrm{val,Ep/m}} \\ & + C_{ij}^{\mathrm{Ep/m}}\left(a^2\tilde{p}^2\right) \times \left[\frac{1}{\left[M_{PS}^{(OS)\mathrm{val,Ep/m}}\right]^2} + \frac{\delta_i}{\left[M_{PS}^{(TM)\mathrm{val,Ep/m}}\right]^2}\right] \\ & + \delta_i D_{ij}^{\mathrm{Ep/m}}\left(a^2\tilde{p}^2\right) \times \left[\frac{1}{\left[M_{PS}^{(OS)\mathrm{val,Ep/m}}\right]^4} + \frac{1}{\left[M_{PS}^{(TM)\mathrm{val,Ep/m}}\right]^4}\right] \end{aligned} \tag{4.4.7}$$

where $\delta_1 = 0$ and $\delta_i = 1$ if $i = 2, 3, 4, 5$ and we are only considering diagonal valence quark masses for the construction of the amputated Green function, i.e $M_1^{\mathrm{val}} = M_2^{\mathrm{val}} = M^{\mathrm{val}}$. In Eq.4.4.7, the last term corresponds to the double GB-pole which may appear in D_{ij} with $i = 2, 3, 4, 5$. In contrast with what we found for the $N_f = 2$ RCs, here the double GB-pole is necessary in order to ensure $\Delta_{ij} \to 0$. The wrong chirality mixing coefficients Δ_{ij} are zero within errors with a deviation of about 0.01 at most (see Figure 4.4.17) if we subtract the double GB-pole. However, if only one GB-pole is subtracted we found that this deviation could reach 0.025-0.050 in the worst cases.

In Figure 4.4.10 to Figure 4.4.15 we display typical examples of the effected of GB-pole subtraction in the matrix elements of the dynamics matrix for the lightest ensemble at each value of β and p/m. As it is shown, for the same β and ensemble p/m data show different behaviour in aM^{val} and their GB-pole contribution should be subtracted with the pseudoscalar meson mass computed in each case. This is the reason why we perform the θ-average after the valence chiral extrapolation. After the GB-pole subtraction a smooth dependence upon M^{val} is observed.

The sea chiral limit is performed at fixed β and $a^2\tilde{p}^2$. As we did in the case of the bilinears, we fit Z_{ij} and Δ_{ij} data to a first order polynomial in $\left(aM^{\mathrm{sea}}\right)^2$, as shown in Figure 4.4.16 for the case of Z_{ij}. We find that the dependence on the sea quark mass is hardly visible within our statistical error bars.

[6] For notation economy, the superindex PC+ has been removed.

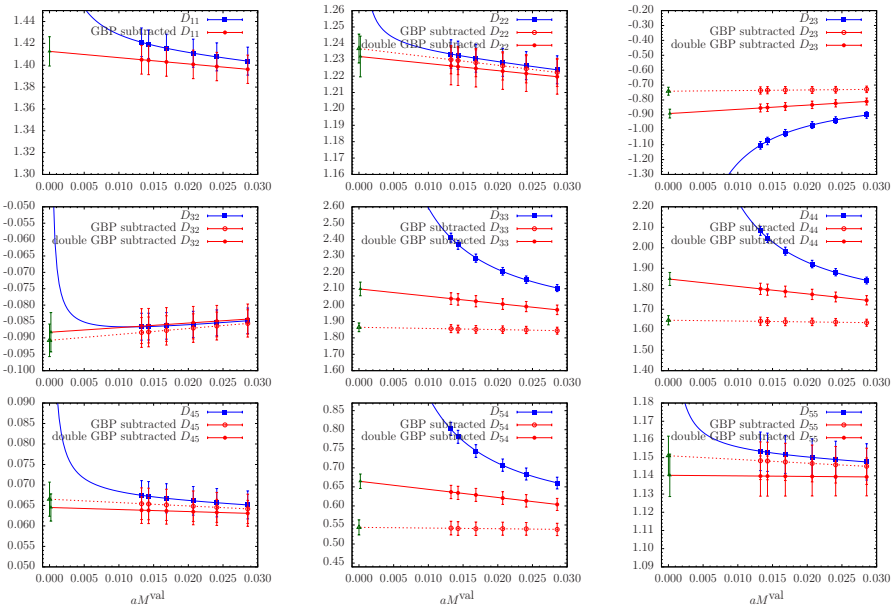

Figure 4.4.10: GB-pole subtraction and valence chiral limit for D_{ij} plotted vs $aM^{\rm val}$ for the A1p ensemble of $\beta = 1.90$ at $(a\tilde{p})^2 \approx 1.565$.

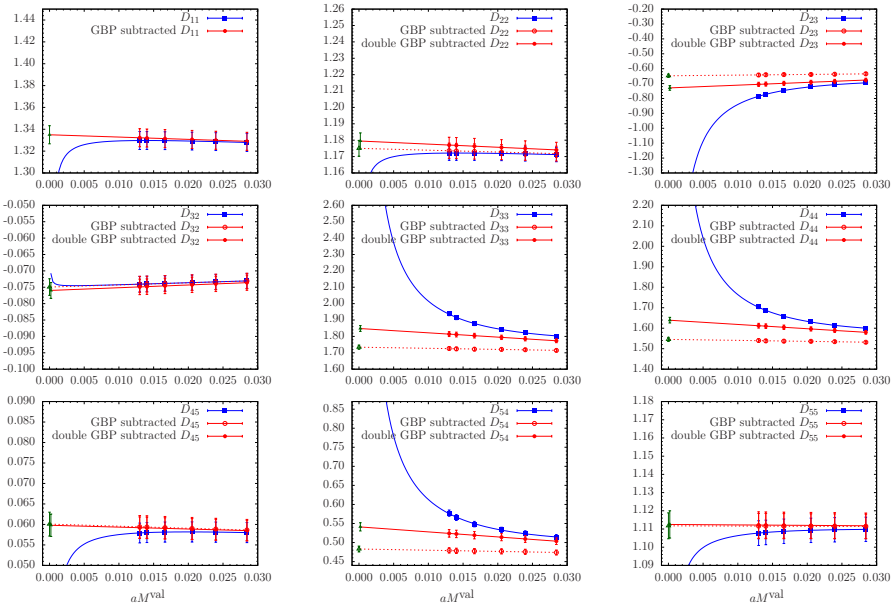

Figure 4.4.11: GB-pole subtraction and valence chiral limit for D_{ij} plotted vs $aM^{\rm val}$ for the A1m ensemble of $\beta = 1.90$ at $(a\tilde{p})^2 \approx 1.565$

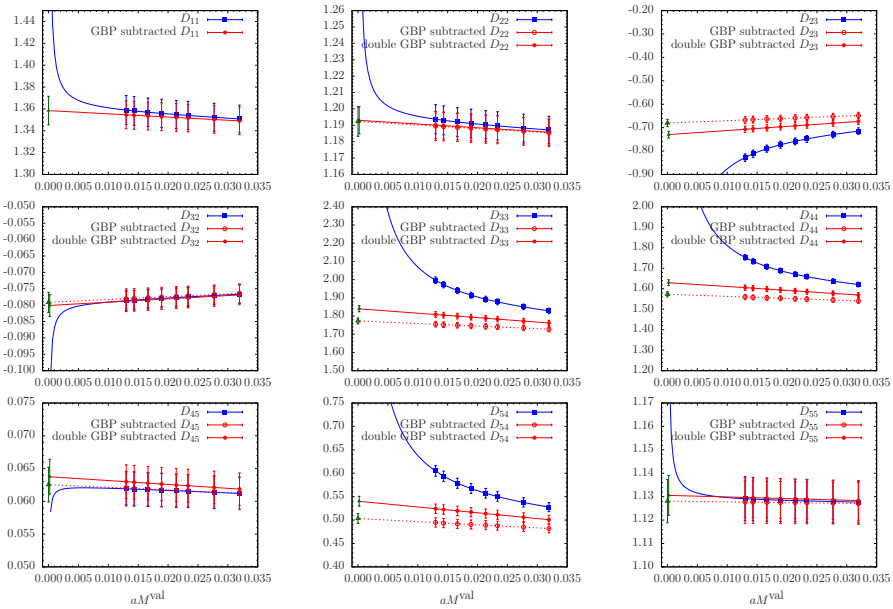

Figure 4.4.12: GB-pole subtraction and valence chiral limit for D_{ij} plotted vs aM^{val} for the 4p ensemble of $\beta = 1.95$ at $(a\tilde{p})^2 \approx 1.565$.

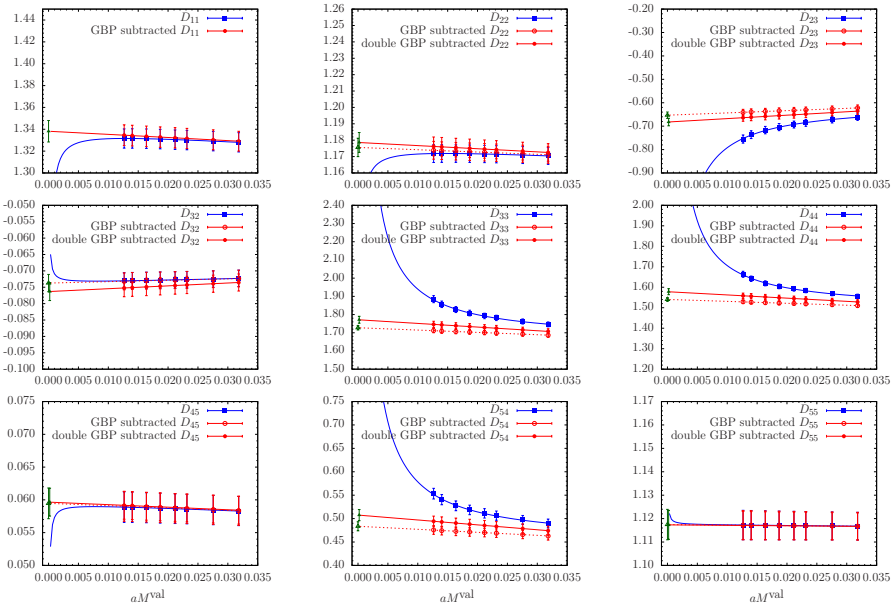

Figure 4.4.13: GB-pole subtraction and valence chiral limit for D_{ij} plotted vs aM^{val} for the 4m ensemble of $\beta = 1.95$ at $(a\tilde{p})^2 \approx 1.565$.

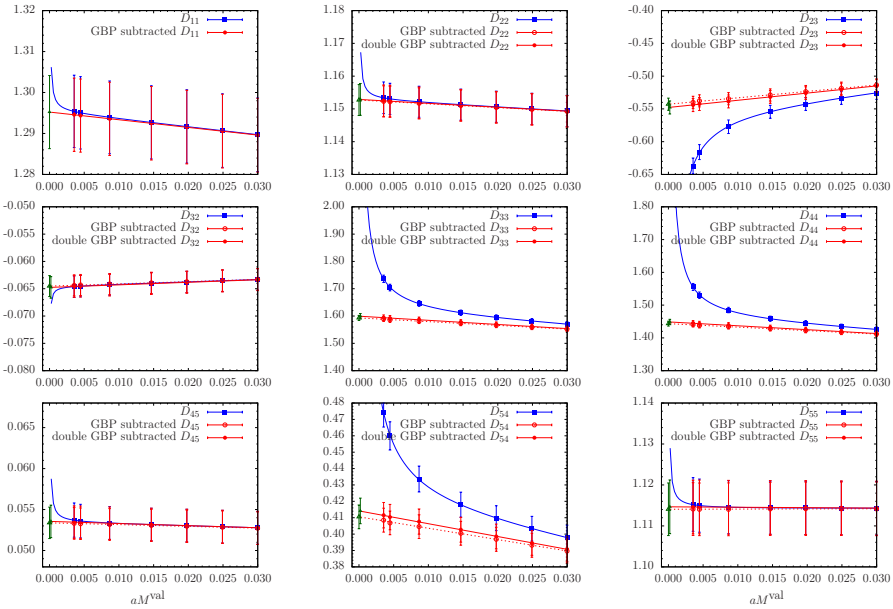

Figure 4.4.14: GB-pole subtraction and valence chiral limit for D_{ij} plotted vs $aM^{\rm val}$ for the 2p ensemble of $\beta = 2.10$ at $(a\tilde{p})^2 \approx 1.573$.

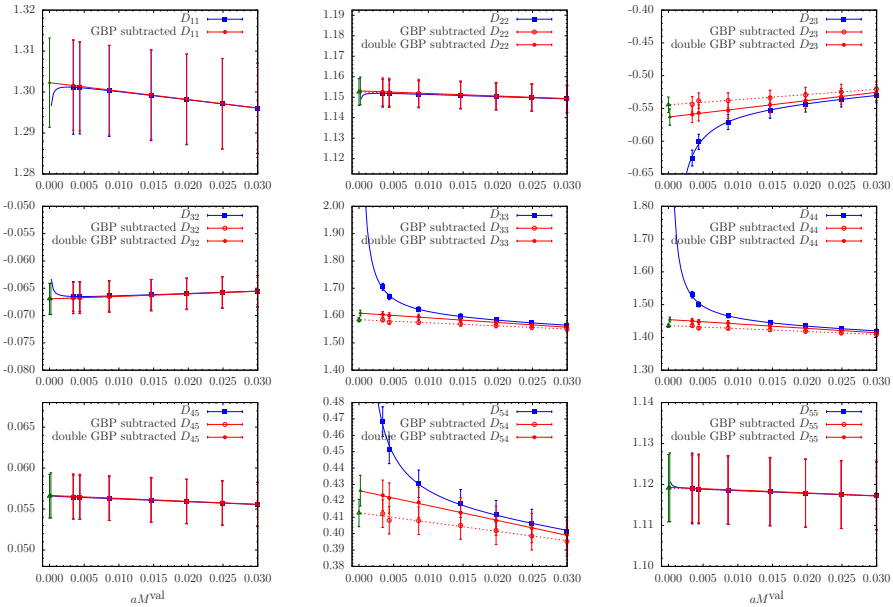

Figure 4.4.15: GB-pole subtraction and valence chiral limit for D_{ij} plotted vs $aM^{\rm val}$ for the 2m ensemble of $\beta = 2.10$ at $(a\tilde{p})^2 \approx 1.573$.

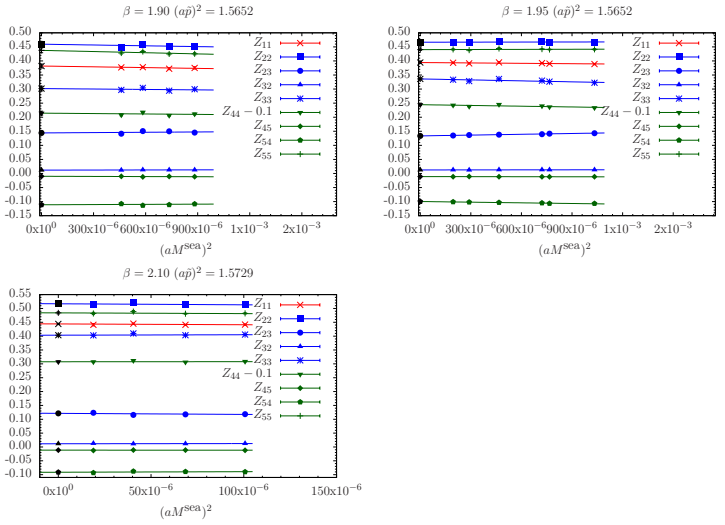

Figure 4.4.16: Sea chiral extrapolation in terms of the polar sea quark mass of the θ-averaged RC estimators for Z_{ij} with $\{ij\} = \{11, 22, 23, 32, 33, 44, 45, 54, 55\}$ at $(a\tilde{p})^2 \simeq 1.5$ for each β .

4.4.4.2 Absence of wrong chirality mixing

In Figure 4.4.17 one can see that for all operators the mixing coefficients Δ_{ij}, θ-averaged and extrapolated to the valence and sea chiral limit, vanish within errors in the range of $(a\tilde{p})^2$ we use. We also checked that this behaviour is systematically clearer as β increases. This indicates that wrong chirality mixing effects are reduced to $\mathcal{O}(a^2)$ artifacts, as expected. For these reasons, the effects of Δ have been neglected in our final RC analysis.

4.4.4.3 Renormalization scale dependence and subtraction of $\mathcal{O}(a^2g^2)$ discretization effects

The procedure to investigate the presence of discretization effects and to study the renormalization scale dependence of the four-fermion RCs is close to the one described subsection 4.4.3.2 for the case of bilinear operators.

In order to disentangle the $\mathcal{O}(a^2\tilde{p}^2)$ cutoff effects from the genuine continuum $\tilde{p}^2$ dependence we evolve the RC estimators computed at each value of $\tilde{p}^2$ to a common scale $\mu_0 = a^{-1}$ by using the known NLO formula for the operators Q_i described in Appendix C.

The residual $\mathcal{O}(a^2)$ discretization effects can be reduced by constructing the improved RC estimators obtained by removing discretization errors up to $\mathcal{O}(a^2g^2)$ by exploiting the one-loop lattice perturbation theory results for the vertices D_{ij} computed in [94]. Including cutoff effects up to second order in a the dynamical matrix has the expression

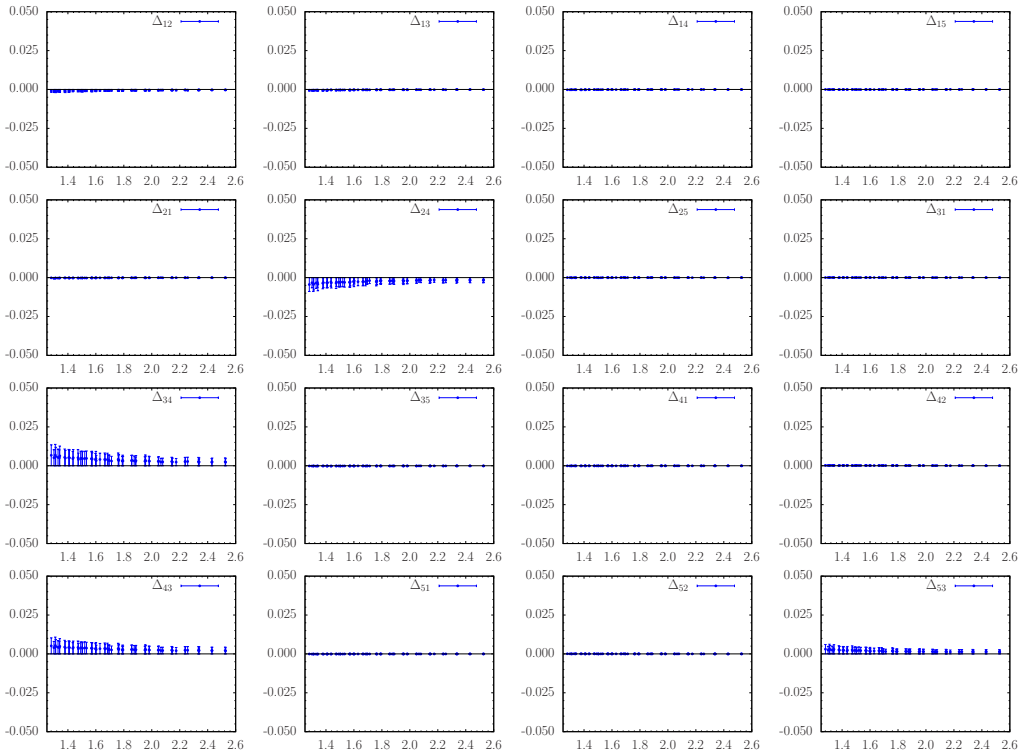

Figure 4.4.17: The behaviour of the mixing coefficients Δ_{ij}, as function of $(a\tilde{p})^2$ for the smallest lattice spacing, corresponding to $\beta = 2.10$.

$$D_{ij}(p)^{\text{pert.}} = 1 + \frac{g^2}{16\pi^2}\left\{ b_{ij}^{(1)} + b_{ij}^{(2)} \log(a^2p^2) + a^2\left[p^2\left(d_{ij}^{(1)} + d_{ij}^{(2)} \log(a^2p^2) \right) + d_{ij}^{(3)} \frac{\sum_\rho p_\rho^4}{p^2} \right] \right\} + \mathcal{O}(a^4g^2, g^4) \tag{4.4.8}$$

where the numerical value of d_{ij} has been computed in [94] for a general covariant gauge, and several popular choices for the Symanzik coefficients. For reader convenience the explicit values for the special choice $c_{SW} = 0$, $\lambda = 0$ (Landau gauge), $r_1 = r_2 = r_3 = -r_4$ and Iwasaki gauge action used for $N_f = 4$ simulation are collected in Appendix D. The calculations in [94] are performed using massless fermions described by the Wilson (or Clover) action. As RI-MOM is implemented in the chiral limit the $d_{ij}^{(k)}$ factors found in the previous reference are identical if we consider the Twisted Mass and the Osterwalder-Seiler action in the twisted basis $\{\bar{\chi}, \chi\}$. Therefore, according to the four-fermion mapping between the twisted basis $\{\bar{\chi}, \chi\}$ and the physical one $\{\bar{\psi}, \psi\}$ with our setup, described

in Eq.3.4.15, the relevant $d_{ij}^{(k)}$ for the PC+ operators in the lattice basis should be

$$\begin{pmatrix} d_{11}^{+} & 0 & 0 & 0 & 0 \\ 0 & d_{22}^{-} & -d_{23}^{-} & 0 & 0 \\ 0 & -d_{32}^{-} & d_{33}^{-} & 0 & 0 \\ 0 & 0 & 0 & d_{44}^{+} & d_{45}^{+} \\ 0 & 0 & 0 & d_{54}^{+} & d_{55}^{+} \end{pmatrix}^{(k)\,\mathtt{PV}}$$

where the $d_{ij}^{(k)}$ elements are directly the ones that we read from [94]. Moreover we know [94]

$$\begin{array}{rclrcl} d_{22}^{\mathtt{PV}+} & = & d_{22}^{\mathtt{PV}-} & d_{23}^{\mathtt{PV}+} & = & -d_{23}^{\mathtt{PV}-} \\ d_{32}^{\mathtt{PV}+} & = & -d_{32}^{\mathtt{PV}-} & d_{33}^{\mathtt{PV}+} & = & d_{33}^{\mathtt{PV}-} \end{array}$$

so finally, the $d_{ij}^{(k)}$ to subtract the PC+ operators with our particular setup can be directly read from the PV+ ones for the Wilson action, i.e those listed in [94]. These $\mathcal{O}(a^2 g^2)$ are analytically subtracted from our numerical computation of the dynamical matrix D_{ij} through

$$D_{ij}(p)^{\text{corr.}} = D_{ij}(p) - \frac{g^2}{16\pi^2} a^2 \left[p^2 \left(d_{ij}^{(1)} + d_{ij}^{(2)} \log(a^2 p^2) \right) + d_{ij}^{(3)} \frac{\sum_\rho p_\rho^4}{p^2} \right]$$

In the numerical evaluation of the perturbative corrections, we take the coupling constant g^2 as the simple boosted coupling $\tilde{g}^2 = g_0/\langle P \rangle$ with $\langle P \rangle$ the non perturbative average plaquette. The important impact of the perturbative corrections in removing the unwanted $(a\tilde{p})^2$ is illustrated in Figure 4.4.18 for the case of $\beta = 1.95$. In this figure the uncorrected values are compared with the corrected values using the boosted coupling.

After the perturbative subtraction, we still allow for a residual dependence on $a^2\tilde{p}^2$. In order to deal with these cutoff effects we use the two M1 and M2 methods presented in subsection 4.4.3.2. In the M1-method we fit data to the linear ansätz

$$Z_{ij}^{RI'}\left(\mu_0^2 = a\,(\beta)^{-2}; a^2\tilde{p}^2\right) = Z_{ij}^{RI'}\left(\mu_0^2 = a\,(\beta)^{-2}\right) + \lambda_{ij}\left(a^2\tilde{p}^2\right) \tag{4.4.9}$$

in the interval $1.5 \leq a^2\tilde{p}^2 \leq 2.2$. Therefore, a simultaneous linear fit extrapolation in $a^2\tilde{p}^2$, where the slope λ_{ij} depend smoothly on each β, should be performed. In Figure 4.4.19 the simultaneous linear fits in $(a\tilde{p})^2$ are reported.

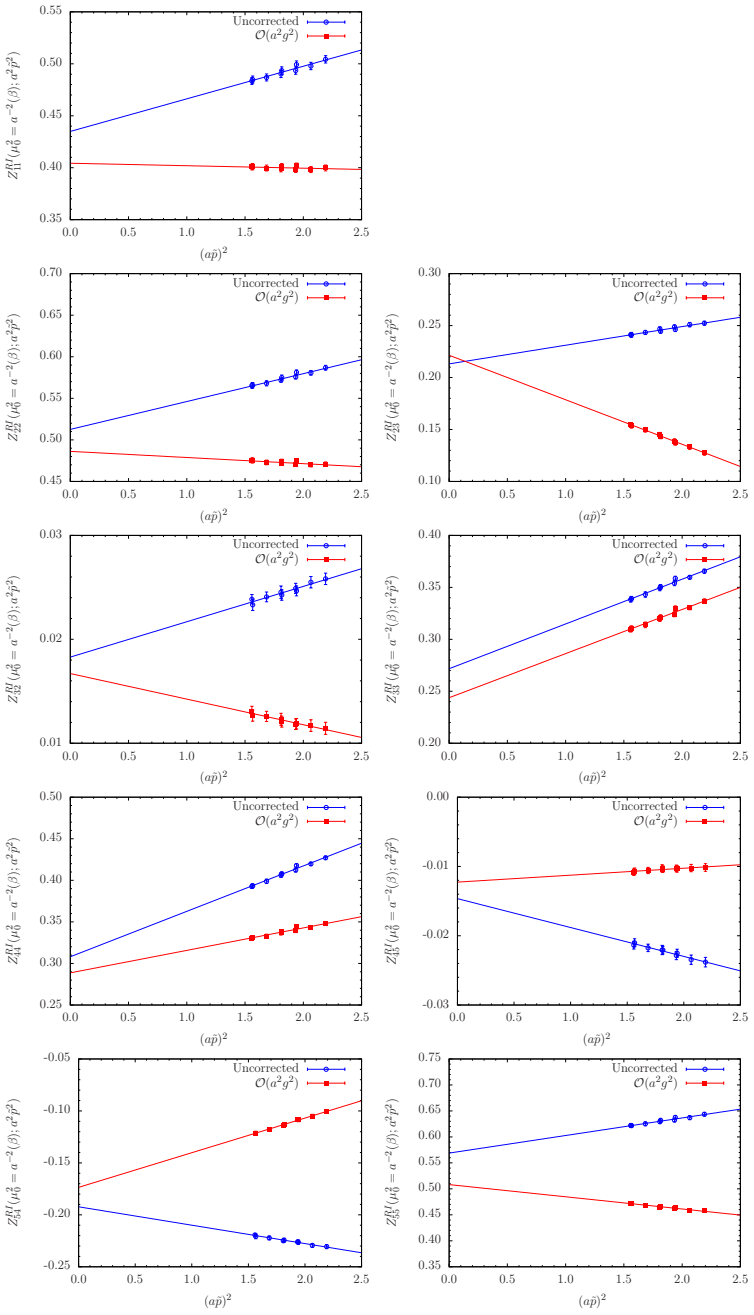

Figure 4.4.18: Effect of the perturbative subtraction from Z_{ij} with $\{ij\} = \{11, 22, 23, 32, 33, 44, 45, 54, 55\}$ renormalized in the RI'-MOM scheme at $\mu_0 = a^{-2}(\beta)$ at $\beta = 1.95$ once they are extrapolated to the valence and sea chiral limit. Only data in the M1 interval and satisfying the cut in Eq.4.4.4 is plotted

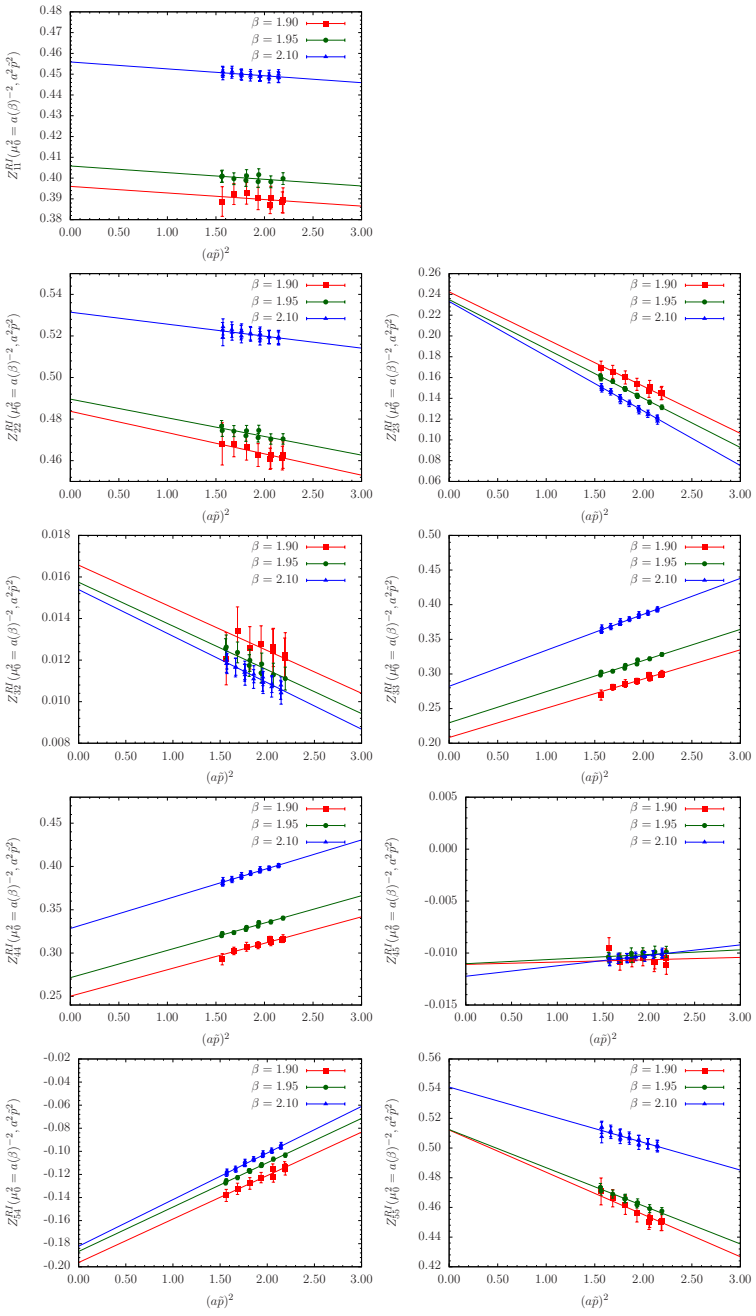

Figure 4.4.19: $Z_{ij}^{RI'}\left(\mu_0^2 = a\,(\beta)^{-2}; a^2\tilde{p}^2\right)$ for $\{ij\} = \{11, 22, 23, 32, 33, 44, 45, 54, 55\}$ as functions of $(a\tilde{p})^2$ for the three β values considered in our study. The straight lines represent the simultaneous linear fit to the lattice data in the interval $1.5 \leq a^2\tilde{p}^2 \leq 2.2$.

Final estimates

The M1 and M2 values of $Z_{ij}^{RI'}\left(\mu_0^2\right)$ are finally used to evaluate, via the NLO continuum QCD evolution discussed in Appendix C, the RC estimates in the $\overline{MS}$ and RI-MOM schemes. The final estimates for the RC matrices of the four-fermion operators in the lattice basis $\{\mathbf{O}_i\}$ are listed below. We present results obtained from both M1 and M2 methods, in $\overline{MS}$ and RI-MOM at 2 GeV.

($\overline{\text{MS}}$, 2 GeV):

$$\mathbf{Z}_\chi{}^{\text{PC+}}(\beta = 1.90; M1) = \begin{pmatrix} 0.407(07) & 0 & 0 & 0 & 0 \\ 0 & 0.473(09) & 0.206(08) & 0 & 0 \\ 0 & 0.024(02) & 0.282(08) & 0 & 0 \\ 0 & 0 & 0 & 0.308(08) & -0.006(01) \\ 0 & 0 & 0 & -0.183(07) & 0.557(11) \end{pmatrix}$$

$$\mathbf{Z}_\chi{}^{\text{PC+}}(\beta = 1.95; M1) = \begin{pmatrix} 0.421(05) & 0 & 0 & 0 & 0 \\ 0 & 0.485(06) & 0.228(04) & 0 & 0 \\ 0 & 0.023(01) & 0.262(05) & 0 & 0 \\ 0 & 0 & 0 & 0.296(05) & -0.004(01) \\ 0 & 0 & 0 & -0.209(03) & 0.586(07) \end{pmatrix}$$

$$\mathbf{Z}_\chi{}^{\text{PC+}}(\beta = 2.10; M1) = \begin{pmatrix} 0.482(04) & 0 & 0 & 0 & 0 \\ 0 & 0.543(05) & 0.262(03) & 0 & 0 \\ 0 & 0.022(01) & 0.287(03) & 0 & 0 \\ 0 & 0 & 0 & 0.325(03) & -0.001(01) \\ 0 & 0 & 0 & -0.255(03) & 0.681(06) \end{pmatrix}$$

($\overline{\text{MS}}$, 2 GeV):

$$\mathbf{Z}_\chi{}^{\text{PC+}}(\beta = 1.90; M2) = \begin{pmatrix} 0.403(05) & 0 & 0 & 0 & 0 \\ 0 & 0.456(05) & 0.104(05) & 0 & 0 \\ 0 & 0.016(01) & 0.399(06) & 0 & 0 \\ 0 & 0 & 0 & 0.379(05) & -0.003(01) \\ 0 & 0 & 0 & -0.091(04) & 0.493(06) \end{pmatrix}$$

$$\mathbf{Z}_\chi{}^{\text{PC+}}(\beta = 1.95; M2) = \begin{pmatrix} 0.415(03) & 0 & 0 & 0 & 0 \\ 0 & 0.469(02) & 0.147(02) & 0 & 0 \\ 0 & 0.017(01) & 0.352(02) & 0 & 0 \\ 0 & 0 & 0 & 0.352(02) & -0.002(01) \\ 0 & 0 & 0 & -0.133(02) & 0.531(03) \end{pmatrix}$$

$$\mathbf{Z}_\chi{}^{\text{PC+}}(\beta = 2.10; M2) = \begin{pmatrix} 0.481(03) & 0 & 0 & 0 & 0 \\ 0 & 0.535(03) & 0.209(02) & 0 & 0 \\ 0 & 0.019(01) & 0.330(02) & 0 & 0 \\ 0 & 0 & 0 & 0.353(02) & -0.000(01) \\ 0 & 0 & 0 & -0.204(02) & 0.657(04) \end{pmatrix}$$

(RI-MOM, 2 GeV):

$$\mathbf{Z}_\chi{}^{\texttt{PC+}}(\beta = 1.90; M1) = \begin{pmatrix} 0.399(07) & 0 & 0 & 0 & 0 \\ 0 & 0.485(010) & 0.224(08) & 0 & 0 \\ 0 & 0.018(01) & 0.233(07) & 0 & 0 \\ 0 & 0 & 0 & 0.279(07) & -0.013(01) \\ 0 & 0 & 0 & -0.183(07) & 0.524(10) \end{pmatrix}$$

$$\mathbf{Z}_\chi{}^{\texttt{PC+}}(\beta = 1.95; M1) = \begin{pmatrix} 0.413(05) & 0 & 0 & 0 & 0 \\ 0 & 0.498(06) & 0.245(04) & 0 & 0 \\ 0 & 0.016(01) & 0.217(04) & 0 & 0 \\ 0 & 0 & 0 & 0.268(05) & -0.012(01) \\ 0 & 0 & 0 & -0.207(03) & 0.550(06) \end{pmatrix}$$

$$\mathbf{Z}_\chi{}^{\texttt{PC+}}(\beta = 2.10; M1) = \begin{pmatrix} 0.473(04) & 0 & 0 & 0 & 0 \\ 0 & 0.557(05) & 0.281(03) & 0 & 0 \\ 0 & 0.016(01) & 0.237(03) & 0 & 0 \\ 0 & 0 & 0 & 0.295(03) & -0.011(01) \\ 0 & 0 & 0 & -0.252(02) & 0.640(06) \end{pmatrix}$$

(RI-MOM, 2 GeV):

$$\mathbf{Z}_\chi{}^{\texttt{PC+}}(\beta = 1.90; M2) = \begin{pmatrix} 0.395(05) & 0 & 0 & 0 & 0 \\ 0 & 0.468(06) & 0.124(05) & 0 & 0 \\ 0 & 0.011(01) & 0.330(05) & 0 & 0 \\ 0 & 0 & 0 & 0.341(04) & -0.010(01) \\ 0 & 0 & 0 & -0.100(04) & 0.463(06) \end{pmatrix}$$

$$\mathbf{Z}_\chi{}^{\texttt{PC+}}(\beta = 1.95; M2) = \begin{pmatrix} 0.407(03) & 0 & 0 & 0 & 0 \\ 0 & 0.481(02) & 0.166(02) & 0 & 0 \\ 0 & 0.012(01) & 0.291(02) & 0 & 0 \\ 0 & 0 & 0 & 0.318(02) & -0.010(01) \\ 0 & 0 & 0 & -0.138(02) & 0.499(03) \end{pmatrix}$$

$$\mathbf{Z}_\chi{}^{\texttt{PC+}}(\beta = 2.10; M2) = \begin{pmatrix} 0.472(03) & 0 & 0 & 0 & 0 \\ 0 & 0.549(03) & 0.228(02) & 0 & 0 \\ 0 & 0.014(01) & 0.273(02) & 0 & 0 \\ 0 & 0 & 0 & 0.319(02) & -0.010(01) \\ 0 & 0 & 0 & -0.205(02) & 0.617(04) \end{pmatrix}$$

Chapter 5

$\overline{K}^0$-K^0 and $\overline{D}^0$-D^0 bag parameters from $\mathbf{N_f = 2}$

In this chapter I will describe the simulation, analysis and results of the first unquenched, continuum extrapolated, lattice QCD results for the matrix elements of the operators describing neutral $\overline{K}^0$-K^0 and $\overline{D}^0$-D^0 oscillations and their possible impact in extensions of the Standard Model. In our non perturbative computation we use a combination of $N_f = 2$ maximally twisted sea quarks and Osterwalder-Seiler valence quarks in order to achieved both $\mathcal{O}(a)$ improvement and continuum-like renormalization pattern for the relevant four-fermion operators as described in chapter 2 and chapter 3. The computation of the renormalization constants has been performed in the RI-MOM scheme described in chapter 4.

The outline of the chapter is as follows. In the first section I will give the details of the ETMC simulation with $N_f = 2$ dynamical sea quarks. In the second section I will discuss the strategy, based on the formulae presented in chapter 3, for obtaining the accurate numerical estimates of the five B_i parameters in the kaon sector. The details and corresponding results for the renormalization of the relevant two- and four-fermion operators following the RI-MOM method described in chapter 4 are collected in Appendix G. In the third section, based on our results for the $\Delta S = 2$ bag parameters, I will briefly discuss the implications for NP of the UTA. The method to obtain the bag parameters in the $\overline{D}^0$-D^0 system follows a similar strategy as in the $\overline{K}^0$-K^0 one. Results of the B_i parameters for the $\overline{D}^0$-D^0 will be presented in the fourth section.

5.1 $\mathbf{N_f = 2}$ simulation

We use, for this analysis, the $N_f = 2$ dynamical gauge configurations with up and down mass degenerate quarks generated by the ETMC. The ETM Collaboration has generated

$N_f = 2$ configuration ensembles using the tree-level Symmanzik improved gauge action and the twisted mass quark action at maximal twist at four values of the inverse bare gauge coupling β and several values of light sea quark masses μ_{sea}. The values of the simulated lattice spacings lie in the interval $[0.05 : 0.1]$fm. We produce stochastic propagators with sources placed at randomly located time-slices. Bare quark mass parameters are chosen such as to get light pseudoscalar meson masses, "pions", in the range $[280 : 500]$ MeV and heavy-light pseudoscalar mesons around the physical K^0 mass and the physical D^0 meson mass. Simulation details are given in Table 5.1.1.

The value of the light quark mass parameter, $a\mu_\ell$, is common for the sea and valence quarks. We simulate three heavy valence quark masses $\mu_{\text{“}s\text{”}}$ around the physical strange mass and three heavy valence quark masses $\mu_{\text{“}c\text{”}}$ around the physical charm one. We also produce a number of heavy quark masses above the charm quark mass in order to extrapolate to the b-quark mass applying the ratio method as it will be described in chapter 6.

Physical values are obtained by interpolating data in $\mu_{\text{“}s\text{”}}$ and $\mu_{\text{“}c\text{”}}$ to the physical value of μ_s and μ_c while chiral and continuum extrapolations ($\mu_\ell \to \mu_{u/d}$ and $a \to 0$) are carried out simultaneously. The physical values for the quark masses μ_s, μ_c and $\mu_{u/d}$ have been previously computed and can be found in [96]. Other quantities entering the data analysis, such as the low energy constants af_0, $a\hat{B}_0$ and the lattice spacing are known from previous ETMC analyses [67, 97, 98].

β	$L^3 \times T$	N_{stat}	$a\mu_\ell = a\mu_{\rm sea}$	$a\mu_{\text{“}s\text{”}}$	$a\mu_{\text{“}c\text{”}}$	$a\mu_h$
3.80	$24^3 \times 48$	128	0.0080 0.0110	0.0175	0.1982	0.3225 0.3793
$a = 0.098(3)(2)$ fm				0.0194	0.2331	0.4461 0.5246
$T_{\rm sep} = 16$				0.0213	0.2742	0.6170 0.7257
						0.8536 1.004
3.90	$24^3 \times 48$	240	0.0040 0.0064	0.0159	0.1828	0.2974 0.3498
$a = 0.085(2)(1)$ fm			0.0085 0.0100	0.0177	0.2150	0.4114 0.4839
$T_{\rm sep} = 18$	$32^3 \times 64$	144	0.0030 0.0040	0.0195	0.2529	0.5691 0.6694
						0.7873 0.9260
4.05	$32^3 \times 64$	144	0.0030 0.0060	0.0139	0.1572	0.2558 0.3008
$a = 0.067(2)(1)$ fm			0.0080	0.0154	0.1849	0.3538 0.4162
$T_{\rm sep} = 22$				0.0169	0.2175	0.4895 0.5757
						0.6771 0.7960
4.20	$32^3 \times 64$	144	0.0065	0.0116	0.13315	0.2166 0.2548
$a = 0.054(1)(1)$ fm				0.0129	0.1566	0.2997 0.3525
$T_{\rm sep} = 28$	$48^3 \times 96$	80	0.0020	0.0142	0.1842	0.4145 0.4876
						0.5734 0.6745

Table 5.1.1: Details of simulation runs at $\beta = 3.80,\ 3.90,\ 4.05$ and 4.20. In the quoted values of the lattice spacing the first uncertainty is statistical and the second systematic.

Smearing techniques are used to improve the determination of the ground state contribution with respect to the case of simpler, local interpolating fields. Details about

smearing are presented in Appendix A.

We have tested several smearing techniques and the main outcome is that, for values around the physical charm mass and above, Gaussian smeared sources improve the quality of the extracted ground-state matrix elements allowing us to detect ground state signals at earlier time slices while for masses around the strange quark mass there is not significant improvement.

We consider Gaussian smeared quark fields [99] using the Jacobi method [100] described in Appendix A. More specifically, in our simulation the smeared quark fields are defined via

$$\psi^S = \left(\frac{1+\kappa_s D^S}{1+6\kappa_s}\right)^{N_s} \psi \tag{5.1.1}$$

where $\kappa_s = 4$ is the Jacobi parameter and $N_s = 30$ is the number of smearing steps. D^S is the smearing covariant derivative defined via

$$D^S(\vec{x},t;\vec{y},t) = \sum_{\mu=1}^{3} \left(U_\mu^{N_a}(\vec{x})\delta_{\vec{x}+\hat{\mu},\vec{y}} + U_\mu^{N_a\dagger}(\vec{x}-\mu)\delta_{\vec{x}-\hat{\mu},\vec{y}}\right)$$

with $U_\mu^{N_a}$ the N_a times APE smeared link [101], defined in terms of (N_a-1) times smeared link $U_\mu^{N_a-1}$ and its surrounding staples $V_{\mu\nu}^{(N_a-1)}$ as detailed in Appendix A

$$U_\mu^{N_a} = \mathrm{Proj}_{\mathrm{SU(3)}}\left[(1-\alpha)U_\mu^{N_a-1} + \frac{\alpha}{6}\sum_{\nu\neq\mu} V_{\mu\nu}^{(n-1)}\right]$$

In our simulation $\alpha = 0.5$ and the number of APE smearing steps is $N_a = 20$.

On the other hand, we found that decreasing the time separation between the sources has the effect of decreasing the statistical error of bare estimators of the bag parameters with heavy quarks around and above the charm quark mass when compared with the standard case where $T_{\mathrm{sep}} = T/2$. The values of T_{sep} we consider are also collected in Table 5.1.1.

It is important to remark that the use of smearing and $T_{\mathrm{sep}} < T/2$ are two features not strictly necessary for the case of $\overline{K}^0 - K^0$ oscillations. In fact, no relevant improvement has been obtained for the $\overline{K}^0 - K^0$ bag parameters with respect to the equivalent ETMC analysis with local sources separated by $T/2$ presented in [102]. The two improvements are introduced in the simulation in order to improve the signal in the study of bag parameters with heavy quark mass around and above the charm quark mass, that is for the $\overline{D}^0 - D^0$ and $\overline{B}^0 - B^0$ oscillations.

5.2 $\overline{K}^0 - K^0$ bag parameters

In order to arrive to the renormalized B_i values at the physical point we need to go through the following steps

1. Identification of the plateau fit of bare B_i estimates from lattice data.
2. Operator renormalization at each lattice spacing.
3. Continuum ($a \to 0$) and chiral extrapolation ($\hat{\mu}_\ell \to \hat{\mu}_{u/d}$) with $\hat{\mu}_{\text{“}s\text{”}}$ set to the strange quark mass μ_s.

5.2.1 Extracting bare estimates from lattice data

Bare estimates for the bag parameters are obtained from the non-renormalized version of Eq.3.4.18

$$\begin{aligned}
&\frac{\left[C^{(3)}_{Q_1}(x_0)\right]_{SS}}{\left[C^{(2)}_{PA}(x_0)\right]_{SL}\left[C'^{(2)}_{PA}(x_0)\right]_{SL}} \xrightarrow[y_0 \ll x_0 \ll y_0+T_{\text{sep}}]{} \xi_1 B_1 \\
&\frac{\left[C^{(3)}_{Q_1}(x_0)\right]_{SS}}{\left[C^{(2)}_{PP}(x_0)\right]_{SL}\left[C'^{(2)}_{PP}(x_0)\right]_{SL}} \xrightarrow[y_0 \ll x_0 \ll y_0+T_{\text{sep}}]{} \xi_i B_i \;\; i = 2, ..., 5
\end{aligned} \tag{5.2.1}$$

where the subindex SS and SL denotes the smearing of the source and sink respectively. For our computation we consider three-point correlators with smeared meson walls while the four-fermion operator always remains at a point source. This choice forces the two-point correlator we have to consider. In order to cancel the pseudoscalar matrix elements appearing in the three-point correlators the smearing of the sources of the two two-point functions must be the same as in the source and sink of the three-point function.

The results for the bare quantities $\xi_i B_i$ at each value of β are collected in section F.3 on Appendix F.

For illustration in Figure 5.2.1 we display some examples of B_i at β =3.8, 3.9, 4.05 and 4.20 for the smallest value of the light quark mass and the simulated strange quark mass around the physical strange one. Vertical dotted lines indicate the plateau region where the K^0 and the $\overline{K}^0$ states dominate the three point correlators: $[T_{\text{sep}}/2 - 2 : T_{\text{sep}}/2 + 2]$.

5.2.2 Renormalization and scaling checks

We have computed the full renormalization matrix of the four-fermion operators RCs for the $N_f = 2$ adopting the RI-MOM scheme discussed in chapter 4. The strategy to compute the four-fermion RCs has been presented in subsection 4.4.4 for the $N_f = 4$ simulations. The implementation for $N_f = 2$ is completely analogous with the main advantage that $\mathcal{O}(a)$ improvement is automatically achieved without θ-average since we are working at maximal twist. Details about the $N_f = 2$ renormalization are collected in Appendix G.

We should mention that in our RC estimators cutoff effects, though parametrically of $\mathcal{O}(a^2)$, are numerically reduced owing to the subtraction of perturbatively evaluated $\mathcal{O}(a^2 g^2)$ contributions. After that, the two different procedures described in chapter 4

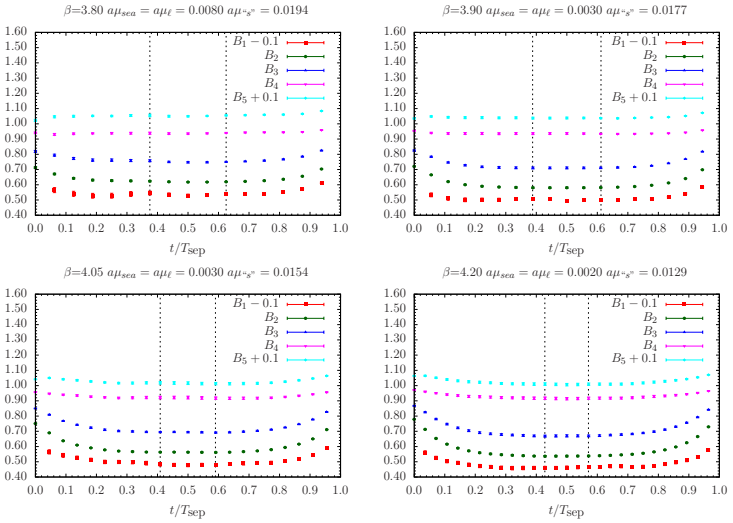

Figure 5.2.1: Data and time plateau for the bare B_i parameters, $(i = 1, 2, 3, 4, 5)$ for the $\overline{K}^0 - K^0$ system plotted vs $t/T_{\rm sep}$ for the lightest sea quark mass at each lattice spacing. B_i parameters have been averaged over the eight possible combinations of Wilson r-parameters satisfying the relation $r_1 = r_2 = r_3 = -r_4$ or equivalent.

are employed to deal with $\mathcal{O}(a^2p^2)$ discretization effects. The first, called M1, consists in linearly extrapolating to $a^2p^2 \to 0$. The second one, called M2, is obtained by averaging data over a fixed in physical units and very narrow momentum interval.

The a^2-scaling of the renormalized operator matrix elements constructed using M2 RCs will be in general different from their M1-type counterparts, but the continuum limit results for these quantities should be consistent with each other. For illustration, in Figure 5.2.2 we show the scaling behavior of $B_1\,(\hat{\mu}^*_\ell, \hat{\mu}_s)$ and $B_5\,(\hat{\mu}^*_\ell, \hat{\mu}_s)$ renormalized in $\overline{MS}$ at 2 GeV. In order to keep the issue of lattice artifacts separated from those related to the extrapolation to the physical quark mass point, the present scaling tests have been performed at fixed reference value of the light quark mass $\hat{\mu}^*_\ell = 46.8$ MeV which correspond to the second sea quark mass at β=4.20. The M1 and M2 methods differ only in the way one deals with the $\mathcal{O}(a^2)$ artifacts. The somewhat different slope in a^2 of the data points in Figure 5.2.2 should be ascribed to these effects. In all cases the a^2-scaling describes correctly the data points and we find that the continuum extrapolated quantities obtained by employing M1 and M2 RCs turn out to be consistent.

5.2.3 Combined continuum-chiral extrapolation

Extracting physical quantities from lattice data requires performing extrapolations and/or interpolations of renormalized lattice estimators to the physical point: continuum limit and physical value of quark masses.

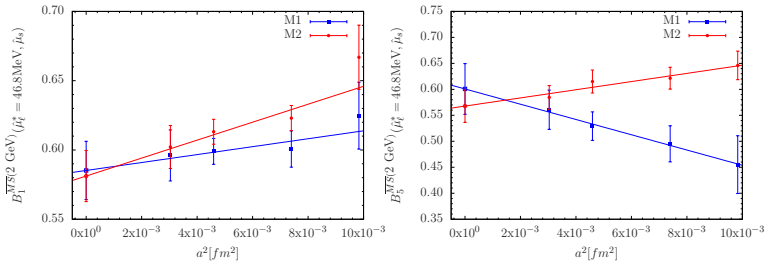

Figure 5.2.2: B_1 (left) and B_5 (right) as function of a^2, at the reference quark mass $\hat{\mu}_\ell^* = 46.8$ MeV for the two a^2p^2 fit procedures M1 and M2. Open symbols correspond to the continuum extrapolated results which are expected to agree. We have assumed a linear fit ansätz in a^2.

Results for each pair of valence quark masses are first interpolated to the physical $\hat{\mu}_s$ value. The renormalized estimates B_i show a smooth dependence on $\mu_{\text{“}s\text{”}}$ and can be interpolated linearly. This interpolation turns out to be under very good control since we have simulated three heavy valence quark masses around the physical strange quark mass, one of them very close to the physical value.

The continuum and chiral extrapolations are carried out in a combined way. For all reormalized bag parameters, we have tried out a linear fit ansätz

$$B_i = A + B\hat{\mu}_\ell + Da^2 \tag{5.2.2}$$

We also studied the case of a quadratic fit in μ_ℓ

$$B_i = A + B\hat{\mu}_\ell + C\hat{\mu}_\ell^2 + Da^2 \tag{5.2.3}$$

Finally, we have also considered infinite volume and continuum Next-to-Leading-Order (NLO) Chiral Perturbation Theory (ChPT) fit functions for B_i based on the formulae given in [103]. Those formulae transformed to NLO SU(2) ChPT read

$$B_i = B_i^\chi \left[1 + b\hat{\mu}_\ell \mp \frac{2\hat{B}_0\hat{\mu}_\ell}{16\pi^2 f_0^2} \log \frac{2\hat{B}_0\hat{\mu}_\ell}{16\pi^2 f_0^2}\right] + Da^2 \tag{5.2.4}$$

with $\hat{B}_0 = 2.84(11)$ GeV (renormalized $\overline{MS}$ at 2 GeV) and $f_0 = 121.0(1)$ MeV [98]. The sign before the logarithmic term is minus for $i = 1, 2, 3$ and plus for $i = 4, 5$.

The u/d and s quark masses have been computed in [96]. Their values in the $\overline{MS}$ scheme at 2 GeV are

$$\mu_{u/d}^{\overline{MS}}(2\ \mathrm{GeV}) = 3.6(2)\ \mathrm{MeV} \qquad \mu_s^{\overline{MS}}(2\ \mathrm{GeV}) = 95(6)\ \mathrm{MeV}$$

In the five panels of Figure 5.2.3 we show the combined chiral and continuum fit for the renormalized B_i estimators. In these plots we have used M1-type RCs expressed in the $\overline{MS}$ scheme of [95] at 2 GeV. Lattice data correspond to points taken at the pair of

quark mass $(\hat{\mu}_\ell, \hat{\mu}_s)$. We display the curves that correspond to the linear fit function at the four β values considered here. The black solid lines represent the continuum limit curve. The dashed black line represents the continuum limit if a quadratic fit in $\hat{\mu}_\ell$ is used. Open circles, squares and stars stand for the results at the physical point corresponding to linear, quadratic and NLO ChPT fit respectively, all of which agree within one sigma deviation.

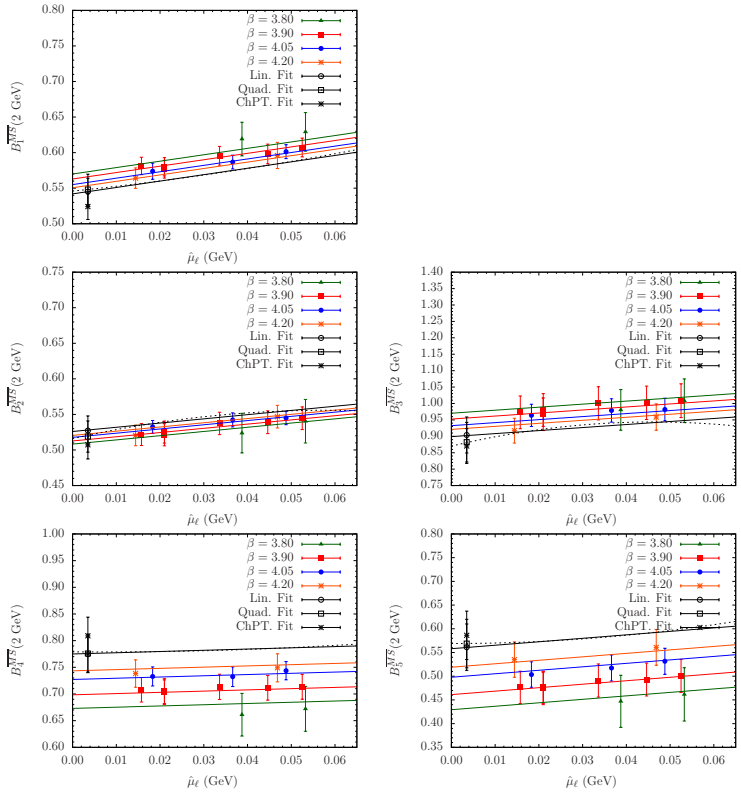

Figure 5.2.3: Solid lines represent the dependence of the B-parameters on the renormalized light quark mass of the combined chiral and continuum limit according to a linear fit for the B_i parameter of $\overline{K}^0 - K^0$ oscillations with $i = 1, 2, 3, 4, 5$ respectively, renormalized in $\overline{MS}$ scheme of [95] at 2 GeV with M1-type RCs. The full black line is the continuum limit curve. The dashed black line represents the continuum limit curve in the case of a quadratic ansätz. Open circles, squares and stars stand for the results at the physical point corresponding to linear, quadratic and NLO ChPT fit respectively.

5.2.4 Final estimates

In Table 5.2.1 and Table 5.2.2 we gather our final continuum results for B_i in the $\overline{MS}$ [95] and RI-MOM at 2 GeV employing M1 and M2 RCs and using a linear, quadratic or ChPT fit formula. The good agreement between the continuum limit results for the bag parameters B_i using M2-type RCs and their counterparts based on M1-type RCs provides a valuable check of the smallness of residual systematic errors in the evaluation of RI-MOM RCs with the M1-method. Possible systematic errors stemming in the M1-method from the inadequacy at non high momenta of the perturbative operator anomalous dimension used in the analysis or from the removal of the leading cutoff effects via linear fit in a^2p^2 are strongly reduced or absent when using the M2-method for RCs. This is so because in the latter approach the RCs are extracted at a rather high p^2 value but comes at the price of generically larger lattice artifacts on the RCs, which we partly suppress by removing the perturbatively known $\mathcal{O}(a^2g^2)$ contributions.

We consider as our final estimates the ones coming from M1-type RCs as it is done in [102]. The final values of B_i for $i = 1, 2, 3, 4, 5$, collected in Table 5.2.3 and Table 5.2.4, have been computed by averaging the estimates obtained from the three kinds of fit ansätz discussed in the previous subsection and using bootstrap error analysis. The half difference between the two more distant results has been taken as an estimate of the systematic error associated to the extrapolation procedure. The total uncertainty is obtained by adding in quadrature the statistical and the systematic error.

Finally we give our continuum results in the $\overline{MS}$ and RI-MOM scheme at 3 GeV, see Table 5.2.5 and Table 5.2.6.

Note that B_K coincides with B_1. The RGI B_K defined in Eq.1.2.12 is obtained using the NLO continuum QCD evolution from RI-MOM to RGI discussed in Appendix C. Our final estimate in this thesis is

$$\hat{B}_K^{\rm RGI} = 0.756(27)(11) \;\rightarrow \hat{B}_K^{\rm RGI} = 0.76(03) \quad @N_f = 2 \tag{5.2.5}$$

where we have averaged the results coming from the several choices of chiral fit ansätz and from M1 and M2 methods[1]. In the first expression the first error quoted is the statistical error for the bare matrix elements and the associated renormalization constants. Its estimate has been obtained via a bootstrap analysis, taking properly into account all possible cross-correlations. As one can see in section F.3 on Appendix F at fixed quark masses and lattice spacing the typical statistical error on the bare lattice estimator is around 1%, while from Appendix G we derive a relative error for the B_K renormalization factor $Z_{11}^{\rm PC+}/(Z_A Z_V)$ of about 2% (slightly larger for $\beta = 3.80$). The extrapolation to the continuum limit and the physical quark masses finally leads to a relative error of about 4% as quoted before. The second error in the first expression on Eq.5.2.5 is a systematic uncertainty. The error budget is detailed below:

- 0.010 from the systematic uncertainty in the chiral and continuum extrapolation. It has been estimated as half of the difference between the two more distant results obtained from the three chiral fit ansätzs, i.e linear, quadratic or ChPT.

[1] Averaging M1 and M2 for B_1 is justified since cutoff effects are under control

- 0.004 from the RI-MOM renormalization due to the spread coming from M1 and M2 methods. It has been estimated as half of the difference between the two results.

Summing in quadrature both systematic uncertainties leads to a total systematic error estimate of ± 0.011. This number is added in quadrature to the statistical error. The final result quoted in the second expression of Eq.5.2.5.

$\overline{MS}$ (2GeV)						
		B_1	B_2	B_3	B_4	B_5
Lin. Fit	M1	0.55(02)	0.53(02)	0.90(06)	0.78(03)	0.56(05)
	M2	0.54(02)	0.51(02)	0.88(04)	0.75(02)	0.54(03)
Quad. Fit	M1	0.55(02)	0.52(02)	0.88(06)	0.78(04)	0.57(05)
	M2	0.54(02)	0.50(02)	0.86(04)	0.75(02)	0.53(03)
ChPT Fit.	M1	0.52(02)	0.51(02)	0.87(05)	0.80(04)	0.59(05)
	M2	0.52(02)	0.49(02)	0.84(04)	0.78(02)	0.56(03)

Table 5.2.1: Continuum limit results for B_i of $\overline{K}^0 - K^0$ oscillations renormalized in $\overline{MS}$ of [95] at 2 GeV using M1- and M2-type RCs for the three kinds of fit functions.

RI-MOM (2GeV)						
		B_1	B_2	B_3	B_4	B_5
Lin. Fit	M1	0.54(02)	0.72(03)	1.24(08)	1.00(04)	0.68(07)
	M2	0.53(02)	0.69(02)	1.20(05)	0.96(02)	0.64(04)
Quad. Fit	M1	0.54(02)	0.70(03)	1.21(09)	1.00(05)	0.69(08)
	M2	0.53(02)	0.68(02)	1.18(05)	0.96(03)	0.64(04)
ChPT Fit.	M1	0.52(02)	0.69(03)	1.20(08)	1.04(04)	0.70(08)
	M2	0.51(02)	0.67(02)	1.15(05)	1.00(03)	0.67(04)

Table 5.2.2: Continuum limit results for B_i of $\overline{K}^0 - K^0$ oscillations renormalized in RI-MOM scheme at 2 GeV using M1- and M2-type RCs for the three kinds of fit functions.

$\overline{MS}$ (2GeV)				
B_1	B_2	B_3	B_4	B_5
0.54(02)	0.52(02)	0.89(06)	0.79(04)	0.57(05)

Table 5.2.3: Continuum limit results for B_i of $\overline{K}^0 - K^0$ oscillations renormalized in $\overline{MS}$ of [95] at 2 GeV with M1-type RCs

RI-MOM (2GeV)				
B_1	B_2	B_3	B_4	B_5
0.53(02)	0.70(03)	1.22(08)	1.01(05)	0.69(07)

Table 5.2.4: Continuum limit results for B_i of $\overline{K}^0 - K^0$ oscillations renormalized in the RI-MOM scheme at 2 GeV with M1-type RCs.

$\overline{MS}$ (3GeV)				
B_1	B_2	B_3	B_4	B_5
0.53(02)	0.48(02)	0.80(04)	0.78(04)	0.60(05)

Table 5.2.5: Continuum limit results for B_i of $\overline{K}^0 - K^0$ oscillations renormalized in $\overline{MS}$ of [95] at 3 GeV with M1-type RCs

RI-MOM (3GeV)				
B_1	B_2	B_3	B_4	B_5
0.52(02)	0.60(02)	1.01(06)	0.92(04)	0.68(06)

Table 5.2.6: Continuum limit results for B_i of $\overline{K}^0 - K^0$ oscillations renormalized in the RI-MOM scheme at 3 GeV with M1-type RCs.

5.3 Model independent constraints on $\Delta S = 2$ operators

Several phenomenological New Physics (NP) analysis of $\Delta F = 2$ processes have been performed in the last years, both for specific NP models and in model-independent frameworks. A generalization of the UT analysis, which allows for NP effects by including the most significant flavor constraints on NP available at the time, was performed in [51]. The result was a simultaneous determination of the CKM parameters and the size of NP contributions to $\Delta F = 2$ processes in the $\overline{K}^0 - K^0$and $\overline{B}^0 - B^0$ meson sectors. In particular, the analysis in [51] shows that the most stringent constrains come from $\overline{K}^0 - K^0$ matrix elements. In this sense, the accurate determination of the $\Delta S = 2$ bag parameters is crucial to the improvement of the NP constrains.

The results for the $\Delta S = 2$ bag parameters computed in this thesis[2] come from unquenched $N_f = 2$ lattice QCD data carefully extrapolated to the continuum limit. They hence represent a significant improvement with respect to the quenched and not continuum-extrapolated input values used in the previous UT analysis of [51].

[2] and the analysis in [102]

As introduced in subsection 1.2.5, the NP generalization of the UT analysis consists in including in the theoretical parametrization of the observables, for instance ϵ_K, the matrix elements of the operators which, although absent in the SM, could appear in NP models. This is implemented by taking into consideration the most general form of the $\Delta S = 2$ effective Hamiltonian in Eq.1.2.16.

Constraints on the NP models can be obtained from the comparison of the lattice determination of $\langle \overline{K}^0 | Q_i(\mu) | K^0 \rangle$ with experimental measurements. In this way, we can constrain the parameters of NP appearing directly in the Wilson coefficients. These constraints can be obtained in a model independent way with the effective weak Hamiltonian parametrized by Wilson coefficients of the form [51]

$$C_i(\Lambda) = \frac{F_i L_i}{\Lambda^2}$$

where F_i is a function of the NP flavor couplings, L_i is a loop factor that is present in models with no tree-level FCNC and Λ is the scale of NP, that is, the typical mass of the new particles mediating the $\Delta S = 2$ transitions. The allowed range for each $C_i(\Lambda)$ can be immediately translated into lower bounds in Λ. Thus an accurate determination of the bag parameters, and with them of the matrix elements, is crucial to the improvement of the NP constraints.

In the updated NP-oriented analysis performed by the UTfit collaboration the bag parameters collected in Table 5.2.4 are employed while for all the other input data the numbers are those quoted in [25]. The results for the lower bounds on the NP scale Λ in a model with $L_i = F_i = 1$ are collected in Table 5.3.1. The analysis is performed by switching on one coefficient at the time in each sector, thus excluding possible accidental cancellations among the contributions of different operators. Two other interesting possibilities are given by loop-mediated NP contributions proportional to either α_s or α_W. To obtain the lower bounds on Λ corresponding to this loop-mediated weak interactions one simply has to multiply the bounds quoted in Table 5.3.1 by $\alpha_s(\Lambda) \sim 0.1$ or $\alpha_W \sim 0.03$.

$F_i \sim L_i \sim 1$	c_1	c_2	c_3	c_4	c_5
$\Lambda(\times 10^4 \text{TeV})$	~ 1.9	~ 24	~ 12	~ 49	~ 29

Table 5.3.1: Updated lower bounds for the scale of NP for a generic strongly interacting NP with generic flavor structure ($L_i = F_i = 1$) coming from the kaon sector.

As a consequence of the recent improved accuracy achieved in the values of the $\Delta S = 2$ bag parameters, the new constrains collected in Table 5.3.1 are more stringent that the previous ones presented in [51].

5.4 $\overline{D}^0$-D^0 bag parameters

The computation of the renormalized B_i parameters controlling the short distance contributions to the $\overline{D}^0 - D^0$ system follows the same steps as in the case of $\overline{K}^0 - K^0$ one

with the difference that now the initial estimator to consider are $B_i\left(\mu_\ell, \mu_{\text{“}c\text{”}}\right)$, instead of $B_i\left(\mu_\ell, \mu_{\text{“}s\text{”}}\right)$. We have to perform an interpolation of $\mu_{\text{“}c\text{”}}$ to the physical charm quark mass previously computed in [96]

$$\hat{\mu}_c\left(\mu_c\right) = 1.28(04)\,\text{GeV} \quad \text{or} \quad \hat{\mu}_c\left(2\,\text{GeV}\right) = 1.14(04)\,\text{GeV}$$

renormalized in $\overline{MS}$ at the μ_c and $\mu = 2$GeV respectively.

However, we have to stress that in the case of $\overline{D}^0 - D^0$ bag parameters both, smearing and the use of $T_{\text{sep}} < T/2$, become relevant in order to get safe plateau signals.

In figure Figure 5.4.1 we show the plateau of the estimator of the B_1 bag parameter at $\beta = 3.80$ on a $24^3 \times 48$ lattice for the lightest quark mass and with the simulated “charm” quark around the physical charm quark mass, i.e $(a\mu_\ell, a\mu_{\text{“}c\text{”}}) = (0.0080, 0.2331)$, for both local and smeared sources. The improvement allows us to extract the D^0- and $\overline{D}^0$-state with more confidence and precision in a wider time interval.

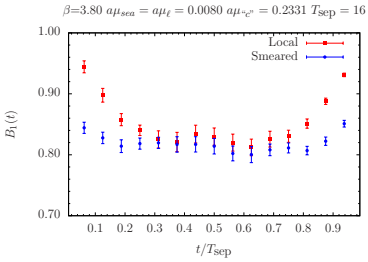

Figure 5.4.1: $B_1(t)$ at $\beta = 3.80$ and $(a\mu_l, a\mu_{\text{“}c\text{”}}) = (0.0080, 0.2331)$ on a $24^3 \times 48$ lattice. Red squares correspond to local source and sink while blue circles correspond to smeared source and sink.

In Figure 5.4.2 we show an exploratory test concerning the effect of locating the source and sink fields at different time slices in the computation of the supersymmetric bare bag parameters using Gaussian smearing at $\beta = 3.80$ and $(a\mu_\ell, a\mu_{\text{“}c\text{”}}) = (0.0080, 0.2331)$ on a $24^3 \times 48$ lattice. Decreasing the time separation between the sources has the effect of decreasing the statistical error of $B_i(t)$ with respect of the standard case where $T_{\text{sep}} = T/2$.

Bare estimates of the bag parameters, obtained from Eq.5.2.1 are collected in section F.3 on Appendix F at each value of β. In Figure 5.4.3, we display some examples of B_i at each β.

Once the bare bag parameters are renormalized adopting the RI-MOM $N_f = 2$ RCs detailed in Appendix G we perform the extrapolation and interpolation of renormalized lattice estimators to the physical point.

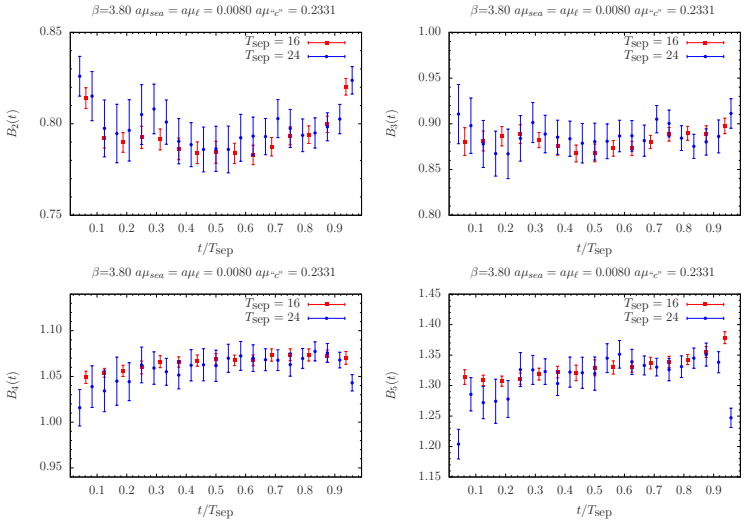

Figure 5.4.2: Bare supersymmetric bag parameters ($i = 2, ..., 5$) at $\beta = 3.80$ and $(a\mu_\ell, a\mu_{\text{“}c\text{”}}) = (0.0080, 0.2331)$ on a $24^3 \times 48$ lattice plotted vs t/T_{sep} for smeared source and sink located at two different time distances.

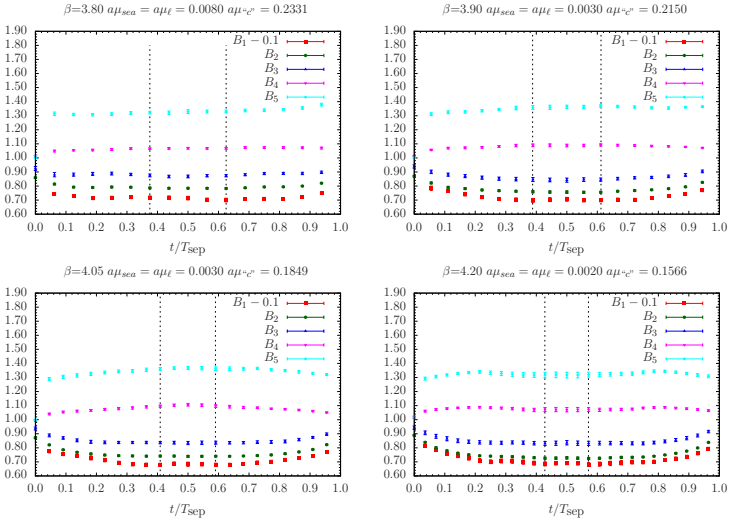

Figure 5.4.3: Data and time plateau for the bare B_i parameters, $(i = 1, 2, 3, 4, 5)$ for the $\overline{D}^0 - D^0$ system plotted vs t/T_{sep} for the lightest sea quark mass at each lattice spacing. Vertical dotted lines indicate the plateau region.

For all bag parameters B_i, the results are firstly interpolated to the physical value of the charm quark mass. As in the case of the $\overline{K}^0 - K^0$, we have simulated three points around the physical charm quark mass, one of them very close to the physical value. Thus the interpolation in $\mu_{\text{“}c\text{”}}$ is under very good control and a linear interpolation describes well the smooth dependence on $\mu_{\text{“}c\text{”}}$.

Continuum and chiral extrapolation ($a \to 0$ and $\mu_\ell \to \mu_{u/d}$) are carried out in a combined way. For all bag parameters, we have tried out the linear and quadratic fit ansätz in Eq.5.2.2 and Eq.5.2.3, and a HMChPT (Heavy Meson Chiral Perturbation Theory) fit ansätz. HMChPT combines the heavy quark effective theory (HQET) with the ChPT which allows us to predict the chiral behaviour of the heavy-light quantities and guide the chiral extrapolation of our lattice results. The implementation is based in the formulae given in [104]

$$B_1 = B_1^\chi \left[1 + b\hat{\mu}_\ell - \frac{(1-3\hat{g}^2)}{2}\frac{2\hat{B}_0\hat{\mu}_\ell}{16\pi^2 f_0^2}\log\frac{2\hat{B}_0\hat{\mu}_\ell}{16\pi^2 f_0^2}\right] + Da^2$$

$$B_i = B_i^\chi \left[1 + b\hat{\mu}_\ell \mp \frac{(1-3\hat{g}^2 Y)}{2}\frac{2\hat{B}_0\hat{\mu}_\ell}{16\pi^2 f_0^2}\log\frac{2\hat{B}_0\hat{\mu}_\ell}{16\pi^2 f_0^2}\right] + Da^2$$

where the sign before the logarithmic term is minus for $i = 2, 3$ and plus for $i = 4, 5$. We take the estimate $Y = 1$ from [104] and the value $\hat{g} = 0.53(4)$ obtained from the lattice measurement of $g_{D^*D\pi}$ coupling [105] where the computation is made on the $N_f = 2$ twisted mass EMTC gauge field configurations using four lattice spacings.

In Figure 5.4.4 we show the combined chiral and continuum fit for the renormalized B_i in the $\overline{MS}$ scheme of [95] at 2 GeV using M1-type RCs. Lattice data corresponds to points taken at the pair of quark masses $(\hat{\mu}_\ell, \hat{\mu}_c)$. The color code is the same as in Figure 5.2.3.

In Table 5.4.1 and Table 5.4.2 we gather our continuum results for B_i in the $\overline{MS}$ [95] and RI-MOM at 2 GeV employing M1 and M2 RCs and using a linear, quadratic or HMChPT fit formula.

$\overline{MS}$ (2GeV)						
		B_1	B_2	B_3	B_4	B_5
Lin. Fit	M1	0.78(02)	0.72(03)	1.08(07)	0.93(04)	1.13(07)
	M2	0.78(02)	0.70(02)	1.02(05)	0.90(03)	1.13(04)
Quad. Fit	M1	0.77(03)	0.71(03)	1.07(08)	0.92(04)	1.12(07)
	M2	0.76(03)	0.69(02)	1.01(06)	0.89(03)	1.13(04)
HMChPT Fit.	M1	0.78(02)	0.71(03)	1.08(07)	0.93(04)	1.13(07)
	M2	0.78(02)	0.69(02)	1.02(05)	0.90(03)	1.14(04)

Table 5.4.1: Continuum limit results for B_i of $\overline{D}^0 - D^0$ oscillations renormalized in $\overline{MS}$ of [95] at 2 GeV using M1- and M2-type RCs for the three kinds of fit functions.

RI-MOM (2GeV)						
		B_1	B_2	B_3	B_4	B_5
Lin. Fit	M1	0.77(02)	0.97(04)	1.48(10)	1.19(05)	1.50(10)
	M2	0.77(02)	0.94(03)	1.39(07)	1.15(03)	1.52(06)
Quad. Fit	M1	0.76(03)	0.96(04)	1.46(11)	1.19(05)	1.49(11)
	M2	0.75(03)	0.93(03)	1.37(07)	1.15(04)	1.51(06)
HMChPT Fit.	M1	0.77(02)	0.97(04)	1.47(10)	1.20(05)	1.51(11)
	M2	0.77(02)	0.94(03)	1.39(07)	1.16(03)	1.52(06)

Table 5.4.2: Continuum limit results for B_i of $\overline{D}^0 - D^0$ oscillations renormalized in the RI-MOM scheme at 2 GeV using M1- and M2-type RCs for the three kinds of fit functions.

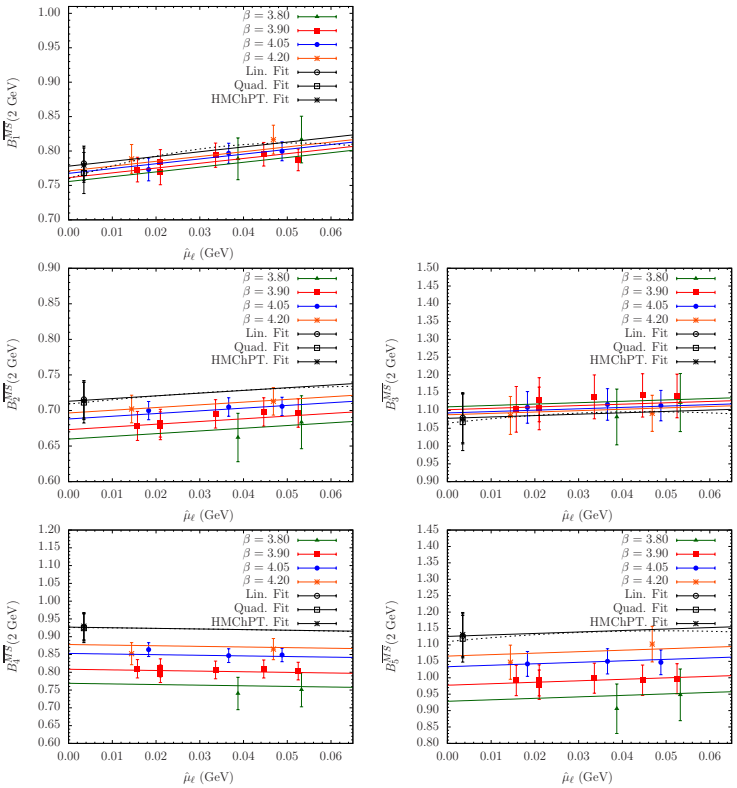

Figure 5.4.4: Behavior vs the renormalized light quark mass of the combined chiral and continuum limit of the B_i parameters of $\overline{D}^0 - D^0$ oscillations with $i = 1, 2, 3, 4, 5$ renormalized in $\overline{MS}$ scheme of [95] at 2 GeV with M1-type RCs. The full black line is the continuum limit curve according to a linear fit. The dashed black line represents the continuum limit curve in the case of a quadratic ansätz.

We consider as our final estimates the ones coming from M1-type RCs. The final values of B_i for $i = 1, 2, 3, 4, 5$, collected in Table 5.4.3 and Table 5.4.4, have been computed by averaging the estimates obtained from the three kinds of fit ansätz. The half difference between the two more distant results has been taken as an estimate of the systematic error and added in quadrature to the statistical error. Finally we give our continuum results in the $\overline{MS}$ and RI-MOM scheme at 3 GeV, see Table 5.4.5 and Table 5.4.6.

$\overline{MS}$ (2GeV)				
B_1	B_2	B_3	B_4	B_5
0.78(03)	0.71(03)	1.07(07)	0.93(04)	1.13(07)

Table 5.4.3: Continuum limit results for B_i of $\overline{D}^0 - D^0$ oscillations renormalized in $\overline{MS}$ of [95] at 2 GeV with M1-type RCs

RI-MOM (2GeV)				
B_1	B_2	B_3	B_4	B_5
0.77(03)	0.97(04)	1.47(10)	1.19(05)	1.50(10)

Table 5.4.4: Continuum limit results for B_i of $\overline{D}^0 - D^0$ oscillations renormalized in the RI-MOM scheme at 2 GeV with M1-type RCs.

$\overline{MS}$ (3GeV)				
B_1	B_2	B_3	B_4	B_5
0.76(03)	0.67(03)	0.99(05)	0.92(04)	1.09(06)

Table 5.4.5: Continuum limit results for B_i of $\overline{D}^0 - D^0$ oscillations renormalized in $\overline{MS}$ of [95] at 3 GeV with M1-type RCs

RI-MOM (3GeV)				
B_1	B_2	B_3	B_4	B_5
0.75(03)	0.83(03)	1.25(08)	1.09(05)	1.33(08)

Table 5.4.6: Continuum limit results for B_i of $\overline{D}^0 - D^0$ oscillations renormalized in the RI-MOM scheme at 3 GeV with M1-type RCs.

Chapter 6

B-physics

Lattice results for B-Physics hadronic parameters play a crucial role in the UTA. Indeed, from the five UTA constraints relying on LQCD, i.e ϵ_K, Br($B \to \tau\nu$), ΔM_{B_d}, $\Delta M_{B_d}/\Delta M_{B_s}$ and V_{ub}/V_{cb}, four of them are B-physics observables.

The computation of B-Physics observables on the lattice is complicated by the presence of $\mathcal{O}(am_b)$ discretization errors which imply that the physical b-quark mass, being approximately 4 GeV, cannot be directly simulated on current lattices where $a^{-1} \leq 4$ GeV. In other words, due to present day computer limitations it is still not possible to simulate directly b-quark mass propagators while keeping at the same time finite volume and discretization errors under control. In order to circumvent this difficulty several methods have been proposed based either on the implementation of the static theory on the lattice or in relativistic simulations in the range of the charm quark mass and then extrapolate to the b-quark mass (for a recent review about the different methods see [106]).

Here, I use a rather new method for B-physics, presented in [24], in which the b quark mass computations are achieved by interpolating, between the accessible charm region and the theoretically known static point, suitable ratios of the desired observable computed at a number of heavy quark mass values. Starting from the safe estimate of the interested observable at the charm region and using the exact asymptotic infinite mass limit we are able to obtain the observable at the b-quark mass point. The main advantage of the method is that the explicit calculation of the B-physics observables and renormalization constants in the static limit, i.e in the infinite heavy-quark mass limit, is not necessary. The only theoretical key ingredient one needs to know is the scaling law of the ratios with the heavy quark mass.

The ratio method has been fully exploited in [107] for the determination of the b-quark mass and the B and B_s decay constants performed with $N_f = 2$ twisted mass quarks at four values of the lattice spacing. Here, in section 6.2, I briefly overview an update of the analysis in [107] including smearing techniques in order to reduce the coupling of the source and sink interpolating fields to excited states and enhance at the same time

their coupling to the ground state as discussed in section 6.1. In particular, we use a linear combination of local and smeared sources in order to extract the relevant signals at smaller time separations. By doing so, we can extend the study to larger values of the heavy quark mass reducing the systematic uncertainty in the interpolation to the b-quark mass.

The application of the ratio method to the determination of the b-quark mass and the pseudoscalar decay constants f_B and f_{B_s} will help me to introduce the technical details of the method. Finally, in the last section of this chapter I extend the ratio method to the evaluation of the B_B and B_{B_s} bag parameters and their supersymmetric contributions.

6.1 Simulation details

This calculation uses the $N_f = 2$ gauge field configurations generated by the ETMC with the tree-level Symanzik gauge action and the twisted mass action at maximal twist, discussed in detail in chapter 2. For simulation details I refer to Table 5.1.1. While, in chapter 5 only the strange and charm quark masses were considered, here a wider range of values for the valence (heavy) quark mass above the charm will be taken into account. The sequence of heavy quark masses $\left\{\mu_h^{(n)}\right\}$ ranges from approximately m_c up to $2.5m_c$. Heavier μ_h values, up to the b-quark mass, have been simulated and were included in Table 5.1.1, but they are excluded in the present analysis due to their large statistical uncertainties in the effective mass, pseudoscalar decay constants and bag parameter signals.

I recall that in this thesis the same ensembles of gauge configurations were used in the $N_f = 2$ analysis of bag parameters for the $\overline{K}^0 - K^0$, $\overline{D}^0 - D^0$ and $\overline{B}^0 - B^0$ systems. This is convenient because the code used by the ETMC is a multi-mass solver (see Appendix A and the references therein). The multi-mass solver allows us to perform inversions over the whole range of masses at once, thus for each ensemble of gauge configurations a single inversion on the lightest quark mass is first performed and then followed by inversions in order to get heavier mass propagators at a very low CPU cost.

6.1.1 Improved interpolating operators

Through the use of smearing techniques, as presented in section 5.1 and the references in it, we are able to project better onto the ground state. The smearing makes possible to extract signal from bare correlators at relatively small time separations were the signal-to-noise ratio is under better control. Because of that, smearing techniques allow us to extend the study of the observables of interest to larger values of the heavy quark mass. This is crucial in order to get closer to the b-quark mass in our B-physics analysis.

To further improve the overlap with the ground state for the heavier quark masses we have constructed the improved source, $\phi(\omega)$, in terms of the local, ϕ_L, and smeared source, ϕ_S

$$\phi(\omega) \propto \omega\phi_L + (1-\omega)\,\phi_S$$

dependent on a tunable parameter ω[1]. We have constructed the correlators where the source is smeared and the sink is $\phi(\omega)$. We call them SL-SS correlators. We then optimize the value of ω to achieve a projection onto the ground state at earlier Euclidean times than with SL correlators. Details on the optimization procedure are given in Appendix F.

In the left plot of Figure 6.1.1 we show the Euclidean time dependence of the effective mass at $\beta = 3.80$, $a\mu_\ell = 0.0080$ and $a\mu_h = 0.5246$ obtained from LL, SL, LS and SS correlators. The impact of smearing compared with local source and sinks is clear. Smearing improves the projection on the ground state and allows us to extract the ground state with more confidence at earlier time-slices where the signal-to-noise ratio is better.

We found that in general the best behaviour corresponds to the SL correlation function. However, although the SL correlator is already substantially improved for a safe extraction of the ground state, a further improvement can be obtained by considering the SL-SS correlators. For illustration in the right plot of Figure 6.1.1 we display the effective mass obtained from SL-SS correlators for several values of ω, one of which is optimal. The optimal value, i.e the one for which the plateau starts earlier, is $\omega \sim 0.6$. In fact, following the algorithm proposed in Appendix F we find $\omega_{\rm opt} = 0.61$ for this β and mass combination.

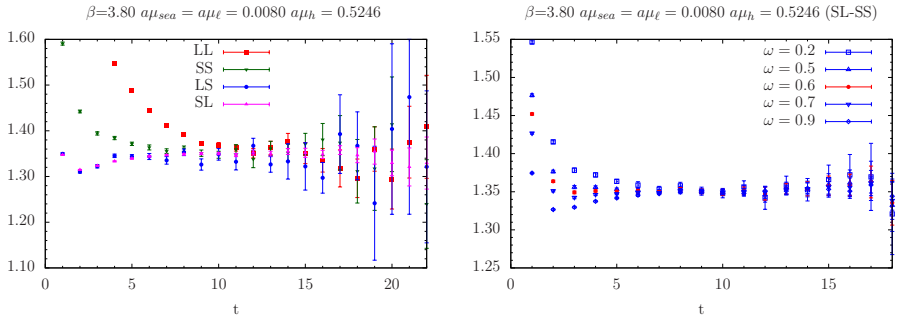

Figure 6.1.1: Left plot: Euclidean time dependence at $\beta = 3.80$, $\mu_\ell = 0.0080$ and $\mu_h = 0.5246$ obtained from LL, SL, LS and SS correlators. Right plot: Linear combination of smeared and local sinks with smeared sources for several ω values.

Following the strategy detailed in Appendix F we have also optimized the pseudoscalar decay constants. In Figure 6.1.2 we display two examples of the pseudoscalar decay constant versus the time, computed with SL or ω-opt improved interpolating operators.

All the results involving pseudoscalar meson masses and pseudoscalar decay constants presented in the following sections take advantage of this ω-improvement.

[1]This notation for ω should not be confused with the twisted angle used in the previous chapters.

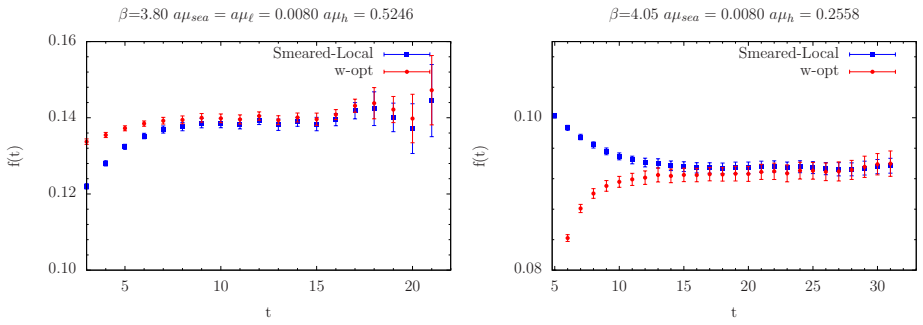

Figure 6.1.2: Euclidean time dependence of the pseudoscalar decay constant at $\beta = 3.80$, $\mu_\ell = 0.0080$ and $\mu_h = 0.5246$ (left) and $\beta = 3.80$, $\mu_\ell = 0.0080$ and $\mu_h = 0.2558$ obtained from smeared-local and improved smeared interpolating fields.

6.2 The ratio method

The b-quark mass and the pseudoscalar decay constants f_B and f_{B_s} can be computed using the ratio method as presented in [107]. Here, I will briefly summarize the basic steps of the method.

6.2.1 The b-quark mass

The ratio method is suggested by the HQET asymptotic behaviour of the heavy-light pseudoscalar meson mass M_{hl} in the pole heavy quark mass $\mu_h^{\rm pole}$

$$M_{hl} = \mu_h^{\rm pole} + \bar{\Lambda} - \left(\frac{\lambda_1}{2} + \frac{3\lambda_2}{2}\right)\frac{1}{\mu_h} + \mathcal{O}(1/\mu_h^2)$$

which implies

$$\lim_{\mu_h \to \infty}\left(\frac{M_{hl}}{\mu_h^{\rm pole}}\right) = 1 \tag{6.2.1}$$

where

$$\rho\big(\log\hat{\mu}_h\big)\hat{\mu}_h = \mu_h^{\rm pole}$$

Here, the function $\rho\,(\log(\hat{\mu}_h))$ is the factor that converts the renormalized $\overline{MS}$ quark mass at 2 GeV into the so-callled *quark pole mass.*

The first step in order to apply the ratio method is to consider an appropriate sequence of heavy quark masses

$$\left\{\mu_h^{(1)}, \mu_h^{(2)}, ..., \mu_h^{(N)}\right\}$$

with a fix ratio between them

$$\frac{\mu_h^{(n)}}{\mu_h^{(n-1)}} = \lambda$$

In our analysis we take initially $\mu_h^{(1)}$ equal to the second value of $\mu_{\text{“}c\text{”}}$ in Table 5.1.1 and we consider the $N = 7$ subsequent values of μ to construct the original sequence of heavy quark masses.

Inspired by the HQET prediction Eq.6.2.1 we consider the chiral and continuum extrapolated ratio

$$y\left(\hat{\mu}_h^{(n)}\right) \equiv \lim_{\hat{\mu}_\ell \to \hat{\mu}_{u/d}} \lim_{a \to 0} y^L\left(\hat{\mu}_h^{(n)}; \hat{\mu}_\ell, a\right) \tag{6.2.2}$$

with $n = 2, ..., N+1$ and

$$y^L\left(\hat{\mu}_h^{(n)}; \hat{\mu}_\ell, a\right) = \frac{M_{hl}\left(\mu_h^{(n)}; \mu_\ell, a\right) / \mu_h^{(n)\text{pole}}}{M_{hl}\left(\mu_h^{(n-1)}; \mu_\ell, a\right) / \mu_h^{(n-1)\text{pole}}}$$

In continuum perturbation theory ρ is known up to N^3LL. The NLL expression reads [92]

$$\rho\left(\hat{\mu}_h\right) = \left[1 + \frac{16}{3}\frac{\alpha(\hat{\mu}_h)}{4\pi}\right]\left(\frac{\alpha(\hat{\mu}_h)}{\alpha(\hat{\mu}_b^*)}\right)^{12/(33-2N_f)} \left[1 + \left(\frac{2(4491 - 252N_f + 20N_f^2)}{3(33-2N_f)^2}\right)\frac{\alpha(\hat{\mu}_h) - \alpha(\hat{\mu}_b^*)}{4\pi}\right]$$

where $\hat{\mu}_b^*$ is a reference heavy scale.

From Eq.6.2.1 it follows that the ratios in Eq.6.2.2 have an exact static limit

$$\lim_{\mu_h \to \infty} y\left(\hat{\mu}_h^{(n)}\right) = 1 \tag{6.2.3}$$

The ratios $y^L\left(\hat{\mu}_h^{(n)}; \hat{\mu}_\ell, a\right)$ introduced in Eq.6.2.2 are expected to have a smoother chiral extrapolation to the light quark mass $\hat{\mu}_{u/d}$ and to the continuum limit than each one of the individual factors. The right panel of Figure 6.2.1 shows the dependence of the third ratio on the light quark mass at the four values of the lattice spacing. A linear fit in the light quark mass and in a^2

$$y^L\left(\hat{\mu}_h^{(n)}; \hat{\mu}_\ell, a\right) = y(\hat{\mu}_h^{(n)}) + C_1(\hat{\mu}_h^{(n)})\hat{\mu}_l + C_2(\hat{\mu}_h^{(n)})a^2$$

turns out to describe lattice data quite well.

After performing the chiral and continuum combined extrapolation of the ratios we study their dependence on the inverse of the heavy quark mass. Inspired by HQET we perform the polynomial fit in $1/\hat{\mu}_h$

$$y\left(\hat{\mu}_h\right) = 1 + \frac{\eta_1}{\hat{\mu}_h} + \frac{\eta_2}{\hat{\mu}_h^2} \tag{6.2.4}$$

in which the static condition in Eq.6.2.3 is explicitly included. The fit is shown in Figure 6.2.2.

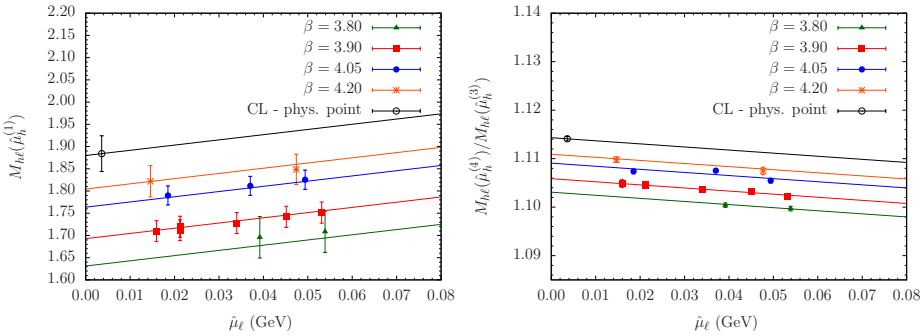

Figure 6.2.1: Left plot: Chiral and continuum extrapolation of the triggering point $M_{hl}\left(\hat{\mu}_h^{(1)}\right)$. Right plot: Chiral and continuum extrapolation of the third ratio of heavy-light meson masses

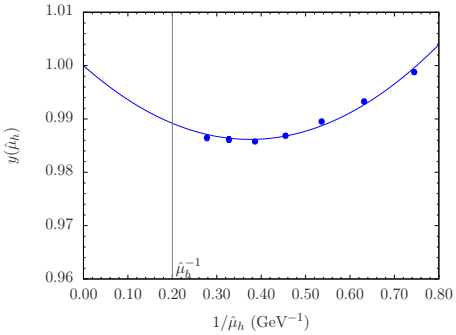

Figure 6.2.2: Heavy quark mass dependence of the ratio $y\left(\mu_h\right)$ extrapolated to the physical value of the light quark mass and to the continuum limit.

The value of the b-quark mass is eventually determined by considering the recursion chain equation

$$y\left(\hat{\mu}_h^{(2)}\right) y\left(\hat{\mu}_h^{(3)}\right) ... y\left(\hat{\mu}_h^{(K+1)}\right) = \lambda^{-K} \left[\frac{M_{hu/d}\left(\hat{\mu}_h^{(K+1)}\right)}{M_{hu/d}\left(\hat{\mu}_h^{(1)}\right)}\right] \left[\frac{\rho\left(\hat{\mu}_h^{(1)}\right)}{\rho\left(\hat{\mu}_h^{(K+1)}\right)}\right] \tag{6.2.5}$$

where $y\left(\hat{\mu}_h^{(i)}\right)$ are the fitted values of $y\left(\hat{\mu}_h\right)$ according to Eq.6.2.4. Eq.6.2.5 relates the heavy-light mass $M_{hu/d}\left(\hat{\mu}_h^{(K+1)}\right)$ to the value at the triggering point $M_{hu/d}\left(\hat{\mu}_h^{(1)}\right)$. In the left panel of Figure 6.2.1 we display the light quark mass dependence of the heavy-light meson mass at the first value of the sequence of heavy quark masses $\hat{\mu}_h^{(1)}$, i.e the triggering mass $M_{hl}\left(\hat{\mu}_h^{(1)}\right)$, at the four values of β. The chiral and continuum extrapolated value gives us the value of $M_{hu/d}\left(\hat{\mu}_h^{(1)}\right)$ that we need in Eq.6.2.5.

The value of the ratio λ is chosen in such a way that after a finite number of steps, K, the heavy-light meson mass $M_{hu/d}\left(\hat{\mu}_h^{(K+1)}\right)$ assumes the experimental value $M_B = 5.279$ GeV

$$M_{hu/d}\left(\hat{\mu}_h^{(K+1)}\right) = M_B \tag{6.2.6}$$

Notice that there are infinite choices of λ, $\mu_h^{(1)}$ and the number of steps K. With the tuning of λ and $\mu_h^{(1)}$ one can always readjust the sequence of heavy quark masses to end up with an integer value of K. In order to implement the condition in Eq.6.2.6, the original lattice data is interpolated to specific values of the heavy quark masses and after an iterative process we find that with $\lambda = 1.1784$ and maintaining the triggering point at $\hat{\mu}_h^{(1)} = \hat{\mu}_c$ we arrive to the B meson mass after $K_B = 9$ steps.

The value of the b-quark mass is now simply obtained from the triggering quark mass

$$\hat{\mu}_b = \hat{\mu}_h^{(K_B+1)} = \lambda^{K_B}\hat{\mu}_h^{(1)}$$

Using the N^{3}LL evolution with $\Lambda_{\rm QCD}(N_f = 2) = 330(23)(^{+22}_{-33})$ MeV [108], our result reads

$$m_b^{\overline{MS}}(m_b)\Big|_{N_f=2} = 4.28(10)(9)\,\text{GeV} \;\rightarrow\; m_b^{\overline{MS}}(m_b)\Big|_{N_f=2} = 4.28(13)\,\text{GeV}$$

where in the first expression the first error includes the statistical error, fits error and the uncertainties of Z_P and the lattice spacing. The second error is the systematic error due to the uncertainty of the lattice spacing. In the second expression both errors have been added in quadrature.

In order to control the systematics we have considered other choices of $\hat{\mu}_h^{(1)}$ and λ. In particular, the pairs of input parameters $\left(\hat{\mu}_h^{(1)}, \lambda\right)$: $(1.20\,\text{GeV}, 1.1720)$ and $(1.08\,\text{GeV}, 1.1855)$ satisfy Eq.6.2.5 with $K = 9$. We find that results obtained from the analyses corresponding to both choices of $\left(\hat{\mu}_h^{(1)}, \lambda\right)$ are perfectly compatible with $\left(\hat{\mu}_h^{(1)}, \lambda\right) = (1.14\,\text{GeV}, 1.1784)$.

6.2.2 f_B and f_{B_s} pseudoscalar decay constants

A strategy very similar to the one described in the previous section is employed to determine the B and B_s meson decay constant. The HQET asymptotic behaviour for the decay constant is

$$\lim_{\mu_h\to\infty} f^{\rm stat}_{hl(s)}\sqrt{\mu_h^{\rm pole}} = \text{constant}$$

where the super index "stat" stands for the static limit and $f_{hl(s)}$ denotes the pseudoscalar decay constant with heavy-light(strange) valence quark mass.

Thus, one should now take

$$\begin{aligned} z_d\left(\hat{\mu}_h^{(n)}\right) &= \lim_{\hat{\mu}_\ell\to\hat{\mu}_{u/d}}\lim_{a\to 0} z_d^L\left(\hat{\mu}_h^{(n)};\hat{\mu}_\ell,a\right) \\ z_s\left(\hat{\mu}_h^{(n)}\right) &= \lim_{\hat{\mu}_{sea}\to\hat{\mu}_{u/d}}\lim_{a\to 0}\lim_{\hat{\mu}_{\text{“}s\text{”}}\to\hat{\mu}_s} z_s^L\left(\hat{\mu}_h^{(n)};\hat{\mu}_{sea},\hat{\mu}_{\text{“}s\text{”}},a\right) \end{aligned}$$

with

$$z_d^L\left(\hat{\mu}_h^{(n)};\hat{\mu}_\ell,a\right) = \frac{f^{\rm stat}_{hl}\left(\hat{\mu}_h^{(n)};\hat{\mu}_\ell,a\right)\sqrt{\mu_h^{(n)\rm pole}}}{f^{\rm stat}_{hl}\left(\hat{\mu}_h^{(n-1)};\hat{\mu}_\ell,a\right)\sqrt{\mu_h^{(n-1)\rm pole}}} \tag{6.2.7}$$

where $f^{\rm stat}_{hl}$ is related to the QCD f_{hl} by

$$f_{hl}\left(\hat{\mu}_h^{(n)};\hat{\mu}_\ell,a\right) = f^{\rm stat}_{hl}\left(\hat{\mu}_h^{(n)};\hat{\mu}_\ell,a\right) C_A^{\rm stat}\left(\hat{\mu}_b^*,\hat{\mu}_h^{(n)}\right)$$

and the analogous one for heavy-strange pseudoscalar decay constants

$$z_s^L\left(\hat{\mu}_h^{(n)};\hat{\mu}_{sea},\hat{\mu}_{\text{“}s\text{”}},a\right) = \frac{f^{\rm stat}_{hs}\left(\hat{\mu}_h^{(n)};\hat{\mu}_{sea},\hat{\mu}_{\text{“}s\text{”}},a\right)\sqrt{\mu_h^{(n)\rm pole}}}{f^{\rm stat}_{hs}\left(\hat{\mu}_h^{(n)};\hat{\mu}_{sea},\hat{\mu}_{\text{“}s\text{”}},a\right)\sqrt{\mu_h^{(n-1)\rm pole}}}$$

Here λ and the triggering point mass $\hat{\mu}_h^{(1)}$ have been previously determined in the analysis of the b-quark mass: $\lambda = 1.1784$ and $\hat{\mu}_h^{(1)} = 1.14$ GeV.

The factor $C_A^{\rm stat}(\hat{\mu}_b^*,\hat{\mu}_h)$ is due to the fact that in HQET the axial current needs to be renormalized. $C_A^{\rm stat}(\hat{\mu}_b^*,\hat{\mu}_h)$ provides the matching between the decay constant in QCD and HQET at the scale $\hat{\mu}_h$ and the running of the static axial current from $\hat{\mu}_h$ to $\hat{\mu}_b^*$, being $\hat{\mu}_b^*$ a reference heavy scale. $C_A^{\rm stat}$ is known up to N^{2}LL [109]. We use the expression up to NLL

$$\begin{aligned} C_A^{\rm stat}(\hat{\mu}_b^*,\hat{\mu}_h) = &\left(\frac{\alpha(\hat{\mu}_h)}{\alpha(\hat{\mu}_b^*)}\right)^{-\frac{6}{33-2N_f}}\left[1-\left(\frac{-3951+300N_f+60N_f^2+(924-56N_f)\pi^2}{9(33-2N_f)^2}\right)\right. \\ &\left.\frac{\alpha(\hat{\mu}_h)-\alpha(\hat{\mu}_b^*)}{4\pi}\right]\left[1-\frac{8}{3}\frac{\alpha(\hat{\mu}_h)}{4\pi}\right] \end{aligned}$$

In order to have a better control on the chiral extrapolation, we consider as primary quantities the decay constant f_{B_s} , where the dependence on the light quark mass occurs

only through sea effects, and the ratio f_{B_s}/f_B. These quantities are obtained from the ratio z_s and the double ratio $z \equiv z_s/z_d$. The decay constant f_B is obtained as a byproduct of both determinations

$$f_B = \frac{f_{B_s}}{f_{B_S}/f_B}$$

Within the ratio method, the value of f_{B_s} is obtained from the pseudoscalar decay constant at the triggering point, $f_{hs}\left(\hat{\mu}_h^{(1)}\right)$, and the fit values according to a HQET ansatz of the ratios z_s at each heavy quark mass in the sequence $\left\{\mu_h^{(i)}\right\}$ using the recursive equation equivalent to Eq.6.2.5

$$z_s\left(\hat{\mu}_h^{(2)}\right)...z_s\left(\hat{\mu}_h^{(K+1)}\right) = \lambda^{K/2}\left[\frac{f_{hs}\left(\hat{\mu}_h^{(K+1)}\right)}{f_{hs}\left(\hat{\mu}_h^{(1)}\right)}\right]\frac{C_A^{\text{stat}}\left(\hat{\mu}_b;\hat{\mu}_h^{(1)}\right)}{C_A^{\text{stat}}\left(\hat{\mu}_b;\hat{\mu}_h^{(K+1)}\right)}\left[\frac{\rho\left(\hat{\mu}_h^{(1)}\right)}{\rho\left(\hat{\mu}_h^{(K+1)}\right)}\right]^{1/2} \tag{6.2.8}$$

The ratios z_s show a smooth chiral continuum extrapolation with cutoff effects under control which turns out to be well described by a linear fit in $\hat{\mu}_\ell$ and a^2 as illustrated in the right panel of Figure 6.2.3. The heavy quark mass dependence of z_s is again well described by a formula as the one in Eq.6.2.4. The corresponding fit is shown in Figure 6.2.4.

By construction, since we fixed $\hat{\mu}_h^{(1)} = \hat{\mu}_c$, $f_{hs}\left(\hat{\mu}_h^{(1)}\right)$ is just f_{D_s}. In the left panel of Figure 6.2.3 we show the chiral and continuum extrapolation of f_{hs} at the triggering mass value $\hat{\mu}_h^{(1)}$. We find

$$f_{D_s} = 250(5)(5)\,\text{MeV} \;\rightarrow f_{D_s} = 250(7)\,\text{MeV}$$

where the first error is statistical and the second one is the systematic error associated to the lattice spacing.

We recall that the coefficients C_A^{stat} and ρ are only introduced in order to construct the ratios with the correct scaling law and they should not be interpreted as a matching to HQET of our results.

The final result, obtained from Eq.6.2.8, is

$$f_{B_s} = 228(5)(5)\ \text{MeV} \;\rightarrow f_{B_s} = 228(7)\ \text{MeV} \tag{6.2.9}$$

where the first error includes the statistical error, fits error and the uncertainties of Z_P and the lattice spacing. The second error denotes the systematic uncertainty for the lattice spacing. In the second expression both errors have been added in quadrature.

On the other hand f_{B_s}/f_B can be obtained from the recursive equation

$$z\left(\hat{\mu}_h^{(2)}\right)...z\left(\hat{\mu}_h^{(K+1)}\right) = \left[\frac{f_{hs}/f_{hl}\left(\hat{\mu}_h^{(K+1)}\right)}{f_{hs}/f_{hl}\left(\hat{\mu}_h^{(1)}\right)}\right] \tag{6.2.10}$$

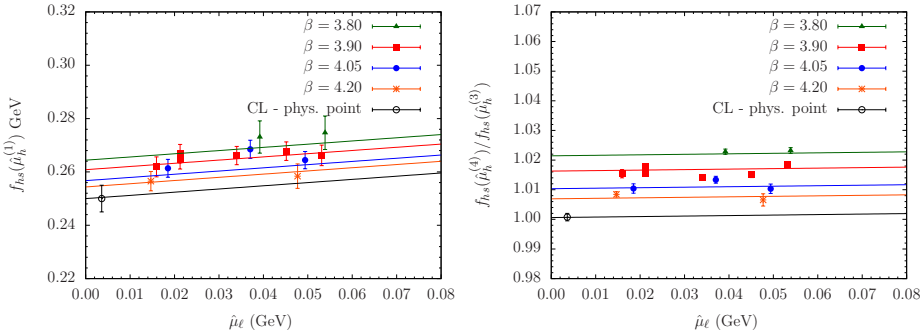

Figure 6.2.3: Left plot: Chiral and continuum extrapolation of the triggering decay constant $f_{hs}\left(\hat{\mu}_h^{(1)}\right)$. Right plot: Chiral and continuum extrapolation of the third ratio $z_s\left(\hat{\mu}_h^{(4)}\right)$.

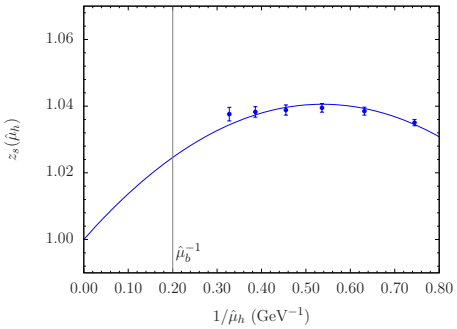

Figure 6.2.4: Heavy quark mass dependence of the ratio $z_s\left(\hat{\mu}_h\right)$.

where the factors C_A^{stat} and ρ are absent because they exactly cancel.

The uncertainty due to the chiral extrapolation at the triggering point is taken into account by considering a linear chiral and continuum extrapolation in $\hat{\mu}_\ell$ and a^2 for $f_{hs}/f_{hl}\left(\hat{\mu}_h^{(1)};\hat{\mu}_\ell,a\right)$ or a HMChPT inspired ansatz given by [110]

$$f_{hs}/f_{hl}\left(\hat{\mu}_h^{(1)};\hat{\mu}_\ell,a\right) = B_h\left[1+\frac{3\left(1+3\hat{g}^2\right)}{4}\frac{2B_0\hat{\mu}_\ell}{16\pi^2 f_0^2}\log\left(\frac{2B_0\hat{\mu}_\ell}{16\pi^2 f_0^2}\right)+C_h\mu_\ell+D_h a^2\right]$$

with $\hat{g} = 0.61(7)$ obtained from the experimental value of $g_{D^*D\pi}$ [111]. We prefer to use this value of $\hat{g}$ instead of $\hat{g} = 0.44(8)$ coming from the lattice measurement of $g_{B^*B\pi}$ coupling [112] because we work close to the charm quark mass. As it is shown in the left plot of Figure 6.2.5 HMChPT predicts a shift of $\simeq 0.08$ with respect to the result obtained from a linear fit. The use of $\hat{g} = 0.53(4)$, obtained from the lattice measurement of

$g_{D^*D\pi}$ in [105], provides a value for the triggering point $f_{hs}/f_{hl}\left(\hat{\mu}_h^{(1)}\right)$ which is comprised between the linear fit and the HMChPT ansatz with $\hat{g} = 0.61(7)$.

Not having the opportunity to work with physical light quark masses, for which the logarithmic term predicted by HMChPT could be significant, we decided to take the average of both fits and we include the half of the difference as a systematic error

$$f_{D_s}/f_D = f_{hs}/f_{hl}\left(\hat{\mu}_h^{(1)}\right) = 1.178(11)(41)$$

where the first error is statistical and the second systematic.

In the right plot of Figure 6.2.5 we study the dependence of the double ratio z on the heavy quark mass. As expected, the dependence on the heavy quark mass is barely visible.

Finally, from Eq.6.2.10 we obtain

$$f_{B_s}/f_B = 1.185(11)(41) \rightarrow f_{B_s}/f_B = 1.185(43) \tag{6.2.11}$$

where in the second value both errors have been added in quadrature.

f_B is finally obtained by combining Eq.6.2.9 and Eq.6.2.11

$$f_B = 193(6)(7)\,\text{MeV} \;\rightarrow f_B = 193(9)\,\text{MeV}$$

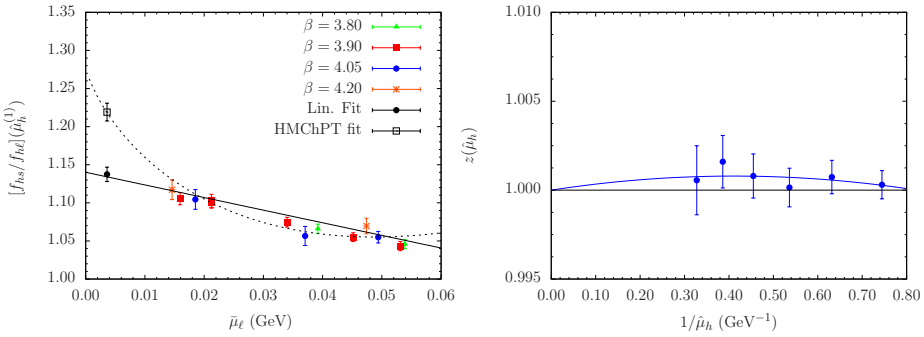

Figure 6.2.5: Left plot: Light quark mass dependence of the ratio $f_{hs}/f_{hl}\left(\hat{\mu}_h^{(1)}\right)$. Right plot: Heavy quark mass dependence of the double ratio $z\left(\mu_h^{(1)}\right)$ extrapolated to the continuum limit and the physical value of the light and strange quark masses.

6.3 $\overline{B}^0 - B^0$ oscillations

For the computation of bag parameters in the $\overline{B}^0 - B^0$ we mimic the procedure followed in the case of $\overline{K}^0 - K^0$ and $\overline{D}^0 - D^0$ using OS fermions in order to achieve both $\mathcal{O}(a)$ improvement and continuum-like renormalization pattern.

The strategy for their computation follows the same basic steps as outlined in chapter 5:

1. Plateau fit of bare B_i estimates from lattice data.
2. Operator renormalization at each lattice spacing. Since we are using only relativistic quarks, the two- and four-fermion renormalization constants needed here have already been computed for the $\overline{K}^0 - K^0$ and $\overline{D}^0 - D^0$ analysis (see Appendix G).
3. Continuum and chiral extrapolations. In the case of the B meson we extrapolate the light valence quark mass equal to the sea quark mass to the physical u/d quark mass: $\hat{\mu}_\ell = \hat{\mu}_{sea} \to \hat{\mu}_{u/d}$. Instead, in the case of the B_s meson the sea quark mass is extrapolated to the physical u/d while the simulated strange quark mass is interpolated to the physical strange: $\hat{\mu}_{sea} \to \hat{\mu}_{u/d}$ and $\hat{\mu}_{\text{“}s\text{”}} \to \hat{\mu}_s$. In practice, we carry out chiral and continuum extrapolation in a combined way over the ratios of bag parameters as it is described in subsection 6.3.1.
4. Extrapolation of the heavy valence quark mass $\hat{\mu}_h$ to the physical b-quark mass by using the ratio method as it will be detailed in subsection 6.3.1.

Decreasing the time separation of the sources and the use of smearing techniques both become relevant when one deals with charmed or heavier mesons.

In Figure 6.3.1 we show the five bare bag parameters computed between smeared sources and sinks at $\beta = 3.80$, $a\mu_\ell = a\mu_{sea} = 0.0080$ and with the simulated heavy quark mass $a\mu_h = 0.5246 \sim 2.25 m_c$ locating the interpolating fields at two different time-slices, $T_{\rm sep} = 24$ and $T_{\rm sep} = 16$. The time separation $T_{\rm sep} = 16$ decreases drastically the relative error of the bare bag parameters. The physical interpretation is the following: with heavier mesons the signal-to-noise ratio get worse at large time-separations, thus in order to overlap the signals of both mesons at each side of the lattice we should decrease the time separations between them.

Similar tests have been performed at the other β's in order to obtain the best $T_{\rm sep}$ as a compromise between signal-to-noise ratio and existence of the plateau around $T_{\rm sep}/2$. As expected the value of $T_{\rm sep}$ scales with the lattice spacing. The selected values for the complete simulation are collected in Table 5.1.1.

In order to obtain the bare B_i values, the plateau for the bag parameters should exist in time-slices around $T_{\rm sep}/2$. In this case smearing techniques are necessary to guarantee that the plateau starts at earlier enough timeslices.

Motivated by the previous observation, we decided that the ω-improvement should also be implemented for the computation of the bag parameters. After some exploratory studies we found that within statistical error the smeared plateau is compatible with the improved one. Figure 6.3.2 illustrates an example of this general observation. The physical reason is that excited state contributions in B_i are negligible within statistical errors. Consequently, in the analysis presented here we do not consider the ω-improvement for the computation of $B_i(t)$. Bag parameters for each lattice spacing and quark masses collected in Appendix B are obtained directly from Eq.5.2.1.

Figure 6.3.3 displays the five bare bag parameters with local and smeared sources and sinks at $\beta = 3.80$ and $(a\mu_\ell = a\mu_{sea}, a\mu_h) = (0.0080, 0.5246)$ with the time separation

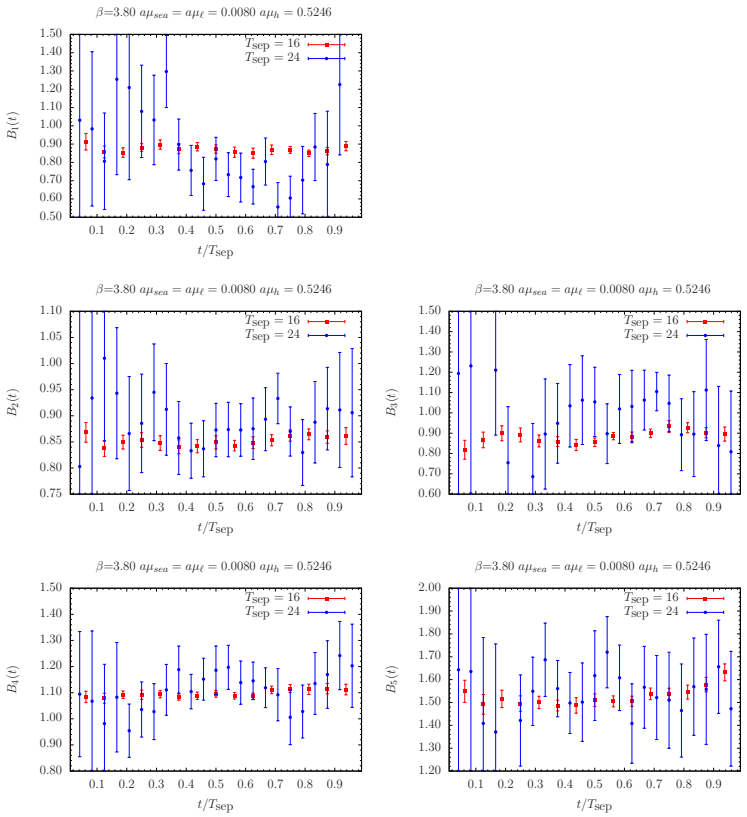

Figure 6.3.1: Bare supersymmetric bag parameters ($i = 1, 2, 3, 4, 5$) at $\beta = 3.80$ and $(a\mu_\ell = a\mu_{sea}, a\mu_h) = (0.0080, 0.5246)$ on a $24^3 \times 48$ lattice plotted vs $t/T_{\rm sep}$ for smeared source and sink located at two different time distances.

between sources fixed to $T_{\rm sep} = 16$. It is clear that thanks to the smeared sources the coupling to excited states is reduced and the quality of the extracted ground state signal is significantly improved in most cases.

For illustration, in Figure 6.3.4 we show examples of B_i at β =3.8, 3.9, 4.05 and 4.20 for the smallest value of the sea quark mass, the light valence quark mass equal to the sea quark mass and with the simulated heavy quark mass $(a\mu_h) \sim 2.25\,(a\mu_c)$. Vertical dotted lines indicate the plateau region where the B^0 and the $\overline{B}^0$ states dominate the three point correlators: $[T_{\rm sep}/2 - 1 : T_{\rm sep}/2 + 1]$. Figure 6.3.5 displays the plateau at each lattice spacing with the lightest sea quark mass, one of the valence quark masses around the physical strange and the heavy quark mass with $(a\mu_h) \sim 2.25\,(a\mu_c)$, relevant for the analysis of $\overline{B}^0_s - B^0_s$ oscillations.

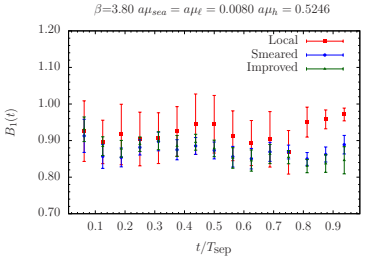

Figure 6.3.2: B_1 bare bag parameter at $\beta = 3.80$ and $(a\mu_\ell = a\mu_{sea}, a\mu_h) = (0.0080, 0.5246)$ on a $24^3 \times 48$ lattice plotted vs $t/T_{\rm sep}$ for local, smeared and improved meson sources and sinks.

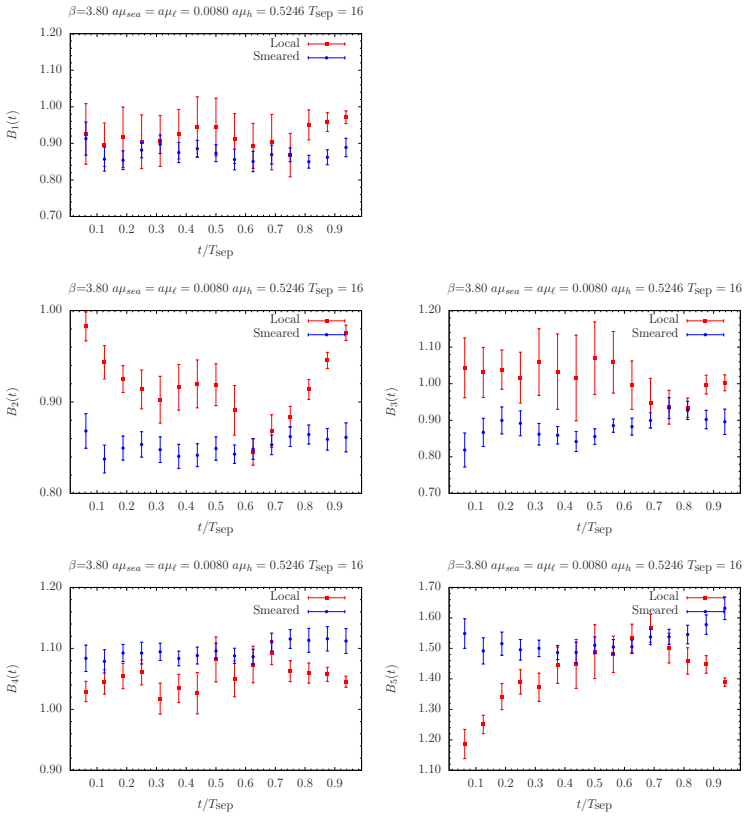

Figure 6.3.3: Bare bag parameters $(i = 1, 2, 3, 4, 5)$ at $\beta = 3.80$ and $(a\mu_\ell = a\mu_{sea}, a\mu_h) = (0.0080, 0.5246)$ on a $24^3 \times 48$ lattice plotted vs $t/T_{\rm sep}$ for smeared and local sources and sinks.

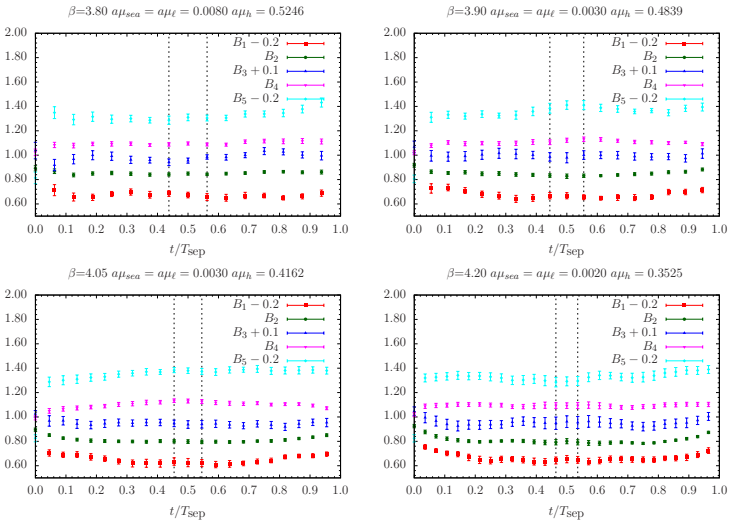

Figure 6.3.4: Data and time plateau for the bare $B_i^{(d)}$ parameters, $(i = 1, 2, 3, 4, 5)$ plotted vs $t/T_{\rm sep}$ with the lightest sea quark mass, $a\mu_\ell = a\mu_{sea}$ and $(a\mu_h) \sim 2.25\,(a\mu_c)$ at each lattice spacing. B_i parameters have been averaged over the eight possible combinations of Wilson parameters satisfying the relation $r_1 = r_2 = r_3 = -r_4$ or equivalent.

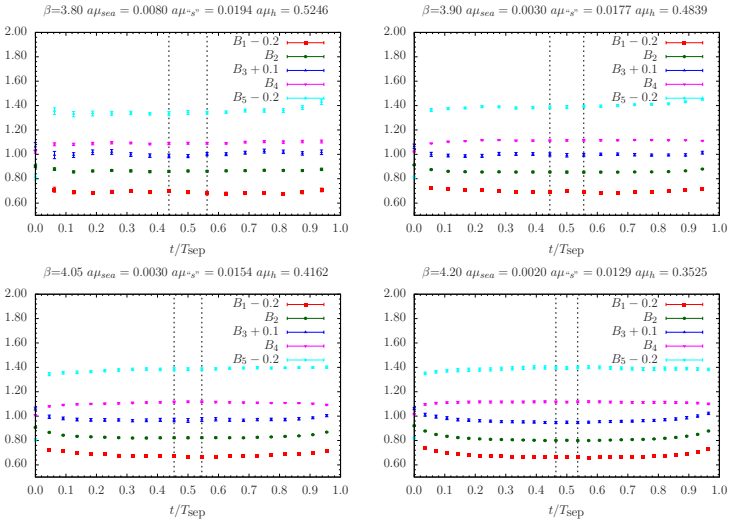

Figure 6.3.5: Data and time plateau for the bare $B_i^{(s)}$ parameters, $(i = 1, 2, 3, 4, 5)$ plotted vs $t/T_{\rm sep}$ with the lightest sea quark mass, $a\mu_{\text{“}s\text{”}} \sim a\mu_s$ and $(a\mu_h) \sim 2.25\,(a\mu_c)$ at each lattice spacing. B_i parameters have been averaged over the eight possible combinations of Wilson parameters satisfying the relation $r_1 = r_2 = r_3 = -r_4$ or equivalent.

6.3.1 B_i bag parameters: the ratio method

The application of the ratio method to the bag parameters follows the same strategy as the one outlined in the case of the pseudoscalar meson masses and decay constants with the handicap that now we are dealing with a vectorial quantity $\vec{B}$ which components mix among themselves under renormalization.

From HQET arguments one expects

$$\lim_{\mu_h \to \infty} \frac{B_i\left(\hat{\mu}_h^{(n)}\right)}{B_i\left(\hat{\mu}_h^{(n-1)}\right)} = 1$$

with some logarithmic leading deviations for small values of $1/\hat{\mu}_h$ of the order

$$\sim 1/\log\left(\hat{\mu}_h/\Lambda_{QCD}\right)$$

Such corrections to the power scaling in $1/\hat{\mu}_h$ are expected to be tiny in the range of $\hat{\mu}_h$ we are working and consequently they can be estimated in perturbation theory by matching HQET and QCD. These logarithmic corrections are removed from our data by considering the bag parameters in HQET

$$\tilde{B}_i\left(\hat{\mu}_h^{(n)}\right) = C_{ij}\left(\hat{\mu}_b^*, \hat{\mu}_h^{(n)}, \mu\right) B_j\left(\hat{\mu}_h^{(n)}\right) \tag{6.3.1}$$

where the C_{ij} factors contain the information on the $1/\log\left(\hat{\mu}_h\right)$ corrections. Bag parameters with tilde refer to the ones computed in HQET renormalized in $\overline{MS}$ at the scale $\hat{\mu}_b^*$ while the ones without tilde will refer to bag parameters computed in QCD and renormalized in $\overline{MS}$ at the scale μ.

The modified ratios

$$\omega_i\left(\hat{\mu}_h^{(n)}\right) = \frac{\tilde{B}_i\left(\hat{\mu}_h^{(n)}\right)}{\tilde{B}_i\left(\hat{\mu}_h^{(n-1)}\right)}$$

should satisfy the scaling law

$$\lim_{\mu_h \to \infty} \omega_i\left(\hat{\mu}_h^{(n)}\right) = 1$$

without logarithmic corrections up to a fixed order in perturbation theory.

The coefficients $C_{ij}\left(\hat{\mu}_b^*, \hat{\mu}_h^{(n)}, \mu\right)$ are computed from the QCD evolution of the bag parameters (from the scheme and the scale where they are computed in QCD (i.e $\overline{MS}$ at μ =2 or 3 GeV) to the heavy quark mass $\hat{\mu}_h^{(n)}$, followed by the matching between QCD and HQET at the reference scale $\hat{\mu}_h$ and the running in HQET to the reference scale $\hat{\mu}_b^*$.

The $\tilde{B}_i\left(\hat{\mu}_h^{(n)}\right)$ parameters obtained after the evolution satisfy the scaling law of HQET and thus they are the candidates to apply the ratio method. Technical details and specific expression for this matrix of matching coefficients are given in Appendix E.

RCs are computed in the RI-MOM scheme at the scale $\mu_0 = a^{-1}$. Since our simulated lattice spacing are close to 3 GeV we prefer to use as input quantities the B-parameter values renormalized in $\overline{MS}$ at μ =3 GeV to avoid the errors due to the truncation in the running from $\mu_0 = a^{-1}$ to μ.

In the numerical implementation we construct the renormalized HQET bag parameters at the reference scale $\hat{\mu}_b^*$ for each lattice spacing, sea quark mass and pair of valence quark masses. The heavy-light static $\tilde{B}_i^{(d)}$ are obtained from the $B_i^{(d)}$ QCD renormalized at the scale μ as

$$\tilde{B}_i^{(d)}\left(\hat{\mu}_h^{(n)};\hat{\mu}_\ell,a\right) = C_{ij}\left(\hat{\mu}_b^*,\hat{\mu}_h^{(n)},\mu\right) B_j^{(d)}\left(\hat{\mu}_h^{(n)};\hat{\mu}_\ell,a\right) \tag{6.3.2}$$

with $n = 1,..,7$ and $a\mu_{sea} = a\mu_\ell$.

Likewise, the heavy-strange static $\tilde{B}_i^{(s)}$ are obtained using the same C-factors[2] as

$$\tilde{B}_i^{(s)}\left(\hat{\mu}_h^{(n)};\hat{\mu}_{sea},\hat{\mu}_{\text{“}s\text{”}},a\right) = C_{ij}\left(\hat{\mu}_b^*,\hat{\mu}_h^{(n)},\mu\right) B_j^{(s)}\left(\hat{\mu}_h^{(n)};\hat{\mu}_{sea},\hat{\mu}_{\text{“}s\text{”}},a\right)$$

Having obtained these renormalized bag parameters we construct the ratios

$$\omega_i^{(d)L}\left(\hat{\mu}_h^{(n)};\hat{\mu}_\ell,a\right) = \frac{\tilde{B}_i^{(d)}\left(\hat{\mu}_h^{(n)};\hat{\mu}_\ell,a\right)}{\tilde{B}_i^{(d)}\left(\hat{\mu}_h^{(n-1)};\hat{\mu}_\ell,a\right)}$$

$$\omega_i^{(s)L}\left(\hat{\mu}_h^{(n)};\hat{\mu}_{sea},\hat{\mu}_{\text{“}s\text{”}},a\right) = \frac{\tilde{B}_i^{(s)}\left(\hat{\mu}_h^{(n)};\hat{\mu}_{sea},\hat{\mu}_{\text{“}s\text{”}},a\right)}{\tilde{B}_i^{(s)}\left(\hat{\mu}_h^{(n-1)};\hat{\mu}_{sea},\hat{\mu}_{\text{“}s\text{”}},a\right)}$$

which should be extrapolated to the continuum limit and physical quark masses

$$\omega_i^{(d)}\left(\hat{\mu}_h^{(n)}\right) = \lim_{\hat{\mu}_\ell\to\hat{\mu}_{u/d}}\lim_{a\to 0}\omega_i^{(d)L}\left(\hat{\mu}_h^{(n)};\hat{\mu}_\ell,a\right)$$
$$\omega_i^{(s)}\left(\hat{\mu}_h^{(n)}\right) = \lim_{\hat{\mu}_{sea}\to\hat{\mu}_{u/d}}\lim_{a\to 0}\lim_{\hat{\mu}_{\text{“}s\text{”}}\to\hat{\mu}_s}\omega_i^{(s)L}\left(\hat{\mu}_h^{(n)};\hat{\mu}_{sea},\hat{\mu}_{\text{“}s\text{”}},a\right)$$

In Figure 6.3.6 and Figure 6.3.7 we show the chiral and continuum extrapolations of the ratio of heavy-light and heavy-strange bag parameters $\omega_i^{(d)}$ and $\omega_i^{(s)}$, respectively. A fit linear in the light quark mass and in a^2 describes data rather well.

[2]Note that $C_{ij}\left(\hat{\mu}_b^*,\hat{\mu}_h^{(n)},\mu\right)$ depends on the initial QCD scale μ, the reference HQET scale $\hat{\mu}_b^*$ and the heavy quark mass $\mu_h^{(n)}$ where we match both theories.

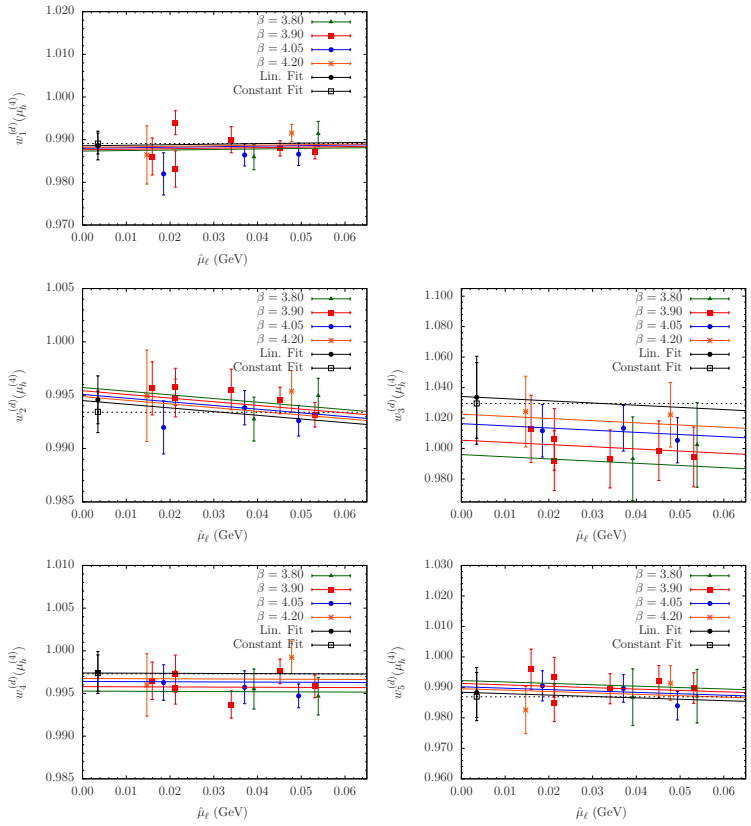

Figure 6.3.6: Solid lines represent the behaviour vs the renormalized light quark mass of the combined chiral and continuum limit according to a linear fit in the light quark mass and a^2 for the $\omega_i^{(d)}$ ratios with $i = 1, 2, 3, 4, 5$ renormalized in the $\overline{MS}$ scheme of [95] at 3 GeV with M1 type RCs. Ratios are computed with NLL matching. The full black line is the continuum limit curve (Lin. Fit). The dashed black line represents the continuum limit curve in the case of a linear fit in a^2 without dependence on the light quark mass (Constant Fit).

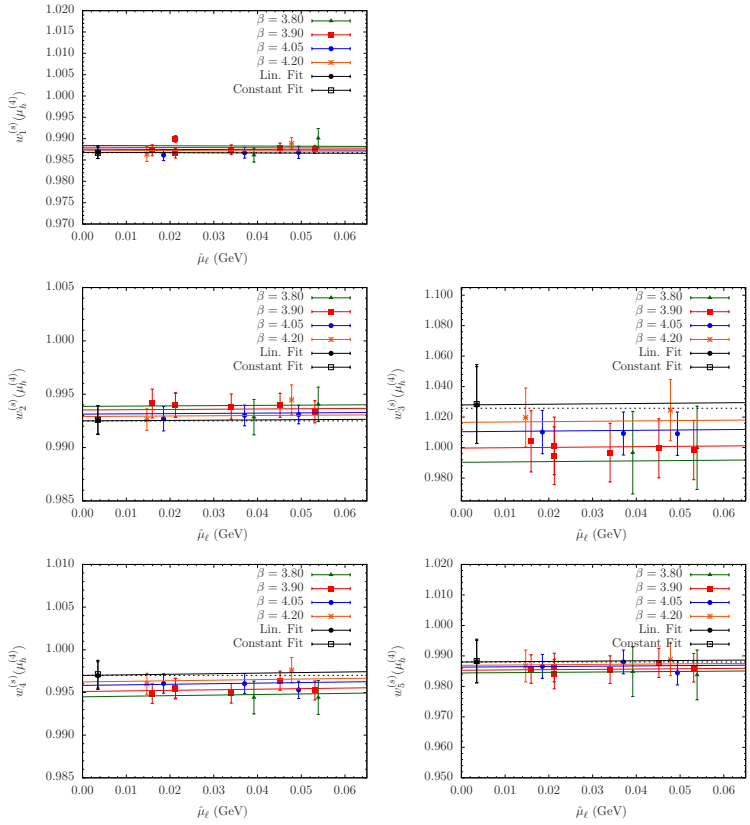

Figure 6.3.7: Solid lines represent the behaviour vs the renormalized light quark mass of the combined chiral and continuum limit according to a linear fit in the light quark mass and a^2 for the $\omega_i^{(s)}$ ratios with $i = 1, 2, 3, 4, 5$ renormalized in $\overline{MS}$ scheme of [95] at 3 GeV with M1 type RCs. Ratios are computed with NLL matching. The full black line is the continuum limit curve (Lin. Fit). The dashed black line represents the continuum limit curve in the case of a linear fit in a^2 without dependence on the light quark mass (Constant Fit).

After performing the chiral and continuum extrapolation we can study the dependence of the heavy-light $\omega_i^{(d)}$ and heavy-strange ratio $\omega_i^{(s)}$ with the heavy quark mass. As we did for the pseudoscalar meson mass and decay constant we consider a quadratic fit in $1/\hat{\mu}_h$

$$\omega_i\left(\hat{\mu}_h\right) = 1 + \frac{\eta_1}{\hat{\mu}_h} + \frac{\eta_2}{\hat{\mu}_h^2} \tag{6.3.3}$$

The quality of these fits for each B_i is illustrated in Figure 6.3.8.

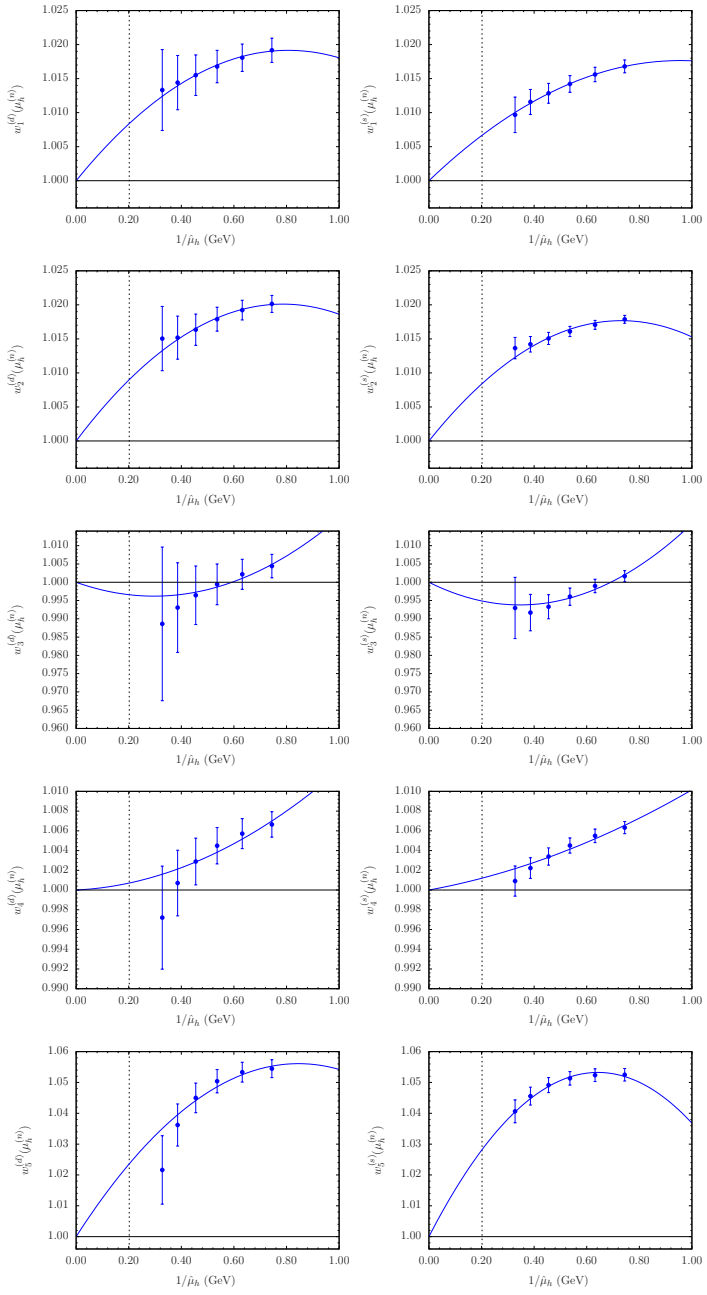

Figure 6.3.8: Heavy quark mass dependence of the ratios $\omega_i^{(d)}$ (left) and $\omega_i^{(s)}$ (right) extrapolated to the physical value of the light and strange quark masses and to the continuum limit. $\omega_i^{(d/s)}\left(\hat{\mu}_h^{(i)}\right)$ are not corrected with the matching (TL matching). The vertical dotted line represents the value of the physical b-quark mass.

In Figure 6.3.9 we show the dependence on $1/\hat{\mu}_h$ of the ratios $\omega_1^{(d)}$ and $\omega_1^{(s)}$ not corrected with the HQET matching (TL), corrected with LL matching and corrected with NLL matching. Despite the different behaviour of the curves at each order of matching, we should remark that this is only an artifact of the construction of the intermediate static quantities $\tilde{B}_i$. Figure 6.3.10 display the effect of the logarithmic corrections on the QCD ratios $B_1\left(\mu_h^{(n)}\right)/B_1\left(\mu_h^{(n-1)}\right)$ [3]. These figures confirm that the logarithmic corrections on the QCD ratios is small and explain the small systematic uncertainty in the final results due to the matching procedure.

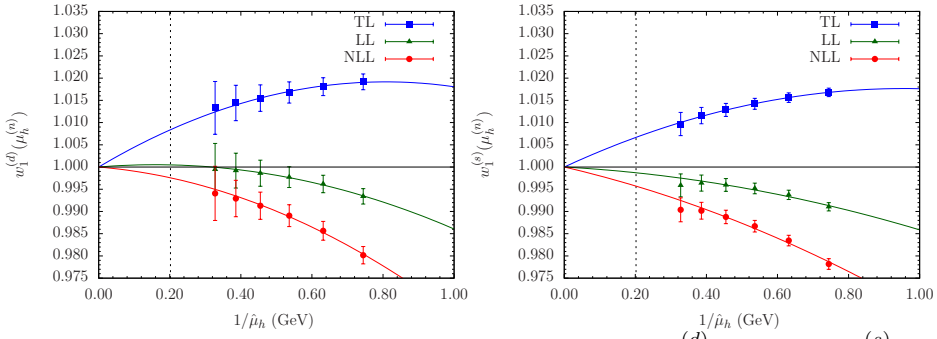

Figure 6.3.9: Heavy quark mass dependence of the ratios $\omega_1^{(d)}$ (left) and $\omega_1^{(s)}$ (right), extrapolated to the physical value of the light and strange quark masses and to the continuum limit, not corrected (TL), corrected with LL matching and corrected with NLL matching. The vertical dotted line represents the value of the physical b-quark mass.

[3] Once the static $\tilde{B}_1\left(\hat{\mu}_h^{(n)}\right)$ is constructed we can use

$$\omega_1\left(\hat{\mu}_h\right) = \frac{\tilde{B}_1\left(\hat{\mu}_h^{(n)}\right)}{\tilde{B}_1\left(\hat{\mu}_h^{(n-1)}\right)} = \frac{\sum_{i=1}^{3} C_{1i}\left(\hat{\mu}_h^{(n)}\right) B_i\left(\hat{\mu}_h^{(n)}\right)}{\sum_{j=1}^{3} C_{1j}\left(\hat{\mu}_h^{(n-1)}\right) B_j\left(\hat{\mu}_h^{(n-1)}\right)}$$

to isolate the QCD ratio $B_1\left(\hat{\mu}_h^{(n)}\right)/B_1\left(\hat{\mu}_h^{(n-1)}\right)$

$$\frac{B_1\left(\hat{\mu}_h^{(n)}\right)}{B_1\left(\hat{\mu}_h^{(n-1)}\right)} = \frac{\tilde{B}_1\left(\hat{\mu}_h^{(n)}\right)}{\tilde{B}_1\left(\hat{\mu}_h^{(n-1)}\right)} \times \frac{\sum_{j=1}^{3} C_{1j}\left(\hat{\mu}_h^{(n-1)}\right) B_j\left(\hat{\mu}_h^{(n-1)}\right)}{\sum_{i=1}^{3} C_{1i}\left(\hat{\mu}_h^{(n)}\right) B_i\left(\hat{\mu}_h^{(n)}\right) B_1\left(\hat{\mu}_h^{(n-1)}\right)/B_1\left(\hat{\mu}_h^{(n)}\right)}$$

where on the r.h.s we introduce the chiral and continuum extrapolated values of the simulated B_i at each $\hat{\mu}_h$. The result on the l.h.s can be considered as the corrected ratio $B_1\left(\mu_h^{(n)}\right)/B_1\left(\mu_h^{(n-1)}\right)$ including the logarithmic corrections in $1/\hat{\mu}_h$.

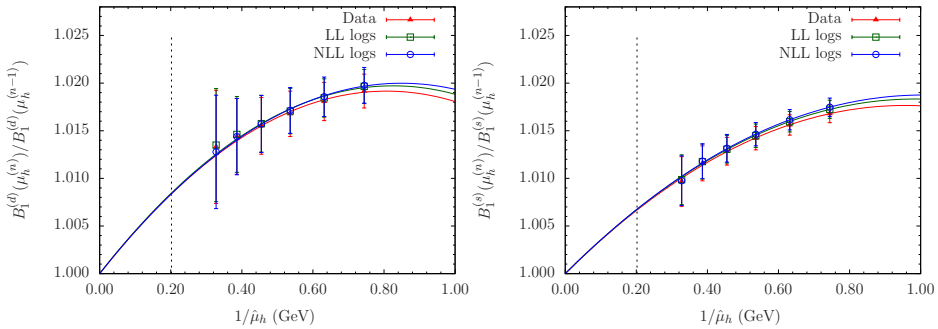

Figure 6.3.10: Ratios $B_1^{(d)}\left(\hat{\mu}_h^{(n)}\right)/B_1^{(d)}\left(\hat{\mu}_h^{(n-1)}\right)$ (left) and $B_1^{(s)}\left(\hat{\mu}_h^{(n)}\right)/B_1^{(s)}\left(\hat{\mu}_h^{(n-1)}\right)$ (right). Red triangles correspond to original data while open green squares and blue circles correspond to data corrected with the logarithmic corrections in $1/\hat{\mu}_h$. Bag parameters are renormalized in $\overline{MS}$ of [95] at 3 GeV.

The value of the bag parameters at the b-quark mass are eventually computed from the recursive chain equation in terms of the fit values of ω_i according to Eq.6.3.3

$$\omega_i\left(\hat{\mu}_h^{(2)}\right)...\omega_i\left(\hat{\mu}_h^{(K+1)}\right) = \frac{C_{ij}\left(\hat{\mu}_b^*, \hat{\mu}_h^{(K+1)}, \mu\right) B_j\left(\hat{\mu}_h^{(K+1)}\right)}{C_{ij}\left(\hat{\mu}_b^*, \hat{\mu}_h^{(1)}, \mu\right) B_j\left(\hat{\mu}_h^{(1)}\right)} \tag{6.3.4}$$

for both $\omega_i^{(d)}$ and $\omega_i^{(s)}$. In Eq.6.3.4 j is a summed index.

In the previous formula, $B_i\left(\hat{\mu}_h^{(1)}\right)$ is the renormalized bag parameter at the triggering point $\hat{\mu}^{(1)} = \hat{\mu}_c$, i.e for the computation of the $B_i^{(d)}$ ($B_i^{(s)}$) it would correspond to the bag parameter of the D (D_s) meson where the chiral and continuum extrapolation are under control. As we have previously tuned λ in order to arrive to the b-quark mass after K steps, $B_i\left(\hat{\mu}_h^{(K+1)}\right) = B_i\left(\hat{\mu}_b\right)$ is the bag parameter at the b-quark mass point renormalized in the same scheme at the same scale as the triggering point $B_i\left(\hat{\mu}_h^{(1)}\right)$, in our case $\overline{MS}$ at μ =3 GeV.

Our results are finally evolved from $\overline{MS}$ at μ =3 GeV to $\overline{MS}$ at the scale m_b using the NLL evolution (see Appendix C) with the updated ETMC value $\Lambda_{\rm QCD}(N_f = 2) = 330(23)(^{+22}_{-33})$ MeV [108].

Estimates for $B_i^{(d)}$ and $B_i^{(s)}$ at TL, LL and NLL are collected in Table 6.3.1 and Table 6.3.2 respectively.

		TL	LL	NLL
$B_1^{(d)}$	M1	0.846(39)	0.856(39)	0.858(39)
	M2	0.841(34)	0.852(35)	0.854(35)
$B_2^{(d)}$	M1	0.720(31)	0.726(32)	0.729(32)
	M2	0.699(23)	0.705(24)	0.708(24)
$B_3^{(d)}$	M1	0.922(70)	0.904(104)	0.892(132)
	M2	0.861(50)	0.836(73)	0.839(87)
$B_4^{(d)}$	M1	0.933(43)	0.934(45)	0.933(44)
	M2	0.904(33)	0.905(32)	0.906(33)
$B_5^{(d)}$	M1	1.455(76)	1.476(80)	1.471(82)
	M2	1.488(60)	1.523(63)	1.521(66)

Table 6.3.1: $B_i^{(d)}$ parameters for $\overline{B}^0 - B^0$ oscillations renormalized in the $\overline{MS}$ of [95] at the scale $\mu = m_b$. The results are obtained assuming a linear fit on $\hat{\mu}_\ell$ and a^2 for the ratios and the triggering point and a quadratic fit in $1/\hat{\mu}_h$.

		TL	LL	NLL
$B_1^{(s)}$	M1	0.848(27)	0.858(27)	0.860(27)
	M2	0.844(20)	0.853(21)	0.857(21)
$B_2^{(s)}$	M1	0.733(27)	0.738(28)	0.741(28)
	M2	0.712(20)	0.718(20)	0.721(20)
$B_3^{(s)}$	M1	0.926(53)	0.901(67)	0.881(95)
	M2	0.867(36)	0.837(43)	0.827(50)
$B_4^{(s)}$	M1	0.935(40)	0.936(40)	0.937(40)
	M2	0.905(28)	0.907(27)	0.907(27)
$B_5^{(s)}$	M1	1.549(66)	1.588(68)	1.598(68)
	M2	1.583(48)	1.625(50)	1.630(51)

Table 6.3.2: $B_i^{(s)}$ parameters for $\overline{B}^0 - B^0$ oscillations renormalized in the $\overline{MS}$ of [95] at the scale $\mu = m_b$. The results are obtained assuming a linear fit on $\hat{\mu}_\ell$ and a^2 for the ratios and the triggering point and a quadratic fit in $1/\hat{\mu}_h$.

We consider the difference between TL, LL and NLL results as a systematic error measuring the impact of the logarithmic corrections in $1/\hat{\mu}_h$. When comparing the results obtained with the TL, LL and NLL matching, the difference in the final estimates of $B_i^{(d)}$ and $B_i^{(s)}$ is found to be small compared with the statistical error. The sensitivity to the $C_{ij}\left(\hat{\mu}_b^*, \hat{\mu}_h^{(n)}, \mu\right)$ factors, introduced in Eq.6.3.1 as intermediate steps, largely cancels in the final determination. In other words, C-factors cancel in Eq.6.3.4 except for the corrections introduced when performing the fit in $1/\hat{\mu}_h$.

Because of that, the dependence on the scale μ, where we renormalize the bare bag

parameters in QCD, and in the reference scale in HQET $\hat{\mu}_b^*$ is expected to cancel in the final estimates. We have repeated the whole analysis with $\hat{\mu}_b^* = \hat{\mu}_b$ or $\hat{\mu}_b^* = 3$GeV. This change resulted in a negligible shift $\lesssim 0.001$ in the central values reported in Table 6.3.1 and Table 6.3.2. We have also checked that fixing $\mu = 2$ GeV or $\mu = 3$GeV for the renormalization of the input B-parameters results in a negligible shift of the final $B_1^{(d)}$ and $B_1^{(s)} \lesssim 0.001$ while for B_i with $i = 2, 3, 4, 5$ the shift is slightly larger, about 1/4 of the statistical σ at maximum.

The uncertainty due to the chiral and continuum extrapolations of the ratios $\omega_i\left(\hat{\mu}_h\right)$ is accounted by considering also linear fit in a^2 without dependence on $\hat{\mu}_\ell$. The use of a constant chiral extrapolation fit yields to a shift of $\sim 0.3\%$ for the final estimate of B_1 while for B_i with $i = 2, 3, 4, 5$ the shift is $\sim 1 - 6\%$.

The systematic error introduced by the chiral and continuum extrapolation of the triggering point $B_i^{(d)}\left(\hat{\mu}_h^{(1)}\right)$ is accounted by a HMChPT (see section 5.4) with $\hat{g} = 0.53(4)$ and $Y = 1$ from [105]. The use of the experimental value $\hat{g} = 0.61$ [111] decreases the systematic error due to the chiral extrapolation of the triggering point.

In order to estimate the uncertainty associated to the interpolation of $\omega_i\left(\hat{\mu}_h\right)$ to $\hat{\mu}_b$ we have repeated the whole analysis by choosing a first order polynomial function in $1/\hat{\mu}_h$ rather than the quadratic fit in Eq.6.3.3. The use of a linear fit in $1/\hat{\mu}_h$ results in a shift of $\sim 2\%$ in the final results.

The final values of $B_i^{(d)}$ and $B_i^{(s)}$ renormalized at $\overline{MS}\left(m_b\right)$ for $i = 1, 2, 3, 4, 5$, collected in Table 6.3.3, correspond to the ones with M1 type RCs and NLL matching. Results have been averaged over the several choices for the chiral extrapolation of the ratios and the triggering point and over the linear or quadratic fit in the inverse of $\hat{\mu}_h$. In the first line the first error is statistical and the second one systematic. The spread between the different results has been considered as an estimate of the systematic error. The statistical error includes the statistical uncertainty on the raw data for the bare matrix elements (~2%), the associated renormalization constants (~2%), the lattice spacing and the value of Z_P.

$B_1^{(d)}$	$B_2^{(d)}$	$B_3^{(d)}$	$B_4^{(d)}$	$B_5^{(d)}$
0.848(33)(16)	0.720(30)(15)	0.867(119)(50)	0.937(42)(08)	1.473(75)(53)
0.85(04)	0.72(03)	0.87(13)	0.94(05)	1.47(09)
$B_1^{(s)}$	$B_2^{(s)}$	$B_3^{(s)}$	$B_4^{(s)}$	$B_5^{(s)}$
0.857(25)(11)	0.740(28)(11)	0.880(95)(37)	0.937(40)(03)	1.598(67)(66)
0.86(03)	0.74(03)	0.88(10)	0.94(04)	1.60(09)

Table 6.3.3: Continuum limit results for $B_i^{(d)}$ and $B_i^{(s)}$ renormalized in $\overline{MS}$ of [95] at $\mu = m_b$ with M1-type RCs and NLL matching coefficients. Results have been averaged over the several choices for the chiral extrapolation of the ratios and the triggering point as well as over the linear or quadratic fit in the inverse of $\hat{\mu}_h$. In the first line the first error is statistical and the second one systematic. The half difference between the two more distant results, coming from the spread of estimates with TL, LL or NLL matching, quadratic or linear fit $1/\hat{\mu}_h$ and different ansatzs of chiral and continuum extrapolation, has been taken as an estimate of the systematic error. In the second line the total uncertainty is obtained by adding in quadrature the statistical and the systematic error.

6.3.2 B_{B_s}/B_B

We can also consider as primary quantities for the application of the ratio method the ratio of $B_1^{(s)}/B_1^{(d)}$, i.e B_{B_s}/B_B. This quantity is obtained from the double ratio

$$\zeta_\omega^L\left(\hat{\mu}_h;\hat{\mu}_\ell,\hat{\mu}_{\text{“}s\text{”}},a\right)=\frac{\omega_s^L\left(\hat{\mu}_h;\hat{\mu}_\ell,\hat{\mu}_{\text{“}s\text{”}},a\right)}{\omega_d^L\left(\hat{\mu}_h;\hat{\mu}_\ell,a\right)}$$

where for notation economy we renamed: $\omega_s^L \equiv \omega_1^{(s)L}$ and $\omega_d^L \equiv \omega_1^{(d)L}$.

In the construction of $\zeta_\omega^L\left(\hat{\mu}_h;\hat{\mu}_\ell,\hat{\mu}_{\text{“}s\text{”}},a\right)$ the logarithmic corrections in $1/\hat{\mu}_h$ contained in the C_{ij} coefficients as defined in Eq.6.3.2 largely cancel out. This is so because $C_{ij}\left(\hat{\mu}_b^*,\hat{\mu}_h,\mu\right)$ depend on the scale in QCD where we renormalize the bare bag parameters, the valence heavy quark mass and the reference scale in HQET but not in the light or strange spectator valence quark mass. In addition, renormalization constants also cancel out in the construction of the double ratio.

The previous argument holds exactly when no mixing occurs, as it happens when we consider TL or LL matching. When considering $C_{ij}\left(\hat{\mu}_b^*,\hat{\mu}_h,\mu\right)$ at NLL a small contribution of B_2 and B_3 appear in $\tilde{B}_1$ and the cancellation of matching coefficients and renormalization constants occurs only in a approximate way. In practice, as it was pointed out and shown numerically in the previous section, they largely cancel numerically in the final estimates within statistical errors. Hence, for the computation of B_{B_s}/B_B I will consider TL matching, i.e $C_{ij}\left(\hat{\mu}_b^*,\hat{\mu}_h,\mu\right)=1$.

Once $\zeta_\omega^L\left(\hat{\mu}_h;\hat{\mu}_\ell,\hat{\mu}_{\text{“}s\text{”}},a\right)$ is interpolated to the physical strange quark mass, we extrapolate them to the continuum and chiral limit. As illustrated in Figure 6.3.11 ζ_ω has a smooth chiral and continuum limit. The results for the double ratio ζ_ω turn out to be well described by both a linear and a constant behaviour in $\hat{\mu}_\ell$ and a^2 (see right plot

in Figure 6.3.11). The impact of considering a linear or a constant fit for the ratio ζ_ω results in a shift $\lesssim 0.005$ over the final estimate of B_{B_s}/B_B which is finally included as a systematic error.

In the left panel of Figure 6.3.11 we show the chiral and continuum extrapolation of the triggering point B_{B_s}/B_B at the initial triggering mass $\hat{\mu}_h^{(1)}$. The black line represent the linear fit in $\hat{\mu}_\ell$ and a^2 while the dotted line corresponds to HMChPT fit which predicts at the NLL a linear plus logarithmic dependence on $\hat{\mu}_\ell$ coming from the chiral logarithmic behaviour of B_B [104]

$$B_{B_s}/B_B\left(\hat{\mu}_h^{(1)};\hat{\mu}_\ell,a\right) = B_h\left[1+\frac{(1-3\hat{g}^2)}{2}\frac{2B_0\hat{\mu}_\ell}{16\pi^2 f_0^2}\log\left(\frac{2B_0\hat{\mu}_\ell}{16\pi^2 f_0^2}\right)+C_h\mu_\ell+D_h a^2\right]$$

with $\hat{g} = 0.53(4)$ [105]. As it is shown in the right panel of Figure 6.3.11 the chiral logs cannot be appreciated with our data so eventually we average the results obtained from the linear chiral and continuum extrapolation and the HMChPT fit ansatz and the difference is included as a systematic error. With the experimental value $\hat{g} = 0.61(7)$ [111] the logarithmic term is smaller and the systematic error due to the light quark mass extrapolation of the triggering point also decreases.

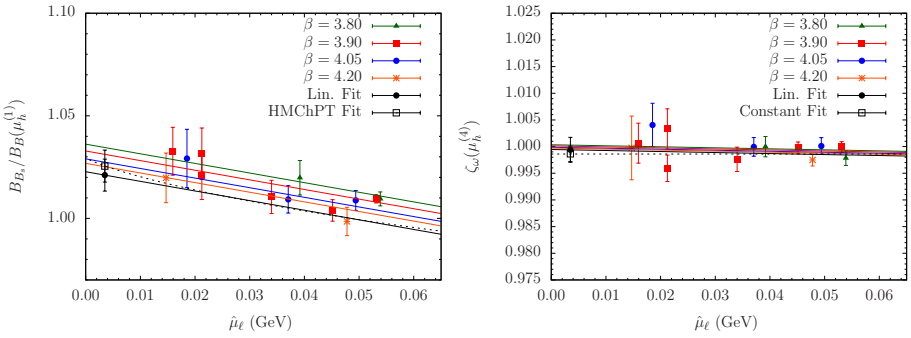

Figure 6.3.11: Light quark mass dependence of the double ratio $\zeta_\omega\left(\hat{\mu}_h^{(4)}\right)$ (right) and the triggering point $B_{B_s}/B_B\left(\hat{\mu}_h^{(1)}\right)$ (left) at the four values of the lattice spacing

Finally, we study the dependence of the ratio ζ_ω on the heavy quark mass as it is shown in Figure 6.3.12. The dependence on the heavy quark mass is barely visible, so in that case we perform either a quadratic or a linear interpolation in $1/\hat{\mu}_h$ or a constant fit which turn out to be compatible with the known static limit $\zeta_\omega = 1$ within statistical error.

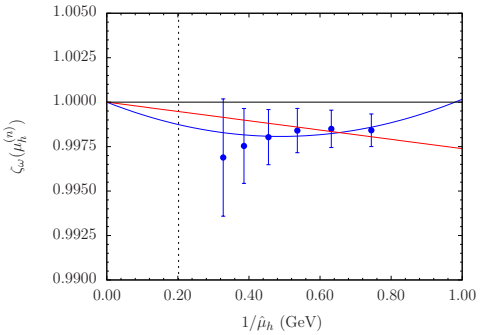

Figure 6.3.12: Heavy quark mass dependence of the ratio $\zeta_\omega\,(\hat{\mu}_h)$ extrapolated to the physical value of the light and strange quark mass and to the continuum limit. The vertical dotted line represents the value of the physical b-quark mass. Blue line corresponds to a quadratic fit in $1/\hat{\mu}_h$ and the red line to a linear fit.

The final estimate is obtained by averaging over the three fit ansatz in $1/\hat{\mu}_h$ (quadratic, linear or constant), the ansatzs for chiral extrapolations of the double ratio ζ_ω (linear or constant) and the ansatz for the chiral extrapolation of the triggering point (linear or HMChPT). The half of the difference between the two more distant results is considered as a systematic uncertainty

$$B_{B_s}/B_B = 1.013(17)(05) \rightarrow B_{B_s}/B_B = 1.013(18) \tag{6.3.5}$$

where the first error is the statistical one coming from a bootstrap analysis and the second is the systematic. In the second result the systematic uncertainty is added in quadrature to the statistical error.

Alternatively, in order to estimate the effect of the NLL matching in the ratio method we can take the ratio of the NLL estimates of B_B and B_{B_s} obtained separately. These values are collected in Table 6.3.3 and lead to

$$B_{B_s}/B_B|_{\rm NLL} = 1.010(19)$$

where only the statistical error has been quoted. The difference with Eq.6.3.5 is a small fraction of one standard deviation. We conclude that, as expected, the effect of the matching in the double ratio are largely canceled and the systematic error associated to the logarithmic corrections in $1/\hat{\mu}_h$ is small.

6.3.3 ξ

The ratio method can also be directly applied to the ξ parameter, relevant in the UT analysis as it is described in subsection 1.2.6. Since the ξ parameter is written in terms of decay constants and bag parameters as

$$\xi = f_{B_S}\sqrt{B_{B_s}}/f_B\sqrt{B_B}$$

we construct the double ratio

$$\zeta_\xi^L\left(\hat{\mu}_h;\hat{\mu}_\ell,\hat{\mu}_{\text{“}s\text{”}},a\right)=\frac{z_s^L\sqrt{\omega_s^L\left(\hat{\mu}_h;\hat{\mu}_\ell,\hat{\mu}_{\text{“}s\text{”}},a\right)}}{z_d^L\sqrt{\omega_d^L\left(\hat{\mu}_h;\hat{\mu}_\ell,a\right)}}$$

As it happens in $\zeta_\omega^L\left(\hat{\mu}_h;\hat{\mu}_\ell,\hat{\mu}_{\text{“}s\text{”}},a\right)$ the logarithmic corrections cancel out when considering the double ratio, exactly up to LL and with negligible contribution in the final results when NLL matching is considered.

As illustrated in Figure 6.3.13 the chiral and continuum limit of the double ratio ζ_ξ presents small cutoff effects and turns out to be well described by both a linear and a constant behaviour in $\hat{\mu}_\ell$ and a^2. The impact of considering a linear or a constant fit for the ratio ζ_ξ is eventually included as a systematic error.

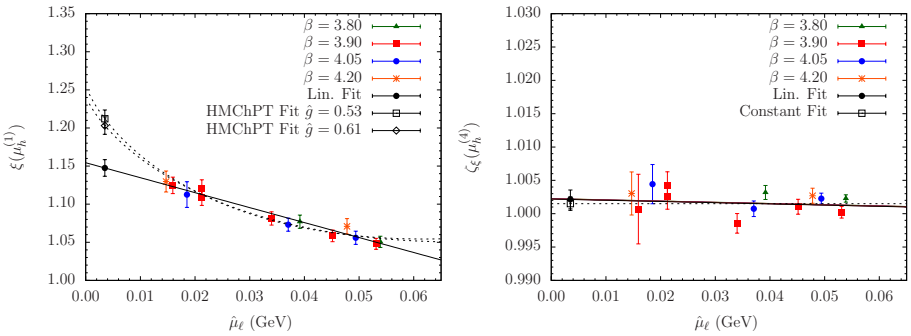

Figure 6.3.13: Light quark mass dependence of the triggering point $\xi\left(\hat{\mu}_h^{(1)}\right)$ and the double ratio $\zeta_\xi\left(\hat{\mu}_h^{(4)}\right)$ at the four values of the lattice spacing

In the left panel of Figure 6.3.13 we show the chiral and continuum extrapolation of ξ at the initial triggering mass $\hat{\mu}_h^{(1)}$. The black line represents the linear fit in $\hat{\mu}_\ell$ and a^2 while the dotted line corresponds to HMChPT fit which predicts at the NLL a linear plus logarithmic dependence on $\hat{\mu}_\ell$ coming from the chiral logarithmic behaviour of f_B and B_B, i.e:

$$\xi\left(\hat{\mu}_h^{(1)};\hat{\mu}_\ell,a\right)=B_h\left[1+\frac{\left(1+3\hat{g}^2\right)}{2}\frac{2B_0\hat{\mu}_\ell}{16\pi^2 f_0^2}\log\left(\frac{2B_0\hat{\mu}_\ell}{16\pi^2 f_0^2}\right)+C_h\mu_\ell+D_h a^2\right]$$

The use of a HMChPT inspired fit for the triggering point instead of a linear fit leads to a shift of $\simeq +0.07$ with $\hat{g}=0.53(4)$ [105] and $\simeq +0.08$ with $\hat{g}=0.61(7)$ [111] in the final estimates. As it is shown in the right panel of Figure 6.3.13 the chiral logs

cannot be appreciated with our data so eventually we average the results at the triggering point obtained from the linear fit and the HMChPT ansatzs with $\hat{g} = 0.61(7)$ (the more conservative) and the difference is included as a systematic error.

Finally, as usual, we study the dependence of the ratio ζ_ξ on the heavy quark mass which turns out to be barely visible as it is shown in Figure 6.3.14.

The final estimate is obtained by averaging over the different chiral and heavy extrapolations and the half of the difference between the two more distant results is considered as a systematic uncertainty. The final result is

$$\xi = 1.192(15)(38) \rightarrow \xi = 1.19(04)$$

where the fist error is the statistical one coming from a bootstrap analysis and the second is the systematic mainly due to the fit ansatz choices for the fit at the triggering point.

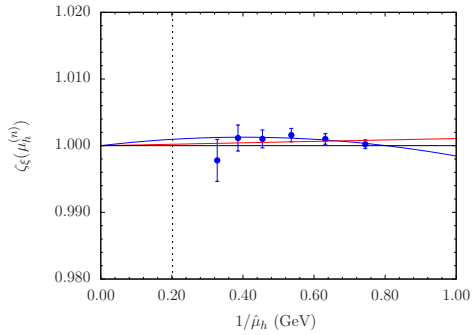

Figure 6.3.14: Heavy quark mass dependence of the ratio $\zeta_\xi(\hat{\mu}_h)$ extrapolated to the physical value of the light and strange quark mass and to the continuum limit. The vertical dotted line represents the value of the physical b-quark mass. Blue line corresponding to a quadratic fit in $1/\hat{\mu}_h$ and the red line to a linear fit are superimposed.

Chapter 7

Neutral kaon oscillations from $\mathbf{N_f = 2 + 1 + 1}$

In this chapter we extend the analysis for the bag parameters by considering the effects of four flavours of quarks in the sea, namely the quantum loop effects of the up, down, strange and charm quarks. This is done by adding a heavy mass-split doublet (c, s) to the light degenerate doublet (u, d) as it is described in chapter 2. We refer to this setup as $N_f = 2+1+1$. The comparison between the physical results obtained with $N_f = 2+1+1$ and $N_f = 2$ would reveal the systematic effect associated to the quenching of the strange and charm quarks in the $N_f = 2$ simulations.

In this chapter, I will present a preliminary analysis of the bag parameters controlling the $\overline{K}^0 - K^0$ oscillations using the $N_f = 2 + 1 + 1$ ensembles generated by the ETMC. In our setup we employ a mixed fermionic action setup with different actions for the sea and valence quarks. As for the $N_f = 2$ mass-degenerate case, we use maximally twisted sea quarks and Osterwalder-Seiler valence quarks in order to achieve both $\mathcal{O}(a)$ improvement and continuum-like renormalization pattern for the four-fermion operators. The computation of the relevant renormalization constants is performed non perturbatively in the RI-MOM scheme using dedicated ensembles with $N_f = 4$ degenerate sea quarks flavours produced by the ETMC and analyzed in chapter 4. The analysis steps for the computation of the bag parameters follows the same standard steps as the ones detailed in chapter 5.

7.1 $\mathbf{N_f = 2 + 1 + 1}$ simulation

The ETM collaboration has generated $N_f = 2 + 1 + 1$ configuration ensembles using the Iwasaki gauge action and the Twisted Mass quark action at maximal twist. The fermionic action for the light doublet and the heavy mass-split doublet are given by Eq.2.2.7 and

Eq.2.2.10 respectively. We have simulations at three values of the lattice spacing in the interval $[0.06 : 0.09]$ fm and with simulated light pseudoscalar meson masses in the range $[230 : 500]$ MeV. These configurations have been used in this analysis.

Simulation details are collected in Table 7.1.1. The value of the light quark mass μ_ℓ is common to sea and valence quarks and we simulate three heavier valence quark masses in the region of the physical strange quark mass.

The mass parameters μ_σ and μ_δ, related to the strange and charm sea quark masses and appearing in Eq.2.2.10, are also reported in Table 7.1.1. They are fixed by requiring the simulated K and D meson masses to approximately take their physical values [69].

For the inversions in the valence sector we used the stochastic method, described in Appendix A, with propagator sources located at random timeslices, y_0. In the $N_f = 2+1+1$ simulation, the two stochastic meson sources are local and separated by $T/2$.

β	$L^3 \times T$	N_{stat}	$a\mu_\ell = a\mu_{\rm sea}$	N_{stat}	$a\mu_{\text{“}s\text{”}}$
1.90 ($a^{-1} \sim 2.19$ GeV)	$24^3 \times 48$	144	0.0040	144	0.0145 0.0185 0.0225
$\mu_\sigma = 0.15$ $\mu_\delta = 0.19$			0.0060	144	
			0.0080	144	
			0.0100	144	
	$32^3 \times 64$	144	0.0030	144	0.0145 0.0185 0.0225
			0.0040	96	
			0.0050	144	
1.95 ($a^{-1} \sim 2.50$ GeV)	$24^3 \times 48$	144	0.0085	224	0.0141 0.0180 0.0219
$\mu_\sigma = 0.135$ $\mu_\delta = 0.17$	$32^3 \times 64$	144	0.0025	144	0.0141 0.0180 0.0219
			0.0035	144	
			0.0055	144	
			0.0075	80	
2.10 ($a^{-1} \sim 3.23$ GeV)	$48^3 \times 96$	96	0.0015	96	0.0118 0.0151 0.0184
$\mu_\sigma = 0.12$ $\mu_\delta = 0.1385$			0.0020	96	
			0.0030	96	

Table 7.1.1: Details of simulation runs at $\beta = 1.90,\ 1.95$ and 2.10.

7.2 Simulation, analysis and final estimates

In order to extract the bare bag parameters we follow the strategy presented in chapter 5. Bare estimates of bag parameters are obtained from the following ratios of local-local (LL) three- and two-point correlators:

$$\frac{\left[C^{(3)}_{Q_1}(x_0)\right]}{\left[C^{(2)}_{PA}(x_0)\right]\left[C'^{(2)}_{PA}(x_0)\right]} \xrightarrow[y_0 \ll x_0 \ll y_0 + T/2]{} \xi_1 B_1$$

$$\frac{\left[C^{(3)}_{Q_i}(x_0)\right]}{\left[C^{(2)}_{PP}(x_0)\right]\left[C'^{(2)}_{PP}(x_0)\right]} \xrightarrow[y_0 \ll x_0 \ll y_0 + T/2]{} \xi_i B_i \;\; i = 2, ..., 5$$

for each β and each couple of $(a\mu_\ell, a\mu_{\text{“}s\text{”}})$. In our analysis, we fit these ratios to a constant in the interval $[T/4 - 2 : T/4 + 2]$. The result remains stable if we use the interval $[T/4 - 3 : T/4 + 3]$, which is a test that indicates that we have isolated the ground state. Since in this analysis $T_{\text{sep}} = T/2$ some reduction of statistical fluctuations comes also from the symmetrization of both sides of the lattice.

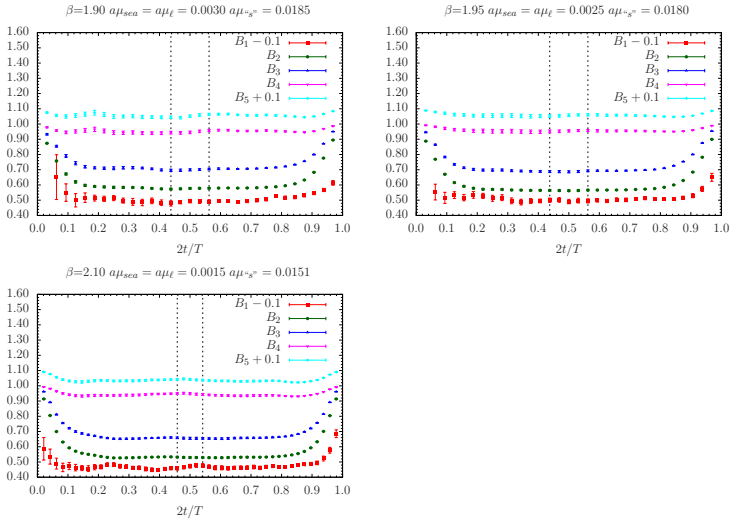

Figure 7.2.1: Data and time plateau for the bare B_i parameters, $(i = 1, 2, 3, 4, 5)$ for the $\overline{K}^0 - K^0$ system plotted vs $2t/T$ for the lightest sea quark mass at each lattice spacing.

The estimators of $\xi_i B_i$ have been averaged over the eight possible combinations of Wilson r-parameters satisfying the relation $r_1 = r_2 = \pm 1$ and $r_3 = -r_4 = \pm 1$ (or the equivalent: $r_1 = -r_2 = \pm 1$ and $r_3 = r_4 = \pm 1$) . These combinations correspond to simulate a K^0 meson with strange-light valence quark content with the same twist angle, $r_1 = r_2$, while the $\overline{K}^0$ meson would contain a strange-light pair of valence quarks with opposite twist angle, $r_3 = -r_4$, or viceversa. For this reason, in order to average over equivalent situations, we have time-inverted the estimators coming from $-r_1 = r_2 = r_3 = r_4$ Wilson r-parameters.

The results for the bare quantities $\xi_i B_i$ are collected in Appendix H. To illustrate their behaviour in Figure 7.2.1 we display examples of B_i as functions of time at $\beta = 1.90$, 1.95 and 2.10 for the lightest simulated sea quark mass and the second strange mass in Table 7.1.1.

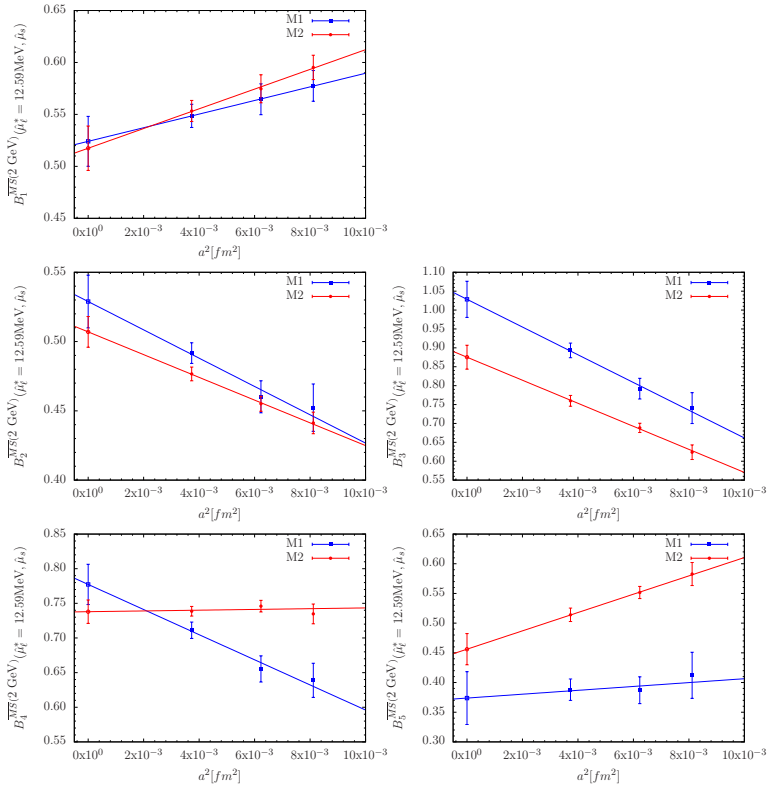

Figure 7.2.2: B_i with $i = 1, 2, 3, 4, 5$ as function of a^2 at the reference quark mass $\hat{\mu}_\ell^* = 12.59$ MeV, corresponding to the second sea quark mass of $\beta = 2.10$, and interpolated to the physical strange quark mass for the two $(ap)^2$ fit procedures: M1 and M2. Open symbols correspond to the continuum extrapolated results. The best linear fit in a^2 is also shown.

The relevant RCs both for the two- and four-fermion operators have been computed non perturbatively in the RI-MOM scheme as it is described in chapter 4. In Figure 7.2.2 we show the scaling behaviour for each B_i using the M1- and M2-type RCs discussed in chapter 4. The scaling test have been performed at a reference quark mass $\hat{\mu}_\ell^* = 12.59$ MeV which corresponds to the second value of the light quark mass at $\beta = 2.10$. The estimators of B_i at $\beta = 1.90$ and $\beta = 1.95$ have been interpolated to this value of $\hat{\mu}_\ell^*$. As expected, the a^2-scaling describes correctly the behaviour of B_i and the continuum

extrapolated results tends to agree. For B_1, B_2 and B_4 the extrapolated results are compatible within 1σ while for B_3 and B_5 the results turn out to be compatible within 2σ.

In order to extract the physical B_i parameters we need to perform the extrapolation and interpolation to the physical quark mass point. This requires the knowledge of the physical masses of up/down and strange quarks with $N_f = 2+1+1$ simulations. Since, at present, these values are still preliminary I prefer to perform an alternative analysis where the role of the renormalized quark masses, $\hat{\mu}_\ell$ and $\hat{\mu}_{\text{“}s\text{”}}$, is played by the Twisted-Mass (TM) masses $(M_{\ell\ell})^2$ and $(M_{hh})^2$.

For all values of β and $(M_{\ell\ell})^2$, data for $B_i\,(M_{\ell\ell}, M_{hh})$ have been first linearly interpolated in $(M_{hh})^2$ to the physical mass $(M_{hh})^2 = 2M_K^2 - M_\pi^2$, with the input values $M_K = 497.7\,\text{MeV}$ and $M_\pi = 135$ MeV. As it is shown for some examples in Figure 7.2.3 this interpolation poses no particular problem. The statistical error on the interpolation results has been estimated by a standard bootstrap procedure.

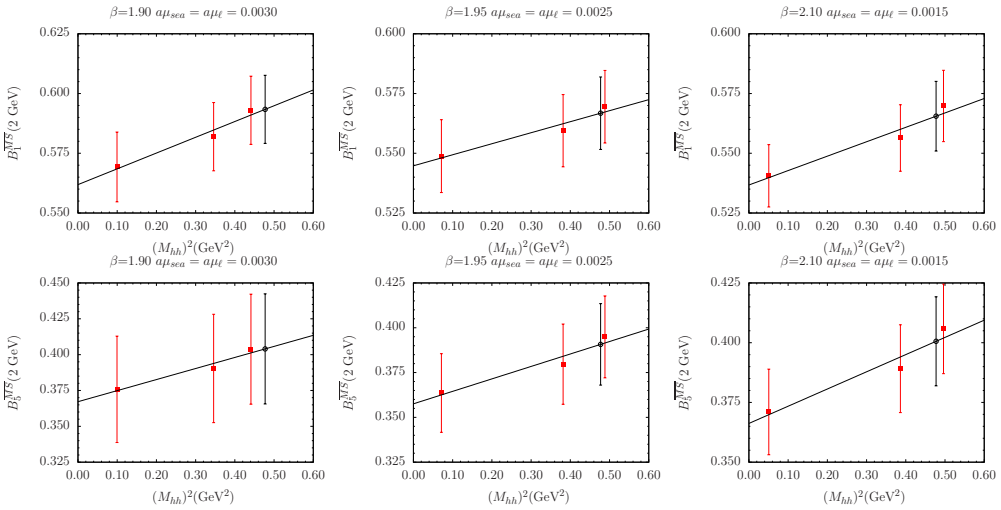

Figure 7.2.3: Examples of the interpolation of B_1 and B_5 to the physical kaon mass, identified as the point where $(M_{hh})^2 = 2M_K^2 - M_\pi^2$, for the lightest sea quark mass at each β. Bag parameters are renormalized in $\overline{MS}$ scheme of [95] at 2 GeV with M1 type RCs. The interpolated value is indicated with an open black circle.

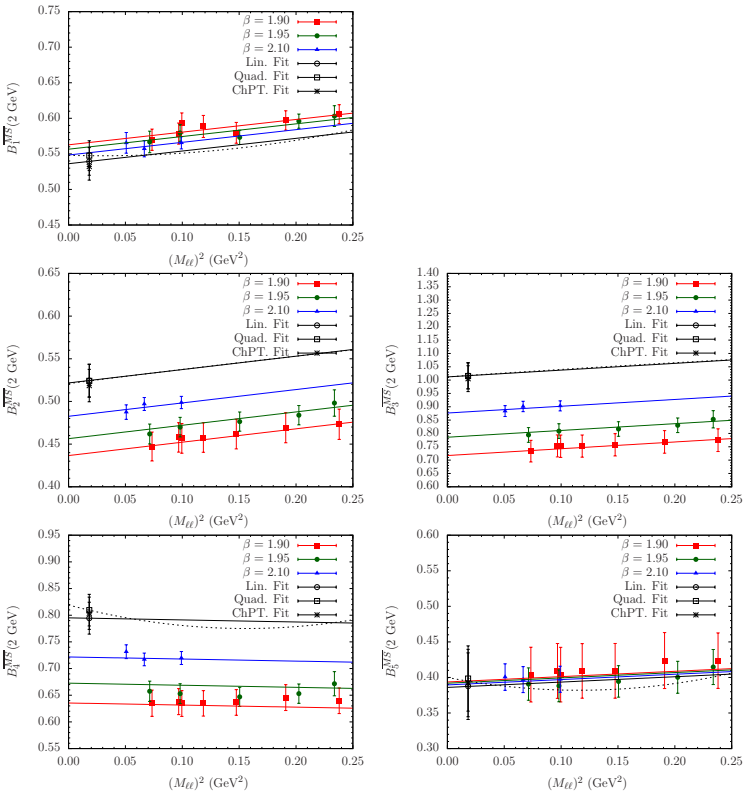

Figure 7.2.4: Solid lines represent the dependence of the B-parameters on the pseudoscalar light meson mass of the combined chiral and continuum limit according to a linear fit for the B_i parameter of $\overline{K}^0 - K^0$ oscillations with $i = 1, 2, 3, 4, 5$ respectively, renormalized in $\overline{MS}$ scheme of [95] at 2 GeV with M1 type RCs. The full black line is the continuum limit curve. The dashed black line represents the continuum limit curve in the case of a quadratic ansätz. Open black circles, squares and stars stand for the results at the physical point corresponding to linear, quadratic and NLO ChPT fit respectively.

Combined chiral and continuum extrapolations are performed using a linear fit in $(M_{\ell\ell})^2$ and a^2, a quadratic fit or the SU(2) Partially Quenched Chiral Perturbation Theory ansätz at NLO. The three ansätze read respectively

$$B_i\left(M_{\ell\ell}\right) = A + B\left(M_{\ell\ell}\right)^2 + Da^2$$

$$B_i\left(M_{\ell\ell}\right) = A + B\left(M_{\ell\ell}\right)^2 + C\left(M_{\ell\ell}\right)^4 + Da^2$$

$$B_i\left(M_{\ell\ell}\right) = B_i\left[1 + b_i\frac{\left(M_{\ell\ell}\right)^2}{f_0^2} - \frac{\left(M_{\ell\ell}\right)^2}{32\pi^2 f_0^2}\log\frac{\left(M_{\ell\ell}\right)^2}{16\pi^2 f_0^2}\right] + Da^2$$

with the input value for the chiral limit pion decay constant

$$f_0 = 120.5(4)\,\text{MeV}$$

obtained from the preliminary ETMC analysis[1] of $N_f = 2+1+1$ light meson masses and decay constants where they use the results on the quark mass renormalization contant $Z_\mu = Z_P^{-1}$ presented in chapter 4.

In Figure 7.2.4 we show the chiral and continuum fit for the renormalized B_i estimators in the $\overline{MS}$ scheme of [95] at 2 GeV. The three fits (linear, quadratic and ChPT) turned out to be of good quality and give good χ^2 values.

With the purpose of estimating the error involved in the extrapolation and interpolation to the physical point we can also use the preliminary ETMC values for the quark masses[2]

$$\mu_{u/d}^{\overline{MS}}(2\text{ GeV}) = 3.68(15) \qquad \mu_s^{\overline{MS}}(2\text{ GeV}) = 102(5) MeV$$

obtained using the Sommer parameter r_0 [72] as the scaling variable and using the value of Z_P presented here in chapter 4. With these values we can follow a parallel analysis to the one performed in chapter 5 for the $N_f = 2$ bag parameters.

We first interpolate the value of the B_i parameters computed at each pair of $(a\mu_\ell, a\mu_{\text{“}s\text{”}})$ to the physical strange quark mass as it is shown in Figure 7.2.5.

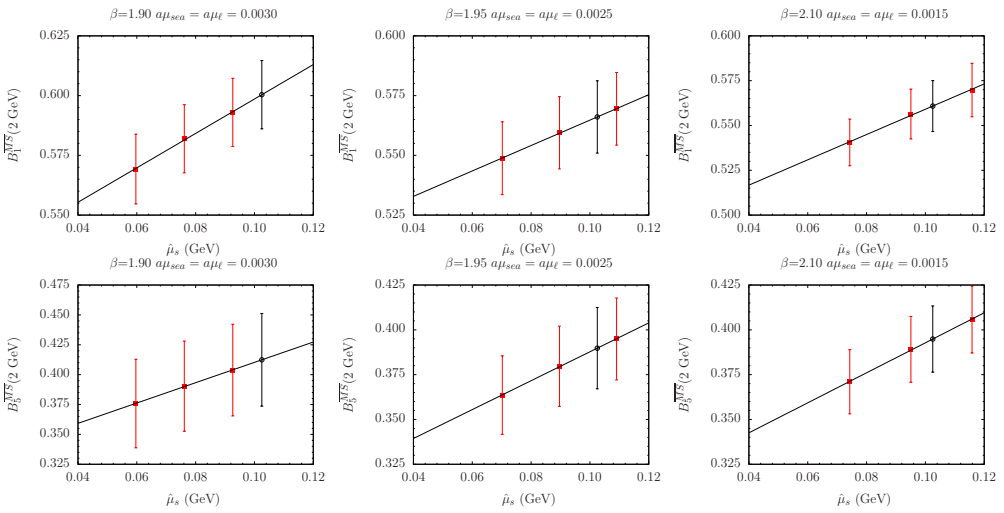

Figure 7.2.5: Examples of the interpolation of B_1 and B_5 to the physical strange quark mass for the lightest sea quark mass at each β. Bag parameters are renormalized in $\overline{MS}$ scheme of [95] at 2 GeV with M1 type RCs. The interpolated value is indicated with an open black circle.

[1] From internal ETMC notes. To be published in a forthcoming ETMC publication.
[2] From internal ETMC notes. To be published in a forthcoming ETMC publication.

The continuum and chiral limit in μ_ℓ are carried out in a combined way using Eq.5.2.2, Eq.5.2.3 and Eq.5.2.4. We have used the still preliminary value[3] for the B_0 quantity renormalized in in $\overline{MS}$ at 2 GeV: $\hat{B}_0 = 2.55(11)$

In Figure 7.2.6 we display the combined chiral and continuum limit for the five B_i parameters renormalized in $\overline{MS}$ scheme of [95] at 2 GeV with M1 type RCs. Open circles, squares and stars stand for the results at the physical point corresponding to linear, quadratic and NLO ChPT fit respectively, which agree within one sigma deviation.

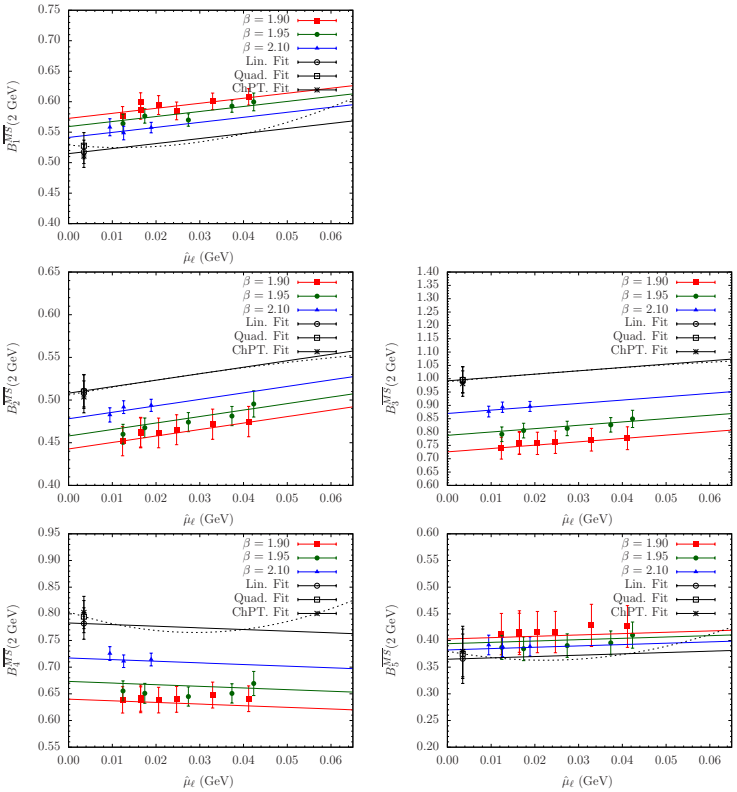

Figure 7.2.6: Solid lines represent the dependence of the B-parameters on the renormalized light quark mass of the combined chiral and continuum limit according to a linear fit for the B_i parameter of $\overline{K}^0 - K^0$ oscillations with $i = 1, 2, 3, 4, 5$ respectively, renormalized in $\overline{MS}$ scheme of [95] at 2 GeV with M1 type RCs. The full black line is the continuum limit curve. The dashed black line represents the continuum limit curve in the case of a quadratic ansätz. Open circles, squares and stars stand for the results at the physical point corresponding to linear, quadratic and NLO ChPT fit respectively.

In Table 7.2.1 I collect the continuum and chiral extrapolated results renormalized in

[3] From internal ETMC notes. To be published in a forthcoming ETMC publication.

the $\overline{MS}$ of [95] at 2 GeV, using $(M_{hh})^2$ and $(M_{\ell\ell})^2$ as fit variables, employing the M1 and M2 RCs and using the three proposed ansätzs for the chiral and continuum extrapolation, i.e linear, quadratic and SU(2) ChPT inspired. In table Table 7.2.2 I collect the analogous results but using $\mu_{\text{“}s\text{”}}$ and μ_ℓ as fit variables. Likewise Table 7.2.3 and Table 7.2.4 contain the renormalized results in the RI-MOM scheme.

The agreement between the B_i results computed using the quark masses $\mu_{\text{“}s\text{”}}$ and μ_ℓ or the pseudoscalar TM meson masses $(M_{hh})^2$ and $(M_{\ell\ell})^2$ as fit variables provides an useful test to evaluate the small systematic errors affecting the interpolation/extrapolations to the physical point. Similarly, the values of the B_i determination from the different chiral ansätzs are perfectly in line within statistical errors. On the other hand, the M1 and M2 methods turn out to provide compatible results for B_1, B_2 and B_4 while for B_3 and B_5 final results are only compatible within 2σ.

$\overline{MS}$ (2GeV)						
		B_1	B_2	B_3	B_4	B_5
Lin. Fit	M1	0.54(02)	0.52(02)	1.02(05)	0.79(03)	0.39(05)
	M2	0.53(01)	0.51(01)	0.88(03)	0.76(02)	0.48(03)
Quad. Fit	M1	0.55(02)	0.52(02)	1.01(05)	0.81(03)	0.40(05)
	M2	0.54(02)	0.50(01)	0.87(03)	0.78(02)	0.49(03)
ChPT Fit.	M1	0.53(02)	0.52(02)	1.00(05)	0.80(03)	0.39(05)
	M2	0.52(01)	0.50(01)	0.87(03)	0.77(02)	0.48(03)

Table 7.2.1: Continuum limit results for B_i of $\overline{K}^0 - K^0$ oscillations renormalized in $\overline{MS}$ of [95] at 2 GeV with M1- and M2-type RCs for the three kinds of fit functions using $(M_{hh})^2$ and $(M_{\ell\ell})^2$ as variables for the extrapolation to the physical point

$\overline{MS}$ (2GeV)						
		B_1	B_2	B_3	B_4	B_5
Lin. Fit	M1	0.52(02)	0.51(02)	1.00(05)	0.79(03)	0.37(05)
	M2	0.51(01)	0.50(01)	0.86(03)	0.75(02)	0.46(03)
Quad. Fit	M1	0.53(02)	0.51(02)	1.00(05)	0.80(03)	0.38(05)
	M2	0.53(02)	0.49(01)	0.86(03)	0.77(02)	0.47(03)
ChPT Fit.	M1	0.51(02)	0.50(02)	0.98(05)	0.80(03)	0.38(05)
	M2	0.50(01)	0.49(01)	0.84(03)	0.77(02)	0.47(03)

Table 7.2.2: Continuum limit results for B_i of $\overline{K}^0 - K^0$ oscillations renormalized in $\overline{MS}$ of [95] at 2 GeV with M1- and M2-type RCs for the three kinds of fit functions using $\mu_{\text{“}s\text{”}}$ and μ_ℓ as variables for the extrapolation to the physical point.

RI-MOM (2GeV)						
		B_1	B_2	B_3	B_4	B_5
Lin. Fit	M1	0.53(02)	0.82(03)	1.66(08)	1.16(05)	0.60(08)
	M2	0.52(01)	0.79(02)	1.42(05)	1.11(02)	0.77(05)
Quad. Fit	M1	0.54(02)	0.82(03)	1.66(08)	1.18(05)	0.62(08)
	M2	0.53(02)	0.79(02)	1.41(05)	1.13(02)	0.79(05)
ChPT Fit.	M1	0.52(02)	0.81(03)	1.64(08)	1.17(05)	0.61(08)
	M2	0.51(01)	0.78(02)	1.40(05)	1.13(02)	0.78(04)

Table 7.2.3: Continuum limit results for B_i of $\overline{K}^0 - K^0$ oscillations renormalized in the RI-MOM scheme at 2 GeV with M1- and M2-type RCs for the three kinds of fit functions using $(M_{hh})^2$ and $(M_{\ell\ell})^2$ as variables for the extrapolation to the physical point

RI-MOM (2GeV)						
		B_1	B_2	B_3	B_4	B_5
Lin. Fit	M1	0.51(02)	0.80(03)	1.63(08)	1.15(05)	0.57(08)
	M2	0.51(01)	0.78(02)	1.40(05)	1.10(02)	0.74(04)
Quad. Fit	M1	0.52(02)	0.80(03)	1.63(08)	1.17(05)	0.59(08)
	M2	0.52(02)	0.77(02)	1.39(05)	1.12(02)	0.76(04)
ChPT Fit.	M1	0.50(02)	0.79(03)	1.59(08)	1.17(05)	0.59(08)
	M2	0.49(01)	0.76(02)	1.37(05)	1.12(02)	0.76(05)

Table 7.2.4: Continuum limit results for B_i of $\overline{K}^0 - K^0$ oscillations renormalized in the RI-MOM scheme at 2 GeV with M1- and M2-type RCs for the three kinds of fit functions using $\mu_{\text{“}s\text{”}}$ and μ_ℓ as variables for the extrapolation to the physical point.

In order to be conservative in this preliminary analysis, I decided to average the estimates obtained from both methods, M1 and M2. The estimators obtained from the different fits and the election of quark masses or pseudoscalar meson masses in the chiral extrapolations have been also averaged. The half of the difference between the two more distant results has been taken as a systematic error associated to renormalization and chiral extrapolation procedure. In Table 7.2.5 and Table 7.2.6 we gather these final estimators where the error is obtained by adding in quadrature the statistical, coming from a standard bootstrap analysis, and the systematic uncertainties.

$\overline{MS}$ (2GeV)				
B_1	B_2	B_3	B_4	B_5
0.53(03)	0.51(02)	0.93(09)	0.78(03)	0.43(06)

Table 7.2.5: Continuum limit results for B_i of $\overline{K}^0 - K^0$ oscillations renormalized in $\overline{MS}$ of [95] at 2 GeV.

RI-MOM (2GeV)				
B_1	B_2	B_3	B_4	B_5
0.52(03)	0.79(03)	1.52(02)	1.14(05)	0.68(11)

Table 7.2.6: Continuum limit results for B_i of $\overline{K}^0 - K^0$ oscillations renormalized in the RI-MOM scheme at 2 GeV.

Finally, in Table 7.2.7 and Table 7.2.8 I also collect the results in the $\overline{MS}$ and RI-MOM schemes renormalized at 3 GeV.

$\overline{MS}$ (3GeV)				
B_1	B_2	B_3	B_4	B_5
0.51(03)	0.46(02)	0.80(07)	0.77(03)	0.48(05)

Table 7.2.7: Continuum limit results for B_i of $\overline{K}^0 - K^0$ oscillations renormalized in $\overline{MS}$ of [95] at 3 GeV.

RI-MOM (3GeV)				
B_1	B_2	B_3	B_4	B_5
0.50(03)	0.63(03)	1.13(12)	0.97(05)	0.64(08)

Table 7.2.8: Continuum limit results for B_i of $\overline{K}^0 - K^0$ oscillations renormalized in the RI-MOM scheme at 3 GeV.

The results in Table 7.2.7 and Table 7.2.8 can be compared with the $N_f = 2$ results presented in Table 5.2.5 and Table 5.2.6 of chapter 5. Estimators for B_i with $i = 1, 2, 3, 4$ are compatible within 1σ-discrepancy while B_5 is compatible only within 2-3σ.

Finally, I discuss the RGI B_K defined in Eq.1.2.12. It is obtained straightforwardly from the B_1 using NLO continuum QCD evolution from RI-MOM to RGI discussed in Appendix C. The final estimate is

$$\hat{B}_K^{\rm RGI} = 0.743(20)(15) \;\; \rightarrow \hat{B}_K^{\rm RGI} = 0.74(03) \quad @N_f = 2 + 1 + 1 \tag{7.2.1}$$

In the first expression the first quoted error is statistical, obtained via a bootstrap analysis, taking into account the possible cross-correlations. It includes the statistical error on the raw data for the bare matrix elements (~1%) and the associated renormalization constants (~2%). The second error in the first expression on Eq.5.2.5 is our systematic uncertainty. The error budget is detailed below:

- 0.011 from the systematic uncertainty in the chiral and continuum extrapolation. It has been estimated as the half of the difference between the two more distant results obtained from the three chiral fit ansätzs, i.e linear, quadratic or ChPT inspired fit.

- 0.009 from varying the choice of the interpolation strange variable ($\mu_{\text{“}s\text{”}}$ or $(M_{hh})^2$) and the extrapolation variable (μ_ℓ or $(M_{\ell\ell})^2$)
- 0.004 from the RI-MOM renormalization due to the spread coming from M1 and M2 methods. It has been estimated as the half of the difference between the two results.

Summing in quadrature both systematic uncertainties leads to a total systematic error estimate of ± 0.015. This number is added in quadrature to the statistical error, leading to the final result quoted in the second expression of Eq.7.2.1.

Chapter 8

Conclusions

Accurate measurements of the $\overline{K}^0 - K^0$, $\overline{D}^0 - D^0$ and $\overline{B}^0 - B^0$ mixing amplitudes provide stringent constrains in the UT analysis and can yield useful constraints on the New Physics scales. One can make precision tests of the SM with the hope of revealing the presence of NP by comparing the theoretical predictions of the mixing amplitudes with their experimental determinations.

This requires precise evaluations of the matrix elements of the full basis of local four-fermion operators entering in the most general $\Delta F = 2$ effective weak Hamiltonian. Therefore, an accurate determination of the $\Delta F = 2$ bag parameters is crucial for the search of New Physics hints. Lattice QCD provides a non perturbative tool to compute these matrix elements with errors at the percent level and with systematic uncertainties under control.

Throughout this thesis I have addressed the computation of the bag parameters from unquenched Twisted Mass Lattice QCD. In addition, we have also computed the b-quark mass and the pseudoscalar decay constants f_B y f_{Bs}. Here, I will summarize the main results and I will compare them with the alternative results obtained by other lattice analyses highlighting the differences between the several computations.

8.1 $\overline{K}^0 - K^0$ oscillations

In chapter 5 I have presented an unquenched lattice QCD determination in the continuum limit of the matrix elements of the full $\Delta S = 2$ four fermion operator basis. I have used the $N_f = 2$ unquenched Twisted Mass gauge configurations produced by the ETMC in combination with the Osterwalder-Seiler valence quarks. This mixed action setup proposed in [23] ensures $\mathcal{O}(a)$ improvement and a continuum-like renormalization pattern at the price of introducing $\mathcal{O}(a^2)$ unitary violations. Using data at four lattice spacing in the interval $[0.05 : 0.1]$ fm and pseudoscalar meson masses, i.e pions, in the range $[260 : 600]$ MeV we are able to safely carry out the continuum and chiral limit. The

analysis and results for B_i @$N_f = 2$ I present here are compatible to the ones recently published by the ETMC in [102][1].

Following the same strategy, in chapter 7 I updated the previous results with the data from the $N_f = 2+1+1$ simulations produced by the ETMC at three values of the lattice spacing in the interval $[0.06 : 0.09]$ fm and working with pseudoscalar meson masses in the range $[230 : 500]$ MeV, thereby controlling the chiral and continuum extrapolations. ETMC preliminary results at one lattice spacing were presented previously in [113].

$N_f = 2 + 1 + 1$ analysis needs non perturbative computation of the relevant $N_f = 4$ two- and four-fermion renormalization constants which has also been addressed in this thesis. As it is discussed in chapter 4, for the case of $N_f = 4$ simulations the implementation of maximal twist, which would guarantee $\mathcal{O}(a)$ improvement, is not a trivial task. Instead we opted to achieve $\mathcal{O}(a)$ improvement for the renormalization constant estimators by averaging simulations with an equal value of the polar mass but opposite value of the twisted angle. It is important to remark that the computation of the four-fermion renormalization constants is still a work in progress and many aspects, regarding the average over equivalent momenta configurations, the chiral extrapolations, the subtraction of the double Goldstone boson pole or the subtraction of discretization effects, should be checked and probably improved. This is the main reason for considering the bag parameters from the $N_f = 2 + 1 + 1$ simulation still preliminary.

Our determination of B_K, i.e B_1 for $\overline{K}^0 - K^0$, agrees rather well with other recent results. Several lattice computations of B_K based on different lattice fermion discretizations have been performed in the last few years. A compilation of recent data is provided in Figure 8.1.1 where the renormalization group invariant (RGI) values of B_K are reported.

A very important conclusion which can be inferred from Figure 8.1.1 is that the quenching of the strange and charm quarks seems to carry an uncertainty which at present is smaller than other systematic uncertainties affecting the computation of B_K.

Our results tend to confirm the tension in the unitarity triangle analysis between the lattice determination and the preferred phenomenological value. Notwithstanding, some theoretical concerns remain about the way of estimating the long distance contributions in the relation between the hadronic parameter B_K and the experimentally well measured quantity ϵ_K which parameterizes the indirect CP violation in the $\overline{K}^0 - K^0$ system. As reviewed in chapter 1, for ϵ_K the short distance effects dominate and the long distance part is estimated to be a few percent correction [47]. Thanks to recent precision lattice calculations, B_K is known with a total uncertainty of less than 4% giving increasing relevance to the unknown long distance contribution.

[1] The same gauge configurations have been used but for this thesis I considered an updated run where the smeared interpolating operators were implemented

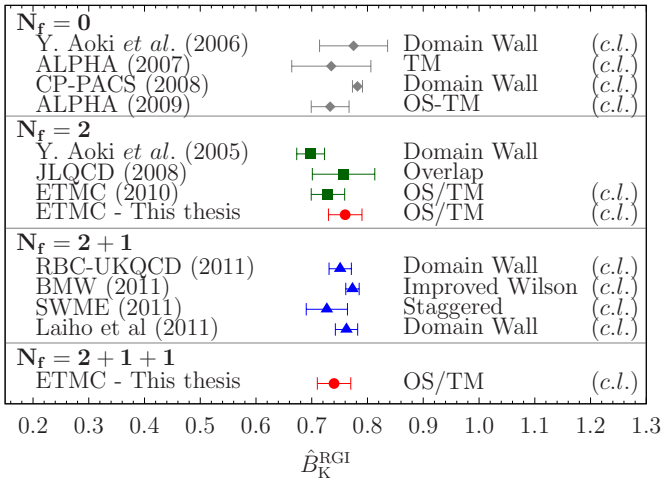

Figure 8.1.1: A compilation of quenched and unquenched results for $\hat{B}_K^{\mathrm{RGI}}$. Data are from [114, 115, 116, 117, 118, 119, 120, 121, 122, 123, 124], respectively. The acronym *c.l* denotes determinations where the continuum extrapolation was carried out.

Our B_i, $i = 2, 3, 4, 5$, for the $\overline{K}^0 - K^0$ oscillations can be compared with the other calculations of these quantities cited in the literature. Previous calculations of the whole set of $\Delta S = 2$ renormalized operators have been performed in the quenched approximation using improved Wilson fermions [125, 126] or the chirallity conserving overlap [127] and domain-wall [128] regularizations.

The quenched computations with overlap [127] and domain-wall [128] fermions, though performed at rather large lattice spacing ($a \sim 0.09$ and $a \sim 0.13$ fm in the first and $a \sim 0.1$ in the second), have the advantage that the four-fermion renormalization constants satisfy a continuum-like pattern and lattice artifacts are $\mathcal{O}(a^2)$. In the calculation presented in [125, 126] the $\mathcal{O}(a)$ improved Wilson fermions were implemented. Simulations were carried out at two values of the gauge coupling corresponding to lattice spacings $a \sim 0.07$ and $a \sim 0.09$ fm and due to the presence of the Clover term matrix elements were affected by $\mathcal{O}(g_0^2 a)$ discretization errors. In this calculation the major source of systematic error was due to the presence of wrong chirallity mixings. All the mixing coefficients and the overall RC were computed in the non-perturbative RI-MOM scheme. In contrast, in our mixed action setup with maximally twisted Wilson fermions on the sea and Osterwalder-Seiler valence quarks we achieve both $\mathcal{O}(a)$ improvement and a continuum-like renormalization pattern.

Only recently a $N_f = 2 + 1$ unquenched calculation using domain-wall fermions at one single value of the lattice spacing appears in [129]. Therefore, the $N_f = 2$[2] and $N_f = 2+1+1$ results presented here are the first unquenched lattice QCD determination

[2] and the equivalent analysis in [102]

in the continuum limit of the matrix elements of the full $\Delta S = 2$ four-fermion operator basis. I remark that, with respect to the other previous calculation, in the present study we have performed simulations at several values of the lattice spacing and pion masses in the chiral regime which provide a better control of the chiral and continuum extrapolation.

In all the quenched works results have been obtained in the RI-MOM scheme at 2 GeV. Table 8.1.1 show a comparison between our unquenched $N_f = 2$ and $N_f = 2+1+1$ results for B_i (in RI-MOM at 2 GeV) and the data at fixed lattice spacing coming from the two old quenched calculations of [125] and [127]. Except for B_1, one finds large differences between the central values of our results and those of [125] and [127] which in addition are not in agreement with each other.

On the other hand, we find a 2-3σ discrepancy between our $N_f = 2$ and $N_f = 2+1+1$ results. However, as pointed out before some technical issues in the $N_f = 2+1+1$ analysis should be controlled before claiming that this is a systematic error related to the quenching of the strange and charm quarks. In addition, this discrepancy is decreased when results are compared at 3 GeV. Table 8.1.2 shows that the results renormalized at 3 GeV are in very good agreement. I stress that our renormalization constants are computed at a^{-1} and they are then converted to RI-MOM or $\overline{MS}$ at 2 or 3 GeV using the NLO perturbative series. As in both cases, $N_f = 2$ and $N_f = 2+1+1$ simulations, a^{-1} is closer to 3 GeV the comparison of final estimates is more reliable when results are renormalized at 3 GeV since the error due to the truncation to NLO of the evolution is smaller.

	This thesis @$N_f = 2$	This thesis @$N_f = 2+1+1$	[127]		[125]	
	CL	CL	$a \sim 0.09$fm	$a \sim 0.13$fm	$a \sim 0.07$fm	$a \sim 0.09$fm
B_1	0.53(02)	0.52(03)	0.56(05)	0.53(04)	0.68(21)	0.70(15)
B_2	0.70(03)	0.79(03)	0.87(07)	0.90(10)	0.67(07)	0.72(09)
B_3	1.22(08)	1.52(02)	1.41(12)	1.53(40)	0.95(15)	1.21(10)
B_4	1.01(04)	1.14(05)	0.94(05)	0.90(13)	1.00(09)	1.15(05)
B_5	0.69(07)	0.68(11)	0.62(05)	0.56(14)	0.66(11)	0.88(06)

Table 8.1.1: Comparison between unquenched results for $\Delta S = 2$ B_i obtained in this thesis and the quenched values of [127] and [125]. Values are renormalized in the RI-MOM scheme at 2 GeV.

It is also very interesting to compare our results with the only other unquenched computation of the B_i parameters by the RBC/UKQCD collaborations [129]. Their computation is performed on a single lattice spacing $a \sim 0.086$fm. In their work final results are collected in $\overline{MS}$ at 3 GeV. For this reason, in Table 8.1.2 I compare our unquenched $N_f = 2$ and $N_f = 2+1+1$ results in $\overline{MS}$ at 3 GeV with the ones in [129]. Our continuum limit results for B_i are in the same ballpark with the results at one lattice spacing given in [129] where $N_f = 2+1$ dynamical quarks are employed.

	This thesis $@N_f = 2$	This thesis $@N_f = 2+1+1$	[129] $@N_f = 2+1$
	CL	CL	$a \sim 0.086$fm
B_2	0.48(02)	0.46(02)	0.43(05)
B_3	0.80(04)	0.80(07)	0.75(09)
B_4	0.74(03)	0.77(03)	0.69(07)
B_5	0.60(05)	0.48(05)	0.47(06)

Table 8.1.2: Comparison between unquenched results for $\Delta S = 2$ B_i obtained in this thesis and the $N_f = 2+1$ results in [129]. Values are renormalized in the $\overline{MS}$ scheme at 3 GeV.

8.2 $\overline{D}^0 - D^0$ oscillations

The analysis procedure followed in the computation of the bag parameters for the $\Delta S = 2$ operators can be mimicked for the analysis of the $\overline{D}^0 - D^0$ oscillations. In chapter 5 we provide the first unquenched computation of the five B_i parameters controlling the $\overline{D}^0 - D^0$ oscillations in the continuum limit using the ETMC $N_f = 2$ simulation. Preliminary results were presented in [130].

Very little has been done in the literature concerning the calculation of the $\Delta C = 2$ physical matrix elements. Only quenched results existed so far in [131] and [132]. In [131] improved Wilson fermions are used and results were presented for a single lattice spacing as intermediate step of the $\overline{B}^0 - B^0$ analysis. The authors of [132] presented results at one lattice spacing using domain-wall fermions for the B_1 parameter. In Table 8.2.1 I compare our results with the quenched results at one lattice spacing presented in [131] .

	B_1	B_2	B_3	B_4	B_5
Quenched [131]	0.87(03)	0.82(03)	1.07(09)	1.08(03)	1.46(09)
This thesis $@N_f = 2$	0.75(03)	0.82(03)	1.23(07)	1.06(03)	1.30(07)

Table 8.2.1: Comparison between unquenched results for $\Delta C = 2$ B_i in the continuum-limit obtained in this thesis and the quenched results at one lattice spacing, $a \sim 0.10$ fm, in [131]. Our results in Table 5.4.4 have been evolved to RI-MOM at 2.8 GeV in order to properly compare with [131].

These values will be used in a forthcoming publication to constrain the parameter space of the Minimal Supersymmetric Standard Model (MSSM) with a generic Flavour structure and update the results published in [133].

8.3 B-physics

Simulating heavy quarks on the lattice implies discretization errors of $\mathcal{O}(am_b)$. With the typical value of the lattice spacing in current lattice simulations these corrections are not negligible since $am_b > 1$. Consequently, it is not possible to simulate the b-quark mass at its physical mass. As I briefly mentioned in the introduction of chapter 6 there are two approaches to overcome this problem: implement a static effective theory on the lattice or simulate relativistic quarks and then extrapolate them up to the physical b-quark mass. The first approach is being used by different lattice collaborations: Alpha implement the Heavy Quark Effective Theory (HQET) on the lattice, HPQCD the non-relativistic QCD (NRQCD), FNAL/MILC the Fermilab action [134] and RBC/UKQCD the non-perturbatively relativistic heavy quark action [135]. On the contrary, HPQCD with the HISQ action [136] uses relativistic quarks. Finally, the ETMC uses relativistic quarks and the ratio method.

In chapter 6 I employed the ratio method proposed within the ETMC [24] in order to deal with the b-quark mass on the lattice. The method consists first of computing suitable ratios of the desired observable in the charm region and then interpolating them between the accessible charm regime to the exactly known static point.

The analysis addressed here has been done using the ETMC $N_f = 2$ gauge configurations. It is important to remind that for this computation we only need the renormalization constants of the two- and four-fermion operators involving relativistic quarks. These renormalization constants have been computed previously and successfully introduced in the computation of the $\overline{K}^0 - K^0$ and $\overline{D}^0 - D^0$ oscillations.

The results discussed in this thesis are also part of the ongoing project, within the ETMC collaboration, to compute the B-physics hadronic parameters. Some systematic effects have to be considered with more accuracy. Therefore, the results presented here are considered to be preliminary.

Thanks to the application of smearing techniques and the construction of improved interpolating fields, the previous ETMC analysis of the b-quark mass, f_B and f_{B_s} presented in [24, 107] have been improved. Preliminary results have already been presented in [137, 138].

In Figure 8.3.1 the recent result of m_b reported in this thesis is compared with other recent computations.

Similarly, our updated results f_B, f_{B_S} and f_{B_s}/f_B are compared with other recent lattice results in Figure 8.3.2.

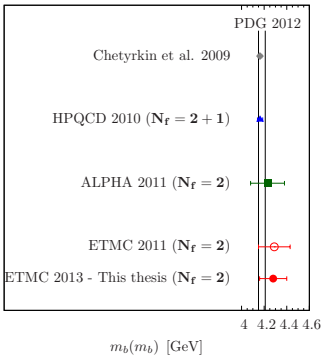

Figure 8.3.1: Recent unquenched results for m_b. Vertical lines corresponds to the PDG 2012 value [45]. Results are from [139, 140, 141] and [107].

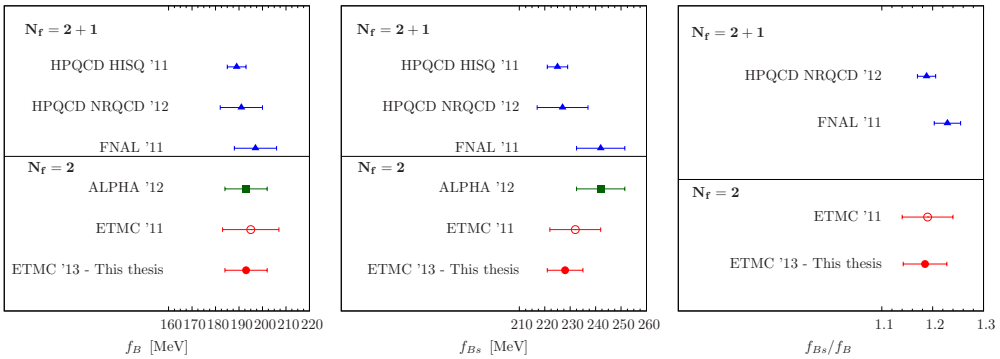

Figure 8.3.2: Collection of recent unquenched results for f_B, f_{B_S} and f_{B_s}/f_B. Results are from [142, 143, 144, 145] and [107].

In this thesis, the ratio method has been extended to the computation of the bag parameters B_B and B_{B_s}, which together with the decay constants f_B and f_{B_s} encode the non perturbative QCD information in the $\overline{B}^0 - B^0$ mixing. The ratio method is also applied to the $SU(3)$ breaking ratio ξ which measures the ratio between the mixing parameters in the B_s and B_d mesons. Preliminary results were presented in [130].

Our result for the ratio B_{B_s}/B_B and ξ together with the RGI values of $\hat{B}_{B_s}$ and $\hat{B}_B$ is compared with the ones provided by the other lattice groups working in B-physics analysis in Table 8.3.1. Our results for $B_1^{(s)}$ and $B_1^{(d)}$ reported in Table 6.3.3 in $\overline{MS}$ at the b-quark mass have been evolved to RGI using $\Lambda_{\rm QCD} = 213(8)$ MeV with $N_f = 5$ flavours [45]. For illustration in Figure 8.3.3 I plot the recent values of ξ with $N_f = 2+1$ together with the estimate obtained in this thesis.

	HPQCD NRQCD '09 [146]	FNAL '12 [147]	RBC-UKQCD '10 [148]	This thesis @$N_f = 2$
ξ	1.26(03)	1.27(06)	1.13(12)	1.19(04)
B_{B_s}/B_B	1.05(07)	1.06(11)	–	1.013(18)
$\hat{B}^{\rm RGI}_{B_s}$	1.33(06)	–	–	1.32(05)
$\hat{B}^{\rm RGI}_{B}$	1.26(11)	–	–	1.30(06)

Table 8.3.1: Recent values for ξ and B_{B_s}/B_B meson mixing parameters.

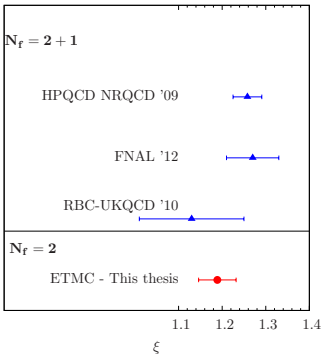

Figure 8.3.3: Comparison between recent results of ξ. The compared results are from [146], [147] and [148].

The non SM bag parameters B_i with $i = 2, 3, 4, 5$ have also been computed in the continuum limit following the ratio method. Quenched results at one lattice spacing can be found in [131] where they use static heavy valence quarks. In Table 8.3.2 and Table 8.3.3 I compare our recent $N_f = 2$ continuum results with the quenched results at one lattice spacing in [131]. This analysis have been performed more than ten years ago and since then there has not been any other unquenched and continuum-limit calculation of the complete basis of $\Delta B = 2$ matrix elements except the present one. Only preliminary (unquenched and continuum-limit) results of the ongoing analysis from the FNAL/MILC collaboration can be found in [149].

	$B_1^{(d)}$	$B_2^{(d)}$	$B_3^{(d)}$	$B_4^{(d)}$	$B_5^{(d)}$
Quenched [131]	0.87(4)(5)	0.83(3)(4)	0.90(6)(8)	1.15(3)(7)	1.72(4)(20)
This thesis @$N_f = 2$	0.85(04)	0.72(03)	0.87(13)	0.94(05)	1.47(09)

Table 8.3.2: Comparison between unquenched results for $\Delta B = 2$ $B_i^{(d)}$ in the continuum-limit obtained in this thesis and the quenched results at one lattice spacing, $a \sim 0.10$ fm, in [131]. Values are renormalized in the $\overline{MS}$ scheme of [95] at the b-quark mass. The results of [131] are accompanied by their statistical and systematic error.

	$B_1^{(s)}$	$B_2^{(s)}$	$B_3^{(s)}$	$B_4^{(s)}$	$B_5^{(s)}$
Quenched [131]	0.87(2)(5)	0.84(2)(4)	0.91(3)(8)	1.16(2)(7)	1.75(3)(21)
This thesis @$N_f = 2$	0.86(03)	0.74(03)	0.88(10)	0.94(04)	1.60(09)

Table 8.3.3: Comparison between unquenched results for $\Delta B = 2$ $B_i^{(s)}$ in the continuum-limit obtained in this thesis and the quenched results at one lattice spacing, $a \sim 0.10$ fm, in [131]. Values are renormalized in the $\overline{MS}$ scheme of [95] at the b-quark mass. The results of [131] are accompanied by their statistical and systematic error.

8.4 Outlook

In this thesis, using $N_f = 2$ simulations, we have computed

- The bag parameters describing the neutral kaon oscillations in the Standard Model and beyond.
- The bag parameters controlling the short distance contributions in the $\overline{D}^0 - D^0$ oscillations.
- Several B-physics observables: the b-quark mass m_b, the pseudoscalar decay constants f_B and f_{B_s}, the ξ parameter, the bag parameters B_B and B_{B_s}, their quotient B_{B_s}/B_B and its supersymmetric contributions $B_i^{(d)}$ and $B_i^{(s)}$.

The next step we have already started is to repeat the whole analysis with the $N_f = 2+1+1$ simulations. The project involves the reanalysis of the observables studied with $N_f = 2$ and the comparison between them. In this way, we intend to quantify the impact of the inclusion of the strange and charm quarks in the sea. Chapters 4 and 7 are moving ahead this direction and the results for the $\Delta S = 2$ bag parameters although preliminary seem very promising.

Other future projects consist in extending the ratio method for the study of other B-physics observables. In particular, we are interested in:

- The form factors describing the semileptonic weak decays of the B and B_s mesons, whose precise knowledge is necessary to extract accurate information on the matrix elements V_{ub} and V_{cb} of the CKM matrix.
- The form factors of exclusive $b \to s\ell^+\ell^-$ decays. These form factors combined with the $\overline{B}^0 - B^0$ oscillations will allow to study many New Physics scenarios.
- Double-heavy hadrons on the lattice: the B_c meson is the only heavy meson consisting of two heavy quarks with different flavour so its decay properties are of special interest since it provides information about strong interaction effects in heavy-heavy systems.

Conclusiones

El análisis del triángulo de unitariedad y la búsqueda de cotas restrictivas sobre las escalas de nueva física requiere medidas precisas de las amplitudes de mezcla de las oscilaciones $\overline{K}^0 - K^0$, $\overline{D}^0 - D^0$ y $\overline{B}^0 - B^0$. Es posible realizar tests de precisión del Modelo Estándar a través de la comparación de las predicciones teóricas para las amplitudes de mezcla con las correspondientes medidas experimentales. Por lo tanto, la medida precisa de los parámetros B es crucial para la búsqueda indirecta de señales de nueva física.

Para ello se requiere el cálculo de los elementos de matriz de la base completa de operadores locales de cuatro fermiones que contribuyen al Hamiltoniano electrodébil $\Delta F = 2$. El retículo proporciona una herramienta no perturbativa para el cálculo de dichos elementos de matriz con incertidumbres del orden del ~1% y con errores sistemáticos bajo control.

A lo largo de esta tesis hemos abordado el cálculo de los parámetros B a partir de QCD simulada en el retículo con la acción Twisted Mass incluyendo quarks dinámicos en el mar. Por otra parte, hemos calculado también la masa del quark b y las constantes de desintegración f_B y f_{Bs}. En estas conclusiones, resumiré los resultados principales, los compararé con otros cálculos alternativos realizados por otras colaboraciones y subrayaré las principales diferencias entre los diferentes análisis.

Oscilaciones $\overline{K}^0 - K^0$

En el capítulo 5 hemos discutido el cálculo de los elementos de matriz de los operadores locales de cuatro fermiones $\Delta S = 2$ a partir de simulaciones en el retículo con sabores dinámicos de quarks. En este análisis, hemos usado las configuraciones de gauge $N_f = 2$ con la acción Twisted Mass generadas por la colaboración ETMC en combinación con fermiones de valencia Osterwalder-Seiler. Esta acción mixta propuesta en [23] garantiza la mejora $\mathcal{O}(a)$ de los efectos de discretización y un patrón de renormalización para los operadores de cuatro fermiones como el que se tendría en una regularización invariante quiral al precio de introducir violaciones de unitariedad $\mathcal{O}(a^2)$. Usando datos a cuatro valores del espaciado del retículo en el intervalo $[0.05 : 0.1]$ fm y masas de mesones pseu-

doscalares, es decir piones, en el rango [260 : 600] MeV somos capaces de llevar a cabo de forma segura las extrapolaciones al continuo y al límite quiral. El análisis y los resultados presentados en esta tesis para B_i @$N_f = 2$ son equivalentes a los publicados recientemente por la ETMC en [102][3].

Siguiendo la misma estrategia, en el capítulo 7 hemos actualizado los resultados del capítulo 5 con datos del retículo provenientes de la simulación $N_f = 2 + 1 + 1$ de la ETMC a tres valores del espaciado del retículo en el intervalo [0.06 : 0.09] fm y con masas de piones en el rango [230 : 500] MeV controlando, por tanto, las extrapolaciones quirales y al continuo. Resultados preliminares a un espaciado del retículo se habían presentado previamente en [113].

Este análisis $N_f = 2 + 1 + 1$ requiere el cálculo de las constantes de renormalización $N_f = 4$ de dos y cuatro fermiones que también ha sido abordado en esta tesis. Como ha sido discutido en el capítulo 4, en el caso de las simulaciones $N_f = 4$, la implementación del llamado *maximal twist*, que garantizaría la mejora $\mathcal{O}(a)$ de forma automática, no es posible. Por ello para conseguir la mejora $\mathcal{O}(a)$ hemos optado por mediar los estimadores de las constantes de renormalización entre simulaciones con igual valor de la masa polar pero valor opuesto del ángulo *twist*. No obstante, es importante subrayar que el cálculo de las constantes de renormalización de los operadores de cuatro fermiones es todavía un trabajo en desarrollo y muchos aspectos, relacionados con el promedio sobre momentos equivalentes, las extrapolaciones quirales, la substracción del doble polo de Goldstone o la substracción de los efectos de discretización, tienen que ser todavía revisados y probablemente mejorados. Esta es la razón principal por la cual consideramos los parámetros B $N_f = 2 + 1 + 1$ preliminares.

Nuestra determinación de B_K, es decir B_1 en las oscilaciones $\overline{K}^0 - K^0$, es compatible con otros resultados recientes obtenidos de forma independiente. En los últimos años diferentes cálculos de B_K basados en diferentes discretizaciones de la acción fermiónica en el retículo han sido llevados a cabo. En la Figura 8.1.1 han sido recopilados los resultados más recientes de B_K en el esquema RGI.

De la Figura 8.1.1 se puede concluir que el efecto de la inclusión dinámica de los quarks *strange* y *charm* en el mar conlleva un error que es más pequeño que otros errores sistemáticos presentes en el cálculo actual del B_K.

Nuestros resultados tienden a confirmar la tensión existente en el triángulo de unitariedad entre la determinación del retículo y el valor fenomenológico del Modelo Estándar. No obstante, todavía quedan por aclarar ciertos aspectos teóricos sobre los efectos de larga distancia que aparecen en la relación entre el parámetro hadrónico B_K y la medida experimental de ϵ_K que parametriza la violación indirecta de CP en el sistema de kaones neutros. Como se recordó en el capítulo 1, en el cálculo de ϵ_K los efectos de corta distancia dominan y la contribución de larga distancia se estima que es una corrección del por ciento. Sin embargo, gracias a la precisión que los cálculos realizados en el retículo están alcanzando en la actualidad, B_K se conoce a día de hoy con una incertidumbre total

[3] En ambos análisis se han usado las mismas configuraciones gauge, pero en esta tesis hemos considerado un *run* de valencia actualizado en el cual se han implementado operadores interpoladores extendidos (smeared).

menor del 4% por lo que las contribuciones de larga distancia comienzan a ser relevantes.

Los estimadores de B_i con $i = 2, 3, 4, 5$ analizados en esta tesis pueden ser comparados con otros citados en la literatura. Cálculos previos del set completo de operadores $\Delta S = 2$ han sido llevados a cabo en la aproximación *quenched* usando fermiones de Wilson mejorados [125, 126] o fermiones quirales *overlap* [127] y *domain-wall* [128].

Los cálculos *quenched* con fermiones *overlap* [127] y *domain-wall* [128], a pesar de haber sido realizados a un espaciado del retículo bastante grande ($a \sim 0.09$ y $a \sim 0.13$ fm en el primero y $a \sim 0.1$ fm en el segundo), tienen la ventaja de que la renormalización de los operadores de cuatro fermiones satisface un patrón como el que se tendría en el continuo (diagonal a bloques) y que los efectos de discretización son $\mathcal{O}(a^2)$. Por otra parte, en el cálculo presentado en [125, 126] se han usado fermiones de Wilson mejorados $\mathcal{O}(a)$. Las simulaciones han sido llevadas a cabo para dos valores de la constante de acoplamiento correspondientes a espaciados del retículo $a \sim 0.07$ y $a \sim 0.09$ fm. Debido a la presencia del término de Clover los elementos de matriz están afectados por efectos de discretización $\mathcal{O}(g_0^2 a)$. En este análisis el mayor error sistemático se debe a la presencia de mezclas con operadores de distinta quiralidad. Todos los coeficientes de mezcla así como las constantes de renormalización de los operadores de cuatro fermiones se calculan no perturbativamente en el esquema RI-MOM. Por el contrario, con la acción mixta que hemos usado a lo largo de esta tesis, con fermiones Wilson al *maximal twist* en el mar y fermiones de valencia de tipo Osterwalder-Seiler, conseguimos al mismo tiempo la mejora $\mathcal{O}(a)$ y un patrón quiral de renormalización.

Solo recientemente se ha presentado otro cálculo de los parámetros B con quarks dinámicos del mar. Se trata de una simulación $N_f = 2+1$ usando fermiones *domain-wall* a un solo valor del espaciado del retículo [129]. Por tanto, los resultados $N_f = 2$ [4] y $N_f = 2 + 1 + 1$ presentados aquí son los primeros resultados *unquenched* en el retículo extrapolados al continuo. Es importante remarcar que, en contraste con otros cálculos previos, en nuestro análisis hemos realizado simulaciones para diversos espaciados del retículo y con masas de piones en la región de la teoría quiral de perturbaciones lo que nos proporciona un mejor control de las extrapolaciones quirales y al continuo.

En todos los trabajos *quenched* los resultados han sido obtenidos en el esquema RI-MOM a 2 GeV. La Tabla 8.1.1 muestra una comparación entre nuestros resultados *unquenched* $N_f = 2$ y $N_f = 2+1+1$ (en RI-MOM a 2 GeV) y los resultados a un espaciado del retículo fijado provenientes de las dos simulaciones *quenched* en [125] y [127]. Excepto para B_1, encontramos grandes diferencias entre los valores centrales de nuestros resultados y los resultados de [125] y [127] que además no están en acuerdo entre ellos.

Por otra parte, encontramos una discrepancia en torno a 2-3σ entre nuestros resultados $N_f = 2$ y $N_f = 2+1+1$. Sin embargo, como se ha indicado anteriormente quedan ciertos aspectos técnicos por controlar en el análisis $N_f = 2 + 1 + 1$ antes de afirmar que se trata de un error sistemático debido a la inclusión de los quarks *strange* y *charm* como quarks dinámicos en el mar. Además esta discrepancia es menor cuando los resultados se comparan a 3 GeV. Esto puede ser explicado por el hecho de que nuestras constantes de renormalización se calculan siguiendo el método RI-MOM a una escala $\mu = a^{-1}$ y después

[4] y el análisis equivalente publicado en [102]

son convertidas a RI-MOM o $\overline{MS}$ a 2 o 3 GeV usando la evolución perturbativa a NLO. Como, tanto en la simulación $N_f = 2$ como en la $N_f = 2 + 1 + 1$, a^{-1} es más cercano a 3 GeV, la comparación de las estimaciones finales es mas creíble cuando los resultados están renormalizados a 3 GeV ya que los errores de truncamiento de la evolución NLO es menor.

Es también muy interesante comparar nuestros resultados con los otros únicos resultados *unquenched,* publicados recientemente por la colaboración RBC/UKQCD [129]. Su cálculo ha sido realizado a un solo valor del espaciado del retículo $a \sim 0.086$ fm. En su trabajo los resultados finales están dados en $\overline{MS}$ a 3 GeV. Por esta razón, en la Tabla 8.1.2 se comparan nuestros resultados $N_f = 2$ y $N_f = 2+1+1$ renormalizados en $\overline{MS}$ a 3 GeV con los publicados en [129].

Oscilaciones $\overline{D}^0 - D^0$

El procedimiento seguido para el cálculo de los parámetros B correspondientes a los operadores $\Delta S = 2$ puede ser extendido para el análisis de las oscilaciones $\overline{D}^0 - D^0$. En el capítulo 5 proporcionamos el primer cálculo *unquenched* con límite al continuo de los cinco parámetros B_i que controlan las oscilaciones $\overline{D}^0 - D^0$ usando la simulación $N_f = 2$ de la ETMC. Resultados preliminares ya fueron presentados en [130].

En la literatura existen muy pocos análisis de los elementos de matriz $\Delta C = 2$. Hasta ahora solo existían resultados sin sabores dinámicos en el mar en [131, 132]. En [131] se usan fermiones de Wilson mejorados $\mathcal{O}(a)$ y los resultados se presentan para un solo valor del espaciado del retículo como un paso intermedio en el análisis de las oscilaciones $\overline{B}^0 - B^0$. En [132] presentan resultados solo para B_1 a un único valor del espaciado del retículo usando fermiones *domain-wall.* En la Tabla 8.2.1 comparamos nuestros resultados con los resultados *quenched* a un valor fijo del espaciado de la red, $a \sim 0.10$ fm, presentados en [131].

Estos valores presentados aquí serán usados en una publicación futura para restringir el espacio de parámetros del *Minimal Supersymmetric Standard Model* (MSSM) con una estructura genérica de sabor y de este modo actualizar los resultados publicados en [133].

Física del quark b

Simular quarks pesados en el retículo implica tratar con errores de discretización $\mathcal{O}(am_b)$. Con los valores típicos del espaciado del retículo en las simulaciones actuales estas correcciones no son despreciables ya que $am_b > 1$. Así pues, no es posible aún simular el quark b con su masa física en el retículo. Como se ha mencionado brevemente en la introducción del capítulo 6 existen dos enfoques para afrontar este problema: implementar la teoría efectiva del quark pesado en el retículo o simular quarks relativistas y después extrapolarlos hasta la masa física del quark b. El primer planteamiento está siendo usado por diferentes colaboraciones: Alpha implementa la teoría efectiva del quark pesado (HQET por sus siglas en inglés) en el retículo, HPQCD usa la acción NRQCD (*non-relativistic*

QCD), FNAL/MILC utiliza la acción Fermilab [134] y RBC/UKQCD la acción del quark pesado relativista no perturbativa [135]. Por el contrario, HPQCD con la acción HISQ [136] utiliza quarks relativistas al igual que la ETMC.

En el capítulo 6 hemos usado el llamado *ratio method* propuesto por la ETMC [24] con el objetivo de tratar el quark b en el retículo. El método consiste primero en calcular cocientes apropiados del observable que nos ocupa en la región del quark *charm* y después interpolar entre el régimen de masas del quark *charm*, accesible directamente, y el limite estático conocido exactamente de modo teórico.

Para el análisis que hemos abordado aquí hemos utilizado las configuraciones de gauge $N_f = 2$ de la ETMC. Es importante volver a remarcar que para nuestro análisis solo necesitamos las constantes de renormalización de dos y cuatro fermiones involucrando quarks relativistas. Estas constantes de renormalización han sido calculadas previamente y utilizadas con éxito en el cálculo de los elementos de matriz que gobiernan las oscilaciones $\overline{K}^0 - K^0$ y $\overline{D}^0 - D^0$.

Los resultados discutidos en esta tesis son también parte del proyecto en marcha, dentro de la colaboración ETMC, dedicado a el cálculo de los parámetros hadrónicos relevantes en la física del b. Algunos errores sistemáticos deben ser todavia considerados con mayor precisión. Por ello, los resultados que han sido presentados aquí deben ser considerados preliminares.

Gracias a la aplicación de las técnicas de smearing y la construcción de campos interpoladores mejorados el análisis previo de la ETMC de la masa del quark b, f_B y f_{B_S} publicado en [24, 107] ha sido actualizado. Resultados preliminares ya han sido presentados en [137, 138].

En la Figura 8.3.1 el valor aquí calculado para m_b, renormalizado en $\overline{MS}$ a la escala $\mu = m_b$, se compara con otros cálculos recientes.

Análogamente los resultados actualizados de f_B, f_{B_s}y f_{B_S}/f_B se comparan en la Figura 8.3.2 con otros resultados recientes del retículo.

En esta tesis el método de los cocientes, o *ratio method*, ha sido extendido al cálculo de los parámetros B relevantes en la física del b, B_B y B_{B_S} que, junto con las constantes de desintegración f_B y f_{B_S}, codifican la información no perturbativa de la mezcla de mesones $\overline{B}^0 - B^0$. El método de los cocientes también ha sido aplicado al parámetro de rotura de SU(3) ξ que mide el cociente entre los parámetros de mezcla en los mesones B_s y B_d. Resultados preliminares de este trabajo han sido presentados en [130].

En la Tabla 8.3.1 comparamos los resultados preliminares de B_{Bs}/B_B, ξ y los valores RGI de $\hat{B}_{Bs}$ y $\hat{B}_B$ con los publicados por otras colaboraciones trabajando en física del quark b en el retículo. Los resultados de $B_1^{(s)}$ y $B_1^{(d)}$ recopilados en el capítulo 6 en $\overline{MS}$ a la masa del quark b han sido evolucionados a RGI usando $\Lambda_{\rm QCD} = 213(8)$ MeV con $N_f = 5$ sabores [45]. En la Figura 8.3.3 hemos comparado los valores más recientes del parámetro ξ con $N_f = 2 + 1$ sabores dinámicos con el obtenido en esta tesis.

Los parámetros B_i con $i = 2, 3, 4, 5$ también han sido estudiados utilizando el método de los cocientes. Resultados sin sabores dinámicos de quarks a un valor del espaciado del retículo se pueden encontrar en [131] donde se usan quarks estáticos de valencia para la simulación. La Tablas 8.3.2 y 8.3.3 comparan los resultados $N_f = 2$ de esta tesis con

los resultados *quenched* sin extrapolación al continuo de [131]. Este análisis fue llevado a cabo hace más de 10 años y, a parte del que hemos presentado en esta tesis, todavía no existe un cálculo alternativo basado en una simulación *unquenched* y con límite al continuo de los elementos de matriz de la base completa de operadores $\Delta B = 2$. Solo existen los resultados preliminares de la colaboración FNAL/MILC discutidos en [149].

Perspectivas futuras

En esta tesis, usando simulaciones $N_f = 2$ en el retículo, hemos calculado

- Los parámetros B que describen las oscilaciones de kaones neutros en el Modelo Estándar y sus extensiones.
- Los parámetros B que controlan las contribuciones de corta distancia en las oscilaciones $\overline{D}^0 - D^0$.
- Diversos observables de la física del b: la masa del quark b m_b, las constantes de desintegración pseudoscalar f_B y f_{B_s}, el parámetro ξ, los parámetros B_B y B_{Bs}, su cociente B_{Bs}/B_B y sus contribuciones supersimétricas $B_i^{(d)}$ y $B_i^{(s)}$.

El siguiente paso, que de hecho ya hemos empezado, consiste en extender el análisis a las simulaciones $N_f = 2+1+1$. Este proyecto involucra el reanálisis de todos los observables estudiados con las simulaciones $N_f = 2$ y la comparación entre ellos. De este modo pretendemos cuantificar el impacto de la inclusión de los quarks *strange* y *charm* como quarks dinámicos en el mar. Los capítulos 4 y 7 ya se mueven hacia esa dirección y los resultados para los parámetros B correspondientes a los operadores $\Delta S = 2$, aunque preliminares, son muy prometedores.

Otros proyectos futuros consisten en extender el método de los cocientes al estudio de otros observables de la física del b. En particular, estamos interesados en:

- Los factores de forma que describen las desintegraciones semiléptonicas de los mesones B y B_s. La medida precisa de éstos es necesaria para la extracción de la información necesaria en la predicción de los elementos V_{ub} y V_{cb} de la matriz CKM.
- Los factores de forma de las desintegraciones exclusivas $b \to s\ell^+\ell^-$. Estos factores de forma combinados con las oscilaciones $\overline{B}^0 - B^0$ permitirán el estudio de distintos escenarios de nueva física.
- Hadrones doblemente pesados en el retículo: el mesón B_c es el único mesón con dos quarks pesados de diferente sabor por lo que sus propiedades de desintegración son de especial interés ya que proporcionan información sobre la interacción fuerte en sistemas con dos quarks pesados.

Appendix A

Smearing and stochastic techniques

In this appendix we briefly describe the construction of quark propagators from smeared quark sources and the smearing in the gauge fields. The construction of stochastic propagators, which fully exploit the information contained in the gauge configuration, is also presented.

The fermionic propagator for each flavor valence quark can be computed by inverting numerically the fermionic matrix for each gauge configuration U

$$S_{ij}^{\alpha\beta}(x,y) = \sum_{z,\gamma,k} \left(Q^{-1}(x,z)\right)_{ik}^{\alpha\gamma} \eta_k^{\gamma}(z) \tag{A.0.1}$$

where we have introduced the *point sources*

$$\eta_k^{\gamma}(z) = \delta_{z,y}\delta_{\gamma\beta}\delta_{kj} \tag{A.0.2}$$

The matrix inversion is usually done using a Krylov space solver as the conjugate gradient (CG) algorithm (see for instance [22]). It is possible to invert the TM operator at a certain twisted mass μ_0 obtaining automatically all the solutions for other twisted masses μ_k with $|\mu_k| \geq |\mu_0|$ [150] . The conjugate gradient multi-mass solver (CGMMS) technique is used in the ETMC inversions to speed up the calculation for ~ 14, 15 valence masses distributed in the light, strange and heavy sectors.

A.1 Smearing

Since mesons are extended objects, cleared correlation signals can be obtained by considering smearing fields. One consider the generalized current

$$J(\vec{x}_1,\vec{x}_2;t) = \bar{\psi}_1(\vec{x}_1,t)F(t,\vec{x}_1,\vec{x}_2)\psi_2(\vec{x}_2,t) \tag{A.1.1}$$

here we have introduced a distribution function $F(t,\vec{x}_1,\vec{x}_2)$ which combines the fields at the lattice sites $(\vec{x}_1,t)$ and $(\vec{x}_2,t)$. The localized current at $(\vec{x},t)$ is recovered with

$$F(t,\vec{x}_1,\vec{x}_2)^{\alpha\beta}_{ij} = \delta_{\vec{x},\vec{x}_1}\Gamma\delta_{\vec{x},\vec{x}_2}\delta_{\alpha\beta}\delta_{ij}$$

where latin and greek indices stand for spin and color indices. A more realistic current can be obtained by choosing a smeared distribution function

$$F(t,\vec{x}_1,\vec{x}_2)^{\alpha\beta}_{ij} = H_1(\vec{x};\vec{x}_1,t)^{\gamma\alpha}_{ki}\Gamma_{\gamma\delta}H_2(\vec{x};\vec{x}_2,t)^{\delta\beta *}_{kj} \tag{A.1.2}$$

Using Eq.A.1.2 one can rewrite Eq.A.1.1 in terms of the *smeared fields*

$$\psi^S(\vec{x},t)^\alpha_i \equiv \sum_{\vec{x}_2} H_2^S(\vec{x};\vec{x}_2,t)^{\alpha\beta *}_{ij}\psi(\vec{x}_2,t)^\beta_j \qquad \bar{\psi}^S(\vec{x},t)^\alpha_i \equiv \sum_{\vec{x}_1} H_1^S(\vec{x};\vec{x}_1,t)^{\alpha\beta}_{ij}\bar{\psi}(\vec{x}_1,t)^\beta_j$$

where the kernel H is chosen to be hermitian and with the correct gauge transformation properties. S is the smearing label, in such a way that no smearing implies $S = L$ and $H^L(\vec{x};\vec{x}_i,t)^{\alpha\beta}_{ij} = \delta_{ij}\delta_{\vec{x}_i\vec{x}}\delta_{\alpha\beta}$. Within this convention, the current operators becomes

$$J(\vec{x},t) = \bar{\psi}^S(\vec{x},t)\Gamma\psi^S(\vec{x},t)$$

And the smeared propagator is

$$\begin{aligned} S^{\alpha\beta}_{ij}(x,y) \quad &\equiv \langle 0|\psi^S(x)^\alpha_i\bar{\psi}^S(y)^\beta_j|0\rangle = \langle 0|\sum_{\vec{x}_2,\vec{y}_1} H_2^S(\vec{x};\vec{x}_2,t)^{\alpha\alpha' *}_{ii'}\psi(\vec{x}_2,t)^{\alpha'}_{i'} H_1^S(\vec{y};\vec{y}_1,t)^{\beta\beta'}_{jj'}\psi(\vec{y}_1,t)^{\beta'}_{j'}|0\rangle \\ &= \sum_{\vec{x}_2,\vec{y}_1} H_2^S(\vec{x};\vec{x}_2,t)^{\alpha\alpha' *}_{ii'}\left(Q^{-1}(\vec{x}_2,t;\vec{y}_1,t)\right)^{\alpha'\beta'}_{i'j'} H_1^S(\vec{y};\vec{y}_1,t)^{\beta\beta'}_{jj'} \end{aligned} \tag{A.1.3}$$

In the construction of the two-point correlators one should replace the original propagator by the one in Eq.A.1.3 to allow for smearing.

Several smearing functions can be used. A gauge covariant source, with a Gaussian shape, is obtained by Jacobi smearing [100]. It is given by

$$\sum_{\vec{x}'} K(\vec{x},t;\vec{x}',t)H^S(\vec{x};\vec{x}',t) = \eta(\vec{x},t) \rightarrow H^S = K^{-1}$$

where η is the local source given in Eq.A.0.2 and $K = 1 - \kappa_s D_s$, with D_s a covariant derivative in the t plane

$$(D_S)^{\alpha\beta}_{ij}(\vec{x},t;\vec{y},t) = \delta_{\alpha\beta}\sum_{\mu=1}^{3}\left[U_{\mu,ij}(\vec{x},t)\delta_{\vec{x}+\hat{\mu},\vec{y}} + U^\dagger_{\mu,ij}(\vec{x}-\hat{\mu},t)\delta_{\vec{x}-\hat{\mu},\vec{y}}\right]$$

here D_S, and therefore H, is hermitian, diagonal in spin and acts only on the color indices connecting different sites of the selected time slice to the central site via the links U_μ. Instead of performing the inversion $H^S = K^{-1}$, the Jacobi method iterates N_S times

$$H^S(\vec{x},t;\vec{y},t) = (\eta(\vec{x},t) + \kappa_s D_S(\vec{x},t;\vec{y},t))^{N_S}$$

Jacobi smearing has two free parameters: the number of smearing steps N_S and a positive real parameter κ_s which is related with the size of the smeared object. Both parameters are tuned to adjust the width of the source.

Smearing of gauge configurations

Smearing of gauge configurations typically consists on replacing the link variables by local averages over products of short paths connecting the endpoints of a given link leading to what is called *fat links*. The propagators and operators are then constructed over these smearing configurations. Three variants of smearing algorithm are the APE [101] , the HYP [151], or the stout one [152].

APE smearing has been exploited in the ETMC production of the bare correlators used in chapter 5 and chapter 6. It replaces in each smearing step n the existing link $U_\mu(n-1)$ by an average over its six perpendicular connecting endpoints

$$U_\mu^{(n)}(x) = \mathrm{Proj}_{\mathrm{SU(3)}}\left[(1-\alpha)U_\mu^{(n-1)}(x) + \frac{\alpha}{6}\sum_{\nu\neq\mu} V_{\mu\nu}^{(n-1)}(x)\right] \equiv \mathrm{Proj}_{\mathrm{SU(3)}}\left[V_\mu^{(n)}\right] \tag{A.1.4}$$

with $V_{\mu\nu}(x) = U_\nu(x)U_\mu(x+\hat{\nu})U_\nu(x+\hat{\mu})^\dagger + U_\nu(x-\hat{\nu})^\dagger U_\mu(x-\hat{\nu})U_\nu(x-\hat{\nu}+\hat{\mu})$. The real parameter α is adjusted depending on the gauge coupling and the projection on $SU(3)$, which guarantees a covariant procedure. This is usually done by maximizing $\mathrm{ReTr}\left[XV_\mu^{(n)}(x)\right]$ for $X \in SU(3)$ and taking X as the new link variable $U_\mu^{(n)}(x) = X$.

A.2 Stochastic all-to-all propagators

Following the notation of [67] we introduce the random sources

$$\xi_{i,\vec{x},x_0} = \delta_{ik}\delta_{x_0,t_0}\delta_{\vec{x},\vec{z}}\eta^{t_0}(k,\vec{z})$$

where i and k are color indices and η is a noise-field. For notation economy, let us denote the sources as ξ_i^r where $i = 1,...V$ spans the set of the source degrees of freedom (colour, spin, space and time). The random sources ξ_i^r are created R times and $r = 1,...R$ denotes the noise samples generated for each gauge configuration. The corresponding average over r is required to satisfy

$$\langle \xi_i^* \xi_j \rangle = \lim_{R\to\infty} \sum_{r=1}^{R} \xi_i^{r*}\xi_j^r = \delta_{ij} \tag{A.2.1}$$

which can be achieved by various choices of ξ_i^r. A typical one is $\xi_i^r = \left(\pm 1 \pm i\right)/\sqrt{2}$ (Z_4 noise) or $\xi_i^r = \pm 1$ (Z_2 noise).

We now invert the lattice Dirac matrix, Q, on each sample of this source

$$\phi_j^r = Q_{jk}^{-1}\xi_k^r$$

The fermion propagator, that is the inverse of the Dirac operator, is estimated by

$$\langle \xi_i^{r*}\phi_j^r\rangle \quad = \lim_{R\to\infty}\frac{1}{R}\sum_{r,k}\xi_i^{r*}Q_{jk}^{-1}\xi_k^r = Q_{ji}^{-1}\big(1+\mathcal{O}(\sqrt{V/R})\big) \tag{A.2.2}$$

Here there is an expected noise $\mathcal{O}(\sqrt{V/R})$ whereas the signal is $\mathcal{O}(1)$ which forces many random sets to obtain a reasonable error.

The *one-end-trick* [153] corrects this behavior. We can recover the product of two propagators joined at the point k from the product $\phi_i^{r*}\phi_j^r$ upon averaging over r

$$\langle \phi_i^{r*}\phi_j^r\rangle = \frac{1}{R}\sum_{r,k,m}\xi_k^{r*}Q_{ki}^{-1*}Q_{jm}^{-1}\xi_m^r = \sum_k Q_{jk}^{-1}Q_{ki}^{-1*}\big(1+\mathcal{O}(\sqrt{V/R})\big)$$

Now contracting with δ_{ij} and summing over all the space at fixed time-slice t_0 where the sources are not zero, we obtain an estimator for the zero three-momentum correlator from t_0 to t, for an interpolating field of the form $\bar{\psi}_1\gamma_5\psi_2$

$$\sum_V\langle \phi_i^{r*}\phi_i^r\rangle = \sum_{i,k}Q_{ik}^{-1}Q_{ki}^{-1*}\big(1+\mathcal{O}(\sqrt{V/R})\big)$$

In this case the signal and the noise are of order V, so the signal-to-noise ratio is more favorable and one sample of noise per gauge configuration ($R=1$) is enough.

A convenient extension of the *one-end-trick* which allow us to compute two and three-point correlators for interpolating fields with any Dirac matrix Γ ($\bar{\psi}_1\Gamma\psi_2$) requires considering the inversion of the lattice Dirac operator on four ($\gamma = 1,2,3,4$) stochastic sources of the form

$$\xi^{(\gamma,t_0)}_{\alpha,i,\vec{x},x_0} = \delta^{\alpha\gamma}\delta_{ik}\delta_{x_0,t_0}\delta_{\vec{x},\vec{z}}\eta^{t_0}(k,\vec{z}) \tag{A.2.3}$$

where now we have splitted the several indices: α (spin) i (colour) x_0 (time) and $\vec{x}$ (space) are free indices while γ and t_0 are fixed as indicated. The η vectors carry only color and three-space indices and according Eq.A.2.1 they should be normalized as

$$\langle \eta^{t_0}(k,\vec{z})\eta^{t_0}(k',\vec{z'})\rangle = \delta_{kk'}\delta_{\vec{z}\vec{z'}}$$

Inserting Eq.A.2.3 in the estimator of the quark propagator Eq.A.2.2, it is possible to evaluate any two- or three-point correlators with any Dirac Matrix. The ϕ-propagator is explicitly given by

$$\phi(\vec{x},x_0)_i^{\alpha\beta} = \sum_{\vec{y},j}\big(Q^{-1}(\vec{x},x_0;\vec{y},y_0)\big)_{ij}^{\alpha\beta}\,\eta^{y_0}(j,\vec{y}) \tag{A.2.4}$$

Therefore, one has to evaluate four separate inversions per gauge configuration, one for each of the four sources corresponding to $\beta = 1,2,3,4$, i.e $\gamma = 1,2,3,4$ in Eq.A.2.3.

Appendix B

Lattice discrete symmetries

B.1 Hermiticity of the propagator

The Wilson operator entering in the Wilson action satisfy

$$\gamma_5 Q^\dagger_{xy} \gamma_5 = Q_{yx} \tag{B.1.1}$$

where Q_{xy} is the expression of the discretized action. This property can be easily shown from the discretized expression of the Wilson action in Eq.2.1.4

$$Q_{xy} = \sum_\mu \frac{1}{2}\gamma_\mu \left([D_{xy}]_\mu + \left[D^*_{xy}\right]_\mu \right) + \frac{a}{2}[\Box_{xy}]_\mu + M\delta_{xy}$$

with the forward and backward derivatives defined as

$$[D_{xy}]_\mu = \frac{1}{a}\left(\delta_{x+a\hat{\mu},y} - \delta_{x,y}\right) \qquad \left[D^*_{xy}\right]_\mu = \frac{1}{a}\left(\delta_{x,y} - \delta_{x-a\hat{\mu},y}\right)$$

and

$$[\Box_{xy}]_\mu = \frac{1}{a^2}\left(\delta_{x+a\hat{\mu},y} + \delta_{x-a\hat{\mu},y} - 2\delta_{xy}\right)$$

The hermitian conjugate of these operators gives

$$\left[D_{xy} + D^*_{xy}\right]^\dagger_\mu = \frac{1}{a}\left(\delta_{y,x+a\hat{\mu}} - \delta_{y,x-a\hat{\mu}}\right)$$

$$[\Box_{xy}]^\dagger_\mu = \frac{1}{a^2}\left(\delta_{y,x+a\hat{\mu}} + \delta_{y,x-a\hat{\mu}} - 2\delta_{yx}\right)$$

and using translational invariance

$$\begin{aligned}\left[D_{xy}+D^{*}_{xy}\right]^{\dagger}_{\mu} &= \frac{1}{a}\left(\delta_{y-a\hat{\mu},x}-\delta_{y+a\hat{\mu},x}\right) &= -\left[D_{yx}+D^{*}_{yx}\right]_{\mu}\\ \left[\Box_{xy}\right]_{\mu} &= \frac{1}{a^2}\left(\delta_{y-a\hat{\mu},x+a\hat{\mu}}+\delta_{y+a\hat{\mu},x}-2\delta_{yx}\right) &= \left[\Box_{yx}\right]_{\mu}\end{aligned}$$

Then

$$Q^{\dagger}_{xy}=-\sum_{\mu}\frac{1}{2}\gamma_{\mu}\left(\left[D_{yx}\right]_{\mu}+\left[D^{*}_{yx}\right]_{\mu}\right)+\frac{a}{2}\left[\Box_{yx}\right]_{\mu}+M\delta_{yx}$$

From where Eq.B.1.1 follows taking into account $\gamma_5\gamma_\mu\gamma_5=-\gamma_\mu$.

As the propagator is $S(x,y,[U])=Q^{-1}_{xy}$ we have

$$S(x,y,[U])=\gamma_5 S^{\dagger}(y,x,[U])\gamma_5$$

The Wilson operator appearing in the TM and OS action reads

$$Q^{f}_{xy}=\sum_{\mu}\frac{1}{2}\gamma_{\mu}\left(\left[D_{xy}\right]_{\mu}+\left[D^{*}_{xy}\right]_{\mu}\right)+\frac{a}{2}\left[\Box_{xy}\right]_{\mu}+m_{0,f}\delta_{xy}+ir_f\mu_f\gamma_5$$

Following the same steps as with the Wilson action

$$\left(Q^{f}_{xy}\right)^{\dagger}=-\sum_{\mu}\frac{1}{2}\gamma_{\mu}\left(\left[D_{yx}\right]_{\mu}+\left[D^{*}_{yx}\right]_{\mu}\right)+\frac{a}{2}\left[\Box_{yx}\right]_{\mu}+m_{0,f}\delta_{yx}-ir_f\mu_f\gamma_5$$

Thus, it satisfies

$$\begin{aligned}\gamma_5\left(Q^{u}_{xy}\right)^{\dagger}\gamma_5 &= Q^{d}_{yx}\\ \gamma_5\left(Q^{d}_{xy}\right)^{\dagger}\gamma_5 &= Q^{u}_{yx}\end{aligned}\tag{B.1.2}$$

and now it is straightforward that

$$\begin{aligned}\gamma_5\left(S^{u}_{xy}\right)^{\dagger}\gamma_5 &= S^{d}_{yx}\\ \gamma_5\left(S^{d}_{xy}\right)^{\dagger}\gamma_5 &= S^{u}_{yx}\end{aligned}$$

B.2 Invariance under time reversal

As we have pointed out in subsection 2.2.2 the action

$$S_F\left[\chi_f,\bar{\chi}_f,U\right]=a^4\sum_{x}\sum_{f=u,d}\bar{\chi}_f(x)\left[D_W\left[U\right]+m_{0,f}+ir_f\mu_f\gamma_5\right]\chi_f(x)$$

which describes a TM doublet if $r_u=-r_d$ or a OS pair if $r_u=r_d$ is invariant under

- Parity with a change of sign of the twisted mass term

$$\tilde{\mathcal{P}} = \mathcal{P}_\omega \times [\mu_f \to -\mu_f]$$

  or equivalently

$$\tilde{\mathcal{P}} = \mathcal{P}_\omega \times [r_f \to -r_f]$$

- Time reversal with a change of sign of the twisted mass term

$$\tilde{\mathcal{T}} = \mathcal{T}_\omega \times [\mu_f \to -\mu_f]$$

  or equivalently

$$\tilde{\mathcal{T}} = \mathcal{T}_\omega \times [r_f \to -r_f]$$

These discrete symmetries can be implemented straightforwardly on quark propagators

$$\begin{array}{l} \tilde{\mathcal{P}} : S_u(x,y,[U]) = \gamma_0 S_d(x^P, y^P, [U]^P)\gamma_0 \\ \tilde{\mathcal{T}} : S_u(x,y,[U]) = \gamma_0\gamma_5 S_d(x^t, y^t, [U]^T)\gamma_5\gamma_0 \end{array} \tag{B.2.1}$$

where $[U]^{P,T}$ denotes the $\tilde{\mathcal{P}}$ or$\tilde{\mathcal{T}}$ transformed links.

Let us now consider the general two point correlation functions with momentum insertion $\vec{p}$

$$\begin{array}{l} C^{(ud)}(\vec{p},t) = -\sum\limits_{\overrightarrow{x}} e^{i\vec{p}\vec{x}} \langle \mathrm{Tr}\left\{ S_u(\overrightarrow{x},t;\overrightarrow{0},0;[U])\Gamma_1 S_d(\overrightarrow{0},0;\overrightarrow{x},t;[U])\Gamma_2 \right\}\rangle \\ C^{(uu)}(\vec{p},t) = -\sum\limits_{\overrightarrow{x}} e^{i\vec{p}\vec{x}} \langle \mathrm{Tr}\left\{ S_u(\overrightarrow{x},t;\overrightarrow{0},0;[U])\Gamma_1 S_u(\overrightarrow{0},0;\overrightarrow{x},t;[U])\Gamma_2 \right\}\rangle \end{array} \tag{B.2.2}$$

where $\langle ... \rangle$ denotes the average over configurations and Γ is a product of gamma matrices $\Gamma = \gamma^{\mu_1}...\gamma^{\mu_k}$ with $\gamma^{\mu_i} \subset \{\gamma^0, \gamma^1, \gamma^2, \gamma^3, \gamma^5\}$. $\tilde{\mathcal{P}}\tilde{\mathcal{T}}$ invariance implies also $\mathcal{PT}$ invariance so

$$\begin{aligned} C^{(ud)}(\vec{p},t) \quad \xrightarrow{\mathcal{PT}} \quad & -\sum_{-\overrightarrow{x}} e^{i\vec{p}\vec{x}} \Big\langle \mathrm{Tr}\Big\{ \gamma_0\gamma_0\gamma_5 S_u(-\overrightarrow{x},-t;\overrightarrow{0},0;[U]^{\mathcal{PT}})\gamma_5\gamma_0\gamma_0\Gamma_1 \\ & \gamma_0\gamma_0\gamma_5 S_d(\overrightarrow{0},0;-\overrightarrow{x},-t;[U]^{\mathcal{PT}})\gamma_5\gamma_0\gamma_0\Gamma_2 \Big\}\Big\rangle \\ = \quad & -\sum_{-\overrightarrow{x}} e^{-i\vec{p}\vec{x}} \Big\langle \mathrm{Tr}\Big\{ \gamma_5 S_u(\overrightarrow{x},-t;\overrightarrow{0},0;[U]^{\mathcal{PT}})\gamma_5\Gamma_1 \\ & \gamma_5 S_d(\overrightarrow{0},0;\overrightarrow{x},-t;[U]^{\mathcal{PT}})\gamma_5\Gamma_2 \Big\}\Big\rangle \end{aligned}$$

as $\gamma_5\gamma^{\mu_1}\gamma_5 = -\gamma^{\mu_1}$ and $\gamma_5\gamma_5\gamma_5$ we have

$$C^{(ud)}(\vec{p},t) = (-1)^N C^{(ud)}(-\vec{p},-t)$$

where N is now the number of indices μ^i in Γ_1 and Γ_2 that differ from 5.

Equivalently one finds

$$C^{(uu)}(\vec{p},t) = (-1)^N C^{(uu)}(-\vec{p},-t)$$

Therefore, imposing invariance under $\mathcal{PT}$ we deduce that the correlator $C^{(2)}_{PP}$ with zero insertion of momentum is even under time reversal while $C^{(2)}_{AP}$ and $C^{(2)}_{PA}$ are odd.

Appendix C

Renormalization Group Analysis

In this appendix I review the basic features of the Renormalization Group equations governing the evolution of the renormalized quantities.

Let us consider a generic amputated Green's function of elementary N fields $q(x)$ with insertion of the operator O. In a covariant gauge the bare amputated Green functions depend on the external momenta $p_1, ..., p_N$, the bare coupling $\alpha = g_0^2/4\pi$, the bare gauge fixing parameter λ_0 and the bare mass of the fields m^0. They have to be regularized, usually in dimensional regularization, in order to parametrize the singularities and then renormalized. Formally the elimination of the divergent parts can be achieved by adding counterterms to the Lagrangian corresponding to each superficially divergent diagram appearing in the theory. Those counterterms can be absorbed in the redefinition of the parameters through the renormalization constants (RCs), determined to cancel the divergences in the Green functions in a specific renormalization scheme.

The relation between the renormalized and bare Green function is [1]:

$$\Gamma^{(R)}(p_i;\alpha,\lambda,m;\mu) = \lim_{\epsilon\to 0} Z_q(\alpha,\lambda,m,\epsilon;\mu)^{N/2} Z_O(\alpha,\lambda,m,\epsilon;\mu)\Gamma^{(0)}(p_i;\alpha^0,\lambda^0,m^0:\epsilon) \tag{C.0.1}$$

where (R) denotes renormalized and (0) bare, μ is the mass scale dependence. The parameters α, m and λ are renormalized, thus, they depend on the scale μ. Different choices of the renormalization scale μ, leads to different definitions of the renormalized parameters, but Γ^0 is independent of μ:

$$\mu\frac{d}{d\mu}\Gamma^{(0)}(p_i;\alpha^0,\lambda^0,m_i^0:\epsilon) = 0 \tag{C.0.2}$$

Defining the anomalous dimension as

[1] assuming dimensional regularization the bare Green function and the renormalization constants depends on ϵ

$$\gamma_\Gamma \equiv \mu \frac{d}{d\mu} \ln Z_\Gamma \tag{C.0.3}$$

And using Eq.C.0.1, Eq.C.0.2 becomes

$$\mu \frac{d}{d\mu} \Gamma^{(R)} = \left(\frac{N}{2} \gamma_q + \gamma_O \right) \Gamma^{(R)}$$

$\Gamma^{(R)}$ depends explicitly on μ and implicitly through α, m and λ, so the derivative $\frac{d}{d\mu}$ can be written more conveniently as

$$\mu \frac{d}{d\mu} = \mu \frac{\partial}{\partial \mu} + \alpha\beta(\alpha, \lambda, x_m) \frac{\partial}{\partial \mu} + \lambda\delta(\alpha, \lambda, x_m) \frac{\partial}{\partial \lambda} - x_m \gamma_m \frac{\partial}{\partial x_m}$$

with $x_m = m/\mu$ and we have defined the following functions depending only on the theory (QCD) but independent of the operator O

$$\mu \frac{d\alpha}{d\mu} \equiv \alpha\beta(\alpha, \lambda, x_m)$$

$$\mu \frac{d\lambda}{d\mu} \equiv \lambda\delta(\alpha, \lambda, x_m)$$

$$-\mu \frac{dx_m}{d\mu} = x_m \gamma_m(\alpha, \lambda, x_m)$$

With this definitions the Renormalization Group Equation reads

$$\left[\mu \frac{\partial}{\partial \mu} + \alpha\beta \frac{\partial}{\partial \alpha} + \lambda\delta \frac{\partial}{\partial \lambda} - x_m \gamma_m \frac{\partial}{\partial x_m} - \left(\frac{N}{2} \gamma_q + \gamma_\Gamma \right) \right] \Gamma^{(R)} = 0$$

The explicit form of γ_Γ, γ_q, β, δ and γ_m depend on the regularization scheme. They can be expanded in terms the gauge coupling. Assuming a gauge and mass-independent scheme (as $\overline{MS}$) they can be written as

$$\beta(\alpha(\mu)) \equiv -\sum_{i \geq 0} \beta^{(i)} \left(\frac{\alpha(\mu)}{4\pi} \right)^{i+1} = \mu \frac{d \ln \alpha}{d\mu} \qquad \gamma_q(\alpha(\mu)) \equiv \sum_{i \geq 0} \gamma_q^{(i)} \left(\frac{\alpha(\mu)}{4\pi} \right)^{i+1}$$

$$\gamma_m(\alpha(\mu)) \equiv \sum_{i \geq 0} \gamma_m^{(i)} \left(\frac{\alpha(\mu)}{4\pi} \right)^{i+1} \qquad \gamma_\Gamma(\alpha(\mu)) \equiv \sum_{i \geq 0} \gamma_\Gamma^{(i)} \left(\frac{\alpha(\mu)}{4\pi} \right)^{i+1} \tag{C.0.4}$$

The first equation in Eq.C.0.4 can be solved iteratively. Up to N^3LO one obtains

$$\frac{\alpha(\mu)}{4\pi} = \frac{1}{\beta_0 L} - \frac{\bar{\beta}_1 \ln L}{(\beta_0 L)^2} + \frac{1}{(\beta_0 L)^3}[\bar{\beta}_1^2(\ln^2 L - \ln L - 1) + \bar{\beta}_2] \tag{C.0.5}$$
$$+\frac{1}{(\beta_0 L)^4}\left[\bar{\beta_1}^3(-\ln^3 L + \frac{5}{2}\ln^2 L + 2\ln L - \frac{1}{2}) - 3\bar{\beta}_1\bar{\beta}_2 \ln L + \frac{\bar{\beta}_3}{2}\right]$$

where $\bar{\beta}_i = \beta_i/\beta_0$, $L = \ln\left(\mu^2/\Lambda^2\right)$ and Λ is called the asymptotic scale parameter of the $\overline{MS}$ scheme.

The scheme-independent coefficients β_i can be found in [92]

$$\begin{aligned}
\beta_0 &= \frac{1}{4}\left(11 - \frac{2}{3}N_f\right) \\
\beta_1 &= \frac{1}{16}\left(102 - \frac{38}{3}N_f\right) \\
\beta_2 &= \frac{1}{64}\left(\frac{2857}{2} - \frac{5033}{18}N_f + \frac{325}{54}N_f^2\right) \\
\beta_3 &= \frac{1}{256}\left[\frac{149753}{6} + 3564\zeta(3) - \left(\frac{1078361}{162} + \frac{6508}{27}\zeta(3)\right)N_f\right. \\
&\quad \left. + \left(\frac{50065}{162} + \frac{6472}{81}\zeta(3)\right)N_f^2 + \frac{1093}{729}N_f^3\right]
\end{aligned} \tag{C.0.6}$$

where N_f is the number of active flavours ζ is the Riemann zeta function.

C.1 Quark bilinears at N^{3}LO

It is usual to solve the evolution of the RC Z_Γ in Eq.C.0.3 in terms of the evolution coefficients C_Γ given by

$$\left[\mu\frac{d}{d\mu} - \gamma_\Gamma\right] C_\Gamma(\mu) = 0 \tag{C.1.1}$$

The solution of the previous equation is standard

$$C_\Gamma(\mu) = \exp\left[\int_{\alpha(\mu_0)}^{\alpha(\mu)} d\alpha_S \frac{\gamma_\Gamma(\alpha)}{\alpha\beta(\alpha)}\right] C_\Gamma(\mu_0) \tag{C.1.2}$$

At N^3LO it gets the explicit form

$$
\begin{aligned}
C_\Gamma(x) = \; & \exp\left\{\int^x dx' \frac{\gamma_\Gamma(x')}{x'\beta(x')}\right\} = \\
& (x)^{\bar{\gamma}_0}\left\{1 + (\bar{\gamma}_1 - \bar{\beta}_1\bar{\gamma}_0)x\right. \\
& + \frac{1}{2}\left[(\bar{\gamma}_1 - \bar{\beta}_1\bar{\gamma}_0)^2 + \bar{\gamma}_2 + \bar{\beta}_1^2\bar{\gamma}_0 - \bar{\beta}_1\bar{\gamma}_1 - \bar{\beta}_2\bar{\gamma}_0\right]x^2 + \\
& + \frac{1}{6}\left[(\bar{\gamma}_1 - \bar{\beta}_1\bar{\gamma}_0)^3 + \frac{1}{2}(\bar{\gamma}_1 - \bar{\beta}_1\bar{\gamma}_0)(\bar{\gamma}_2 + \bar{\beta}_1^2\bar{\gamma}_0 - \bar{\beta}_1\bar{\gamma}_1 - \bar{\beta}_2\bar{\gamma}_0) + \right. \\
& \left.\left. + \frac{1}{3}(\bar{\gamma}_3 - \bar{\beta}_1^3\bar{\gamma}_0 + 2\bar{\beta}_1\bar{\beta}_2\bar{\gamma}_0 - \bar{\beta}_3\bar{\gamma}_0 + \bar{\beta}_1{}^2\bar{\gamma}_1 - \bar{\beta}_2\bar{\gamma}_1 - \bar{\beta}_1\bar{\gamma}_2)\right]x^3 + \mathcal{O}\left(x^4\right)\right\}
\end{aligned}
\tag{C.1.3}
$$

with $x = \alpha(\mu)/(4\pi)$ and

$$
\bar{\gamma}_i^{(i)} = \gamma_\Gamma^{(i)}/\beta_0 \tag{C.1.4}
$$

The coefficients $\gamma_{S/P}^{(i)}$ in Eq.C.0.4 computed in the and RI'-MOM scheme are [92][2]

$$
\gamma_{S/P}^{(0)} = -1 \tag{C.1.5}
$$

$$
(\gamma_{S/P}^{(1)})^{RI'} = -\frac{1}{16}(126 - \frac{52}{9}N_f)
$$

$$
(\gamma_{S/P}^{(2)})^{RI'} = -\frac{1}{64}\left[\frac{20174}{3} - \frac{3334}{3}\zeta(3) + \left(-\frac{17588}{27} + \frac{128}{9}\zeta(3)\right)N_f + \frac{856}{81}N_f^2\right]
$$

$$
\begin{aligned}
(\gamma_{S/P}^{(3)})^{RI'} = -\frac{1}{256}\; & \left[\frac{141825253}{324} - \frac{7230017}{54}\zeta(3) + \frac{6160}{3}\zeta(5)\right. \\
& + \left(-\frac{3519059}{54} + \frac{298241}{27}\zeta(3) + \frac{4160}{3}\zeta(5)\right)N_f \\
& \left. + \left(\frac{611152}{243} - \frac{5948}{27}\zeta(3)\right)N_f^2 - \frac{16024}{729}N_f^3\right]
\end{aligned}
$$

For the tensorial operator the anomalous dimension operator is known up to N^{2}LO [93]

[2] Due to the Ward Identities, $m(\mu)S(\mu)$ and $m(\mu)P(\mu)$ are renormalization group invariant quantities. Thus $\gamma_S = \gamma_P$.

$$\gamma_T^{(0)} = \frac{4}{3} \tag{C.1.6}$$

$$(\gamma_T^{(1)})^{RI'} = -\frac{1}{16}\frac{2}{27}(26N_f - 543)$$

$$(\gamma_T^{(2)})^{RI'} = \frac{1}{64}\frac{2}{243}\left[572N_f^2 + (1152\zeta(3) - 29730)\,N_f - 58824\zeta(3) + 269259\right]$$

The quark anomalous dimension in the RI'-MOM scheme are [92]

$$\gamma_q^{(0)} = 0 \tag{C.1.7}$$

$$(\gamma_q^{(1)})^{RI'} = -\frac{1}{16}(-\frac{67}{3} + \frac{4}{3}N_f)$$

$$(\gamma_q^{(2)})^{RI'} = -\frac{1}{64}\left[-\frac{52321}{36} + \frac{607}{2}\zeta(3) + \left(+\frac{4472}{27} - 16\zeta(3)\right)N_f - \frac{104}{27}N_f^2\right]$$

$$\begin{aligned}(\gamma_q^{(3)})^{RI'} = -\frac{1}{256}\ \Bigg[&-\frac{8966278}{81} + \frac{15631129}{324}\zeta(3) - \frac{15846715}{1296}\zeta(5)\\ &+\left(\frac{1537880}{81} - \frac{121558}{27}\zeta(3) + 830\zeta(5)\right)N_f\\ &+\left(-\frac{75355}{81} + 80\zeta(3)\right)N_f^2 - \frac{1000}{81}N_f^3\Bigg]\end{aligned}$$

Finally, Z_V and Z_A are protected by the Ward Identities so they are $\mu-$independent and they do not evolve with the renormalization scale $C_A(\mu,\mu_0) = C_V(\mu,\mu_0) = 1$, or equivalently $\gamma_A = \gamma_V = 0$.

The renormalization group invariant (RGI) RCs are defined as

$$Z_\Gamma^{\rm RGI} = \frac{Z_\Gamma(\mu)}{C_\Gamma(\mu)}$$

Consequently, the RCs computed in the RI'-MOM scheme at some values of $\mu^2 = p^2$ are evolved to a reference scale $\mu_0 = a^{-1}$ with

$$Z_\Gamma^{\rm RI'}(\mu_0 = a^{-1}) = C_\Gamma^{\rm RI'}(\mu_0 = a^{-1})Z_\Gamma^{\rm RGI} = \frac{C_\Gamma^{\rm RI'}(\mu_0 = a^{-1})}{C_\Gamma^{\rm RI'}(\mu^2 = p^2)}Z_\Gamma^{\rm RI'}(\mu^2 = p^2)$$

Now it is straightforward to compute the function $C_\Gamma^{\rm RI'}(\mu)$ in the RI'-MOM scheme given the number of active flavors. Explicitly one finds

$$C_{S/P}^{\text{RI'}}(N_f=2;\mu)=\left(\frac{\alpha(\mu)}{4\pi}\right)^{-12/29}\left[1-8.55727\left(\frac{\alpha(\mu)}{4\pi}\right)-125.423\left(\frac{\alpha(\mu)}{4\pi}\right)^2-3797.71\left(\frac{\alpha(\mu)}{4\pi}\right)^3\right]$$

$$C_{S/P}^{\text{RI'}}(N_f=4;\mu)=\left(\frac{\alpha(\mu)}{4\pi}\right)^{-12/25}\left[1-9.38987\left(\frac{\alpha(\mu)}{4\pi}\right)-96.2883\left(\frac{\alpha(\mu)}{4\pi}\right)^2-2403.82\left(\frac{\alpha(\mu)}{4\pi}\right)^3\right]$$

$$C_{T}^{\text{RI'}}(N_f=2;\mu)=\left(\frac{\alpha(\mu)}{4\pi}\right)^{4/29}\left[1+2.66852\left(\frac{\alpha(\mu)}{4\pi}\right)+47.9701\left(\frac{\alpha(\mu)}{4\pi}\right)^2\right]$$

$$C_{T}^{\text{RI'}}(N_f=4;\mu)=\left(\frac{\alpha(\mu)}{4\pi}\right)^{4/25}\left[1+2.91662\left(\frac{\alpha(\mu)}{4\pi}\right)+37.9471\left(\frac{\alpha(\mu)}{4\pi}\right)^2\right]$$

$$C_{q}^{\text{RI'}}(N_f=2;\mu)=1+2.0345\left(\frac{\alpha(\mu)}{4\pi}\right)+35.9579\left(\frac{\alpha(\mu)}{4\pi}\right)^2+1199.16\left(\frac{\alpha(\mu)}{4\pi}\right)^3$$

$$C_{q}^{\text{RI'}}(N_f=4;\mu)=1+2.4000\left(\frac{\alpha(\mu)}{4\pi}\right)+29.6724\left(\frac{\alpha(\mu)}{4\pi}\right)^2+719.141\left(\frac{\alpha(\mu)}{4\pi}\right)^3$$

From RGI we can also evolve to $\overline{MS}$ at some scale μ

$$Z_\Gamma^{\overline{MS}}(\mu)=C_\Gamma^{\overline{MS}}(\mu)Z_\Gamma^{\text{RGI}}$$

In particular, for the study of quark masses and bag parameters, we are interested in the scalar and pseudoscalar bilinears renormalized in $\overline{MS}$. The anomalous dimension are [92]

$$\begin{aligned}
(\gamma_{S/P}^{(1)})^{\overline{MS}}&=-\frac{1}{16}\left(\frac{202}{3}-\frac{20}{9}N_f\right)\\
(\gamma_{S/P}^{(2)})^{\overline{MS}}&=-\frac{1}{64}\left[1249-\left(\frac{2216}{27}+\frac{160}{3}\zeta(3)\right)N_f-\frac{140}{81}N_f^2\right]\\
(\gamma_{S/P}^{(3)})^{\overline{MS}}&=-\frac{1}{256}\left[\frac{4603055}{162}-\frac{135680}{27}\zeta(3)-8800\zeta(5)\right.\\
&\quad+\left(-\frac{91723}{27}-\frac{34192}{9}\zeta(3)+880\zeta(4)+\frac{18400}{9}\zeta(5)\right)N_f\\
&\quad\left.+\left(\frac{5242}{243}+\frac{8006}{9}\zeta(3)-\frac{160}{3}\zeta(4)\right)N_f^2-\left(\frac{332}{243}-\frac{64}{27}\zeta(3)\right)N_f^3\right]
\end{aligned}\tag{C.1.8}$$

and the corresponding evolution functions are

$$C_{S/P}^{\overline{MS}}(N_f=2;\mu)=\left(\frac{\alpha(\mu)}{4\pi}\right)^{-12/29}\left[1-3.22394\left(\frac{\alpha(\mu)}{4\pi}\right)-12.0214\left(\frac{\alpha(\mu)}{4\pi}\right)^2-63.6449\left(\frac{\alpha(\mu)}{4\pi}\right)^3\right]$$

$$C_{S/P}^{\overline{MS}}(N_f=4;\mu)=\left(\frac{\alpha(\mu)}{4\pi}\right)^{-12/25}\left[1-4.05653\left(\frac{\alpha(\mu)}{4\pi}\right)-5.77185\left(\frac{\alpha(\mu)}{4\pi}\right)^2-43.7847\left(\frac{\alpha(\mu)}{4\pi}\right)^3\right]$$

C.2 $\Delta F=2$ operators at NLO

Let us now generalize the previous formalism to the complete basis of $\Delta F=2$ operators, which mix among themselves in the renormalization procedure. The effective Hamiltonian is written as a linear combination of the complete basis $\vec{O}$ trough $\mathcal{H}_{\text{eff}}\sim\sum_j C_{ij}O_j=\vec{O}^T\vec{C}$ where $\vec{C}$ are the Wilson coefficients. In the matrix form Eq.C.1.1 reads

$$\left[\mu\frac{d}{d\mu}-\gamma^T\right]\vec{C}_O(\mu)=0 \tag{C.2.1}$$

The solution is

$$\vec{C}_O(\mu)=\exp\left[\int_{\alpha(\mu_0)}^{\alpha(\mu)}d\alpha_S\frac{\gamma^T(\alpha_S)}{\alpha\beta(\alpha)}\right]\vec{C}_O(\mu_0) \tag{C.2.2}$$

which is usually written in terms of the matrix $W(\mu,\mu_0)$ as

$$\vec{O}(\mu)=\left(W^T(\mu,\mu_0)\right)^{-1}\vec{O}(\mu_0) \tag{C.2.3}$$

It is convenient to write the evolution matrix in the following form

$$W\left(\mu,\mu_0\right)=\omega\left(\mu\right)\omega^{-1}\left(\mu_0\right)$$

where

$$\omega\left(\mu\right)=M\left(\mu\right)\alpha\left(\mu\right)^{-\gamma^{(0)T}/2\beta_0}$$

and

$$M\left(\mu\right)=I+J\frac{\alpha\left(\mu\right)}{4\pi}$$

$\gamma^{(0)}$ is the one-loop anomalous dimension matrix. It is independent of the renormalization scheme. In the lattice basis of $\left\{\vec{O}^{\text{PC+}}\right\}$, the one-loop anomalous dimension matrix of the PC+ operators reads [154][3]

[3]The $\gamma^{(0)}$ value quoted here differs from the one directly read in [154] because of the factor 4 due to the sum in $\mu>\nu$ in our definition of O^{TT}. Our $\gamma^{(0)}$ is obtained by applying $S\gamma^{(0)}S^{-1}$ over the one in [154] with $S=\text{diag}\{1,1,1,1,1/4\}$.

$$\gamma^{(0)} = \begin{pmatrix} 4 & 0 & 0 & 0 & 0 \\ 0 & 2 & 12 & 0 & 0 \\ 0 & 0 & -16 & 0 & 0 \\ 0 & 0 & 0 & -10 & 2/3 \\ 0 & 0 & 0 & -10 & 34/3 \end{pmatrix} \tag{C.2.4}$$

The expression for J can be found by inserting Eq.C.2.2 into Eq.C.2.1. In the lattice basis defined by $\left\{\vec{O}^{\text{PC}+}\right\}$, the matrix J in the Feynman-gauge RI scheme is computed in [154]

$$J^{+}_{\text{FRI}} = \begin{pmatrix} J^{+}_{11} & 0 & 0 & 0 & 0 \\ 0 & J_{22} & J^{+}_{23} & 0 & 0 \\ 0 & J^{+}_{32} & J_{33} & 0 & 0 \\ 0 & 0 & 0 & J^{+}_{44} & J^{+}_{45} \\ 0 & 0 & 0 & J^{+}_{54} & J^{+}_{55} \end{pmatrix}$$

The non zero J matrix elements are[4]

$$\begin{aligned} J^{+}_{11} &= \frac{-23931 + 2862N_f - 128N_f^2}{6\,(33 - 2N_f)^{\,2}} \\ J_{22} &= \frac{1437345 - 221058N_f + 13488N_f^2 - 256N_f^3}{24\,(33 - 2N_f)^{\,2}\,(-30 + N_f)} \\ J_{23} &= \frac{45}{480 - 16N_f} \\ J_{32} &= \frac{-4347675 + 2468583N_f - 294786N_f^2 + 14928N_f^3 - 256N_f^4}{4\,(33 - 2N_f)^{\,2}\left(90 - 33N_f + N_f^2\right)} \end{aligned}$$

[4]The J^{+}_{45} quoted here differ from the one in [154] because of the factor 4 in our definition of O_{TT}. With our definition J can be obtained directly from [154] after applying $\left\{S\left\{J^{T}\right\}S^{-1}\right\}^{T}$ with $S = \text{diag}\{1,1,1,1,1/4\}$.

$$
\begin{aligned}
J_{33} &= \frac{-15575085 + 2142036N_f - 115572N_f^2 + 2048N_f^3}{24\,(33-2N_f)^{\,2}\,(-30+N_f)} \\
J_{44}^{+} &= \frac{4176675 - 5048688N_f + 669548N_f^2 - 36624N_f^3 + 640N_f^4}{3\,(33-2N_f)^{\,2}\left(125 - 132N_f + 4N_f^2\right)} \\
J_{45}^{+} &= \frac{5\left(-277425 - 767424N_f + 118876N_f^2 - 7056N_f^3 + 128N_f^4\right)}{3\,(33-2N_f)^{\,2}\left(125 - 132N_f + 4N_f^2\right)} \\
J_{54}^{+} &= \frac{-898695 + 1066800N_f - 142204N_f^2 + 7632N_f^3 - 128N_f^4}{36\,(33-2N_f)^{\,2}\left(125 - 132N_f + 4N_f^2\right)} \\
J_{55}^{+} &= \frac{11915775 + 14548416N_f - 2050844N_f^2 + 119952N_f^3 - 2176N_f^4}{9\,(33-2N_f)^{\,2}\left(125 - 132N_f + 4N_f^2\right)}
\end{aligned}
$$

In the RI'-MOM scheme the corresponding J is

$$J_{RI'} = J_{FRI} + r_{RI'}^{T}$$

and in the $\overline{MS}$

$$J_{\overline{MS}} = J_{FRI} + r_{RI'}^{T} - r_{\overline{MS}}^{T} \tag{C.2.5}$$

where r_{RI} can be found in [154]

$$
r_{RI'} = \begin{pmatrix}
1 + 8\log(2) & 0 & 0 & 0 & 0 \\
0 & \frac{1}{6} - \frac{2\log(2)}{3} & 1 - 4\log(2) & 0 & 0 \\
0 & -\frac{1}{2} - \log(2) & -\frac{13}{3} - \frac{2\log(2)}{3} & 0 & 0 \\
0 & 0 & 0 & \frac{10\log(2)}{3} - \frac{23}{6} & \frac{11}{72} + \frac{7\log(2)}{18} \\
0 & 0 & 0 & \frac{56\log(2)}{3} - \frac{14}{3} & \frac{43}{18} + \frac{58\log(2)}{9}
\end{pmatrix}
$$

The $\overline{MS}$ scheme we use is the one defined by Buras et al. in [95]. Their definition of $\overline{MS}$, which has become standard, differs from the one in [154] proposed by Ciuchini et al. in the treatment of the four-fermion evanescent operators appearing in the calculation of the anomalous dimension. The $r_{\overline{MS}}$ matrix can be read from [95]:

$$r_{\overline{MS}} = \begin{pmatrix} 8\log(2) - \frac{14}{3} & 0 & 0 & 0 & 0 \\ 0 & -\frac{2}{3} - \frac{2\log(2)}{3} & -4 - 4\log(2) & 0 & 0 \\ 0 & 1 - \log(2) & \frac{34}{3} - \frac{2\log(2)}{3} & 0 & 0 \\ 0 & 0 & 0 & \frac{10}{3} + \frac{10\log(2)}{3} & \frac{7\log(2)}{18} - \frac{1}{18} \\ 0 & 0 & 0 & \frac{56\log(2)}{3} & \frac{58\log(2)}{9} - \frac{16}{9} \end{pmatrix}$$

Armed with this information, $Z_O(\mu)$ can be obtained from the RGI quantity as

$$Z_O(\mu) = (\omega(\mu))^T \, Z_O^{\mathrm{RGI}}$$

Appendix D

Renormalization Constants $\mathcal{O}(a^2g^2)$ corrections

In this appendix I collect the $\mathcal{O}(a^2g^2)$ corrections to the fermion propagator, Green's functions of all fermion bilinear operators and four-fermion matrix element. Results for several choices of the value for the Symanzik coefficients can be obtained from [91] for bilinear and [94] for four-fermion operators. Here I only collect the values of the relevant coefficients for the lattice action used in the present study, namely the Twisted Mass action at maximal twist with the tree-level Symanzik improved and the Iwasaki gluon action.

D.1 Propagator and bilinears

Up to 1-loop and up to $\mathcal{O}(a^2)$, the corrected amputated projected Green function and the corrected form factor, of the quark field have the simple expression in Eq.4.4.5. The explicit value of the coefficients $c_{\Gamma,q}$ can be obtained from the perturbative expressions of $S_q^{-1}(p)$ and the amputated Green function Λ_Γ in equations 4.1, 5.3, 5.4, 5.5, 5.6, 5.8 and 5.9 of [91] [1] with the coefficients c_i defined in Eq.2.1.14, λ=0 (Landau gauge) and the clover term fixed to $c_{SW} = 0$ in the two gauge actions considered along this work: tree-level improved Symanzik (*tlsym)* for $N_f = 2$ and the *Iwasaki* one for $N_f = 2+1+1$. Finally, the quantities $\epsilon^{(i,j)}$ are numerical coefficients depending on the Symanzik parameters which should be calculated for each action and are specified in the appendix of [91]. The value of the coefficients entering in the corrected quark propagator and in the amputated projected Green function Eq.4.4.5 are collected in Table D.1.1.

[1] The coefficient listed here are obtained from the corrected expressions up to 1-loop in [91] through:
$\Sigma_1(p) = -\frac{i}{12N(p)}\mathrm{Tr}\left[\sum'_\rho \left(\gamma_\rho S_q(p)^{-1}\right)/\tilde{p}_\rho\right]$
$\mathcal{V}_\Gamma(p) = \mathrm{Tr}\left[\Lambda_\Gamma P_\Gamma\right]$,

	tlsym				Iwasaki		
	$c^{(1)}$	$c^{(2)}$	$c^{(3)}$		$c^{(1)}$	$c^{(2)}$	$c^{(3)}$
q	1.14716 $+\frac{1}{N(p)}$2.07733	-0.20278 $-\frac{1}{N(p)}$0.87222	0.02917	q	0.62002 $+\frac{1}{N(p)}$1.84904	-0.07482 $-\frac{1}{N(p)}$0.96303	0.00440
V	0.69992	-0.33333	-0.43403	V	0.28814	-0.20950	-0.51658
A	1.52408	-0.33333	-0.43403	A	0.96380	-0.20950	-0.51658
S	2.35473	-0.25000	0.50000	S	2.02123	-0.25000	0.37617
P	0.70641	-0.25000	0.50000	P	0.66908	-0.25000	0.37617
T	0.97248	-0.36111	-0.74537	T	0.38610	-0.19600	-0.81417

Table D.1.1: Numerical values of the perturbative coefficients correcting the quark propagator and bilinear operators obtained from [91]. $N(p)$ is the number of Lorentz indices for which p_ρ is different from zero.

D.2 Four-fermion dynamical matrix

The $\mathcal{O}(a^2g^2)$ are analytically subtracted from our numerical computation of the dynamical matrix trough Eq.4.4.8 where the explicit value of $d_{ij}^{(k)}$ are obtained in [94]. We provide here, the results for $c_{SW} = 0$, $\lambda = 0$, $N_c = 3$ and *tlsym* and *Iwasaki* actions. As described in subsection 4.4.4.3, with our setup, $r_1 = r_2 = r_3 = -r_4$, the relevant $d_{ij}^{(k)}$ are obtained from the PV+ ones computed for the Wilson action in [94]. Their numerical values are collected in Table D.2.1.

tlsym				Iwasaki			
(i,j)	$d_{ij}^{(1)}$	$d_{ij}^{(2)}$	$d_{ij}^{(3)}$	(i,j)	$d_{ij}^{(1)}$	$d_{ij}^{(2)}$	$d_{ij}^{(3)}$
(1 , 1)	-2.79899	2.64223	-1.05556	(1 , 1)	-3.05067	0.36480	0.01767
(2 , 2)	-0.87361	1.84679	-0.69444	(2 , 2)	-1.04823	0.76500	-0.40550
(2 , 3)	0.89270	-1.46854	0.33333	(2 , 3)	0.94036	-0.99659	0.20950
(3 , 2)	1.70276	-6.71131	1.16667	(3 , 2)	1.97594	-5.42558	0.91900
(3 , 3)	1.92847	3.10250	-0.44444	(3 , 3)	1.63002	2.92381	-0.52700
(4 , 4)	2.01567	-0.28621	0.05556	(4 , 4)	1.80953	-0.40753	0.34450
(4 , 5)	-1.07855	4.60271	-0.77778	(4 , 5)	-1.28920	3.65074	-0.48883
(5 , 4)	-0.98220	1.25519	-0.31481	(5 , 4)	-1.02490	0.73718	-0.13594
(5 , 5)	-3.06216	0.82895	-0.85185	(5 , 5)	-3.21610	-1.33185	0.20761

Table D.2.1: Numerical values of the $d_{ij}^{(k)}$ obtained from [94]

Appendix E

QCD-HQET matching of bag parameters

The coefficients $C_{ij}\left(\hat{\mu}_b^*, \hat{\mu}_h^{(n)}, \mu\right)$ appearing in Eq.6.3.1 are estimated from the evolution of the bag parameters in QCD in the scheme and the scale where they are computed in QCD usually $\overline{MS}$ at 2 or 3 GeV, followed by the matching between QCD and HQET at the reference scale $\hat{\mu}_h$, corresponding to the heavy mass quark of the simulated meson, and the running in HQET to the reference scale $\hat{\mu}_b^*$.

We can separate the evolution and matching of the bag parameters in two sectors: the bilinear and the four-fermion operators.

Instead of the five operators we listed in Eq.3.2.8, in Heavy Quark Effective Theory (HQET) one deals with only four of them

$$\begin{aligned}
\tilde{Q}_1 &= \left[\bar{H}^a\gamma^\mu(1-\gamma_5)l^a\right]\left[\bar{H}^b\gamma_\mu(1-\gamma_5)l^b\right] \\
\tilde{Q}_2 &= \left[\bar{H}^a(1-\gamma_5)l^a\right]\left[\bar{H}^b(1-\gamma_5)l^b\right] \\
\tilde{Q}_4 &= \left[\bar{H}^a(1-\gamma_5)l^a\right]\left[\bar{H}^b(1+\gamma_5)l^b\right] \\
\tilde{Q}_5 &= \left[\bar{H}^a(1-\gamma_5)l^b\right]\left[\bar{H}^b(1+\gamma_5)l^a\right]
\end{aligned} \tag{E.0.1}$$

where H stands for the infinitely heavy static quark and in order to avoid confusions we use tilde symbols over the operators and bag parameters computed in HQET.

In the HQET, the operator $\tilde{Q}_3$ is related to $\tilde{Q}_1$ and $\tilde{Q}_2$ by the equation of motion

$$\tilde{Q}_3 = -\tilde{Q}_2 - \frac{1}{2}\tilde{Q}_1 \tag{E.0.2}$$

However, in order to work with 5×5 squared matrix also in HQET, we consider the basis of five operators $\left\{\tilde{Q}_i\right\}$ by adding $\tilde{Q}_3$ to Eq.E.0.1.

Following the notation in [131], the matching of QCD operators, renormalized at the scale μ, and the HQET ones renormalized at some reference scale $\hat{\mu}_b^*$ is made at $\hat{\mu}_h$ by using Eq.C.2.3

$$\langle \vec{\tilde{Q}}\left(\hat{\mu}_b^*\right)\rangle = \left[\mathbf{W}^T\left(\hat{\mu}_h,\mu\right)\mathbf{C}\left(\hat{\mu}_h\right)\left(\tilde{\mathbf{W}}^T\left(\hat{\mu}_h,\hat{\mu}_b^*\right)\right)^{-1}\right]^{-1}\langle \vec{Q}\left(\mu\right)\rangle \tag{E.0.3}$$

where $\mathbf{W}^T\left(\mu,\hat{\mu}_h\right)$ is the matrix encoding the full QCD evolution from the scale μ to the scale $\hat{\mu}_h$ in $\overline{MS}$ for the five operators $\Delta F=2$ collected in $\vec{Q}(\mu)$, $\tilde{\mathbf{W}}^T\left(\hat{\mu}_h,\hat{\mu}_b^*\right)$ encodes the evolution from $\hat{\mu}_h$ to $\hat{\mu}_b^*$ in the static limit and $\mathbf{C}(\mu_h)$ is the matching matrix which match the HQET operators with the QCD ones, both computed in $\overline{MS}$. It can be written as a power expansion

$$\mathbf{C}(\hat{\mu}_h) = 1 + \sum_n \mathbf{c}^{(n)}\left[\alpha(\hat{\mu}_h)/4\pi\right]^n$$

From Appendix C, we know that at next-to-leading log (NLL) the renormalization group evolution is given by[1]

$$\mathbf{W}(\mu,\mu_0) = \omega\left(\mu\right)\omega^{-1}\left(\mu_0\right) = \left[1+\frac{\alpha(\mu)}{4\pi}\mathbf{J}\right]\left[\frac{\alpha(\mu)}{\alpha(\mu_0)}\right]^{\frac{-\gamma^{(\mathbf{0})T}}{2\beta_0}}\left[1-\frac{\alpha(\mu_0)}{4\pi}\mathbf{J}\right] \tag{E.0.4}$$

One can proceed similarly for the bilinear operators appearing in the bag parameters definition. As we will see in detail in the following sections:

$$\begin{aligned}\langle \tilde{P}\left(\hat{\mu}_b^*\right)\rangle &= \left[c_P\left(\hat{\mu}_h\right)\tilde{W}_A^T\left(\hat{\mu}_h,\hat{\mu}_b^*\right)\right]^{-1}\langle A\rangle \\ \langle \tilde{P}\left(\hat{\mu}_b^*\right)\rangle &= \left[W_P^T\left(\hat{\mu}_h,\mu\right)c_A\left(\hat{\mu}_h\right)\tilde{W}_A^T\left(\hat{\mu}_h,\hat{\mu}_b^*\right)\right]^{-1}\langle P\left(\mu\right)\rangle\end{aligned} \tag{E.0.5}$$

E.1 QCD-HQET matching

The matching coefficient for the pseudoscalar and axial operators can be found by comparing the two-point amputated function with an insertion of a light-heavy current in QCD and HQET. At NLL the information in the $\overline{MS}$ scheme can be extracted from [155]

$$\begin{aligned}P\left(\mu\right) &= \left(1+\left(\frac{\alpha(\mu)}{4\pi}\right)\left[-2\log\left(\mu_h^2/\mu^2\right)+8/3\right]\right)\tilde{A}(\mu) \\ A &= \left(1+\left(\frac{\alpha(\mu)}{4\pi}\right)\left[2\log\left(\mu_h^2/\mu^2\right)-8/3\right]\right)\tilde{A}(\mu)\end{aligned}$$

from where the c_P and c_A coefficient for the matching at $\mu=\mu_h$ can be directly read

$$c_P^{(1)}\left(\hat{\mu}_h\right) = 8/3 \qquad c_A^{(1)}\left(\hat{\mu}_h\right) = -8/3$$

[1] Note the factor 2 before β_0 with respect to the definition in Eq.C.1.4. We introduce it in order to follow the notation in [155, 156, 131]

Let us now consider the $\Delta F = 2$ operators in the basis $\{O^V_{LL}, O^S_{LL}, O^V_{LR}, O^S_{LR}\}$ defined in equation 5.1 of [156]

$$\begin{aligned} O^V_{LL} &= \left[\bar{H}^a\gamma^\mu(1-\gamma_5)l^a\right]\left[\bar{H}^b\gamma_\mu(1-\gamma_5)l^b\right] \\ O^S_{LL} &= \left[\overline{H}^a(1-\gamma_5)l^a\right]\left[\overline{H}^b(1-\gamma_5)l^b\right] \\ O^V_{LR} &= \left[\overline{H}^a\gamma^\mu(1-\gamma_5)l^a\right]\left[\bar{H}^b\gamma_\mu(1+\gamma_5)l^b\right] \\ O^S_{LR} &= \left[\bar{H}^a(1-\gamma_5)l^a\right]\left[\bar{H}^b(1+\gamma_5)l^b\right] \end{aligned}$$

Rhe explicit expression for the matching coefficients from HQET to QCD is given in equations 6.1 and 6.5 of [156]. For reader convenience we collect here the explicit results for the Landau gauge-fixing parameter and in the regularization scheme $\overline{MS}$-NDR, which implies $z_{\rm QCD} = 1$, $x = 0$ and $z = 1$ in the formulae presented in [156]

$$\begin{aligned} C^{(1)}_{O^V_{LL}}(\mu) &= \{-14 + 6\log({\mu_h}^2/\mu^2), -8, 0, 0\} \\ C^{(1)}_{O^S_{LL}}(\mu) &= \{\frac{13}{8} - \log({\mu_h}^2/\mu^2), \frac{25}{3} - 4\log({\mu_h}^2/\mu^2), 0, 0\} \\ C^{(1)}_{O^{(F)S}_{LL}}(\mu) &= \{\frac{121}{24} - 4\log({\mu_h}^2/\mu^2), \frac{11}{3} - 4\log({\mu_h}^2/\mu^2), 0, 0\} \\ C^{(1)}_{O^V_{LR}}(\mu) &= \{0, 0, -\frac{21}{2} + \frac{9}{2}\log({\mu_h}^2/\mu^2), -7 + 3\log({\mu_h}^2/\mu^2)\} \\ C^{(1)}_{O^S_{LR}}(\mu) &= \{0, 0, \frac{11}{4} - \frac{3}{4}\log({\mu_h}^2/\mu^2), \frac{17}{2} - \frac{9}{2}\log({\mu_h}^2/\mu^2)\} \end{aligned} \tag{E.1.1}$$

where we also define $O^{(F)S}_{LL}$ as the Fierz transformed of O^S_{LL}. The previous operators are related with the supersymmetric basis as

$$\begin{aligned} &\tilde{Q}_1 = O^V_{LL} = -2\left(O^S_{LL} + O^{(F)S}_{LL}\right) \\ &\tilde{Q}_2 = O^S_{LL} \qquad\qquad \tilde{Q}_3 = O^{(F)S}_{LL} \\ &\tilde{Q}_4 = O^S_{LR} \qquad\qquad \tilde{Q}_5 = -\frac{O^V_{LR}}{2} \end{aligned} \tag{E.1.2}$$

By performing the change of basis defined by Eq.E.1.2 over the matching coefficients at LL in Eq.E.1.1 we can obtain the matching at $\mu = \mu_h$ for the operators $\{\tilde{Q}_i\}$

$$\mathbf{c}^{(1)}(\hat{\mu}_h) = \begin{pmatrix} -14 & -8 & 0 & 0 & 0 \\ 0 & 61/12 & -13/4 & 0 & 0 \\ 0 & -77/12 & -121/12 & 0 & 0 \\ 0 & 0 & 0 & 17/2 & -11/2 \\ 0 & 0 & 0 & 7/2 & -21/2 \end{pmatrix} \tag{E.1.3}$$

E.2 Renormalization evolution in HQET

The anomalous dimension in the static limit for all two fermion currents independently of the Dirac structure is [155]:

$$\tilde{\gamma}_A^{(0)} = -4 \qquad \tilde{\gamma}_A^{(1)} = \tilde{\gamma}_A^{(1)} = \frac{254}{9} + \frac{56}{27}\pi^2 - \frac{20}{9}N_f \tag{E.2.1}$$

from which we can construct

$$\tilde{J}_A = \frac{\tilde{\gamma}_A^{(0)}\beta_1}{2\beta_0^2} - \frac{\tilde{\gamma_A}^{(1)}}{2\beta_0} = 12\frac{153 - 19N_f}{(33 - 2N_f)^2} - \frac{1}{9}\frac{381 + 28\pi^2 - 30N_f}{33 - 2N_f}$$

with β_0 defined as in [155, 156, 131]: $\beta_0 = 11 - 2/3N_f$.

Dealing now with the $\Delta F = 2$ operators in the HQET basis $\{O_{LL}^V, O_{LL}^S, O_{LR}^V, O_{LR}^S\}$ the explicit formula of $\tilde{\gamma}^{(0)}$ is computed in [156]

$$\tilde{\gamma}_O^{(0)} = \begin{pmatrix} -8 & 0 & 0 & 0 \\ 4/3 & -8/3 & 0 & 0 \\ 0 & 0 & -7 & 6 \\ 0 & 0 & 3/2 & -7 \end{pmatrix}$$

But we are interested in the anomalous dimension matrix in the supersymmetric basis. Operators $\{\tilde{Q}_1, \tilde{Q}_2, \tilde{Q}_4, \tilde{Q}_5\}$ are related with $\{O_{LL}^V, O_{LL}^S, O_{LR}^V, O_{LR}^S\}$ through

$$\begin{array}{ll} O_{LL}^V = \tilde{Q}_1 & O_{LL}^S = \tilde{Q}_2 \\ O_{LR}^V = -2\tilde{Q}_5 & O_{LR}^S = \tilde{Q}_4 \end{array}$$

By performing the change of basis from $\{O_{LL}^V, O_{LL}^S, O_{LR}^V, O_{LR}^S\}$ to $\{\tilde{Q}_1, \tilde{Q}_2, \tilde{Q}_4, \tilde{Q}_5\}$ and adding the anomalous dimension of $\tilde{Q}_3$ through the dependence in Eq.E.0.2, we obtain $\tilde{\gamma}^{(0)}$ in the usual supersymmetric basis $\{\tilde{Q}_1, \tilde{Q}_2, \tilde{Q}_3, \tilde{Q}_4, \tilde{Q}_5\}$

$$\tilde{\gamma}^{(0)} = \begin{pmatrix} -8 & 0 & 0 & 0 & 0 \\ 0 & -16/3 & -8/3 & 0 & 0 \\ 0 & -8/3 & -16/3 & 0 & 0 \\ 0 & 0 & 0 & -7 & -3 \\ 0 & 0 & 0 & -3 & -7 \end{pmatrix} \tag{E.2.2}$$

Regarding now the anomalous dimension matrix at NLL, non-zero elements of J matrix in the HQET basis$\{O_{LL}^V, O_{LL}^S, O_{LR}^V, O_{LR}^S\}$ are given in equation 6.24 of [156] with $z_{\text{QCD}} = 1$, $x = 0$ and $z = 1$, which corresponds to the $\overline{MS}$ scheme we are interested. As we did for $\gamma^{(0)}$, we perform the change of basis between $\{O_{LL}^V, O_{LL}^S, O_{LR}^V, O_{LR}^S\}$ and $\{\tilde{Q}_1, \tilde{Q}_2, \tilde{Q}_4, \tilde{Q}_5\}$ having in mind that operators transform with $\tilde{\mathbf{J}}^T$. The operator $\tilde{Q}_3$ is added imposing the dependence in Eq.E.0.2. The non-zero elements of $\tilde{\mathbf{J}}$ in the supersymmetric basis are

$$
\begin{aligned}
\tilde{J}_{11} &= \frac{156N_f^2 - 4\left(75+34\pi^2\right)N_f + 3\left(748\pi^2-951\right)}{9(33-2N_f)^2} \\
\tilde{J}_{22} &= \frac{364N_f^2 - 148\left(4\pi^2-9\right)N_f + 9768\pi^2 - 28629}{36(33-2N_f)^2} \\
\tilde{J}_{23} &= \frac{260N_f^2 + 12\left(4\pi^2-211\right)N_f - 792\pi^2 + 17217}{36(33-2N_f)^2} \\
\tilde{J}_{32} &= \frac{284N_f^2 + 12\left(4\pi^2-277\right)N_f - 792\pi^2 + 23751}{36(33-2N_f)^2} \\
\tilde{J}_{33} &\quad \frac{340N_f^2 + \left(2124-592\pi^2\right)N_f + 9768\pi^2 - 35163}{36(33-2N_f)^2} \\
\tilde{J}_{44} &= \frac{174N_f^2 + \left(2169-296\pi^2\right)N_f + 4884\pi^2 - 22491}{18(33-2N_f)^2} \\
\tilde{J}_{45} &= \frac{66N_f^2 + \left(8\pi^2-925\right)N_f - 132\pi^2 + 5961}{6(33-2N_f)^2} \\
\tilde{J}_{54} &= \frac{66N_f^2 + \left(8\pi^2-925\right)N_f - 132\pi^2 + 5961}{6(33-2N_f)^2} \\
\tilde{J}_{55} &= \frac{174N_f^2 + \left(2169-296\pi^2\right)N_f + 4884\pi^2 - 22491}{18(33-2N_f)^2}
\end{aligned}
\tag{E.2.3}
$$

E.3 C-factor

The $\mathbf{C}\left(\hat{\mu}_b^*, \hat{\mu}_h^{(n)}, \mu\right)$ coefficient, as defined in Eq.6.3.1, at LL reads

$$
\mathbf{C}^{\mathrm{LL}}\left(\hat{\mu}_b^*, \hat{\mu}_h^{(n)}, \mu\right) = \xi^{-1}\left[\frac{\alpha\left(\hat{\mu}_b^*\right)}{\alpha\left(\hat{\mu}_h\right)}\right]^{\frac{\tilde{\gamma}_B^{(0)}}{2\beta_0}}\left[\frac{\alpha\left(\hat{\mu}_h\right)}{\alpha\left(\mu\right)}\right]^{\frac{\gamma_B^{(0)}}{2\beta_0}}\xi
$$

where $\xi = \mathrm{diag}\left\{8/3, -5/3, 1/3, 2, 2/3\right\}$ has been introduced because $\xi\vec{B}$ (and not $\vec{B}$) evolves as $\vec{Q}$. By construction

$$
\begin{aligned}
\left\{\tilde{\gamma}_B^{(0)}\right\}_{ij} &= \tilde{\gamma}_{ij}^{(0)} - 2\tilde{\gamma}_A^{(0)}\delta_{ij} \\
\left\{\gamma_B^{(0)}\right\}_{ij} &= \gamma_{ij}^{(0)} - 2\gamma_P^{(0)}\sum_{k=2}^{k=5}\delta_{ik}\delta_{jk}
\end{aligned}
$$

where $\tilde{\gamma}^{(0)}$ and $\gamma^{(0)}$ are the anomalous dimension matrix at one loop in HQET and QCD respectively of the complete basis of four fermion operator. Their numerical values can be found in Eq.E.2.2 and Eq.C.2.4[2] . $\tilde{\gamma}_A^{(0)}$ and $\gamma_P^{(0)}$ are the anomalous dimension at one loop of the bilinear operators in HQET and the pseudoscalar operator in QCD respectively which numerical values have been specified in Eq.E.2.1 and Eq.C.1.5[3].

At NLL the anomalous-dimension matrices at NLL and the matching between HQET and QCD are also involved. Using Eq.E.0.4 the evolution coefficient reads

$$\begin{aligned}\mathbf{C}^{\text{NLL}}\left(\hat{\mu}_b^*,\hat{\mu}_h^{(n)},\mu\right)=\xi^{-1}\quad&\left\{\left[1-\frac{\alpha\left(\hat{\mu}_b^*\right)}{4\pi}\tilde{\mathbf{J}}_B^T\right]\left[\frac{\alpha\left(\hat{\mu}_b^*\right)}{\alpha\left(\hat{\mu}_h\right)}\right]^{\frac{\tilde{\gamma}_B^{(0)}}{2\beta_0}}\left[1+\frac{\alpha\left(\hat{\mu}_h\right)}{4\pi}\tilde{\mathbf{J}}_B^T\right]\right.\\&\times\left[1-\mathbf{c}_B^{(1)}\frac{\alpha\left(\hat{\mu}_h\right)}{4\pi}\right]\\&\left.\times\left[1-\frac{\alpha\left(\hat{\mu}_h\right)}{4\pi}\mathbf{J}_B^T\right]\left[\frac{\alpha\left(\hat{\mu}_h\right)}{\alpha\left(\hat{\mu}\right)}\right]^{\frac{\gamma_B^{(0)}}{2\beta_0}}\left[1+\frac{\alpha\left(\hat{\mu}\right)}{4\pi}\mathbf{J}_B^T\right]\right\}\xi\end{aligned}$$

where $\mathbf{J}_B$, $\tilde{\mathbf{J}}_B$ and $\mathbf{c}_B^{(1)}$ are

$$\begin{aligned}\left\{\tilde{J}_B\right\}_{ij}=&\quad\tilde{J}_{ij}-2J_P\delta_{ij}\\\left\{J_B\right\}_{ij}=&\quad J_{ij}-2J_P\sum_{k=2}^{k=5}\delta_{ik}\delta_{jk}\\\left\{c_B^{(1)}\right\}_{ij}=&\quad c_{ij}^{(1)}-2c_A\delta_{i1}\delta_{j1}-2c_P\sum_{k=2}^{k=5}\delta_{ik}\delta_{jk}\end{aligned}$$

Here J_{ij} can be read from the $J_{\overline{MS}}$ in Eq.C.2.5[4] while $\tilde{J}_{ij}$ is collected in Eq.E.2.3.

[2]Note that in Eq.C.2.4 the one-loop anomalous dimension matrix is expressed in the lattice basis (LAT). Instead, here we are working in the supersymmetric basis (SUSY). The SUSY $\gamma^{(0)}$ we need to insert here is obtained from $\left\{\gamma^{(0)}\right\}_{\text{SUSY}}=R\left\{\gamma^{(0)}\right\}_{\text{LAT}}R^{-1}$, where R is defined in Eq.3.2.14.

[3]Note that for convenience in the matching formulae we are using the conventions in [131] where $\beta_0=11-2N_f/3$ instead of Eq.C.0.6 and $\bar{\gamma}_i^{(i)}=\gamma_\Gamma^{(i)}/2\beta_0$ instead of Eq.C.1.4. Therefore, using the conventions defined here, the value of $\gamma_P^{(0)}$ in Eq.C.1.5 reads $\gamma_P^{(0)}=-8$

[4]Following the notation in [131], here we are working directly in the supersymmetric basis. The J matrix in the supersymmetric basis (SUSY) is obtained from the one in the lattice basis (LAT) collected in Appendix C through $\left\{J^T\right\}_{\text{SUSY}}=R\left\{J^T\right\}_{\text{LAT}}R^{-1}$, where we have taken into account that operators transform with the J^T (see Eq.C.2.3)

Appendix F

$\mathbf{N_f = 2}$ Lattice data on masses and matrix elements

In this appendix I collect the tables for pseudoscalar meson masses, decay constants and bare bag parameters for each β and each couple of $(a\mu_\ell = a\mu_{sea}, a\mu_h)$ and $(a\mu_s, a\mu_h)$ relevant for the $N_f = 2$ analysis in the K, D and B sector.

F.1 Pseudoscalar meson masses

In tables from Table F.1.2 to Table F.1.7 I collect our results for the pseudoscalar TW meson mass computed from $C^{(2)}_{PP}(t)$ correlators with smeared-local (SL) source and sink, using Eq.3.1.13, and improved smeared-optimized (SL-SS) correlators. I collect results for heavy-light and heavy-strange mesons. In the case of heavy-strange to simplify tables we only consider the second of the simulated strange quark mass which have been previously fixed to be close to the physical strange. The error over each value has been evaluated using the jacknife method (see subsection 2.3.2). For some β's we have also compared our improved determination with the GEVP [157], obtaining consistent results. The time fit intervals are summarized in Table F.1.1.

The optimal value of ω is also reported in each case. The values of $\omega_{\rm opt}$ have been obtained by requiring that the optimized operator projects onto the ground state at earlier Euclidean time slices. In practice the algorithm to find $\omega_{\rm opt}$is:

1. Compute $\left[C^{(2)}_{PP}(t)\right]_{SL-SS}$ as

$$\left[C^{(2)}_{PP}(t)\right]_{SL-SS} = \omega \frac{\left[C^{(2)}_{PP}(t)\right]_{SL}}{\left[C^{(2)}_{PP}(t_0)\right]_{SL}} + (1-\omega)\frac{\left[C^{(2)}_{PP}(t)\right]_{SS}}{\left[C^{(2)}_{PP}(t_0)\right]_{SS}}$$

β	V	SL	SL-SS	$\omega_{\rm opt}$ search	t_0
3.80	$24^3 \times 48$	8:13	6:13	5:8 6:9 7:10 8:11 9:12	2
3.90	$24^3 \times 48$	12:16	9:16	8:11 9:12 10:13 11:14 12:15	4
	$32^3 \times 48$	12:20	10:20	8:11 9:12 10:13 11:14 12:15	4
4.05	$32^3 \times 48$	13:23	10:20	9:14 10:15 11:16 12:17 13:18 14:19	6
4.20	$32^3 \times 48$	20:30	15:25	10:16 11:17 12:18 13:19 14:20	7
	$48^3 \times 96$	20:30	15:25		7

Table F.1.1: Time fit intervals for SL and SL-SS correlators. The last columns contains the considered $t_{\rm min} : t_{\rm max}$ intervals in the $\omega_{\rm opt}$ algorithm and the value of the normalizing time t_0.

for a sequence of ω_i values. The normalization at t_0 is necessary in order to normalize the SL and SS correlators to quantities of the same order. The values of t_0 are collected in Table F.1.1 and they have been chosen in order to have as monotonal values of $\omega_{\rm opt}$ as possible.

2. For each ω_i we compute the effective mass $M_{PS}(t)$ using Eq.3.1.13. By performing a fit for several choices of early and short time intervals $[t_{\rm min}, t_{\rm max}]_j$, collected in Table F.1.1,we obtain different estimators of M_{PS}.

3. The quasi-optimal value of ω_i is the one for which the condition $\mathrm{MAX}\{M_{PS}\} \simeq \mathrm{MIN}\{M_{PS}\}$ between the estimator obtained at different $[t_{\rm min}, t_{\rm max}]_j$ is better fulfilled.

Finally, in order to avoid a monotonic behavior in the values of M_{PS} implying that the plateau is still not achieved, we also require that at least one oscillation is found between the several choices of $[t_{\rm min}, t_{\rm max}]_j$. That is, we require that for the $\omega_{\rm opt}$ value exist at least one $[t_{\rm min}, t_{\rm max}]_j$ for which

$$M_{PS}\left([t_{\rm min}, t_{\rm max}]_{j-1}\right) < M_{PS}\left([t_{\rm min}, t_{\rm max}]_{j}\right) < M_{PS}\left([t_{\rm min}, t_{\rm max}]_{j+1}\right)$$

or

$$M_{PS}\left([t_{\rm min}, t_{\rm max}]_{j-1}\right) > M_{PS}\left([t_{\rm min}, t_{\rm max}]_{j}\right) > M_{PS}\left([t_{\rm min}, t_{\rm max}]_{j+1}\right)$$

β=3.80 $L^3 \times T = 24^3 \times 48$					
			SL	SL-SS	
μ_{sea}	μ_1	μ_2	M	ω	M
0.0080	0.0080	0.1982	0.7714(11)	1.28	0.7715(9)
		0.2331	0.8432(12)	1.08	0.8432(9)
		0.2742	0.9235(13)	0.92	0.9236(10)
		0.3225	1.0133(14)	0.79	1.0135(11)
		0.3793	1.1135(16)	0.70	1.1139(12)
		0.4461	1.2253(17)	0.64	1.2260(13)
		0.5246	1.3493(19)	0.61	1.3504(13)
		0.6170	1.4864(20)	0.62	1.4876(15)
		0.7257	1.6363(25)	0.67	1.6371(18)
		0.8536	1.7981(40)	0.82	1.7964(21)
0.0110	0.0110	0.1982	0.7778(8)	0.89	0.7780(7)
		0.2331	0.8493(9)	0.74	0.8496(7)
		0.2742	0.9294(10)	0.66	0.9297(8)
		0.3225	1.0189(11)	0.60	1.0194(9)
		0.3793	1.1188(13)	0.56	1.1197(10)
		0.4461	1.2300(15)	0.52	1.2318(12)
		0.5246	1.3534(19)	0.51	1.3562(15)
		0.6170	1.4896(24)	0.52	1.4935(18)
		0.7257	1.6386(33)	0.58	1.6430(23)
		0.8536	1.8003(49)	0.66	1.8045(31)

(a)

β=3.80 $L^3 \times T = 24^3 \times 48$					
			SL	SL-SS	
μ_{sea}	μ_1	μ_2	M	ω	M
0.0080	0.0194	0.1982	0.7982(8)	0.96	0.7982(6)
		0.2331	0.8689(8)	0.81	0.8690(7)
		0.2742	0.9483(9)	0.71	0.9486(8)
		0.3225	1.0371(9)	0.63	1.0377(8)
		0.3793	1.1364(10)	0.56	1.1375(9)
		0.4461	1.2473(11)	0.50	1.2491(11)
		0.5246	1.3704(12)	0.46	1.3732(12)
		0.6170	1.5063(14)	0.44	1.5104(14)
		0.7257	1.6552(18)	0.52	1.6587(18)
		0.8536	1.8159(29)	0.65	1.8169(21)
0.0110	0.0194	0.1982	0.7978(6)	0.64	0.7981(6)
		0.2331	0.8687(6)	0.55	0.8691(6)
		0.2742	0.9481(7)	0.50	0.9488(7)
		0.3225	1.0371(8)	0.45	1.0380(7)
		0.3793	1.1365(9)	0.42	1.1379(9)
		0.4461	1.2472(11)	0.40	1.2496(10)
		0.5246	1.3701(13)	0.39	1.3738(13)
		0.6170	1.5058(17)	0.42	1.5106(16)
		0.7257	1.6541(24)	0.47	1.6599(20)
		0.8536	1.8149(35)	0.55	1.8208(27)

(b)

Table F.1.2: Heavy-light (a) and heavy-strange (b) meson masses with SL and SL-SS correlators at $\beta = 3.80$ and $L^3 \times T = 24^3 \times 48$

β=3.90 $L^3 \times T = 32^3 \times 64$					
			SL	SL-SS	
μ_{sea}	μ_1	μ_2	M	ω	M
0.0030	0.0030	0.1828	0.6675(16)	1.00	0.6711(10)
		0.2150	0.7323(19)	1.00	0.7366(11)
		0.2529	0.8050(23)	1.00	0.8100(13)
		0.2974	0.8865(27)	1.00	0.8923(16)
		0.3498	0.9780(33)	2.72	0.9860(23)
		0.4114	1.0808(39)	1.92	1.0895(23)
		0.4839	1.1964(47)	1.47	1.2054(28)
		0.5691	1.3262(59)	1.18	1.3349(33)
		0.6694	1.4735(80)	1.08	1.4787(36)
		0.7873	1.6440(140)	1.10	1.6355(46)
0.0040	0.0040	0.1828	0.6737(8)	0.43	0.6746(6)
		0.2150	0.7393(10)	0.41	0.7402(7)
		0.2529	0.8130(12)	0.38	0.8138(10)
		0.2974	0.8956(15)	0.31	0.8963(12)
		0.3498	0.9884(18)	0.43	0.9886(16)
		0.4114	1.0924(23)	1.67	1.0906(25)
		0.4839	1.2085(29)	1.31	1.2073(27)
		0.5691	1.3367(38)	1.78	1.3333(39)
		0.6694	1.4757(60)	1.83	1.4737(54)
		0.7873	1.6222(118)	1.58	1.6298(90)

(a)

β=3.90 $L^3 \times T = 32^3 \times 64$					
			SL	SL-SS	
μ_{sea}	μ_1	μ_2	M	ω	M
0.0030	0.0177	0.1828	0.7040(5)	1.00	0.7053(4)
		0.2150	0.7681(5)	1.00	0.7695(4)
		0.2529	0.8403(5)	2.27	0.8417(6)
		0.2974	0.9214(6)	1.60	0.9228(5)
		0.3498	1.0127(6)	1.50	1.0142(6)
		0.4114	1.1151(8)	1.12	1.1168(7)
		0.4839	1.2298(11)	0.92	1.2318(9)
		0.5691	1.3579(16)	0.84	1.3603(12)
		0.6694	1.5007(30)	0.80	1.5032(15)
		0.7873	1.6576(57)	0.78	1.6601(20)
0.0040	0.0177	0.1828	0.7067(5)	1.00	0.7068(5)
		0.2150	0.7712(6)	0.62	0.7714(5)
		0.2529	0.8438(6)	0.71	0.8439(5)
		0.2974	0.9253(6)	0.82	0.9252(6)
		0.3498	1.0171(7)	1.03	1.0169(7)
		0.4114	1.1202(8)	0.89	1.1198(8)
		0.4839	1.2357(10)	0.80	1.2352(9)
		0.5691	1.3643(14)	0.64	1.3641(13)
		0.6694	1.5069(23)	0.59	1.5073(22)
		0.7873	1.6634(49)	0.58	1.6649(43)

(b)

Table F.1.3: Heavy-light (a) and heavy-strange (b) meson masses with SL and SL-SS correlators at $\beta = 3.90$ and $L^3 \times T = 32^3 \times 64$

β=3.90 $L^3 \times T = 24^3 \times 48$					
			SL	SL-SS	
μ_{sea}	μ_1	μ_2	M	ω	M
0.0040	0.0040	0.1828	0.6769(15)	0.72	0.6765(11)
		0.2150	0.7420(18)	0.69	0.7417(11)
		0.2529	0.8152(20)	0.68	0.8150(12)
		0.2974	0.8972(23)	0.69	0.8971(13)
		0.3498	0.9894(27)	0.73	0.9896(14)
		0.4114	1.0931(31)	1.17	1.0937(13)
		0.4839	1.2096(38)	1.05	1.2098(16)
		0.5691	1.3405(48)	1.14	1.3400(19)
		0.6694	1.4888(66)	1.20	1.4856(26)
		0.7873	1.6605(121)	2.20	1.6445(53)
0.0064	0.0064	0.1828	0.6791(13)	0.19	0.6800(10)
		0.2150	0.7442(13)	0.18	0.7452(11)
		0.2529	0.8173(14)	0.21	0.8185(11)
		0.2974	0.8993(15)	0.30	0.9006(12)
		0.3498	0.9916(16)	0.45	0.9929(13)
		0.4114	1.0952(19)	0.64	1.0963(13)
		0.4839	1.2116(22)	0.86	1.2124(16)
		0.5691	1.3419(29)	0.93	1.3424(21)
		0.6694	1.4863(42)	0.84	1.4878(30)
		0.7873	1.6427(75)	0.79	1.6499(50)
0.0085	0.0085	0.1828	0.6851(10)	0.68	0.6864(9)
		0.2150	0.7502(10)	0.75	0.7514(9)
		0.2529	0.8233(11)	1.30	0.8245(11)
		0.2974	0.9054(11)	1.21	0.9064(12)
		0.3498	0.9979(13)	1.09	0.9986(12)
		0.4114	1.1017(15)	0.97	1.1022(13)
		0.4839	1.2181(20)	1.00	1.2181(15)
		0.5691	1.3475(28)	0.97	1.3474(16)
		0.6694	1.4906(49)	1.01	1.4908(18)
		0.7873	1.6462(98)	1.03	1.6490(23)
0.0100	0.0100	0.1828	0.6891(9)	0.21	0.6901(8)
		0.2150	0.7543(9)	0.39	0.7553(8)
		0.2529	0.8277(10)	0.57	0.8285(7)
		0.2974	0.9101(10)	0.78	0.9106(7)
		0.3498	1.0028(12)	1.09	1.0027(7)
		0.4114	1.1071(14)	1.28	1.1061(8)
		0.4839	1.2241(18)	1.56	1.2215(10)
		0.5691	1.3551(27)	1.58	1.3504(13)
		0.6694	1.5012(47)	0.32	1.5026(21)
		0.7873	1.6632(100)	0.35	1.6650(38)

(a)

β=3.90 $L^3 \times T = 24^3 \times 48$					
			SL	SL-SS	
μ_{sea}	μ_1	μ_2	M	ω	M
0.0040	0.0177	0.1828	0.7070(7)	1.28	0.7070(6)
		0.2150	0.7712(7)	1.26	0.7713(6)
		0.2529	0.8435(8)	1.25	0.8435(6)
		0.2974	0.9247(9)	1.26	0.9247(6)
		0.3498	1.0162(10)	1.32	1.0161(7)
		0.4114	1.1191(11)	1.25	1.1188(7)
		0.4839	1.2347(14)	1.25	1.2339(8)
		0.5691	1.3643(18)	1.27	1.3625(9)
		0.6694	1.5096(26)	1.38	1.5052(10)
		0.7873	1.6706(52)	0.56	1.6691(30)
0.0064	0.0177	0.1828	0.7056(9)	0.12	0.7064(8)
		0.2150	0.7698(10)	0.09	0.7708(8)
		0.2529	0.8422(10)	0.27	0.8432(8)
		0.2974	0.9234(11)	0.60	0.9242(8)
		0.3498	1.0149(12)	0.86	1.0154(9)
		0.4114	1.1177(13)	1.15	1.1175(10)
		0.4839	1.2331(15)	1.07	1.2329(11)
		0.5691	1.3622(18)	1.07	1.3616(12)
		0.6694	1.5052(24)	1.04	1.5050(16)
		0.7873	1.6608(40)	0.85	1.6651(26)
0.0085	0.0177	0.1828	0.7064(8)	1.55	0.7075(8)
		0.2150	0.7707(8)	1.67	0.7718(9)
		0.2529	0.8430(8)	1.68	0.8439(9)
		0.2974	0.9243(8)	1.65	0.9249(10)
		0.3498	1.0160(9)	1.57	1.0161(10)
		0.4114	1.1190(10)	1.29	1.1190(10)
		0.4839	1.2345(12)	1.02	1.2346(11)
		0.5691	1.3633(17)	0.95	1.3633(12)
		0.6694	1.5058(30)	1.00	1.5058(14)
		0.7873	1.6616(59)	1.04	1.6629(16)
0.0100	0.0177	0.1828	0.7064(8)	1.00	0.7073(4)
		0.2150	0.7709(8)	0.14	0.7717(7)
		0.2529	0.8435(8)	0.29	0.8443(7)
		0.2974	0.9251(8)	0.77	0.9256(5)
		0.3498	1.0171(9)	1.09	1.0170(5)
		0.4114	1.1205(10)	1.43	1.1194(6)
		0.4839	1.2366(12)	1.62	1.2341(8)
		0.5691	1.3664(17)	0.39	1.3677(11)
		0.6694	1.5111(30)	0.38	1.5129(16)
		0.7873	1.6718(64)	0.43	1.6734(26)

(b)

Table F.1.4: Heavy-light (a) and heavy-strange (b) meson masses with SL and SL-SS correlators at $\beta = 3.90$ and $L^3 \times T = 24^3 \times 48$

β=4.05 $L^3 \times T = 32^3 \times 64$					
			SL	SL-SS	
μ_{sea}	μ_1	μ_2	M	ω	M
0.0030	0.0030	0.1572	0.5538(16)	-0.72	0.5535(15)
		0.1849	0.6089(18)	-0.73	0.6084(16)
		0.2175	0.6708(19)	-0.76	0.6702(17)
		0.2558	0.7405(20)	-0.81	0.7398(19)
		0.3008	0.8190(22)	-0.89	0.8182(21)
		0.3538	0.9077(24)	-1.06	0.9066(24)
		0.4162	1.0078(25)	-1.47	1.0061(30)
		0.4895	1.1206(26)	-0.59	1.1211(28)
		0.5757	1.2474(27)	-0.96	1.2478(38)
		0.6771	1.3904(41)	-0.66	1.3927(46)
0.0060	0.0060	0.1572	0.5622(8)	-1.59	0.5606(7)
		0.1849	0.6172(8)	-1.39	0.6158(8)
		0.2175	0.6793(8)	-1.19	0.6781(9)
		0.2558	0.7492(8)	-1.05	0.7481(9)
		0.3008	0.8282(8)	-0.70	0.8275(9)
		0.3538	0.9176(9)	-0.27	0.9172(9)
		0.4162	1.0186(10)	0.18	1.0185(8)
		0.4895	1.1323(13)	0.58	1.1321(8)
		0.5757	1.2604(21)	1.00	1.2593(8)
		0.6771	1.4040(38)	1.00	1.4014(10)
0.0080	0.0080	0.1572	0.5658(12)	-0.69	0.5655(12)
		0.1849	0.6208(11)	-0.39	0.6205(12)
		0.2175	0.6829(11)	-0.39	0.6821(13)
		0.2558	0.7529(11)	-0.41	0.7514(14)
		0.3008	0.8317(10)	-0.43	0.8296(15)
		0.3538	0.9206(11)	-0.43	0.9181(17)
		0.4162	1.0207(13)	-0.54	1.0179(20)
		0.4895	1.1330(18)	-0.63	1.1305(24)
		0.5757	1.2587(28)	0.30	1.2598(18)
		0.6771	1.3992(45)	0.66	1.4039(15)

(a)

β=4.05 $L^3 \times T = 32^3 \times 64$					
			SL	SL-SS	
μ_{sea}	μ_1	μ_2	M	ω	M
0.0030	0.0154	0.1572	0.5807(10)	-0.55	0.5805(7)
		0.1849	0.6348(10)	-0.53	0.6346(7)
		0.2175	0.6959(11)	-0.51	0.6957(8)
		0.2558	0.7648(11)	-0.51	0.7646(8)
		0.3008	0.8427(12)	-0.51	0.8424(9)
		0.3538	0.9310(13)	-0.49	0.9305(10)
		0.4162	1.0308(13)	-0.04	1.0311(10)
		0.4895	1.1434(14)	-0.11	1.1434(11)
		0.5757	1.2703(16)	-0.31	1.2694(13)
		0.6771	1.4129(22)	0.52	1.4137(13)
0.0060	0.0154	0.1572	0.5827(5)	-1.24	0.5815(4)
		0.1849	0.6370(5)	-1.13	0.6358(5)
		0.2175	0.6984(5)	-1.01	0.6973(5)
		0.2558	0.7677(6)	-0.88	0.7667(5)
		0.3008	0.8460(6)	-0.77	0.8451(6)
		0.3538	0.9348(7)	-0.59	0.9340(6)
		0.4162	1.0352(8)	-0.12	1.0348(6)
		0.4895	1.1483(10)	0.45	1.1480(6)
		0.5757	1.2756(12)	1.00	1.2747(6)
		0.6771	1.4182(18)	1.00	1.4162(7)
0.0080	0.0154	0.1572	0.5810(9)	-0.70	0.5811(9)
		0.1849	0.6353(9)	-0.70	0.6352(9)
		0.2175	0.6966(8)	-0.74	0.6961(10)
		0.2558	0.7658(8)	-0.66	0.7651(10)
		0.3008	0.8439(8)	-0.55	0.8431(11)
		0.3538	0.9322(9)	-0.56	0.9311(13)
		0.4162	1.0319(10)	-0.66	1.0305(15)
		0.4895	1.1439(12)	-0.99	1.1421(20)
		0.5757	1.2697(17)	0.15	1.2708(15)
		0.6771	1.4102(28)	0.52	1.4141(13)

(b)

Table F.1.5: Heavy-light (a) and heavy-strange (b) meson masses with SL and SL-SS correlators at $\beta = 4.05$ and $L^3 \times T = 32^3 \times 64$

β=4.20 $L^3 \times T = 32^3 \times 64$					
			SL	SL-SS	
μ_{sea}	μ_1	μ_2	M	ω	M
0.0065	0.0065	0.13315	0.4628(10)	-1.42	0.4621(8)
		0.1566	0.5079(11)	-1.40	0.5071(9)
		0.1842	0.5590(12)	-1.39	0.5580(10)
		0.2166	0.6166(13)	-1.39	0.6155(11)
		0.2548	0.6821(14)	-1.40	0.6808(12)
		0.2997	0.7564(16)	-1.44	0.7548(14)
		0.3525	0.8407(17)	-1.51	0.8390(17)
		0.4145	0.9363(19)	-1.62	0.9346(20)
		0.4876	1.0449(23)	-1.82	1.0433(26)
		0.5734	1.1678(33)	-2.10	1.1649(41)

(a)

β=4.20 $L^3 \times T = 32^3 \times 64$					
			SL	SL-SS	
μ_{sea}	μ_1	μ_2	M	ω	M
0.0065	0.0129	0.13315	0.4769(8)	-1.24	0.4763(7)
		0.1566	0.5219(9)	-1.21	0.5212(7)
		0.1842	0.5728(9)	-1.18	0.5721(8)
		0.2166	0.6304(10)	-1.16	0.6296(8)
		0.2548	0.6959(10)	-1.15	0.6951(9)
		0.2997	0.7703(11)	-1.16	0.7693(10)
		0.3525	0.8548(12)	-1.19	0.8536(11)
		0.4145	0.9504(14)	-1.26	0.9491(12)
		0.4876	1.0590(16)	-1.39	1.0577(15)
		0.5734	1.1817(22)	-1.57	1.1802(25)

(b)

Table F.1.6: Heavy-light (a) and heavy-strange (b) meson masses with SL and SL-SS correlators at $\beta = 4.20$ and $L^3 \times T = 32^3 \times 64$

β=4.20 $L^3 \times T = 48^3 \times 96$					
			SL	SL-SS	
μ_{sea}	μ_1	μ_2	M	ω	M
0.0020	0.0020	0.13315	0.4524(12)	-2.07	0.4517(11)
		0.1566	0.4982(13)	-1.96	0.4973(13)
		0.1842	0.5499(15)	-1.86	0.5488(15)
		0.2166	0.6082(16)	-1.78	0.6067(17)
		0.2548	0.6743(18)	-1.71	0.6724(19)
		0.2997	0.7490(20)	-1.67	0.7467(21)
		0.3525	0.8336(24)	-1.67	0.8308(23)
		0.4145	0.9293(28)	-1.71	0.9260(25)
		0.4876	1.0378(36)	-1.82	1.0341(31)
		0.5734	1.1602(48)	-2.04	1.1555(43)

(a)

β=4.20 $L^3 \times T = 48^3 \times 96$					
			SL	SL-SS	
μ_{sea}	μ_1	μ_2	M	ω	M
0.0020	0.0129	0.13315	0.4760(4)	-1.61	0.4754(5)
		0.1566	0.5212(5)	-1.54	0.5204(5)
		0.1842	0.5723(5)	-1.47	0.5713(6)
		0.2166	0.6301(5)	-1.41	0.6289(6)
		0.2548	0.6959(5)	-1.36	0.6943(7)
		0.2997	0.7704(6)	-1.32	0.7685(7)
		0.3525	0.8551(7)	-1.31	0.8527(8)
		0.4145	0.9510(8)	-1.31	0.9480(9)
		0.4876	1.0600(10)	-1.34	1.0562(10)
		0.5734	1.1832(14)	-1.39	1.1786(13)

(b)

Table F.1.7: Heavy-light (a) and heavy-strange (b) meson masses with SL and SL-SS correlators at $\beta = 4.20$ and $L^3 \times T = 48^3 \times 96$

F.2 Pseudoscalar decay constants

Pseudoscalar decay constants are computed from the WI definition

$$f = \frac{(\mu_1 + \mu_2)}{M_{PS} \sinh M_{PS}} \langle 0 | P_5^\dagger | M \rangle$$

with TM correlators, which not require renormalization as shown in subsection 3.3.2. Here, the $\sinh M_{PS}$ have been introduced in order to take into account finite size effects.

The matrix element of the local pseudoscalar correlator appears explicitly in $C^{(2)}_{PP}(t)$, see Eq.3.1.10. Therefore, the pseudoscalar decay constant can be obtained from

$$f(t) = (\mu_1 + \mu_2) \sqrt{\frac{e^{M_{PS} T/2}}{M_{PS}^2 \sinh(M_{PS})}} \frac{1}{\sqrt{\cosh\left[M_{PS}\left(\frac{T}{2} - t\right)\right]}} \sqrt{\left[C^{(2)}_{PP}(t)\right]_{LL}}$$

introducing the previous determined value of M_{PS} through the effective mass equation and performing a fit for $0 \ll t \ll T$.

Using smearing correlators one can extract the signal at earlier time-slices. With smearing sources the previous equation reads

$$f(t) = (\mu_1 + \mu_2) \sqrt{\frac{e^{M_{PS} T/2}}{M_{PS}^2 \sinh(M_{PS})}} \frac{1}{\sqrt{\cosh\left[M_{PS}\left(\frac{T}{2} - t\right)\right]}} \frac{\sqrt{\left[C^{(2)}_{PP}(t)\right]_{SL}}}{\left[C^{(2)}_{PP}(t)\right]_{SS}} \tag{F.2.1}$$

And finally, with improved interpolating operators

β	V	$[t_{\min}, t_{\max}]$
3.80	$24^3 \times 48$	8:16
3.90	$24^3 \times 48$	12:20
	$32^3 \times 48$	12:20
4.05	$32^3 \times 48$	12:20
4.20	$32^3 \times 48$	15:25
	$48^3 \times 96$	15:25

Table F.2.1: Time fit intervals for $f(t)$.

$$f(t) = (\mu_1 + \mu_2)\sqrt{\frac{e^{M_{PS}T/2}}{M_{PS}^2 \sinh(M_{PS})}}\frac{1}{\sqrt{\cosh\left[M_{PS}\left(\frac{T}{2} - t\right)\right]}}\frac{\sqrt{\left[C_{PP}^{(2)}(t)\right]_{\omega L}}}{\left[C_{PP}^{(2)}(t)\right]_{\omega\omega}} \tag{F.2.2}$$

where we have defined the ωL, or SL-LL, optimized correlator as

$$\left[C_{PP}^{(2)}(t)\right]_{\omega L} = \omega\frac{\left[C_{PP}^{(2)}(t)\right]_{SL}}{\left[C_{PP}^{(2)}(t_0)\right]_{SL}} + (1-\omega)\frac{\left[C_{PP}^{(2)}(t)\right]_{LL}}{\left[C_{PP}^{(2)}(t_0)\right]_{LL}} \tag{F.2.3}$$

and the double-optimized correlator[1]

$$\left[C_{PP}^{(2)}(t)\right]_{\omega\omega} = \omega_1\omega_1\left[C_{PP}^{(2)}(t)\right]_{SS} + \omega_1\omega_2\left(\left[C_{PP}^{(2)}(t)\right]_{SL} + \left[C_{PP}^{(2)}(t)\right]_{LS}\right) + \omega_2\omega_2\left[C_{PP}^{(2)}(t)\right]_{LL}$$

with

$$\omega_1 = \frac{\omega'_{\text{opt}}}{\left[C_{PP}^{(2)}(t_0)\right]_{SL}} \qquad \omega_2 = \frac{\omega'_{\text{opt}}}{\left[C_{PP}^{(2)}(t_0)\right]_{LL}}$$

Here ω'_{opt} is by construction the value of ω optimizing SL-LL correlators in Eq.F.2.3.

Our estimates for the pseudoscalar decay constant are collected in tables from Table F.2.2 to Table F.2.7. The time fit intervals are indicated in Table F.2.1.

[1] coming from $\left[C^{(2)}\right]_{\omega\omega} \sim \langle\phi_\omega\phi_L\rangle + \langle\phi_L\phi_\omega\rangle$

β=3.80 $L^3 \times T = 24^3 \times 48$				
μ_{sea}	μ_1	μ_2	ω'	f
0.0080	0.0080	0.1982	1.08	0.1246(8)
		0.2331	1.02	0.1273(8)
		0.2742	0.97	0.1299(7)
		0.3225	0.93	0.1325(8)
		0.3793	0.88	0.1350(8)
		0.4461	0.85	0.1375(8)
		0.5246	0.82	0.1399(10)
		0.6170	0.80	0.1421(12)
		0.7257	0.81	0.1437(15)
		0.8536	0.87	0.1430(17)
0.0110	0.0110	0.1982	0.99	0.1278(10)
		0.2331	0.95	0.1306(10)
		0.2742	0.92	0.1332(11)
		0.3225	0.88	0.1359(11)
		0.3793	0.85	0.1385(11)
		0.4461	0.83	0.1411(12)
		0.5246	0.80	0.1438(12)
		0.6170	0.79	0.1465(13)
		0.7257	0.78	0.1488(13)
		0.8536	0.79	0.1512(15)

(a)

β=3.80 $L^3 \times T = 24^3 \times 48$				
μ_{sea}	μ_1	μ_2	ω'	f
0.0080	0.0194	0.1982	0.99	0.1326(8)
		0.2331	0.94	0.1357(8)
		0.2742	0.90	0.1388(8)
		0.3225	0.86	0.1419(8)
		0.3793	0.82	0.1450(8)
		0.4461	0.78	0.1484(9)
		0.5246	0.75	0.1519(10)
		0.6170	0.73	0.1556(14)
		0.7257	0.71	0.1585(17)
		0.8536	0.73	0.1601(19)
0.0110	0.0194	0.1982	0.93	0.1334(10)
		0.2331	0.90	0.1365(10)
		0.2742	0.86	0.1396(11)
		0.3225	0.83	0.1427(11)
		0.3793	0.80	0.1459(11)
		0.4461	0.77	0.1492(12)
		0.5246	0.74	0.1527(13)
		0.6170	0.73	0.1561(14)
		0.7257	0.71	0.1596(14)
		0.8536	0.71	0.1634(15)

(b)

Table F.2.2: Heavy-light (a) and heavy-strange (b) pseudoscalar decay constant at $\beta = 3.80$ and $L^3 \times T = 24^3 \times 48$ obtained from Eq.F.2.2. The value of ω'_{opt} is also reported.

β=3.90 $L^3 \times T = 32^3 \times 64$			
μ_{sea}	μ_1	μ_2	f
0.0030	0.0030	0.1828	0.1001(6)
		0.2150	0.1021(7)
		0.2529	0.1039(7)
		0.2974	0.1055(8)
		0.3498	0.1074(9)
		0.4114	0.1085(8)
		0.4839	0.1092(11)
		0.5691	0.1098(14)
		0.6694	0.1105(17)
		0.7873	0.1112(21)
0.0040	0.0040	0.1828	0.1020(6)
		0.2150	0.1041(6)
		0.2529	0.1060(6)
		0.2974	0.1078(7)
		0.3498	0.1092(7)
		0.4114	0.1093(8)
		0.4839	0.1107(9)
		0.5691	0.1092(14)
		0.6694	0.1076(21)
		0.7873	0.1059(35)

(a)

β=3.90 $L^3 \times T = 32^3 \times 64$			
μ_{sea}	μ_1	μ_2	f
0.0030	0.0177	0.1828	0.1105(6)
		0.2150	0.1128(6)
		0.2529	0.1150(6)
		0.2974	0.1170(6)
		0.3498	0.1187(6)
		0.4114	0.1203(7)
		0.4839	0.1217(8)
		0.5691	0.1231(10)
		0.6694	0.1244(12)
		0.7873	0.1257(17)
0.0040	0.0177	0.1828	0.1115(5)
		0.2150	0.1141(6)
		0.2529	0.1164(6)
		0.2974	0.1185(6)
		0.3498	0.1204(5)
		0.4114	0.1223(6)
		0.4839	0.1240(8)
		0.5691	0.1258(12)
		0.6694	0.1277(20)
		0.7873	0.1295(40)

(b)

Table F.2.3: Heavy-light (a) and heavy-strange (b) pseudoscalar decay constant at $\beta = 3.90$ and $L^3 \times T = 32^3 \times 64$ obtained from Eq.F.2.1.

β=3.90 $L^3 \times T = 24^3 \times 48$			
μ_{sea}	μ_1	μ_2	f
0.0040	0.0040	0.1828	0.1025(8)
		0.2150	0.1043(9)
		0.2529	0.1059(9)
		0.2974	0.1074(10)
		0.3498	0.1086(11)
		0.4114	0.1100(10)
		0.4839	0.1106(12)
		0.5691	0.1114(12)
		0.6694	0.1124(15)
		0.7873	0.1124(23)
0.0064	0.0064	0.1828	0.1045(7)
		0.2150	0.1067(7)
		0.2529	0.1087(8)
		0.2974	0.1105(8)
		0.3498	0.1120(8)
		0.4114	0.1133(9)
		0.4839	0.1145(10)
		0.5691	0.1160(11)
		0.6694	0.1186(14)
		0.7873	0.1221(28)
0.0085	0.0085	0.1828	0.1065(6)
		0.2150	0.1086(6)
		0.2529	0.1106(6)
		0.2974	0.1124(6)
		0.3498	0.1142(7)
		0.4114	0.1158(9)
		0.4839	0.1171(13)
		0.5691	0.1181(21)
		0.6694	0.1184(37)
		0.7873	0.1174(71)
0.0100	0.0100	0.1828	0.1083(9)
		0.2150	0.1106(9)
		0.2529	0.1127(9)
		0.2974	0.1146(9)
		0.3498	0.1162(8)
		0.4114	0.1177(8)
		0.4839	0.1186(9)
		0.5691	0.1196(10)
		0.6694	0.1267(16)
		0.7873	0.1306(30)

(a)

β=3.90 $L^3 \times T = 24^3 \times 48$			
μ_{sea}	μ_1	μ_2	f
0.0040	0.0177	0.1828	0.1127(6)
		0.2150	0.1150(7)
		0.2529	0.1171(7)
		0.2974	0.1191(7)
		0.3498	0.1209(7)
		0.4114	0.1225(7)
		0.4839	0.1239(7)
		0.5691	0.1252(8)
		0.6694	0.1266(9)
		0.7873	0.1328(28)
0.0064	0.0177	0.1828	0.1122(7)
		0.2150	0.1147(7)
		0.2529	0.1169(7)
		0.2974	0.1189(7)
		0.3498	0.1205(7)
		0.4114	0.1218(7)
		0.4839	0.1234(7)
		0.5691	0.1249(8)
		0.6694	0.1270(9)
		0.7873	0.1309(16)
0.0085	0.0177	0.1828	0.1123(6)
		0.2150	0.1146(6)
		0.2529	0.1168(6)
		0.2974	0.1189(6)
		0.3498	0.1209(7)
		0.4114	0.1227(7)
		0.4839	0.1245(9)
		0.5691	0.1260(13)
		0.6694	0.1272(23)
		0.7873	0.1277(46)
0.0100	0.0177	0.1828	0.1129(7)
		0.2150	0.1152(10)
		0.2529	0.1176(10)
		0.2974	0.1196(9)
		0.3498	0.1214(8)
		0.4114	0.1228(8)
		0.4839	0.1239(8)
		0.5691	0.1292(12)
		0.6694	0.1323(14)
		0.7873	0.1360(25)

(b)

Table F.2.4: Heavy-light (a) and heavy-strange (b) pseudoscalar decay constant at $\beta = 3.90$ and $L^3 \times T = 24^3 \times 48$ obtained from Eq.F.2.1.

β=4.05 $L^3 \times T = 32^3 \times 64$				
μ_{sea}	μ_1	μ_2	ω'	f
0.0030	0.0030	0.1572	1.63	0.0800(16)
		0.1849	1.62	0.0814(16)
		0.2175	1.60	0.0826(16)
		0.2558	1.59	0.0835(17)
		0.3008	1.59	0.0841(17)
		0.3538	1.62	0.0843(18)
		0.4162	1.69	0.0839(21)
		0.4895	1.86	0.0845(20)
		0.5757	1.00	0.0851(22)
		0.6771	1.00	0.0863(27)
0.0060	0.0060	0.1572	1.00	0.0845(6)
		0.1849	1.00	0.0861(6)
		0.2175	1.00	0.0876(6)
		0.2558	1.82	0.0889(7)
		0.3008	1.62	0.0901(7)
		0.3538	1.44	0.0911(8)
		0.4162	1.28	0.0919(9)
		0.4895	1.17	0.0927(10)
		0.5757	1.07	0.0935(14)
		0.6771	0.99	0.0945(25)
0.0080	0.0080	0.1572	1.81	0.0823(16)
		0.1849	1.72	0.0838(15)
		0.2175	1.63	0.0851(13)
		0.2558	1.55	0.0860(13)
		0.3008	1.49	0.0868(12)
		0.3538	1.44	0.0873(12)
		0.4162	1.43	0.0873(13)
		0.4895	1.45	0.0872(14)
		0.5757	1.51	0.0884(11)
		0.6771	1.65	0.0887(10)

(a)

β=4.05 $L^3 \times T = 32^3 \times 64$				
μ_{sea}	μ_1	μ_2	ω'	f
0.0030	0.0154	0.1572	1.61	0.0877(12)
		0.1849	1.57	0.0893(11)
		0.2175	1.54	0.0907(11)
		0.2558	1.51	0.0918(11)
		0.3008	1.48	0.0926(11)
		0.3538	1.46	0.0932(11)
		0.4162	1.45	0.0940(11)
		0.4895	1.46	0.0940(11)
		0.5757	1.49	0.0936(12)
		0.6771	1.48	0.0948(11)
0.0060	0.0154	0.1572	1.00	0.0902(5)
		0.1849	1.88	0.0920(5)
		0.2175	1.74	0.0937(5)
		0.2558	1.60	0.0952(5)
		0.3008	1.48	0.0965(6)
		0.3538	1.36	0.0976(6)
		0.4162	1.24	0.0986(7)
		0.4895	1.15	0.0995(7)
		0.5757	1.08	0.1005(9)
		0.6771	1.04	0.1015(13)
0.0080	0.0154	0.1572	1.89	0.0866(17)
		0.1849	1.80	0.0881(16)
		0.2175	1.71	0.0895(15)
		0.2558	1.63	0.0907(14)
		0.3008	1.56	0.0917(13)
		0.3538	1.50	0.0923(12)
		0.4162	1.46	0.0926(13)
		0.4895	1.45	0.0924(14)
		0.5757	1.45	0.0940(12)
		0.6771	1.47	0.0951(10)

(b)

Table F.2.5: Heavy-light (a) and heavy-strange (b) pseudoscalar decay constant at $\beta = 4.05$ and $L^3 \times T = 32^3 \times 64$ obtained from Eq.F.2.2. The value of ω'_{opt} is also reported.

β=4.20 $L^3 \times T = 32^3 \times 64$				
μ_{sea}	μ_1	μ_2	ω'	f
0.0065	0.0065	0.13315	2.13	0.0647(13)
		0.1566	2.05	0.0655(12)
		0.1842	1.97	0.0661(11)
		0.2166	1.89	0.0665(11)
		0.2548	1.82	0.0666(10)
		0.2997	1.74	0.0666(10)
		0.3525	1.66	0.0663(10)
		0.4145	1.59	0.0659(11)
		0.4876	1.52	0.0655(13)
		0.5734	1.46	0.0645(19)

(a)

β=4.20 $L^3 \times T = 32^3 \times 64$				
μ_{sea}	μ_1	μ_2	ω'	f
0.0065	0.0129	0.13315	2.01	0.0693(11)
		0.1566	1.93	0.0704(10)
		0.1842	1.86	0.0713(9)
		0.2166	1.78	0.0719(8)
		0.2548	1.71	0.0724(8)
		0.2997	1.64	0.0726(7)
		0.3525	1.57	0.0726(7)
		0.4145	1.51	0.0723(7)
		0.4876	1.44	0.0720(7)
		0.5734	1.38	0.0716(12)

(b)

Table F.2.6: Heavy-light (a) and heavy-strange (b) pseudoscalar decay constant at $\beta = 4.20$ and $L^3 \times T = 32^3 \times 64$ obtained from Eq.F.2.2. The value of ω'_{opt} is also reported.

β=4.20 $L^3 \times T = 48^3 \times 96$				
μ_{sea}	μ_1	μ_2	ω'	f
0.0020	0.0020	0.13315	1.96	0.0612(10)
		0.1566	1.91	0.0620(10)
		0.1842	1.86	0.0627(11)
		0.2166	1.82	0.0631(11)
		0.2548	1.77	0.0633(12)
		0.2997	1.71	0.0632(12)
		0.3525	1.66	0.0627(12)
		0.4145	1.61	0.0620(13)
		0.4876	1.55	0.0611(14)
		0.5734	1.48	0.0599(19)

(a)

β=4.20 $L^3 \times T = 48^3 \times 96$				
μ_{sea}	μ_1	μ_2	ω'	f
0.0020	0.0129	0.13315	1.83	0.0684(8)
		0.1566	1.78	0.0694(8)
		0.1842	1.73	0.0703(7)
		0.2166	1.68	0.0709(7)
		0.2548	1.63	0.0713(7)
		0.2997	1.57	0.0714(7)
		0.3525	1.52	0.0713(7)
		0.4145	1.46	0.0709(7)
		0.4876	1.41	0.0704(6)
		0.5734	1.35	0.0699(7)

(b)

Table F.2.7: Heavy-light (a) and heavy-strange (b) pseudoscalar decay constant at $\beta = 4.20$ and $L^3 \times T = 48^3 \times 96$ obtained from Eq.F.2.2. The value of $\omega'_{\rm opt}$ is also reported.

F.3 Bare bag parameters

In the following tables I gather the bare results for the quantities $\xi_i B_i$ at all values of β and combination of light-strange, light-charm, light-heavy and strange-heavy, relevant for the computation of B_i in the K^0, D^0, B^0 and B_s^0 system respectively. As before, in order to simplify tables only the second simulated strange is shown here.

All values have been obtained from Eq.5.2.1, i.e they correspond to correlators computed with smeared sources and sinks and local four-fermion operator. The fit time interval has taken to be $[T_{\rm sep}/2 - 2 : T_{\rm sep}/2 + 2]$ for the strange-light combinations and $[T_{\rm sep}/2 - 1 : T_{\rm sep}/2 + 1]$ for the light-charm, light-heavy and strange-heavy combinations. The systematic error which would come from considering a variation of one time-slice in the time fit interval is negligible compared with the statistical error.

$\beta = 3.80$ $L^3 \times T = 24^3 \times 48$							
μ_{sea}	μ_ℓ	μ_h	$\xi_1 B_1$	$\xi_2 B_2$	$\xi_3 B_3$	$\xi_4 B_4$	$\xi_5 B_5$
0.0080	0.0080	0.0080	1.627(25)	0.986(07)	0.241(02)	1.819(11)	0.602(04)
		0.0175	1.684(21)	1.026(06)	0.249(01)	1.867(09)	0.630(03)
		0.0194	1.695(20)	1.033(06)	0.250(01)	1.875(09)	0.635(03)
		0.0213	1.705(20)	1.039(06)	0.251(01)	1.883(09)	0.639(03)
		0.1982	2.126(30)	1.285(09)	0.289(03)	2.120(10)	0.860(06)
		0.2331	2.160(32)	1.307(09)	0.291(03)	2.135(11)	0.884(07)
		0.2742	2.193(35)	1.329(10)	0.291(03)	2.148(12)	0.909(08)
		0.3225	2.225(39)	1.350(12)	0.292(04)	2.159(13)	0.933(09)
		0.3793	2.256(44)	1.371(13)	0.291(04)	2.168(15)	0.957(10)
		0.4461	2.286(50)	1.390(15)	0.290(05)	2.175(18)	0.979(12)
		0.5246	2.314(58)	1.408(18)	0.288(06)	2.177(23)	0.999(16)
		0.6170	2.335(71)	1.421(24)	0.285(10)	2.168(33)	1.014(23)
		0.7257	2.320(122)	1.427(35)	0.280(21)	2.129(50)	1.016(43)
		0.8536	2.163(367)	1.417(70)	0.280(53)	1.994(85)	0.986(96)
0.0110	0.0110	0.0110	1.656(43)	1.034(20)	0.251(05)	1.867(33)	0.625(11)
		0.0175	1.709(40)	1.059(20)	0.256(05)	1.899(33)	0.643(11)
		0.0194	1.722(40)	1.066(20)	0.258(05)	1.907(33)	0.648(11)
		0.0213	1.735(39)	1.072(20)	0.259(05)	1.914(34)	0.653(11)
		0.1982	2.196(43)	1.326(24)	0.299(05)	2.153(35)	0.884(15)
		0.2331	2.236(44)	1.349(24)	0.301(05)	2.168(36)	0.910(15)
		0.2742	2.277(45)	1.373(24)	0.303(05)	2.181(37)	0.936(16)
		0.3225	2.318(47)	1.397(25)	0.304(05)	2.192(38)	0.963(17)
		0.3793	2.362(50)	1.421(26)	0.306(05)	2.202(39)	0.989(18)
		0.4461	2.410(56)	1.447(26)	0.308(05)	2.210(40)	1.015(19)
		0.5246	2.466(67)	1.475(27)	0.312(05)	2.214(42)	1.038(21)
		0.6170	2.538(92)	1.511(29)	0.320(08)	2.210(46)	1.058(26)
		0.7257	2.637(158)	1.562(37)	0.332(17)	2.183(57)	1.065(40)
		0.8536	2.777(364)	1.642(70)	0.342(53)	2.084(93)	1.037(84)

Table F.3.1: Strange-light and heavy-light $\xi_i B_i$ at $\beta = 3.80$ and $L^3 \times T = 24^3 \times 48$

$\beta = 3.80$ $L^3 \times T = 24^3 \times 48$							
μ_{sea}	μ_ℓ	μ_h	$\xi_1 B_1$	$\xi_2 B_2$	$\xi_3 B_3$	$\xi_4 B_4$	$\xi_5 B_5$
0.0080	0.0194	0.1982	2.168(18)	1.312(06)	0.295(02)	2.122(09)	0.877(04)
		0.2331	2.204(19)	1.333(07)	0.296(02)	2.136(09)	0.902(05)
		0.2742	2.239(19)	1.355(07)	0.298(02)	2.149(10)	0.927(05)
		0.3225	2.273(20)	1.377(08)	0.299(02)	2.160(11)	0.953(06)
		0.3793	2.305(22)	1.398(09)	0.299(03)	2.169(12)	0.978(06)
		0.4461	2.337(23)	1.417(10)	0.299(03)	2.175(13)	1.003(07)
		0.5246	2.365(26)	1.436(12)	0.298(04)	2.177(14)	1.026(08)
		0.6170	2.386(30)	1.451(14)	0.296(06)	2.174(15)	1.047(10)
		0.7257	2.392(52)	1.461(18)	0.293(12)	2.158(18)	1.063(17)
		0.8536	2.355(161)	1.464(26)	0.295(28)	2.108(31)	1.075(41)
0.0110	0.0194	0.1982	2.219(42)	1.342(23)	0.302(05)	2.158(35)	0.893(14)
		0.2331	2.259(42)	1.365(24)	0.304(05)	2.172(35)	0.919(15)
		0.2742	2.299(43)	1.388(24)	0.305(05)	2.185(35)	0.944(15)
		0.3225	2.339(45)	1.412(25)	0.307(05)	2.196(36)	0.971(16)
		0.3793	2.380(47)	1.435(25)	0.308(05)	2.206(37)	0.996(17)
		0.4461	2.423(50)	1.459(26)	0.309(05)	2.213(37)	1.021(18)
		0.5246	2.470(57)	1.484(26)	0.311(05)	2.217(38)	1.044(19)
		0.6170	2.523(70)	1.513(28)	0.314(06)	2.216(40)	1.062(21)
		0.7257	2.580(105)	1.550(31)	0.321(11)	2.202(45)	1.073(28)
		0.8536	2.623(218)	1.598(47)	0.327(33)	2.152(62)	1.068(53)

Table F.3.2: Heavy-strange $\xi_i B_i$ at $\beta = 3.80$ and $L^3 \times T = 24^3 \times 48$

$\beta = 3.90$ $L^3 \times T = 32^3 \times 64$							
μ_{sea}	μ_ℓ	μ_h	$\xi_1 B_1$	$\xi_2 B_2$	$\xi_3 B_3$	$\xi_4 B_4$	$\xi_5 B_5$
0.0030	0.0030	0.0030	1.486(37)	0.876(09)	0.217(03)	1.756(12)	0.567(04)
		0.0159	1.589(14)	0.960(07)	0.235(02)	1.861(10)	0.619(03)
		0.0177	1.602(13)	0.968(07)	0.237(02)	1.872(10)	0.625(03)
		0.0195	1.615(13)	0.975(07)	0.238(02)	1.882(10)	0.631(03)
		0.1828	2.099(28)	1.238(12)	0.279(04)	2.165(16)	0.881(07)
		0.2150	2.134(30)	1.262(13)	0.282(04)	2.179(17)	0.908(08)
		0.2529	2.168(32)	1.286(14)	0.284(05)	2.193(19)	0.937(09)
		0.2974	2.200(33)	1.310(15)	0.286(06)	2.205(21)	0.966(10)
		0.3498	2.230(35)	1.334(17)	0.288(07)	2.216(23)	0.997(12)
		0.4114	2.259(39)	1.359(19)	0.292(09)	2.227(26)	1.028(15)
		0.4839	2.285(47)	1.387(21)	0.298(11)	2.238(31)	1.060(20)
		0.5691	2.302(67)	1.420(26)	0.309(14)	2.249(39)	1.094(27)
		0.6694	2.281(118)	1.464(36)	0.336(22)	2.259(58)	1.134(39)
		0.7873	2.108(281)	1.541(66)	0.413(53)	2.271(109)	1.200(68)
0.0040	0.0040	0.0040	1.449(28)	0.900(07)	0.223(02)	1.761(15)	0.571(05)
		0.0159	1.574(16)	0.967(06)	0.237(01)	1.850(11)	0.617(04)
		0.0177	1.589(16)	0.975(06)	0.239(01)	1.860(11)	0.623(04)
		0.0195	1.604(15)	0.982(06)	0.240(01)	1.870(11)	0.628(04)
		0.1828	2.119(25)	1.239(06)	0.281(02)	2.128(16)	0.868(05)
		0.2150	2.165(26)	1.262(07)	0.282(02)	2.142(17)	0.895(05)
		0.2529	2.212(27)	1.285(07)	0.283(02)	2.155(18)	0.923(06)
		0.2974	2.260(28)	1.309(07)	0.284(03)	2.166(19)	0.951(07)
		0.3498	2.311(30)	1.333(08)	0.284(03)	2.176(21)	0.981(09)
		0.4114	2.365(34)	1.357(10)	0.283(04)	2.185(23)	1.010(12)
		0.4839	2.425(42)	1.383(12)	0.281(05)	2.193(26)	1.039(17)
		0.5691	2.501(61)	1.409(17)	0.278(07)	2.202(30)	1.067(23)
		0.6694	2.626(105)	1.437(26)	0.268(13)	2.220(38)	1.096(33)
		0.7873	2.925(226)	1.455(49)	0.237(31)	2.277(78)	1.132(64)

Table F.3.3: Strange-light and heavy-light $\xi_i B_i$ at $\beta = 3.90$ and $L^3 \times T = 32^3 \times 64$

$\beta = 3.90$ $L^3 \times T = 32^3 \times 64$							
μ_{sea}	μ_ℓ	μ_h	$\xi_1 B_1$	$\xi_2 B_2$	$\xi_3 B_3$	$\xi_4 B_4$	$\xi_5 B_5$
0.0030	0.0177	0.1828	2.168(12)	1.287(06)	0.291(02)	2.164(08)	0.896(04)
		0.2150	2.205(13)	1.310(07)	0.293(02)	2.178(08)	0.922(04)
		0.2529	2.242(14)	1.333(07)	0.294(02)	2.191(09)	0.950(04)
		0.2974	2.277(15)	1.356(08)	0.296(03)	2.202(09)	0.977(04)
		0.3498	2.312(16)	1.378(09)	0.297(03)	2.212(10)	1.005(05)
		0.4114	2.345(18)	1.401(10)	0.298(03)	2.220(10)	1.033(06)
		0.4839	2.378(21)	1.424(12)	0.299(04)	2.228(11)	1.059(07)
		0.5691	2.410(26)	1.448(14)	0.302(05)	2.234(13)	1.084(09)
		0.6694	2.442(37)	1.477(16)	0.308(06)	2.241(16)	1.106(14)
		0.7873	2.477(74)	1.519(22)	0.324(10)	2.259(24)	1.125(25)
0.0040	0.0177	0.1828	2.165(10)	1.280(04)	0.290(01)	2.143(07)	0.887(03)
		0.2150	2.206(11)	1.303(04)	0.291(01)	2.159(08)	0.914(04)
		0.2529	2.247(11)	1.325(04)	0.293(01)	2.173(08)	0.942(04)
		0.2974	2.288(12)	1.348(05)	0.293(02)	2.185(08)	0.970(04)
		0.3498	2.329(12)	1.370(05)	0.293(02)	2.197(09)	0.998(05)
		0.4114	2.370(13)	1.392(06)	0.293(02)	2.206(09)	1.026(06)
		0.4839	2.413(15)	1.413(06)	0.291(03)	2.213(11)	1.052(07)
		0.5691	2.458(18)	1.435(08)	0.288(04)	2.217(13)	1.077(08)
		0.6694	2.509(28)	1.455(11)	0.283(05)	2.220(19)	1.100(11)
		0.7873	2.578(66)	1.471(19)	0.274(12)	2.220(36)	1.128(19)

Table F.3.4: Heavy-strange $\xi_i B_i$ at $\beta = 3.90$ and $L^3 \times T = 32^3 \times 64$

$\beta = 3.90$ $L^3 \times T = 24^3 \times 48$							
μ_{sea}	μ_ℓ	μ_h	$\xi_1 B_1$	$\xi_2 B_2$	$\xi_3 B_3$	$\xi_4 B_4$	$\xi_5 B_5$
0.0040	0.0040	0.0040	1.431(48)	0.890(14)	0.218(03)	1.759(21)	0.569(07)
		0.0159	1.583(21)	0.960(09)	0.234(02)	1.854(15)	0.617(05)
		0.0177	1.599(19)	0.967(08)	0.236(02)	1.865(14)	0.623(05)
		0.0195	1.613(18)	0.975(08)	0.237(02)	1.875(14)	0.628(05)
		0.1828	2.089(28)	1.245(07)	0.284(02)	2.169(14)	0.883(08)
		0.2150	2.125(31)	1.269(07)	0.287(03)	2.186(15)	0.910(08)
		0.2529	2.157(34)	1.292(08)	0.289(03)	2.202(16)	0.938(10)
		0.2974	2.187(38)	1.315(08)	0.292(03)	2.216(18)	0.966(11)
		0.3498	2.213(44)	1.337(09)	0.294(04)	2.230(21)	0.993(14)
		0.4114	2.233(53)	1.358(11)	0.296(05)	2.243(25)	1.017(17)
		0.4839	2.250(70)	1.377(14)	0.299(07)	2.257(31)	1.037(21)
		0.5691	2.271(103)	1.397(20)	0.303(12)	2.269(41)	1.044(26)
		0.6694	2.336(166)	1.423(30)	0.311(23)	2.276(59)	1.025(34)
		0.7873	2.562(329)	1.482(55)	0.336(56)	2.265(109)	0.940(58)
0.0064	0.0064	0.0064	1.527(24)	0.942(07)	0.232(02)	1.813(17)	0.595(06)
		0.0159	1.626(17)	0.990(05)	0.242(01)	1.877(13)	0.629(05)
		0.0177	1.641(16)	0.997(05)	0.244(01)	1.887(13)	0.635(05)
		0.0195	1.655(16)	1.004(05)	0.245(01)	1.897(13)	0.640(04)
		0.1828	2.152(24)	1.269(08)	0.288(02)	2.159(16)	0.884(07)
		0.2150	2.192(26)	1.293(08)	0.290(02)	2.171(16)	0.910(07)
		0.2529	2.231(28)	1.317(08)	0.291(03)	2.182(16)	0.936(07)
		0.2974	2.270(31)	1.341(08)	0.292(03)	2.190(16)	0.963(07)
		0.3498	2.311(35)	1.365(09)	0.293(03)	2.197(16)	0.990(07)
		0.4114	2.357(40)	1.389(10)	0.291(04)	2.201(16)	1.018(08)
		0.4839	2.412(47)	1.414(12)	0.288(06)	2.204(17)	1.047(10)
		0.5691	2.490(57)	1.440(15)	0.281(09)	2.207(21)	1.078(14)
		0.6694	2.620(77)	1.472(22)	0.269(15)	2.210(35)	1.115(24)
		0.7873	2.899(144)	1.529(40)	0.251(34)	2.216(75)	1.164(51)
0.0085	0.0085	0.0085	1.569(26)	0.956(08)	0.235(02)	1.829(08)	0.606(03)
		0.0159	1.634(20)	0.993(07)	0.243(02)	1.873(08)	0.629(03)
		0.0177	1.648(20)	1.000(07)	0.244(02)	1.883(08)	0.635(03)
		0.0195	1.662(19)	1.007(07)	0.246(02)	1.892(08)	0.640(03)
		0.1828	2.155(18)	1.274(06)	0.289(01)	2.160(14)	0.881(07)
		0.2150	2.196(20)	1.298(07)	0.291(02)	2.178(15)	0.908(07)
		0.2529	2.235(21)	1.322(07)	0.293(02)	2.194(16)	0.937(08)
		0.2974	2.273(23)	1.345(08)	0.294(02)	2.210(18)	0.967(09)
		0.3498	2.310(25)	1.368(09)	0.294(02)	2.224(19)	0.997(10)
		0.4114	2.346(27)	1.391(10)	0.294(02)	2.239(21)	1.028(11)
		0.4839	2.381(27)	1.412(11)	0.293(03)	2.252(24)	1.059(12)
		0.5691	2.414(27)	1.431(13)	0.290(05)	2.266(29)	1.093(16)
		0.6694	2.441(39)	1.449(17)	0.283(10)	2.277(38)	1.132(25)
		0.7873	2.442(117)	1.466(34)	0.268(30)	2.277(61)	1.183(47)
0.0100	0.0100	0.0100	1.619(20)	0.980(06)	0.240(02)	1.846(10)	0.615(03)
		0.0159	1.662(16)	1.004(06)	0.245(01)	1.879(09)	0.634(03)
		0.0177	1.674(15)	1.011(06)	0.246(01)	1.888(08)	0.639(03)
		0.0195	1.685(14)	1.017(05)	0.247(01)	1.897(08)	0.644(03)
		0.1828	2.136(12)	1.273(05)	0.288(02)	2.148(11)	0.880(05)
		0.2150	2.173(12)	1.295(06)	0.291(02)	2.163(12)	0.907(06)
		0.2529	2.209(13)	1.318(06)	0.292(02)	2.176(13)	0.934(06)
		0.2974	2.243(15)	1.340(07)	0.293(03)	2.187(14)	0.962(07)
		0.3498	2.276(17)	1.361(07)	0.293(03)	2.197(15)	0.990(08)
		0.4114	2.307(20)	1.380(08)	0.292(04)	2.207(16)	1.019(09)
		0.4839	2.337(25)	1.398(08)	0.289(05)	2.216(17)	1.048(10)
		0.5691	2.363(31)	1.411(10)	0.282(08)	2.227(19)	1.079(14)
		0.6694	2.371(44)	1.413(13)	0.266(14)	2.244(25)	1.119(24)
		0.7873	2.292(84)	1.385(28)	0.226(30)	2.276(43)	1.192(53)

Table F.3.5: Strange-light and heavy-light $\xi_i B_i$ at $\beta = 3.90$ and $L^3 \times T = 24^3 \times 48$

$\beta = 3.90$ $L^3 \times T = 24^3 \times 48$							
μ_{sea}	μ_ℓ	μ_h	$\xi_1 B_1$	$\xi_2 B_2$	$\xi_3 B_3$	$\xi_4 B_4$	$\xi_5 B_5$
0.0040	0.0177	0.1828	2.148(14)	1.283(06)	0.292(02)	2.155(07)	0.891(03)
		0.2150	2.185(15)	1.306(06)	0.294(02)	2.170(07)	0.917(04)
		0.2529	2.221(16)	1.328(07)	0.296(02)	2.184(07)	0.945(04)
		0.2974	2.255(16)	1.350(07)	0.298(02)	2.196(07)	0.972(05)
		0.3498	2.289(17)	1.372(07)	0.299(03)	2.207(08)	0.999(05)
		0.4114	2.320(18)	1.394(08)	0.300(03)	2.217(09)	1.025(07)
		0.4839	2.349(20)	1.415(08)	0.300(04)	2.224(10)	1.049(08)
		0.5691	2.376(23)	1.435(09)	0.300(06)	2.229(13)	1.068(11)
		0.6694	2.401(35)	1.457(12)	0.299(09)	2.228(19)	1.076(15)
		0.7873	2.423(85)	1.481(20)	0.296(20)	2.211(37)	1.060(24)
0.0064	0.0177	0.1828	2.176(13)	1.292(05)	0.292(02)	2.157(11)	0.893(05)
		0.2150	2.214(13)	1.315(05)	0.294(02)	2.170(11)	0.919(05)
		0.2529	2.251(14)	1.337(05)	0.295(02)	2.183(11)	0.946(06)
		0.2974	2.286(14)	1.359(05)	0.296(02)	2.194(11)	0.973(06)
		0.3498	2.322(15)	1.382(05)	0.296(02)	2.203(11)	1.001(06)
		0.4114	2.359(16)	1.403(05)	0.296(03)	2.212(11)	1.028(06)
		0.4839	2.400(18)	1.425(06)	0.294(03)	2.219(11)	1.056(07)
		0.5691	2.448(21)	1.446(07)	0.289(05)	2.224(11)	1.082(09)
		0.6694	2.518(27)	1.469(09)	0.281(07)	2.230(14)	1.109(13)
		0.7873	2.641(49)	1.496(16)	0.266(15)	2.239(26)	1.137(24)
0.0085	0.0177	0.1828	2.168(12)	1.292(05)	0.292(01)	2.155(10)	0.889(04)
		0.2150	2.207(13)	1.315(05)	0.295(01)	2.171(10)	0.916(05)
		0.2529	2.244(14)	1.338(06)	0.296(01)	2.186(11)	0.944(05)
		0.2974	2.282(16)	1.360(06)	0.297(02)	2.200(11)	0.972(06)
		0.3498	2.318(18)	1.383(07)	0.298(02)	2.213(12)	1.002(06)
		0.4114	2.353(20)	1.405(08)	0.298(02)	2.225(13)	1.031(07)
		0.4839	2.388(21)	1.426(08)	0.297(03)	2.236(14)	1.060(08)
		0.5691	2.420(22)	1.447(10)	0.295(04)	2.246(16)	1.089(10)
		0.6694	2.446(27)	1.467(11)	0.291(07)	2.253(21)	1.119(15)
		0.7873	2.455(68)	1.488(19)	0.282(19)	2.255(33)	1.152(26)
0.0100	0.0177	0.1828	2.157(12)	1.288(05)	0.292(02)	2.146(09)	0.887(04)
		0.2150	2.194(12)	1.311(06)	0.294(02)	2.160(10)	0.913(05)
		0.2529	2.230(13)	1.333(06)	0.295(02)	2.172(10)	0.939(05)
		0.2974	2.265(14)	1.354(06)	0.296(02)	2.183(11)	0.967(05)
		0.3498	2.299(16)	1.376(07)	0.297(02)	2.193(11)	0.994(06)
		0.4114	2.332(17)	1.396(07)	0.296(03)	2.202(12)	1.021(06)
		0.4839	2.366(19)	1.416(07)	0.295(03)	2.210(12)	1.048(07)
		0.5691	2.400(22)	1.434(08)	0.291(05)	2.217(13)	1.074(09)
		0.6694	2.431(28)	1.448(09)	0.283(08)	2.225(16)	1.103(15)
		0.7873	2.438(42)	1.447(15)	0.261(18)	2.235(29)	1.145(33)

Table F.3.6: Heavy-strange $\xi_i B_i$ at $\beta = 3.90$ and $L^3 \times T = 24^3 \times 48$

$\beta = 4.05$ $L^3 \times T = 32^3 \times 64$							
μ_{sea}	μ_ℓ	μ_h	$\xi_1 B_1$	$\xi_2 B_2$	$\xi_3 B_3$	$\xi_4 B_4$	$\xi_5 B_5$
0.0030	0.0030	0.0030	1.349(44)	0.848(10)	0.211(02)	1.702(24)	0.547(08)
		0.0139	1.530(23)	0.930(06)	0.230(01)	1.828(17)	0.604(06)
		0.0154	1.547(23)	0.938(06)	0.231(01)	1.841(17)	0.610(05)
		0.0169	1.564(23)	0.945(05)	0.233(01)	1.853(16)	0.616(05)
		0.1572	2.058(29)	1.213(08)	0.277(03)	2.183(16)	0.881(07)
		0.1849	2.088(32)	1.234(10)	0.279(03)	2.202(17)	0.910(07)
		0.2175	2.114(36)	1.255(12)	0.280(04)	2.219(19)	0.940(08)
		0.2558	2.137(42)	1.275(14)	0.281(05)	2.232(20)	0.969(09)
		0.3008	2.157(50)	1.295(17)	0.281(06)	2.243(22)	0.998(10)
		0.3538	2.175(61)	1.313(19)	0.282(07)	2.249(25)	1.025(12)
		0.4162	2.191(76)	1.331(22)	0.282(09)	2.252(29)	1.050(14)
		0.4895	2.211(97)	1.349(24)	0.281(12)	2.250(35)	1.071(18)
		0.5757	2.244(133)	1.370(27)	0.277(17)	2.246(46)	1.085(24)
		0.6771	2.316(206)	1.402(42)	0.262(28)	2.241(77)	1.084(45)
0.0060	0.0060	0.0060	1.476(20)	0.911(11)	0.226(03)	1.753(28)	0.574(09)
		0.0139	1.567(15)	0.949(09)	0.234(03)	1.829(22)	0.610(07)
		0.0154	1.582(15)	0.955(09)	0.235(02)	1.841(21)	0.616(07)
		0.0169	1.597(15)	0.962(08)	0.236(02)	1.851(21)	0.622(07)
		0.1572	2.115(23)	1.221(08)	0.279(03)	2.144(15)	0.875(07)
		0.1849	2.151(25)	1.243(09)	0.281(03)	2.160(16)	0.904(08)
		0.2175	2.185(28)	1.265(10)	0.282(04)	2.175(18)	0.933(09)
		0.2558	2.218(30)	1.287(11)	0.283(04)	2.188(20)	0.963(10)
		0.3008	2.249(33)	1.309(12)	0.284(05)	2.199(22)	0.993(12)
		0.3538	2.281(37)	1.329(13)	0.284(06)	2.207(26)	1.022(14)
		0.4162	2.315(41)	1.348(15)	0.283(07)	2.212(30)	1.049(17)
		0.4895	2.354(49)	1.366(17)	0.280(09)	2.212(35)	1.071(20)
		0.5757	2.407(67)	1.379(23)	0.273(13)	2.207(43)	1.086(25)
		0.6771	2.497(113)	1.385(34)	0.254(20)	2.196(57)	1.086(35)
0.0080	0.0080	0.0080	1.552(18)	0.922(08)	0.228(02)	1.815(12)	0.599(04)
		0.0139	1.609(16)	0.953(07)	0.235(02)	1.860(10)	0.623(04)
		0.0154	1.622(15)	0.960(06)	0.236(02)	1.870(10)	0.628(03)
		0.0169	1.635(15)	0.966(06)	0.237(02)	1.879(10)	0.633(03)
		0.1572	2.121(20)	1.223(08)	0.279(02)	2.149(11)	0.877(05)
		0.1849	2.158(22)	1.245(08)	0.280(02)	2.165(12)	0.904(06)
		0.2175	2.195(25)	1.266(09)	0.281(03)	2.179(12)	0.931(07)
		0.2558	2.230(29)	1.287(10)	0.282(03)	2.190(13)	0.959(08)
		0.3008	2.262(34)	1.307(12)	0.281(03)	2.197(15)	0.985(10)
		0.3538	2.292(39)	1.326(13)	0.280(04)	2.200(17)	1.008(12)
		0.4162	2.319(46)	1.343(15)	0.278(05)	2.197(19)	1.027(14)
		0.4895	2.341(55)	1.358(17)	0.275(07)	2.185(24)	1.040(18)
		0.5757	2.356(67)	1.368(20)	0.269(10)	2.161(34)	1.045(24)
		0.6771	2.358(93)	1.370(29)	0.257(17)	2.125(56)	1.041(38)

Table F.3.7: Strange-light and heavy-light $\xi_i B_i$ at $\beta = 4.05$ and $L^3 \times T = 32^3 \times 64$

$\beta = 4.05$ $L^3 \times T = 32^3 \times 64$							
μ_{sea}	μ_ℓ	μ_h	$\xi_1 B_1$	$\xi_2 B_2$	$\xi_3 B_3$	$\xi_4 B_4$	$\xi_5 B_5$
0.0030	0.0154	0.1572	2.119(10)	1.248(05)	0.285(01)	2.159(10)	0.887(04)
		0.1849	2.155(11)	1.269(05)	0.287(02)	2.176(11)	0.914(04)
		0.2175	2.189(12)	1.291(06)	0.289(02)	2.191(11)	0.942(04)
		0.2558	2.222(13)	1.312(07)	0.290(03)	2.204(11)	0.971(04)
		0.3008	2.253(16)	1.332(08)	0.290(03)	2.215(12)	1.000(05)
		0.3538	2.283(18)	1.352(09)	0.290(04)	2.224(12)	1.029(06)
		0.4162	2.313(21)	1.371(10)	0.290(05)	2.232(14)	1.057(07)
		0.4895	2.345(25)	1.389(12)	0.289(06)	2.238(16)	1.084(09)
		0.5757	2.380(33)	1.408(14)	0.287(08)	2.244(20)	1.109(13)
		0.6771	2.424(51)	1.427(19)	0.283(11)	2.246(28)	1.133(21)
0.0060	0.0154	0.1572	2.137(15)	1.244(07)	0.284(02)	2.152(11)	0.888(05)
		0.1849	2.173(16)	1.266(07)	0.286(02)	2.168(12)	0.916(05)
		0.2175	2.208(17)	1.287(07)	0.288(02)	2.183(13)	0.946(06)
		0.2558	2.241(18)	1.308(08)	0.289(02)	2.196(14)	0.976(07)
		0.3008	2.274(19)	1.329(08)	0.289(03)	2.208(15)	1.007(08)
		0.3538	2.305(20)	1.349(08)	0.289(03)	2.218(17)	1.037(09)
		0.4162	2.337(22)	1.368(09)	0.288(03)	2.226(19)	1.066(10)
		0.4895	2.369(24)	1.387(11)	0.286(04)	2.230(22)	1.093(12)
		0.5757	2.402(30)	1.403(13)	0.283(06)	2.230(26)	1.115(15)
		0.6771	2.438(48)	1.418(20)	0.279(09)	2.223(33)	1.132(19)
0.0080	0.0154	0.1572	2.140(12)	1.245(06)	0.284(02)	2.154(09)	0.887(04)
		0.1849	2.178(13)	1.267(06)	0.286(02)	2.170(10)	0.914(05)
		0.2175	2.214(14)	1.289(07)	0.287(02)	2.184(10)	0.942(05)
		0.2558	2.249(16)	1.311(07)	0.288(02)	2.197(10)	0.971(06)
		0.3008	2.282(18)	1.331(08)	0.288(02)	2.207(11)	0.999(06)
		0.3538	2.313(20)	1.352(08)	0.288(03)	2.213(12)	1.025(07)
		0.4162	2.342(23)	1.371(09)	0.287(03)	2.215(13)	1.048(08)
		0.4895	2.367(26)	1.388(09)	0.286(04)	2.211(15)	1.067(10)
		0.5757	2.388(32)	1.404(11)	0.282(05)	2.198(18)	1.080(12)
		0.6771	2.405(45)	1.415(16)	0.276(09)	2.174(27)	1.085(18)

Table F.3.8: Heavy-strange $\xi_i B_i$ at $\beta = 4.05$ and $L^3 \times T = 32^3 \times 64$

$\beta = 4.20$ $L^3 \times T = 32^3 \times 64$							
μ_{sea}	μ_ℓ	μ_h	$\xi_1 B_1$	$\xi_2 B_2$	$\xi_3 B_3$	$\xi_4 B_4$	$\xi_5 B_5$
0.0065	0.0065	0.0065	1.505(40)	0.906(17)	0.226(04)	1.797(19)	0.591(06)
		0.0116	1.570(37)	0.935(13)	0.232(03)	1.849(18)	0.616(05)
		0.0129	1.584(36)	0.941(13)	0.234(03)	1.860(17)	0.622(05)
		0.0142	1.599(36)	0.948(12)	0.235(03)	1.870(17)	0.627(05)
		0.13315	2.128(32)	1.205(12)	0.278(04)	2.157(20)	0.878(10)
		0.1566	2.174(33)	1.229(13)	0.280(05)	2.178(20)	0.908(11)
		0.1842	2.220(33)	1.253(15)	0.282(05)	2.199(21)	0.940(12)
		0.2166	2.265(34)	1.277(16)	0.283(06)	2.219(23)	0.974(13)
		0.2548	2.310(35)	1.301(18)	0.284(07)	2.238(25)	1.008(15)
		0.2997	2.353(37)	1.324(20)	0.284(08)	2.255(27)	1.042(17)
		0.3525	2.395(39)	1.345(22)	0.283(10)	2.269(30)	1.074(19)
		0.4145	2.438(41)	1.365(24)	0.279(12)	2.280(35)	1.104(23)
		0.4876	2.483(46)	1.380(26)	0.272(15)	2.287(43)	1.131(30)
		0.5734	2.529(65)	1.389(29)	0.257(21)	2.295(58)	1.151(44)

Table F.3.9: Strange-light and heavy-light $\xi_i B_i$ at $\beta = 4.20$ and $L^3 \times T = 32^3 \times 64$

$\beta = 4.20$ $L^3 \times T = 32^3 \times 64$							
μ_{sea}	μ_ℓ	μ_h	$\xi_1 B_1$	$\xi_2 B_2$	$\xi_3 B_3$	$\xi_4 B_4$	$\xi_5 B_5$
0.0065	0.0129	0.13315	2.128(21)	1.221(08)	0.282(03)	2.159(15)	0.887(07)
		0.1566	2.169(22)	1.244(09)	0.284(03)	2.178(16)	0.916(08)
		0.1842	2.209(22)	1.267(10)	0.286(03)	2.195(17)	0.947(09)
		0.2166	2.248(23)	1.290(11)	0.287(04)	2.212(18)	0.979(10)
		0.2548	2.285(24)	1.312(12)	0.288(04)	2.227(19)	1.011(11)
		0.2997	2.321(25)	1.334(13)	0.289(05)	2.241(20)	1.044(12)
		0.3525	2.355(26)	1.355(14)	0.288(06)	2.253(22)	1.076(13)
		0.4145	2.389(27)	1.375(16)	0.287(08)	2.262(24)	1.106(14)
		0.4876	2.423(28)	1.392(17)	0.284(10)	2.268(27)	1.133(17)
		0.5734	2.456(34)	1.407(19)	0.277(13)	2.274(32)	1.155(22)

Table F.3.10: Heavy-strange $\xi_i B_i$ at $\beta = 4.20$ and $L^3 \times T = 32^3 \times 64$

$\beta = 4.20$ $L^3 \times T = 48^3 \times 96$							
μ_{sea}	μ_ℓ	μ_h	$\xi_1 B_1$	$\xi_2 B_2$	$\xi_3 B_3$	$\xi_4 B_4$	$\xi_5 B_5$
0.0020	0.0020	0.0020	1.352(36)	0.812(11)	0.205(03)	1.661(24)	0.533(08)
		0.0116	1.480(26)	0.888(08)	0.221(02)	1.818(16)	0.599(05)
		0.0129	1.499(25)	0.896(08)	0.223(02)	1.832(16)	0.605(05)
		0.0142	1.516(25)	0.903(08)	0.225(02)	1.845(15)	0.612(05)
		0.13315	2.068(33)	1.187(12)	0.275(04)	2.130(28)	0.853(12)
		0.1566	2.100(33)	1.211(13)	0.278(05)	2.143(29)	0.879(13)
		0.1842	2.131(34)	1.234(15)	0.280(06)	2.156(31)	0.905(14)
		0.2166	2.160(36)	1.256(18)	0.282(08)	2.168(34)	0.931(15)
		0.2548	2.189(42)	1.278(21)	0.284(10)	2.178(37)	0.956(16)
		0.2997	2.217(54)	1.299(27)	0.285(12)	2.185(42)	0.980(19)
		0.3525	2.246(72)	1.321(34)	0.285(16)	2.189(48)	0.999(24)
		0.4145	2.272(101)	1.342(44)	0.284(21)	2.189(56)	1.014(32)
		0.4876	2.292(148)	1.363(58)	0.281(27)	2.185(67)	1.023(44)
		0.5734	2.296(226)	1.390(79)	0.278(38)	2.180(85)	1.024(64)

Table F.3.11: Strange-light and heavy-light $\xi_i B_i$ at $\beta = 4.20$ and $L^3 \times T = 48^3 \times 96$

$\beta = 4.20$ $L^3 \times T = 48^3 \times 96$							
μ_{sea}	μ_ℓ	μ_h	$\xi_1 B_1$	$\xi_2 B_2$	$\xi_3 B_3$	$\xi_4 B_4$	$\xi_5 B_5$
0.0020	0.0129	0.13315	2.112(12)	1.213(05)	0.280(01)	2.161(10)	0.887(05)
		0.1566	2.146(12)	1.235(05)	0.282(01)	2.177(11)	0.915(05)
		0.1842	2.180(12)	1.256(05)	0.283(01)	2.191(12)	0.944(06)
		0.2166	2.212(12)	1.276(05)	0.284(02)	2.205(12)	0.974(06)
		0.2548	2.242(13)	1.296(06)	0.284(02)	2.216(13)	1.005(07)
		0.2997	2.272(15)	1.315(06)	0.284(02)	2.226(14)	1.036(07)
		0.3525	2.300(17)	1.334(06)	0.283(03)	2.234(15)	1.065(08)
		0.4145	2.326(20)	1.352(07)	0.282(04)	2.239(16)	1.093(09)
		0.4876	2.350(25)	1.370(08)	0.281(06)	2.242(18)	1.118(11)
		0.5734	2.367(35)	1.390(10)	0.283(08)	2.242(21)	1.141(13)

Table F.3.12: Heavy-strange $\xi_i B_i$ at $\beta = 4.20$ and $L^3 \times T = 48^3 \times 96$

Appendix G

$\mathbf{N_f = 2}$ Renormalization Constants

In this appendix I summarize the results for the $N_f = 2$ bilinear and four-fermion RCs used in chapter 5 and chapter 6. The procedure to compute them is similar to the one followed in chapter 4 for the $N_f = 4$ RCs with the advantage that in this case θ-average is not necessary since we are working at maximal twist. For that reason, here I focus only on the main output of the $N_f = 2$ RC analysis.

G.1 Simulation details

In Table G.1.1 we give the details about the ETMC $N_f = 2$ simulation for the RC computation. The smallest sea quark mass corresponds to a pion of about 300 MeV. The highest sea quark mass is around half of the strange quark mas. The inversions in the valence sector for the RI-MOM study have been performed using point-like sources randomly located on the lattice for each gauge configurations in order to reduce the autocorrelation time.

For the computation of Z_V using the WI method, as explained in subsection 4.4.3.3, the lattice parameters are those used also in the RI-MOM determination and collected in Table G.1.1.

The selected momenta for the RI-MOM study are in the interval

$$n_\nu = \begin{cases} ([0,2],[0,2],[0,2],[0,3]) \\ ([2,3],[2,3],[2,3],[4,7]) \end{cases} \quad , \text{ for } \beta = 3.8 \text{ and } 3.9$$

and

$$n_\nu = \begin{cases} ([0,2],[0,2],[0,2],[0,3]) \\ ([2,5],[2,5],[2,5],[4,9]) \end{cases} \quad , \text{ for } \beta = 4.05 \text{ and } 4.20$$

β	V	$\mu_{\rm sea}$	$\mu_{\rm val}$	N_{stat}
3.80	$24^3 \times 48$	{0.0080 0.0110 0.0165}	{0.0080,0.0110,0.0165, 0.0200}	400/240
3.90	$24^3 \times 48$	{0.0080 0.0064 0.0085 0.0100}	{0.0080 0.0064 0.0085 0.0100 0.0150}	240/240
4.05	$32^3 \times 64$	{0.0030 0.0060 0.0080}	{0.0030 0.0060 0.0080 0.0120}	128/240
4.20	$24^3 \times 48$	0.0020	{0.0020 0.0045 0.0065 0.0100}	208/208
		0.0050	{0.0020 0.0050 0.0065 0.0100}	176/176

Table G.1.1: Details of the simulations performed for computing the RCs. The number of configuration N_{stat} analyzed is given for the case of the WI determination and the RI-MOM analysis.

Furthermore, only momenta satisfying the cut $\Delta_4(p) < 0.28$ are considered.

Our RC estimators of bilinear operators have been computed for all combinations of valence quark masses appearing in Table G.1.1 while for the four-fermion operators only diagonal combinations in valence quark mass have been considered for simplicity.

G.2 Bilinear operators

In tables Table G.2.1 and Table G.2.2 we collect values of Z_P and Z_S calculated in the RI-MOM scheme. Results are obtained with the methods M1 and M2 described in chapter 4 at each value of the gauge coupling in $\overline{MS}$ and RI-MOM at 2 GeV. We have used the three-loop conversion formula from RI-MOM to $\overline{MS}$ described in Appendix C with $\Lambda_{\rm QCD} = 250$ MeV [158]. For illustration, in Figure G.2.1 the simultaneous best linear fits in $a^2\tilde{p}^2$of our β for Z_P are shown.

RC(M1)	$\beta = 3.80$	$\beta = 3.90$	$\beta = 4.05$	$\beta = 4.20$
$\overline{\rm MS}$ at 2 GeV				
Z_P	0.413(12)	0.437(07)	0.477(06)	0.498(05)
Z_S	0.728(16)	0.712(10)	0.702(05)	0.694(08)
RI-MOM at 2 GeV				
Z_P	0.339(09)	0.359(06)	0.391(04)	0.409(04)
Z_S	0.598(13)	0.585(09)	0.576(04)	0.570(07)

Table G.2.1: Z_P and Z_S results using the M1 method at β =3.80, 3.90, 4.05 and 4.20 in $\overline{MS}$ and RI-MOM at 2 GeV.

The values of the scale independent constants Z_A and Z_V are collected in Table G.2.3. The collected values of Z_V are the ones computed from the WI formula which turn to be more precise than the ones computed from the RI-MOM procedure.

RC(M2)	$\beta = 3.80$	$\beta = 3.90$	$\beta = 4.05$	$\beta = 4.20$
$\overline{\text{MS}}$ at 2 GeV				
Z_P	0.532(05)	0.518(06)	0.520(04)	0.503(05)
Z_S	0.813(07)	0.776(06)	0.735(04)	0.708(10)
RI-MOM at 2 GeV				
Z_P	0.437(04)	0.426(05)	0.427(04)	0.413(04)
Z_S	0.668(06)	0.637(05)	0.603(04)	0.582(08)

Table G.2.2: Z_P and Z_S results using the M2 method at β =3.80, 3.90, 4.05 and 4.20 in $\overline{MS}$ and RI-MOM at 2 GeV.

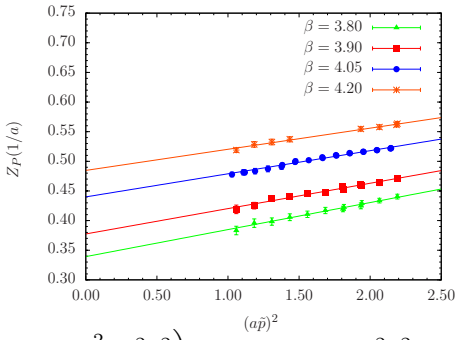

Figure G.2.1: $Z_P^{RI'}\left(\mu_0^2 = a\,(\beta)^{-2}; a^2\tilde{p}^2\right)$ as function of $a^2\tilde{p}^2$ for the four β values considered in our study at $N_f = 2$. The straight lines represent the simultaneous linear fit to the lattice data interval in $1.0 \leq a^2\tilde{p}^2 \leq 2.2$ at the four βs.

β	$Z_A(M1)$	$Z_A(M2)$	$Z_V(WI)$
3.80	0.750(10)	0.727(07)	0.5816(02)
3.90	0.747(06)	0.730(03)	0.6103(03)
4.05	0.769(05)	0.758(04)	0.6451(03)
4.20	0.776(05)	0.779(05)	0.6736(02)

Table G.2.3: Final estimates of Z_A with the M1 and M2 method and Z_V computed from the WI as described in subsection 4.4.3.3, for the four values of interest here.

G.3 Four-fermion operators

Here, I summarize the results of the procedure detailed in section 4.3 to compute the four-fermion RCs. First of all, for each β and choice of the scale $\tilde{p}^2$, the condition Eq.4.3.8 is enforced at all values of μ_{val} and μ_{sea}. By doing so, one obtains the lattice estimators at non zero masses of Z_{ij} which are extrapolated to $\mu_{val} = 0$ using the ansatz in Eq.4.4.7. A typical example is illustrated in Figure G.3.1. There we display the effect of the Goldstone Boson (GB) pole subtractions in the matrix elements of the dynamics matrix at two values of β. We do not find clear numerical evidence for single GB-pole in the valence mass chiral extrapolations and thus, we decide to ignore them.

The sea chiral limit is taken at fixed β and $a^2\tilde{p}^2$ by fitting Z_{ij} to a first order polynomial fit in $a^2\mu_{sea}^2$. We find that, as expected, the Δ_{ij} coefficients are compatible with zero and systematically smaller when β increases. Consequently, the effects of Δ have been neglected in our final RC analysis assuming a continuum-like renormalization pattern.

Improved estimates are obtained by removing the perturbatively leading cutoff effects. This can be done up to $\mathcal{O}(a^2g^2)$ exploiting the one-loop perturbative results in [91, 94] with the explicit coefficients for the tree-level Symmanzik improved action (tlsym) collected in Appendix D. In our numerical evaluation of the perturbative corrections, we take the coupling constant g^2 as the simple boosted coupling $\tilde{g}^2 \equiv g_0^2/\langle P\rangle$, where $\langle P\rangle$ is the non perturbative plaquette. The numerical values are [0.5689, 0.5825, 0.6014, 0.6200] for β =3.80, 3.90, 4.05 and 4.20 respectively.

The remaining $a^2\tilde{p}^2$ dependence is taken into account by employing either the M1 or M2 method introduced in chapter 4. RC estimators are brought to a reference scale value $\mu_0 = a^{-1}$ using the known NLO QCD evolution from [154, 95], sketched in Appendix C, with $\Lambda_{\rm QCD} = 250$ MeV [158]. Method M1 consists in fitting Z_{ij} to the linear ansatz in Figure G.3.2, where in the case of $N_f = 2$ the fit momentum region is taken to be $1.0 \leq a^2\tilde{p}^2 \leq 2.2$. As expected the slopes λ_{ij} depend smoothly on β. According to Eq.4.4.9 a simultaneous linear extrapolation in $a^2\tilde{p}^2 = 0$ at each β is performed. In Figure G.3.2 the best linear fits in $a^2\tilde{p}^2$ are shown.

Instead, the M2 method average at each β the value of $Z_{ij}^{RI'}\left(\mu_0^2 = a\,(\beta)^{-2}; a^2\tilde{p}^2\right)$ over a narrow interval of momenta, fixed in physical units. We have chosen $\tilde{p}^2 \in [8.0 : 9.5]$ GeV^2. The M1 and M2 final estimates are finally used to evaluate via the NLO running matrix formula of Buras et al. [95], the $Z_{ij}^{\overline{MS}}$quantities.

Final estimates

The RC matrices of the four-fermion operators in the lattice basis $\{\mathbf{O}_i\}$ are listed below. We present results obtained from both M1 and M2 methods, in $\overline{MS}$ and RI-MOM at 2 GeV.

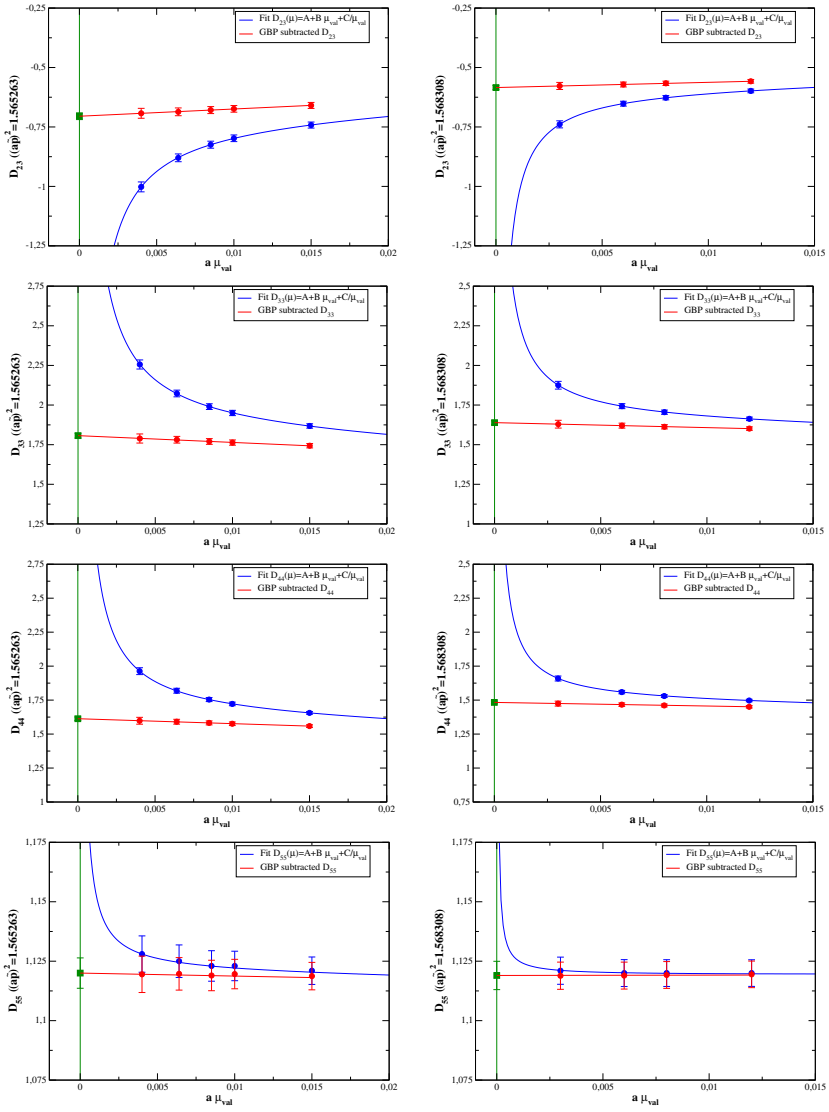

Figure G.3.1: Goldstone Boson pole subtraction and valence chiral limit of D_{23}, D_{33}, D_{44} and D_{55} plotted vs $a\mu_{val}$ for $\beta = 3.90$, $a\mu_{sea} = 0.0040$ and $(a\tilde{p})^2 \sim 1.565$ (left column) and $\beta = 4.05$, $a\mu_{sea} = 0.0030$ and $(a\tilde{p})^2 \sim 1.568$ (right column)

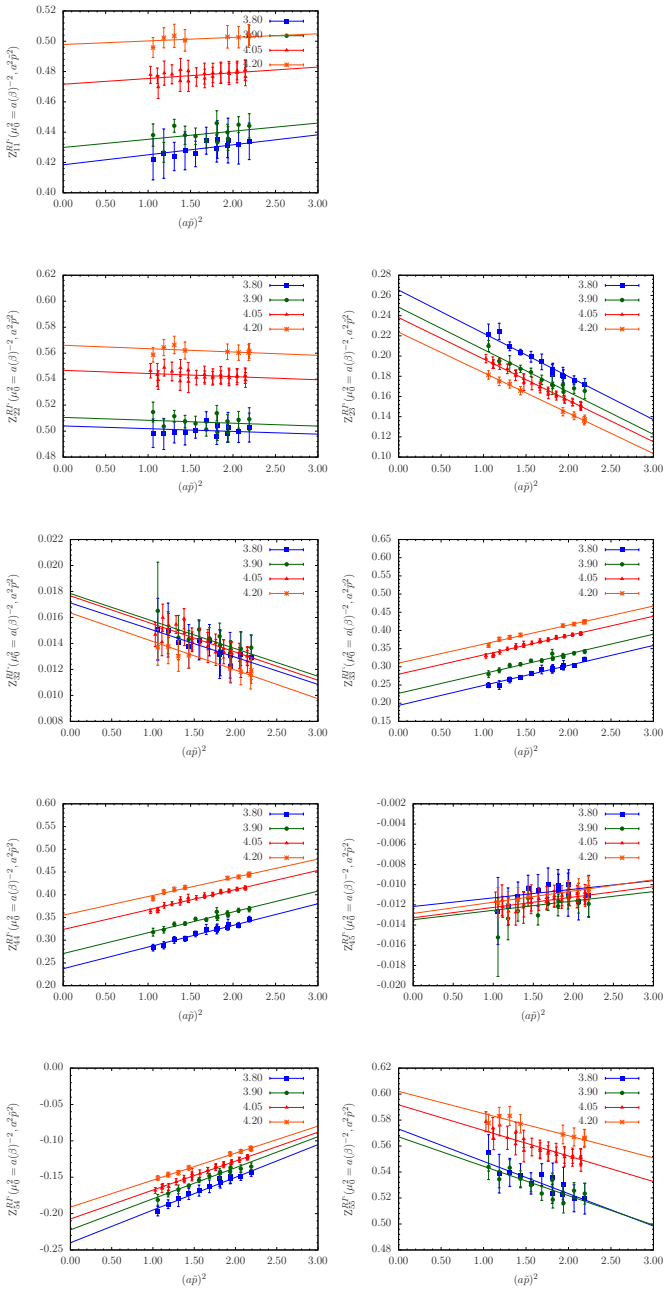

Figure G.3.2: $Z_{ij}^{RI'}\left(\mu_0^2 = a\,(\beta)^{-2}; a^2\tilde{p}^2\right)$ for $\{ij\} = \{11, 22, 23, 32, 33, 44, 45, 54, 55\}$ as functions of $a^2\tilde{p}^2$ for the four β values considered in our study. The straight lines represent the simultaneous linear fit to the lattice data in the interval $1.0 \leq a^2\tilde{p}^2 \leq 2.2$ at the four β's.

($\overline{\mathbf{MS}}$, 2 GeV):

$$\mathbf{Z}_{\chi}{}^{\mathtt{PC+}}(\beta = 3.80; M1) = \begin{pmatrix} 0.425(15) & 0 & 0 & 0 & 0 \\ 0 & 0.492(13) & 0.238(07) & 0 & 0 \\ 0 & 0.022(02) & 0.227(10) & 0 & 0 \\ 0 & 0 & 0 & 0.257(09) & -0.005(02) \\ 0 & 0 & 0 & -0.246(08) & 0.600(14) \end{pmatrix}$$

$$\mathbf{Z}_{\chi}{}^{\mathtt{PC+}}(\beta = 3.90; M1) = \begin{pmatrix} 0.440(08) & 0 & 0 & 0 & 0 \\ 0 & 0.503(08) & 0.231(04) & 0 & 0 \\ 0 & 0.023(01) & 0.250(06) & 0 & 0 \\ 0 & 0 & 0 & 0.282(06) & -0.006(01) \\ 0 & 0 & 0 & -0.244(05) & 0.617(11) \end{pmatrix}$$

$$\mathbf{Z}_{\chi}{}^{\mathtt{PC+}}(\beta = 4.05; M1) = \begin{pmatrix} 0.490(06) & 0 & 0 & 0 & 0 \\ 0 & 0.546(06) & 0.240(05) & 0 & 0 \\ 0 & 0.023(01) & 0.281(05) & 0 & 0 \\ 0 & 0 & 0 & 0.319(04) & -0.004(01) \\ 0 & 0 & 0 & -0.258(05) & 0.681(09) \end{pmatrix}$$

$$\mathbf{Z}_{\chi}{}^{\mathtt{PC+}}(\beta = 4.20; M1) = \begin{pmatrix} 0.523(010) & 0 & 0 & 0 & 0 \\ 0 & 0.571(09) & 0.243(07) & 0 & 0 \\ 0 & 0.021(01) & 0.292(08) & 0 & 0 \\ 0 & 0 & 0 & 0.335(07) & -0.002(02) \\ 0 & 0 & 0 & -0.266(06) & 0.726(010) \end{pmatrix}$$

($\overline{\mathbf{MS}}$, 2 GeV):

$$\mathbf{Z}_{\chi}{}^{\mathtt{PC+}}(\beta = 3.80; M2) = \begin{pmatrix} 0.439(12) & 0 & 0 & 0 & 0 \\ 0 & 0.489(09) & 0.136(05) & 0 & 0 \\ 0 & 0.017(02) & 0.362(05) & 0 & 0 \\ 0 & 0 & 0 & 0.369(07) & -0.005(02) \\ 0 & 0 & 0 & -0.144(05) & 0.544(11) \end{pmatrix}$$

$$\mathbf{Z}_{\chi}{}^{\mathtt{PC+}}(\beta = 3.90; M2) = \begin{pmatrix} 0.446(05) & 0 & 0 & 0 & 0 \\ 0 & 0.496(05) & 0.158(04) & 0 & 0 \\ 0 & 0.019(01) & 0.348(05) & 0 & 0 \\ 0 & 0 & 0 & 0.362(04) & -0.005(01) \\ 0 & 0 & 0 & -0.167(04) & 0.573(05) \end{pmatrix}$$

$$\mathbf{Z}_{\chi}{}^{\mathtt{PC+}}(\beta = 4.05; M2) = \begin{pmatrix} 0.495(05) & 0 & 0 & 0 & 0 \\ 0 & 0.543(06) & 0.197(04) & 0 & 0 \\ 0 & 0.020(01) & 0.333(06) & 0 & 0 \\ 0 & 0 & 0 & 0.361(05) & -0.003(01) \\ 0 & 0 & 0 & -0.211(04) & 0.660(09) \end{pmatrix}$$

$$\mathbf{Z}_{\chi}{}^{\mathtt{PC+}}(\beta = 4.20; M2) = \begin{pmatrix} 0.531(06) & 0 & 0 & 0 & 0 \\ 0 & 0.579(06) & 0.239(03) & 0 & 0 \\ 0 & 0.019(01) & 0.299(05) & 0 & 0 \\ 0 & 0 & 0 & 0.334(05) & -0.000(01) \\ 0 & 0 & 0 & -0.259(04) & 0.733(08) \end{pmatrix}$$

(RI-MOM, 2 GeV):

$$\mathbf{Z}_{\chi}{}^{\text{PC+}}(\beta = 3.80; M1) = \begin{pmatrix} 0.418(15) & 0 & 0 & 0 & 0 \\ 0 & 0.504(13) & 0.265(07) & 0 & 0 \\ 0 & 0.017(02) & 0.195(09) & 0 & 0 \\ 0 & 0 & 0 & 0.238(08) & -0.012(02) \\ 0 & 0 & 0 & -0.240(08) & 0.573(14) \end{pmatrix}$$

$$\mathbf{Z}_{\chi}{}^{\text{PC+}}(\beta = 3.90; M1) = \begin{pmatrix} 0.434(08) & 0 & 0 & 0 & 0 \\ 0 & 0.515(08) & 0.260(05) & 0 & 0 \\ 0 & 0.018(01) & 0.215(05) & 0 & 0 \\ 0 & 0 & 0 & 0.261(06) & -0.013(01) \\ 0 & 0 & 0 & -0.239(05) & 0.589(11) \end{pmatrix}$$

$$\mathbf{Z}_{\chi}{}^{\text{PC+}}(\beta = 4.05; M1) = \begin{pmatrix} 0.483(06) & 0 & 0 & 0 & 0 \\ 0 & 0.559(06) & 0.273(05) & 0 & 0 \\ 0 & 0.017(01) & 0.242(04) & 0 & 0 \\ 0 & 0 & 0 & 0.295(03) & -0.012(01) \\ 0 & 0 & 0 & -0.253(05) & 0.650(08) \end{pmatrix}$$

$$\mathbf{Z}_{\chi}{}^{\text{PC+}}(\beta = 4.20; M1) = \begin{pmatrix} 0.516(010) & 0 & 0 & 0 & 0 \\ 0 & 0.585(09) & 0.278(07) & 0 & 0 \\ 0 & 0.016(01) & 0.251(07) & 0 & 0 \\ 0 & 0 & 0 & 0.310(06) & -0.011(02) \\ 0 & 0 & 0 & -0.261(06) & 0.693(010) \end{pmatrix}$$

(RI-MOM, 2 GeV):

$$\mathbf{Z}_{\chi}{}^{\text{PC+}}(\beta = 3.80; M2) = \begin{pmatrix} 0.433(12) & 0 & 0 & 0 & 0 \\ 0 & 0.501(09) & 0.175(05) & 0 & 0 \\ 0 & 0.013(02) & 0.311(05) & 0 & 0 \\ 0 & 0 & 0 & 0.339(06) & -0.011(02) \\ 0 & 0 & 0 & -0.146(05) & 0.520(11) \end{pmatrix}$$

$$\mathbf{Z}_{\chi}{}^{\text{PC+}}(\beta = 3.90; M2) = \begin{pmatrix} 0.440(05) & 0 & 0 & 0 & 0 \\ 0 & 0.508(05) & 0.196(04) & 0 & 0 \\ 0 & 0.015(01) & 0.299(04) & 0 & 0 \\ 0 & 0 & 0 & 0.334(03) & -0.012(01) \\ 0 & 0 & 0 & -0.168(03) & 0.547(05) \end{pmatrix}$$

$$\mathbf{Z}_{\chi}{}^{\text{PC+}}(\beta = 4.05; M2) = \begin{pmatrix} 0.487(05) & 0 & 0 & 0 & 0 \\ 0 & 0.556(06) & 0.234(04) & 0 & 0 \\ 0 & 0.015(01) & 0.287(05) & 0 & 0 \\ 0 & 0 & 0 & 0.333(04) & -0.011(01) \\ 0 & 0 & 0 & -0.210(04) & 0.630(08) \end{pmatrix}$$

$$\mathbf{Z}_{\chi}{}^{\text{PC+}}(\beta = 4.20; M2) = \begin{pmatrix} 0.523(06) & 0 & 0 & 0 & 0 \\ 0 & 0.593(06) & 0.274(04) & 0 & 0 \\ 0 & 0.014(01) & 0.257(04) & 0 & 0 \\ 0 & 0 & 0 & 0.308(04) & -0.009(01) \\ 0 & 0 & 0 & -0.254(04) & 0.700(07) \end{pmatrix}$$

Appendix H

$\mathbf{N_f = 2 + 1 + 1}$ Lattice data on masses and matrix elements

In this appendix I present the tables with our estimates for the pseudoscalar masses and bare bag parameters with the $N_f = 2 + 1 + 1$ simulation.

H.1 Pseudoscalar meson masses

For each β, each μ_{sea} and each couple $(a\mu_\ell, a\mu_\ell)$ and $(a\mu_h, a\mu_h)$ we have computed the Twisted-Mass, i.e $r_1 = r_2$, pseudoscalar meson mass $aM_{\ell\ell}$ and aM_{hh} relevant in the interpolation/extrapolation of the $N_f = 2 + 1 + 1$ bag parameters to the physical point. Table H.1.1 summarize the ranges $[t_{\rm min} : t_{\rm max}]$ where the constant fit to the effective mass in Eq.3.1.13 has been performed.

β	V	$[t_{\rm min} : t_{\rm max}]$
1.90	$24^3 \times 48$	11:20
	$32^3 \times 48$	11:28
1.95	$24^3 \times 48$	13:20
	$32^3 \times 48$	13:28
2.10	$48^3 \times 96$	17:44

Table H.1.1: Time fit intervals used in the analysis

$\beta = 1.90$ $L^3 \times T = 24^3 \times 48$				
$a\mu_{sea}$	$aM_{\ell\ell}$	aM_{11}	aM_{22}	aM_{33}
0.0040	0.1441(13)	0.2686(9)	0.3032(8)	0.3347(7)
0.0060	0.1754(8)	0.2684(6)	0.3030(6)	0.3345(6)
0.0080	0.1995(7)	0.2668(7)	0.3015(7)	0.3331(7)
0.0100	0.2228(6)	0.2673(6)	0.3020(5)	0.3336(5)

Table H.1.2: $aM_{\ell\ell}$ and aM_{hh} for the three simulated strange valence quark masses at $\beta = 1.90$ and $L^3 \times T = 24^3 \times 48$

$\beta = 1.90$ $L^3 \times T = 32^3 \times 64$				
$a\mu_{sea}$	$aM_{\ell\ell}$	aM_{11}	aM_{22}	aM_{33}
0.0030	0.1237(7)	0.2668(6)	0.3015(5)	0.3329(5)
0.0040	0.1421(4)	0.2669(4)	0.3017(4)	0.3332(4)
0.0050	0.1572(4)	0.2654(4)	0.3003(3)	0.3320(3)

Table H.1.3: $aM_{\ell\ell}$ and aM_{hh} for the three simulated strange valence quark masses at $\beta = 1.90$ and $L^3 \times T = 32^3 \times 64$

$\beta = 1.95$ $L^3 \times T = 24^3 \times 48$				
$a\mu_{sea}$	$aM_{\ell\ell}$	aM_{11}	aM_{22}	aM_{33}
0.0085	0.1934(9)	0.2484(8)	0.2810(8)	0.3107(8)

Table H.1.4: $aM_{\ell\ell}$ and aM_{hh} for the three simulated strange valence quark masses at $\beta = 1.95$ and $L^3 \times T = 24^3 \times 48$

$\beta = 1.95$ $L^3 \times T = 32^3 \times 64$				
$a\mu_{sea}$	$aM_{\ell\ell}$	aM_{11}	aM_{22}	aM_{33}
0.0025	0.1068(5)	0.2471(5)	0.2795(5)	0.3090(5)
0.0035	0.1253(4)	0.2468(3)	0.2793(3)	0.3089(3)
0.0055	0.1551(3)	0.2473(3)	0.2799(3)	0.3095(3)
0.0075	0.1800(6)	0.2467(6)	0.2794(6)	0.3092(6)

Table H.1.5: $aM_{\ell\ell}$ and aM_{hh} for the three simulated strange valence quark masses at $\beta = 1.95$ and $L^3 \times T = 32^3 \times 64$

$\beta = 2.10$ $L^3 \times T = 48^3 \times 96$				
$a\mu_{sea}$	$aM_{\ell\ell}$	aM_{11}	aM_{22}	aM_{33}
0.0015	0.0697(4)	0.1924(3)	0.2181(3)	0.2414(3)
0.0020	0.0799(4)	0.1919(4)	0.2176(4)	0.2410(4)
0.0030	0.0975(3)	0.1923(3)	0.2181(3)	0.2416(3)

Table H.1.6: $aM_{\ell\ell}$ and aM_{hh} for the three simulated strange valence quark masses at $\beta = 2.10$ and $L^3 \times T = 48^3 \times 96$

H.2 Bare bag parameters

In the following tables I collect the bare results for the quantities $\xi_i B_i$ at all values of β and each couple of $(a\mu_\ell = a\mu_{sea}, a\mu_{\text{“}s\text{”}})$ valence quark masses relevant for the $N_f = 2+1+1$ analysis of $\overline{K}^0 - K^0$. The fit time interval has taken to be $[T/4 - 2 : T/4 + 2]$.

$\beta = 1.90$ $L^3 \times T = 24^3 \times 48$							
$a\mu_{sea}$	$a\mu_\ell$	$a\mu_h$	$\xi_1 B_1$	$\xi_2 B_2$	$\xi_3 B_3$	$\xi_4 B_4$	$\xi_5 B_5$
0.0040	0.0040	0.0145	1.605(22)	0.963(08)	0.235(02)	1.867(13)	0.620(04)
		0.0185	1.642(19)	0.982(08)	0.239(02)	1.892(12)	0.633(04)
		0.0225	1.674(18)	0.999(07)	0.242(02)	1.914(12)	0.646(04)
0.0060	0.0060	0.0145	1.567(21)	0.978(07)	0.238(02)	1.874(09)	0.625(03)
		0.0185	1.601(19)	0.994(06)	0.241(02)	1.896(08)	0.637(03)
		0.0225	1.630(18)	1.008(05)	0.244(01)	1.914(08)	0.648(03)
0.0080	0.0080	0.0145	1.624(19)	0.991(05)	0.241(01)	1.900(08)	0.638(03)
		0.0185	1.653(16)	1.008(04)	0.244(01)	1.921(07)	0.649(03)
		0.0225	1.679(14)	1.022(04)	0.247(01)	1.938(07)	0.660(03)
0.0100	0.0100	0.0145	1.640(10)	0.998(05)	0.242(01)	1.884(09)	0.634(03)
		0.0185	1.670(10)	1.014(04)	0.246(01)	1.903(09)	0.645(03)
		0.0225	1.696(10)	1.029(04)	0.249(01)	1.920(08)	0.655(03)

Table H.2.1: Strange-light $\xi_i B_i$ at $\beta = 1.90$ and $L^3 \times T = 24^3 \times 48$

$\beta = 1.90$ $L^3 \times T = 32^3 \times 64$							
$a\mu_{sea}$	$a\mu_\ell$	$a\mu_h$	$\xi_1 B_1$	$\xi_2 B_2$	$\xi_3 B_3$	$\xi_4 B_4$	$\xi_5 B_5$
0.0030	0.0030	0.0145	1.536(26)	0.943(08)	0.230(02)	1.877(17)	0.623(05)
		0.0185	1.572(23)	0.961(08)	0.233(02)	1.898(15)	0.635(05)
		0.0225	1.606(22)	0.977(07)	0.237(02)	1.916(15)	0.646(05)
0.0040	0.0040	0.0145	1.563(23)	0.965(05)	0.235(01)	1.871(13)	0.623(04)
		0.0185	1.606(21)	0.983(04)	0.239(01)	1.895(13)	0.636(04)
		0.0225	1.643(21)	0.999(04)	0.242(01)	1.915(14)	0.648(04)
0.0050	0.0050	0.0145	1.577(24)	0.965(04)	0.235(01)	1.867(06)	0.622(02)
		0.0185	1.614(22)	0.983(04)	0.239(01)	1.890(06)	0.635(02)
		0.0225	1.648(21)	0.998(04)	0.242(01)	1.910(06)	0.646(02)

Table H.2.2: Strange-light $\xi_i B_i$ at $\beta = 1.90$ and $L^3 \times T = 32^3 \times 64$

$\beta = 1.95$ $L^3 \times T = 24^3 \times 48$							
$a\mu_{sea}$	$a\mu_\ell$	$a\mu_h$	$\xi_1 B_1$	$\xi_2 B_2$	$\xi_3 B_3$	$\xi_4 B_4$	$\xi_5 B_5$
0.0085	0.0085	0.0141	1.660(35)	0.993(19)	0.242(05)	1.934(39)	0.649(13)
		0.0180	1.691(35)	1.012(20)	0.246(05)	1.955(39)	0.661(13)
		0.0219	1.720(35)	1.028(20)	0.250(05)	1.974(39)	0.672(13)

Table H.2.3: Strange-light $\xi_i B_i$ at $\beta = 1.95$ and $L^3 \times T = 24^3 \times 48$

$\beta = 1.95$ $L^3 \times T = 32^3 \times 64$							
$a\mu_{sea}$	$a\mu_\ell$	$a\mu_h$	$\xi_1 B_1$	$\xi_2 B_2$	$\xi_3 B_3$	$\xi_4 B_4$	$\xi_5 B_5$
0.0025	0.0025	0.0141	1.560(35)	0.922(08)	0.226(02)	1.884(15)	0.624(05)
		0.0180	1.592(34)	0.940(08)	0.230(02)	1.911(15)	0.638(05)
		0.0219	1.622(34)	0.956(08)	0.233(02)	1.934(15)	0.651(05)
0.0035	0.0035	0.0141	1.589(24)	0.936(07)	0.229(02)	1.877(13)	0.622(04)
		0.0180	1.623(23)	0.955(07)	0.233(02)	1.900(13)	0.635(04)
		0.0219	1.653(23)	0.972(07)	0.237(02)	1.921(13)	0.647(04)
0.0055	0.0055	0.0141	1.569(18)	0.951(05)	0.232(01)	1.859(09)	0.621(03)
		0.0180	1.604(15)	0.968(05)	0.236(01)	1.881(09)	0.633(03)
		0.0219	1.635(14)	0.984(05)	0.239(01)	1.901(08)	0.645(03)
0.0075	0.0075	0.0141	1.643(16)	0.964(04)	0.236(01)	1.880(08)	0.629(03)
		0.0180	1.672(16)	0.981(04)	0.239(01)	1.901(08)	0.641(03)
		0.0219	1.699(16)	0.997(04)	0.242(01)	1.920(08)	0.652(03)

Table H.2.4: Strange-light $\xi_i B_i$ at $\beta = 1.95$ and $L^3 \times T = 32^3 \times 64$

$\beta = 2.10$ $L^3 \times T = 48^3 \times 96$							
$a\mu_{sea}$	$a\mu_\ell$	$a\mu_h$	$\xi_1 B_1$	$\xi_2 B_2$	$\xi_3 B_3$	$\xi_4 B_4$	$\xi_5 B_5$
0.0015	0.0015	0.0118	1.472(29)	0.865(08)	0.215(02)	1.863(12)	0.611(04)
		0.0151	1.518(31)	0.884(08)	0.219(02)	1.895(12)	0.627(04)
		0.0184	1.556(33)	0.900(08)	0.222(02)	1.923(13)	0.641(04)
0.0020	0.0020	0.0118	1.452(22)	0.880(05)	0.218(01)	1.827(08)	0.602(03)
		0.0151	1.499(23)	0.899(05)	0.222(01)	1.859(08)	0.617(03)
		0.0184	1.540(23)	0.916(05)	0.226(01)	1.886(08)	0.631(03)
0.0030	0.0030	0.0118	1.477(16)	0.886(04)	0.220(01)	1.839(08)	0.606(03)
		0.0151	1.519(14)	0.903(03)	0.223(01)	1.868(09)	0.620(03)
		0.0184	1.557(13)	0.919(03)	0.227(01)	1.893(09)	0.633(03)

Table H.2.5: Strange-light $\xi_i B_i$ at $\beta = 2.10$ and $L^3 \times T = 48^3 \times 96$

Acronyms list

ChPT ..... Chiral Perturbation Theory
CKM ..... Cabibbo-Kobayashi-Maskawa
ETMC ..... European Twisted Mass Collaboration
FCNC ..... Flavour Changing Neutral Currents
GB ..... Goldstone Boson
HMChPT ..... Heavy Meson Chiral Perturbation Theory
HQET ..... Heavy Quark Effective Theory
LL ..... Leading Log
LO ..... Leading Order
LQCD ..... Lattice QCD
NLL ..... Next to Leading Log
NLO ..... Next to Leading Order
NP ..... New Physics
OPE ..... Operator Product Expansion
OS ..... Osterwalder-Seiler
PC ..... Parity Conserving
PV ..... Parity Violating
QCD ..... Quantum Chromodynamics
QED ..... Quantum Electrodynamics
RC ..... Renormalization Constants
RGI ..... Regularization Group Invariant
RI-MOM ..... Regularization Independent Momentum subtraction
SM ..... Standard Model
TL ..... Tree Level
TM ..... Twisted Mass
UT ..... Unitarity Triangle
UTA ..... Unitarity Triangle Analysis
VIA ..... Vacuum Insertion Approximation

Bibliography

[1] Steven Weinberg. A model of leptons. *Phys. Rev. Lett.*, 19:1264–1266, Nov 1967.

[2] A.Salam. *Elementary Particle Physics ed. N. Svartholm (Stockholm: Almqvist and Wiksells)*, 1968.

[3] Georges Aad et al. Observation of a new particle in the search for the Standard Model Higgs boson with the ATLAS detector at the LHC. *Phys.Lett.*, B716:1–29, 2012, 1207.7214.

[4] Serguei Chatrchyan et al. Observation of a new boson at a mass of 125 GeV with the CMS experiment at the LHC. *Phys.Lett.*, B716:30–61, 2012, 1207.7235.

[5] J.H. Christenson, J.W. Cronin, V.L. Fitch, and R. Turlay. Evidence for the 2 pi Decay of the k(2)0 Meson. *Phys.Rev.Lett.*, 13:138–140, 1964.

[6] H. Burkhardt et al. First Evidence for Direct CP Violation. *Phys.Lett.*, B206:169, 1988.

[7] A. Alavi-Harati et al. Observation of direct CP violation in K(S,L)-> pi pi decays. *Phys.Rev.Lett.*, 83:22–27, 1999, hep-ex/9905060.

[8] V. Fanti et al. A New measurement of direct CP violation in two pion decays of the neutral kaon. *Phys.Lett.*, B465:335–348, 1999, hep-ex/9909022.

[9] Bernard Aubert et al. Observation of CP violation in the B^0 meson system. *Phys.Rev.Lett.*, 87:091801, 2001, hep-ex/0107013.

[10] K. Abe et al. Observation of large CP violation in the neutral B meson system. *Phys.Rev.Lett.*, 87:091802, 2001, hep-ex/0107061.

[11] R. Aaij et al. Evidence for CP violation in time-integrated $D^0 \to h^- h^+$ decay rates. *Phys.Rev.Lett.*, 108:111602, 2012, 1112.0938.

[12] Makoto Kobayashi and Toshihide Maskawa. CP Violation in the Renormalizable Theory of Weak Interaction. *Prog.Theor.Phys.*, 49:652–657, 1973.

[13] Patrick Huet and Eric Sather. Electroweak baryogenesis and standard model *CP* violation. *Phys. Rev. D*, 51:379–394, Jan 1995.

[14] P.G. Harris, C.A. Baker, K. Green, P. Iaydjiev, S. Ivanov, et al. New experimental limit on the electric dipole moment of the neutron. *Phys.Rev.Lett.*, 82:904–907, 1999.

[15] The UTfit collaboration (summer 2012): http://www.utfit.org/utfit/results.

[16] A. Lenz, U. Nierste, J. Charles, S. Descotes-Genon, H. Lacker, et al. Constraints on new physics in $B - \bar{B}$ mixing in the light of recent LHCb data. *Phys.Rev.*, D86:033008, 2012, 1203.0238.

[17] Bernard Aubert et al. Evidence for D^0 -anti-D0 Mixing. *Phys.Rev.Lett.*, 98:211802, 2007, hep-ex/0703020.

[18] K. Abe et al. Measurement of D0 - anti-D0 Mixing Parameters in D0 ; K(s)0 pi+ pi- decays. *Phys.Rev.Lett.*, 99:131803, 2007, 0704.1000.

[19] M. Staric et al. Evidence for D^0 - $\bar{D}^0$ Mixing. *Phys.Rev.Lett.*, 98:211803, 2007, hep-ex/0703036.

[20] R Aaij et al. Observation of D0-D0bar oscillations. 2012, 1211.1230.

[21] I.Montway and G. Muntster. *Quantum Fields on a Lattice*. Cambridge University Press, 1974.

[22] T. De Grand and C. DeTar. *Lattice methods for quantum chromodynamics*. World Scientific Lecture Notes in Physics, 2006.

[23] R. Frezzotti and G. C. Rossi. Chirally improving Wilson fermions. II: Four-quark operators. *JHEP*, 10:070, 2004, hep-lat/0407002.

[24] B. Blossier et al. A Proposal for B-physics on current lattices. *JHEP*, 1004:049, 2010, 0909.3187.

[25] The UTfit collaboration: http://utfit.org.

[26] Marco Ciuchini, G. D'Agostini, E. Franco, V. Lubicz, G. Martinelli, et al. 2000 CKM triangle analysis: A Critical review with updated experimental inputs and theoretical parameters. *JHEP*, 0107:013, 2001, hep-ph/0012308.

[27] Karl Jansen and Rainer Sommer. O(alpha) improvement of lattice QCD with two flavors of Wilson quarks. *Nucl.Phys.*, B530:185–203, 1998, hep-lat/9803017.

[28] G.P. Dubois-Felsmann, D.G. Hitlin, F.C. Porter, and G. Eigen. Sensitivity of CKM fits to theoretical uncertainties and their representation. 2003, hep-ph/0308262.

[29] http://ckmfitter.in2p3.fr/.

[30] Enrico Lunghi and Amarjit Soni. Possible Indications of New Physics in B_d -mixing and in sin(2 beta) Determinations. *Phys.Lett.*, B666:162–165, 2008, 0803.4340.

[31] Enrico Lunghi and Amarjit Soni. Hints for the scale of new CP-violating physics from B-CP anomalies. *JHEP*, 0908:051, 2009, 0903.5059.

[32] Andrzej J. Buras and Diego Guadagnoli. On the consistency between the observed amount of CP violation in the K^- and Bd-systems within minimal flavor violation. *Phys.Rev.*, D79:053010, 2009, 0901.2056.

[33] Cecilia Tarantino. Flavor Lattice QCD in the Precision Era. 2012, 1210.0474.

[34] Murray Gell-Mann and A. Pais. Behavior of neutral particles under charge conjugation. *Phys.Rev.*, 97:1387–1389, 1955.

[35] H. Albrecht et al. Observation of B0 - anti-B0 Mixing. *Phys.Lett.*, B192:245, 1987.

[36] A. Abulencia et al. Observation of B0(s) - anti-B0(s) Oscillations. *Phys.Rev.Lett.*, 97:242003, 2006, hep-ex/0609040.

[37] T. Aaltonen et al. Evidence for $D^0 - \bar{D}^0$ mixing using the CDF II Detector. *Phys.Rev.Lett.*, 100:121802, 2008, 0712.1567.

[38] Collins. *Renormalization*. Cambridge University Press, 1984.

[39] T. Inami and C.S. Lim. Effects of Superheavy Quarks and Leptons in Low-Energy Weak Processes ... *Prog.Theor.Phys.*, 65:297, 1981.

[40] Stefan Herrlich and Ulrich Nierste. Indirect CP violation in the neutral kaon system beyond leading logarithms. *Phys. Rev.*, D52:6505–6518, 1995, hep-ph/9507262.

[41] Andrzej J. Buras, Matthias Jamin, and Peter H. Weisz. LEADING AND NEXT-TO-LEADING QCD CORRECTIONS TO epsilon PARAMETER AND B0 - anti-B0 MIXING IN THE PRESENCE OF A HEAVY TOP QUARK. *Nucl.Phys.*, B347:491–536, 1990.

[42] Stefan Herrlich and Ulrich Nierste. The Complete |Delta S|=2 Hamiltonian in the Next-To- Leading Order. *Nucl. Phys.*, B476:27–88, 1996, hep-ph/9604330.

[43] Joachim Brod and Martin Gorbahn. $Epsilon_K$ at Next-to-Next-to-Leading Order: The Charm-Top-Quark Contribution. *Phys.Rev.*, D82:094026, 2010, 1007.0684.

[44] Ling-Lie Chau. Quark Mixing in Weak Interactions. *Phys. Rept.*, 95:1–94, 1983.

[45] Review of particle physics. *Phys. Rev. D*, 86:010001, Jul 2012.

[46] Andrzej J. Buras. Weak Hamiltonian, CP violation and rare decays. pages 281–539, 1998, hep-ph/9806471.

[47] Andrzej J. Buras, Diego Guadagnoli, and Gino Isidori. On $epsilon_K$ beyond lowest order in the Operator Product Expansion. *Phys.Lett.*, B688:309–313, 2010, 1002.3612.

[48] Gilberto Colangelo, Stephan Durr, Andreas Juttner, Laurent Lellouch, Heinrich Leutwyler, et al. Review of lattice results concerning low energy particle physics. *Eur.Phys.J.*, C71:1695, 2011, 1011.4408.

[49] D. Asner et al. Averages of b-hadron, c-hadron, and τ-lepton Properties. 2010, 1010.1589.

[50] E. Lunghi and Amarjit Soni. Possible evidence for the breakdown of the CKM-paradigm of CP-violation. *Phys.Lett.*, B697:323–328, 2011, 1010.6069.

[51] M. Bona et al. Model-independent constraints on Δ F=2 operators and the scale of new physics. *JHEP*, 0803:049, 2008, 0707.0636.

[52] Gerhard Buchalla. Renormalization of delta B = 2 transitions in the static limit beyond leading logarithms. *Phys.Lett.*, B395:364–368, 1997, hep-ph/9608232.

[53] Heinz J.Rothe. *Lattice Gauge Theories, An Introduction*. World Scientific Lecture Notes in Physics, 1994.

[54] Andrea Shindler. Twisted mass lattice QCD. *Phys. Rept.*, 461:37–110, 2008, 0707.4093.

[55] Stefan Sint. Lattice QCD with a chiral twist. 2007, hep-lat/0702008.

[56] K. Yoshida G. Immirzi. Generalized lattice fermion actions and applications. *Nuclear Physics*, B(210):499–512, 1982.

[57] Roberto Frezzotti, Stefan Sint, and Peter Weisz. O(a) improved twisted mass lattice QCD. *JHEP*, 0107:048, 2001, hep-lat/0104014.

[58] Kenneth G. Wilson. Quarks and Strings on a Lattice. New Phenomena In Subnuclear Physics. Part A. Proceedings of the First Half of the 1975 International School of Subnuclear Physics, Erice, Sicily, July 11 - August 1, 1975, ed. A. Zichichi, Plenum Press, New York, 1977, p. 69, CLNS-321.

[59] Commun D.Friedan. *Math.Phys*, (85):481, 1982.

[60] Martin Luscher, Stefan Sint, Rainer Sommer, and Peter Weisz. Chiral symmetry and O(a) improvement in lattice QCD. *Nucl. Phys.*, B478:365–400, 1996, hep-lat/9605038.

[61] P. Weisz and R. Wohlert. Continuum Limit Improved Lattice Action for Pure Yang-Mills Theory. 2. *Nucl. Phys.*, B236:397, 1984.

[62] Martin Luscher, Stefan Sint, Rainer Sommer, Peter Weisz, and Ulli Wolff. Non-perturbative O(a) improvement of lattice QCD. *Nucl. Phys.*, B491:323–343, 1997, hep-lat/9609035.

[63] Y. Iwasaki. RENORMALIZATION GROUP ANALYSIS OF LATTICE THEORIES AND IMPROVED LATTICE ACTION. 1. TWO-DIMENSIONAL NONLINEAR O(N) SIGMA MODEL. UTHEP-117.

[64] Tetsuya Takaishi. Heavy quark potential and effective actions on blocked configurations. *Phys. Rev.*, D54:1050–1053, 1996.

[65] Sinya Aoki and Andreas Gocksch. SPONTANEOUS BREAKING OF PARITY IN QUENCHED LATTICE QCD WITH WILSON FERMIONS. *Phys.Lett.*, B231:449, 1989.

[66] R. Frezzotti and G. C. Rossi. Chirally improving Wilson fermions. I: O(a) improvement. *JHEP*, 08:007, 2004, hep-lat/0306014.

[67] Philippe Boucaud et al. Dynamical Twisted Mass Fermions with Light Quarks: Simulation and Analysis Details. *Comput.Phys.Commun.*, 179:695–715, 2008, 0803.0224.

[68] R. Frezzotti and G.C. Rossi. Twisted mass lattice QCD with mass nondegenerate quarks. *Nucl.Phys.Proc.Suppl.*, 128:193–202, 2004, hep-lat/0311008.

[69] R. Baron et al. Light hadrons from lattice QCD with light (u,d), strange and charm dynamical quarks. *JHEP*, 06:111, 2010, 1004.5284.

[70] K. Osterwalder and E. Seiler. Gauge Field Theories on the Lattice. *Annals Phys.*, 110:440, 1978.

[71] K. Jansen and C. Urbach. tmLQCD: A Program suite to simulate Wilson Twisted mass Lattice QCD. *Comput.Phys.Commun.*, 180:2717–2738, 2009, 0905.3331.

[72] R. Sommer. A New way to set the energy scale in lattice gauge theories and its applications to the static force and alpha-s in SU(2) Yang-Mills theory. *Nucl.Phys.*, B411:839–854, 1994, hep-lat/9310022.

[73] Lüscher M. Volume dependence of the energy spectrum in massive quantum field theories. *Math.Phys*, 104:177–206, 1986.

[74] M. Luscher. Construction of a Selfadjoint, Strictly Positive Transfer Matrix for Euclidean Lattice Gauge Theories. *Commun.Math.Phys.*, 54:283, 1977.

[75] A. Donini, V. Gimenez, G. Martinelli, M. Talevi, and A. Vladikas. Non-perturbative renormalization of lattice four-fermion operators without power subtractions. *Eur. Phys. J.*, C10:121–142, 1999, hep-lat/9902030.

[76] G. Martinelli and Yi-Cheng Zhang. The Connection Between Local Operators on the Lattice and in the Continuum and Its Relation to Meson Decay Constants. *Phys.Lett.*, B123:433, 1983.

[77] G. Martinelli. THE FOUR FERMION OPERATORS OF THE WEAK HAMILTONIAN ON THE LATTICE AND IN THE CONTINUUM. *Phys.Lett.*, B141:395, 1984.

[78] G. Martinelli and Yi-Cheng Zhang. ONE LOOP CORRECTIONS TO EXTENDED OPERATORS ON THE LATTICE. *Phys.Lett.*, B125:77, 1983.

[79] R. Frezzotti, E. Gabrielli, C. Pittori, and G.C. Rossi. Four fermion operators with improved nearest neighbor action. *Nucl.Phys.*, B373:781–794, 1992.

[80] Luuk H. Karsten and Jan Smit. Lattice Fermions: Species Doubling, Chiral Invariance, and the Triangle Anomaly. *Nucl.Phys.*, B183:103, 1981.

[81] Marco Bochicchio, Luciano Maiani, Guido Martinelli, Gian Carlo Rossi, and Massimo Testa. Chiral Symmetry on the Lattice with Wilson Fermions. *Nucl.Phys.*, B262:331, 1985.

[82] G. Martinelli, C. Pittori, Christopher T. Sachrajda, M. Testa, and A. Vladikas. A General method for nonperturbative renormalization of lattice operators. *Nucl. Phys.*, B445:81–108, 1995, hep-lat/9411010.

[83] Karl Jansen, Chuan Liu, Martin Luscher, Hubert Simma, Stefan Sint, et al. Nonperturbative renormalization of lattice QCD at all scales. *Phys.Lett.*, B372:275–282, 1996, hep-lat/9512009.

[84] M. Constantinou et al. Non-perturbative renormalization of quark bilinear operators with Nf=2 (tmQCD) Wilson fermions and the tree- level improved gauge action. *JHEP*, 08:068, 2010, 1004.1115.

[85] Y. Aoki, P.A. Boyle, N.H. Christ, C. Dawson, M.A. Donnellan, et al. Nonperturbative renormalization of quark bilinear operators and B(K) using domain wall fermions. *Phys.Rev.*, D78:054510, 2008, 0712.1061.

[86] C. Sturm, Y. Aoki, N.H. Christ, T. Izubuchi, C.T.C. Sachrajda, et al. Renormalization of quark bilinear operators in a momentum-subtraction scheme with a nonexceptional subtraction point. *Phys.Rev.*, D80:014501, 2009, 0901.2599.

[87] R. Frezzotti, G. Martinelli, M. Papinutto, and G.C. Rossi. Reducing cutoff effects in maximally twisted lattice QCD close to the chiral limit. *JHEP*, 0604:038, 2006, hep-lat/0503034.

[88] S. Petrarca. Remarks on lattice gauge fixing. 1999, hep-lat/9912037.

[89] B. Blossier et al. Renormalisation constants of quark bilinears in lattice QCD with four dynamical Wilson quarks. *PoS*, LATTICE2011:233, 2011, 1112.1540.

[90] P. Dimopoulos et al. Renormalization constants for Wilson fermion lattice QCD with four dynamical flavours. *PoS*, LATTICE2010:235, 2010, 1101.1877.

[91] M. Constantinou, V. Lubicz, H. Panagopoulos, and F. Stylianou. O(a**2) corrections to the one-loop propagator and bilinears of clover fermions with Symanzik improved gluons. *JHEP*, 0910:064, 2009, 0907.0381.

[92] K. G. Chetyrkin and A. Retey. Renormalization and running of quark mass and field in the regularization invariant and MS-bar schemes at three and four loops. *Nucl. Phys.*, B583:3–34, 2000, hep-ph/9910332.

[93] J. A. Gracey. Three loop anomalous dimension of non-singlet quark currents in the RI' scheme. *Nucl. Phys.*, B662:247–278, 2003, hep-ph/0304113.

[94] Martha Constantinou et al. Perturbative renormalization factors and O(a^2) corrections for lattice 4-fermion operators with improved fermion/gluon actions. *Phys. Rev.*, D83:074503, 2011, 1011.6059.

[95] Andrzej J. Buras, Mikolaj Misiak, and Jorg Urban. Two loop QCD anomalous dimensions of flavor changing four quark operators within and beyond the standard model. *Nucl.Phys.*, B586:397–426, 2000, hep-ph/0005183.

[96] B. Blossier et al. Average up/down, strange and charm quark masses with Nf=2 twisted mass lattice QCD. *Phys.Rev.*, D82:114513, 2010, 1010.3659.

[97] Ph. Boucaud et al. Dynamical twisted mass fermions with light quarks. *Phys.Lett.*, B650:304–311, 2007, hep-lat/0701012.

[98] Remi Baron et al. Light Meson Physics from Maximally Twisted Mass Lattice QCD. *JHEP*, 1008:097, 2010, 0911.5061.

[99] S. Gusken. A Study of smearing techniques for hadron correlation functions. *Nucl.Phys.Proc.Suppl.*, 17:361–364, 1990.

[100] C. Best et al. Pion and rho structure functions from lattice QCD. *Phys. Rev.*, D56:2743–2754, 1997, hep-lat/9703014.

[101] M. Albanese et al. Glueball Masses and String Tension in Lattice QCD. *Phys. Lett.*, B192:163–169, 1987.

[102] V. Bertone et al. Kaon Mixing Beyond the SM from Nf=2 tmQCD and model independent constraints from the UTA. *JHEP*, 1303:089, 2013, 1207.1287.

[103] Damir Becirevic and Giovanni Villadoro. Remarks on the hadronic matrix elements relevant to the SUSY K0 - anti-K0 mixing amplitude. *Phys.Rev.*, D70:094036, 2004, hep-lat/0408029.

[104] Damir Becirevic, Svjetlana Fajfer, and Jernej F. Kamenik. Chiral behavior of the $B^0_{d,s} - \bar{B}^0_{d,s}$ mixing amplitude in the standard model and beyond. *JHEP*, 0706:003, 2007, hep-ph/0612224.

[105] Damir Becirevic and Francesco Sanfilippo. Theoretical estimate of the $D^* \to D\pi$ decay rate. 2012, 1210.5410.

[106] C. Aubin. Lattice studies of hadrons with heavy flavors. *PoS*, LAT2009:007, 2009, 0909.2686.

[107] P. Dimopoulos et al. Lattice QCD determination of m_b, f_B and $f_B s$ with twisted mass Wilson fermions. *JHEP*, 1201:046, 2012, 1107.1441.

[108] B. Blossier et al. Ghost-gluon coupling, power corrections and $\Lambda_{\overline{\rm MS}}$ from twisted-mass lattice QCD at Nf=2. *Phys.Rev.*, D82:034510, 2010, 1005.5290.

[109] K.G. Chetyrkin and A.G. Grozin. Three loop anomalous dimension of the heavy light quark current in HQET. *Nucl.Phys.*, B666:289–302, 2003, hep-ph/0303113.

[110] Stephen R. Sharpe and Yan Zhang. Quenched Chiral Perturbation Theory for Heavy-light Mesons. *Phys. Rev.*, D53:5125–5135, 1996, hep-lat/9510037.

[111] K. Nakamura et al. Review of particle physics. *J. Phys.*, G37:075021, 2010.

[112] Damir Becirevic, Benoit Blossier, Emmanuel Chang, and Benjamin Haas. g(B*Bpi)-coupling in the static heavy quark limit. *Phys.Lett.*, B679:231–236, 2009, 0905.3355.

[113] N. Carrasco, V. Gimenez, P. Dimopoulos, R. Frezzotti, D. Palao, et al. $K^0 - \bar{K}^0$ mixing in the Standard Model from Nf=2+1+1 Twisted Mass Lattice QCD. *PoS*, LATTICE2011:276, 2011, 1111.1262.

[114] Y. Aoki, T. Blum, N.H. Christ, C. Dawson, T. Izubuchi, et al. The Kaon B-parameter from quenched domain-wall QCD. *Phys.Rev.*, D73:094507, 2006, hep-lat/0508011.

[115] P. Dimopoulos, J. Heitger, F. Palombi, C. Pena, S. Sint, et al. Flavour symmetry restoration and kaon weak matrix elements in quenched twisted mass QCD. *Nucl.Phys.*, B776:258–285, 2007, hep-lat/0702017.

[116] Yousuke Nakamura, Sinya Aoki, Yusuke Taniguchi, and Tomoteru Yoshie. Precise determination of B(K) and right quark masses in quenched domain-wall QCD. *Phys.Rev.*, D78:034502, 2008, 0803.2569.

[117] P. Dimopoulos, H. Simma, and A. Vladikas. Quenched B(K)-parameter from Osterwalder-Seiler tmQCD quarks and mass-splitting discretization effects. *JHEP*, 0907:007, 2009, 0902.1074.

[118] Y. Aoki, T. Blum, N. Christ, C. Dawson, K. Hashimoto, et al. Lattice QCD with two dynamical flavors of domain wall fermions. *Phys.Rev.*, D72:114505, 2005, hep-lat/0411006.

[119] S. Aoki et al. BK with two flavors of dynamical overlap fermions. *Phys.Rev.*, D77:094503, 2008, 0801.4186.

[120] M. Constantinou et al. BK-parameter from Nf = 2 twisted mass lattice QCD. *Phys. Rev.*, D83:014505, 2011, 1009.5606.

[121] S. Durr, Z. Fodor, C. Hoelbling, S.D. Katz, S. Krieg, et al. Precision computation of the kaon bag parameter. *Phys.Lett.*, B705:477–481, 2011, 1106.3230.

[122] Jack Laiho and Ruth S. Van de Water. Pseudoscalar decay constants, light-quark masses, and B_K from mixed-action lattice QCD. 2011, 1112.4861.

[123] Christopher Kelly. Continuum Results for Light Hadronic Quantities using Domain Wall Fermions with the Iwasaki and DSDR Gauge Actions. 2012, 1201.0706. 7 pages, 3 figures. Contribution to The XXIX International Symposium on Lattice Field Theory, July 10-16, 2011.

[124] Taegil Bae, Yong-Chull Jang, Chulwoo Jung, Hyung-Jin Kim, Jangho Kim, et al. Kaon B-parameter from improved staggered fermions in $N_f = 2 + 1$ QCD. 2011, 1111.5698.

[125] A. Donini, V. Gimenez, Leonardo Giusti, and G. Martinelli. Renormalization group invariant matrix elements of Delta S = 2 and Delta I = 3/2 four fermion operators without quark masses. *Phys.Lett.*, B470:233–242, 1999, hep-lat/9910017.

[126] C.R. Allton, L. Conti, A. Donini, V. Gimenez, Leonardo Giusti, et al. B parameters for Delta S = 2 supersymmetric operators. *Phys.Lett.*, B453:30–39, 1999, hep-lat/9806016.

[127] Ronald Babich, Nicolas Garron, Christian Hoelbling, Joseph Howard, Laurent Lellouch, et al. K0 - anti-0 mixing beyond the standard model and CP-violating electroweak penguins in quenched QCD with exact chiral symmetry. *Phys.Rev.*, D74:073009, 2006, hep-lat/0605016.

[128] Y. Nakamura et al. Kaon B-parameters for Generic Delta S=2 Four-Quark Operators in Quenched Domain Wall QCD. *PoS*, LAT2006:089, 2006, hep-lat/0610075.

[129] P.A. Boyle, N. Garron, and R.J. Hudspith. Neutral kaon mixing beyond the standard model with $n_f = 2{+}1$ chiral fermions. *Phys.Rev.*, D86:054028, 2012, 1206.5737.

[130] N. Carrasco et al. Neutral meson oscillations in the Standard Model and beyond from Nf=2 Twisted Mass Lattice QCD. *PoS*, LATTICE2012:105, 2012, 1211.0565.

[131] D. Becirevic, V. Gimenez, G. Martinelli, M. Papinutto, and J. Reyes. B parameters of the complete set of matrix elements of delta B = 2 operators from the lattice. *JHEP*, 0204:025, 2002, hep-lat/0110091.

[132] Huey-Wen Lin, Shigemi Ohta, Amarjit Soni, and Norikazu Yamada. Charm as a domain wall fermion in quenched lattice QCD. *Phys.Rev.*, D74:114506, 2006, hep-lat/0607035.

[133] M. Ciuchini, E. Franco, D. Guadagnoli, V. Lubicz, M. Pierini, et al. D - $\bar{D}$ mixing and new physics: General considerations and constraints on the MSSM. *Phys.Lett.*, B655:162–166, 2007, hep-ph/0703204.

[134] Aida X. El-Khadra, Andreas S. Kronfeld, and Paul B. Mackenzie. Massive fermions in lattice gauge theory. *Phys.Rev.*, D55:3933–3957, 1997, hep-lat/9604004.

[135] Yasumichi Aoki et al. Nonperturbative tuning of an improved relativistic heavy-quark action with application to bottom spectroscopy. *Phys.Rev.*, D86:116003, 2012, 1206.2554.

[136] E. Follana et al. Highly improved staggered quarks on the lattice, with applications to charm physics. *Phys.Rev.*, D75:054502, 2007, hep-lat/0610092.

[137] N. Carrasco, P. Dimopoulos, R. Frezzotti, V. Gimenez, G. Herdoiza, et al. B-physics from the ratio method with Wilson twisted mass fermions. *PoS*, LATTICE2012:104, 2012, 1211.0568.

[138] N. Carrasco, P. Dimopoulos, R. Frezzotti, V. Gimenez, G. Herdoiza, et al. B-physics from lattice QCD...with a twist. *PoS*, ICHEP2012:428, 2012, 1212.0301.

[139] K.G. Chetyrkin, J.H. Kuhn, A. Maier, P. Maierhofer, P. Marquard, et al. Charm and Bottom Quark Masses: An Update. *Phys.Rev.*, D80:074010, 2009, 0907.2110.

[140] C. McNeile, C.T.H. Davies, E. Follana, K. Hornbostel, and G.P. Lepage. High-Precision c and b Masses, and QCD Coupling from Current-Current Correlators in Lattice and Continuum QCD. *Phys.Rev.*, D82:034512, 2010, 1004.4285.

[141] Benoit Blossier, John Bulava, Michele Della Morte, Michael Donnellan, Patrick Fritzsch, et al. M_b and f_B from non-perturbatively renormalized HQET with Nf=2 light quarks. *PoS*, LATTICE2011:280, 2011, 1112.6175.

[142] C. McNeile, C.T.H. Davies, E. Follana, K. Hornbostel, and G.P. Lepage. High-Precision f_{B_s} and HQET from Relativistic Lattice QCD. *Phys.Rev.*, D85:031503, 2012, 1110.4510.

[143] Heechang Na, Chris J. Monahan, Christine T.H. Davies, Ron Horgan, G. Peter Lepage, et al. The B and B_s Meson Decay Constants from Lattice QCD. *Phys.Rev.*, D86:034506, 2012, 1202.4914.

[144] A. Bazavov et al. B- and D-meson decay constants from three-flavor lattice QCD. *Phys.Rev.*, D85:114506, 2012, 1112.3051.

[145] F. Bernardoni, B. Blossier, J. Bulava, M. Della Morte, P. Fritzsch, et al. B-physics from HQET in two-flavour lattice QCD. *PoS*, LATTICE2012:273, 2012, 1210.7932.

[146] Elvira Gamiz, Christine T.H. Davies, G. Peter Lepage, Junko Shigemitsu, and Matthew Wingate. Neutral B Meson Mixing in Unquenched Lattice QCD. *Phys.Rev.*, D80:014503, 2009, 0902.1815.

[147] A. Bazavov, C. Bernard, C.M. Bouchard, C. DeTar, M. Di Pierro, et al. Neutral B-meson mixing from three-flavor lattice QCD: Determination of the SU(3)-breaking ratio ξ. *Phys.Rev.*, D86:034503, 2012, 1205.7013.

[148] C. Albertus, Y. Aoki, P.A. Boyle, N.H. Christ, T.T. Dumitrescu, et al. Neutral B-meson mixing from unquenched lattice QCD with domain-wall light quarks and static b-quarks. *Phys.Rev.*, D82:014505, 2010, 1001.2023.

[149] C.M. Bouchard, E.D. Freeland, C. Bernard, A.X. El-Khadra, E. Gamiz, et al. Neutral B mixing from $2+1$ flavor lattice-QCD: the Standard Model and beyond. *PoS*, LATTICE2011:274, 2011, 1112.5642.

[150] Beat Jegerlehner. Krylov space solvers for shifted linear systems. 1996, hep-lat/9612014.

[151] Anna Hasenfratz and Francesco Knechtli. Flavor symmetry and the static potential with hypercubic blocking. *Phys. Rev.*, D64:034504, 2001, hep-lat/0103029.

[152] Colin Morningstar and Mike J. Peardon. Analytic smearing of SU(3) link variables in lattice QCD. *Phys. Rev.*, D69:054501, 2004, hep-lat/0311018.

[153] M. Foster and Christopher Michael. Quark mass dependence of hadron masses from lattice QCD. *Phys. Rev.*, D59:074503, 1999, hep-lat/9810021.

[154] Marco Ciuchini, E. Franco, V. Lubicz, G. Martinelli, I. Scimemi, et al. Next-to-leading order QCD corrections to Delta F = 2 effective Hamiltonians. *Nucl.Phys.*, B523:501–525, 1998, hep-ph/9711402.

[155] V. Gimenez. Two loop calculation of the anomalous dimension of the axial current with static heavy quarks. *Nucl.Phys.*, B375:582–624, 1992.

[156] Juan Reyes Gámez. *Cálculo de elementos de matriz débiles para hadrones B con la HQET en el retículo*. PhD thesis, Universitat de València. Departamento de Física Teórica, Mayo 2001.

[157] Benoit Blossier, Michele Della Morte, Georg von Hippel, Tereza Mendes, and Rainer Sommer. On the generalized eigenvalue method for energies and matrix elements in lattice field theory. *JHEP*, 0904:094, 2009, 0902.1265.

[158] Michele Della Morte et al. Computation of the strong coupling in QCD with two dynamical flavors. *Nucl.Phys.*, B713:378–406, 2005, hep-lat/0411025.